The Development and Evaluation of Next-Generation Metallic Nanomedicines for Oncology

by

Brian Christopher Youden

A thesis
presented to the University of Waterloo
in fulfilment of the
thesis requirement for the degree of
Doctor of Philosophy
in
Biology

Waterloo, Ontario, Canada, 2024

Examining Committee Membership

The following served on the Examining Committee for this thesis. The decision of the Examining Committee is by majority vote.

External Examiner	**Dr. Devika Chithrani** Professor; Department of Physics and Astronomy & Department of Medical Physics, University of Victoria
Supervisor(s)	**Dr. Mark Servos** Professor; Canada Research Chair in Water Quality Protection, Department of Biology, University of Waterloo
	Dr. Runqing (Renee) Jiang Medical Physicist; Department of Medical Physics, Grand River Regional Cancer Centre Adjunct Professor; Department of Biology & Department of Physics, University of Waterloo Adjunct Professor; Department of Clinical Studies, University of Guelph
Internal Member	**Dr. Brian Dixon** Professor; Canada Research Chair in Fish and Environmental Immunology, Department of Biology, University of Waterloo
Internal-External Member	**Dr. Juewen Liu** Professor; Department of Chemistry, University of Waterloo
Other Member(s)	**Dr. Xu (Shine) Zhang** Professor; Canada Research Chair in Healthy Environments and Communities & Industrial Research Chair in Applied Nanotechnology, Department of Chemistry, Cape Breton University Adjunct Professor; Department of Biology, University of Waterloo

Author's Declaration

This thesis consists of material all of which I authored or co-authored: see *Statement of Contributions* included in the thesis. This is a true copy of the thesis, including any required final revisions, as accepted by my examiners.

I understand that my thesis may be made electronically available to the public.

Statement of Contributions

I was the sole author for Chapters 1 and 7, which were written under the supervision of Drs. Xu (Shine) Zhang, Runqing (Renee) Jiang, and Mark Servos. This thesis also consists of five manuscripts written with scientific collaborators for publication in peer-reviewed journals. Exceptions to the sole authorship of materials are as follows:

Chapter 2:

The work in Chapter 2 has been published as: Youden, B., Jiang, R., Carrier, A., Servos, M., Zhang, X. A Nanomedicine Structure-Activity Framework for Research, Development, and Regulation of Future Cancer Therapies. *ACS Nano* (Impact Factor: 17.1), **2022**, 16 (11), pp. 17497–17551. DOI: 10.1021/acsnano.2c06337.

As the primary author of this article, I was responsible for data collection, literature analysis, figure selection/design, and writing of the manuscript. Drs. Xu Zhang, Runqing Jiang, Andrew Carrier, and Mark Servos assisted in manuscript editing and provided their expert opinions on nanotechnology, radiology, chemistry, and biology, respectively. Drs. Xu Zhang, Runqing Jiang, and Mark Servos provided projection supervision and assisted in funding acquisition.

Chapter 3:

The work in Chapter 3 has been published as: Youden, B., Wang, F., Zhang, X., Curry, D., Majtenyi, N., Shaaer, A., Bingham, K., Nguyen, Q., Bragg, L., Liu, J., Servos, M., Zhang, X., and Jiang, R. Degradable Multifunctional Gold-Liposomes as an All-in-One Theranostic Platform for Image-Guided Radiotherapy. *International Journal of Pharmaceutics* (Impact Factor: 5.8), **2022**, 629, 122413. DOI: 10.1016/j.ijpharm.2022.122413.

Preliminary data for this work was also presented and published as a conference abstract (The American Association of Physicists in Medicine (AAPM), 2018 Annual Meeting): Youden, B., Jiang, R., Zhang, X. and Servos, M. Radio-Photothermal Therapy of Prostate Cancer Cells Using Gold-Lipid Nanoshells. In *Medical Physics* (Impact Factor: 3.8), **2018**, 45 (6), E342-E343. 111 River St., Hoboken 07030-5774, NJ USA: Wiley.

As the primary author of this work, I was responsible for experimental design, data collection, literature review, figure design, and writing of the manuscript. Dr. Feng Wang, Xiaohan Zhang, and Dr. Dennis Curry assisted in experimental design. Drs. Runqing Jiang, Nicholas Majtenyi, and Amani Shaaer assisted in operating radiation sources and data collection. Kenneth Bingham and Quang Nguyen provided HPLC analysis of iohexol. Leslie Bragg provided technical assistance and contributed to manuscript

editing. Drs. Xu Zhang, Runqing Jiang, Juewen Liu, and Mark Servos assisted in manuscript editing and provided their expert opinions on nanotechnology, radiology, chemistry, and biology, respectively. Dr. Juewen Liu also generously provided experimental facilities and materials. Drs. Xu Zhang, Runqing Jiang, and Mark Servos provided projection supervision and assisted in funding acquisition.

Chapter 4:

The work in Chapter 4 has been published as: Youden, B., Singh, P., Yang, Y., Chen, Y., Carrier, A., Cui, S., Oakes, K., Servos, M., Jiang, R. and Zhang, X. Synergistic multimodal cancer therapy using glucose oxidase@CuS nanocomposites. *ACS Applied Materials & Interfaces* (Impact Factor: 9.5), **2021**, 13 (35), pp.41464-41472. DOI: 10.1021/acsami.1c12235.

I and Dr. Parbeen Singh were shared first-authors for this work, contributing equally to experimental design, data collection, and manuscript preparation. I performed in vitro and mechanistic analysis of the CuS@Gox nanocomposites, while Dr. Parbeen Singh performed in vivo analysis. Drs. Yikun Yang and Yongli Chen also assisted in in vivo experimental design and data collection. Drs. Xu Zhang and Andrew Carrier assisted in manuscript editing and provided their expert opinions on nanotechnology and chemistry, respectively. Drs. Xu Zhang, Runqing Jiang, and Mark Servos provided projection supervision and assisted in funding acquisition.

Chapter 5:

The work in Chapter 5 has been published as: Youden, B., Singh P., Carrier, A., Oakes, K., Servos, M., Jiang, R., Sujing, L. Nguyen, T.D., and Zhang, X. Photo-Responsive Microneedles: An Innovative Way to Treat Diseases. *Journal of Controlled Release* (Impact Factor: 10.8), **2023**, 353, 1050-1067. DOI: 10.1016/j.jconrel.2022.12.036.

I and Dr. Parbeen Singh were shared first-authors for this work, contributing equally to literature review and manuscript preparation. Drs. Xu Zhang, Mark Servos, Runqing Jiang, Andrew Carrier, and Ken Oakes assisted in manuscript editing and provided their expert opinions on nanotechnology, radiology, chemistry, and biology. Drs. Xu Zhang, Runqing Jiang, and Mark Servos provided projection supervision and assisted in funding acquisition.

Chapter 6:

The work in Chapter 6 has been published as: Singh, P., Chen, Y., Youden, B., Oakley, D., Carrier, A., Oakes, K., Servos, M., Jiang, R., and Zhang, X. Accelerated Cascade Melanoma Therapy using Enzyme-Nanozyme-Integrated Dissolvable Polymeric Microneedles. *International Journal of Pharmaceutics* (Impact Factor: 5.8), **2024**, 652, 123814. DOI: 10.1016/j.ijpharm.2024.123814.

I and Drs. Parbeen Singh and Yongli Chen were shared first-authors for this work, contributing equally to literature review and manuscript preparation. I performed mechanistic analysis of the CuS@Gox nanocomposites as well as supplementary in vitro data, while Drs. Parbeen Singh and Yongli Chen performed in vivo analysis. Drs. Xu Zhang, Mark Servos, Runqing Jiang, Andrew Carrier, and Ken Oakes assisted in manuscript editing and provided their expert opinions on nanotechnology, radiology, chemistry, and biology. David Oakley assisted in data collection and experimental design. Drs. Xu Zhang, Runqing Jiang, and Mark Servos provided projection supervision and assisted in funding acquisition.

Additional publications which I have contributed to during my graduate studies but are not contained within this thesis include:

Chen, Y., Xian, Y., Carrier, A., Youden, B., Servos, M., Cui, S., Luan, T., Lin, S. and Zhang, X. A simple and cost-effective approach to fabricate tunable length polymeric microneedle patches for controllable transdermal drug delivery. *RSC Advances* (Impact Factor: 3.9), **2020**, 10 (26), pp.15541-15546. DOI: 10.1039/D0RA01382J

Chen, Y., Tyagi, D., Lu, M., Carrier, A., Nganou, C., Youden, B., Wang, W., Cui, S., Servos, M., Oakes, K. and He, S. A regenerative NanoOctopus based on multivalent-aptamer functionalized magnetic microparticles for effective cell capture in whole blood. *Analytical Chemistry* (Impact Factor: 7.4), **2019**, 91 (6), pp.4017-4022. DOI: 10.1021/acs.analchem.8b05432

Curry, D., Andrea, K., Carrier, A., Nganou, C., Scheller, H., Yang, D., Youden, B., Zhang, Y., Nicholson, A., Cui, S. and Oakes, K. 2018. Surface interaction of doxorubicin with anatase determines its photodegradation mechanism: insights into removal of waterborne pharmaceuticals by TiO2 nanoparticles. *Environmental Science: Nano* (Impact Factor: 7.3), **2018**, 5, 1027-1035. DOI: 10.1039/C7EN01171G

Abstract

Nanoparticles (NPs) are ultrasmall objects with profound applications in research, industry, and medicine. Next-generation nanomedicines, such as gold, hafnium, iron, and copper nanoparticles, are particularly interesting due to their excellent physical, chemical, and quantum properties that can be exploited for cancer diagnosis and therapy. However, despite their demonstrated preclinical effectiveness, the potential of these inorganic nanomedicines, both in oncology and the broader medical field, is hampered by mechanistic uncertainty and a lack of detailed regulatory guidance. Together, these factors have resulted in many failed clinical trials and unexpected and sometimes severe side effects for approved formulations. The therapeutic efficacy and toxicity of nanomedicines are controlled by an extremely complex interplay of nanoparticle physicochemical properties and individual patient biology, where many confounding factors exist. This makes designing and evaluating nanomedicines a challenging task. To progress metal-based nanomedicines to the clinic and for them to be considered safe, even in the life-or-death circumstances of cancer, a deep understanding of nano-bio interactions is necessary across different stakeholders. This includes physicians, academia, industry, and government. By understanding and utilizing these in vivo behaviors, powerful nanomedicines and novel treatments can be applied to oncology.

This thesis begins with a summary of the fundamental concepts relating to nanotechnology and the origins, properties, and treatment of cancer. Chapter 2 expands this discussion for a comprehensive analysis of cancer nanomedicines and their structure-activity relationships (SARs) in the body, which are central to both treatment efficacy and safety. Fundamentally, SARs describe the interactions between NP properties and the biological systems that ultimately produce their effects. To assist in the communication of this information, identified SARs were integrated into a simple, adaptable, and guiding framework composed of a parameter space, a pathway model, and various evaluation metrics. By resolving the complexity of nanomedicine into three parts, representing the interactions of NPs with 1) whole organs, 2) individual cells, and 3) fundamental biochemical pathways, this framework provides a clear illustration of how to fine-tune nanomedicines via pathway analysis. This framework and SARs were then used to guide the design, application, and evaluation of next-generation nanomedicines containing gold and copper.

Gold nanoparticles (GNPs) have long been proposed as promising agents for cancer phototherapy and image-guided radiation therapy (IGRT) due to their strong absorption of near-infrared (NIR) light and X-rays. GNPs are also among the most studied NPs owing to their general biocompatibility and easy synthesis. Despite this, only one GNP has been approved for clinical use owing to long-term safety concerns. Among various SARs, those related to size are often the most critical parameters for both efficacy and safety. This stems from both the nanoparticles themselves and the size-restrictive nature of kidney, liver, and tumor filtration of blood. To optimize the use of GNPs for enhanced IGRT, drug delivery, and

photothermal therapy (PTT), drug-loadable lipid NPs were utilized as a scaffold for GNP assembly, forming a versatile nanocomposite (Lipogold). Overall, this allows small NPs to function collectively as one larger nanoshell with plasmonic properties. Over time, this shell will degrade as the soft liposome core is stressed and deformed, resulting in renal-clearable NPs that can be cleared by the body following treatment. This thin shell of gold also optimizes the Auger process for RT and enables PTT, while the hollow core allows for encapsulation and delivery of drugs and molecular contrast agents. Thus, Lipogold nanocomposites demonstrate the advantages of both large and small NPs while adding multifunctionality. In this work (Chapter 3), medical radiation sources and cellular models were used to test their ability to sensitize cancer cells to megavoltage X-ray radiation therapy, provide contrast for computed tomographic (CT) imaging, deliver drugs, and engage in NIR-based PTT.

In addition to GNPs, plasmonic copper sulfide ($Cu_{2-X}S$ or just CuS) NPs are also emerging as increasingly popular nanomedicine candidates due to their photothermal properties, biodegradability, an ability to convert less-toxic H_2O_2 into more potent reactive oxygen species (ROS) for chemodynamic therapy (CDT). However, this approach in cancer therapy is fundamentally limited by several factors, principally the low concentration of H_2O_2 in the body. To overcome this issue, the properties of the tumor microenvironment (TME) were exploited for nanomedicine design, where CuS NPs were combined with the enzyme glucose oxidase (Gox) for a synergistic combination of starvation therapy, CDT, and PTT. Gox was used to convert glucose, which is upregulated in the TME, into H_2O_2 and acid, starving the cancerous cells and activating the Fenton-like reactivity of the CuS NPs. Deep-penetrating NIR could then be used for PTT and to enhance reaction kinetics specifically at the tumor site. The fundamental reaction mechanism was also investigated, highlighting the accelerative effect of chloride ions on the copper-Fenton reaction, which are present at high concentrations within skin and individual cells. In Chapter 4, the therapeutic efficacy and biocompatibility of the Gox@CuS nanocomposite were demonstrated using in vitro and in vivo melanoma models.

To further improve the safety profile of the Gox@CuS nanocomposite, the emerging technology of microneedle patches were explored as a transdermal drug delivery approach. Since conventional injections can lead to off-target uptake and toxicity, transdermal delivery may improve both efficacy and safety by maximizing local delivery and limiting blood exposure. This approach was extensively reviewed (Chapter 5) to determine the viability, design considerations, and fabrication methods of MNs containing light-responsive NPs such as Gox@CuS. Applications outside oncology were also reviewed to fully understand the advantages and limitations of this delivery system. Gox@CuS were then integrated into dissolvable polymeric microneedle (DPMN) patches and compared to hypodermic injection using another mouse melanoma model. In this study (Chapter 6), the microneedle patches were demonstrated to deliver

a higher amount of Gox@CuS to the tumor site and reduce the risk of systemic toxicity. Further mechanistic insight into the catalytic behavior of CuS NPs was also collected, specifically identifying the effect of chloride ions on the generation of both hydroxyl radicals and singlet oxygen.

Overall, this thesis contributes to our overall understanding of cancer nanomedicine and demonstrates several novel next-generation treatment strategies using metal-containing NPs. The framework proposed in this work is an adaptable and potentially valuable resource for researchers and regulators to understand SARs. Additionally, the pathway modelling used by this framework can assist in the development and integration of machine learning models that will increasingly play a role in the regulatory and industrial development of nanomedicine formulations.

Acknowledgements

I am eternally grateful for the support of my family and the mentorship and supervision of Drs. Xu (Shine) Zhang, Mark Servos, and Runqing (Renee) Jiang. I would also like to thank Leslie Bragg her administrative support and advice during experiment and manuscript preparation, Dr. Andrew Carrier for his expert knowledge on chemistry, Drs. Brian Dixon and Ken Oakes for their expert knowledge on biology and environmental science, Dr. Juewen Liu and his laboratory for their equipment use and technical assistance, Drs. Parbeen Singh and Yongli Chen for their collaborative efforts, Dongchang Yang, David Oakley, Dr. Nicholas Majtenyi, Dr. Amani Shaaer, Kenneth Bingham, Quang Nguyen, and Xiaohan Zhang for their help in data collection, and Dr. Brenda Lee from CyroDragon Inc. for her assistance in graphics design.

Financial support for this thesis was generously provided by the University of Waterloo, the Canada Research Chairs program, the NSERC Discovery Development Program, Canada's Telus Ride for Dad (RFD) and The Prostate Cancer Fight Foundation (PCFF), the Mitacs Accelerate program, the Ontario Graduate Scholarship (OGS) program, the China Postdoctoral Science Foundation, the Guangdong Province Higher Vocational College & School's Pearl River Scholar Funded Scheme, the Project of Scientific and Technological Foundation of Shenzhen, the Cape Breton University RISE program, the New Frontiers in Research Fund-Exploration program, and the Post-doctoral Foundation Project of Shenzhen Polytechnic.

Table of Contents

List of Figures and Schemes

List of Tables

List of Abbreviations

AA:	Ascorbic Acid	**CNS:**	Central Nervous System
ABC:	Accelerated Blood Clearance	**Col III:**	Recombinant Human Type III Collagen
ABTS:	2,2'-Azino-bis(3-ethylbenzothiazoline-6-sulfonic acid)	**CPO:**	Chloroperoxidase
AI:	Artificial Intelligence	**CPP:**	Cell Penetrating Peptide
ALA:	5-Aminolevulinic Acid	**CQ:**	Chloroquine
ALT:	Alanine transaminase	**CQA:**	Critical Quality Attributes
AOP:	Adverse Outcome Pathway	**CT:**	Computed Tomography
API:	Active Pharmaceutical Ingredients	**CW:**	Continuous Wave
AST:	Aspartate transaminase	**DAD:**	Diode Array Detector
ATTC:	American Type Culture Collection	**DAMP:**	Damage-Associated Molecular Pattern
AUC:	Area Under the Time Concentration Curve	**DHE:**	Dihydroethidium
BBB:	Blood-Brain Barrier	**DLS:**	Dynamic Light Scattering
BE:	Biological Event	**DMA:**	Dimethylmaleic Anhydride
BMPO:	5-tert-butoxycarbonyl-5-methyl-1-pyrroline-N-oxide	**DMEM:**	Dulbecco's Modified Eagle Medium
BP:	Black Phosphorus	**DMSO:**	Dimethyl Sulfoxide
CARPA:	Complement Activation-Related Pseudo-Allergy	**DOX:**	Doxorubicin
CAT:	Catalase	**(DP)MN:**	(Dissolvable Polymeric) Microneedle
CDT:	Chemodynamic Therapy	**DPPC:**	Dipalmitoyl Phosphatidylcholine
CED:	Convection-Enhanced Delivery	**EDTA:**	Ethylenediaminetetraacetic Acid
CMC:	Carboxymethyl Cellulose	**EMA**	European Medicines Agency
CME:	Clathrin-Mediated Endocytosis	**EMEM:**	Eagle's Minimum Essential Medium

EPR	Enhanced Permeability & Retention	**LED:**	Light Emitting Diode
ESR	Electron Spin Resonance	**LSEC:**	Liver Sinusoidal Endothelial Cell
FBS:	Fetal Bovine Serum	**LSP(R):**	Localized Surface Plasmon (Resonance)
FFF:	Flattening Filter Free	**LPPC:**	Long-Persistent Photocatalysis
GM-CSF:	Granulocyte-Macrophage Colony-Stimulating Factor	**MINBE:**	Minimum Information About Nanomaterial Biocorona Experiments
GNPr:	Gold Nanoprism	**MIRIBEL:**	Minimum Information Reporting in Bio–Nano Experimental Literature
GNR:	Gold Nanorod	**MDR:**	Multidrug Resistance
(r)GO:	(Reduced) Graphene Oxide	**MES:**	2-(N-morpholino)ethanesulfonic Acid
Gox:	Glucose Oxidase	**MIE:**	Molecular Initiating Event
GSH:	Glutathione	**ML:**	Machine Learning
GUI:	Graphical User Interface	**MN:**	Microneedle
(M)HA:	(Methacrylated) Hyaluronic acid	**MOF:**	Metal-Organic Framework
HIFU	High-Intensity Focused Ultrasound	**MP:**	Microparticle
ICG:	Indocyanine Green	**MPS:**	Mononuclear Phagocyte System
Ig:	Immunoglobulin	**MRI:**	Magnetic Resonance Imaging
IGRT:	Imaged-guided Radiation Therapy	**MRSA:**	Methicillin-Resistant *Staphylococcus aureus*
IIE:	Intrinsic Initiating Event	**MTT:**	Thiazolyl Blue Tetrazolium Bromide
IPA:	Isopropyl Alcohol	**MWCO**	Molecular Weight Cutoff
KC:	Kupffer Cell	**NC:**	Nanocomposite
KE:	Key Event	**NaOAc**	Sodium Acetate
LA:	Lauric Acid	**NIR:**	Near-Infrared
LAL:	Limulus Amoebocyte Lysate	**NLS:**	Nuclear Localization Signal

NO:	Nitric Oxide	**PRMN:**	Photoresponsive Microneedle
(G)NP:	(Gold) Nanoparticle	**PRR:**	Pattern-Recognition Receptor
NPC:	Nuclear Pore Complex	**PS:**	Parameter Space
OCED:	Organisation for Economic Co-Operation and Development	**PTT:**	Photothermal therapy
OSM:	Organic Semiconducting Material	**PVA:**	Polyvinyl Alcohol
PACT:	Photodyanmic Antimicrobial Therapy	**PVP:**	Polyvinylpyrrolidone
PAMAM:	Polyamidoamine	**PVPVA:**	Vinylpyrrolidone—Vinyl Acetate Copolymer
PAMP:	Pathogen-Associated Molecular Pattern	**QD:**	Quantum Dot
PB:	Prussian Blue	**REACH:**	Registration, Evaluation, Authorisation and Restriction of Chemicals
(D)PBS:	(Dulbecco's) Phosphate Buffered Saline	**RES:**	Reticuloendothelial System
PDA:	Polydopamine	**RFA:**	Radiofrequency Ablation
PDI:	Polydispersity Index	**RNS:**	Reactive Nitrogen Species
PDT:	Photodynamic Therapy	**ROS:**	Reactive Oxygen Species
PEG:	Polyethylene Glycol	**RPMI:**	Roswell Park Memorial Institute
PEGDA:	Polyethylene Glycol Diacrylate	**RT:**	Radiation Therapy / Radiotherapy
PET:	Positron Emission Tomography	**(Q)SAR:**	(Quantitative) Structure-Activity Relationship
PLGA:	Poly(Lactic-co-Glycolic Acid)	**SARS-CoV-2**	Severe Acute Respiratory Syndrome Coronavirus 2
PLLA:	Poly-L-lactic Acid	**SDT:**	Sonodynamic Therapy
PMMA:	Polymethylmethacrylate	**SERS**	Surface Enhanced Raman Spectroscopy
Pox:	Polyoxazolines	**SLS:**	Sentinel Lymph Node
PRM:	Photoresponsive Material	**SOP:**	Standard Operating Procedure

SOSG: Singlet Oxygen Sensor Green

SPION: Superparamagnetic Iron Oxide Nanoparticle

SSD: Source-to-Surface Distance

ST: Starvation Therapy

STS: Soft Tissue Sarcoma

TAT: Transactivator of Transcription

TDDS: Transdermal Drug Delivery System

TEM: Transmission Electron Microscopy

TMB: 3,3',5,5'-Tetramethylbenzidine

TME: Tumor Microenvironment

TNM: Tumor-Node-Metastasis

TPA: Terephthalic Acid

TPP: Triphenylphosphonium

US: Ultrasound

UV: Ultraviolet

VEGF: (Vascular) Endothelial Growth Factor

VIS: Visible

List of Symbols

λ, λ_{EM}, and λ_{EX} – Absorbance, Emission, and Excitation Wavelengths: Photon wavelengths used for optical absorbance and fluorescence spectroscopy…….....

γ-Ray – Gamma Ray: A high energy photon produced by the radioactive decay of an isotope, as opposed to X-rays produced by particle collisions. The term can also be used to denote X-rays of particularly high energy. Commonly measured in kilovolts (kV) or megavolts (MV)…….

γ-Fe_2O_3 – Maghemite: A specific form of iron oxide……..

$^1O_2$ – Singlet Oxygen: An excited state of molecular oxygen produced by the spin-pairing of the molecule's electrons. It can exist in two unstable and highly reactive forms, $^1\Delta_g$ and $^1\Sigma_g^+$, which are 0.98 and 1.63 eV above the ground state……..

$^3O_2$ – Triplet Oxygen: The stable ground state of molecular oxygen containing 2 unpaired electrons with the same spin state. Also denoted with the symbol $^3\Sigma_g^-$……..

ζ – Zeta Potential: The magnitude of the electrostatic or charge repulsion/attraction between particles; one of the fundamental parameters known to affect stability. Commonly measured in millivolts (mV)…….

“How do I know that I know this, except that I've always been taught this and never heard anything else? It's always worth establishing first principles. […] Don't take refuge in the false security of consensus and the feeling that whatever you think you're bound to be okay because you're in the safely moral majority.”

-Christopher Hitchens, April 13, 1949 – December 15, 2011

~ Chapter 1 ~

Cancer & Nanomedicine: Foundational Concepts

Chapter Summary

Cancer is a broad category of diseases involving abnormal and rapid cell growth with the potential to invade and damage healthy organs. Cancer is also among the top medical concerns globally owing to its variability and aggression. To manage this disease, significant efforts are put into the research of new drugs and treatments with improved efficacy and safety. Among these, nanotechnology has emerged as a powerful approach to improve the diagnosis and treatment of tumors, both as drug delivery vehicles and active pharmaceutical ingredients (APIs). This thesis serves to examine this field, particularly as it relates to the emerging next-generation of metal-based nanoparticles. This Chapter introduces the foundational concepts necessary for understanding cancer biology and the application of nanomedicine, and outlines the specific objectives of this thesis.

1.1 Cancer as a Disease: Properties & Pathogenesis

Cancer is a group of diseases involving abnormal cell growth that afflicts almost all living species. It is a progressive and potentially fatal condition that stems from the accumulation of genetic and epigenetic mutations in genes regulating metabolism and replication.[1] Once an individual cell becomes cancerous (oncogenesis), it will rapidly replicate into a mass, i.e., a tumor, that will excessively consume nutrients, manipulate surrounding tissue and the immune system,[2] and grow into and damage healthy organs.[3] At later stages, cancerous tumors can also release cells into the blood or lymph wherein they can spread the disease to secondary sites (metastasis).[4,5] By comparison, benign tumors, e.g., moles and fibroids, are cellular masses with a slow replication rate and without the capacity to invade; however, benign tumors can occasionally progress into cancerous tumors or cause health effects on their own.[6] Currently, various cancers are estimated to cause up to 10 million deaths each year and 16% of deaths overall,[7,8] with approximately 26.3% of men and 24.0% of women being expected to develop cancer in their lifetimes.[9]

Cancer can develop in any tissue type, although the most common forms are those affecting the lungs, colorectal tissue, stomach, prostate, and breasts.[8] Cancers can also be classified according to the cell type from which the disease originated, such as carcinoma (epithelial cells), sarcoma (connective tissue), melanoma (pigment cells), lymphoma (lymphocytes), leukemia (hematopoietic (blood-forming) cells), glioma (brain/glial cells), or blastoma (immature "precursor" cells or embryonic tissue). Despite occurring in widely different tissue types, cancerous cells and tumors can be generally defined by 8 hallmarks: 1) enhanced proliferative signaling, 2) evasion of growth suppressors, 3) resistance cell death mechanism, 4)

replicative immortality, 5) induced angiogenesis, i.e., vasculature formation, 6) tissue invasion and metastasis, 7) altered cellular metabolism, and 8) evasion of the immune system.[10–12] Individually, these hallmarks and the mutations that cause them do not define a cell as cancerous, but collectively they represent an aggressive and highly adaptive disease. Cells can become cancerous through both random replication errors as well as through exposure to ionizing radiation, particular pathogens, and carcinogens (chemicals known to be capable of either directly damaging DNA or reducing the efficiency of DNA repair).[13] While cells are remarkable for their ability to accurately transcribe DNA, this process is not perfect and will gradually result in the buildup of mutations over time, even in the absence of DNA damaging agents. In conditions of inflammation and genetic instability, such as during infection, the likelihood of developing mutations is significantly increased.[14,15] If these mutations occur in germ cells, then these mutations can be passed on, increasing the cancer risk in offspring.

The main risk factors for developing cancer are genetics/family history, age, and environmental exposure, with the later having the most significant and controllable impact[16–18]; however, as the average lifespan continues to increase throughout the world, the incidence of cancer can also be expected to increase significantly.[19,20] Notably, for some common carcinogens, single-to-moderate exposures can have low or negligible risks and it is primarily through chronic exposure that cancer arises. The chronic consumption of tobacco or cannabis products is the most well-known example as the burning of plant matter releases a wide range of toxic compounds,[21] although the development of cancer often takes several years or decades to occur. Overall, it is estimated that ~20-25% of all cancers can be attributed to long-term tobacco use,[22] ~10-20% can be attributed to infections by pathogens such as *Helicobacter pylori*, hepatitis B and C, and human immunodeficiency virus,[23,24] ~10-15% can be attributed to obesity, diet, and alcohol consumption,[25,26] and ~5-10% to genetics.[27] Other cancers are likely to be the result of several risk factors in combination,[28] although it is important to note that some risk factors will be more or less important for individuals depending on their genetic and metabolic profiles. Additionally, some cancers are more likely to be induced by some risk factors than others.[29]

The progression and survival rate of different cancers can be defined according to various stages of development, with the most common systems being the tumor-node-metastasis (TNM) and Roman numeral systems.[30–33] In the TNM system, each tumor can be classified by letters according to its size (Tx, Tis, or T0-4), degree of lymph node invasion (Nx or N0-3), and metastasis (M0-1), with additional parameters occasionally being noted by other letters and prefixes. In the Roman numeral system, cancers are simply classified by their size and degree of spread (stages 0-IV), although like the TNM system some modifiers are occasionally used to provide further detail. Stage 0 includes both benign and pre-cancerous tumors that not yet seen significant growth (are in situ) and have high cure rates. Stage I cancers are defined

by their small and localized size, while stages II and III indicate larger locally advanced cancers. The difference between stages II-III depends on the specific type of cancer and the organ it is affecting. At stage IV, defined by metastasis, many cancers become terminal and the focus of treatment switches from curative to palliative care. Additional classification systems, often using similar notations, also exist for specific cancers such as blood,[34] brain,[35] and pediatric cancers,[36] which can not be adequately described using conventional staging systems. In both cases, as the stages progress and the numerical values increase, the odds of survival decrease and the available treatment options become more limited. The rate of progression of different cancers, even of the same tissue type, is often patient specific owing to unique combinations of oncogenes,[1] although cancers originating from fast-replicating tissue can be expected to grow and spread faster than cancers from slow-replicating tissue.

1.2 Oncology: Cancer Diagnosis & Therapy

The field of oncology includes the diagnosis and treatment of both benign and cancerous tumors; however, this goal is challenging due to the complexity of cancer and its similarity to normal healthy tissue. While cancerous cells possess unique hallmarks that can be targeted for treatment, these are often based on the up- or down-regulation of molecular features that are also expressed in normal cells to some degree.[10–12] As such, most diagnostic and treatments that respond to cancerous tissue will also affect healthy tissue to some degree. Cancers can also be highly variable in their treatment sensitivity due to different combinations of mutations that alter cellular responses to drugs and/or radiation.[37] Additionally, since cancers emerge from a small population of cells, very few symptoms are initially produced or observed, making early detection and treatment difficult for non-superficial tumors. After further growth, a wide range of symptoms can emerge depending on which organ(s) are affected and how. Many of these symptoms can present similarly to other diseases, further complicating detection.[38] Ultimately, most patients are diagnosed only after the onset of symptoms and many present to emergency care services with life-threatening manifestations of the disease.[39]

Cancer diagnosis has increasingly focused on early screening methods including DNA and RNA testing, routine physical checks, blood and urine tests for cancer biomarkers or circulating tumor cells, and medical imaging.[40–44] This is because early-stage tumors are far easier to treat than late-stage tumors. Collectively, these advances in screening have produced significant improvements in cancer detection and treatment, although each method has limitations.[45] DNA testing, for example, can be slow, only provides an expectation or estimate of risk, and still requires routine checkups for detection. Other methods, including physical checks, biomarkers, and imaging can all be subject to false positives and negatives due to the high variability of individual patients, limited sensitivities, co-morbidities, and the dynamic nature of cancer.[46]

Conventional cancer therapies include chemotherapy, immunotherapy, hormone therapy, radiation therapy/radiotherapy, and surgery.[47–49] More recently, other techniques including phototherapies (light/photon-based treatments), ultrasound-based treatments, anti-cancer vaccinations, and gene therapies have entered clinical use as well.[50–54] Surgery is the most direct approach to the removal of tumors; however, it is also highly invasive, requires the removal of surrounding heathy tissue, and can not be used against small metastasises that can not be easily visualized. Many tumors can also grow in, on, or near highly sensitive and important locations, e.g., near a major artery or within the brain, which further increases the risks of surgery. As such, the delivery of therapeutics and/or radiation therapy are often used in combination with, or as an alternative to, surgery.

Radiotherapy and similar methods, including phototherapies and ultrasound-based methods, damage tissue via the delivery of energy (ionizing radiation, magnetic fields, light, or ultrasound) to the tumor site by an external, implanted, or injected source.[50–53,55–61] By comparison, chemotherapy, immunotherapy, and hormone therapy, etc. can all be viewed under the simplified lens of 'drug delivery', with the key difference laying in the type of compound(s) delivered and their mechanisms of action. Chemotherapy normally involves the use of cytotoxic agents that are preferential in some way for cancerous cells.[62] In the case of hormone therapy, the delivered therapeutics target either the endocrine system broadly or the tumors cells directly to suppress tumor growth.[49] Immunotherapy involves the delivery of agents that modulate immune cell behavior at or towards tumors.[48] Notably, immune cells can both target cancerous cells for destruction or promote their growth, depending on the immune cell type/polarization and the cytokines/chemokines release by cancerous cells.[63] As such, most cancer treatments can be expected to induce some immunological effects due to the release of cellular components and inflammation following tumor cell death.[64,65] Immunogenic cell death refers to when immune cells are primed to target tumors as a response to a prior treatment. The immune system is also heavily implicated in rare cases of spontaneous remission.[66,67]

The main limitation of radiotherapy and drug delivery strategies for oncology is the high potency, and thus side effects, of the delivered energy or active pharmaceutical ingredients (APIs). Overall, drugs, hormones, proteins, and other compounds (APIs) delivered via injections to the blood are effective at treating widespread cancers, including metastasis and blood cancers, but also produce systemic side effects.[68] When APIs, including radiation sources, are delivered locally, i.e., intratumorally injections,[69] topical creams,[70] or transdermal delivery,[71,72] cancers and other disease can be treated more effectively and reduce systemic exposure, although some tumors are not directly accessible for such applications and consistent dosing is also a concern. Various forms of oral and nasal/pulmonary delivery are also explored as relevant to specific tumor types.[73,74] In the case of delivering radiation, light, and sound, factors relating

to energy attenuation and beam accuracy must be considered. Depending on the treatment and tumor types, different delivery strategies may be appropriate.

Despite several treatment techniques at our disposal, cancer is a difficult disease to detect and treat, and the currently approved methods possess many limitations and risks. Owing to its genetic nature, cancer is not a disease that can be eliminated from the population or prevented entirely. Additionally, the same random mutations that lead to oncogenesis can also alter cell signalling and responses to APIs, light, oxygen-deprivation, oxidative stress, and radiation. While some tumors respond exceptionally well to one or many treatments, others can be or become highly resistant. For these reasons, cancer research has consistently sought new APIs, treatment mechanisms, and improvements to traditional approaches. Among the various approaches to improve oncology, nanotechnology-based strategies have become increasingly prominent.

1.3 Nanotechnology, Nanomaterials, & Nanomedicine

Nanotechnology is a billion-dollar research field and industry that has provided significant advances in engineering, electronics,[75] agriculture,[76] energy storage,[77] homeland security,[78] and medicine.[79] This includes the diagnosis and treatment of cancers (cancer nanomedicine), the focus of this thesis. However, considerable overlap and ambiguity exists in the terminology used to described nanotechnology, which can result in significant confusion for those unfamiliar with the field. Thus, this section will be devoted to defining and clarifying these terms while the greater detail of mechanisms, challenges, knowledge gaps, applications, progress, and opportunities of nanomedicine will be discussed in Chapter 2.

Nanotechnology can be considered a catch-all term for both the matter/materials and techniques that operate on the nanoscale. The nanoscale can be broadly defined between 0.1-1000 nm, although most sources use a stricter definition of 1-500 nm.[80] Any material with at least one physical dimension in this range is therefore a nanomaterial. Materials below this size range (≤2 nm) are classified as nanoclusters or as simple chemical compounds and ions,[81] while those above this range (≥0.5-1000 μm) are broadly described as microparticles. Quantum dots (QDs) are a special category of small nanomaterials (~1-20 nm) wherein the electrical and optical properties are determined by quantum confinement.[82] Importantly, these three categories exist on a size spectrum and share overlapping features. Therefore, no arbitrary size can be used to define them and some nanomaterials at or near the defining size boundaries may be classified as either microparticles or quantum dots by different sources. Nanomaterials and nanoparticles (NPs) are similarly broad terms that can describe any nanoscale material and are often interchangeable, although NP is also widely used specifically for spherical nanomaterials (nanospheres or nanocrystals).[80] For non-

spherical nanomaterials, specific names such as nanocubes, nanotriangles, nanowires, nanofilms, and nanostars are commonly used.

Nanomaterials can be composed of either organic (composed of carbon/silicon and other light elements) or inorganic (composed of metals, metalloids, or carbon/silicon allotropes) compounds, including noble metals, semiconductors, carbon, lipids, proteins, and DNA.[79,83] Importantly, there is no official delineation between nanomaterials that are natural, i.e., proteins and ultrasmall minerals, and those are that engineered by humans, although it is common to only refer to the latter as nanomaterials in biological contexts to avoid confusion. Thus, whole living cells, organelles, and biomolecules with diameters in the nanoscale, e.g., mycoplasma, mitochondria, and chromosomes, are excluded from the definition of nanomaterials while modified proteins, aptamers, and non-living cell-like membranes, e.g., lipid NPs and modified endosomes, are included. By comparison, both synthesized and naturally occurring metal NPs, e.g., small rust particles, are both considered nanomaterials.[84]

Inorganic nanomaterials have a long history with humans, largely through their accidental discovery and production. Copper, gold, and silver NPs, for example, have been widely used across the world since ancient times for producing highly coloured red, purple, and yellow glass.[85] In both western and eastern alchemy (the precursor to modern chemistry), gold NPs (GNPs) and salts in particular played notable parts in the production of glass, dyes/glazes, medicines, and the mythical philosopher's stone (of which GNPs may have inspired its purported ruby red color).[86] Inorganic carbon nanomaterials, i.e., nanotubes and nanowires, have also been reported to be among the defining features of Damascus steel.[87] By contrast, nanomaterials made of organic compounds are a recent invention originating from fields of medicine, biochemistry, and biotechnology.[83,88] Organic nanomaterials, such as lipid NPs (liposomes) and fusion proteins, closely resemble their biological counterparts in form and function, i.e., vesicles and enzymes, respectively. As such, their behavior and toxicity are comparatively simple to understand from a biological or medical background. In contrast, inorganic nanomaterials utilize the emergence of quantum mechanical phenomena, particularly those that relate to quasiparticles (a collective behavior of a group of particles, e.g., plasmons (electrons), phonons (vibrational modes), electron vacancies (holes), and excitons (electron-hole pairs)), electron movement (excitation and conductivity), and photon-electron interactions (adsorption, scattering, and emission). Thus, inorganic nanomaterials have traditionally been the focus of chemical engineers, physicists, and materials scientists. For both organic and inorganic nanomaterials, the ultimate capabilities, stability, and reactivity of NPs are fundamentally dependant on their structure.[89–94] In the case of organic nanomaterials, these structure-activity relationships (SARs) can be compared to the nature of proteins, antibodies, enzymes, and biological membranes. In inorganic nanomaterials, SARs,

including quantum effects, depend on crystalline and surface structure (including defects), elemental and chemical composition, and morphology.[95–98]

By finely tuning the SARs of nanomaterials, a wide range of applications, including cancer therapy, are unlocked. Nanomedicine, therefore, simply refers to nanotechnology and nanomaterials used for various medical purposes. This can include the use of individual nanomaterials or composites of several nanomaterials (nanocomposites) for a wide range of treatment strategies.[79] Notably, nanomedicine has its primary origins in oncology with the development of liposomes for drug delivery, i.e., Doxil®.[88] In the decades since, liposomes have been expanded for the treatment of several different diseases as well as nutrient supplementation and medical imaging.[99–103] Cancer nanomedicine has also evolved to include other nanomaterials including fusion proteins, organic polymers, and inorganic NPs, making it a highly interdisciplinary field.[104–106] Owing to its large-scale implementation during the SARS-CoV-2 pandemic, nanomedicine is now a well-established medical field and is likely to continue to grow significantly in the next few decades.[107–109] Nevertheless, significant knowledge gaps in the interactions of nanomaterials with biological systems remain.

1.4 Thesis Objectives

Currently, a large volume of research has been conducted on nanomedicines; however, the majority of this has been performed on simple organic nanomaterials. Despite their long history, highly unique properties, considerable research efforts, and promising preliminary results, nanomaterials composed of metals have only just begun to enter the market for a limited number of applications. To progress additional next-generation materials to the clinic, fundamental research into the engineering and application of nanomedicine SARs to cancer biology is needed. This research must then be effectively synthesized, communicated, and applied. Therefore, this work seeks to provide foundational insights, resources, and improvements to the development and application of next-generation metal-based nanomedicines for oncology. To accomplish this, the objectives of this thesis were to: 1) perform a comprehensive and up-to-date literature review of nanomaterial SARs in vivo, 2) propose a simple, adaptable, and novel theoretical framework (nanomedicine structure-activity framework (NSAF)) to guide the design and study of cancer nanomedicines for a broad audience, including researchers, industry, and regulators, 3) apply the insights of the NSAF and the unique SARs of copper and gold to develop novel next-generation metal-based nanomedicines, and 4) evaluate the integration of emerging microneedle delivery technologies with NSAF-inspired nanomedicines. This thesis is composed of seven Chapters (**Scheme 1**), including an introduction of foundational concepts (Chapter 1), two literature reviews (Chapters 2 and 5) and three experimental research articles published in high-impact journals (Chapters 3, 4, and 6), and a concluding summary and outlook (Chapter 7).

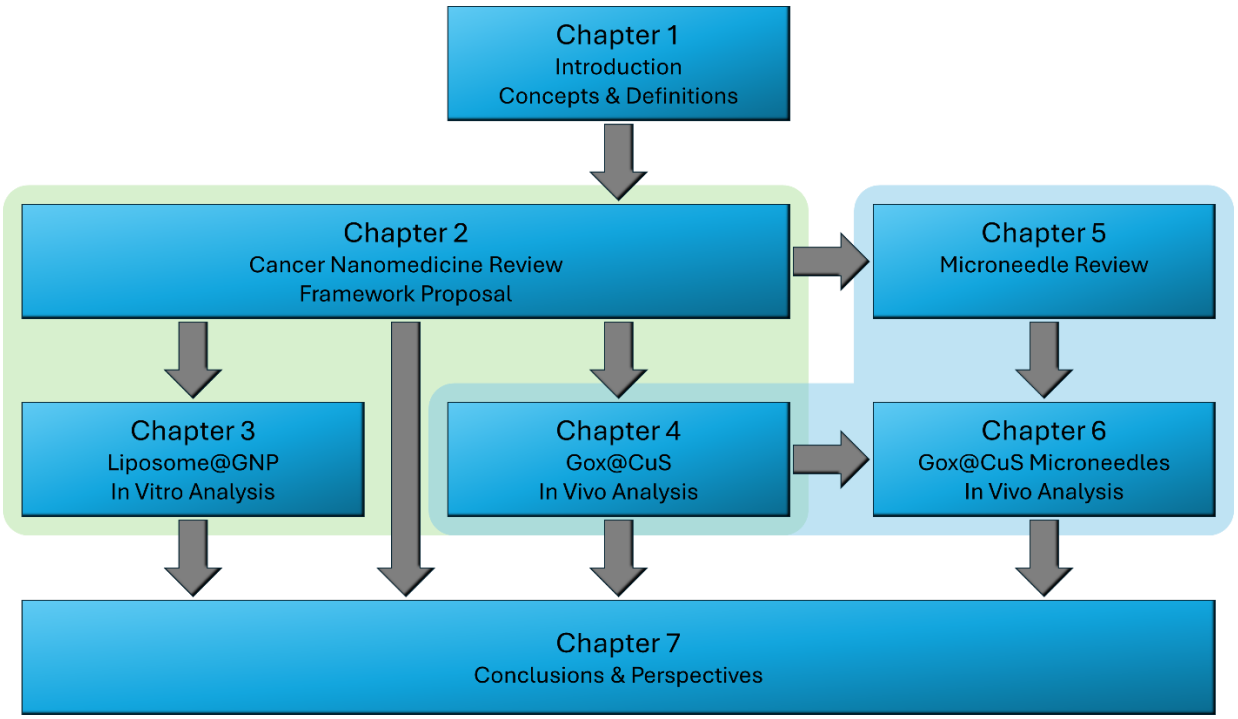

Scheme 1: Simplified thesis structure.

In Chapter 2, a comprehensive review of the overall field of cancer nanomedicine is presented.[110] This information is then summarized into a simplified and adaptable framework that divides the complexity of nanomedicine into three levels, representing the interactions of NPs with 1) whole organs, 2) individual cells, and 3) fundamental biochemical pathways. Collectively, this provides an illustration of how nanomedicines can be fine-tuned for efficacy and safety. Importantly, since this is a knowledge framework, the bulk of the literature review for this thesis was provided in Chapter 2 to support the design and integration of different mechanisms. Particular attention is also given to the mechanisms of metal-based nanomedicines due to their more recent emergence in the fields of medicine and toxicology. Additionally, as nanomedicine research attempts to move away from large-scale animal testing, the need for computer-assisted solutions for evaluation will increase. To facilitate this, the proposed framework utilizes a machine-learning inspired structure, including an input parameter space and feedback system, to organize and integrate different SARs. This provides a valuable guide for nanomedicine development and evaluation for a wide range of researchers and regulators. In the following Chapters, the NSAF was utilized as a guide when designing and applying novel nanomedicines for in vivo applications.

In Chapter 3, SARs were applied in the design and testing of a novel liposome@GNP core-shell nanocomposite for enhanced image-guided radiotherapy, drug delivery, and photothermal therapy.[111] Since physical size is a key parameter governing NP's optical properties, circulation half-life, biological retention, and excretion/removal (affecting imaging, potency, drug delivery, and toxicity), soft biodegradable

liposomes were employed as a scaffold for renal-clearable GNPs. In this way, the advantages of both large and small GNPs are combined while adding further multifunctionality via a loadable hollow core. The large overall size of the nanocomposite enables a localized surface plasmon resonance that can be used for photothermal therapy and drug release, and long circulation times following injection. Following the treatment, the degradation of the nanocomposite in vivo can then facilitate rapid clearance of GNPs from the body, improving safety. During X-ray radiation therapy, the thin-shell of gold also maximizes the emission of dose-amplifying Auger electrons into the cellular environment. The potential and validity of this approach was established using in vitro assays and patient-relevant radiation and light sources.

In Chapters 4-6, the preclinical development and investigation of a simple organic-inorganic hybrid nanocomposite for the treatment of superficial tumors was completed in a collaboration with Shenzhen Polytechnic.[112–114] Chapter 4 details the initial development of the nanocomposite using SARs.[112] The enzyme glucose oxidase (Gox) was combined with (photo-)catalytic copper sulfide (CuS) nanoparticles and evaluated for its ability to produce cytotoxic reactive oxygen species (ROS) from glucose, which is upregulated in tumors. The optical properties of CuS also enabled the use of deeply-penetrating near-infrared (NIR) light for combination photothermal therapy. Following chemical and in vitro analysis, the nanocomposite was then applied for in vivo combination therapy of mouse melanoma xenografts with positive results. The safety profile of the nanocomposite was then enhanced using a microneedle delivery system. In Chapter 5, the potential of this approach over intratumoral injection was examined by reviewing the integration of phototherapeutics, including nanomedicines, with microneedle technologies.[113] This review also served to establish the necessary microneedle design principles. In Chapter 6, the nanocomposite was encapsulated within a dissolvable microneedle patch and evaluated using a more extensive lineup of chemical, in vitro, and in vivo assays.[114] The results of these experiments provided additional insights into the nanocomposites mechanisms and improvements to both the efficacy and safety profile. The original and unique contributions of this thesis include the characterization and mechanistic analysis of the nanocomposite, which are critical for treatment optimization and further expansion, e.g., the use of the composite in combination with radiotherapy.

Finally, Chapter 7 serves to summarize the results of this thesis, update the NSAF developed in Chapter 2, and explore future research directions. Insights from the application of nanomedicines in the SARS-CoV-2 pandemic are also briefly discussed. In its totality, this thesis provides contributions to the general understanding of nanomedicines and nanotoxicology via the development of a guiding knowledge framework, the proof-of-concept development of a novel platform for image-guided radiotherapy, and the preclinical and mechanistic analysis of a highly effective combination strategy.

~ Chapter 2 ~

A Nanomedicine Structure-Activity Framework for Research, Development, and Regulation of Future Cancer Therapies

The work presented in this chapter has been published as:

Youden, B., Jiang, R., Carrier, A., Servos, M., Zhang, X. A Nanomedicine Structure-Activity Framework for Research, Development, and Regulation of Future Cancer Therapies. *ACS Nano*, **2022**, 16 (11), pp. 17497–17551. DOI: 10.1021/acsnano.2c06337.

Chapter Summary

Despite their clinical success in drug delivery applications, the potential of theranostic nanomedicines is hampered by mechanistic uncertainty and a lack of science-informed regulatory guidance. Both the therapeutic efficacy and the toxicity of nanoformulations are tightly controlled by the complex interplay of the nanoparticle's physicochemical properties and the individual patient/tumor biology; however, it can be difficult to correlate such information with observed outcomes. Additionally, as nanomedicine research attempts to gradually move away from large-scale animal testing, the need for computer-assisted solutions for evaluation will increase. Such models will depend on a clear understanding of structure–activity relationships. This review provides a comprehensive overview of the field of cancer nanomedicine and provides a knowledge framework and foundational interaction maps that can facilitate future research, assessments, and regulation. By forming three complementary maps profiling nanobio interactions and pathways at different levels of biological complexity, a clear picture of a nanoparticle's journey through the body and the therapeutic and adverse consequences of each potential interaction are presented.

2.1 Introduction to Nanomedicine

Cancer is a leading cause of premature death worldwide and both its incidence and mortality are currently increasing.[115,116] Despite many advances in conventional treatments, nonspecific antitumor drug distribution, intolerable cytotoxicity/side effects, and the development of radiation resistance and multiple drug resistance (MDR) remain challenging roadblocks.[47] There is therefore an urgent need to develop more effective approaches to cancer treatments. Nanomedicine, the medical use of engineered nanomaterials, *i.e.*, materials containing at least one dimension on the nanoscale (broadly 1–500 nm), has emerged as a means of transforming the current treatment paradigm in oncology.[117] Nanomaterials, often simply referred to as just nanoparticles (NPs) in the context of nanomedicine, can be engineered to act as multifunctional therapeutics, diagnostic tools, and drug carriers in a myriad of clinical applications. (**Figure 1**).[61,118]

Following the approval of Doxil® /Caelyx™ in 1995 for the treatment of Kaposi's sarcoma and ovarian cancer, over 50 additional nanomedical products have been approved,[99–103] including several recent SARS-CoV-2 mRNA vaccines that have seen widespread use.[107–109] Currently, 24 different nanomedicines are approved worldwide for cancer treatment, and significantly more are undergoing clinical trials.[119–123]

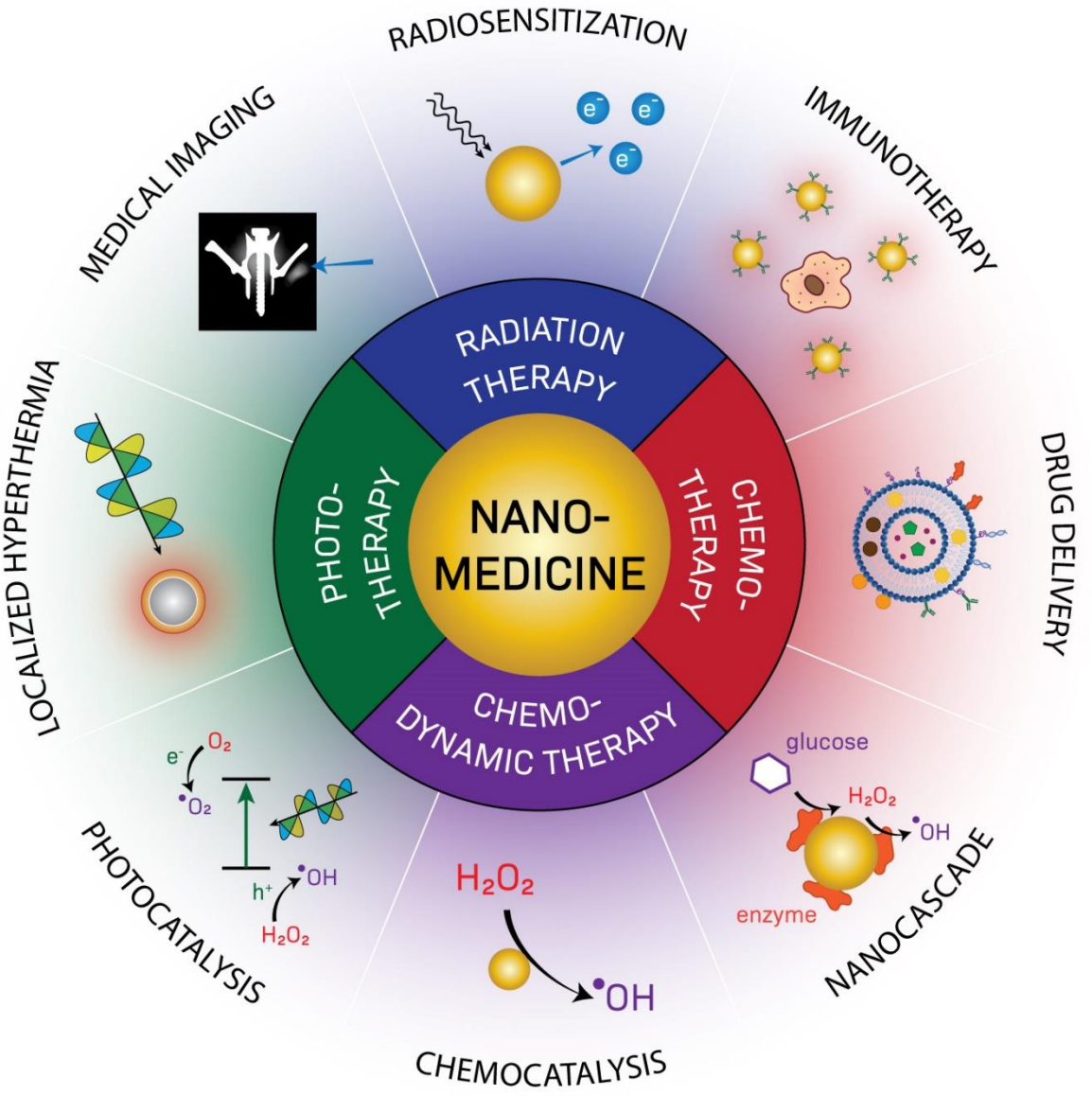

Figure 1: The advanced anticancer paradigm of nanomedicine. Nanoparticles (NPs) have been widely exploited for phototherapies and chemodynamic therapies, in addition to sensitized radiotherapy and drug delivery. To eliminate cancer, chemodynamic therapy (CDT) uses reactive oxygen species (ROS) catalytically generated in situ whereas phototherapies use non-ionizing light and radio-waves to generate heat and ROS. As these applications stem from overlapping physicochemical properties, they can be combined for synergistic treatments. NP-enabled drug delivery

can be combined with many treatments, such as radiation therapy to enhance immunogenic cell death, or CDT to produce more ROS by cascade reactions. CDT can synergize phototherapy to accelerate ROS production via heat and photocatalysis. High resolution medical imaging, such as photoacoustic, X-ray, and magnetic-resonance imaging, can be facilitated by NPs with different optical properties.

Anticancer nanomedicines can be broadly categorized as organic, inorganic, or hybrid formulations depending on their primary composition and function.[124,125] Such formulations can be composed of either NPs that possess therapeutic functions or a combination of inert NP carriers (nanocarriers) and active pharmaceutical ingredients (APIs) that possess a different pharmacodynamic or pharmacokinetic profile from the API alone. Organic nanomedicines are primarily composed of biomolecules, such as lipids, proteins, or synthesized biopolymers, and have seen the most clinical success because of their overall biocompatibility, biodegradability, and/or their ability to encapsulate different APIs.[99,119–121] Comparatively, inorganic nanomedicines, containing nanomaterials such as carbon-based NPs, metallic NPs, and quantum dots (QDs), have seen less progress because of uncertainty regarding their biological persistence and toxicity.[124,126,127] Inorganic NPs often have distinct physicochemical properties from their corresponding bulk materials because of quantum confinement effects and surface defects inherent to nanoscale crystal structures.[95–98] As such, these NPs possess varying degrees of activity, potentially leading to chronic side effects. However, the manipulation of these properties also enables future therapeutic strategies, which have shown encouraging results in early preclinical studies and clinical trials. For example, the strong interactions of some inorganic NPs with light (visible, infrared, or ionizing radiation) have been exploited for phototherapies or to improve radiation therapy. Most recently, the European Medicines Agency's (EMA's) approved Hensify®, a solution of 50 nm hafnium oxide (HfO_2) NPs that has seen clinical success when used in combination with radiation therapy for the treatment of locally advanced soft tissue sarcoma.[102,106] Clinical trials in the US are currently underway for liver, lung, pancreatic, and squamous cell cancers, including a phase III trial for locally advanced squamous cell cancers in combination with cetuximab immunotherapy.

Despite the preclinical and clinical success of both organic and inorganic nanomedicines, major questions and challenges remain that hinder their further development. Herein, a conceptual framework is presented for assembling existing knowledge. This framework provides a structural understanding of nanomedicine, focusing on the fundamental design principles and mechanisms governing their functions and toxicity. An emphasis is placed on clinically approved formulations and next-generation inorganic nanomedicines, which we believe will significantly contribute to oncology in near future. Through this framework, we aim to facilitate nanomedicine research, development, and regulation by providing a useful efficacy and risk assessment tool for cancer treatments.

2.1.1 Organic Nanomedicine: Advanced Drug Delivery Strategies

Of the 24 currently recognized and approved nanomedicines for anticancer applications, 22 (92%) contain organic NPs (**Table 1**).[120,122,123,128–130] Generally, many therapeutic biomolecules, including antibodies, hormones, and synthetic polymers, naturally qualify as nanomedicines because of their size alone.[131,132] However, most researchers and this work limit the term nanomedicine to only those materials that have been engineered (including simple chemical modifications) to possess additional therapeutic functions or pharmacokinetic properties. Using this definition, there have been clinical successes for cancer treatment in the forms of lipid vesicles, biodegradable polymers, engineered proteins, and antibody-drug conjugates (Table 1, **Figure 2**).[104,105] In addition, organic NPs made of dendrimers or polysaccharides such as chitosan and hyaluronic acid have also gained intense research interest.[133,134] While some organic NPs are designed to be therapeutic agents, most are designed as drug delivery vehicles to improve API circulation and targeting. Among these, lipid NPs, *i.e.*, liposomes and micelles, have seen the most attention and success.

Table 1: Nanomedical products currently in clinical use for the treatment of cancer.[120,122,123,128–130]

Category	Type	Brand Name	Composition	Application
Organic	Liposome	DaunoXome®	Liposomal daunorubicin	Drug Delivery: increased delivery to the tumour site, prolonged circulation time, and/or lower systemic toxicity
		DepoCyt®	Liposomal cytarabin	
		Marqibo®	Liposomal vincristine	
		Onivyde®	Liposomal irinotecan (PEGylated)	
		Doxil® /Caelyx®	Liposomal doxorubicin (PEGylated)	
		LipoDox®		
		Mepact®	Liposomal mifamurtide	
		Myocet®	Liposomal doxorubicin	
		Vyxeos®	Liposomal cytarabine & daunorubicin (5:1 Molar ratio)	
		Lipusu®	Liposomal paclitaxel	
	Micelle	Apealea®	Micellar paciltaxel	
		Genexol-PM®		
	Antibody-Drug Conjugates	Kadcyla®	Ado-trastuzumab emtansine & anti-HER2	
		Adcetris®	Brentuximab vedotin & anti-CD30	
		Besponsa®	Inotuzumab ozogamicin & anti-CD22	
		Mylotarg®	Gemtuzumab ozogamicin & anti-CD33	

	Polymer-Drug Conjugates	Eligard®	Leuprolide acetate & PLGH (poly (DL-lactide-co-glycolide)) polymer	
	Engineered Proteins	Oncaspar®	PEGylated L-asparaginase	
		Asparlas®		
		Abraxane®	Albumin-bound paclitaxel NPs	
		Ontak®	Interleukin 2 & diphtheria toxin fusion protein	
		Zinostatin stimalamer®	Poly(styrene-co-maleic acid) conjugated neocarzinostatin	
Inorganic	Nanospheres	Nanotherm®	Iron oxide NPs (~15 nm, aminosilane coated)	Magnetic hyperthermia therapy: thermal ablation of tumor
		Hensify®	Hafnium oxide NPs (~50 nm, phosphate coated)	Radiation therapy: enhanced dose deposition

Liposomes are small spherical vesicles composed of at least one phospholipid bilayer that can encapsulate hydrophilic drugs in the aqueous core and hydrophobic compounds in the lipid lamellae (Figure 2A(I)). Micelles are similar structures lacking an aqueous core, preferentially encapsulating hydrophobic compounds. Many conventional anticancer drugs exhibit poor pharmacokinetics, limited bioavailability, and high systemic toxicity, which severely limit their use in clinical settings.[120] Being encapsulated within liposomes or other nanocarriers, such drugs are protected from early degradation during circulation and delivered at high concentrations to their target sites, improving their efficacy profile relative to the free drug.[100,135–137] This enhanced permeability and retention (EPR) effect was initially believed to occur because of poor angiogenesis in solid tumors, producing fenestrae that nanoscale objects could enter selectively, and rapid tumor growth preventing lymphatic drainage.[138–141] As such, NPs could passively target and be retained by tumors. However, recent observations have shown that NPs may accumulate in tumors primarily *via* active endo-/transcytosis mechanisms induced by absorbed serum proteins.[142,143] Regardless, the EPR mechanism cannot be discounted entirely, and both mechanisms likely co-occur at varying rates. Adsorbed serum proteins were also shown to determine NP interactions with the immune system and organs responsible for blood filtration.[144,145] This discovery led to the development of the 'second generation' of nanomedicine, most known in the form of 'stealth liposomes'. These formulations contain surface coatings, such as polyethylene glycol (PEG), which prolong their circulation time by altering protein absorption (Figure 2A(II)).[146–149] Approved PEGylated liposomes include Doxil® /Caelyx® (liposomal doxorubicin (DOX)) and Onivyde® (liposomal irinotecan). PEGylated forms of L-asparaginase (Oncaspar® and Asparlas®) have also been approved.[150] Although PEG increases blood circulation times, some drugs have an increased incidence of side effects when encapsulated in PEGylated liposomes. For example, extended

circulation times allow Doxil® to permeate from microcapillaries in the hands and feet, producing blistering and inflammation (known as palmar-plantar erythrodysesthesia).[151] Comparatively, non-PEGylated DOX (Myocet®) does not promote this side effect while maintaining a similar efficacy profile.[152,153] Therefore, conventional non-PEGylated liposomes are not obsolete and have seen more approvals by the US Food and Drug Administration (FDA) and EMA.

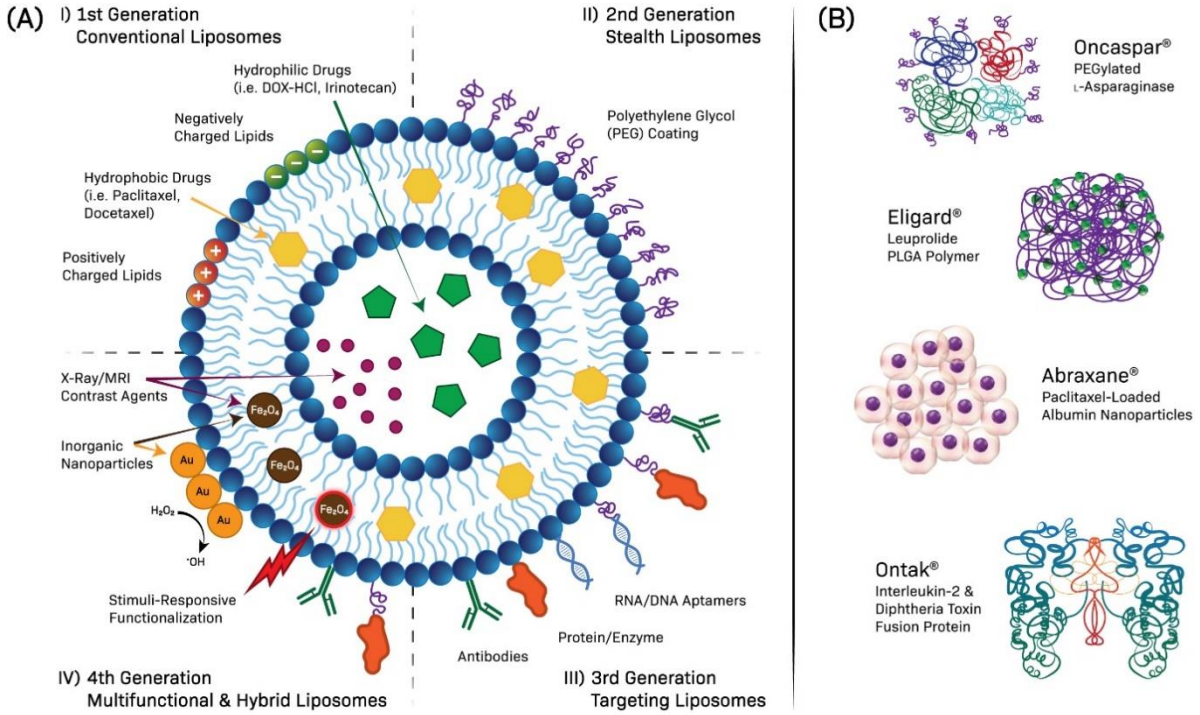

Figure 2: Organic nanoparticles (NPs) used in anticancer treatment strategies. A) Liposomes are the most widely used NPs and are categorized into four distinct generations based on incremental developments. These include (I) conventional liposomes made of phospholipids encapsulating hydrophobic and/or hydrophobic drugs, (II) PEGylated/stealth liposomes containing a surface polyethylene glycol (PEG) layer for reduced clearance, (III) targeted liposomes containing specific ligands to target the tumor site, and (IV) multifunctional liposomes, such as hybrid organic-inorganic composites, which can be used for both the diagnosis and treatment of solid tumors. Adapted with permission under a Creative Commons CC BY License (https://creativecommons.org/licenses/by/4.0/) from ref [149]. Copyright 2015 The Authors. B) Examples of clinically approved non-liposomal organic nanoparticles.

2.1.2 Inorganic Nanomedicine: Reactive & Multifunctional NPs for Oncology

Inorganic nanomedicines are primarily composed of solid NPs with various shapes and structures. Unlike organic NPs, which are usually inert or possess limited activities, inorganic NPs often possess inherent reactivities due to their specific composition, high surface energy, and distinct optical properties resulting from quantum-mechanical effects.[154] As size decreases and particle curvature increases, the

number of surface atoms (relative to the NP core) and defects to the NP's lattice structure increase as well. The nanoscale introduces lattice rearrangements that favour the confinement of electrons and the formation of discrete electronic states.[155] Altogether, these nanoscale effects produce reactive surface sites and distinct interactions with light and radio-waves. This gives inorganic NPs the potential to be used as therapeutics and imaging contrast agents.[156,157] Importantly, because these effects are enabled by overlapping properties, many nanomedicines can be design as multifunctional packages combing multiple imaging and treatment modes. Currently, several inorganic nanomedicine clinical trials are underway, including several phase III trials (**Table 2**). For inorganic nanomedicine, understanding how composition and structure impacts activity is key for clinical success, both in cancer therapy and in other medical applications.

Table 2: Inorganic nanomedicines currently in active clinical trials for imaging and cancer therapies.

Nanomaterial	Application	Disease	Clinical Trial	Phase
Silica NPs labelled with cyanine 5.5, human prostate-specific membrane antigen inhibitor, and ^{64}Cu	Magnetic Resonance Imaging (MRI) and Positron Emission Tomography (PET)	Prostate Cancer	NCT04167969	I
Gold@Silica Nanoshells (AuroLase®)	Photothermal Therapy	Prostate Cancer	NCT04240639	N/A
Gold NP-drug conjugates (MTX110)	Convection-Enhanced Delivery (CED) of Solubilized Panobinostat	Brain Cancers	NCT04264143	I
Cadmium sulfide@zinc sulfide Quantum dot-drug conjugates	Fluorescence Bioimaging & Chemotherapy (Veldoreotide)	Breast Cancer	NCT04138342	I
Hafnium oxide NPs (Hensify® or NBTXR3)	Radiation Therapy (RT)	Lung Cancer	NCT04505267	I
		Pancreatic Cancer	NCT04484909	I
	RT & Immunotherapy (Pembrolizumab)	Recurrent or Metastatic Head and Neck Squamous Cell Cancer	NCT04862455	II
		Recurrent Head and Neck Squamous Cell Cancer	NCT04834349	II
	RT & Immunotherapy (Ipilimumab and Nivolumab)	Lung and Liver Metastases	NCT05039632	I/II
	RT & Immunotherapy (Cetuximab)	Locally Advanced Squamous Cell Cancer	NCT04892173	III
Gadolinium-chelated polysiloxane NPs (AGulX®)	Brachytherapy (RT) & Chemotherapy (Cisplatin)	Locally advanced Cervical Cancer	NCT03308604	I
	RT & Chemotherapy (Temozolomide)	Glioblastoma	NCT04881032	I/II
	RT	Lung and Pancreatic Cancer	NCT04789486	I/II
		Multiple Brain Metastases	NCT03818386	II
	Stereotactic RT	Multiple Brain Metastases	NCT04899908	II
	Proton RT	Recurrent Cancers	NCT04784221	II
Superparamagnetic iron oxide NPs (SPIONS)	Magnetic Thermoablation	Prostate Cancer	NCT05010759	N/A

(e.g., NanoTherm®, FerroTrace®, Ferraheme®, Magseed®, Magtrace®, Ferrotran®)	Magnetic Thermoablation	Osteosarcoma	NCT04316091	I
	Diagnostic MRI	Bladder Cancer	NCT04369560	I
		Prostate Cancer	NCT04261777	III
	MRI for RT Planning	Liver Cancer	NCT04682847	N/A
	Sentinel Lymph Node (SLN) Monitoring by MRI	Colorectal Cancer	NCT05092750	I/II
		Breast Cancer	NCT05161507	N/A
			NCT05359783	I/II
			NCT04722692	III

Therapies commonly enabled by inorganic NPs include photodynamic, photothermal, and chemodynamic therapies.[158–160] Phototherapies kill cancerous cells by utilizing heat or reactive oxygen and nitrogen species (ROS and RNS) generated *via* low-energy photons.[58,161] Chemodynamic therapy (CDT), in contrast, does not require a light source, but instead uses catalytic NPs to generate ROS.[154,162] These approaches can serve as monotherapies or be combined with other treatment modes such as radiation therapy (RT) and small-molecule chemotherapy.[163] However, these properties are also implicated in the toxicity of NPs to healthy tissue as undesired ROS generation could induce oxidative stress and inflammation. Several iron-based NPs approved for magnetic resonance imaging (MRI) were subsequently discontinued due to such toxicity concerns.[164] Reactive NPs used in CDT possess the greatest risk of ROS generation due to their readily available substrates, *e.g.*, endogenous H_2O_2, while photoresponsive NPs could be activated by ambient light near the skin surface. As a result, only a handful of inorganic nanomedicines are currently clinically available (Table 1).

Some inorganic NPs may draw interest due to distinct properties associated with their atomic composition.[53,156,163,165,166] Gold and iron NPs, for example, are often chosen for cancer diagnostics and therapies due to their interactions with radiation and magnetic fields. Radiation therapy (RT) is widely used to diagnose and treat tumors, with ~50% of all cancer patients receiving RT in some form.[167,168] Clinical RT uses targeted doses of high-energy ionizing radiation to damage malignant cells and inhibit tumor growth, and can be explained through direct and indirect mechanisms.[169] The direct mechanism involves the interaction of ionizing radiation with DNA to form lesions, whereas the indirect mechanism involves the production of ROS to damage DNA and other cellular components such as lipid membranes.[170,171] Despite RT's general efficacy, limitations arise through a combination of the exposure of healthy tissue to high doses of damaging radiation and the development of radiation-resistant tumor subpopulations.[172–174] One method to overcome these issues is combining RT with other treatment strategies. As defined by Steel and Peckham, there are four mechanisms by which adjunctive chemotherapy can enhance RT: (1) the spatial cooperation of two independent treatments; (2) the combined toxicity of chemotherapy and RT; (3) protection of normal tissue from radiation; and (4) the sensitization of cancerous tissue to radiation.[172,175] These approaches have collectively resulted in significant improvements in overall cancer survival, with

the critical contribution of radiosensitizers.[172,176,177] By sensitizing cancerous tissue, lower radiation doses can be applied to minimize side effects to the surrounding healthy tissue while maximizing local tumor destruction. Traditional methods of cancer radiosensitization include the use of conventional chemotherapeutics, such as fluoropyrimidines, which deregulate S-phase cell cycle checkpoints and DNA repair, and cisplatin, which forms DNA adducts to inhibit replication.[178,179] Since resistance to these drugs can arise, the development of small molecule-based radiosensitizers has slowed significantly in recent years.[180–182] However, the rapid development of nanotechnology has evoked great interest in using low toxicity metallic NPs, particularly those containing high-Z elements such as gadolinium, hafnium, and gold NPs (GNPs), to enhance RT because of their strong photoelectric interactions with X- and γ-rays compared to biological tissue.[124,166,183–187] These interactions result in a more localized dose of radiation energy. Recently, lower-Z metals, such as titanium, iron, and copper, have also piqued interest for sensitized RT through synergistic mechanisms based on chemodynamic and photothermal therapies, among others.[159,163]

2.1.3 Current Challenges & Gaps for Regulators & Researchers

Regulatory agencies, such as the FDA and EMA, assess medical products containing nanomaterials for both clinical trials and market use.[188,189] However, despite the early success in nanomedicine, there is currently little regulatory guidance available to support the development of future products.[190–192] While the FDA has released some documents related to nanomedicines, these are non-legally binding and do not provide specific guidelines for evaluations of NP-based efficacy or toxicity.[193–195] Rather, these articles simply reflect the FDA's current thinking. Presently, medical products containing NPs are cautiously reviewed by regulatory bodies on a case-by-case basis according to their primary mechanisms of action and are subject to conventional regulations related to small drug molecules, biologics, or medical devices.[189,190] This process typically involves three phases of clinical trials in addition to post-market surveillance studies to ensure long-term safety. However, the conventional classification systems used to determine appropriate experimental guidelines are challenging for NPs because of their distinct properties and cross-category features.[99,196] The FDA has thus routinely classified nanomedicines as combination products, assigning each a primary regulatory category, *e.g.*, a drug or device, and then supplementing additional requirements when considered necessary. While this approach gives regulatory agencies flexibility to cope with the challenges and uncertainties associated with NPs, it also makes it more difficult to provide general regulations for nanomedicine development and evaluation. Furthermore, nanomedicines often require special assays to evaluate their efficacy and toxicity. For example, several NP formulations have been found to interfere with conventional assays such as those for endotoxins (Limulus amoebocyte lysate (LAL) assay),[197] cell viability (MTT assay),[198] and cytokine production (Interleukin-8 ELISA).[199] In the case of liposomes and other nanocarriers, their pharmacokinetics must consider the encapsulated, free, and leaked API fractions;

however, it is highly challenging to accurately measure non-encapsulated API levels as their in vivo concentrations are often very low in comparison to NP- and protein-bound forms.[200]

In addition to the normal pathway for approval, nanomedicines developed for unmet health needs or to treat life-threatening diseases may qualify for an accelerated review under breakthrough therapy status or emergency use.[189] There are also approval routes for copies of approved brand-name products after patent expiry, *i.e.*, generics or similars. In the context of nanomedicine, the term nanosimilars is used for nanoformulations with identical physicochemical properties compared to an original product. Importantly, the approval route for generics does not require full-scale clinical trials, but only evidence showing therapeutic equivalence. Therefore, generics and nanosimilars can theoretically be approved at a faster rate and enter a competitive market, increasing supplies and reducing costs for patients. However, compared to small-drug molecules with easily characterizable structures, nanomedicines are far more complex and difficult to synthesis consistently. In addition, there has been inconsistencies among regulatory agencies in regard to defining and determining the equivalence of NPs due to their distinct behaviors.[188,201,202] For example, the FDA and EMA have taken different stances on the approval of LipoDox, a generic version of Doxil. Lipodox was approved by the FDA but rejected by the EMA because no bioequivalence study for unencapsulated/leaked DOX was provided. As such, nanomedicine or nanosimilar applications intended for international markets may be subjected to different approval criteria with different data requirements in different areas.

Without clear and specific regulatory guidelines supporting nanomedicine development, strategic financial investments cannot be properly weighed, which may result in slow development of nanomedicines .[182,203,204] Conventional drug development programs are time-consuming and expensive, taking ~5-12 years (out of a 20 year patent) and costing >350 million USD (not including marketing costs and liabilities) to produce a single product for a specific application under one regulatory agency.[205] As nanomedicines are physically complex, likely subject to inconsistent regulations, and can require alternative testing methods for evaluation, the time and cost for their development may be significantly higher.[206] Additionally, while phase I trials for nanomedicine are often promising (>90% successful), the success rate of phase II and III trials, which measure safety and efficacy, is only at 48% and 14%, respectively.[207] For most clinical trials, failure has been reportedly due to a low efficacy in patients, although many results contain proprietary information and are thus not publicly available.[207,208] The most detailed advice on NP development and approval can only be offered after the FDA or other agencies perform clinical trial reviews[182]; however, it is challenging for regulators to issue guidance because of significant uncertainty regarding the incidence and mechanisms of NP toxicity.[99,191] In addition to clinical trial failures, some nanomedicines have been discontinued after approval due to arising safety concerns. For example, in 2006 it was found that Ontak, a

protein-based anticancer nanomedicine, could result in vision loss through an unknown mechanism and received a black box warning, which is the FDA's highest safety-related warning.[209] In addition, several iron oxide NPs designed for iron replacement therapy and MRI imaging (e.g., Feridex and Feraheme) were also discontinued due to limited benefits and fatal anaphylactic reactions.[190,210] Most recently, side effects including fatal heart issues (myo/pericarditis) associated with the emergency use SARS-CoV-2 vaccines have caused public controversy.[211] Such cases underscore the cautious approach of regulatory agencies and reflect the difficulty in predicting NP behaviors in human patients relative to cell or animal models. While phase II and III studies are designed to detect side effects, these trials only include a limited number of patients (~300-3000 individuals required including controls),[212,213] which may cause rarer side effects to go unnoticed until larger post-market/phase IV trials. In order to enact a safe-by-design approach, maintain or improve treatment efficacy, and be commercially viable, a firm mechanistic understanding of nanomedicine is critical to predict outcomes early in development. To accomplish this, regulatory agencies and researchers require an comprehensive decision framework linking the physicochemical characteristics of nanomedicines to their toxicological effects.[214]

The remaining uncertainty surrounding nanomedicine is partially caused by insufficient efforts spent in studying fundamental structure-activity relationships (SARs).[99,172,188,215] Contemporary research has identified that the physicochemical properties of a NP, such as size, shape, composition, surface properties, and crystal structure/phase, ultimately control its biological fate, chemical reactivity, and toxicity.[89–94] A recent meta-analysis by Labouta *et al*. found that NP cytotoxicity could be primarily predicted from the material's chemistry, followed by NP concentration, size, cell type, and the cytotoxicity screening indicators.[216] Other factors, such as surface charge and redox potentials, are also valuable parameters, although they are often insufficiently reported.[217–219] Labouta *et al*.'s meta-analysis, for example, observed that 64% and 56% of the representative publications lacked appropriate reporting of surface chemistry and zeta-potential (surface charge), respectively.[216] Other reviews have also noted that a lack of consideration of NP transformations in the biological environment can result in incorrect identification of the relevant characteristics.[196,220–223] When investigating NP size effects, the formation of an adsorbed protein layer on the NP surface is often not accounted for, leading to incorrect assumptions about the NP's in vivo size and behavior. In addition, differences between techniques and experimental conditions can also make identifying SARs difficult as these do not allow for replication and comparison. Therefore, some researchers have proposed implementing minimum reporting standards to harmonize nanomedicine research,[224] although others have worried that applying overly strict publication requirements may slow down research progress.[94] Regardless, understanding how key physicochemical parameters influence NP activity and their interactions with biological systems is essential to developing accurate decision frameworks for future nanomedicine development and regulation. These mechanisms are

particularly important for RT because of the significant overlap between the radiosensitization mechanisms and NP toxicity, which can further complicate treatment optimization and risk-benefit assessments.[225]

In addition to their direct toxicological significance, studying SARs are of special interest for *in silico* modeling to address the ethical concerns of large-scale animal testing and the development of nanosimilars following market expansion.[226–228] The FDA noted that while the current animal-testing paradigm is unlikely to end soon, alternative methodologies, such as quantitative structure-activity relationship (QSAR) computational models, have successfully predicted some toxicological endpoints, and thus their submission in combination with traditional studies is encouraged.[229] The development and application of computational methods are also supported by the EU's *Registration, Evaluation, Authorisation and Restriction of Chemicals* (REACH) regulation as exploratory and predictive tools in risk assessment.[230] In 2012, the *Organisation for Economic Co-operation and Development* (OECD) launched a program on the development of *Adverse Outcome Pathways* (AOPs; **Figure 3**) to facilitate these efforts.[231]

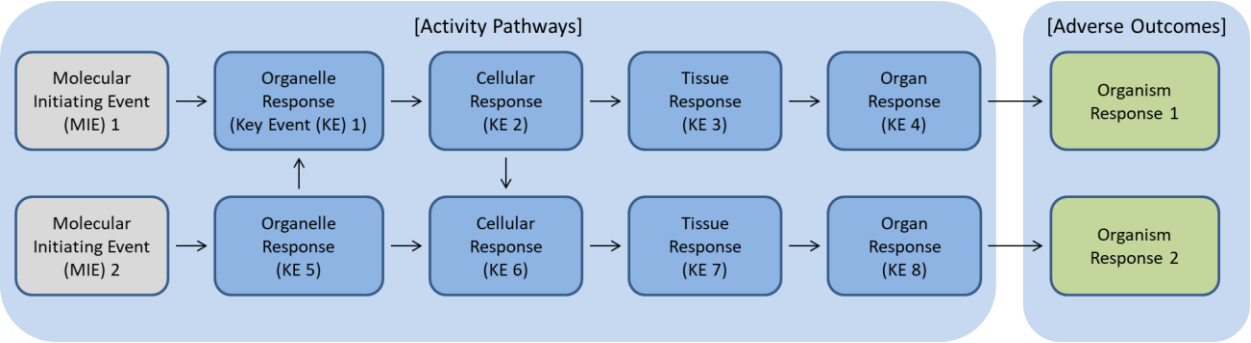

Figure 3: A schematic of an adverse outcome pathway (AOP) network in toxicology. In the AOP framework, a molecular initiating event (MIE) is linked to adverse outcomes (Aos) through a series of downstream biochemical key events (KEs).

The AOP framework reflects an evolution of pathway-based concepts for assembling toxicological data across different biological organization levels. An AOP describes a chain of biological and chemical events starting from a molecular initiating event (MIE), continuing through several downstream linked key events (Kes), and ending at an observable adverse health or ecotoxicological outcome (adverse outcome, AO).[232] According to the OECD, AOPs are a central element of modern toxicological knowledge and significant attention has been brought towards their use for nanotoxicity evaluations.[220,233,234] As a "map" of the key nano-bio interactions, AOPs can serve as a scaffold for assembling knowledge associated with a given AO, inform the development of in vitro toxicological assays, and guide the interpretation of KE measurements. While several researchers have created early AOPs for nanotoxicity analysis,[231,232,235–239] a

generalized framework suitable for evaluating both the safety and efficacy of therapeutic nanomedicines has yet to be developed.

Notably, the AOP framework, which was designed for the toxicological assessment of small drug molecules and bulk materials, has fundamental limitations in evaluating of the efficacy and toxicity of nanomedicines. First, compared to conventional drug molecules that only have a few medically relevant structural modifications, NPs possess much more tunable properties that can dramatically alter their pharmacodynamic and pharmacokinetic behavior.[240,241] These overlapping properties can result in many common features not seen among different drug molecules. Second, AOPs are simplified activity pathways describing a link from an MIE to an AO and do not consider material-specific properties or kinetics.[231] As such, medically relevant factors such as effective dose (including specific organ uptake and excretion) and structural changes to the nanomedicine including NP dissolution, protein adsorption, and NP aggregation, are ignored. Importantly, next-generation metallic nanomedicines generally do not exert their primary effects *via* the activation of specific receptors or pathways but through a complex dysregulation of cellular redox homeostasis.[242,243] Therefore, conventional AOPs cannot be used as predictive models for nanomedicines; instead, more complex pathway networks that account for the interactions between nanomedicines and their local physiological environment are required.[231,244,245] In this regard, a QSAR-like understanding of nanomedicine is critical. Finally, a focus solely on adverse outcomes is insufficient when evaluating nanotherapeutics. To treat life-threatening diseases, such as cancer, the safety considerations must be balanced against various therapeutic endpoints, such as tumor reduction and radiosensitivity. To accurately reflect this complexity and create a foundation for nanomedicine assessments, we propose a multi-phase framework (herein referred to as the *Nanomedicine Structure-Activity Framework* (NSAF)), which can be broadly applied to nanomedicines for cancer treatment strategies.

2.1.4 The Nanomedicine Structure-Activity Framework

The proposed framework is composed of three distinct but interconnected phases that represent three different levels of biological complexity, through which the nanomedicine moves from the point of administration to its therapeutic target. These phases include 1) the biodistribution phase accounting for systemic distribution, blood clearance, and overall tissue impact; 2) the internalization phase detailing the cellular level interactions involved in NP uptake and intracellular trafficking; and 3) the dysregulation phase encompassing the molecular interactions between delivered therapeutic agents and intracellular biomolecules or organelles, which ultimately result in therapeutic and toxic effects. Within each phase, an AOP-like network (the *Activity Network*) is constructed to mechanistically link a virtual *Parameter Space*, composed of the structural and environmental parameters used for modeling and assessment, to one or more *Evaluation Metrics* through a series of *Intrinsic Initiating Events* and *Biological Events* (**Table 3** and **Figure**

4). The logical structure of each phase diagram is based on the principles of QSAR design and computational modeling, featuring an identifiable input of known data and an output of predictable outcomes. Feedback parameters are incorporated into the schemes to reflect the continually evolving physiological state and physicochemical changes to the nanomedicine in vivo. Compared to small-molecule drugs, nanomedicines possess distinct pharmacokinetics and pharmacodynamics, which are primarily determined by the physicochemical properties of the nano-ingredients. However, such properties are often strongly interconnected and it is difficult to modify one parameter while maintaining the rest constant in mechanistic and predictive analysis.[220] For example, altering the NP shape can simultaneously impact its size, the spatial distribution of surface defects and functionalizations, and the propensity for surface adsorption. While further research is required to identify the contribution of each parameter for accurate *in silico* modeling, generalized trends can be identified and refined. As such, this framework should possess widespread utility for research in both nanomedicine and nanotoxicology.

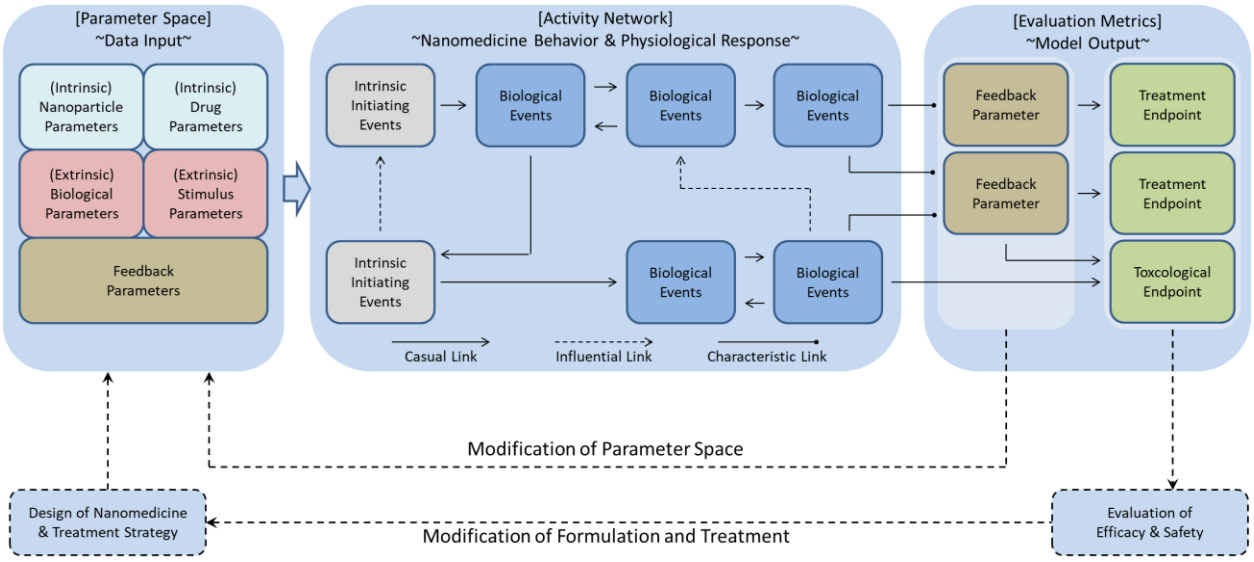

Figure 4: The structure of the Nanomedicine Structure-Activity Framework (NSAF). Nanomedicine and patient characteristics are first entered into a Parameter Space (PS), which represents the in vivo conditions and reactivity of the nanoparticles at different levels of biological complexity. Based on these properties, one or more Intrinsic Initiating Events (IIEs) occur at various rates that result in a series of physiological responses leading to measurable or predictable outcomes. The links between different events and outcomes are classified into three types: casual, influential, and characteristic.

Table 3: Description of the different components of the Nanomedicine Structure-Activity Framework (NSAF).

Section	Component(s)		Definition/Description
Parameter Space	Intrinsic Parameters	Nanoparticle (NP) Parameters	•The physical or chemical properties of the nanomedicine, specifically the active NP or inert nanocarrier components.

			•Common critical quality attributes (CQAs) defining NP structure and stability.
		Drug Parameters	•Pharmacokinetic and mechanistic properties of loaded drug molecules (when distinct from an active NP or inert nanocarrier in the formulation).
	Extrinsic Parameters	Biological Parameters	•Parameters describing patient biology that can interact with the administered nanomedicine. •Includes parameters related to the aqueous carrier, *e.g.*, blood and interstitial fluid, individual cell/tissue types, patient comorbidities, *etc*.
		Stimulus Parameters	•Parameters describing externally applied medical stimuli, *e.g.*, ionizing radiation, UV-Vis-NIR light, applied magnetic fields, *etc*.
	Feedback Parameters		•Parameters informed from observed or predicted outcomes, *e.g.*, NP dose distribution, changes to NP surface over time, tumor volume reduction, *etc*. •Can have kinetic (affecting the rate) or mechanistic (affecting or enabling/disabling pathways) effects on different events in the Activity Network.
Activity Network	Intrinsic Initiating Events (IIEs)		•An initial physical or biochemical event caused by the nanomedicine after administration, which can lead to one or more specific outcomes. •Highly dependent on the physicochemical properties of the nanomedicine and its components.
	Biological Events (BEs)		•A downstream change to a physical or biological state that is essential, but not necessarily sufficient, for the progression of an IIE towards an outcome. •Can affect the rate of IIEs and other BEs through biochemical feedback cycles.
Evaluation Metrics	Treatment and Toxicological Endpoints		•Common clinical, regulatory, or research and design endpoints that are typically considered in evaluating the performance or risks of anticancer medicines. •Can be informed from one or more events, as well as feedback parameters.
	Phase Feedback Parameters		•Changes to the nanomedicine or patient (including the disease site) that can be characterized quantitatively or qualitatively. •Can be used to assess endpoints or modify the Parameter Space. •Can inform how the events of one phase influence another.

The first component of the NSAF, the *Parameter Space*, provides a distinct advantage over other pathway-based models, such as conventional AOPs, for nanomedicine. Currently, confusion and misconceptions exist over the generalized nature of AOPs and their application. Because chemical-specific properties, such as toxicokinetics, must be considered to predict specific outcomes in real applications, there is a tendency to represent AOPs in a chemical-specific manner.[246] However, small-molecule pharmaceuticals can possess drastically different modes of action and thus any specialized AOP might not apply to other molecules. As such, chemical-specific models can be perceived too limited in scope. In contrast, generalized AOP models linking outcomes to a simplified cause, *e.g.*, an MIE such as enzyme

inhibition, regardless of the chemical initiator itself, have more widespread utility, but cannot be used to assess any specific risk.[246] Within each Phase of the NSAF, the *Activity Network* can be viewed as a generalized model describing all possible interactions for various nanomedicines. While nanomedicines can have many different functions based on their APIs, their NP components possess many common behaviors. The *Parameter Space* then determines the events that occur in the *Activity Network* by linking them to the characteristics of both the nanomedicine and the patients rather than only the specific category of APIs. The NSAF, therefore, combines the desired traits of both generalized and specialized pathway models for evaluating nanomedicine. The components of the *Parameter Space* include (1) *intrinsic parameters* such as relevant *critical quality attributes* (CQAs) describing the nanomedicine's physicochemical structure and stability, (2) *extrinsic parameters* characterizing the biological and physical stimuli that interact with the nanomedicine, and (3) *feedback parameters* used to connect the different Phases for holistic evaluations and fine-tune of the NSAF over time.[247] Altogether, these parameters reflect the in vivo conditions of a nanomedicine at any given time, and thus how it behaves. While the exact mathematical descriptions of such behavior are beyond this review, the NSAF provides a map guiding their development and integration.

Within the *Activity Network*, *Intrinsic Initiating Events* (IIEs) are the starting points of one or more pathways that are directly caused by the specific physicochemical properties of the nanomedicine. These initial events reflect the strongest structure-function relationships for the nanomedicine and are of particular importance for *in silico* modeling and the development of diagnostic assays. *Biological Events* (BEs) are downstream biological responses to IIEs, which can be independent of the NP characteristics. However, BEs can produce feedback loops that then affect the kinetic rate of IIEs. The links between events and outcomes can be categorized as either causal, influential, or characteristic. For casual links, the preceding events directly causing the later events to occur. Influential links indicate that a prior event can affect subsequent events but is not a prerequisite for their occurrence. Finally, characteristic links are used for events that generate measurable feedback parameters. These parameters describe significant changes to the nanomedicine or patient physiology in the Parameter Space, and therefore have the potential to influence multiple apparently unrelated events, including those in other Phases. As feedback parameters describe the characteristics of the nanoformulation and patient physiology at any time point, they can also be used to assess treatment endpoints. Importantly, the NSAF should be viewed as a living document as additional evidence either supporting or rejecting a particular event emerges. This makes the NSAF an evolving but foundational map to model the behavior of nanomedicine.

Finally, more than the AOP framework, which only focuses on adverse toxicological effects, the NSAF's *Evaluation Metrics* also represent therapeutic outcomes and pharmacokinetic data. As any single

endpoint is insufficient for evaluating the overall pros and cons of a nanoformulation, conclusions can only be drawn by evaluating various pharmacokinetic and pharmacodynamic endpoints obtained through multi-phase assessments. Focusing on one or a limited subset of metrics risks overlooking important side effects and applications. Thus, the NSAF should be used not only to solve specific questions, but also as a support framework to integrate and guide future research and regulations.

2.2 Phase I: Nanomedicine Biodistribution & Clearance

The *Biodistribution Phase* (Phase I) primarily accounts for the nanomedicine's behavior at the blood and tissue levels following intravenous or intratumoral injection (**Figure 5**). Phase I is the highest-level overview of nano-bio interactions, with the key cellular and molecular interactions being explored in Phases II and III, respectively. The interphase connections are accounted for by feedback parameters. For example, Phase II parameters can improve predictions of NP uptake by accounting for uptake routes and transport rates within the tumor volume,[248] while Phase III highlights the mechanisms underlying cell death and inflammation. However, both later phases are dependent on the events outlined in Phase I, in particular the surface protein adsorption and the EPR effect, which influence overall localization and cellular uptake of nanomedicines.

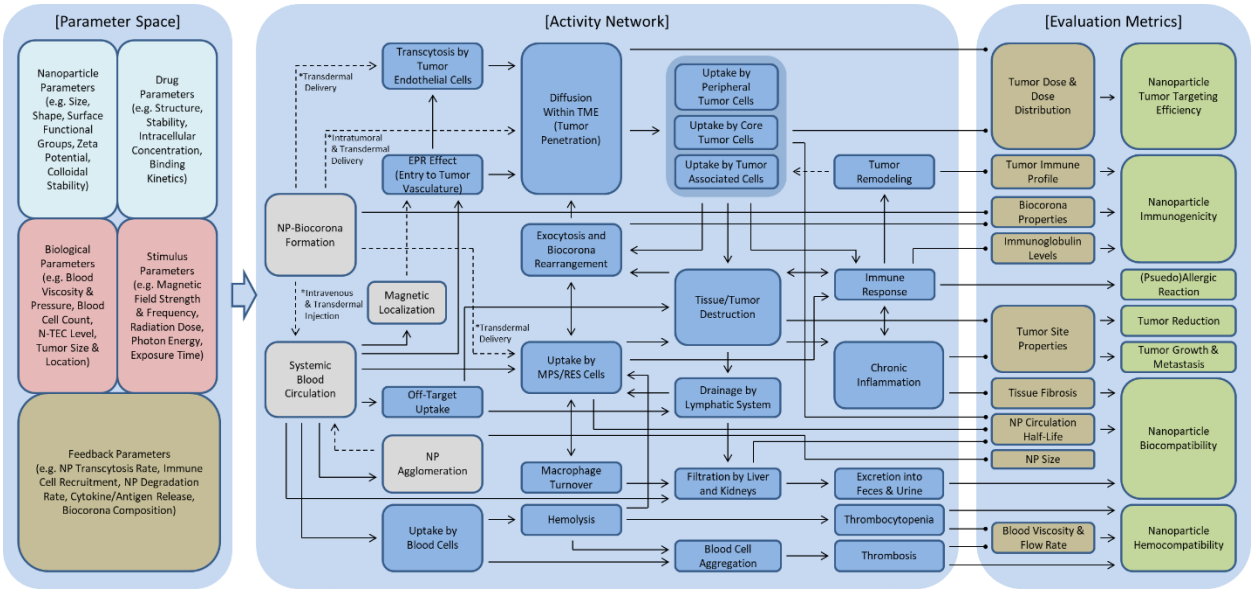

Figure 5: Phase I (Biodistribution) of the NSAF for anticancer strategies, representing the highest level of biological complexity. The Parameter Space includes intrinsic parameters relating to the pristine nanoformulation (Critical Quality Attributes (CQAs)), extrinsic parameters such as blood pressure and tumor definition, and finally feedback parameters, e.g., the identity of the protein corona or the specific NP dissolution rate. Phase I focuses on the behavior and fate of the nanomedicine in the patient's blood, tumor, and organs, including both the beginning of the treatment

(injection of the nanomedicine) and its final assessment (endpoints representing the overall biocompatibility and efficacy of the nanomedicine).

The events outlined in this section combine to generate several outcomes, including clinical responses that are key for the overall assessment of treatments. In contrast to AOPs that are only used to measure 'adverse' outcomes, such as tissue fibrosis, carcinogenesis, and (pseudo)allergic responses, measurements of therapeutic efficacy such as tumor reduction are considered in NSAF to provide beneficial outcomes.[249–251] This allows the weighing of both risks and rewards within the same model. Additionally, pharmacokinetic endpoints are assessed. Similar to regular pharmaceuticals, nanomedicines possess dose-dependent effects that must be considered to accurately predict patient outcomes. Selective, sufficient, and homogenous dose delivery to the tumor site are the primary nanomedicine design considerations, but early removal and off-target accumulation by defensive systems are significant barriers to these goals. As such, the conventional design paradigm for nanomedicine has mainly focused on engineering NP structure for extended circulation *via* macrophage evasion and avoiding organ accumulation. However, nanomedicines with low biodegradability (primarily inorganic NPs) must be removable by the body's defensive systems to prevent chronic toxicity following treatment, and therefore cannot simply bypass them entirely.[252,253] Within pharmaceutical applications, regulations favor API clearance within a certain timeframe.[254] Therefore, ideal nanomedicine design must consider the change of NP properties across different biological systems, as focussing on only one tissue type will lead to sub-optimal clinical performance.

2.2.1 The Biocorona: Biological Identity

A key element for both Phases I and II is the natural formation of the '*biocorona*' (often referred to as the protein corona) that mediates NP-cell interactions including uptake, intracellular transport, and clearance.[144,145,255] Upon contact with biological media, such as blood, interstitial fluid, or cytoplasm, organic and inorganic NPs rapidly adsorb native biomolecules (including proteins, sugars, nucleic acids, and lipids) forming nanoconjugates.[256–259] These conjugates can then further bind to different cellular receptors, which confer the NP with an additional 'biological identity', or alter the NP properties including the hydrodynamic size, colloidal stability, and reactivity.[260,261] The biocorona is commonly comprised of at least two layers: the 'hard' inner layer biomolecules absorb with a high affinity and low dissociation rate (allowing them to mediate NP-cell interactions) and the 'soft' outer corona of weakly adsorbed biomolecules that undergo rapid and continuous exchange (**Figure 6**).[144,262] The inner hard corona is the more interesting layer because the biocorona of a particle migrating from one biological fluid/space can carry a "fingerprint" *via* strongly adsorbed serum proteins.[263,264] This provides a means of characterizing, predicting, and engineering the biocorona's composition and effects. Because of the rapid exchange in the soft corona, the outer layer does not influence NP-cell interactions so much as the hard corona; however, it

can act as a transient blocking agent for cell recognition or the adsorption of other molecules.[265] PEGylated NPs were initially believed to improve circulation by preventing protein adsorption, although recent research has shown that PEG merely reduces protein binding rather than complete inhibition.[266,267]

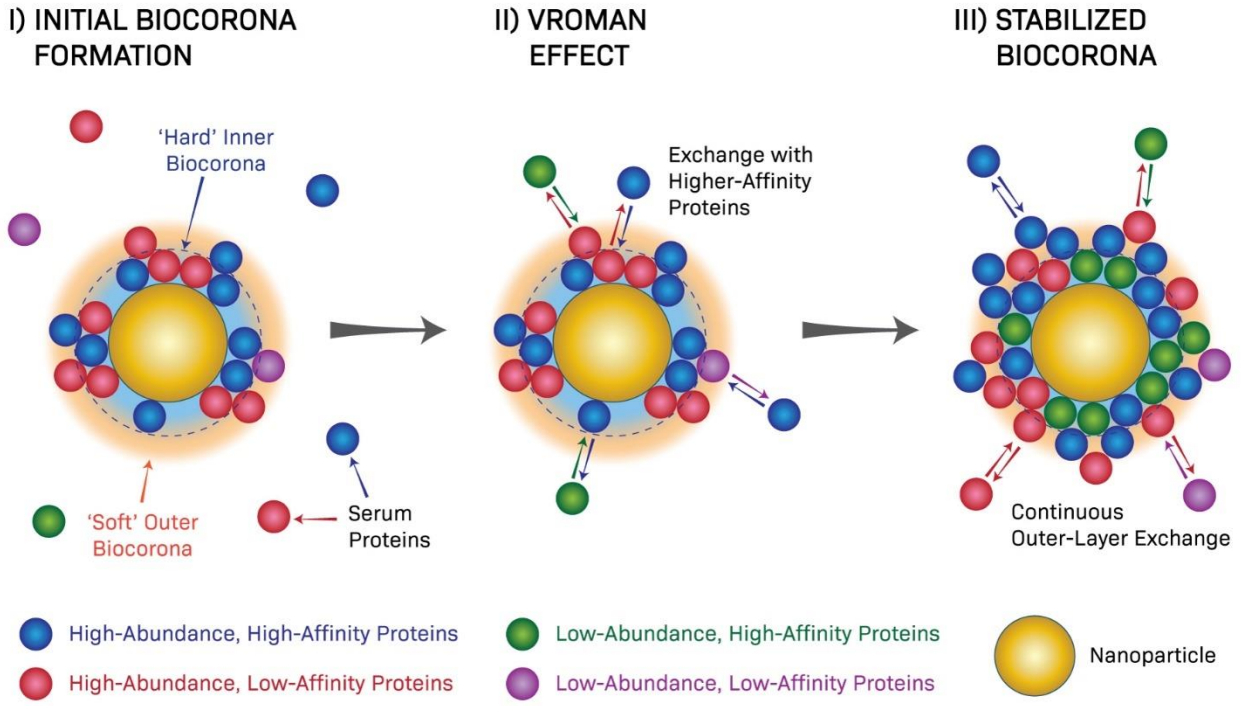

Figure 6: The formation and composition of the NP biocorona. The biocorona is commonly composed of two layers: the hard and soft coronae composed of tightly bound and rapidly exchanging proteins, respectively. The biocorona formation depends on intrinsic and extrinsic parameters and is subject to layer instabilities because of the Vroman effect. Adapted with permission from ref [268]. Copyright 2019 Springer Nature.

The nature of the biocorona formation and fate depends on the intrinsic properties of the pristine NPs, *e.g.*, size, charge, and functional groups, and extrinsic parameters relating to the route of entry, local protein concentration, incubation/circulation time, and disease and patient characteristics.[258,262,269–271] These observations indicate that NPs form biocoronae distinct to each individual's physiology.[272] Cancerous cells also have their own "secretomes" containing hundreds of tumor-derived proteins that can further complicate the biocorona's composition.[273] The structure and concentration of human plasma proteins are altered by lifestyle choices and comorbidities including cancer, obesity, diabetes, smoking, and pregnancy.[259,274,275] These differences can have a subtle yet significant impact on the biocorona formation as NP protein adsorption evolves based on the local protein concentration.[276,277] Proteins additionally undergo reorientation and conformational changes on the NP surface in a "hardening" process, yielding a partially denatured state with a reduced dissociation rate.[278–280] Therefore, both protein composition and conformation on the NP surface can significantly influence its interaction with important cellular

receptors.[281,282] Conformational changes producing 'unnatural' conformations during opsonization can initiate phagocytosis and inflammatory reactions from macrophages.[283] Although there are thousands of different human serum proteins with concentrations spanning 9-10 orders of magnitude, only ~350–500 proteins have been observed bound to various NPs. Among these, some NPs only selectively bind an even smaller number of proteins at any given time.[258,284,285] Because of this selectivity, strongly absorbed hard corona proteins remain relatively constant, providing NPs with a 'fingerprint' of their initial environment when administered.[263,264,286] This fingerprint is useful for nanomedicine design and the prediction of NP fate as it can mediate tumor targeting and immune evasion.[287,288] To facilitate the use of the biocorona to predict NP delivery and efficacy, several early computational-based tools have been developed for modeling biocorona formation and effects.[289–292]

The hard and soft coronae form rapidly in contact with biological media and show biological fingerprints, but are unstable and dynamically change *via* the Vroman effect and other physical forces.[293] The Vroman effect is a time-dependent phenomenon where certain initially associated proteins are competitively exchanged with others possessing higher affinities for the NP surface or extant corona.[255,262,294–296] This is not limited to serum proteins, as even engineered surface functionalization can be replaced. For example, native cysteines can replace thiolated mPEG on GNPs.[297] The Vroman effect has conventionally been explained solely in terms of physical diffusion, with small fast-diffusing proteins adsorbing first while large slow-diffusing proteins with stronger NP surface interactions are preferred at equilibrium. However, this simplistic model ignores the contributions of electrostatic, hydrophobic, and other protein-protein interactions. Angioletti-Uberti *et al*. calculated that proper consideration of additional interactions, including steric and electrostatic interactions, through dynamic density functional theory (DDFT), produces Vroman-like, *i.e.*, non-monotonic, adsorption on polymethyl methacrylate (PMMA) NPs in various scenarios. Moreover, consideration of energetic terms predicted both competitive and cooperative NP surface adsorption.[298] As such, these complex models may provide a richer understanding of biocorona formation and composition. The Vroman effect impacts the early development of both the hard and soft corona; however, long-term effects during circulation and distribution (and thus changing the local proteome) are largely limited to the transient soft layer while the hard layer remains relatively constant as noted above. Shear stresses and catch-and-slip bonds within changing blood vessels diameters may partially explain the differences in biocoronae formed in vitro and in vivo, although this is difficult to confirm.[299–301] Because of these effects, the biocorona should be viewed as dynamic when considering the design and modeling of nanomedicines.

2.2.2 Administration, Circulation, & Physiological Response

The administration route of nanomedicines can alter their biodistribution and clearance.[274,302–305] For example, Dölen *et al*., showed that intravenously administered poly(lactic-co-glycolic acid) (PLGA) NPs accumulate primarily in the liver and spleen, whereas NPs delivered subcutaneously or intranodally accumulated in local lymph nodes.[306] Currently, the most common administration routes for nanomedicine include intravenous, intratumoral, and transdermal delivery.[307] Other methods tailored for specific disease sites, such as pulmonary or oral delivery, are also examined.[308–310] The circulation and clearance of intravenously injected NPs is mainly determined by their interactions with blood- and tissue-resident macrophages of the mononuclear phagocyte and reticuloendothelial systems (MPS/RES) within the liver, kidneys, lymph nodes, and spleen.[251,252,303,311–313] However, NP interactions with blood cells and platelets should be considered. Several studies have found that NPs can perturb the coagulation system and cause thrombi (clots) and thrombocytopenia (low platelet count) that can lead to life-threatening conditions.[314–317] Intratumoral injections can bypass many issues associated with blood circulation; however they are still limited by barriers present at the tumor site. Additionally, methods for topical and transdermal delivery must overcome barriers associated with skin penetration, with polymeric microneedles emerging as a promising delivery platform.[70,318–320] Furthermore, NPs targeting central nervous system tumors must contend with the blood brain barrier (BBB). Ultimately, to successfully model nanomedicine, we must consider all the possible interactions during the NPs' journey to the target site, and not simply disease properties alone (Figure 5).

NP hemocompatibility is an emerging topic with limited understanding. The main cellular constituents of blood are red blood cells (erythrocytes), white blood cells (leukocytes), and platelets (thrombocytes). Numerous NPs, including silica, hydroxyapatite, and especially silver NPs (AgNPs), cause significant hemolysis, with other NPs inducing blood cell aggregation or deformation despite having little hemolytic activity.[314,321–323] As such, hemocompatibility evaluations for nanomedicine should include erythrocyte aggregation and deformation, in addition to hemolysis assays. Most NP hemolytic activity is concentration-, structure-, size-, and shape-dependent, with smaller NPs appearing more hemolytic than larger ones, likely because of their greater reactivity and uptake.[314,324] Hemolysis causes anemia but is also associated with thrombi formation through nitric oxide (NO) sequestration by released hemoglobin.[325–327] In addition, the effect of NPs on blood viscosity should be considered. Under physiological shear rates, erythrocytes form linear face-to-face cell arrays (rouleaux) that contribute to the non-Newtonian behavior of blood and can easily be dispersed.[314,328,329] However, enhanced erythrocyte aggregates are difficult to disperse and can block small blood vessels and increase blood viscosity.[330] Erythrocytes travel down the center of the blood vessel, pushing platelets and NPs towards the periphery.[331,332] This phenomenon, called

axial margination, is blood viscosity dependent and influences the platelet and nanoformulation distribution within the vasculature. Increased blood viscosity enhances platelet margination, intensifying collisions with the vascular wall and increasing the thrombus formation risk. Similar effects on blood viscosity are seen for less deformable erythrocytes, a condition that can be induced by some NPs.[333,334]

The size effect of nanomedicine is a key factor in determining NP circulation time, biodistribution, tumor targeting efficacy, and toxicity. To leverage the EPR effect and maximize tumor accumulation, the sizes of nanomedicines are generally limited by upper and lower bounds determined by the filtration cut-offs of the kidneys, liver, and spleen, and the vascular sizes of different tumors. The lower size limit for NPs is specifically imposed by the renal filtration cut-off of 5.5–10 nm.[312,335–337] In the glomerulus of the kidneys, blood is rapidly filtered through three overlapping membranous layers containing slits >30 nm wide that form ~5.5 nm pores through which NPs and other compounds are rapidly excreted into the urine. These pores are also charge selective for cationic compounds, which is the mechanism that allows the kidneys selectively maintain some anionic proteins in the bloodstream.[253,338] While renal clearance is essential because it prevents the accumulation of NPs in healthy tissue, rapidly cleared NPs do not accumulate in the target tumors at high levels. The upper size limits are imposed by the highly variable tumor vasculature (~300 nm–4.7 μm) and the spleen, which has intercellular slits that preferentially filter NPs >200 nm.[141,339–341] In general, the ideal size for optimal blood circulation and MPS/RES evasion is estimated at ~100 nm.[342,343] However, to prevent chronic toxicity, the size of non-biodegradable and reactive NPs is further limited by their accumulation in the liver. Phagocytes, such as those produced in the spleen, preferentially ingest particles between 2–3 μm and uptake smaller NPs to a lower extent. For example, well-dispersed 20–200 nm AgNPs were taken up by THP-1 macrophages less than by nonphagocytic A549 and HepG2 cancer cells.[344,345] AgNP aggregates, however, were taken up by macrophages to a higher extent. A similar size effect is observed for organic NPs, such as liposomes, which are often designed with the EPR effect in mind. An early study by Liu *et al*. investigating the biodistribution of liposomes from 30–400 nm observed that 100–200 nm liposomes were up to 4-fold more concentrated in tumors compared to those <50 and >300 nm.[340,346] The liver uptake of particles <50 and >300 nm was observed to be 25% of the injection dose, compared to 10% for 100 nm liposomes. 40–50% of the injection dose of particles >400 nm was cleared by the spleen. It should be noted that organic NPs, such as liposomes, are more flexible and deformable than inorganic NPs and can therefore possess different size optima despite having a similar pristine size.[347,348] Additionally, some tumor treatments may benefit from the targeting of tumor-associated or antibody-producing macrophages, and thus the concept of ideal NP size is treatment-specific.[349]

Liver and spleen uptake are generally undesirable for nanomedicines; however, those NPs that are not degraded at the target site or removed by the kidneys must eventually be cleared *via* the liver or spleen

to avoid chronic toxicity. Thus, a detailed understanding of NP sequestration and clearance is crucial for the effective optimization of NP delivery. Usually, organic NPs, such as liposomes, are readily degraded. Therefore the concerns over long-term toxicity and clearance are focused on inorganic/metallic NPs, which have a wide range of responses.[252,350–353] So far, the observed toxic effects of such NPs appear to resemble their microparticle analogs, e.g., tissue fibrosis *via* long-term inflammation and immune cell recruitment.[251,354–356] As blood passes through the liver sinusoids, NPs can be taken up by hepatocytes, liver sinusoidal endothelial cells (LSECs), B cells, and Kupffer cells (KCs).[252,311] KCs and LSECs are typically the first cells to interact with NPs and uptake the majority that pass through the liver through phago- and endocytosis, respectively.[335,357–360] However, circulating NPs smaller than the diameter of liver sinusoidal fenestrations (~100–150 nm) can extravasate into the space of Disse and interact directly with hepatocytes.[361,362] Hepatocytes are responsible for metabolizing compounds and releasing the products back into the bloodstream or the bile and feces. NP filtration and clearance from the liver and spleen into the feces is a slow, NP degradation rate dependant process.[252,303,363–366] Sadauskas *et al*. found that 91% of uncoated 4 nm GNPs accumulated in mouse livers the first day after injection remained after 6 months.[367] More recently, Disdier *et al*. found that 33% of the Ti burden from intravenous TiO_2 NP injections remained in Fischer F344 rat livers after 1 y.[368] However, Chevallier *et al*. reported that 70% of an injected dose of PEGylated MnO NPs was excreted within 48 h.[369] KC turnover could partially explain the slow clearance of some NPs. KCs are completely replaced after 21 d and therefore some NPs may escape while dying KCs are consumed by other cells and accumulate in the bile.[335,357]

In addition to mediating clearance, interactions between NPs and macrophages or other immune cells may initiate systemic toxicity because of host immune reactions such as complement activation and thrombolytic events. These induce the release of cytokines and chemokines that regulate inflammation and immune cell recruitment, cellular differentiation and activation, and allergic and pseudo-allergic responses.[274,341,370] When such reactions occur shortly after administration they are termed infusion reactions, hypersensitivity reactions, or anaphylaxis.[371] The four main types of relevant immunological reactions include immediate/type I (developing within 15–30 min), type II (minutes to hours), type III (3–8 h), and delayed/type IV (48–72 h).[372] Type I–III reactions are mediated by pre-existing immunoglobulins (IgM, IgG, and IgE) specific to at least one component of an antigen or drug product and specific immune cells that recognize these antibodies.[370] Conversely, Type IV reactions involve T-helper and antigen-presenting cells. Type I reactions, which pose the most risk to patients, are mediated by IgE and mast cells, whose activation can lead to hay fever, allergic asthma, and anaphylactic shock. Outside of these classifications, an additional IgE-independent reaction with symptoms resembling a Type I reaction can occur *via* activation of the complement system. This system is composed of several dozen proteins found in plasma and is responsible for non-specific immune responses. Upon activation, which can be triggered

by binding to the NP surface or certain components of the biocorona, particularly those rich in hydroxyl and amino groups,[373,374] the complement proteins are enzymatically cleaved to generate bound and free fragments. Among them, the fragments that remain bound can both mark the NP for uptake by immune cells and trigger additional complement cascade reactions.[374,375] Meanwhile, the free fragments include several anaphylatoxins that can trigger cell degranulation, similar to IgE antibodies. Although antibodies can activate complement proteins, they are not the only trigger for inducing a severe hypersensitivity reaction *via* the complement system. Therefore, this pathway is known as a complement activation-related pseudo-allergy (CARPA).[376–379] As mentioned earlier, significant complement-related side-effects observed for several iron oxide NPs ultimately resulted in their discontinuation.[251,370,380] A recent review also identified that ~50% of investigated NPs induced immune response among published in vivo studies.[381] The immune system is incredibly robust and can produce antibodies against many foreign substances, including nano-sized viruses, fullerenes, gold surfaces, liposomes, metal-ion-induced autoantigens, and even cholesterol crystals.[382–384] Like molecular antigens with distinct epitopes, NP have chemically and geometrically distinct surfaces that antibodies and cellular receptors can recognize to induce an immune response.[378,385] These receptors, including pattern recognition receptors (PRRs), may unintentionally crossreact with misfolded proteins or surface functionalizations that structurally resemble pathogen or damage-associated molecular patterns (PAMPs and DAMPs).[386] As such, both surface functionalizations and biocoronae should be taken into account for immunogenicity evaluation. Given the significant reports of CARPA and other hypersensitivity reactions due to NPs, immunogenicity testing should become a required standard for nanomedicine development.

PEGylation is considered the gold standard to form 'stealth' NPs for in vivo applications because PEG is generally regarded as non-toxic.[150,265,387] However, PEGylation has been found to induce immune responses and hypersensitivity through anti-PEG antibody production by liver and spleen cells.[388,389] Recent clinical trials of a PEGylated-aptamer, for example, found that several patients experienced anaphylaxis due to pre-existing anti-PEG antibodies.[390] Importantly, Armstrong *et al*. observed anti-PEG antibodies in as many as 25% of healthy donors without a known exposure to PEGylated drugs.[391] This contrasts with studies in the 1980s that indicated only a 0.2% occurrence.[392] Most recently, allergic reactions have been reported as a potential risk of several SARS-CoV-2 vaccines that contain PEG and similar compounds, *e.g.*, polysorbate 80, as a liposome stabilizer.[393–395] This increase in allergic responses among the general population is likely due to the expanded use of PEG in cosmetics and food preservatives; however, the widespread use of PEGylated nanomedicines may further increase this risk.[388,396] Importantly, anti-PEG antibodies can also produce the accelerated blood clearance (ABC) phenomena, which results in diminishing returns for subsequent doses as the body can better recognize and remove PEGylated compounds.[397–399] These results indicate that alternative options for controlling blood circulation are needed

to reduce dependence on PEG. Otherwise, common nanomedicine designs could become increasingly less effective and more dangerous as generated anti-PEG antibodies may significantly increase the risk of early clearance and hypersensitivity reactions.[400] Even if the risk is relatively small, such effects could significantly impact public perception and use. Candidate ligands such as polyamino acids, glycopolymers, and polyoxazolines (Pox) have been suggested as potential options.[401–403] However, as these compounds could poise a similar risk in the future, their immunogenicity and safety must be carefully evaluated over time.

The development of biomimetic NPs and erythrocyte hitchhiking represent emerging methods for extending blood circulation and facilitating targeted delivering of NPs.[404,405] Biomimetic NP formulations incorporate cell-derived membrane proteins or vesicles to mimic the biological characteristics and functions of native cells, enabling them to evade immune cell recognition.[406–408] Furthermore, these NPs can deliver cellular components that favorably modulate immune responses.[409,410] In contrast, erythrocyte hitchhiking uses intact cells as a delivery vehicle.[411,412] Unlike small molecule drugs, whose half-life is typically a day or less, cells can circulate in vivo for months. Therefore, when nanoparticles are adsorbed onto or are internalized in circulating cells, their blood half-life can be substantially prolonged. NPs are typically dislodged in capillary beds where the red blood cell must deform to fit through, and this strategy can result in extremely efficient delivery to organs such as the lungs and brain without any additional targeting moieties.[413] However, as mentioned previously, the hemocompatibility of NPs is a concern and must be balanced against delivery efficiency.

2.2.3 Tumor Targeting & Penetration

Most approved organic nanomedicines benefit patients *via* the reduction of severe side effects with only a moderate increase in overall survival compared to standard therapies.[135,414] While these benefits are welcome, such small increases in survival limit the potential clinical translation value of nanomedicine.[208] This apparently insignificant improvement is likely caused by many factors, such as an incomplete knowledge about nano-bio interactions, limited regulatory guidance for nanomedicine design, and the poor reliability of existing preclinical models.[100,415] One factor that has gained significant research attention has been the tumor uptake of injected NPs via the EPR effect, which has served as a foundational design principle for nanomedicine and drug delivery. Although NPs possess inherent tumor-targeting properties through the EPR effect, there are many EPR-related parameters that can vary between tumor subtypes, resulting in suboptimal uptake.[141,416–419] For example, different tumor possess vasculature fenestrations of different dimensions and these can further vary between primary and metastatic tumors as well.[420–422] Tumors also have varying degrees of functional lymphatics and macrophage infiltration that can affect NP uptake. These EPR parameters can further vary based on patient characteristics such as age, sex, body

composition, comorbidities, and co-medications, which are extrinsic, i.e. non-NP, parameters in Figure 5.[422] As such, there has been considerable debate over its role relative to active uptake methods. One meta-analysis concluded that only ~0.7% of injected NP doses (%ID) reached selected tumor sites even in high-EPR xenografted tumors[423]; however, more accurately, this metric represents the amount of NPs detected in the tumors at every 1-hour interval throughout the evaluation period.[424,425] After using established pharmacokinetics calculations based upon area under the time concentration curves (AUCs), Price *et al*. determined that the overall NP exposure to the tumor (AUC_{tumor}) was 76.12% of that of the blood plasma (AUC_{blood}). These two metrics from the same dataset possess a difference of ~113-fold, highlighting how metric selection influences the interpretation of results.[425] Importantly, since NPs can either deliver or act as APIs, no single metric suits all nanoformulations. Furthermore, the EPR effect and high NP uptake may not be a significant factor for some types of nanomedicines. For example, liposomal formulations can extend API circulation and increase tumor exposure without requiring a high delivery efficiency of the NPs themselves. Because each liposome NP contains many API molecules, only a small fraction of the total injected NPs may be sufficient to deliver a therapeutic dose. Furthermore, since nanoformulations have much longer circulation times than small molecule APIs, both encapsulated and leaked drugs have an overall longer exposure time to the tumor than a high-concentration injection of the molecule drug alone. Therefore, a low %ID does not necessarily indicate poor drug delivery. Conversely, for NPs that act as APIs by themselves, such as light-responsive NPs, the number of NPs accumulated within a tumor site can directly determine their efficacy. For such NPs, either established pharmacokinetics or the EPR effect alone may not be sufficient to evaluate nanomedicines.

Active tumor targeting is now a major topic in nanomedicine through engineering specific surface ligands and manipulating the native biocorona.[287,291,426] To reach solid tumors, NPs rely on a combination of passive size-based diffusion through tumor fenestrae, *i.e.*, the EPR effect, and active endocytotic mechanisms, with recent research focusing more on the latter. Kingston *et al*. recently identified an endothelial tumor cell subset with a specific preference for NP transport and vessel permeability.[427] Such cells (termed nanoparticle transport endothelial cells, or N-TECs) were proposed to control NP uptake and distribution within the tumor; however, whether these cells exist in all or only a small subset of tumors is currently unknown. This highlights that understanding tumor cellular heterogeneity is key for proper nanomedicine design. Although ligands, such as PEG, significantly reduce macrophage uptake, this shielding also limits the NP-cell interactions that mediate tumor cell uptake.[428] In addition, the serum and biocorona effects on endocytic uptake, *i.e.*, the primary uptake mechanism for cancer cells, has caused debate among researchers.[429,430] Receptor-mediated endocytosis is widely accepted as a common pathway for NP internalization and for this to occur *via* the biocorona, NPs must adsorb specific protein species of the proper orientation and conformation. Enhanced NP uptake by cancer cells was commonly observed in

serum-containing media; however, recent studies have also found enhanced uptake in serum-free media.[431–434] As such, some researchers believe that the biocorona may actually limit NP uptake by inhibiting non-specific membrane interactions, which is another important mechanism facilitating NP internalization.[429,430,435]

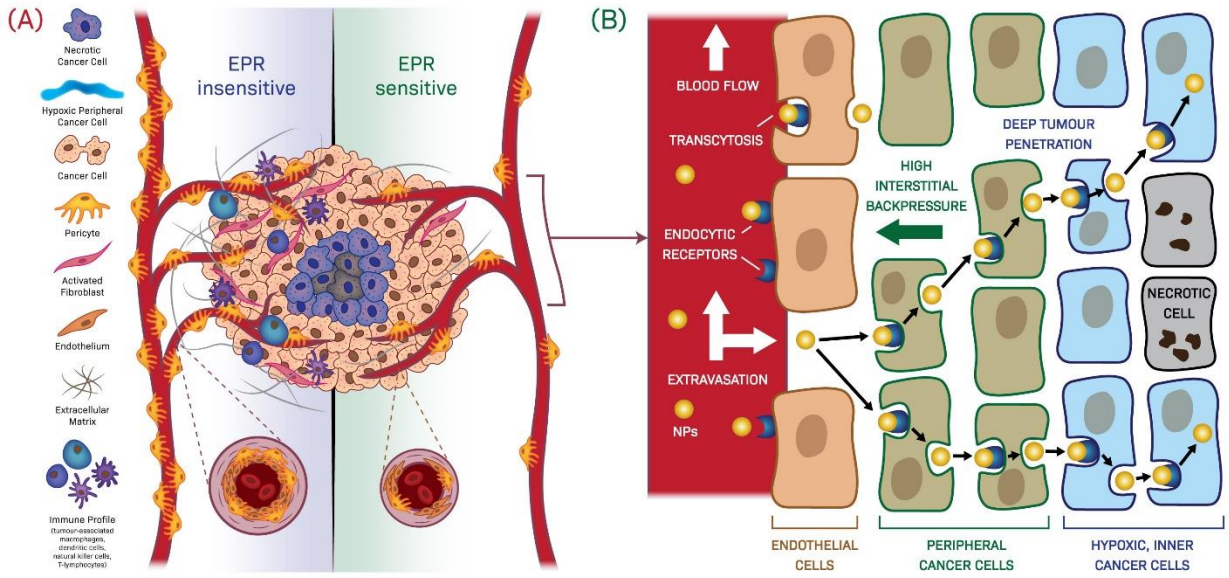

Figure 7: A) The structure of a representative solid tumor and the barriers present for efficient NP penetration via the EPR effect. Adapted with permission under a Creative Commons CC BY License (https://creativecommons.org/licenses/by/4.0/) from ref [414]. Copyright 2019 The Authors. B) Active and passive mechanisms involved in NP tumor penetration.

Once nanomedicines reach the tumor site they must diffuse across the whole tumor mass to achieve a homogenous dose distribution and minimize the risk of disease reoccurrence from spared cell subpopulations.[436] Like the process of the NP reaching the tumor, the interstitial transport of NPs is governed by both passive diffusion and active endo-/transcytosis mechanisms (**Figure 7**).[437–439] Transcytosis is a process where molecules are actively transported from one side of a cell to the other side and is implicated in the regulation of plasma constituents and micronutrients among other processes.[440,441] However, several factors limit the overall NP diffusion in the tumor microenvironment (TME). Because of their rapid growth, tumor blood vessels are often malformed and lack the fundamental architecture of normal blood vessels, reducing blood perfusion and increasing interstitial back-pressure.[436,442–444] As tumors often lack functional lymphatic drainage, this back-pressure is further increased, forcing NPs to concentrate at the tumor periphery.[445,446] Low perfusion commonly induces hypoxic and anoxic TMEs, which are defined as having O_2 levels <2% (in contrast to normal tissue that typically rests between 2–9%) and are strongly related to further tumor angiogenesis and metastasis.[447–449] Cancer cells can sustain themselves in

hypoxic conditions *via* changes to their metabolic pathways, resulting in a focus on glycolysis and lactic acid fermentation as opposed to normal aerobic respiration.[450] Hypoxic conditions are implicated in the induction of chemo- and radioresistance, and are a crucial factor in cancer relapse because of their effects on cell cycle regulation, apoptosis, stem cell maintenance and quiescence, and treatment-resistant noncycling cancer cell selection.[451–454] However, because acidic and hypoxic conditions are typically associated with the TME, such characteristics have been widely explored to design approaches for selective tumor targeting.[455,456]

Tumors are composed of a thick extracellular matrix that contains several cell types, including tumor-associated macrophages (TAMs) and stromal cells that can sequester NPs and limit their uptake.[443,457–460] During inflammation or immune-based treatment strategies, additional phagocytic cells are recruited to the tumor site, further increasing its complexity and the degree of NP sequestration.[461–464] Therefore, the patient and tumor are dynamic systems and active targeting strategies must overcome barriers associated both with reaching and distributing within the tumor. Next-generation nanomedicines will likely feature formulations with a mixture of engineered surface coatings designed to balance challenges associated with uptake, immune response, and clearance. By understanding the key parameters and events that occur in vivo, combination treatments using immunomodulatory and TME modifying compounds can be further developed, which have obtained promising progress for increasing drug delivery and uptake to cancer cells (Figure 5).[141,465–468]

Some specific tumors can have particular barriers associated with their locations. The proper delivery of medications to tumors of the central nervous system (CNS), for example, is often limited by the blood-brain barrier (BBB). Compared to other endothelial cells, the brain capillary endothelial cells show a lack of fenestrations, tight junctions complexes, minimal transcytosis and micropinocytosis, a high electric resistance (1500-2000 Ω), and additional efflux transporters.[469,470] This makes delivery across the BBB extremely difficult. Only small molecules (<500 Da) such as water, some gases, and some lipid-soluble compounds can passively penetrate through the BBB, while most other materials require active transport via receptor-mediated transcytosis. In this way, delivery of NPs through the BBB partially resembles tumor penetration. In order to efficiently release drugs into the brain, various strategies have been developed. These include chemical modifications of drug and prodrugs, temporary disruption of tight junctions, and local delivery into the brain by neurosurgery.[471,472] However, the temporary disruption of the BBB is risky and can cause an uncontrolled influx of molecules into the CNS. Therefore, the ideal method to transport drugs across the BBB should be controlled and not damage the barrier. Many types of nanomedicines have been extensively studied for delivery to the brain including liposomes, synthetic polymer NPs, and inorganic NPs such as GNPs and QDs.[470,473,474] One promising technique to facilitate NP

uptake across the BBB and other barriers is the use of focused ultrasound (US) together with gas bubbles.[475] Owing to the compressibility of gas, lipid- and protein-stabilized microbubbles can oscillate and backscatter US more strongly than solid particles of the same size. In addition to US scattering, microbubble oscillations also generate mechanical shear forces (including shock waves and microjetting) that can temporarily disrupt cell membranes, the tumor extracellular matrix, and vascular walls, thus improving NP extravasation and uptake by tumors or across the BBB (sonoporation).[476–478] Nanobubbles can also be engineered; however, because the internal Laplace pressure strengthens and bubble resonance weakens with decreasing size, their design and utility are still under early investigation.[479] Nevertheless, caution should be taken in the development of brain-targeted NPs since some NPs have been observed to be amyloidogenic and may be able to induce neurodegenerative diseases such as Alzheimer's disease.[480–482]

2.3 Phase II: Internalization and Subcellular Localization

The second phase of assessment, the *Internalization Phase*, accounts for the individual cellular events involved in NP biodistribution as opposed to the organ-level or blood-level responses in Phase I (**Figure 8**). While the overall effects of active transcytosis and different passive factors on NP biodistribution are accounted for in Phase I in the framework *via* their overall diffusion rate across the tumor mass, the specific cellular level mechanisms should not be ignored.[483] Tumors have a highly heterogeneous composition and different cells have varying levels of expressed surface and intracellular receptors. Thus, understanding how NPs interact with these components is critical for the optimization of treatment efficacy as outlined in Phases I and III.[251,484,485] Macrophages and other immune cells typically uptake larger NPs through phagocytosis whereas cancer cells preferentially use other endocytotic routes.[486] Cancer cells possess different surface protein expression patterns that have been extensively investigated for their use in diagnostics and drug targeting.[487] Ultrasmall and engineered NPs can also enter the cell through membrane diffusion because of their small size or special surface functionalization.[488,489] Thus, both the biocorona formed in Phase I and the bare NPs contribute at this level of biological complexity. Once internalized, most NPs are first trapped within endosomes or other similar vesicles. Depending on how the cell recognizes the NP through its biocorona, these vesicles can fuse with lysosomes for degradation, be trafficked to specific organelles, or be transported out of the cell.[490] Exocytosis or transcytosis can be exploited for deep tumor penetration because these active-transport processes bypass the diffusion barriers encountered in the tumor stroma.[437,438,491,492] Regarding subcellular trafficking, many anticancer targets are located at specific cellular locations, resulting in both organelle targeting and endosomal escape emerging as key areas of research.[487,493,494] More accurate assessments of NP toxicological impacts (as detailed in Phase III) can be obtained by understanding the subcellular dose.[495] Estimates of NP degradation by lysosomes or external stimuli can assist in Phase III assessments with knowledge of the release of

encapsulated therapeutics, reactive metal ions, or other compounds of interest.[496–498] Thus Phase II is a key mediator for design and assessment, as the overall biodistribution and activity of the administered nanomedicines are dependent on the cellular events outlined here.

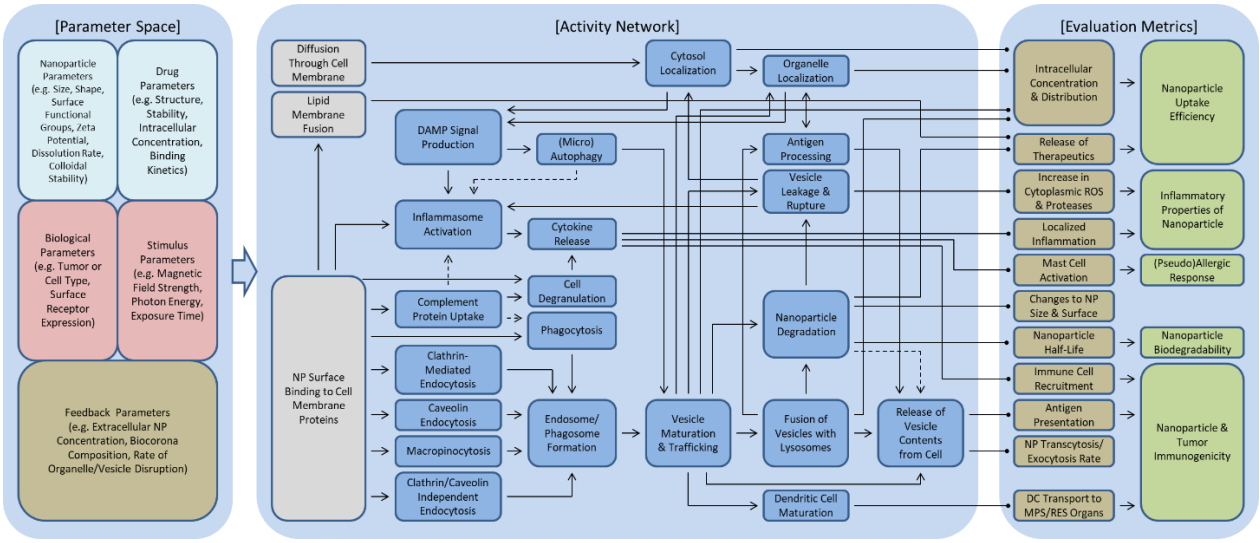

Figure 8: Phase II (Internalization) of the NSAF for anticancer strategies. Herein, the extrinsic parameters focus on cell type-dependent parameters such as the expression level of specific cellular receptors. Feedback parameters include factors relating to the NPs location and biological identity (Phase I), and organelle damage (Phase III). Phase II focuses on the mechanisms of NP uptake, transport, and subcellular localization.

2.3.1 Nanomedicine Uptake Routes

Nanomedicines interact with components of the plasma membrane upon contact with individual cells and trigger cellular uptake *via* various mechanisms.[499] Endocytosis, the primary uptake route for all cells, leads to NP engulfment in membrane invaginations, which then fuse with early endosomes for further processing. Overcoming the intrinsic tension of the lipid bilayer in a controlled manner is a crucial step towards membrane budding. Because this is a highly entropic process, it requires the aid of several scaffolding or destabilizing agents that disrupt the ordered and compact structure of the membrane.[500,501] Depending on the cell type and the biomolecules involved in the uptake and sorting process, endocytosis can be broadly classified into five main types: phagocytosis, clathrin-mediated endocytosis, caveolin-mediated endocytosis, clathrin/caveolin-independent endocytosis, and macropinocytosis (**Figure 9**).[282,502–504] Compared to phagocytosis, which occurs mainly in phagocytes responsible for clearance and antigen presentation, the other endocytic mechanisms are more common and occur at varying levels in many cell types, including cancer.[484,499] Some NPs, such as liposomes, can directly fuse with the plasma membrane due to their similar structure/components, resulting in releasing their cargo into the cytoplasm.[488] Other NPs

can directly diffuse across the plasma membrane or escape endocytic vesicles and directly enter the cytoplasm because of their small size or engineered surface properties.[489,505–507]

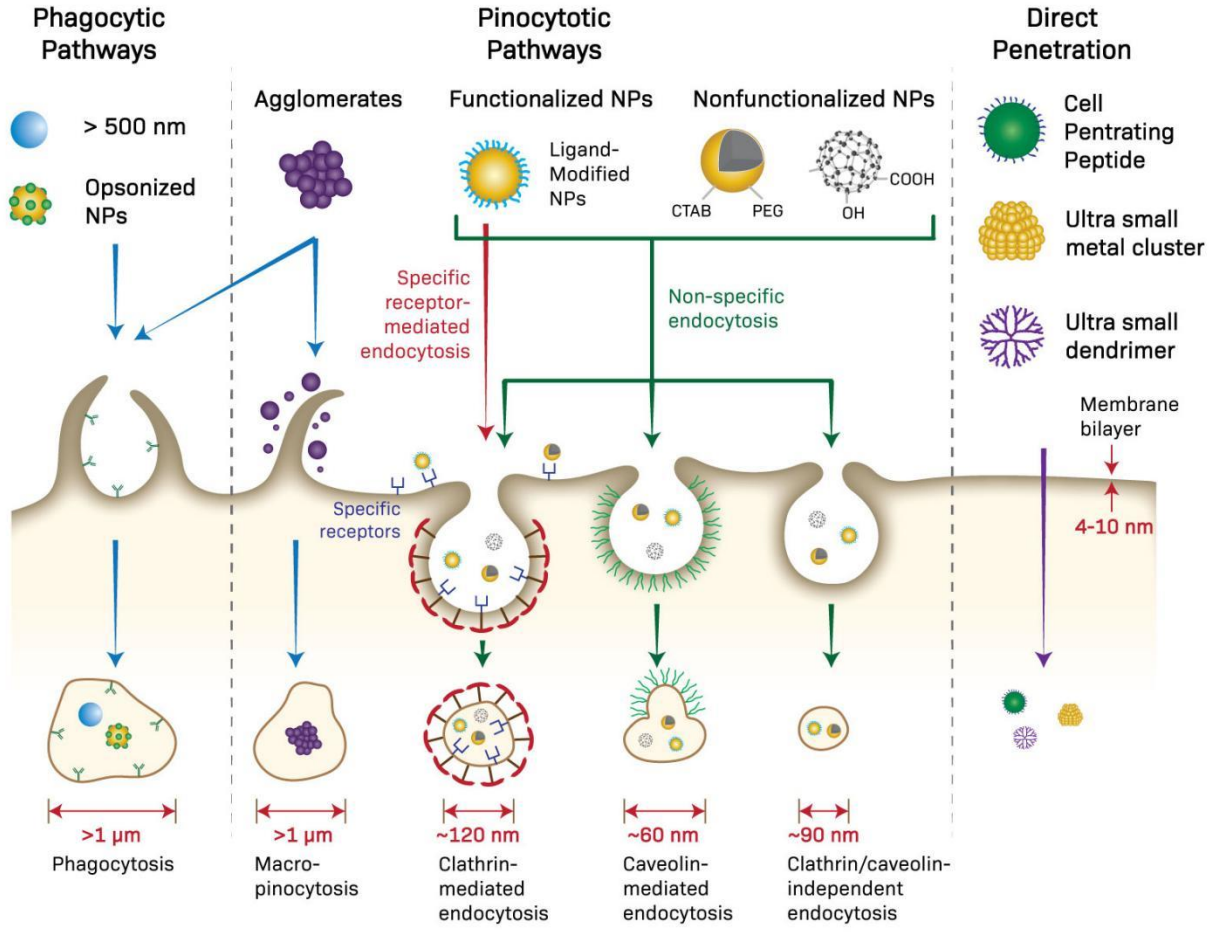

Figure 9: The endocytotic uptake routes for various NP types. Phagocytosis is preferred for larger and aggregated NPs, while ultrasmall NPs can directly diffuse through lipid membranes. Most NPs, however, will be internalized through one or more of the main endocytotic routes depending on the interplay of their various properties. Adapted with permission from ref [508]. Copyright 2013 American Chemical Society.

NP phagocytosis is usually initiated by biocorona proteins interacting with specific receptors on the phagocyte surface.[251,509] This initiates a signaling cascade triggering actin assembly, the formation of cell membrane extensions, and the engulfment and internalization of NPs into a vesicle known as a phagosome that functions similarly to late endosomes.[510,511] This process can take several hours to complete depending on the cell type and the NP surface.[503] Phagocyte receptors involved in this process commonly include Fc receptors, complement receptors, and other receptors, such as mannose/fructose receptors.[484,503,512] Depending on the uptake receptors used, macrophages can release anti- or pro-inflammatory mediators that induce several effects on cells.[63,251,513–515] Therefore, even NPs designed to

exploit phagocytic uptake for targeting macrophage populations or the RES/MPS organs should consider the role of the protein corona and its influence on different uptake routes.

Clathrin-mediated endocytosis (CME) is the main mechanism by which most cells obtain nutrients and plasma membrane components, such as cholesterol.[510,516] CME occurs either by receptor-specific or non-specific adsorptive uptake, also called receptor-independent CME. Non-specific hydrophobic or electrostatic interactions drive receptor-independent CME.[517] CME occurs at plasma membrane domains (typically covering about 0.5–2% of the cell surface) that are rich in clathrin and adapter proteins acting as recognition sites for different cargoes and sorting signals.[503,510,518–520] During CME, ~70–150 nm vesicles are formed, engulfing extracellular fluid proportional to the internal volume of the vesicle.[521,522] Vesicle fission is coordinated by the recruitment of dynamin, a GTPase.[523] Once inside the cell, these vesicles are stripped of their clathrin-coating before fusing with early endosomes.[522,524] While CME is a major route of entry for many NPs, vesicles produced by this route are frequently degraded by lysosomes and thus may be unsuitable for such types of drug delivery wherein early degradation is undesirable.[503,525–527] In contrast, the degradative and acidic lysosome environment can act as a switch for NP activity or drug release, and thus the 'ideal' uptake route depends on the specific clinical application and the corresponding design of the nanoformulation.[154,528]

Caveolae-dependent endocytosis is critical in many biological processes, including cell signaling, transcytosis, and cellular plasma membrane regulation.[499,529–531] Because caveolae-dependent endocytosis often results in the transcytosis of smaller NPs (<60 nm) and evasion of lysosome fusion, this route has potential for deep tumor penetration and the delivery of degradable drugs/compounds, such as genes or proteins.[484,487,492,532] This non-degradative transport has typically been ascribed to a pH-neutral vesicle known as a caveosome; however, recent research has cast doubt on its existence and the role of caveolae in transcytosis remains controversial.[533–535] Caveolae are 50–80 nm flask-shaped membrane invaginations present in epithelial and non-epithelial cells.[502,503,510,536] In non-epithelial cells, such as adipocytes and smooth muscle cells, caveolae constitute a substantial proportion of the cell membrane (up to 75%).[503,537–539] Caveolae contain several cell receptors usable by NPs. For example, Abraxane®, an albumin-bound form of paclitaxel, is taken up by cells primarily by caveolae-mediated endocytosis *via* gp60, an albumin receptor present in endothelial cell caveolae that facilitates transport into the interstitial space.[540] After entering the interstitial spaces the Abraxane® NPs are captured by SPARC (secreted protein, acidic and rich in cysteine) that is selectively secreted by tumors.[541] The resulting complex is selectively internalized by the cancerous cells leading to increased drug delivery.

Although CME and caveolae are the principal endocytic pathways, other less-studied mechanisms can internalize cargos, such as extracellular fluid, Interleukin-2, folate, and growth hormones, through

various (and perhaps redundant) receptors.[510,542,543] These mechanisms are usually cholesterol-dependent and require specific lipid compositions.[503] Currently, caveolae- and clathrin-independent pathways are classified as Arf6-, flotillin-, Cdc42-, or RhoA-dependent.[544,545] Because the altered cancerous cell metabolism often leads to increased folate demand and upregulation of the GPI-anchored folate receptor FRα, the use of folic acid as a surface ligand has gained some interest for active tumor targeting strategies.[546] Though clathrin- and caveolae-independent mechanisms have been observed for several NPs, they typically only contribute a small proportion to overall nanomedicine uptake and further analysis is needed to fully elucidate their role.[543,547–549]

Macropinocytosis is a special case of clathrin-, caveolae-, and dynamin-independent endocytosis that is often initiated by the activation of receptor tyrosine kinases by growth factors.[550,551] Receptor activation mediates a signaling cascade that produces changes in the actin cytoskeleton and the formation of protruding membrane ruffles that entrap extracellular material as they fuse back with the membrane. Endocytic vesicles formed during this process (termed macropinosomes) are typically larger (0.5–10 μm) and allow for non-specific uptake of larger NPs in cells that lack phagocytosis.[552,553] This bulk pathway is possible for virtually any cell with only a few exceptions, such as macrophages and brain microvessel endothelial cells.[554]

Several experimental studies have suggested that ~30–60 nm is the optimum NP size range for uptake in cancerous cells.[324,486,503,555–557] Chithrani *et al*., for example, showed that 50 nm GNPs were internalized by HeLa cells more effectively than GNPs in the 14–100 nm range.[558] Increasing NP size, and thus the number of surface ligands, allows each NP to bind to more receptors on an individual cell simultaneously, causing them to associate more firmly with the cell and initiate internalization.[559,560] The lower enthalpic limit for a spherical NP occurs at ~30 nm, indicating that smaller NPs should not as effectively drive the membrane-wrapping process.[560] However, further increasing the NP size yields diminishing returns as this increases the free energy required for uptake and reduces the remaining receptors available for other NPs.[559,561,562] Although an ideal size range has been identified for general uptake, the relationship between NP size and specific endocytic pathways is inconsistent.[282,510] These contradictions are related to the complexity of controlling other uptake parameters such as the cell phenotype, surface charge, shape, hydrophobicity, and the specific biocorona composition. NP aggregation following administration also has distinct effects on uptake as aggregates contain small subunits with higher surface curvatures than spherical NPs of the same overall size.[563,564] These subunits can alter the aspect ratio and ligand density of the aggregates, which in turn affects binding avidity. Albanese *et al*. showed the uptake of aggregated GNPs in HeLa and A549 cells were on average 25% lower than for non-aggregated GNPs.[565] However, there was a 2-fold increase in MDA-MB-435 cell uptake for the largest aggregates.

In addition to surface properties, NP shape and morphology can significantly influence cellular uptake.[566–569] For >100 nm NPs, Gratton *et al*. observed that rod-shaped NPs exhibited the highest uptake followed by spheres, cylinders, and cubes.[552] Herd *et al*. investigated the uptake of worm-like (232 × 1348 nm), cylindrical (214 × 428 nm), and spherical (178 nm) silica NPs in relation to the different internalization mechanisms.[570] Chemical inhibitor experiments suggested that CME was the primary mechanism for spherical NPs whereas the worm-like NPs preferentially underwent macropinocytosis or phagocytosis as they were too large for CME. For NPs <100 nm, spherical NPs have the highest uptake, and increasing the aspect ratio of nanorods decreases uptake.[504,571,572] Carnovale *et al*. observed that the surface area of different GNPs (prisms > cubes > rods) was inversely correlated with the number of particles internalized.[429] These observations may be explained based on the particle wrapping principles noted above. The point of contact of a sphere with a cell is significantly lower than a shape with flat sides. Thus, to be internalized, smaller spherical NPs require less free energy and fewer cellular receptors than larger particles. This increases the internalization rate with less negative feedback due to limited receptor availability. Notably, simulations and experimental results indicate a higher energy barrier for the internalization of soft, easily deformable NPs, *e.g.*, liposomes, than for rigid NPs.[573–576] Consequently, soft NPs generally possess longer circulation times but reduced cellular uptake.

2.3.2 Intracellular Trafficking & Degradation

Following NP internalization, endocytic vesicles become uncoated and fuse with early endosomes for further processing.[577,578] Nanomedicine fate once inside early endosomes depends on the NP properties and proteins involved in the uptake and transport process (Figure 8).[504,579,580] Early endosomes can transport NPs across the cell membrane, to the trans-Golgi network or other organelles, or late endosomes (**Figure 10**).[581–583] The endosome development stages are typically accompanied by acidification of the intra-vesicle pH (5.0–6.5), which may eventually fuse with lysosomes for additional acid (pH 4.5–5.0) and enzymatic digestion of the vesicle contents.[499,584–586] Another important and overlapping pathway involved in NP trafficking and degradation is autophagy, where cytoplasmic contents and dysfunctional organelles are encapsulated into autophagosomes that later fuse with lysosomes.[587–589] Autophagy can be triggered by NPs in the cytoplasm by oxidative stress and damaging signals from organelles including the mitochondria, Golgi, and other endosomal vesicles.[590–595] Ultimately, the degraded contents within lysosomes and similar degradative vesicles are released *via* exocytosis.[596,597] As noted above, some internalization mechanisms, such as caveolae-dependant endocytosis, commonly bypass lysosomal degradation. Such uptake methods can confer mechanistic advantages. Zhang *et al*. recently used caveolae-dependant transcytosis for deep tumor penetration using small (5–10 nm) NPs composed of polyamidoamine (PAMAM) dendrimers modified with dimethylmaleic anhydride (DMA).[491] Under normal physiological conditions, the NPs were

negatively charged, minimizing macrophage uptake and clearance; however, the NPs underwent a charge reversal in the acidic tumor microenvironment, causing internalization and transcytosis at a greater rate *via* caveolae.

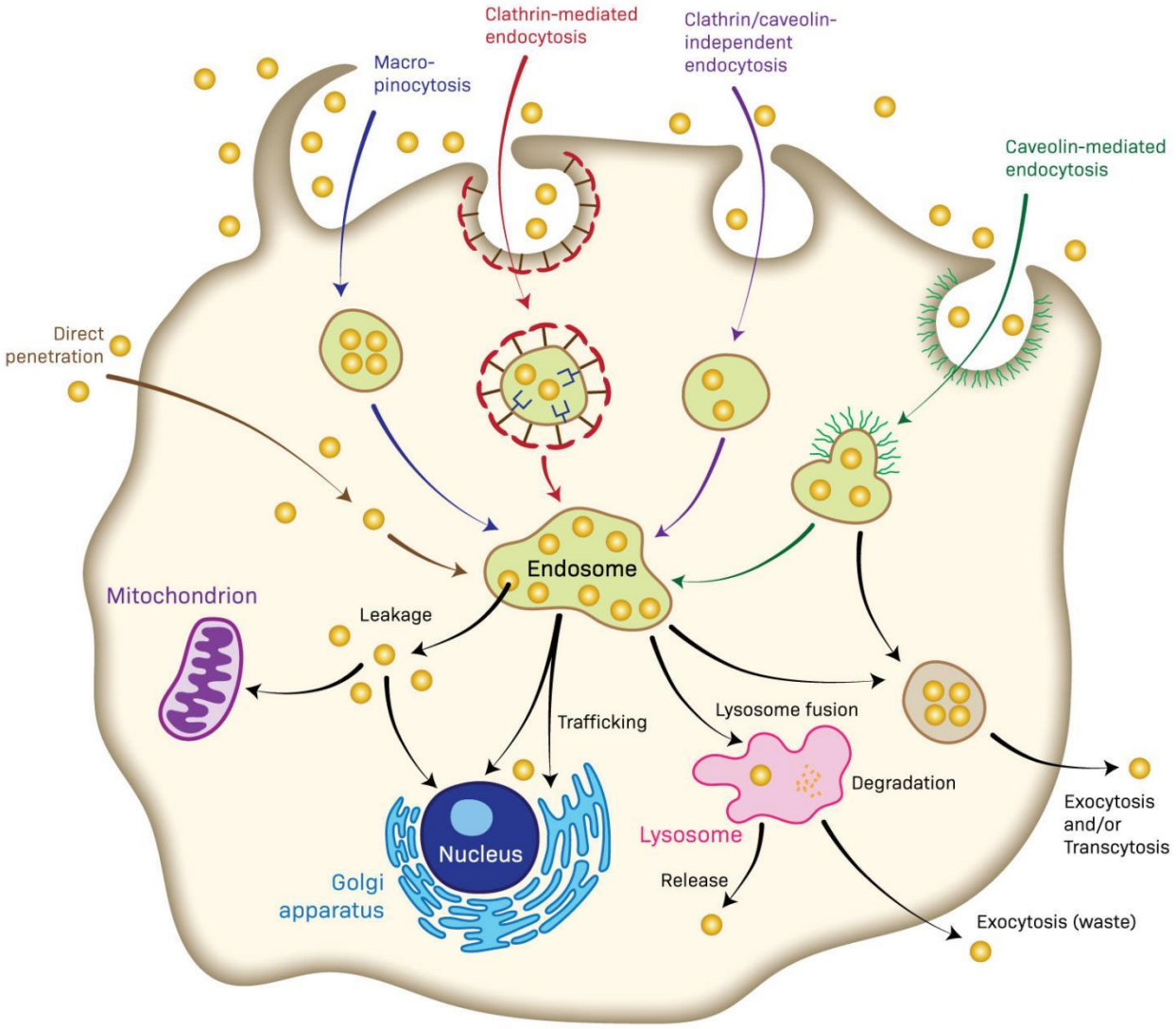

Figure 10: Endocytic pathways for internalized NPs. Following internalization, NPs are mostly trafficked into endosomes before merging with lysosomes for degradation or release. Depending on the uptake and endosome processing factors involved, NPs can be trafficked to different organelles or escape into the cytoplasm.

Endosomal entrapment is a common challenge for many nanomedicines as endosomal localization and lysosomal degradation can prevent the intended API interactions with therapeutic targets.[598] In some cases, however, endocytosed NPs may escape typical trafficking pathways at any stage and be released into the cytoplasm because of their size or engineered surface properties.[501] If this precedes lysosome fusion,

the NPs bypass lysosomal degradation and enter the cytoplasm or other target destinations intact. Some methods of engineering endosomal escape include the use of polycationic polymers, cell-penetrating peptides (CPPs), and stimuli-responsive designs to generate disruptive forces, *e.g.*, ROS, localized heat, or osmotic pressure, to damage the vesicles.[455,505,599–602] The intrinsic NP properties that lead to endosomal escape relate to their pristine surface properties, primarily regarding their ability to bind lipid membranes and generate ROS.[603–605] Electrostatic and hydrophobic interactions between NPs and cellular membranes are key parameters influencing uptake and transport, with positively charged and hydrophobic NPs typically having higher cellular uptake rates because of their affinity for the negatively charged plasma membrane.[507,606–609] Conversely, localized membrane disruptions induced by such NPs may contribute to their higher observed toxicity in contrast to neutral or negatively charged hydrophilic NPs.[610] Positively charged NPs readily induce membrane disruption, stimulating intracellular oxidative stress *via* lysosome destruction and $^{\bullet}O_2^-$ release from mitochondria.[611–613] Other research suggests that the surface charge magnitude is more critical than whether the NP possesses an overall positive or negative charge.[614,615] Because the biocorona forms an NP surface layer in the extracellular environment, the effective surface charge is significantly screened by adsorbed proteins during NP uptake.[431,616–618] However within maturing endosomes and lysosomes, the adsorbed proteins may be degraded, leading to an increased role of the pristine NP characteristics, such as composition, charge, hydrophobicity, and surface reactivity.[498,619–622]

NP organelle localization can largely be categorized into two main pathways: (1) direct, passive diffusion into the organelle compartments from the cytoplasm, and (2) active transport using targeting moieties.[623–626] For many anticancer therapies, the nucleus is the main organelle target as it contains the DNA and its repair enzymes. Passive NP or drug delivery to the nucleus requires entering *via* either nuclear pores (<10 nm) or during periods of compromised membrane integrity, such as mitosis.[495,627–629] This size-dependency was exemplified by Huo *et al*. who observed that despite better cellular uptake for 14 nm GNPs, smaller 2 nm GNPs delivered DNA payloads to the nucleus 20× more efficiently.[630] 2–6 nm NPs were observed within the nucleus, whereas those between 10–16 nm were present outside the nucleus. Within cells, large endogenous molecules destined for the nucleus contain a nuclear localization signal (NLS) that simultaneously binds to the protein cargo and transport proteins (importins) that shuttle the cargo to the nuclear pore complex (NPC).[631] The NPC then actively translocates the cargo (even those >10 nm) into the nucleus.[632] The canonical NLS is a short, positively-charged CPP rich in basic amino acids, *e.g.*, the transactivator of transcription (TAT) peptide (YGRKKRRQRRR).[633] NPs and drugs bearing such TAT motifs can translocate to the cell nucleus, which can dramatically improve their efficacy, mitigate multidrug resistance, and reduce off-target toxicity.[631,634–638] Peng *et al*. showed that transferrin and TAT-functionalized NPs showed a 45-fold higher accumulation to A549 lung cancer cell nuclei in vitro and better photothermal therapy outcomes in A549 tumor-bearing mice compared to non-targeted iron oxide

NPs.[639] Interestingly, like the biocorona, the effect of functionalized TAT motifs appears to be partially dependent on surface density.[640] Dalal and Jana examined the uptake of CdSe/ZnS core-shell QDs coated in a polyacrylate shell modified with PEG and varying amounts of TAT (CGRKKRRQRRR) peptides.[641] These NPs entered HeLa cells through a lipid-raft mediated endocytotic pathway and possessed different trafficking patterns based on the TAT peptide density. QDs with a lower TAT peptide surface density induced endosomal escape and localization at the Golgi apparatus and the perinuclear region, whereas a higher density led to exocytosis. Similar results were obtained for mesoporous silica NPs conjugated with the same TAT peptide sequence.[632] Tang *et al*. observed that the nuclear transport of 2–8 nm CdSeS/ZnS QDs containing a different TAT sequence (DRQIKIWFQNRRMKWKK) plateaued at a ligand density of ~20%.[642,643]

Another key target for many anticancer strategies is the mitochondria. In normal mammalian cells, the mitochondria execute a controlled regulation over the growth-death cycle through the mediation of apoptosis, energy production, amino acid metabolism, and redox signaling, among other roles. In cancerous cells, however, the Warburg effect, where the anaerobic glycolysis rate in the mitochondria dramatically increases to accommodate cancerous growth, plays a fundamental role in cancer initiation and progression.[644–646] Furthermore, tumors frequently produce high mitochondrial ROS levels that invoke genetic instability and tumorigenesis.[647] Consequently, mitochondrial dysfunction is a metabolic hallmark of cancer cells.[11] Anticancer nanomedicines that selectively disrupt cancerous mitochondria can be achieved by designing NPs that inhibit glycolysis, depolarize the membrane potential to release ROS and pro-apoptotic signals, and inhibit the mitochondrial permeability transition pore.[648–650] Many clinically approved anticancer drugs, such as paclitaxel, etoposide, betulinic acid, lonidamine, and CD-437, act directly on the mitochondria to trigger apoptosis; however, compounds that specifically localize to the mitochondria have yet to be fully developed.[624,651–653] Drug access into the mitochondria is challenging because of their complex membrane structure coupled with a highly negative membrane potential (−150−180 mV) that prohibits the entry of small anionic materials into the inner matrix.[625] These properties are often further enhanced in cancerous cells.[654–656] Currently, bioactive molecule transport into mitochondria is based on two key parameters: the mitochondrial membrane potential and its protein import machinery. One successful strategy is the use of cationic and lipophilic molecules that facilitate NP accumulation to the anionic mitochondrial membrane *via* electrostatic interactions, followed by translocation through the membrane to the inner mitochondrial matrix.[657–659] So far, triphenylphosphonium (TPP) surface coatings have shown particular promise for mitochondrial targeting.[660–663] The advantages of TPP-based systems include their biological stability, the combination of lipophilic and hydrophilic moieties, low chemical reactivity toward cellular components, and simple synthesis and purification.[650]

2.4 Phase III: Molecular Mechanisms of Activity

Finally, the *Dysregulation Phase* concerns molecular level events and details the mechanisms by which nanomedicines directly exert their toxicological or therapeutic effects on cells (**Figure 11**). Organic NPs, such as liposomes, being composed primarily of biocompatible materials, rarely possess their own pharmacodynamic effects but instead have their activities attributed to their loaded drug payloads. As each loaded drug possesses a distinct mechanism of action, a comprehensive analysis of every possible pathway and interaction is beyond the scope of this review. Nevertheless, drug delivery and drug combination strategies are key in the fight against cancer and their mechanisms must be integrate into the NSAF as appropriate. We have therefore chosen to use Doxil® as a model to integrate drug delivery strategies into the framework outlined in Figure 11.[664–666] DOX is one of the earliest drugs to be used in clinical nanoformulations and it remains widely used in drug delivery research.[88,667] In contrast to organic NPs, inorganic NPs may possess quantum-mechanical properties that warrant in-depth examinations to establish both efficacy and safety. Thus, herein we have chosen to focus on the activities of nanomedicines typically containing next-generation materials, such as metallic NPs. Regardless of the main mode(s) of action, the common goals of anticancer compounds are to outright kill cancerous cells or sensitize them to further treatments such as radiotherapy and immunotherapy. Although many strategies exist, these are fundamentally born from common mechanisms, *e.g.*, ROS/heat production, drug delivery, and downstream effects such as DNA damage, macrophage polarization, and caspase activation, which can be described by the network outlined herein. The Evaluation Metrics of this phase primarily represent therapeutic endpoints, such as the development of drug resistance and radiosensitivity, or the production of pro-inflammatory conditions that exacerbate the overall cancerous state as outlined in prior Phases.

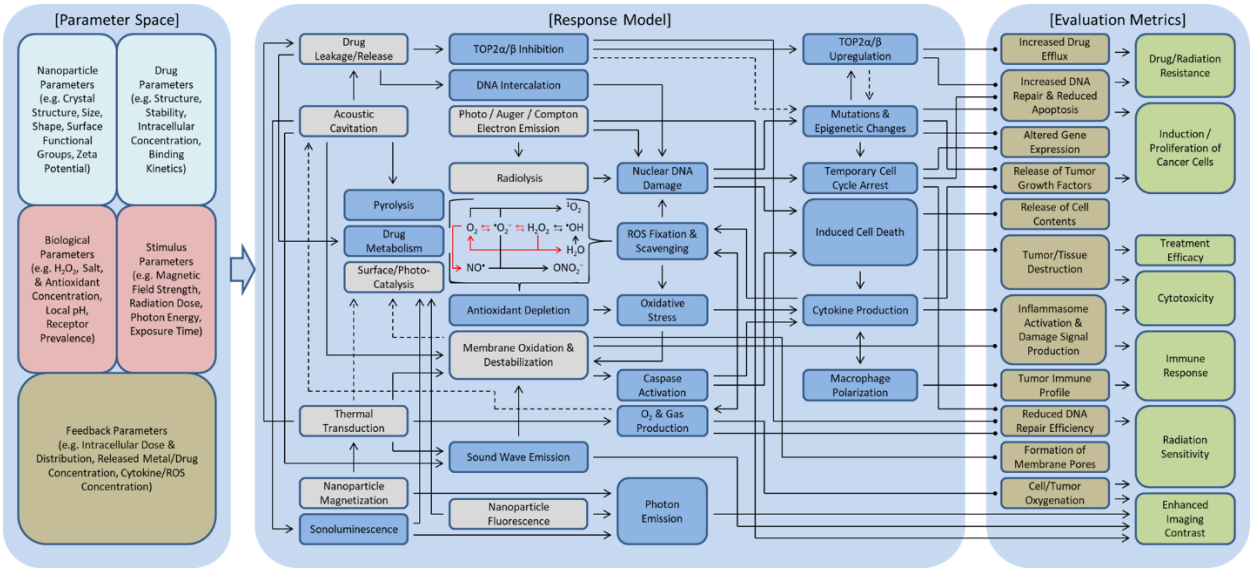

Figure 11: Phase III (Dysregulation) of the NSAF for anticancer strategies. Herein, the extrinsic parameters include those related to the internal conditions of the cell, such as native ROS and protein levels, as well as external stimuli such as X-Rays. Both treatment efficacy and toxicity are primarily determined by ROS, which can be generated or scavenged by the NP surface, by released drugs or other therapeutic compounds, or by the cell upon the initiation of damage. ROS pathways associated with major cellular enzymes/antioxidants are noted in red.

2.4.1 Chemodynamic Therapy: Intrinsic ROS Catalysis

The primary driver of nanomedicine efficacy and toxicity following delivery is the production and of reactive oxygen and nitrogen species (ROS and RNS respectively, generalized as ROS for simplicity). Low ROS levels produced by cellular metabolism are omnipresent in all cells and are essential for effective cell signaling and function in combination with antioxidants, such as glutathione (GSH).[60,668–670] Increased ROS generation within cells, however, can overwhelm the antioxidant and redox equilibrium, triggering oxidative stress, biomolecular damage, such as DNA double-strand breaks and lipid peroxidation, membrane depolarization, and apoptosis.[243,668,671] Because of their altered growth and metabolism, cancer cells possess an altered redox environment characterized by a high basal rate of both ROS production and scavenging.[669,672–674] Despite their toxicity, elevated ROS levels have long been associated with many cancer types and were initially believed to be oncogenic by promoting genome instability.[668,675–677] Recent research has suggested that cancer cells maintain this altered redox equilibrium to exploit ROS in pro-tumorigenic signaling pathways.[15,669,678,679] However, like normal cells, cancer cells are sensitive to redox environment changes, and ROS overproduction during RT and chemotherapy contributes significantly to the overall tumor/tissue response.[170,680–683] Many inorganic NPs and loaded drugs can produce ROS through redox reactions at the NP surface, by released metal ions, or during drug metabolism.[671,684–690] The highly curved surfaces of inorganic NPs lead to inherent surface defects, causing the disruption of the continuous

bulk electronic configurations and generation of ROS-producing redox sites (**Figure 12**A).[691–693] The radiolysis of water during RT is also aided by the reduction of its ionization energy when adsorbed on NP surfaces, *e.g.*, from 465 kJ mol^{-1} to 256 kJ mol^{-1} on a bare gold surface.[694–697] Because of these redox sites and the dysregulation of endogenous substrate molecules in cancer cells, metallic NPs can damage or kill tumor cells even at ambient conditions.[163,217,698] Though apoptosis induction *via* ROS is ideal for cancer reduction, ROS and ionizing-radiation-induced DNA damage possess additional, dose-dependant, cellular effects.[591] Sublethal DNA damage can promote oncogenic mutations and chromosomal aberrations, which can worsen the overall tumor state.[671] Conversely, excessive damage can induce necrosis, resulting in inflammation and exacerbating the ROS feedback cycle.[699] While for most nanomedicines the exact mechanisms and parameters involving ROS generation still need to be elucidated and optimized for medical use, significant progress has been made in the development of ROS-based treatments; meanwhile several widely accepted assumptions, such as the chemical inertness of GNPs, have been challenged.[162,172,700–702] Yang *et al*. recently published an excellent review covering the latest studies that primarily exploit ROS-based nanomedicines to treat cancers with an important emphasis on the underlying materials' chemistry.[154]

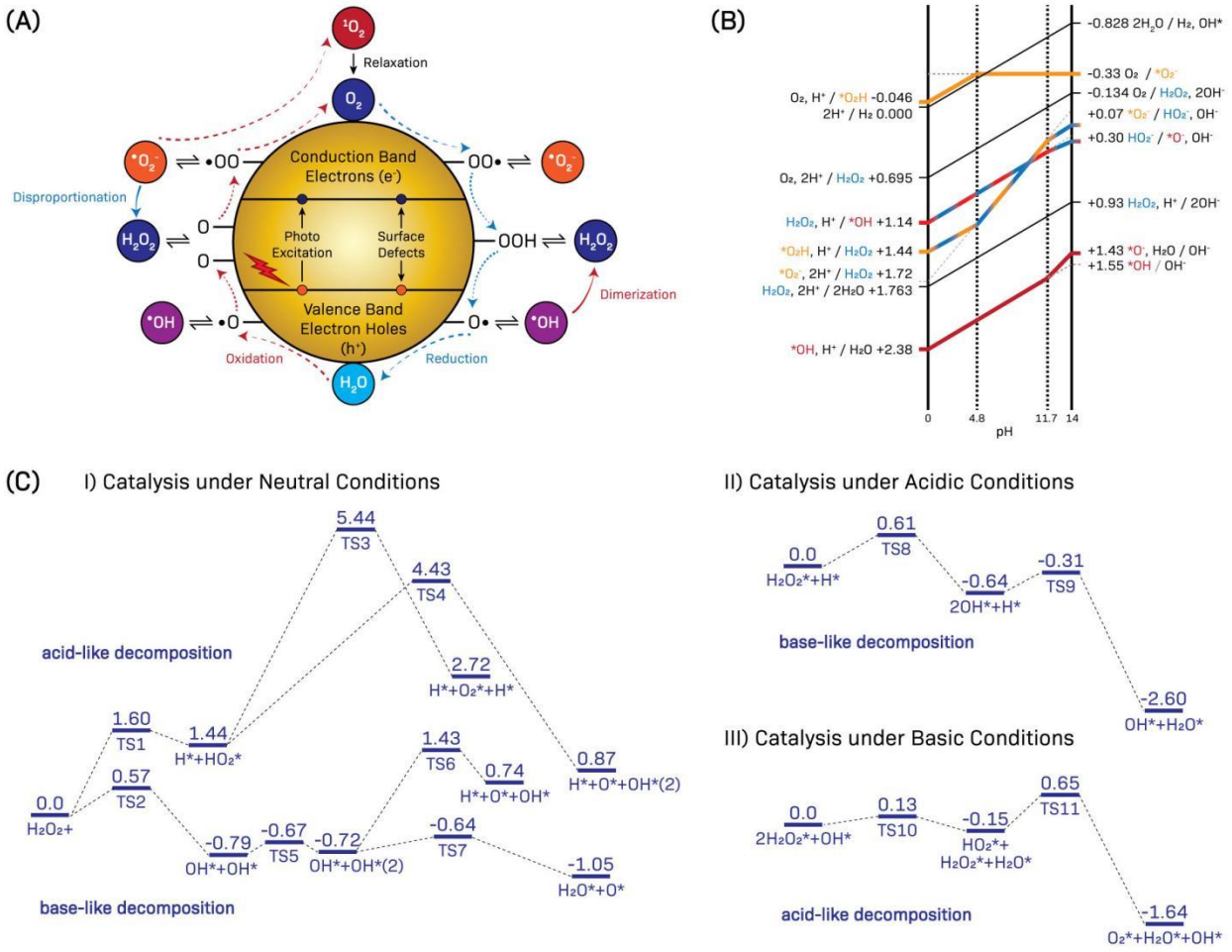

Figure 12: A) The catalytic reactions prevalent on inorganic NPs surfaces because of their crystal structures, surface defects, and photoexcitation. B) pH dependence of one-electron redox of H_2O, H_2O_2, and O_2. Black lines show two-electron ($2e^-$) processes that correspond to the average of the redox potentials at each step. The redox potential of O_2 (−0.33 V) is for the standard gas state of 1 atm. For 1 M in water, the redox potential is estimated to be −0.16 V. Adapted with permission from ref [703]. Copyright 2017 American Chemical Society. C) Calculated reaction energy profiles (eV) for H_2O_2 decomposition on an Au(111) surface in (I) neutral, (II) acidic, and (III) basic conditions. Adapted with permission from ref [704]. Copyright 2015 Elsevier.

The most classic examples of metal-based ROS catalysis are the Fenton-like reactions, wherein metals ions, such as iron or copper, undergo redox cycling to decompose H_2O_2, forming various ROS, such as singlet oxygen ($^1O_2$), superoxide ($^{\bullet}O_2^-$), and hydroxyl radicals ($^{\bullet}OH$).[705–708] Many NPs of various compositions, shapes, and surface coatings have been found to possess Fenton-like and catalase-like activities.[709–712] In addition to hypoxia, one common consequence of the altered redox conditions of cancer cells is a persistently elevated level of H_2O_2 compared to normal cells.[713,714] While H_2O_2 is a strong oxidant, it is not very reactive because of its slow reaction kinetics and thus it can accumulate and act as a secondary

signaling molecule, or be catalytically decomposed to effectively produce O_2 or more reactive oxidants, such as $^{\bullet}OH$.[715–718] As H_2O_2 levels serve as an important precursor for ROS generation and a potential hallmark of cancer, it likely acts as a key molecule in the activity and toxicity profiles of many NPs, and understanding these catalytic pathways may assist in future nanomedicine design and assessments.[719–722] Many treatment strategies exploit native tumor H_2O_2 levels, either through ROS generation (chemodynamic therapy (CDT)), photodynamic therapy (PDT) to selectively damage cancer cells, or through O_2 generation for enhanced RT.[455,723–728] Importantly, NPs that possess high oxygen scavenging properties are likely ineffective radiosensitizers in comparison to those that preferentially use other substrates, such as H_2O_2, to compensate for their oxygen consumption.[713,729,730]

It is often assumed that metal ion dissolution from NPs is the primary cause of both therapeutic ROS generation and cellular toxicity; however, this may not be the case for all NPs or that it may only be one of several mechanisms.[243,721,731] In semiconductor NPs, an excess of conduction band electrons (n-type) or valance holes (p-type) can be inherent the nanostructure based on its composition. Because of this and the high curvature of NPs, reactive defects can readily occur and induce redox reactions with endogenous molecules such as H_2O_2. The peroxidase-like activity of copper sulfide (CuS) NPs (a p-type semiconductor) has optimal activity in acidic conditions, which contrasts with the Fenton-like reaction of Cu ions that are most active at circumneutral pH.[112,732–734] An investigation of the peroxidase-like activity of CuS nanorods by Guan *et al*. found that the nanorod activities were concentrated on the particle surface, with negligible activity resulting from leached Cu^{2+} ions.[112,735] The authors hypothesized that absorbed H_2O_2/HO_2^- reacts with surface-bound Cu^{2+} to generate $^{\bullet}OH$, which are stabilized *via* partial electron exchange interactions. The bound $^{\bullet}OH$ could then oxidize nearby molecules to induce cellular damage.[735] A further study using selective spin-trapping of $^{\bullet}OH$ produced by γ-Fe_2O_3 NPs showed that similar to CuS NPs, leached Fe ions from the NPs had insignificant peroxidase-like activity, leading to the conclusion that the active surface sites are at least 50-fold more effective at $^{\bullet}OH$ production than iron salts.[97] Similarly, Angelé-Martínez *et al*. reported that 50–60 nm CuO NP surfaces contribute significantly to the generation of ROS from H_2O_2 decomposition.[686] Another recent study provided evidence that many commercial copper, silver, and titania NPs have a reduced leaching in hypoxic environments, making the role of surface reactions potentially more important in tumors.[736]

Titanium dioxide (TiO_2) NPs have photocatalytic properties capable of producing ROS under UV; however, because of their large band-gap (3.2 eV) and stable +4 oxidation state of Ti, they are generally perceived as inert absent irradiation.[737–740] Though materials with large band gaps are unlikely to generate ROS photocatalytically, wide bandgap NPs (>3 eV) have been observed to possess some level of intrinsic catalytic activity resulting from their high surface areas and defect sites.[741–743] There is a growing body of

work suggesting that non-photocatalytic reactions occur on TiO_2 surfaces that may contribute to cancer radiosensitization or long-term toxicity in healthy tissue.[739,744–749] ROS have been implicated in TiO_2 cytotoxicity and the use of ROS scavengers, such as N-acetylcysteine, have limited TiO_2 cytotoxicity in vitro.[747,750–752] Gurr *et al*., for example, showed that 10 and 20 nm anatase TiO_2 NPs, absent UV-vis irradiation, induced oxidative DNA damage, lipid peroxidation, micronuclei formation, and H_2O_2 and nitric oxide production in BEAS-2B cells, a human bronchial epithelial cell line.[753] Treatment with ≥200 nm anatase NPs did not induce oxidative stress, suggesting that smaller NPs, with a higher effective surface area and rate of uptake, may be more likely to induce oxidative damage. In contrast to the generally accepted notion that anatase TiO_2 NPs are more photocatalytically active than rutile TiO_2, Gurr *et al*.'s results indicated that 200 nm rutile NPs, unlike the 200 nm anatase NPs, induced H_2O_2 production and oxidative DNA damage in the dark. A later electron spin resonance (ESR) investigation of 50 nm anatase and rutile TiO_2 NPs by Lipovsky *et al*. detected the formation of both $^{\bullet}OH$ and $^{\bullet}O_2^-$ without UV-Vis irradiation.[754] Fenoglio *et al*. observed no ESR signals from anatase or rutile NPs in water under ambient light; however, they did detect significant ROS signals resulting from the degradation of H_2O_2 and carboxylate radicals ($^{\bullet}CO_2^-$) from the cleavage of formate.[755] In the dark, <10 nm anatase and 20–80 nm anatase-rutile NPs (Degussa Aeroxide P25; ~80:20 anatase:rutile) became inactive toward H_2O_2 after 10 min and were reactivated by sunlight, whereas 35 nm rutile NPs showed comparable activity in the dark to that observed under illumination. For rutile NPs under ambient conditions, $^{\bullet}OH$ predominated over $^{\bullet}O_2^-$, whereas for anatase only $^{\bullet}O_2^-$ was detected. Using Degussa P25 NPs, $^{\bullet}O_2^-$ contributed to 79% of the ESR signal while 21% was attributed to $^{\bullet}OH$.[755] Additional ESR measurements by Sánchez *et al*. and Wiedmer *et al*. demonstrated that non-irradiated Degussa P25 NPs generated both $^{\bullet}OH$ and $^{\bullet}O_2^-$ from H_2O_2 and that the ratio between the NP effective surface area and the liquid volume controlled the prevalence of the radical species formed.[756,757] High values of this ratio promoted $^{\bullet}O_2^-$ production while lower values favored $^{\bullet}OH$. This effect was independent of particle size with both 21 nm Degussa P25 NPs and 100–180 μm Kronos anatase microparticles showing consistent alterations in ROS production with particle concentration.[756,758] Further in vivo studies have investigated the effects of non-irradiated TiO_2 and some have identified evidence of ROS production and oxidative stress.[759] Long-term exposure to ultrasmall TiO_2 NPs in mice (administered by nasal instillation) without photoirradiation was investigated by Li *et al*. and resulted in increased ROS production, lipid, protein, and DNA peroxidation, inflammatory cell response, and alterations in gene expression.[760]

While the toxicity and reactivity of gold salts are well documented, GNPs are often considered inert. However, GNPs supported on metal oxides are widely used as catalysts and many studies have demonstrated that colloidal GNPs undergo catalytic reactions and induce oxidative stress in cells without irradiation, showing that this assumption of inertness is not justified.[165,761–765] Pan *et al*., for instance,

showed that high concentrations of 1.4 nm triphenylphosphine monosulfonate-coated GNPs were cytotoxic to HeLa cells without irradiation through the induction of oxidative stress.[766] Elevated ROS levels were measured *via* a fluorescein derivative and flow cytometry. The GNP toxicity was inhibited by pre-treatment with thiol-containing antioxidants/reducing agents or replacing the capping agent with the more strongly binding glutathione. Overall, the GNP toxicity profiles closely resembled previously reported catalytic profiles related to gas-phase or organic-phase oxidation and halogen abstraction reactions, which led to the hypothesis that the activation of molecular oxygen to produce ROS was involved.[766–769] The authors also observed mitochondrial membrane depolarization, which can itself amplify ROS production through the leakage of $^{\bullet}O_2^-$ and H_2O_2. Elevated ROS, DNA damage, and mitochondrial membrane depolarization and oxidation were also observed by Taggart *et al*. using 1.9 nm Aurovist™ GNPs in MDA-MB-231, DU-145, and T98G cancer cells.[770] The authors further observed that irradiation of GNP-treated cells with 2 Gy of 225 kVp X-rays resulted in a temporary increase in membrane polarity, which returned to pre-irradiated GNP-treated levels within 4 h, while cardiolipin oxidation remained elevated but steady pre- and post-irradiation. A key step in intrinsic apoptotic pathway initiation is mitochondrial membrane oxidation that then releases cytochrome c into the cytosol.[771,772] These observations emphasize the significance of the cellular events occurring before irradiation and the role of the mitochondria as a key target for cancer therapies.[773]

Direct evidence for GNP reactivity has also been obtained by methods including ESR and the use of ROS-specific probes.[769] Zhang *et al.* showed that nitroxyl radicals could be quenched in a dose-dependent manner by absorption on the NP surface, a process facilitated by unpaired electron exchange interactions between the nitroxyl radicals and GNP surface electrons. They further observed that, in the presence of oxygen, adsorbed TEMPAMINE radicals were catalytically oxidized to the carbonyl derivative, TEMPONE. Additional ESR-based studies by Ionita *et al*. and Conte *et al*. observed that phosphine- and amine-coated GNPs could abstract hydrogen and halogen atoms from halogenated compounds.[767,768] GNP reactions with chloroform had an inverse kinetic isotope effect wherein a trichloromethyl spin adduct was observed when GNPs were mixed with $CDCl_3$ but not $CHCl_3$. GNP treatment with oxidizing or reducing reagents tuned the selectivity of radical formation from halogen to hydrogen (deuterium) abstraction. Jv *et al*. later found that positively charged GNPs catalyzed the oxidation of the peroxidase substrate 3,3',5,5'-tetramethylbenzidine (TMB) by H_2O_2 and subsequent studies have shown similar activities by other types of nanogold.[774,775] He *et al*., for example, found that 10–100 nm GNPs coated with polyvinylpyrrolidone (PVP) or tannic acid decomposed H_2O_2 into either $^{\bullet}OH$ or O_2 depending on the pH in the dark.[776] Lower pH (<4.6) produced $^{\bullet}OH$ while higher pH (>6.0) produced O_2. The GNPs catalyzed conversion of $^{\bullet}O_2^-$ to H_2O_2 through a SOD-like activity at physiological pH. Similar activities were observed for other noble metal NPs, most notably PtNPs.[85,704,777–779] Collectively, these results demonstrate that nanogold is not inert.

Importantly, significant but often overlooked factors, such as pH, temperature, and the ionic strength of the medium/tissue can affect ROS production and may contribute to the variability observed between different methods and cell lines.[741,780] The redox potentials for water, oxygen, H_2O_2, and other ROS change with pH according to the Nernst equation for the release of one proton, except for the reduction of O_2 into $^{\bullet}O_2^-$ (Figure 12B).[703,781] However, because the actual redox reactions occur at adsorbed sites on the NP surface, the redox properties will differ from these predictions depending on the degree of the stabilization and alterations to the crystal structure, such as oxygen deficiencies and surface hydroxyl groups. Li *et al*., for example, found that the switch from peroxidase to catalase activity observed for Au, Ag, Pd, or PtNPs were the result of pre-adsorbed $^{\bullet}OH$ groups, which are only favorably formed in basic conditions (Figure 12C).[704] While the extracellular environment of tumors are often acidic, the intracellular environment is often basic. Thus, a simply difference in location can alter the NP's surface properties and function.[782,783] In our own work, we have identified that chloride ions, which vary dramatically in concentration inside and outside cells, can accelerate the production of ROS by Cu-based NPs.[112,784]

Overall, most inorganic nanomedicines possess some inherent chemical reactivity, which can be enhanced or inhibited in different physiological conditions. These conditions are determined in prior Phases and can be described using feedback parameters, such as tissue and subcellular location. The resulting reactivities can produce effects that, in turn, affect outcomes at those higher biological levels. For example, ROS production from local H_2O_2 levels can trigger damage signals from the oxidation of organelles, eventually initiating inflammasome activation and a cytokine burst (Phase II; Figure 8). This triggers local inflammation via the immune system. If the conditions are consistent and widespread, chronic inflammation at the tissue can occur leading to fibrosis (Phase I, Figure 5). Therefore, even a simple treatment, *i.e.*, killing cancerous cells via ROS, requires a multidisciplinary understanding of nanomedicine behavior.

2.4.2 Radiology

High Z-number elements such as gold have long been identified as potential contrast agents and radiosensitizers because of their strong interactions with X- and γ-rays.[184–187] Medical X-rays are generated by accelerating electrons across a high voltage tube to collide with an anode composed of a high-Z, high melting point material, such as tungsten. The emitted spectrum of X-rays is a combination of bremsstrahlung/braking radiation (kinetic energy losses caused by electron deceleration) and characteristic X-rays resulting from post-ionization electron transitions in the anode.[55,56] In contrast, medical γ-rays are produced by the radioactive decay of radionuclides such as ^{131}Cs and ^{192}Ir and typically range in energy from 20 to 1060 kilovolts (kV).[57] The radiosensitization ability of high-Z elements was first observed in patients with reconstructive metallic implants undergoing RT for head and neck cancers, wherein significant increases in the effective radiation dose received by patients were observed at the tissue-metal

interface.[529,785,786] Pioneering work by Hainfeld *et al*., demonstrated that 1.9 nm GNPs injected intravenously in mice (2.7 g Au kg^{-1} body weight) enhanced the radiosensitivity of subcutaneous EMT-6 mammary carcinomas under 250 peak kV (kVp) irradiation.[186] The 1-year survival rate for mice treated with both GNPs and RT was 86% compared to 20% and 0% for X-rays and GNPs alone, respectively. The GNPs showed no observable toxicity to the mice and were cleared effectively through the kidneys. These results led to a massive surge in research related to the possible clinical use of GNPs and other high-Z metals.

High-Z elements were initially expected to produce useful effects only using kV photons, which are used for X-ray imaging and treating skin/surface tumors. This is because the photoelectric effect, which scales with atomic number, primarily occurs in this energy range, with random Compton scattering dominating at megavoltage (MV) energy levels.[172,184,690,787–790] Of particular interest for kV irradiation is the K-edge, which is the binding energy of an element's innermost 1s core electrons. For gold, this is 80.7 kV, which is close to the mean energy output of orthovoltage X-ray beams (**Figure 13**A). For lower energy X-ray beams (~70–80 kVp), iodine and barium are commonly used as contrast agents because of their lower K-edges of 33.2 and 37.4 kV, respectively; however, high-Z elements can also have good X-ray attenuation in this energy range due to trailing from their L-edges (2p orbital electrons; Figure 13A).[791] When an emitted photoelectron from an inner electron shell leaves behind a vacancy, it can be filled by an electron from a higher energy shell resulting in the release of excess energy. This energy is typically released as a characteristic X-ray; however, it can also be directly transferred to another electron, which is then ejected from the atom as a secondary Auger, Coster-Kronig, or Super-Coster-Kronig electron (Figure 13B).[792–794] This process can repeat, ultimately resulting in an Auger cascade that produces ~10–20 secondary electrons from a single X-ray.[795,796] Since electrons are far more reactive than X-rays, this process can effectively amplify the radiation dose received by the tumor and enables what is known as Auger therapy. Importantly, this amplification to a few nm around the NP.[797–799] Thus, cells without internalized NPs do not receive this amplified dose. In addition, because low-energy electrons produced in the NP core are more likely to react with nearby gold atoms rather than escaping into the environment, Auger therapy is primarily determined by the NP surface, even if the core contains substantially more high-Z atoms.[184,797] However, for imaging, the contrast effect depends only on X-ray absorption that is correlated to the total amount of high-Z atoms instead of just those on the NP surface.[800]

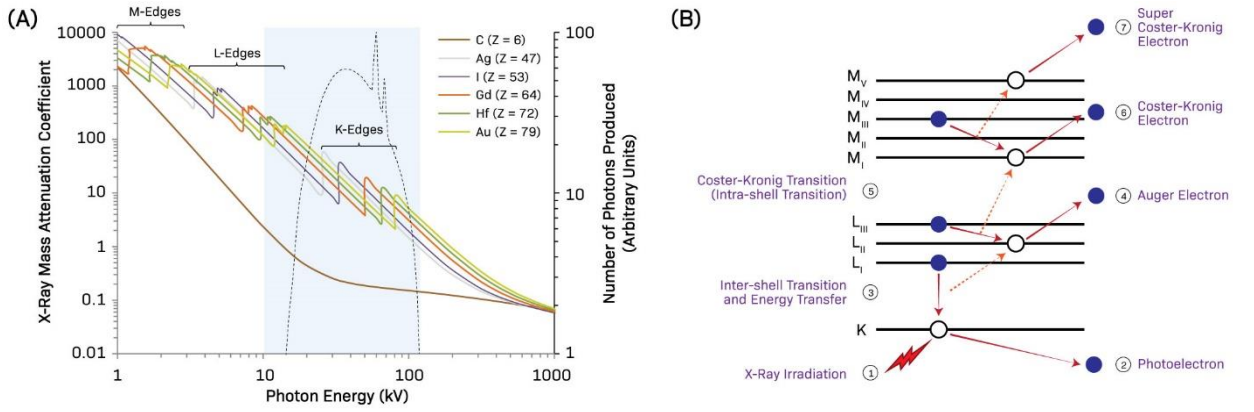

Figure 13: A) X-ray mass attenuation coefficients for several elements relevant to radiation therapy (with carbon acting as a representative element of biological tissue) over an energy range of 1–1000 kV.[791] The diagnostic range for clinically relevant X-ray tubes is highlighted in blue with an overlay of a representative 120 kVp photon spectra produced from a tungsten anode. B) A schematic visualization of the Auger effect. When an X-ray is absorbed by a K-shell electron in a metal such as gold (①), both an ejected photoelectron and an electron-hole are generated (②). This hole is then be filled by electrons from the metal's L or M shells (③), releasing excess energy that can be emitted as a photon or secondary Auger electron (④). If the electron vacancy is filled by an electron from a higher subshell (⑤), then the effect is known as a Coster-Kronig transition (⑥). If the emitted secondary electron also originates from the same shell, then this becomes a Super Coster-Kronig transition (⑦).

Despite the theoretical predictions of high-Z NPs, higher sensitizations than expected have been observed experimentally using both kV and MV energy sources.[690,801] This is valuable as MV photons are the most commonly used for cancer treatments due to their deep tissue penetration. One factor to consider in modeling the sensitization with high-Z elements is that an MV X-ray tube's output contains a significant portion of low energy kV photons due to bremsstrahlung radiation, which is further enhanced by scattering ("beam softening") as the X-rays travel through biological tissue.[802–804] In the air, the fraction of low energy (<150 keV) photons is only ~0.5% but this increases to 13% at a depth of 10 cm (or 20% using a flattening filter-free (FFF) beam).[184] Thus, the Auger effect may be more prominent than expected using MV beams. Additional modifications/variations of the treatment beam or filters can further change the percentage of low energy photons and the sensitization efficacy caused by NPs.[805,806] Further research has identified additional chemical and biological mechanisms, *e.g.*, enhanced ROS production and cell cycle arrest, that can enhance cancer cell radiosensitivity. Tumor oxygen levels, for example, are a critical factor in determining RT efficacy. Without sufficient oxygen, the amount of ROS generated and their ability to induce non-repairable damage are severely reduced.[683,807] Hypoxic tumors, therefore, show a greater rate of radioresistance, metastasis, and relapse than non-hypoxic tumors.[808,809] As a result, many conventional RT schemes are fractionated into smaller doses (<2 Gy fraction^{-1}) to provide sufficient time for reoxygenation

and the recovery of healthy tissue.[169] High-Z metals have shown great promise over a range of treatment energies; however, their efficacy at very high doses of clinically relevant radiation is unknown. The use of extremely high doses (stereotactic radiotherapy; >10 Gy fraction^{-1} of MV sources) is an emerging field owing to improved imaging and beam technology and has shown great success in the clinic for many tumors.[810–813] With many clinics moving towards stereotactic radiotherapies due to their high speed and efficacy, more efforts should be spent towards analyzing nanomedicine for these applications.[814–816] Another important aspect of enhanced RT responses include the bystander and abscopal effects, wherein the effects of localized irradiation can affect unirradiated cells or organs. These effects are believed to be mediated primarily by the immune system and cell-to-cell communication, in particular *via* released tumor antigens and cytokines.[817] Therefore, even cancer cells without internalized NPs could be influenced by NPs elsewhere.

Most recent pre-clinical work on radiosensitization has focused on GNPs due to their high K-edge, facile and controllable synthesis, and low toxicity.[818] Despite this, there has been very little translation of GNPs from proof-of-concept experiments to clinical trials (Table 2). There is a broad consensus that gold, along with other high-Z elements, can significantly enhance the radiosensitivity of cancerous tissue using both kV and MV radiation sources.[184,819–821] However, specific conclusions regarding NP efficacy, design, treatment location, long-term toxicity, *etc.*, are difficult to make because of the wide range of GNP formulations and treatment methods being employed. To date, there have been no clinical trials investigating GNP radiosensitizers; although GNPs have been employed in clinical trials for other purposes, including drug delivery and photothermal therapy.[822–825] Though many studies demonstrated the radiosensitizing effects of GNPs based on the principles of Auger therapy, far less studies have evaluated the role of ROS production and the specific species generated.[185,826] An early in vitro study documented that low concentrations (5 nM) of 14 nm thio-glucose-bound GNPs enhanced intracellular ROS production in SKOV-3 human ovarian cancer cells when irradiated with either 90 kVp or 6 MV X-rays.[827] Misawa and Takahashi later identified the ROS generated in aqueous suspensions of 5–250 nm citrate-capped GNPs following either X-ray (100 kVp) or UV irradiation.[689] Using the fluorescent probes 2-[6-(4-amino)phenoxy-3H-xanthen-3-on-9-yl]benzoic acid (APF) to detect $^{\bullet}OH$ and hydroethidine-dihydroethidium (DHE) to measure $^{\bullet}O_2^-$, it was observed that 20 nm GNPs enhanced the production of $^{\bullet}OH$ and $^{\bullet}O_2^-$ by factors of 1.46 and 7.68, respectively, under X-ray irradiation. Ethanol, an $^{\bullet}OH$ scavenger, significantly reduced X-ray + GNP induced APF fluorescence, but only marginally reduced DHE fluorescence, supporting both $^{\bullet}OH$ and $^{\bullet}O_2^-$ production by irradiated GNPs. The generation of $^{\bullet}O_2^-$ was NP size-dependent, while $^{\bullet}OH$ production was not. Using the $^{\bullet}OH$-mediated hydroxylation of coumarin-3-carboxylic acid (3-CCA) to 7-hydroxycoumarin-3-carboxylic acid (7-OH-CCA) as a probe, Cheng *et al.* observed that under 100 kVp irradiation, the reaction yield was enhanced ~2000 times over that predicted

based on a physical dose enhancement by the GNPs alone due to Auger electron production.[688] This enhancement depended on both the NP surface area and X-ray dose rate, reaching a 2-fold enhancement at 20 Gy min^{-1}. The ROS scavengers SOD ($^{\bullet}O_2^-$), $NaNO_3$ (e^{solv}), NaN_3 ($^1O_2$), and ascorbic acid were used to identify that $^{\bullet}O_2^-$ was the primary contributor to the overall enhancement of 3-CCA oxidation. The authors proposed a catalytic enhancement mechanism wherein electron transfer from radiolytically generated $^{\bullet}O_2^-$ to the GNPs enabled the intermediate 3-OH-CCA radical adduct to react on the surface to form 7-OH-CCA either sequentially or simultaneously. Similar results were observed for PtNPs.[688] Conversely, ESR measurements of aqueous 89 nm PEGylated GNP suspensions showed that the amount of ROS generated and measured directly *via* 5-tert-butoxycarbonyl-5-methyl-1-pyrroline-N-oxide (BMPO) were within the levels predicted by physical dose enhancement models, with no observable secondary catalytic reactions.[828] While Chang *et al*. only observed BMPO-OH adducts, they could not exclude the role of $^{\bullet}O_2^-$ and further experiments suggested that the ratio of generated $^{\bullet}OH$ to $^{\bullet}O_2^-$ was approximately equal.

In contrast to the popular GNPs, significant clinical progress has been made with Hensify®, HfO_2 NPs developed by Nanobiotix for RT.[106,829–831] Hensify®'s rational basis is the physical dose enhancement mechanisms outlined above.[832,833] Hafnium possesses a K-edge of 65.4 kV and L-edges between 9.5 and 11.3 kV.[791] In April of 2019, Hensify® received European market approval (CE Marking) for intratumoral administration and treatment of locally advanced soft tissue sarcoma (STS) following positive Phase II/III clinical trials. In the Phase II/III trial, a total of 180 adult patients with locally advanced STS of the extremities or trunk wall were randomly allocated to either a test group receiving a single intratumoral injection of Hensify® followed by RT, or a control group treated with RT alone.[106] In both groups, RT was followed by surgery. Follow-ups showed that the pathological complete response rate (<5% viable cancer cells) was 16.1% in the Hensify® group *vs* 7.9% in the control. In the patient subgroup with more advanced disease (histologic grade 2 and 3), the pathological complete response rate was 17.1% in the Hensify® group *vs* 3.9% in the control. Despite Hensify®'s clinical trial success, there are relatively few experimental or computational studies available on the mechanisms of HfO_2 radiosensitization. A recent study by Shiryaeva *et al*. of X-ray irradiated (45 kVp) 84 nm HfO_2 NPs in methanol identified that HfO_2 significantly increased the $^{\bullet}OH$ production rate.[834] Like TiO_2, HfO_2 NPs are believed to be chemically inert in biological media/tissue absent irradiation because of their large ~6 eV bandgap, stable +4 oxidation state, and a lack of clonogenic and in vivo toxicity.[697,832,834–837] However, Jayaraman *et al*. observed that high concentrations of <10 nm HfO_2 NPs (>1 mg mL^{-1}) were cytotoxic to 3T3 fibroblast cells, with larger NPs (~8.79 nm) showing higher toxicities than smaller NPs (~7.16 and 6.78 nm).[838] Comparatively, Kumar *et al*. observed that <10 nm HfO_2 NPs were minimally toxic in WS1 normal fibroblasts but toxic in MCF-7 breast cancer cells. The authors proposed ROS production as the toxicity mechanism, which was supported by increased caspase 3/7 activities.[839–841] Recently, Li *et al*. showed that ~65 nm HfO_2 nanoassemblies, designed for

intratumoral and intravenous injections, increased ROS production in 4T1 mammary carcinoma cells.[842] While further analysis is needed, these results suggest that, like GNPs, HfO_2 and other 'inert' NPs may not act solely through a physical enhancement mechanism and may induce cytotoxicity and radiosensitivity under specific conditions. Similar observations of ROS production have been made for ZrO_2, another insulating material that resembles HfO_2 in terms of physical and chemical properties.[779,843–845]

2.4.3 Phototherapies

As mentioned earlier, some inorganic NPs can utilize non-ionizing radiation and magnetic fields to produce anticancer effects and imaging contrast. Treatments derived from these effects are broadly classified into either photodynamic therapy (PDT; photocatalysis), magnetic hyperthermia, or photothermal therapy (PTT), which produce ROS or heat to damage cancerous cells.[58–61] Like intrinsic ROS production, photocatalytic reactions in PDT can overwhelm cellular redox homeostasis and induce varying degrees of oxidative stress. Owing to the spatiotemporal control of light delivery, ROS can be generated *via* PDT with precise control in NP-containing tumor cells while minimizing the adverse effects to healthy tissue.[846,847] PDT is further divided into Type-I and Type-II photocatalysis.[59,703,848] Type-I photocatalysis involves the generation of electron-hole pairs, *i.e.*, excitons, after absorbing photons that induce many redox reactions at the NP surface to produce ROS (Figure 12A).[849,850] Although electron-hole pairs generated by NPs are short-lived, they can still participate in many chemical reactions, particularly if the reactants absorb directly on the NP surface. Type-II photocatalysis, in contrast, involves the direct energy transfer from photo-responsive NPs to ground-state molecular triplet oxygen to form $^1O_2$.[847,851] Compared to triplet oxygen, $^1O_2$ is highly reactive and can readily oxidize biomolecules.[852,853] However, the O_2 dependence of Type-II photocatalysis reduces its effectiveness for hypoxic tumors or in combination with RT.[713,849] Heat generated during PTT and magnetic hyperthermia, in comparison, can also significantly damage and kill cells by altering lipid membrane fluidity and denaturing proteins and DNA. Additionally, several clinical trials have shown that the effectiveness of RT and some chemotherapeutics is significantly enhanced through local hyperthermia (elevated temperatures between 39–45 °C).[854–857] In the context of RT, hyperthermia is believed to sensitize tumors through a combination of macromolecule denaturation and improved blood flow to facilitate tumor oxygenation.[58,858] For chemotherapy, increased temperatures improve drug perfusion, drug release rates, and reaction kinetics.[468,859–861] Phototherapies have gathered significant interest over the past two decades and have great potential to change the current treatment paradigm in oncology.[58,61]

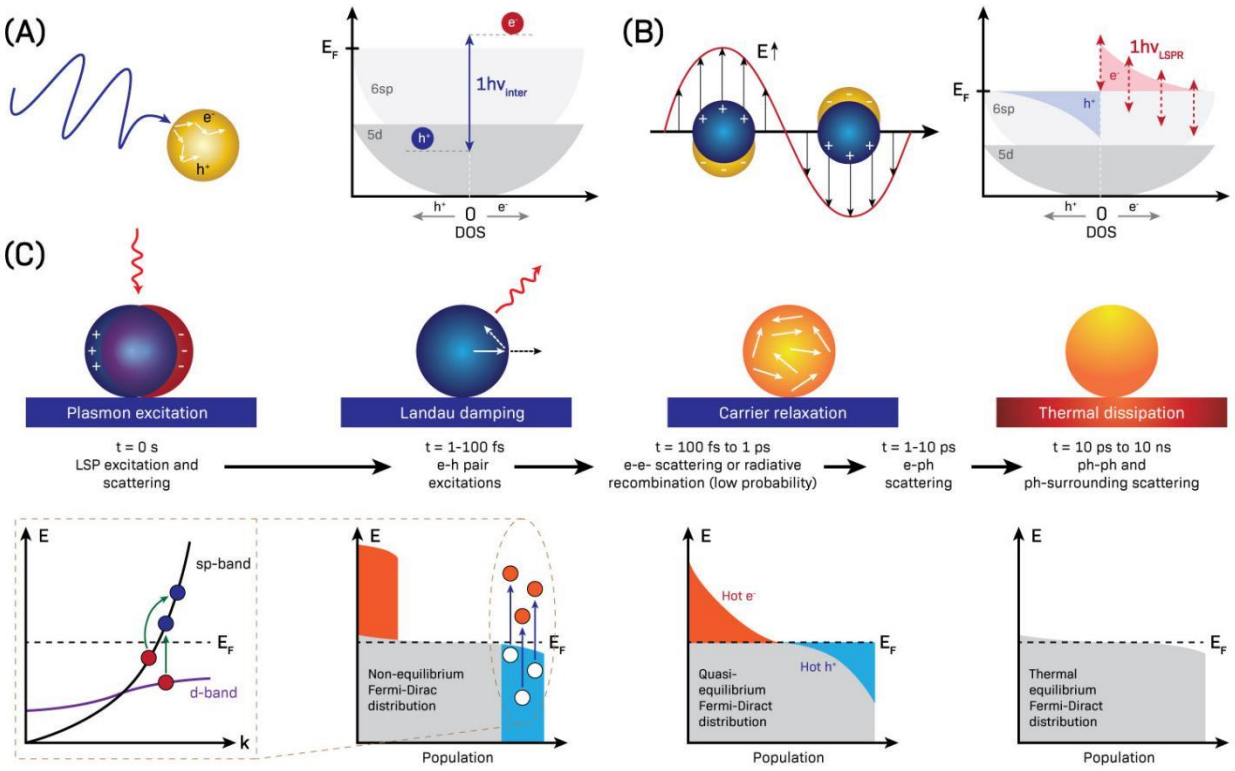

Figure 14: Photoexcitation of inorganic NPs. In semiconductor and plasmonic nanomaterials, photon absorption can occur via (A) inter- or (B) intraband excitations, which produce reactive electron-hole pairs. Adapted with permission from ref [862]. Copyright 2017 American Chemical Society. (C) More specifically, excitations are produced because of Landau damping adding kinetic energy to electrons from the excited plasmon, which then relax via scattering and recombination and generate heat. Adapted with permission from ref [863]. Copyright 2015 Springer Nature.

To generate ROS or heat from light, electrons must first gain energy from the incident photons and undergo either interband or intraband transitions (**Figure 14**A and B). These transitions generate electron-hole pairs, with the electrons gaining kinetic energy and becoming 'hot.' Hot electrons and holes can participate in redox reactions, which can be predicted based on the redox potentials of the NP's bands and the substrate molecule.[217] In insulating and semiconductor NPs, the valance band is typically completely filled and the conduction band empty, and thus only interband transitions are possible. These transitions require high energy UV or visible photons to excite electrons across the bandgap, as opposed to intraband transitions which utilize lower energy NIR photons.[864,865] In degenerate semiconductors and plasmonic materials, *e.g.*, CuS and Ag NPs, the valance and conduction bands are unfilled and possess a small or zero bandgap, allowing both interband and intraband transitions.[865] Though UV-Vis photons have higher energy than NIR photons, NIR irradiation has drastically improved tissue penetration and has less mutagenic effects on non-target tissue.[866,867] Therefore, NIR-responsive nanoformulations are more attractive for treating non-surface tumors. Means of providing alternative excitation and decay pathways for electron-

hole pairs is a widely explored field through the use of dopants and intentional defects that extend the valance or conduction band (forming p-doped or n-doped NPs).[868–870] These additional energy levels in the nanostructure allow lower energy photons to excite electrons, and the formation of unfilled conduction and valance bands. ZnO, ZrO_2, and TiO_2 NPs, for example, gain strong NIR absorbance through hydrogenation and the introduction of oxygen vacancies; turning the normally white colored NPs black, blue, or green and causing them to behave more like plasmonic nanomaterials.[157,871–873]

When plasmonic nanomaterials such as gold or copper NPs are exposed to light the conduction band electrons located on the particle's surface are excited and oscillate with the incident photon waves (Figure 14B).[874,875] This collective oscillation of conduction band electrons at the metal/dielectric interface is also known as a localized surface plasmon (LSP); a bosonic quasiparticle that corresponds to a quantum of plasma oscillation.[876] Because the LSP resonance (LSPR) originates from electron movement localized to the NPs, the LSPR is highly dependent on factors affecting electron density, such as size, shape, and the dielectric properties of the NPs and their surrounding medium. Excited plasmons can decay radiatively (scattering) or non-radiatively (absorption).[877,878] The former process is significant for surface-enhanced Raman spectroscopy (SERS) and fluorescence imaging because of the local enhancement of electric fields and the emission of photons, while the latter process is of interest for phototherapeutics.[877,879] Non-radiative decay of the plasmon initially proceeds through Landau damping (in simple terms, the transfer of energy from the incident electric field/photons to the electrons) to produce intraband electron-hole pairs in a non-thermal distribution (1–100 fs), which then quickly relax to a Fermi-Dirac electron distribution *via* electron-electron scattering (100 fs–1 ps, Figure 14C).[863,877,880] These hot electron-hole pairs can be used for photocatalysis; however they have a very short lifetime and rapidly lose their energy as heat. For nanomaterials, photocatalysis and heat generation are tightly linked, and for plasmonic materials, both can be expected to occur in some ratio. Some plasmonic NPs can directly be used for photocatalysis, however in most cases hot electrons are utilized by trapping them in a semiconductor to extend their lifetime.[881–883] At the interface of these two materials, such as in a composite NP, a potential energy barrier (a Schottky barrier) is formed between the different NP's conduction bands, allowing electrons to move into the semiconductor when excited and become trapped. For photocatalytic nanomedicine, understanding band-structure and plasmon decay is necessary to obtain good quantum efficiencies and target specific redox molecules.

Following the initial production and redistribution of electron-hole pairs (thermalization), the energy generated during photoexcitation is then transferred to the nanoparticle crystal lattice *via* electron-phonon scattering (1–10 ps) and finally to the local environment through phonon-phonon scattering to generate heat (10 ps–10 ns; Figure 14C).[879,884] This heat is the basis behind photothermal therapy and

photoacoustic imaging.[885–887] In addition to killing cancer cells, heat induces the thermo-elastic expansion of the local environment. If the irradiation is pulsed to produce rapid heating and cooling cycles, PTT can produce pressure waves that may be detected and converted into ultrasound images.[888] Because NIR light does not possess the mutagenicity of UV or X-/γ-rays and the effects are localized, PTT has attracted considerable interest as a standalone monotherapy and in combination with chemotherapy and RT.[889] The classical view of PTT is that hyperthermic temperatures induce radiosensitivity and apoptosis, whereas higher or more sustained temperatures trigger necrosis (thermal ablation).[890] More recently, a third pathway, necroptosis, was observed during PTT.[891] Necroptosis is a controlled form of necrotic cell death, and unlike apoptosis, has inflammatory and immunogenic properties that are useful for inducing immunogenic cell death.[892] As many tumors develop resistance to apoptosis to assist in their rapid growth the induction of alternative cell death routes has emerged as a treatment strategy.[893,894] A study by Zhang *et al*. showed that for folic-acid-functionalized GNRs, localized temperatures of ~43 °C induced approximately equal levels of apoptosis, necroptosis, and necrosis in B16-BL6 murine melanoma cells (10.2%, 18.3%, and 17.6% respectively).[891] When the local temperature induced by PTT reached a moderate temperature of ~46 °C necroptosis was significantly increased (35.1%) and at ~49 °C necrosis became the dominant mechanism (52.8%). So far only limited investigations have been performed to understand the cellular mechanisms of PTT after the induction of hyperthermia, although it is known that the biological environment, *i.e.*, the local extrinsic parameters, impacts the photothermal response.[892,895,896] Moros *et al*. recently examined GNP-based PTT in B16-F10 melanoma cells and the small freshwater polyp *H. vulgaris* in combination with selective inhibitors of the various death pathways.[895] At levels inducing the same degree of cell death (~50% inhibition), gold nanoprisms (GNPrs) led to rapid necrosis under almost all tested conditions while GNRs led to a simultaneous combination of apoptosis and necroptosis. When examined in vivo, although both types of GNPs provoked sublethal hyperthermia, only GNPrs induced cell death through regulated death pathways. Therefore, like with all other treatments, heat-based therapies require an integrated view of both the NP and the local physiology to model.

Currently, clinical trials are underway for PTT of prostate tumors using PEGylated gold@silica nanoshells (AuroLase®). Preliminary results published in 2019 for a pilot trial of patients with low or intermediate-grade focal prostate cancer showed that AuroLase® proved considerably effective for 94% (15/16) of patients without serious complications or loss of sexual health.[897] Follow-up biopsies of the treatment areas were negative for tumors in 62.5% (10/16) of lesions after 3 months, which increased to 87.5% (14/16) at 12 months. The study postulated the increase in apparent effectiveness could be due to undersampling; however, it has been postulated that time is required for resolution of the inflammatory response and this could be associated with an abscopal effect.[897] In addition to plasmonic PTT, localized hyperthermia can be used for controlled drug release by organic or hybrid organic-inorganic

nanomedicines. One such organic nanoformulation developed is ThermoDox®, a thermosensitive liposome formulation that has undergone Phase III testing for advanced hepatocellular carcinoma with radiofrequency ablation (RFA).[121] This treatment translated to an approximate survival benefit of 25.4 months (2.1 years) in patients given a combination of optimized RFA and ThermoDox® compared to RFA alone. When heated under RFA, the lipid membranes of ThermoDox® transition from the gel-phase to the liquid-crystalline phase, causing a triggered increase in DOX leakage rate to the tumor site.[898,899] The transition temperatures of phospholipids is a key parameter for drug release for both thermosensitive and conventional liposomes.[900] GNP-coated liposomes, similarly, work based on the photothermal effect of the GNP shell.[901]

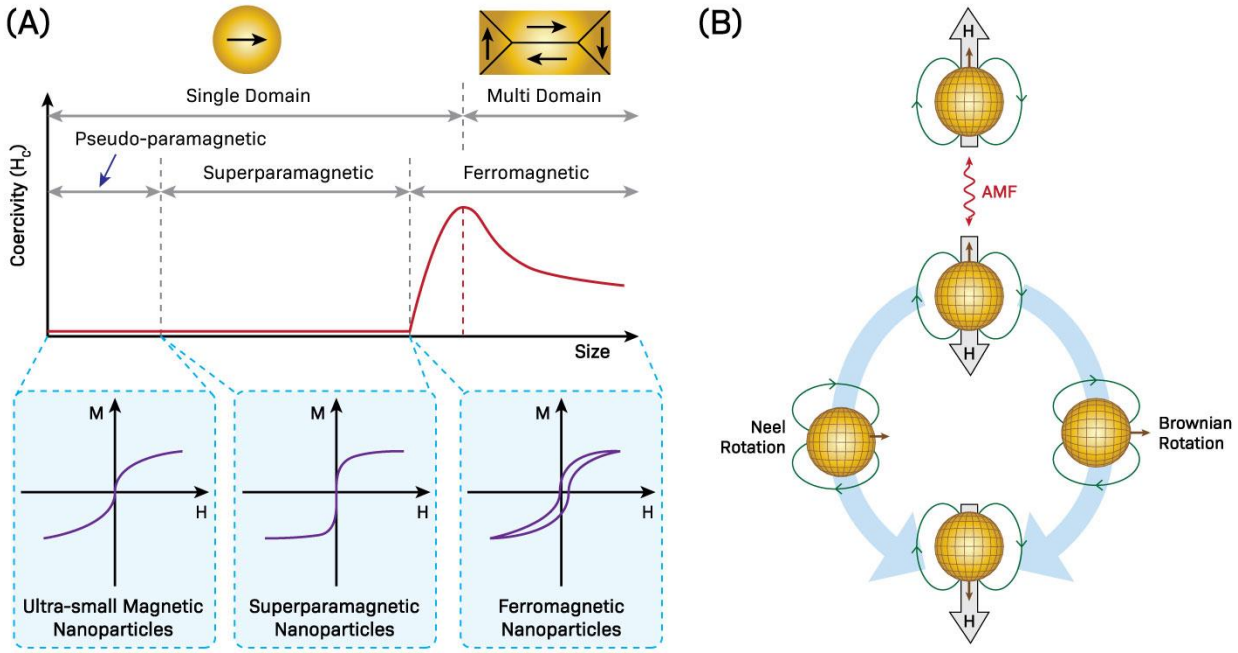

Figure 15: (A) Representation of typical hysteresis loops of ferromagnetic/ferrimagnetic and superparamagnetic nanomaterials and the dependence of coercivity on particle size. Adapted with permission under a Creative Commons CC BY License (https://creativecommons.org/licenses/by/4.0/) from ref [902]. Copyright 2020 The Authors. (B) Néel and Brownian relaxation mechanisms for superparamagnetic NPs.

Comparable to PTT, heat generation by magnetic hyperthermia has been examined for anticancer treatments using magnetic NPs, such as iron oxide, subjected to alternating magnetic fields (AMFs).[52,53] Because tissue is weakly diamagnetic, it does not attenuate or scatter static or low-frequency magnetic fields, enabling imaging and treatments using magnetic energy; however, AMFs at high frequencies (>10^6 Hz) induce non-specific heating *via* eddy currents, which limits the range of energies that are clinically feasible.[902,903] Within this limitation, the ability of magnetic NPs to induce therapeutic effects depends on their thermal conversion efficiency. The heating mechanism of single or multi-domain magnetic materials

in the presence of an AMF differs, but in both cases, it is related to a lag in magnetization (a hysteresis cycle; **Figure 15**A).[161] Magnetic materials possess magnetic moments or dipoles that depend on their physicochemical parameters, such as composition, size, shape, and volume.[161,904] In larger materials, multiple randomly-oriented magnetic moments are separated by boundaries called domain walls. When an external magnetic field is applied to such materials, the magnetic domains align and the domain walls disappear, causing the material to be magnetically saturated.[905] Ferromagnetic materials have some memory of the applied field called remanence, which then requires a coercive force to remove.[906] When a material possessing multiple domains is exposed to an AMF, a hysteresis loop occurs as a result of domain wall reorganization, the area of which roughly equals the amount of possible heat generated during one cycle of an AMF.[907] As the domain sizes decrease with NP size, domain wall maintenance becomes too energy-intensive, and a single functional domain forms. Further decreasing NP size causes the remanence and coercivity to drop below the local thermal energy and thus the NPs revert to a non-magnetic state when the external magnetic field is removed; these NPs are classified as superparamagnetic.[161] For such NPs, the heat generation mechanism mainly comes from the energy loss caused by overcoming the rotational energy barrier of the single magnetic moment (Néel relaxation) or the particle itself (Brownian relaxation; Figure 15B).[903] Additionally, because superparamagnetic NPs lack residual magnetism they are less likely to agglomerate than other magnetic NPs, enhancing their blood circulation and phagocyte evasion.[904] Among the various magnetic NPs, superparamagnetic iron oxide nanoparticles (SPIONs) have garnered the most research attention and clinical success.[902] SPIONs are composed of either γ-Fe_2O_3 (maghemite), Fe_3O_4 (magnetite), or α-Fe_2O_3 (hematite) particles with a core size ranging from 10–100 nm in diameter.[904] In 2010, Nanotherm® (~15 nm aminosilane-coated SPIONs; produced by MagForce) was approved by the EMA for the treatment of glioblastoma *via* local hyperthermia and has since received approval for clinical testing by the FDA for the treatment of prostate and pancreatic cancers.[161]

The combination of nanomedicines with ultrasound (US) is another promising approach for cancer therapy.[50,51] In its simplest use, US alone can be focused to deposit energy as heat for high-intensity focused US (HIFU) thermal ablation. In contrast to UV-Vis-NIR light for PTT, therapeutic US, *i.e.*, low frequency sound/pressure pulses (~1 MHz), can be easily delivered to tissues at depths exceeding 10 cm. This makes HIFU an excellent tool for treating deep-seated tumors using hyperthermia and thermosensitive NPs such as liposomes. Alternatively, US waves can be rapidly pulsed to kill cancerous cells *via* histotripsy, which is the mechanical damage produced by gas bubble oscillation/cavitation.[908] In combination with nanomedicines, this approach can be used for sonodynamic therapy (SDT). In response to acoustic waves with low intensities, delivered or catalytically generated gases may be fused into nano- and microbubbles that can expand and contract without breaking (stable cavitation). With increasing US intensity, nonlinear bubble oscillations arise, creating strong mechanical shear forces near the surface of the bubble that can

disrupt tissue. Eventually, these bubbles can be forced to grow and oscillate beyond the maximum resonant size, leading to implosion (inertial cavitation). This process results in a powerful shockwave containing transient (350 ps to <2 μs) hotspots with modeled temperatures of 2,000–25,000 K and pressures >800 atm.[908] In addition to damaging cells *via* pressure waves, this quick release of thermal energy can trigger sonochemical reactions generating ROS and other energetic free radicals (pyrolysis).[50,909] Importantly, during cavitation, brief bursts of light are also produced, *i.e.*, sonoluminescence, that can be utilized by photocatalytic NPs or photosensitizers to produce additional ROS.[50] As such, nanomedicines for SDT and PDT usually rely on the same fundamental principles and design considerations. Importantly however, it should be noted that the mechanisms behind sonoluminescence and SDT are still under investigation. Currently, hypothesis for sonoluminescence primarily include ion-electron recombination and bremsstrahlung radiation from heated ions.[51] The spectrum of emitted light tends to peak in the UV, but it is greatly affected by trace dissolved gases or other contaminants. For SDT, the contributions of the various cavitation effects are still unknown.[50] Therefore, further fundamental research is required to understand the interaction of NPs and gas bubbles with US.

2.5 NSAF Applications & Outlook

Anticancer nanomedicine has continued to grow over the decades with additional materials and treatment strategies published each year; however, only a limited number of nanoformulations have gained clinical success so far. Key to this issue is the lack of mechanistic understanding on how nanomedicine structure interacts with and impacts the human body. As a result, many nanoformulations ultimately underperform or produce unexpected side effects when translated from animal to human models. Meanwhile, it is challenging for researchers and regulators to identify potential risks and develop appropriate toxicological assays to evaluate nanomedicines. For effective clinical translation, the physicochemical properties of nanomedicines must be designed to balance treatment efficacy and toxicity. As both beneficial and adverse outcomes can stem from the same key parameters, *e.g.*, NP size, tumor permeability, or biocorona properties, slight changes of those parameters can result in dramatically different results. This complexity highlights the need for standardized experimental protocols, collaborative efforts from various fields, and large-scale knowledge base of nano-bio interactions to identify mechanisms of action. By systematically examining the key nano-bio interactions, the NSAF provides comprehensive maps of the underlying SARs of nanomedicines across different levels of biological complexity and various treatment strategies (Figure 5, Figure ***8***, and Figure ***11***). As it becomes increasingly challenging for researchers to sort out ever-growing research data, such knowledge maps can allow for more effective use of the literature and better engagement in collaborative efforts. By using a simple visual framework, the NSAF allows researchers to understand the intersection of various mechanisms, identify knowledge gaps, and

integrate their own work into the broader field, which is particularly beneficial to junior researchers and groups with limited resources. Although the NSAF is not an exhaustive description of every nanoformulation or therapy, the framework is applicable to most NPs of medical interest to illustrate their functions.

Similar to using AOPs in nanotoxicology, the NSAF can be used to identify events and predict outcomes (Figure 3). When an endpoint is observed during (pre-)clinical testing, the map function of the NSAF allows researchers to trace back the likely mechanisms and determine upstream events, including intrinsic initiating events and key biological events. Meanwhile, known or observed events can be used to predict outcomes. When the exact mechanisms are unclear, potential intermediate events can be examined to design assays for pathway identification or validation. Therefore, from a regulatory perspective, the NSAF can be used to identify endpoints and develop testing methods. For comparing different NPs, the maps for each NP can be used to differentiate common behaviors and specific events. Such knowledge may allow researchers to identify mechanisms initially overlooked and thereby uncover additional treatment modes for a given formulation. Furthermore, different maps and their Parameters Spaces can also be compared to elucidate critical parameters between formulations. Therefore, from a research perspective, the NSAF can be used to facilitate SAR identification and improve nanomedicine design. Importantly, the NSAF handles the complexity of nanomedicine by organizing information into interconnected layers covering different biological levels. Drug delivery, for example, can be studied from various perspectives: tumor accumulation and the evasion of non-target organs (Phase I), trans-/endocytosis and endosomal escape (Phase II), and drug release and tumor destruction mechanisms (Phases III). Each Phase alone can provide valuable information; however, only after all these perspectives are combined, can a treatment be properly designed to maximize efficacy and minimize toxicity. This requires each Phase to communicate with others *via* a feedback system, normally represented as loops within a self-contained pathway network. Within the NSAF (Figure 4), feedback mechanisms can also be represented as parameters and outcomes that do not visually overlap with events in the Activity Network, allowing them to be incorporated both within and between Phases.

In our view, one of the largest challenges for nanomedicine moving forward is the development of mathematical descriptions of SARs to enable quantitative *in-silico* modeling. While many papers have collectively examined NPs of different sizes, shapes, and other properties, these studies are often done using different assays, models, doses, and experimental conditions. Thus, it is difficult to accurately model how subtle differences between NP and patient properties impact treatment efficacy and toxicity, even when the effect is broadly understood. The characterization of both patient and NP parameters is widely recognized as necessary for nanomedicine development; however, it can be difficult to correlate such information,

often unmentioned or buried within text or tables, with observed outcomes. In addition, unlike conventional drug doses, which contain identical molecules, nanoformulations typically possess a certain degree of composition variability, such as the polydispersity of the constituent NPs, further complicating their mechanistic understanding.

One important advancement for studying SARs and predicting nanomedicine outcomes has been the adoption of machine learning (ML) platforms.[910,911] ML constitutes a subset of artificial intelligence (AI) that learns underlying trends from data to make informed decisions or predictions. Most often, ML platforms utilize classic algorithmic approaches, such as clustering and regression, to identify or make predictions from complex patterns. Using these tools, previously unknown SARs can be identified from large datasets, which can then be used to make clinical predictions without the traditional trial-and-error approach of animal testing. Importantly, ML algorithms for predicting outcomes must be trained using known datasets and outcomes from past experiments to infer a casual relationship between the input parameters and the output metrics.[912] Once trained, they must also be validated against real experimental and clinical data. However, a key challenge with AI and ML platforms is organizing a dataset that will not overfit. Overfitting occurs when a model is trained to only predict training samples, perhaps due to a bias in the data, and becomes unsuccessful when given unknown samples. Conversely, underfitting can occur if the dataset is too large and an overly simplistic parametric model is used. Currently, significant efforts have been made in establishing nanomaterial and nano-bio interaction databases *via* the use of big data mining algorithms and other methods.[913] As such, the quantity of data is usually less of an issue than the quality of the datasets chosen. Effectively curating comprehensive datasets to train any ML model remains a key challenge for AI platforms, largely due to a lack of standardization in the source literature.

Recently, the minimum information reporting in bio–nano experimental literature (MIRIBEL) was proposed for the standardization of nanomaterial characterization and the development of standard operating procedures (SOPs),[224] as standardisation is a key step in enabling comparisons of different NPs and the establishment of evaluation metrics. Under these standards, data to be published is divided into three groups: material characterisation, biological characterisation, and the details of experimental protocols. The first group describes the important parameters for the characterization of the NPs and the establishment of CQAs, such as size, zeta potential, aggregation behavior, and possible drug loading. The second group describes the basic characteristics of the selected biological model, such as general cell characteristics and proteins present in serum. The final group describes the details of the experiments performed, including cell culture dimensions, dosage, and measured cellular uptake. These categories correspond to the various components of the NSAF's Parameter Space; however, the MIRIBEL standards currently do not account for many nanomedicine applications such as RT.[94] Additionally, Florindo et al.

recently reviewed 100 articles in multidisciplinary journals from 2018 and found that only a small fraction satisfied all the proposed requirements.[914] In order to develop complex predictive tools using ML learning, significant effort is still needed to improve the scope and implementation of reporting standards in nanomedicine research. Like the NSAF, the MIRIBEL standards are a living document and they have been recently updated using the minimum information about nanomaterial biocorona experiments (MINBE).[915] Further work will likely update these checklists for specific applications such as immunotherapy or RT and include other important but missing parameters. However, since not all research groups have the resources to perform comprehensive characterizations, either due to equipment limitations or funding, reports containing incomplete datasets according to the MIRIBEL checklist should not be necessarily dismissed as this may slow down basic research efficiency[94]. Rather, emphasis should simply be placed on accurately characterizing as many properties as possible, with collective efforts and replication be used to overcome the weakness of data collected by any individual group.

For predictions of complex nanomedicine problems, such as their performance in the human body, ML models can be made using techniques such as random forest decision tress and deep learning artificial neural networks.[912,916] Tree-based algorithms are function around simple flowchart-type diagrams connecting possible outcomes to a series of decisions about the experimental conditions. Predictions are made by following a linear path along the diagram and making key decisions based on fundamental properties or thresholds, e.g., is the exposure concentration high enough to induce a specific effect? By comparison, neural networks rely on a more complicated combination of multiple nonlinear functions. A single nonlinear relationship is referred to as an artificial neuron, and multiple neurons can process the same input information to form a layer. Additional mathematical functions may then be applied to the output of the first layer, causing it to become the input of multiple other layers. Thus, each layer transforms the function, breaking the complex task down into smaller and simpler pieces. The network of neurons can also be flexibly rearranged and many different deep learning architectures can be developed, each suited to specific prediction tasks. Such predictive ML models can be incredibly powerful and have found success in predicting nanomedicine properties. For example, Lazarovits *et al.* used neural networks to predict the organ accumulation and blood half-life of PEGylated GNPs based on their size and biocorona composition.[291] When validating the model using two unknown GNPs, the organ accumulation and blood half-life were successfully predicted with an accuracy of 77–94%. Furthermore, Ban *et al.* utilized a random forest method to successfully predict biocorona composition based on various physicochemical parameters with an accuracy at least 75%.[917] Most recently, Boehnke *et al.*, combined ML and high-throughput screening to evaluate the influence of biological heterogeneity on NP delivery, an important consideration for the development of targeted and personalized nanomedicines. Using this approach, the authors were able to construct genomic and protein-protein interaction networks to identify several cellular biomarkers

for NP uptake and subcellular trafficking.[918] While further work is still needed to improve the training and validation of these models, these early results are key steps to improving nanomedicine development. Importantly however, nanomedicines interact with many biological systems, including the immune system, and thus must be evaluated using multiple tools and endpoints. By serving as a knowledge map of when, where, and how key decision nodes may occur, the NSAF framework can be used as an evolving template to guide the development and integration of these complex ML platforms.[916,919] Fundamentally, these collective ML algorithms and the NSAF describe the same predictive pathways from various input parameters to potential in vivo outcomes, one mathematically and one visually. As such, powerful ML toolboxes could be constructed by combining and updating the NSAF, MIRIBEL, and large nano-bio databases produced by data mining.

In summary, in addition to providing clarity on NP interactions, the broader concept behind the NSAF can directly assist nanomedicine development by providing an intuitive way to organize key parameters and SARs into a system that is compatible with computer algorithms. As medical research attempts to gradually move away from traditional animal testing, the need for computer-assisted solutions for both development and evaluation will increase. As such, the QSAR-inspired design of the NSAF should facilitate this transition. Similar to a computer algorithm, the NSAF describes how input information is transformed to an output. We envision that clinicians and researchers will eventually be able to input patient and NP parameters into an algorithm that can then provide a personalized nanoformulation design for the patient. While such a future is still a long way off, we are rapidly acquiring a much deeper understanding of the challenges and opportunities in anticancer nanomedicine. To facilitate this progress, we propose our knowledge framework, the NSAF, as a foundational tool for future research and regulation of nanomedicine. Through its usage, we hope to provide enhanced clarity and focus for researchers and regulators.

~ Chapter 3 ~

Degradable Multifunctional Gold-Liposomes as an All-in-One Theranostic Platform for Image-Guided Radiotherapy

The work presented in this chapter has been published as:

Youden, B., Wang, F., Zhang, X., Curry, D., Majtenyi, N., Shaaer, A., Bingham, K., Nguyen, Q., Bragg, L., Liu, J., Servos, M., Zhang, X., and Jiang, R. Degradable Multifunctional Gold-Liposomes as an All-in-One Theranostic Platform for Image-Guided Radiotherapy. *International Journal of Pharmaceutics*, **2022**, 629 (15), 122413. DOI: 10.1016/j.ijpharm.2022.122413.

Preliminary data for this work was also presented and published as a conference abstract (The American Association of Physicists in Medicine, 2018 Annual Meeting):

Youden, B., Jiang, R., Zhang, X. and Servos, M. Radio-Photothermal Therapy of Prostate Cancer Cells Using Gold-Lipid Nanoshells. In *Medical Physics*, **2018**, 45 (6), E342-E343. 111 River St., Hoboken 07030-5774, NJ USA: Wiley.

Chapter Summary

To improve tumor destruction and minimize adverse effects to healthy tissues, image-guided radiation therapy (IGRT) has been developed to allow for the accurate delivery of radiation energy to tumor sites facilitated by real-time imaging. Nevertheless, the current IGRT platform still suffers from the limitation of poor tissue contrast, resulting in the incidental irradiation of healthy tissue. Gold nanoparticles (GNPs) have been identified as promising candidates to simultaneously improve both radiotherapy and imaging, thereby improving both the accuracy and safety of IGRT. However, despite much preclinical study, little clinical progress has been made due to uncertainty over GNP toxicity. Herein, we demonstrate the great potential of using GNP-coated liposomes, *i.e.*, Lipogold, which combine the advantages of both large and small nanoparticles into one multifunctional formulation, as an ideal platform for IGRT. When irradiated with low doses (<2 Gy) of therapeutic X-rays, Lipogold induced a significant radiosensitization effect for PC-3 prostate cancer cells, which are moderately radiation-resistant. When imaged with computed tomography (CT), Lipogold was also found to possess consistent X-ray contrast of ~18–23 HU/mg across tube X-ray voltages (70–140 kVp), which could be boosted *via* the encapsulation of a small-molecule contrast agent containing iodine.

3.1 Background

Within the current landscape of oncology, radiation therapy (RT) is one of the major treatment options used today, with approximately 50% of all patients receiving RT in some form.[920,921] Although RT

is highly effective, it suffers from a lack of tissue selectivity, leading to numerous adverse effects in healthy tissues surrounding the tumor target. To improve tumor destruction and minimize adverse effects to healthy tissues, image-guided RT (IGRT) has been developed to allow for to adjustments of beam position based on tumor location and movement before or during treatment.[922] Three-dimensional X-ray imaging (computed tomography (CT)) of the patient prior to treatment is a common IGRT procedure; however, like stand-alone imaging procedures, it is limited by poor soft tissue contrast, making accurate identification of tumor boundaries extremely difficult. As such, a combination of other imaging techniques is usually needed to accurately define the tumor volume. While iodine-based small molecule contrast agents can be used to partially alleviate this issue, they are rapidly cleared from circulation and are known to be toxic to the kidneys, limiting their practicality for most treatments that rely upon the application of daily doses of radiation.[923–925] Nanomedicines, owing to their multifunctionality and extended biological half-life, offer a means to further enhance the efficacy and safety of IGRT.

Amongst nanomedicines studied for RT and X-ray imaging, those based on gold nanoparticles (GNPs) have gathered the most attention. GNPs offer the benefits of being easy to synthesize into different sizes and shapes, having relatively low toxicity, and being light-responsive in the visible-to-near infrared (NIR) range.[185,818,820,891] In addition to these benefits, there is a broad consensus that gold and other high-Z elements can simultaneously function as both contrast agents and radiosensitizers due to their greater absorbance/attenuation of X-ray energy compared to biological tissue. This absorption by the atom's innermost (1s or k-shell) electrons produces contrast *via* the photoelectric effect, and then releases additional energy into the local tissue through the Auger effect; a cascade of emitted secondary electrons resulting from electron recombination.[166,172,798,825,926] Through this 'Auger therapy,' lower doses of radiation can be applied to spare healthy tissue while maintaining treatment efficacy. Thus, GNPs are ideal candidates for use in IGRT and related combination therapies. However, despite the abundance of primary literature demonstrating the use of GNPs, there has been a noticeable lack of progress of GNPs into the clinic, particularly in the context of radiology.

One reason for this has been the lack of a consensus opinion on the optimal nanomedicine design and the influence of different physicochemical parameters.[215,927–929] Size alone, for example, can significantly alter nanomedicine performance and has been subject to much investigation.[929] Smaller GNPs typically possess the highest rates of cellular uptake and can penetrate into intracellular compartments such as the nucleus; however, they are limited by their rapid clearance through the kidneys similar to small molecules. Importantly, small GNPs possess a very high surface area-to-volume ratio, resulting in strong and fast surface reactions. In the context of radiation therapy, this high ratio maximizes Auger electron emission by reducing electron re-absorption by the GNP core.[930] Since Auger electrons can only travel a

short distance before reacting, only those produced near the NP surface can be emitted and cause cellular damage. Larger GNPs, by comparison with smaller ones, tend to have longer circulation times (based on the slower removal of the NPs by the liver, spleen, and immune system), which allows for greater blood circulation and tumor accumulation and retention.[343] For imaging, a greater circulation time allows for longer imaging windows, increasing the flexibility of patient preparation, while increased accumulation and retention reduces the need for repeated doses. Additionally, larger NPs can possess additional properties such as hollow, drug-loadable cores or localized surface plasmons that can extend into the infrared. Unlike ultraviolet (UV) or visible (Vis) light, near-infrared (NIR) light possesses good tissue penetration, allowing for deep-activated phototherapies.[931] As a plasmonic material, GNPs with infrared absorbance (typically nanorods and nanoshells) have been widely explored for photothermal therapy and controlled drug release, offering combination therapies and enhanced imaging modes to create multifunctional designs.[932,933] However, due to their larger size, concerns exist over their immune response and chronic toxicity to the liver, spleen, and heart due to a high in vivo retention.[343]

Previously, Romanowski and colleagues discovered that liposomes could be used for the formation of plasmonic gold nanoshells.[934–936] Similar to conventional nanoshell cores made of solid SiO_2, the presence of the liposome serves as both a stabilizing agent (together with the capping agent) and a scaffold for GNP formation.[937] This results in the GNPs forming a thin coating over the liposome surface and generating a localized surface plasmon resonance which can be utilized to generate heat under visible or infrared irradiation.[938,939] Importantly, liposomes, unlike solid NP cores, are hollow and highly sensitive to temperature, providing a means for the triggered release of encapsulated drugs such as oleanolic acid, doxorubicin (DOX), or photosensitizers that can be used for photodynamic therapy.[901,940–947] The light-induced degradation of the liposome scaffold also causes the GNP coating to disassemble into smaller NPs that can then be cleared by the kidneys.[948] Altogether these gold-lipid nanoshells, termed 'Lipogold,' offer the benefits of both large and small NPs in a single design without sacrificing its broad multifunctionality (**Figure 16**). However, all examinations of Lipogold thus far have been limited to photothermal-chemotherapy combinations, with the use of Lipogold for Auger radiation therapy being unexplored. Due to the high surface area of the GNPs making up the Lipogold coating, this formulation may prove particularly effective for use with RT. Additionally, as a liposome, the hollow core of Lipogold can also be loaded with X-ray responsive materials for an additive contrast effect and extended circulation. Thus, we hypothesize that Lipogold could function as a powerful agent for IGRT, optimally enhancing both RT and imaging through its unique structure.

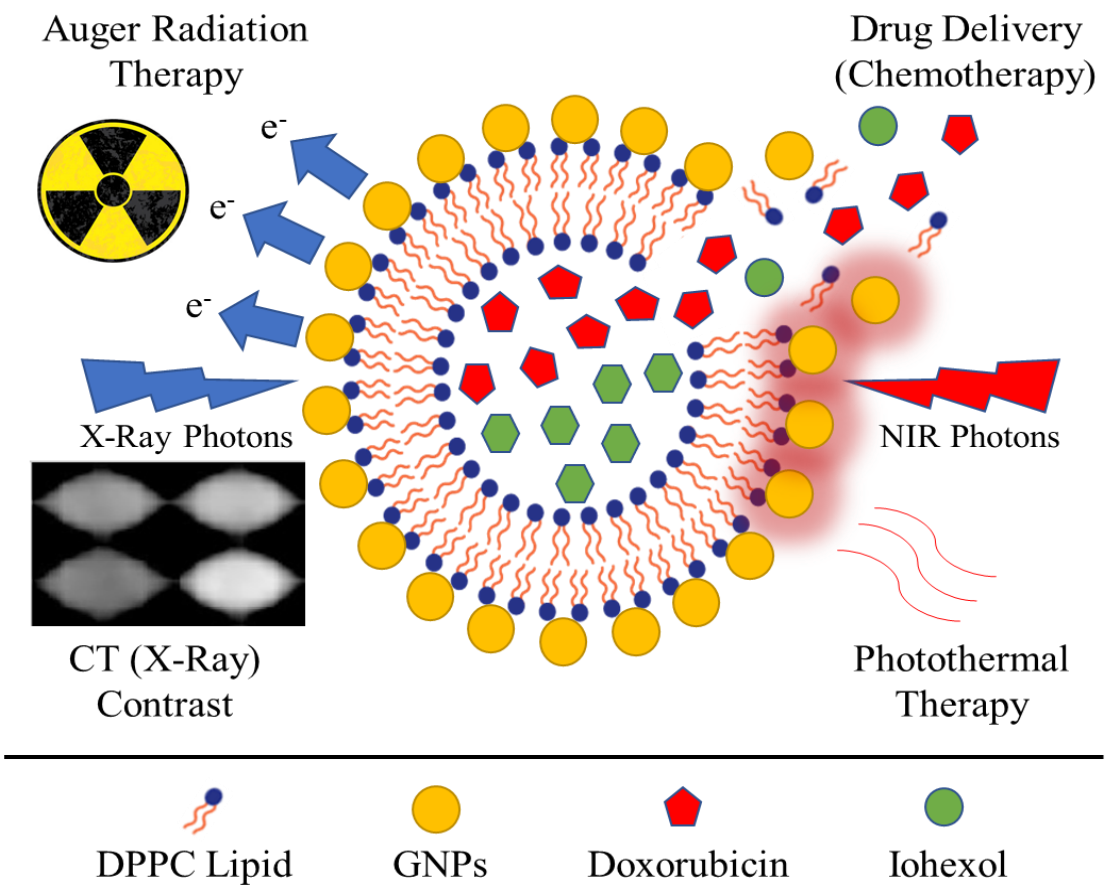

Figure 16: Gold nanoparticle-coated liposomes (i.e., Lipogold) as an all-in-one platform for cancer therapies.

Herein, we demonstrate the potential viability of Lipogold as an all-in-one platform for sensitized IGRT using modern clinical platforms. Radiosensitization of PC-3 cells was observed using clinically relevant megavoltage X-rays, with both biological (oxidative stress) and physical responses (Auger electron emission) suspected to play a role. In addition, we show that Lipogold can be used as an effective contrast agent for computed tomography (CT) imaging and could be enhanced *via* the encapsulation of iohexol, an FDA approved iodine-based small molecule contrast agent.

3.2 Methods

3.2.1 Materials

The prostate cancer cell lines PC-3 and DU-145 were purchased from American Type Culture Collection (ATCC) *via* Cedarlane, Burlington, ON, Canada. The Avanti Mini-Extruder, dipalmitoylphosphatidylcholine (DPPC; 25 mg/mL in chloroform), Sephadex G-50 powder, ascorbic acid, doxorubicin hydrochloride (DOX), thiazolyl blue tetrazolium bromide (MTT), iohexol, polyethylene glycol (PEG-20k), Triton X-100, tetrachloroauric acid and methanol were purchased from Sigma Aldrich,

Oakville, ON, Canada. Dulbecco's phosphate-buffered saline (DPBS), RPMI-1640 Cell Media, heat-inactivated fetal bovine serum (FBS), penicillin-streptomycin, TrypLE Express, trypsin-EDTA, trypan blue, citric acid, sodium carbonate, acetonitrile, and crystal violet were purchased from Fisher Scientific, Mississauga, ON, Canada.

3.2.2 Cell Culture

All cell lines were cultured in RPMI-1640 cell media supplemented with 10% fetal bovine serum (FBS) and 2% penicillin/streptomycin. They were subcultured when the cells reached 80-100% confluency, approximately 1-2 times per week. TrypLE Express or trypsin–EDTA enzymes were used for cell dissociation, with passage numbers 7-30 being used for experiments. Cells were counted on a glass hemocytometer and a splitting ratio of 1:10 was used.

3.2.3 Preparation of Liposomes

Uncoated DPPC Liposomes were prepared using the well-described thin-film hydration method followed by extrusion. Briefly, 100-200 µL of DPPC (dissolved in chloroform; 25 mg/mL) was manually rotary evaporated in a clear 4 mL glass vial using gentle stream of dry nitrogen or argon gas. The stream was applied until a visible and consistent white film formed on the bottom of the tubes. The thin film was then rehydrated in 70°C MilliQ water to form large, multilamellar liposomes (5 mg/mL) which were then converted to small, unilamellar liposomes *via* 11 passes through an Avanti Mini-Extruder equipped with a 0.1 µm polycarbonate membrane. The liposomes were allowed to cool to room temperature before further processing.

For iohexol-encapsulated liposomes, the rehydration solution was replaced with a 140 mg /mL solution of iohexol and was additionally subjected to 10 freeze-thaw cycles prior to extrusion. To prepare DOX-encapsulated liposomes, a previously described method employing a transmembrane pH gradient was used.[949] Briefly, citric acid (300 mM, pH 4) was used as the rehydration medium for the DPPC thin-film, and a pH gradient was established following extrusion by titrating sodium carbonate (17.4 mg/mL) until the external pH reached 7.4. Next, DOX (1 mM) and PEG-20k (100 ppm) were added to the liposomes mixture and incubated at 50ºC for 10 minutes. Finally, the liposomes were centrifuged at 12,000 RPM for 8 minutes and washed with MilliQ water up to 5 times to remove unencapsulated and leaked DOX.

3.2.4 Synthesis and Characterization of Lipogold

To coat the DPPC liposomes (with or without DOX) with gold nanoparticles (GNPs), different ratios of tetrachloroauric acid (Au) and ascorbic acid (AA) were used.[901] Briefly, to a 200 µL solution of DPPC (2 mg/mL), 100 µL of varied concentrations of Au were added and mixed, followed by the rapid

addition of 400 µL of ascorbic acid (5 mM). Upon mixing, the solutions rapidly changed from a pale yellow to different shades of red, blue, and green depending on the amount of gold reduced. The solutions were then centrifuged at 12,000 RPM for 8 minutes to remove the unused reactants and concentrate the samples for CT analysis. For stability analysis, samples were stored at 4ºC for 48 h in 0.1X or 0.5X PBS buffer. Dynamic light scattering (DLS) and ζ-potential measurements were performed using a Malvern Zetasizer Nano ZS90. UV-Vis and fluorescence measurements were collected with a Molecular Devices SpectraMax M5e microplate reader.

3.2.5 Drug Leakage and Release

The in vitro leakage profile for iohexol from Lipogold was assessed by a dialysis method.[950–952] In short, 200 µL of iohexol-encapsulated Lipogold (iohexol@Lipogold) was placed in a dialysis bag (MWCO 10,000 kDA) suspended in 40 mL of 0.1X PBS and incubated at 4°C or 37°C. At specific time points over the course of 7 days, 400 µL of the dialysate was removed for measurement, and 400 µL of fresh buffer was added to maintain constant volume. The diffusion of free iohexol (140 mg/mL) across the dialysis membrane was also examined. Measurements of released iohexol were conducted *via* HPLC using an Agilent 1260 LC with a diode array detector (DAD) at 254 nm.[953] An Agilent Zorbax Eclipse XDB-C18 column (4.6 x 150 mm; 5 µm particle size) was used with an isocratic mobile phase consisting of 10% acetonitrile in water. The flow rate was 0.4 mL/min throughout the total run time of 10 minutes. An injection volume of 35 µL was used and during separation the column temperature was held at 30°C. To achieve 100% release, Triton X-100 was added to the Lipogold (10% final volume) and incubated at 50°C for 10 minutes. Afterwards, the sample was centrifuged at 12,000 RPM and the supernatant was analyzed using HPLC-DAD.

For DOX-loaded Lipogold (DOX@Lipogold), passive drug leakage was analyzed using fluorescence spectroscopy (λ_{ex} = 486, λ_{em} = 592) over the course of 72 h. At each time point, DOX@Lipogold samples were centrifuged for 8 minutes at 12,000 RPM and the DOX in the supernatant was quantified. To examine the potential of NIR-induced drug release from the Lipogold, triplicate samples of DOX-encapsulated liposomes and DOX@Lipogold were exposed to an 808 nm diode laser (5 min, 1500 mW/cm^2) in a 96-well prior to centrifugation. To obtain 100% release, Triton X-100 was added as described above for iohexol@Lipogold.

3.2.6 Cellular Toxicity

To understand the toxicity of Lipogold and the effect of different treatment conditions, we performed 3 separate viability assays (Trypan Blue Exclusion (TBE), MTT, and Clonogenic) using PC-3 prostate cancer cells. For both the MTT and TBE assay, 10,000 cells/well were seeded in triplicate and

allowed to attach to the surface of a 96-well plate overnight. For clonogenic assays, cells were prepared as above when treated with radiation doses of up to 3 Gy or seeded at a higher density of 50,000 or 100,000 cells/well in a 24-well plate for treatments with 5 and 10 Gy, respectively. The next day, the media was replaced with supplemented RPMI medium containing serial dilutions of Lipogold. The cells were then incubated for an additional 24-48 h, after which they were washed 2-3 times with 1X DPBS to remove any remaining extracellular Lipogold. Following this, the cells were taken for treatment or toxicological analysis.

For the TBE assay, following incubation or photothermal therapy (PTT), the cells were trypsinized, diluted with RPMI medium, and then mixed with an equal volume of 0.4% trypan blue for 10 min. Following this, the cells were examined on a glass hemocytometer and the ratio of viable to dead cells was determined.

For MTT analysis, the washing of the cells was followed by the addition of RPMI medium containing 5 mg/mL MTT for 2 h. After incubation, the media was removed, and the formazan end-product was solubilized using 200 uL of DMSO and vigorous pipetting. The absorbance at 570 nm was then measured immediately after.

For clonogenic analysis, cells were trypsinized and reseeded in 6-well plates at a density of 200 cells/well. After 10 days of growth, the colonies were fixed with ice-cold methanol and stained with 0.5% crystal violet (in 20% methanol). The plating efficiency and surviving fraction were then determined relative to non-treated or sham-irradiated samples.

3.2.7 In Vitro Photothermal Therapy

The response of Lipogold to NIR was evaluated by the increase in solution temperature (photothermal transduction), liposome degradation, DOX drug release, and photothermal therapy (PTT). Initially, triplicate samples of Lipogold were prepared at a ratio of 2:1 AA:Au (0.25 mg/mL Au, 0.5 mg/mL DPPC), uncoated DPPC liposomes (0.5 mg/mL DPPC), and MilliQ water were exposed to an 808 nm diode laser (1500 mW/cm^2) in a 96-well plate. The peak temperature of the solutions was then recorded at 0, 1, 3, and 5 minutes using a digital thermometer. To analyze the degradation of the liposome over time, the UV-vis spectra was collected after 0-15 min of continuous irradiation, or 5 on/off cycles of 2 min of irradiation and cooling. Before scanning or between cycles, MilliQ water was added to the samples to account for evaporation. For PTT, laser exposure was performed after washing the cells with DPBS and reintroducing fresh RPMI medium. Cell viability was determined *via* a clonogenic assay.

3.2.8 CT Imaging

To evaluate the potential of Lipogold to function as a contrast agent for CT imaging, serial dilutions of Lipogold (synthesized using an AA:Au ratio of 2:1), iohexol-encapsulated Lipogold, or pure iohexol were prepared, well mixed, and then placed in a patient phantom composed of a 96-well plate surrounded by 4 cm thick bolus and sandwiched between 4 and 5 cm thick blocks of solid water, placed above and below respectively. Sample wells without contrast material were filled with an equivalent volume of MilliQ water. The final dimension of the phantom was 30 x 30 x 13 cm. This CT phantom was then loaded and positioned onto the gantry of a Siemens SOMATOM Definition AS 64-slice CT scanner for imaging. A 2D topogram was first performed to define the scan range for the whole phantom, followed by imaging at 70, 80, 100, 120, and 140 kVp using 1 mm slices. The collected images were then loaded into analysis software, wherein the mean attenuation was calculated using a minimum of 8 measurements focused across the center of the wells. Measurements at the edge of the well were excluded to minimize overlapping signals from the plastic and air between wells.

3.2.9 In Vitro Radiation/Auger Therapy

To apply radiation therapy (RT), 96- and 24-well plates containing PC-3 prostate cancer cells treated with or without Lipogold were sealed with parafilm and transported to the Grand River Regional Cancer Centre for irradiation. Plates were placed in a patient phantom as described above, and then irradiated with 0-10 Gy of 6 MV X-rays produced by a Varian TrueBeam at 600 MU/minute (1.03 MU/cGy). Irradiations were focused on a 10 x 10 cm field with a source to surface distance (SSD) of 94 cm. After treatment, cells were immediately returned to the laboratory, unsealed, trypsinized, and then reseeded in either 6-well (200-2500 cells/well for 0-5 Gy) or T25 cell culture flasks (50,000-100,000 cells/flask for 10 Gy). The treated cells were then incubated for 10 d, after which they were fixed, stained, and analyzed as described above. Independent replicates were collected on separate days.

3.2.10 Statistical Analysis

Statistical analysis of all data was performed in SigmaPlot 13.0 using one-way or two-way ANOVAs followed by Holm-Sidak post-hoc tests. P-values of less than 0.05 were considered significant.

3.3 Results

3.3.1 Synthesis and Characterization of Lipogold

To prepare Lipogold NPs, we adapted a robust method invented by Troutman *et al.*[934] Using extruded pure DPPC liposomes as a template, the GNP shell was created by sequentially adding different ratios of gold chloride precursor and ascorbic acid. By varying the ratio of gold to ascorbic acid, a variety

of blue-green colored nanoshells were produced, with more gold resulting in more intense and red-shifted plasmons (**Figure 17**A and B). For consistency, we selected Lipogold prepared at an AA:Au ratio of 2:1 for further experiments. The mean ζ-potential was found to be very close to neutral (-0.7 ± 1.1 mV). The intensity-weighed DLS results indicated that the average size of the uncoated DPPC liposomes was ~137 ± 40 nm, while the Lipogold NPs were ~422 ± 166 nm **Figure S2**A). However, a small number of aggregates can skew DLS measurements using intensity alone (scattering power increases with size to the 6th power), the number-weighted values were also compared, suggesting the bare liposomes were ~87 ± 23 nm, which increased slightly to 96 ± 20 nm following GNP coating (Figure S2B).[954] Thus, the majority of the liposomes were around 100 nm, regardless of gold deposition. The polydispersity index (PDI) of the Lipogold NPs was measured at 0.266 ± 0.056. Transmission electron microscopy (TEM) of the Lipogold suggested an average particle size of 134 ± 43 nm (Figure S17C). Following storage at 4 ºC, small changes in plasmon intensity were observed, suggesting Lipogold agglomeration (***Figure S1***).[941] Additionally, during storage, Lipogold was observed to settle at the bottom of the tubes and aggregate to form a semi-stable gel like substance. This gel could easily be redispersed with pipetting (Figure S2C). In contrast, repeated centrifugation (2+ times) could result in more significant agglomeration.

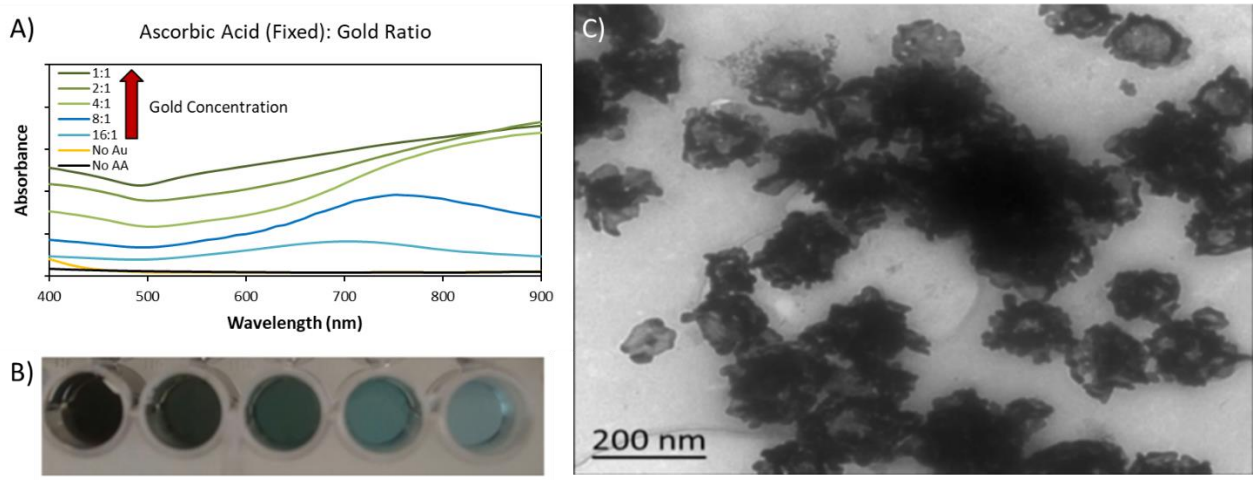

Figure 17: Characterization of Lipogold. A) UV-vis spectra of Lipogold prepared with different ratios of tetrachloroauric acid (Au) to a fixed concentration of ascorbic acid (AA). B) Visual depiction of the Lipogold samples (from left to right; 1:1, 2:1, 4:1, 8:1, and 16:1 AA:Au ratio) following synthesis. C) TEM images of Lipogold prepared at an AA:Au ratio of 2:1.

3.3.2 Acute and Chronic Cytotoxicity

Next, we evaluated the toxicity of the Lipogold using the MTT assay, a commonly used approach to measuring cytotoxicity *via* cellular metabolism (**Figure 18**A).[901] When incubated with Lipogold for 24 h, cytotoxicity was observed through a decreased rate of MTT reduction; however, interestingly, a longer

incubation period (48 h) showed no significant toxicity. Since the reduction of MTT can be confounded by NPs and stress,[955–958] we thus aimed to corroborate these results using the Trypan blue and clonogenic assays, which measure cell membrane integrity and reproductive capacity, respectively (Figure 18B). When examined under the microscope after incubation with Trypan blue, the total number and ratio of live-to-dead cells following incubation with Lipogold was found to be unchanged, suggesting that while the cells may possess acute metabolic responses to Lipogold, their membrane integrity is largely uncompromised. Light microscopy without staining also indicated that clusters of Lipogold NPs could be observed in the cells, with different cells showing various levels of Lipogold uptake (Figure 18C and D). Using the clonogenic assay, we found no significant inhibition to growth and replication for both PC-3 and DU-145 cells (Figure 18B and **Figure *S3***B). Together, these results suggest that Lipogold alone is largely non-toxic, although oxidative stress following uptake may occur and impact the radiation response.

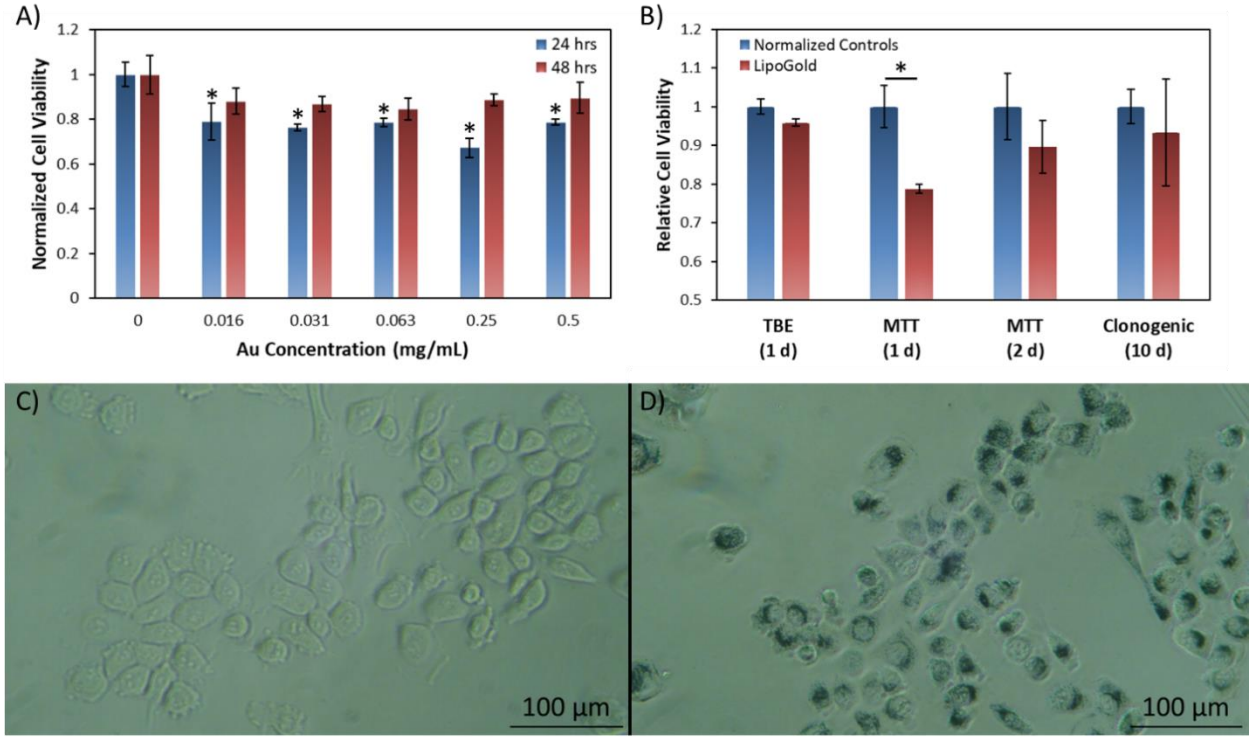

Figure 18: In vitro toxicity of Lipogold to PC-3 cells. A) MTT assay performed after 24 and 48 h of incubation. B) Comparison of toxicity markers (cell membrane integrity, metabolism, and reproductive capacity) using different assays. $n = 3$ with errors bars representing the standard deviation. $n \geq 3$ with errors bars representing the standard deviation. $*p < 0.05$. Visual appearance of PC-3 cells before (C) or after (D) incubation with 125 µg Au/mL Lipogold for 24 h.

3.3.3 NIR-Activated Photothermal Therapy and Drug Release

We evaluated the *in-vitro* photothermal performance of the Lipogold using the PC-3 cell model. Compared to water or bare DPPC liposomes, NIR irradiation of Lipogold had a significant effect, rapidly raising the solution temperature to hyperthermic levels capable of inducing cell death (**Figure 19**A). For Lipogold (0.5 mg/mL of DPPC and 0.25 mg/mL of Au), one minute of irradiation (1.5 W/cm^2) was sufficient to increase the temperature above the phase-transition temperature of pure DPPC (41.3°C), allowing for degradation of the nanostructure to form small GNPs (≤ 5 nm) (Figure 19B-C and **Figure *S4***), consistent with previous observations.[936,940,941,959] After 5 minutes of irradiation, photothermal therapy alone was sufficient to kill 62.2 ± 5.4% of the cells as determined *via* the clonogenic assay (Figure 19D). Similarly, 5 minutes of irradiation was sufficient to fully release encapsulated DOX from the Lipogold (Figure 19E), whereas non-irradiated DOX@Lipogold showed a slow-release profile over the course of 72 h at 37°C (**Figure S5**). When stored at 4°C, only minimal leakage was observed (~5-7%).

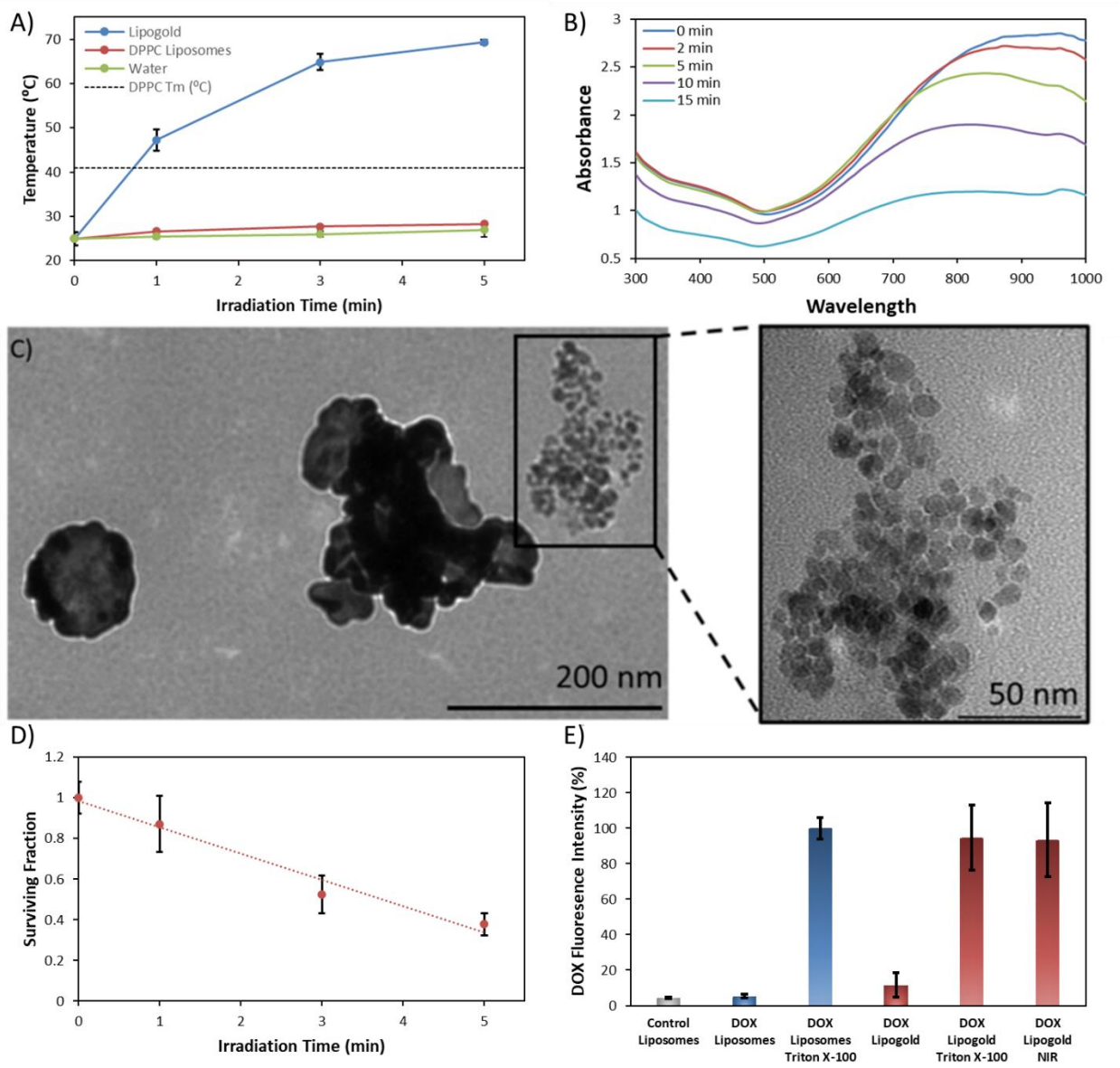

Figure 19: Photothermal performance of Lipogold. A) Temperature increase under NIR irradiation. B) Degradation of Lipogold as measured via the loss of the LSPR during continuous exposure to an 808 nm laser. C) TEM image of irradiated Lipogold, showing an intact nanoshell, a degraded/burst nanoshell, and the individual GNPs making up the nanoshell. The small GNPs are highlighted at a higher resolution. D) Clonogenic survival of PC-3 cells following PTT. E) Comparison of DOX release efficiency. n = 3 with errors bars representing the standard deviation.

3.3.4 CT Contrast Efficacy

Previously, it was demonstrated in proof-of-concept experiments that concentrated Lipogold could provide CT contrast; however, its performance has not yet been quantitatively evaluated.[901,960] Importantly, this quantification depends not only on the elemental composition of the contrast agent, but also the X-ray

energies produced by the scanner (**Figure 20**A).[961,962] When compared to iohexol, a widely used clinical contrast agent, gold (and Lipogold) at the same weight concentration (w/v% of Au or I) produced lower CT contrast than iodine at low tube voltages (e.g., 21 HU/mg of Au vs 51 HU/mg of I at 70 kVp), and comparable contrast with iodine at high tube voltages (e.g., 24 HU/mg of Au vs 26 HU/mg of I at 120 kVp) (Figure 20C and D). Notably, although lower tube voltages can provide a smaller radiation dose to the patient, generating less harm, they also produce significantly noisier images than those gathered at higher voltages (**Figure S6**A and B).

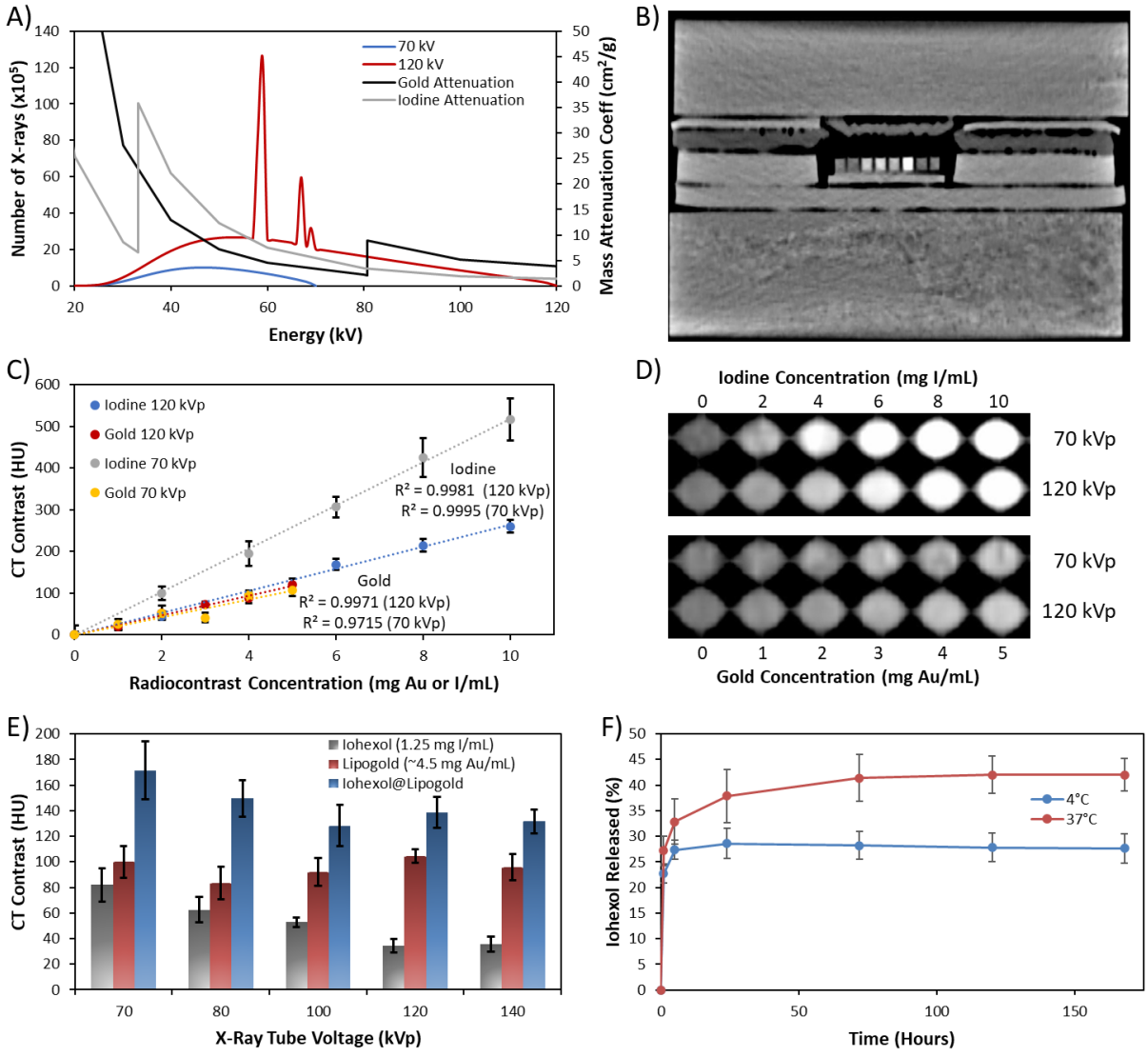

Figure 20: Performance of Lipogold as a platform for radiology. A) X-ray spectrum produced at 70 and 120 kVp with the mass attenuation coefficients of iodine (33.2 kV) and gold (80.7 kV) plotted separately for reference. B) Scan of the X-ray phantom showing the physical setup for irradiation, with chloroauric acid, iohexol@Lipogold, Lipogold, and iohexol in the center wells from left to right. The outer wells contain water. The image was taken at a tube voltage

of 120 kVp. C) Measured CT contrast of iodine (iohexol) and gold ($HAuCl_4$) at 70 and 120 kVp. D) Representative images of contrast provided by iodine and gold. E) CT contrast provided by Lipogold, and iohexol@Lipogold at 70-140 kVp. $n \geq 8$ slices. F) The in vitro release profile for iohexol from Lipogold at 4C and 37C. $n = 3$. Errors bars represent standard deviation.

Importantly, Lipogold can encapsulate many different small molecules to enhance its therapeutic and diagnostic efficacy. Therefore, to improve the X-ray contrast effect of Lipogold, which normally is dependent on the GNP coating alone, we prepared iohexol-encapsulated Lipogold (iohexol@Lipogold). By having both gold and iodine combined into a single formulation with extended circulation, iohexol-encapsulated Lipogold may provide better contrast and limit the toxicity risks associated with high concentrations of either element on its own. Interestingly, when GNP synthesis was conducted in the presence of high concentrations of free iohexol, the color of the Lipogold was found to blueshift and greatly increase in intensity (**Figure S9**). Based on the UV-NIR spectra, no characteristic signals from individual GNPs (characteristically between 500-600 nm) were observed except in the absence of the liposome template, suggesting the iohexol can alter, but not inhibit gold nanoshell formation. Calibration with iohexol and gold salts at 70 and 120 kVp respectively indicated that the coating efficiency of the Lipogold was approximately 89.6 ± 10.4% and the total lipid:GNP:drug molar ratio was ~1:1.69:0.17. During CT scanning, encapsulation was found to significantly improve the contrast effect of the Lipogold through an additive effect of gold and iodine (Figure 20E). Leakage analysis showed that the release kinetics of Lipogold exhibited a two-phase pattern, with a fast release of ~20-30% of the entrapped iohexol within the first 6 h prior to a slower leakage of the remaining amount (Figure 20). Similar release profiles have been previously observed for non-GNP coated liposomes loaded with iohexol and iodixanol.[950,951,963,964] After 1 week of storage at 37°C, ~58% of the iohexol remained within the Lipogold. Iohexol release was significantly lowered by storing Lipogold at 4°C, with ~72% remaining after 1 week.

3.3.5 X-Ray Radiosensitization / Auger Radiation Therapy

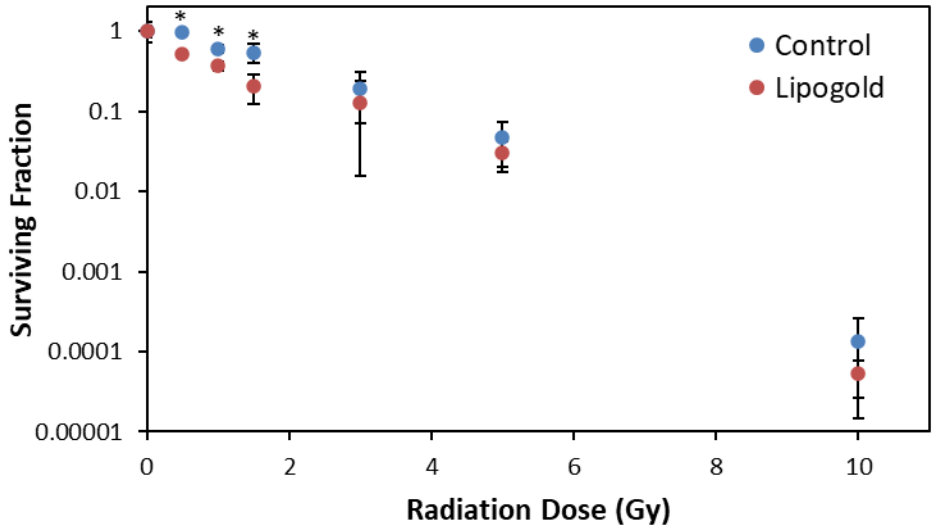

Figure 21: Dose survival curve under different doses of 6 MV X-ray irradiation. $n \geq 5$ with errors bars representing the standard deviation. *$p < 0.05$.

While the overall size of Lipogold is relatively large (100-200 nm), the individual GNPs forming the nanoshell are small (<5-10 nm; Figure 19C). As a result, when irradiated, more Auger electrons can be released to the environment rather than being re-adsorbed in the bulk NP core (**Table 4**).[930] Therefore, it was hypothesized that Lipogold may serve as an effective platform for tumor radiosensitization *via* Auger therapy. To confirm this, we employed a clinical linear accelerator (a Varian TrueBeam) to irradiate PC-3 cells treated with or without Lipogold and then evaluated their survival *via* clonogenic assays. Since many of the effects of radiation are delayed, MTT or other assays for acute cytotoxicity would be unsuitable for evaluating the efficacy of RT.[965,966] As seen in **Figure 21**, Lipogold was found to be a highly effective radiosensitizer under low doses of radiation, with the largest decrease in survival (~2.65 fold difference) observed at 1.5 Gy. Above 10 Gy of irradiation, no survival was observed for PC-3 with or without Lipogold using seeding densities of 100,000 cells per flask. It is important to note this limitation given the increasing use of stereotactic RT, wherein the behavior of both conventional and new radiosensitizers under high radiation doses are poorly understood.

Table 4: Comparison of different gold nanomaterials for X-ray-based imaging and radiotherapy.

Nanomaterial	Advantages	Disadvantages
Large Spherical GNP	-Longer circulation time -Large Au content per NP for imaging	-High organ retention -Large core reabsorbs many Auger electrons

	-Lower Toxicity	-Low cellular uptake
Small Spherical GNP	-High surface area-to-volume for Auger electron emission -Low organ retention -High cellular uptake	-Short circulation time -Low Au content per NP for imaging -Higher toxicity
Gold Nanoshell	-Longer circulation time -Plasmonic (NIR) -Moderate surface area-to-volume for Auger electron emission -Moderate Au content per NP for imaging	-High organ retention -Some Auger electrons absorbed by NP core -Non-biodegradable metal/silica core
Lipogold	-Longer circulation time -Plasmonic (NIR) -Moderate surface area-to-volume for Auger electron emission -Moderate Au content per NP for imaging -Degradable into small NPs -Can load secondary contrast agents or drugs in hollow core -Biodegradable liposome core	-Some Auger electrons absorbed by liposome

3.4 Discussion

Currently, one significant limitation of IGRT is a lack of viable contrast materials that can provide accurate delineation of the tumor's margins, with large gold-based implants being the current method of choice; however, these large physical markers come with side effects such as inflammation, swelling, and bleeding that can complicate treatment prognosis.[922] Small molecule contrast agents containing iodine, while common in regular X-ray and CT imaging, have limited use in IGRT due to their poor biological half-life, lack of tumor targeting, and potential renal toxicity.[967] An ideal CT contrast agent for IGRT should not only maximize the contrast provided for a tumor, but also sufficiently maintain that contrast throughout the course of the daily IGRT application, which usually takes several hours. As most RT schedules are fractionated, this period can be extended to several days or a month. As such, even if a tumor could be seen using iodine, extremely high concentrations of iodine would need to be injected over a long period of time, resulting in kidney toxicity.[968] To further advance the technology of IGRT, CT contrast agents that can overcome these deficiencies are needed. Furthermore, as contrast agents will nevertheless have some limit to their ability to accurately define the tumor volume, radiosensitizers that can simultaneously reduce the therapeutic radiation dosage required will further advance this treatment option. Herein, we demonstrate

the viability of Lipogold for IGRT by enhancing both 3D CT imaging and Auger RT using modern clinical tools.

Under therapeutic X-ray irradiation (6 MV from a Varian TrueBeam), Lipogold was found to have the strongest effects on cells exposed to lower doses (<2 Gy) of radiation. At higher doses, a greater variation in survival was observed and the effects of Lipogold were far less significant. Due to the low survival under higher levels of irradiation, a large number of cells is required to observe small effects. Additionally, as the uptake of Lipogold among different cells was uneven (Figure 18D), the radiosensitizing effect will also be unequal amongst the cells. While uptake could be improved using various targeting ligands, the difficultly of low survival remains for quantifying stereotactic doses. In our observations, irradiation with 10 Gy yielded <10 colonies when 50-100,000 cells were plated, and no colonies were observed above 10 Gy, regardless of the presence of Lipogold. Many cell lines exhibit variable or low plating efficiencies, and further scale-up of clonogenic assays can present several issues. In addition to the larger volumes and plating dishes required, we observed that many clustered dead cells, appearing enlarged but still with an intact structure, could remain attached to the plates/flasks and be stained at the end of the assay, thus being miscounted as living colonies. For PC-3 cells, the clusters of dead cells were clearly distinguishable from the smaller living colonies; however, this difference may not be as pronounced for other cell lines or at higher seeding densities. Due to the increasing popularity of stereotactic RT, further research is clearly needed to identify if radiosensitization can be consistently observed at very high doses. However, a lack of access to clinically relevant radiation facilities (such as the Varian TrueBeam utilized in our work) can prevent researchers from such screening assays. As such, radiosensitization research is often performed using orthovoltage units that produce only X-rays with kV energies. These units have the advantage of availability, imaging modes, and an output energy most likely to excite the k-edges of different elements; however, kV X-rays have poor tissue penetration and thus can only be used for treating tumors close to the surface. For most cancers, MV X-rays are used due to their deep tissue penetration and these beams contain only a small fraction of kV photons produced by scattering. As such, the influence of the Auger effect is much smaller during MV RT than during kV RT. Under MV irradiation, the chemical and biological effects of NP uptake (e.g., reactive oxygen species (ROS) dysregulation, metabolic changes, cell cycle arrest, etc.) likely play a much greater, but less understood role.

In addition to radiosensitization, Lipogold was also able to load a high concentration of gold and iodine for CT imaging and IGRT. As shown in Figure 20D, very low concentrations of iodine or gold do not provide notable contrast over the noise, and thus a minimum concentration of ~4 mg/mL of Au, 2-4 mg/mL of I, or a combination of both, is required to provide at least 100 HU at any given tube voltage. For iohexol, sold under the tradename Omnipaque, concentrations of 140-300 mg I/mL are typically used due

to its rapid dilution and excretion from the blood and into the urine. This high dose can present renal toxicity for at-risk patients, and thus by combining both elements into a single formulation with extended circulation, lower concentrations of each individual element are needed to generate the same level of contrast.[951,969] As such, Lipogold could limit the toxicity of traditional iodinated contrast agents, and the potential toxicity of high concentrations of gold.[970] Importantly, as noted in Figure 20F, iohexol leakage from the liposomes during dialysis was significant, even when stored at 4 ℃; however, since the blood half-life of iohexol is only 2 h, this retention in the Lipogold, even at 37 ℃, still marks an improvement over the free drug and allows for extended imaging windows.[963] Previous studies have reported different leakage rates of iohexol liposomes, with some showing very low levels of leakage.[964,971] These differences are likely due to differences in liposome composition, such as using mixtures of different lipids and the inclusion of cholesterol and PEG. Additionally, since dialysis produces a concentration gradient across the liposome membrane, the first phase of iohexol leakage may be mitigated by storing liposomes without removing the unencapsulated iohexol molecules. Interestingly, as iohexol does not appear to inhibit GNP formation on the liposome surface, it does not have to be removed prior to the nanoshell synthesis, thus minimizing the purification steps required for Lipogold. In our experiments, the presence of iohexol could even enhance the formation of the surface plasmon (Figure S9). Since Lipogold can also be prepared from a wide range of liposomes in a simple and easy one-step reaction (combine liposomes, gold, and ascorbic acid) following drug encapsulation, other liposomal formulations may also be used as templates to form Lipogold to boost their performance under radiation without significant changes to their preparation. Since iohexol@Lipogold samples were prepared in small amounts (25 mmol lipids/batch) and the loading method of iohexol is passive (unlike DOX) the encapsulation efficiency was relatively low (~2%); however, the drug-to-lipid ratio indicates the loading capacity of the Lipogold NPs was similar to liposomes prepared at higher lipid concentrations (200 mmol lipids/batch).[950] Herein, increasing or decreasing the iohexol concentration did not significantly change drug% encapsulation, and thus lipid concentration, *i.e.,* the volume available for drug entrapment, may act as the dominant factor. More recently, other preparation methods such as microfluidics have also emerged as an option to produce high-encapsulation efficiency liposomes without requiring excessive drug concentrations.[951]

The Lipogold formulation was found to be relatively non-toxic, consistent with previous works, although a stress mechanism was implied *via* the reduced metabolism of MTT at 24 h compared to 48 h (for comparison, the doubling time of PC-3 cells range from ~24-36 h).[901,940,942,945,947,948] Gold is known to be highly reactive to antioxidants containing sulfur moieties and can also catalyze the breakdown of molecules such as H_2O_2 into ROS when the surface is fully exposed.[972] As such, Lipogold can likely induce some level of sub-lethal oxidative stress during uptake, which may even contribute to its radiosensitization

effect. As such, care should be taken in following in vivo studies, although encouraging work by Rengan *et al.* and Luo *et al.* showed that PEGylated DPPC/cholesterol-based Lipogold was largely non-toxic in mice.[940,948] As each patient's tumor is unique, the need to develop customizable NPs to target different tumor phenotypes becomes apparent. In the case of Lipogold, customization can be made to the API encapsulated, the liposome composition, and the GNP shell functionalization. Importantly however, once NPs enter the body they rapidly absorb blood components onto their surface, affecting their uptake and immunogenicity.[973,974] The proteins that absorb and their effects can heavily depend on the NP's composition as well as the patient's individual proteome.[975] In addition, such parameters can also affect drug loading and leakage, NP agglomeration/aggregation, and plasma stability.[976,977] Thus, while Lipogold is a highly customizable platform, enabling it to adapt to different needs, each potential application of Lipogold must consider how the selected NP parameters will affect its performance.

3.5 Conclusions

In this work, our results indicate that Lipogold can be a powerful and highly customizable nanomedicine for IGRT in addition to phototherapy and chemotherapy. By combining gold and iodine for broad-spectrum CT imaging and maximizing Auger electron emission, Lipogold is an ideal platform for IGRT and its related combination strategies. While further work is needed to validate its efficacy in vivo, improve its tumor targeting, and identify the optimal formulations for encapsulating different small molecules, the application of Lipogold to clinic could significantly improve patient outcomes.

~ Chapter 4 ~

Synergistic Multimodal Cancer Therapy Using Glucose Oxidase@CuS Nanocomposites

The work presented in this chapter has been published as:

Singh, P.*, **Youden, B.***, Yang, Y., Chen, Y., Carrier, A., Cui, S., Oakes, K., Servos, M., Jiang, R. and Zhang, X. Synergistic multimodal cancer therapy using glucose oxidase@CuS nanocomposites. *ACS Applied Materials & Interfaces*, **2021**, 13 (35), pp.41464-41472. DOI: 10.1021/acsami.1c12235.

**These authors contributed equally to this work.*

Chapter Summary

Multimodal nanotherapeutic cancer treatments are widely studied but are often limited by their costly and complex syntheses that are not easily scaled up. Herein, a simple formulation of glucose-oxidase-coated CuS nanoparticles was demonstrated to be highly effective for melanoma treatment, acting through a synergistic combination of glucose starvation, photothermal therapy, and synergistic advanced chemodynamic therapy enabled by near-infrared irradiation coupled with Fenton-like reactions that were enhanced by endogenous chloride.

4.1. Introduction

Cancer is a family of complex and dynamic diseases that evolves as it progresses.[978,979] Therefore, effective monomodal treatment is challenging because of cellular heterogeneity, rapid metastasis, and the strong possibility of developing resistance to therapeutics. However, these challenges can be addressed through multimodal synergistic therapies that employ combinations of treatments.[61] Combination therapies are ideal as they can maximize treatment efficacy while minimizing adverse side effects. Among these treatments, glucose oxidase (Gox)-based catalytic nanomedicine is has emerged as an excellent technical platform for powerful multimodal cancer therapies.[980–983]

An important hallmark of most cancerous cells is an increase in glucose uptake.[11] Unlike normal cells, which often rely on mitochondrial oxidative phosphorylation to obtain energy, cancerous cells exhibit a preference towards aerobic glycolysis to drive their proliferation.[984] However, this process is much less efficient at generating ATP overall and thus requires higher levels of glucose to meet the same energy demands. Gox catalyzes glucose oxidation by molecular oxygen to form gluconic acid and hydrogen peroxide (H_2O_2) (Equation 1). Gox can therefore suppress tumor growth by depleting glucose, i.e., cancer starvation therapy.[985,986] This also lowers the local pH of tumor sites and generates H_2O_2, which not only is

toxic by itself to tumor cells but also serves as the precursor to generate even more toxic reactive oxygen, chlorine, and nitrogen species (ROS, RCS, and RNS), e.g., singlet oxygen ($^1O_2$),[987,988] hydroxyl radicals ($^{\bullet}OH$),[989] hypochlorous acid (HOCl),[990] and nitric oxide (NO)[991] through Fenton-like reactions. These reactive species can kill tumor cells more efficiently than H_2O_2. Therefore, as recently reviewed by Wang et al., combining Gox with a nano-catalyst to form a catalytic nanomedicine formulation that accelerates H_2O_2 decomposition for reactive species generation, may present an effective multimodal synergistic cancer treatment.[992]

$$Glucose + O_2 + H_2O \xrightarrow{Gox} Gluconic\ acid + H_2O_2 \quad (1)$$

Compared to conventional chemotherapeutics, catalytic nanomedicine may be better tolerated by patients because the constituting therapeutic agents (Gox and nano-catalyst) are not toxic until combined. Thereafter, powerful short-lived reactive species are generated in situ to attack tumor cells in the tumor microenvironment (TME), which minimizes systemic toxicity while remaining effective in the tumor sites. Thus far, catalysts used in combination with Gox are either encapsulated enzymes, e.g., chloroperoxidase, catalase,[993] peroxidase,[994] or catalytic nanoparticles (NPs), e.g., Fe_3O_4 NPs,[701,995] amorphous Fe NPs, single-atom Fe nanocatalysts,[996,997] porous hollow Prussian blue NPs,[998] Mn-doped $Ca_3(PO_4)_2$ NPs,[999] Ag NPs,[1000] Pt NPs,[1001] MnO_2 NPs,[1002] Fe_5C_2 NPs,[1003] etc. (more examples in **Table S2**). Although these catalysts are effective cancer therapeutics, they have technical and economic concerns, e.g., complex materials synthesis and high cost, which hinder their translation to large-scale clinical applications.

Copper sulfide nanoparticles (CuS NPs) are an emerging theranostic platform that have great translational potential because of their excellent photothermal properties,[1004] consistent near infrared (NIR) absorption from the d-d energy transition of Cu^{2+} ions that is independent of the NP size, shape, and surrounding environment, low toxicity, biodegradability, and scalable and cost-effective synthesis.[1005] CuS NPs are promising low-temperature photothermal and photodynamic therapeutics,[1006] excellent contrast agents for photoacoustic and magnetic resonance imaging,[1004,1007] and a promising radiotherapy sensitizer.[1008] Recently, our group discovered that chloride ions accelerate Cu-based Fenton chemistry (Cl-Cu Fenton),[1009] generating reactive species including hydroxyl and chlorine radicals, and singlet oxygen.[784,987,1010] This effect was observed for both Cu ions and CuO NPs, and the effect of chloride on ROS production has been further investigated in other systems with differing results.[1011–1013] We hypothesize chloride-accelerated Cu-Fenton may also apply to the catalytic activity of CuS NPs in the tumor sites, especially when Gox is introduced simultaneously to produce H_2O_2 in situ. In addition, because NIR irradiation can generate electron-hole pairs[1014] and the Cu-Fenton reaction rate increases with temperature,[1015] we believe the photothermal effect from NIR irradiation of CuS NPs will enhance the

radical generation, resulting in a more effective and efficient treatment (**Scheme 2**). In this work, we validated these hypotheses, resulting in a very simple, safe, and highly effective novel nano-formulation, i.e., Gox-coated CuS nanocomposites (Gox@CuS) that integrates cancer starvation therapy (ST), Cl-accelerated CuS-Fenton based chemodynamic therapy (CA-CDT), and dual photothermal-photodynamic therapy (PTT-PDT) into a simple nanoplatform.

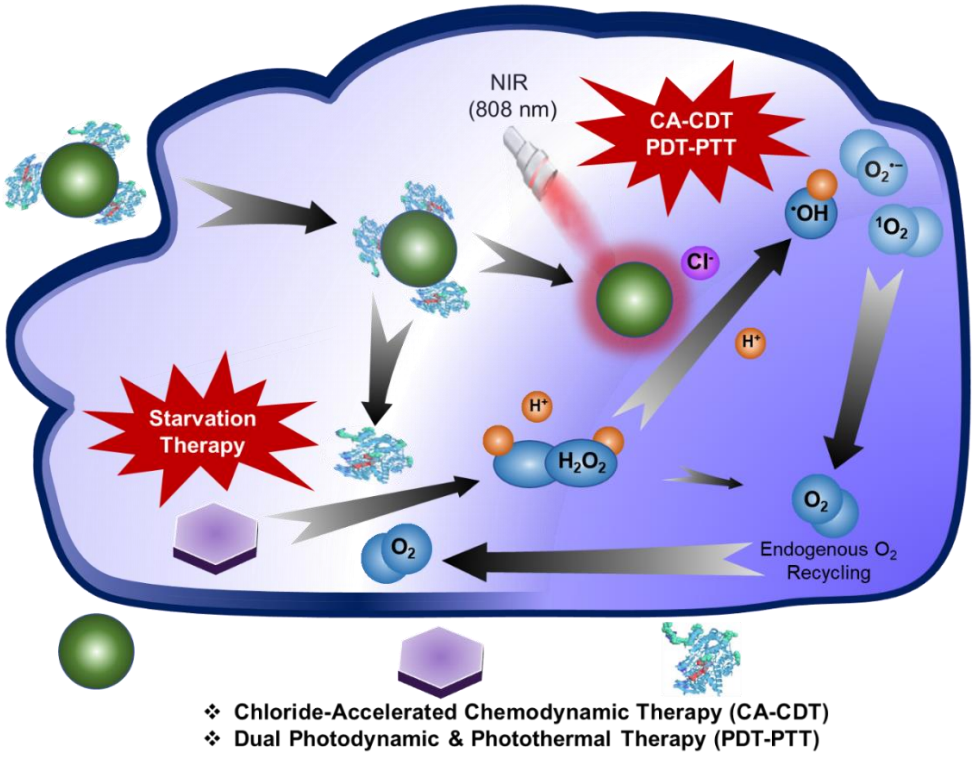

Scheme 2: The catalytic therapeutic mechanisms of Gox@CuS NPs for the generation of lethal reactive oxygen species (ROS) and glucose depletion for tumor therapy.

4.2 Materials and Methods

4.2.1 Materials

Copper chloride dihydrate ($CuCl_2 \cdot 2H_2O$) was purchased from Shanghai Medin Co., Ltd. (Shanghai, China). Sodium citrate and glucose oxidase (Gox, Lot No. L470S90) were purchased from J&K Chemical Co., Ltd. (Beijing, China). Sodium sulfide nonahydrate ($Na_2S \cdot 9H_2O$), 2,2′-azino-bis(3-ethylbenzothiazoline-6-sulfonate) (ABTS), fluorometric H_2O_2 assay kit (Sigma-Aldrich, catalog No. 187037), and HEPES buffer were purchased from Sigma Aldrich Co., Ltd. (Shanghai, China). Cell growing media (DMEM and RPMI-1640) were purchased from Thermo Fisher Scientific (Waltham, MA, USA). CCK-8 and (3-(4,5-Dimethylthiazol-2-yl)-2,5-Diphenyltetrazolium Bromide (MTT) were purchased from Beyotime Co., Ltd. (Jiangsu, China). Liver toxicity assay kits (ALT and AST assay kits) were obtained

from Elabscience Biotechnology Co. Ltd. (Wuhan, China). Fetal bovine serum (FBS) was obtained from Invitrogen Life Technologies (Carlsbad, CA, USA). Human breast cancer MD-MB-231 and melanoma cell line B16F10 were obtained from China Infrastructure of Cell Line Resource (Beijing, China). CellROX® green reagent was purchased from Life Technologies Inc. (Grand Island, NY, USA). Hoechst 33258 was obtained from ThermoScientific (Waltham, MA, USA).

4.2.2 Gox@CuS NPs fabrication

Citrate-capped CuS NPs were synthesized using a previously reported method with slight modification.[1016] Briefly, $CuCl_2 \cdot 2H_2O$ (10.77 mg) and trisodium citrate (10 mg) were dissolved in 30 mL of nanopure water (prepared by using MilliQ water purification system, Merck). After 15 min of stirring, 50 µL of aqueous $Na_2S \cdot 9H_2O$ (743.92 mg/mL) was rapidly added to the solution under vigorous stirring. The solution was transferred to a water bath (90°C) and stirred for an additional 30 min until the solution turned dark green, indicating the formation of CuS NPs. The synthesized NPs were purified from the crude mixture via overnight dialysis against nanopure water. The amount of synthesized CuS was determined by measuring the free Cu ions remaining in the crude mixture using the colorimetric method previously developed by our group.[1009] Briefly, to separate the free Cu ions from the highly dispersible NPs, an equal volume of ethanol containing 100 mM NaCl was added to the crude NP mixture and centrifuged at 10,000 RPM for 10 minutes. The clear supernatant was carefully removed, diluted, and then added to a series of $CuCl_2$ standards solutions (final concentration 0-200 nM) for analysis. Afterwards, 20 µL of each standard solution was added to a mixture containing the substrate 3,3',5,5'-tetramethylbenzidine (TMB, 750 mM), NaCl (100 mM), and MES Buffer (2 mM, pH 5.5). As a result of the TMB, DMSO composed 10% of the final reaction volume. To this, 50 µL of 3% H_2O_2 was then added to bring the final volume to 200 µL. Immediately after adding H_2O_2, the oxidation of TMB was monitored at 650 nm using a Tecan Infinite M1000 Pro microplate reader (Mannedorf, Switzerland) and the concentration of Cu in the sample was calculated (n = 3).

Gox (10 mg) was conjugated onto the CuS NPs by adding it to 30 mL of the prepared CuS NPs and shaking for 10 min. The conjugate material was then separated from the free NPs and enzymes by size-exclusion chromatography using Sephadex G-50 pre-equilibrated with MilliQ water, and 0.1X PBS (pH 7.4). After separation, the nanocomposite was freeze-dried and stored in a freezer (-20 °C) for future use. To determine the loading capacity of Gox on the CuS NPs, the Bradford assay was used to calculate the unconjugated protein remaining following conjugate synthesis and separation (n = 3).

4.2.3 Characterization of CuS NPs

4.2.3.1 Particle size and zeta potential measurement

The particle size and surface charge of the freshly synthesized CuS NPs and Gox@CuS NPs were measured using a Malvern Zetasizer, Nano series (Nano ZS90) in triplicate.

4.2.3.2 Optical characterization

The UV-Vis and IR spectra of CuS NPs and Gox@CuS NPs were measured using a UV-Vis-NIR spectrophotometer (Shimazdu, UV-3600 plus 220/230 VC) and FTIR spectrometer Thermo-scientific system Nicolet FT-IR spectrophotometer (FTIR) in the region of 4000 to 400 cm^{-1}, respectively. The data were processed using Origin Pro 8 software.

4.2.3.3 Gox@CuS NPs structure and composition

The morphological characterization of as-synthesized NPs was performed with transmission electron microscopy (TEM, JEM-1400 TEM, 40–120 kV). To check the composition of Gox@CuS NPs energy dispersive X-ray analysis (EDX) was also performed.

4.2.4 pH Effect of Gox@CuS NPs

To measure the ability of the Gox@CuS conjugates to reduce the pH of the local environment (n = 3), 500 µL of the Gox@CuS conjugates was added to 4.5 mL of 0.1X PBS (pH 7.44) containing various concentrations of glucose (0–5 mM). The solutions were incubated for 2 h at ambient temperature with gentle shaking and the pH was monitored using a pH meter.

4.2.5 CuS NPs in vitro photothermal activity

To determine the photothermal activity of the NPs, 200 µL of Gox, CuS NPs, or Gox@CuS NPs were added to a 96 well plate and irradiated with an 808 nm diode laser (1.5 W/cm^2) for up to 10 min. The temperature of the various solutions was measured using a digital thermometer. For thermal imaging, solutions of PBS, CuS NPs, and Gox@CuS NPs were taken into an microtube and subjected to NIR irradiation (980 nm, 5 W/cm^2) for 5 min. Then the temperature change of the NP solutions was recorded by a forward-looking IR Camera (class 2 laser product, FDA approved). The thermal images were further processed by Image J software.

For analysis of PC-3 cells (n = 3), 5000 cells were seeded per well in a 96-well plate and allowed to attach for 24 h before being introduced to CuS NPs (30 µg/mL). After a further 24 h, the cells were

exposed to an 808 nm diode laser (1 W/cm^2) for 5 min. The cells were then washed with PBS and allowed to grow for another 24 h, after which viability was assessed via the MTT assay with cells not exposed to CuS NPs serving as a comparison.

4.2.6 The Fenton-like catalytic activity of CuS NPs

To evaluate the catalytic properties of CuS NPs under various conditions, the kinetics of the oxidation of the chromogenic substrate molecule ABTS (2,2′-azino-bis(3-ethylbenzothiazoline-6-sulfonate)) was recorded with light absorbance at λ = 420 nm using a Tecan Infinite M1000 Pro microplate reader (Mannedorf, Switzerland) for the oxidized ABTS. The kinetics of this reaction were investigated at different pH values, H_2O_2 and glucose concentrations, in the presence or absence of NaCl, and with or without NIR irradiation.

Generally, all experiments (n = 3) were performed in 96-well microplates with final reaction volumes of 200 µL. The oxidation of 250 µM ABTS was monitored at 420 nm in the presence or absence of one or more of the following: CuS NPs or Gox@CuS NPs (10 µg/mL), NaCl (100 mM), and H_2O_2 (200 mM). The pH was adjusted between 3.6–5.6 using differently buffered 0.1 M acetate buffers. Reactions at pH 6-8 were conducted using 0.1X phosphate buffer. NIR excitation was achieved by exposing the sample wells to a diode laser (808 nm, 1.5 W/cm^2) continuously for 3 min. An appropriate amount of water was added following laser excitation to account for evaporation from the photothermal effect.

To study if the Fenton reactivity was from Gox@CuS nanocomposite or leached Cu^{2+}, the separated Gox@CuS nanocomposite was added into acetate buffer (10 mM, pH 4.0) containing 300 mM NaCl and incubated for 30 min at ambient temperature before centrifuging the solutions to precipitate the Gox@CuS NPs and collect the supernatant. The precipitated Gox@CuS NPs were redispersed in the same volume of acetate buffer. Afterwards the same volume of Gox@CuS NPs and supernatant were tested for their catalytic reactivity in the Fenton reaction with or without a 5 min NIR irradiation, where the final concentrations of ABTS, H_2O_2, and NaCl were 250 µM, 200 mM, and 300 mM, respectively.

A H_2O_2 assay was performed to determine the H_2O_2 production by Gox at different glucose concentrations. Briefly, 30 µL of different glucose concentrations and 20 µL of 10 µg/mL of Gox or an equivalent amount of Gox@CuS was added to 50 µL of H_2O_2 assay buffer (Sigma Aldrich, USA) and the fluorescence of the samples was measured at λ_{em} 590 nm (λ_{ex} 540 nm). The catalytic properties of the CuS NPs were also measured for different time periods. All the samples were measured in triplicate.

4.2.7 The cell-killing activity of CuS NPs

MDA-MB-231 and PC-3 cells were cultured in the complete RPMI-1640 medium, containing 2000 mg/L glucose, 10% FBS, 100 U/mL of penicillin and streptomycin. B16F10 cells were cultured in high glucose (4500 mg/L) DMEM supplemented with 10% FBS, 100 U/mL penicillin and streptomycin. The cells were incubated at 37 °C in a humidified 5% CO_2 atmosphere. The media was changed every 2 d during incubation. Cells for experiments were taken from an exponentially growing phase and harvested from plates with trypsin–EDTA. The cells were counted using a hemocytometer.

To check the in vitro cytotoxicity of Gox@CuS NPs (n = 3), B16F10 and MDA-MB-231 cells were seeded into 96 well plates (5000 cells/well) and incubated for 24 h in cell media for attachment. Subsequently, the media was replaced and supplemented with 10 µL of Gox@CuS NPs (0.25, 0.5, 1, 2.5, 5, 10, 25, and 50 nM) prepared in HEPES buffer. After 12 h of incubation, MTT reagent was added to each well and incubated for another 4 h. Afterwards, the cells were gently washed with PBS three times and replaced with 200 µL of DMSO to dissolve the formazan crystals whose absorbance was measured at 590 nm and 650 nm using a microplate reader (SpectraMax M5e, Molecular Devices, San Jose, CA, USA). Similarly, we analyzed the cytotoxicity at different glucose concentrations.

4.2.8 H_2O_2 production by Gox

The H_2O_2 concentration produced in cell medium by Gox was quantified with a fluorometric H_2O_2 assay kit. B16F10 cells were cultured in DMEM (containing 4.5 g/L of glucose) and seeded into 96 well plates (5000 cells/well; n = 3). After 24 h, Gox solutions of different concentrations were added to each well and incubated for a further 12 h. Then, 20 µL of the medium was added to another 96 well plate containing 30 µL of nanopure water. To quantify H_2O_2, 50 µL of the H_2O_2 detection reagent was added and incubated in the dark for 30 min. The fluorescence intensity of the samples was finally measured at 590 nm (λ_{ex} 540 nm) using a microplate reader. The concentration was quantified against H_2O_2 standard solutions.

4.2.9 Intracellular ROS levels

The detection of intracellular ROS analysis was performed with B16F10 cells. After the B16F10 cells were incubated with Gox, CuS with or without laser (30 s irradiation without increasing the medium temperature), and Gox@CuS with or without laser, they were treated with CellROX® Green Reagent according to the manufacturer's instructions. Then, the treated cells were fixed in 4% (w/v) paraformaldehyde for 10 min and stained with Hoechst 33258 staining solution (5 µg/mL). After rinsing with PBS, images were taken under a confocal laser scanning microscope (Nikon, Japan) with the excitation

channels at 405 and 488 nm for the quantitative determination of ROS levels. The fluorescence intensity was analyzed using ImageJ software.

4.2.10 In-vitro Uptake

Quantification of the amount of CuS NPs internalized by cells was performed using PC-3 cells. To detect the NPs, a variation of our method for detecting Cu^{2+} ions was used. Briefly, after incubating the CuS NPs for 24 h in RPMI-1640 media (10% FBS) with or without cells (5000 cells/well in triplicate), the media was carefully removed and analyzed for the oxidation of TMB at 652 nm. NPs incubated without cells were serially diluted to form a standard curve and the amount of CuS NPs not internalized or degraded by cells (i.e. remaining in the media) was calculated based on the relative rate of oxidation.

4.2.11 *In-vivo* evaluation of the synergistic cancer therapy

All of the animal studies were performed in the laboratory animal center, Cancer Hospital, Chinese Academy of Medical Sciences, Shenzhen Center. The experimental procedures were based on the guidelines on animal care and use of Principles of Laboratory Animal Care (NIH publication no. 86-23, revised 1985) and approved by the institutional animal care committee at Cancer Hospital, Chinese Academy of Medical Sciences, Shenzhen Center (No. NCC2019A006).

Male BALB/c-nu/nu mice (11–13 g, 21–28 days) were supplied by the Southern Medical School Laboratory Animal Center (No. 44002100020556). When their body weight reached 15–18 g, 0.1 mL of B16F10 cells (10^6 cells/mL) were injected into the back of each mice to establish the subcutaneous tumor xenografts. The tumors were allowed to grow to a size of 80–100 mm^3 before the start of the experiment. For therapeutic evaluation, all of the mice were randomly assigned into 7 groups (n=6): (1) Saline, (2) Saline with NIR irradiation, (3) Gox, (4) CuS NPs, (5) CuS-NPs with NIR laser irradiation, (6) Gox@CuS NPs, and (7) Gox@CuS NPs with NIR laser irradiation. The mice were injected with 100 µL saline solution from the tail vein.

The Gox@CuS NPs along with control (saline solution) were injected into the mice intravenously via the tail-vein. The body weight and tumor volumes were measured on alternate days to evaluate the therapeutic efficacy. The Gox (2.2 mg/kg body weight) and Gox@CuS NPs (200 nM, 100 µL, dosage: 2 µg/kg body weight) were injected on alternate days. After 1 h of drug administration, NIR laser irradiation was applied on the tumor site for 10 min at a setting of 5 W/cm^2. After 10 d, the mice were sacrificed, and the tumors were separated from the skin. Their blood was collected for liver toxicity and blood glucose level determination. The blood glucose level of the mice was measured with a glucometer before and after administration of the therapeutics.

4.2.12 Liver toxicity assay

The day after the last treatment, the blood of each group's mice was collected directly from the eyes 24 h post-injection. The blood samples were stored at 4 °C overnight and centrifuged at 3000 rpm for 20 min to separate the plasma. The plasma levels of AST and ALT in mice were assayed according to the protocols recommended by the manufacturer. The absorbance was measured with a plate reader at 510 nm.

4.2.13 Histological analysis

Histological analysis of different organs was performed using a microscope for which tissue samples of different organs were collected and fixed with paraformaldehyde (3%). The biopsies were embedded into paraffin blocks and then sliced into the sections (~4 μm). These sections were stained with H&E stains for histological examination. The stained sections were observed under a bright light field with a microscope (Leica DM6b, Germany) and the images were processed using Leica LAS X software.

4.2.14 Statistical analysis

Data were expressed as mean values with standard deviation. One-way ANOVA was used to compare two or multiple groups, and $p < 0.05$ was considered significant.

4.3 Results and Discussion

The synthesized CuS NPs were spherical with an average size of 8 ± 2 nm (**Figure S10** and **Figure *22***B) as measured by transmission electron microscopy (TEM) and dynamic light scattering (DLS). The citrate capping ligand yielded a negative surface charge (ξ = -28 mV, **Figure S11**), but displacement by Gox conjugation greatly reduced this (ξ = -2 mV). Gox conjugation also increased the hydrodynamic size up to 13 ± 3 nm (**Figure S12**) and was further supported by FTIR (**Figure S13**) and energy dispersive X-Ray (EDX) spectroscopy showing increased C, N, and O signals from the protein together with Cu and S (inset in Figure 22B and **Table S1**). As Cu^{2+} ions can be detected using a highly sensitive colorimetric assay based on the Cu-Cl Fenton reaction (**Figure S14**), the concentration of the CuS NPs was determined by measuring the free Cu^{2+} left over from the NP synthesis via the standard addition calibration method.[1009] Approximately 73% of the free Cu was consumed during particle synthesis, and the Bradford assay indicated a high loading capacity of the CuS NPs (0.61 g of Gox per g of CuS, **Figure S15**), likely owing to the formation of disulfide bonds between the comparably sized particle and enzyme. Importantly, Gox

adsorption did not significantly change the NIR absorption ($\lambda > 800$ nm) of the plasmonic CuS NPs (Figure 22A), which is responsible for their strong photothermal effect (**Figure S16**).

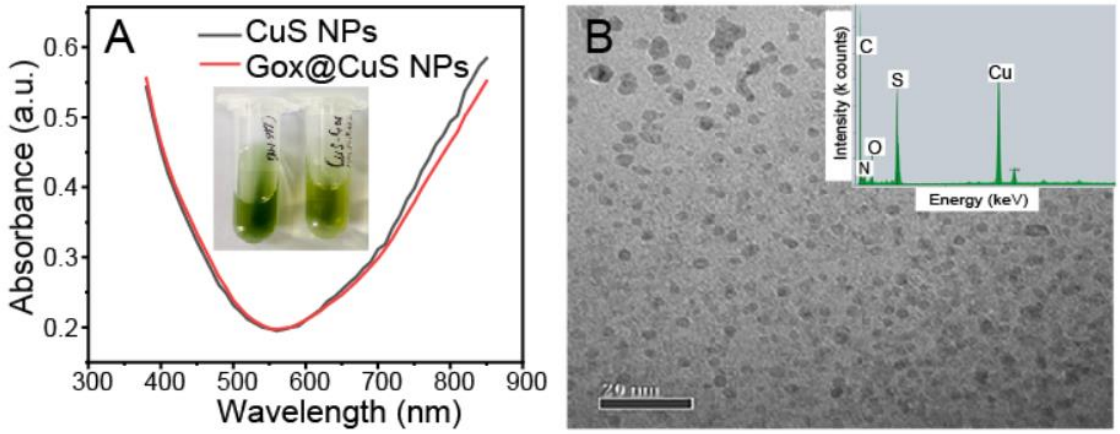

Figure 22: Characterization of CuS and Gox@CuS nanoparticles (NPs). (A) UV-Vis spectra of CuS and Gox@CuS NPs. Inset: a photograph of the NP solutions. (B) Transmission electron micrograph of Gox@CuS NPs showing ultrasmall particle size (scale bar = 20 nm). Inset: Energy dispersive X-ray spectrum of the Gox@CuS NPs.

The Fenton activity of the CuS and Gox@CuS NPs was examined by monitoring the oxidation of the chromogenic substrate 2,2-azino-bis(3-ethylbenzothiazoline-6-sulfonate) (ABTS, $\lambda = 420$ nm) by ROS in the presence or absence of H_2O_2 and Cl^- (**Figure 23**A and **Figure *S17***). As previously observed by Liu et al.,[1017] ROS produced on the surface of CuS show negligible activity towards the negatively charged ABTS compared to other substrates; however, the presence of Cl^- in this study demonstrates the accelerated oxidation of this probe by ROS under mildly acidic conditions provided by the glucose oxidation reaction catalyzed by Gox as described in Equation 1 (**Figure S18**). Importantly, we observed that this catalytic activity was primarily from the reactions facilitated by the NP surface and not from the acid-led degradation of H_2O_2, surface adsorption of ABTS, or leached Cu^{2+} (**Figure S19**).[735] The Cl-accelerated Fenton reaction could be further enhanced via NIR irradiation, owing to the combination of local heating and electron-hole pairs generated by the excitation of the CuS plasmon (Figure 23B). Though conjugation with Gox did inhibit the Fenton reaction significantly by blocking reactive sites on the NP surface, NIR irradiation was able to restore this activity (Figure 23B).

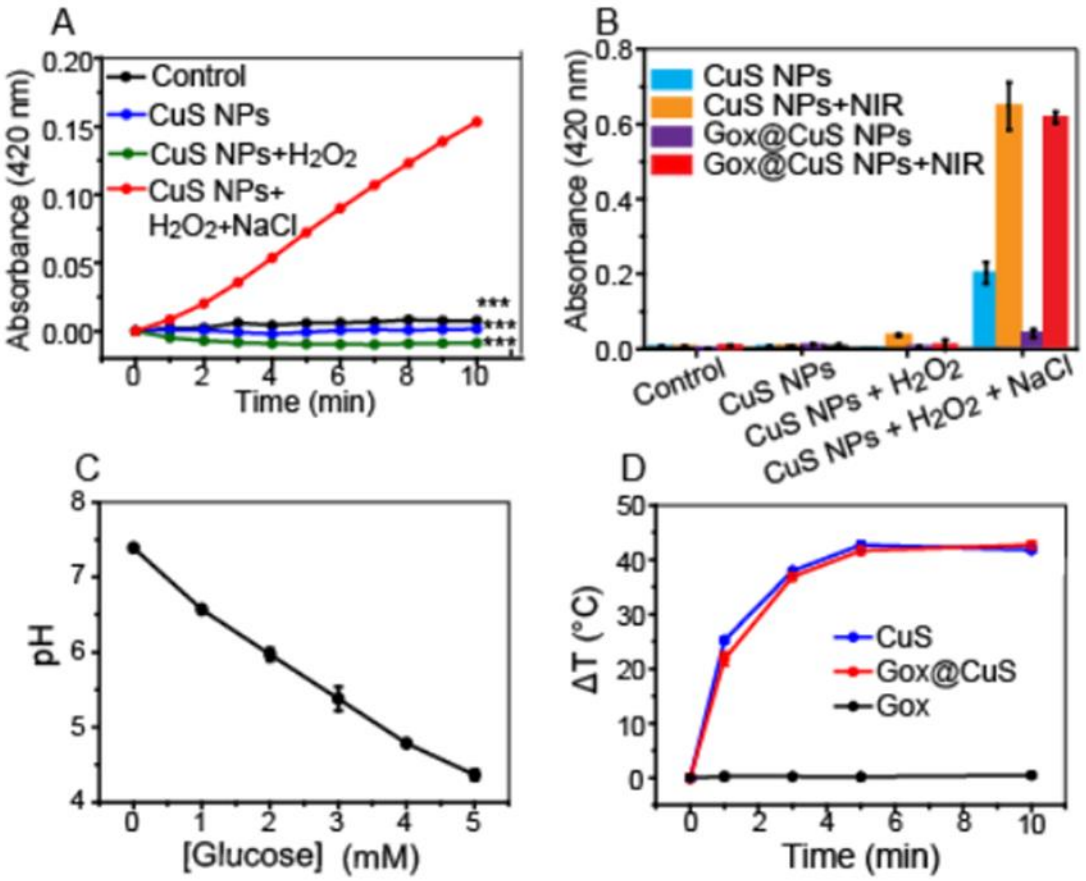

Figure 23: The catalytic activity of Gox@CuS nanoparticles (NPs). ABTS oxidation catalyzed by CuS NPs (10 μg/mL) (A) in the presence and absence of NaCl, and (B) with or without NIR irradiation (λ = 808 nm, 1.5 W/cm^2). (C) The decrease in pH over 2 h as a function of glucose concentration. (D) The temperature change of the CuS NP solutions under NIR irradiation over 10 min. Error bars indicate standard deviation (n = 3).

The catalytic activity of the surface-adsorbed Gox was confirmed by the reduction of pH resulting from gluconic acid generation (Figure 23C). In the presence of typical blood-glucose concentrations, the Gox@CuS NPs were able to reduce the pH of the buffered sample volume from physiological to mildly acidic conditions sufficient to activate the NP's Fenton-like activity. Meanwhile, H_2O_2 production also increased in a glucose dose-dependent manner (**Figure S20**). The H_2O_2 produced by Gox was catalytically decomposed by CuS NPs or Cu^{2+} within 1 h through Fenton-like chemistry (**Figure S21**), generating intermediate ROS, including superoxide radical anion ($O_2^{\bullet-}$), $^{\bullet}OH$, and $^1O_2$, which could induce oxidative damage to local biological structures. When considering the high levels of endogenous glucose and Cl^- in the interstitial fluid of solid tumors (~100–110 mM)[1018] as well as select organelles (e.g. ~118 mM in human lysosomes),[1019] Gox@CuS shows promise as a powerful nanocascade system. The ultimate products of H_2O_2 degradation catalyzed by the CuS NPs are H_2O and O_2, the latter of which is recycled back into glucose oxidation by Gox and the reformation of H_2O_2 (Scheme 2). Cancerous cells featuring normal or

elevated levels of antioxidant enzymes, such as catalase and superoxide dismutase, are also expected to partially contribute to H_2O_2 production, degradation, and O_2 recycling through these enzymes.[1020] In addition to the catalytic activity of the NPs, the CuS and Gox@CuS NPs solution temperatures increased ~40 ºC within 5 min during NIR irradiation (Figure 23D), indicating a strong photothermal effect. The temperature increase not only kills cells directly, but also enhances the Fenton reaction as previously mentioned (Figure 23B), contributing to the multimodal cancer therapy.

The synergistic therapeutic effects of Gox@CuS NPs were first demonstrated in two human cancer cell lines, i.e., melanoma (B16F10 cell line) (**Figure 24**) and triple negative breast cancer MDA-MB-231 cell line (**Figure S22**). The cells were treated with Gox, CuS NPs, or Gox@CuS nanocomposite in the presence of various supplemented glucose concentrations (0–5 mM). Only the Gox@CuS nanocomposite exhibited high cytotoxicity, which increased with higher glucose or nanocomposite concentrations (Figure 24). The anticancer effect of the nanocomposite was quite strong, with 2.5 nM (~0.19 μg/mL) of Gox@CuS NPs capable of eliminating ~90% of the B16F10 cells during the short treatment period (Figure 24B). The composite also showed toxicity to cancerous cells when no exogenous glucose was added, where we presume the toxicity was from depletion of endogenous glucose and oxidative stress generated in the chain reaction that we would expect in vivo.

The Gox@CuS composite was significantly more effective than either CuS or Gox alone, with a calculated combination index of ~0.19 using the Chou-Talalay method, indicating the strong synergy of the chain reaction mechanism.[1021,1022] The H_2O_2 production in B16F10 cell medium was dependent on the Gox concentration (Figure 24C). The IC50s for B16F10 and MDA-MB-231 cells were calculated to be ~0.14 and 0.38 μg/mL, respectively. We then tested the activity enhancement of a brief NIR irradiation (5 s) with Gox@CuS treatment using confocal microscopy (**Figure S23**), which showed fewer viable cells after treatment than those treated with Gox, CuS, or Gox@CuS NPs alone. More ROS was generated inside cells treated with Gox@CuS NPs (with or without NIR irradiation), which was visible as bright green fluorescence and could be attributed to Cl-accelerated Fenton reactions. The uptake and photothermal performance of the CuS NPs by PC-3 prostate cancer cells was also evaluated. Following a 24 h incubation period with 30 μg/mL CuS, ~17.7% (~5.3 μg/mL) was found to have been internalized or degraded by the cells using the CA-Fenton reaction in the media for quantification, of which the standard curve was shown in Figure S14B. Following NIR irradiation (808 nm) at a power setting of 1 W/cm^2 for 5 min, cell viability was reduced from 61.7 ± 7.26% to 26.2 ± 3.36% (**Figure S24**). In comparison, NIR treatment alone showed no reduction in viability.

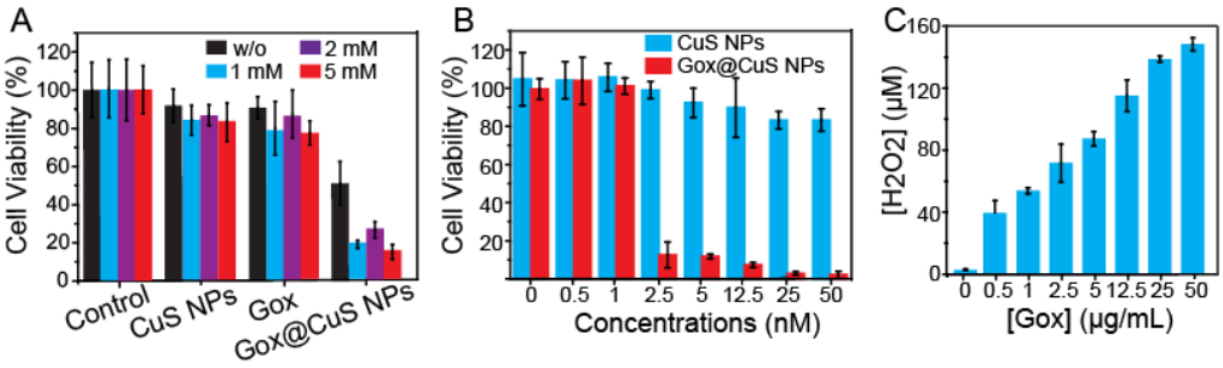

Figure 24: The toxicity of Gox@CuS nanoparticlrs (NPs) with different (A) glucose and (B) Gox@CuS NPs concentrations, towards B16F10 melanoma cells. (C) H_2O_2 produced by different Gox concentrations in the cell medium. Error bars indicate standard deviation (n = 3).

Because B16F10 cells showed a higher susceptibility towards the Gox@CuS treatment than MDA-MB-231 cells, we next tested the therapeutic efficacy of the Gox@CuS nanocomposite using a mouse model of the melanoma B16F10 cells (**Figure 25**A). Tumor-bearing mice were randomly placed into seven groups (6 mice per group) and were treated with the following strategies: saline (negative control), saline + NIR irradiation, Gox, CuS NPs, CuS NPs + NIR irradiation, Gox@CuS, and Gox@CuS + NIR irradiation. Saline and the three individual therapeutic solutions (CuS and Gox@CuS NPs, 200 nM, 100 μL, Gox = 2.2 mg/kg of body weight) were intravenously (IV) introduced to the mice. NIR irradiation (10 min, 5 W/cm^2) was applied to the tumor area of the mice 1 h after injection. The change in body temperature was recorded with a forward-looking infrared camera. Although the camera measured the mouse skin temperature, their body temperature should exceed their skin temperature, and the images showed the accumulation of CuS and Gox@CuS NPs in the melanoma, which significantly increased the local tissue temperature under NIR irradiation (**Figure S25**). This low-temperature photothermal effect improved the suppression of tumor growth significantly (Figure 25B), attributable to both the locally produced heat and the NIR-enhanced catalytic activity of the CuS NPs and Gox@CuS nanocomposites (Figure 23B and D). In contrast, without NIR irradiation, CuS NPs did not inhibit tumor growth. When combined with the NIR irradiation, the Gox@CuS nanocomposite showed the highest efficacy compared with the other groups, further demonstrating the synergistic effect of ST, Cl-accelerated Fenton-based CDT, and dual PDT-PTT for melanoma treatment (Figure 25B, Figure ***25***C, and **Figure *S26***).

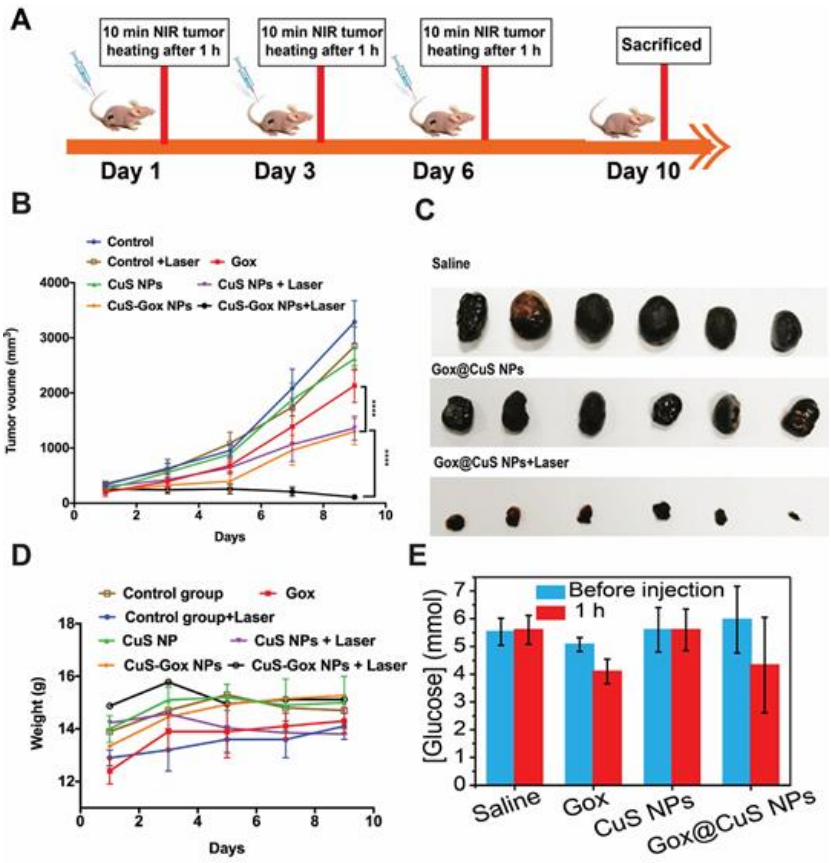

Figure 25: In vivo mouse model for efficacy evaluation of the Gox@CuS nanocomposite. (A) Schematic representation of in vivo antitumor experiments. (B) Tumor volume during the treatment. (C) Extracted tumor images after 9 d of treatment from sacrificed mice. (D) The mouse body weight during treatment. (E) Observed changes in blood glucose level 1 h after treatment. Error bars indicate standard deviation (n = 6).

No signs of acute systemic toxicity were observed as a result of treatment with Gox@CuS during the 10-day treatment period. First, no significant loss of body weight was observed (Figure 25D). Second, the nanocomposite did not induce a noticeable or persistent drop of peripheral blood glucose after 1 h of IV injection (Figure 25E). Third, the blood aspartate aminotransferase (AST) and alanine aminotransferase (ALT) levels, indicators of liver function, were not elevated (**Figure 26**A and B), indicating no harmful effect on the liver. Last, potential pathological damage to the major organs, i.e., the heart, lungs, liver, spleen, and kidneys by the Gox@CuS + NIR treatment was evaluated using the histological images of the dissected organs. Compared to the saline treated control group, no significant tissue damage was observed (Figure 26C), which further substantiated the biosafety of Gox@CuS NPs during treatment. After 10 d of treatment using Gox@CuS NPs + NIR, all tumor bearing mice were cured (**Figure S27**) with only residual scar tissue remaining, while all other treatment groups retained some level of tumor growth. Overall, the results suggest the effectiveness and biosafety of the Gox@CuS nanocatalyst for tumor treatment.

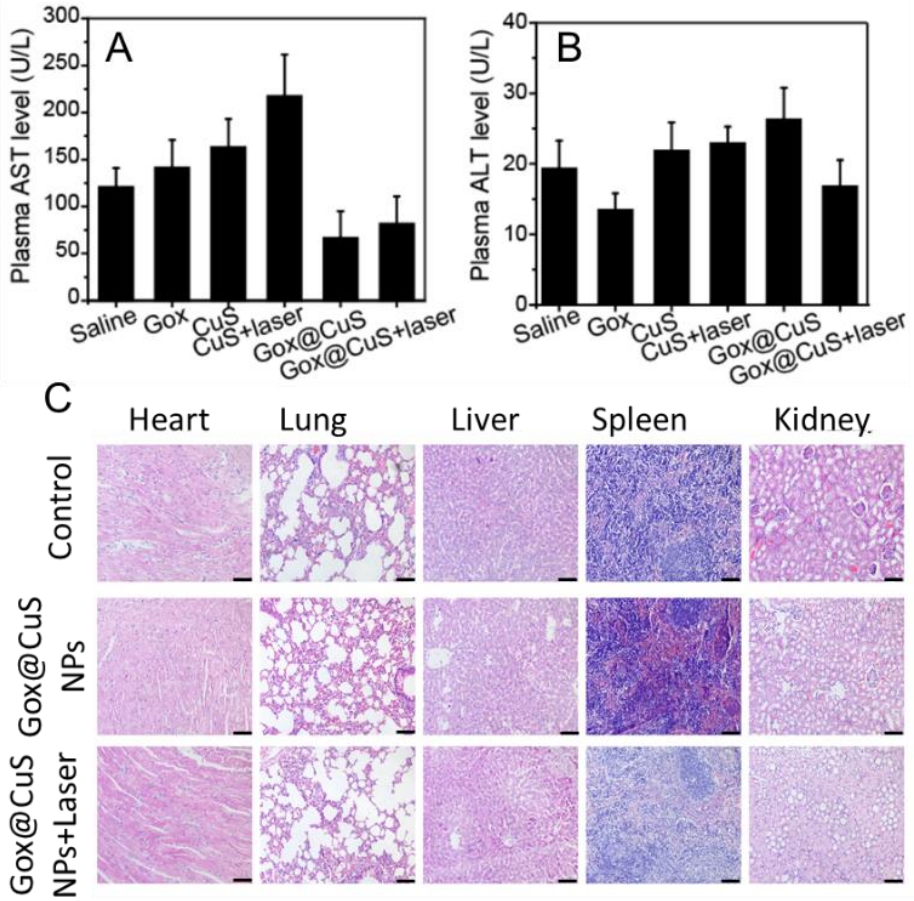

Figure 26: The (A) AST and (B) ALT concentrations of healthy nude mice after 10 d of treatment to evaluate liver function. (C) H&E staining of different organs of B16F10 tumor bearing mice after 10 d of treatment. Scale bar = 100 μm. Error bars indicate standard deviation (n = 6).

4.4 Conclusions

Altogether, by integrating ST, Cl-accelerated CDT/PDT, and PTT using the Gox@CuS nanocomposite, a very simple, highly effective, and non-toxic nanomedicine formulation was demonstrated for synergistic combinatory cancer therapy. These unique attributes, especially the cost-effectiveness and scalable fabrication, make the nanoformulation very promising for industrial manufacturing and clinical applications.

~ Chapter 5 ~

Photoresponsive Polymeric Microneedles: An Innovative Way to Monitor and Treat Diseases

The work presented in this chapter has been published as:

Singh P.*, **Youden, B.***, Carrier, A., Oakes, K., Servos, M., Jiang, R., Sujing, L. Nguyen, T.D., and Zhang, X. Photo-Responsive Microneedles: An Innovative Way to Treat Diseases. *Journal of Controlled Release*, **2023**, 353, 1050-1067. DOI: 10.1016/j.jconrel.2022.12.036.

**These authors contributed equally to this work.*

Chapter Summary

Microneedles (MN) technology is an emerging technology for the transdermal delivery of therapeutics. When combined with photoresponsive (PR) materials, MNs can deliver therapeutics precisely and effectively with enhanced efficacy or synergistic effects. This review systematically summarizes the therapeutic applications of PRMNs in cancer therapy, wound healing, diabetes treatment, and diagnostics. Different PR approaches to activate and control the release of therapeutic agents from MNs are also discussed. Overall, PRMNs are a powerful tool for stimuli-responsive controlled-release therapeutic delivery to treat various diseases.

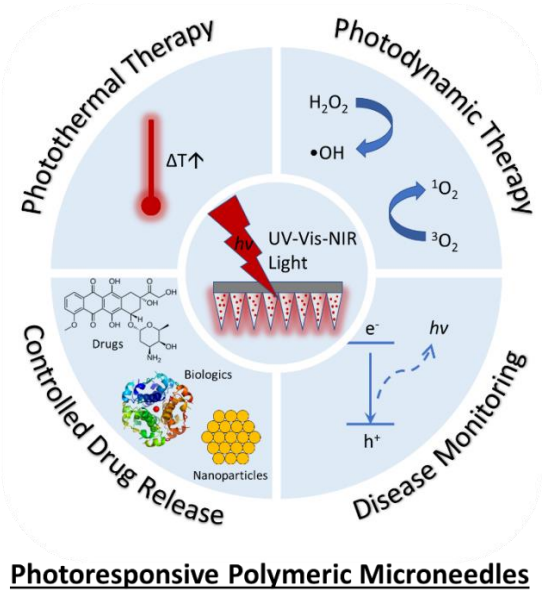

Scheme 3: The light activation and medical applications of photoresponsive microneedles.

5.1 Introduction

Photosynthesis, circadian periodicity, sight, and melanin secretion are a few examples of photoresponsive biochemical reactions.[1023] Inspired by nature, biomedical researchers have gained an increased understanding of light-matter interactions and their effects on biological systems, developing phototherapies (or light therapies) for medical applications.[1024] Phototherapies are used to treat diseases, such as skin wounds and cancer, through the conversion of light energy into reactive oxygen species (ROS; photodynamic therapy (PDT)) or heat (photothermal therapy (PTT))[1025–1029]. These therapies are highly effective and have motivated further exploration in the field of photomedicine.[1024,1030–1032] This is especially empowered by nanotechnology, materials sciences, advanced micro- and nano-engineering, and artificial-intelligence-assisted design.[110,885,910,1025,1033–1035] For example, organic semiconducting materials (OSMs) consisting of optically active π-conjugated building blocks have emerged as promising phototherapeutics because of their excellent optical properties, high photostability, and great biocompatibility.[1036] Additionally, thermosensitive lipid nanoparticles (NPs), which are widely used for drug delivery,[1037] have also been found to be highly effective for controlled drug release in combination with various types of PTT.[948]

Visible and near-infrared (NIR) lasers are the most common light sources for phototherapies because of their low ionizing potential and greater tissue penetration than UV light (up to 5 mm vs <0.2 mm).[1038,1039] As such, phototherapies are best used for transdermal and subcutaneous drug delivery for the treatment of superficial diseases. Microneedles (MNs), in combination with phototherapies, are therefore a promising drug delivery technology. Conventional transdermal delivery, e.g., topical gels/creams, is limited by the diffusion of drugs across the outermost skin layer, the stratum corneum.[1040] Therefore, polymeric MNs use arrays of hundreds-to-thousands of micron-scale needles (<4 μm) made of degradable polymers containing encapsulated therapeutics, or non-degradable structures coated with drug formulations, to deliver therapeutic cargos through the superficial layers of the skin to treat diseases.[1041,1042] Compared to subcutaneous injections, MN technologies offers painless, self-administrable, and effective treatments of both local and systematic diseases with minimal skin damage.[1043,1044] MNs also avoid mucosal irritation, first-pass hepatic metabolism, gastrointestinal degradation of therapeutics, systemic side-effects, and the need for specialized practitioner training.[1045] Its advantages over traditional transdermal drug delivery systems (TDDSs) also include highly uniform dose distributions and controlled drug-release profiles.[1043] Interest in MNs has grown significantly over the last four decades, with many preclinical and clinical studies showing that MNs effectively deliver vaccines, insulin, and hormones through the skin.[1046–1049]

Recently, polymeric MN technologies have successfully used photoresponsive materials (PRMs) for disease treatment and controlled transdermal drug delivery. These photoresponsive microneedles (PRMNs), as a novel TDDS, can minimize the toxicity of active pharmaceutical ingredients (APIs), trigger drug release on command, and enhance therapeutic efficacy through synergistic mechanisms. In 2020, Zhi et al. published the first instructive review on the use of PRMNs for PDT, PTT, and combination therapies.[1050] Many novel PRMN formulations and strategies have emerged over the last three years. However, the photoresponsive mechanisms, PRMN design considerations, and the focused applications of PRMNs have not been systematically reviewed. To fill the gap, this critical review focuses on the fundamental mechanisms and principles behind PRMN development and summarizes the most common applications of PRMNs in cancer therapy, wound healing, diabetes treatments, and diagnostics.

5.2 PRMN Fundamentals

The use of PRMs for phototherapies, both with and without MNs, depends on many factors relating to light-matter interactions. Different wavelengths of light correspond to the energy of photons, with longer wavelengths indicating lower energy. Photons with high energies, including X-rays (<10 nm) and ultraviolet (UV, <400 nm) light, are ionizing and can directly break chemical bonds. These forms of light can therefore be used for the treatment of malignant tissues and pathogens because of their cytotoxic effects, e.g., radiation therapy.[169,1051,1052] By comparison, visible and NIR light typically do not have enough energy to degrade molecules, and instead only interact with a small number of endogenous PRMs, such as melanin, cytochrome C oxidase, or heme, which can absorb visible or NIR photons to indirectly exert physical or chemical effects.[1053] Depending on the PRM properties and the light source, these effects are primarily induced by luminescence (scattered light), heat (photothermal transduction), or ROS generation (photocatalysis).[703,1054–1056] The use of light alone for phototherapies (photobiomodulation) has been explored for many years, although many studies report conflicting levels of efficacy.[1057,1058] One method to increase the efficacy of phototherapies is to introduce specific PRMs that act as an antenna and amplifier, preferentially absorbing and converting the light energy.[1024,1059] Additionally, delivered PRMs can be designed to interact with photons of certain wavelengths that have minimal biological absorbance to increase penetration depth.[1060–1062] In this section, we review the fundamental principles governing the use of PRMNs, including light-matter interactions, light-sources, and the design and functions of PRMN patches. These principles determine the efficacy and safety of PRMNs for each application.

5.2.1 Phototherapy Mechanisms & Materials

PRMs are broadly classified as either organic or inorganic materials. Organic PRMs commonly include dye molecules, pigments, and polymers containing aromatic chromophore groups whereas

inorganic PRMs are most often metal- or carbon-based nanomaterials.[110,1054,1063,1064] Both categories of materials can absorb visible (400–700 nm) and near-infrared (NIR, >700 nm) light, although the wavelengths involved can differ significantly between molecule or particle types.[1065] Fundamentally, the light spectrum absorbed by a PRM is determined by the specific arrangement of its molecular orbitals and therefore the ability of the photons to excite an electron into a higher energy state (**Figure 27**A and B). Such excited states are unstable and quickly relax either radiatively, emitting the absorbed energy as a photon (fluorescence), or non-radiatively (vibrationally), generating heat.[110] They can also be used as redox sites to react with dissolved O_2 and H_2O_2 to produce ROS via photocatalysis for type-I PDT.[703,1066–1069] Excited organic PRMs can also undergo intersystem crossing, enabling type-II PDT through non-radiative energy transfer.[1070] In most situations, molecular oxygen is involved in this reaction, being converted from the triplet ground state to an excited singlet state.[1068] Without a molecule to absorb the energy, phosphorescence can occur, emitting the photon at a longer wavelength. Depending on both the photon energy and the PRM's electronic structure, one or more of the above mechanisms may dominant. Heat and ROS can have both stimulatory and inhibitory effects on cells,[110] and therefore significant efforts are needed to optimize the photoresponsive mechanisms for each application.

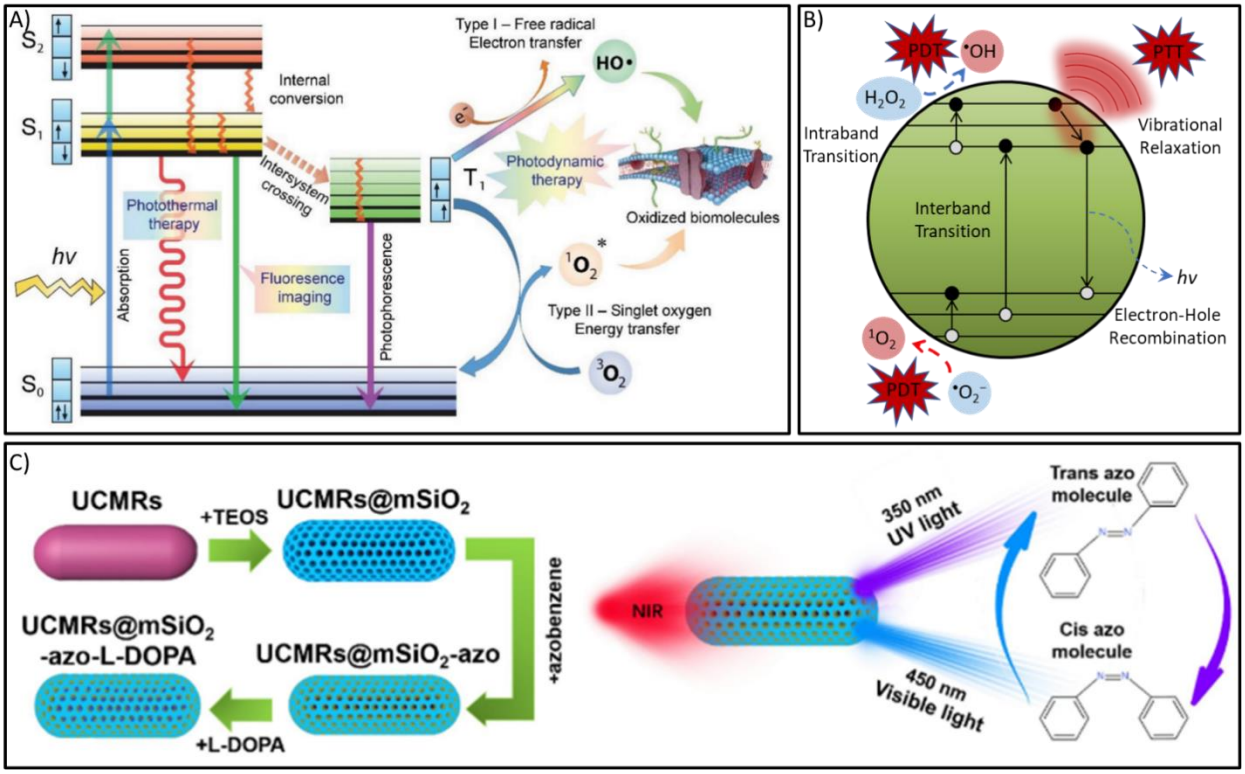

Figure 27: Photoresponsive mechanisms. A) Excitation and relaxation of organic photoresponsive materials: generating heat, luminescence, or reactive oxygen species. Reprinted with permission from Ref [1054] (Copyright John Wiley & Sons, 2018). B) Excitation and relaxation of inorganic photoresponsive materials. C) Synthesis of

upconverting mesoporous silica microrods with controlled release via azobenzene isomerization. Reprinted with permission from Ref [1071] (Copyright Elsevier, 2022).

In addition to delivering PRMs for phototherapies, the fluorescence, heat, or ROS produced may enable physical or chemical changes of other components of the PRMN. Photocleavage, photoisomerization, and photopolymerization are such photoresponsive mechanisms that can be used for PRMNs, of which the latter is only used for MN casting.[1072] Photocleavage uses specific wavelengths of ionizing UV light to break the linker bond of a drug conjugate to liberate and activate the drug molecules for controlled release.[1073] Conversely, photoisomerization uses light to produce reversible conformational changes of drug molecules.[1071,1074] Both strategies can be induced directly by irradiation; however, this may damage healthy tissue. By comparison, upconverting PRMs can use these mechanisms safely through luminescence. For example, Zhou et al. used upconverting mesoporous-silica microrods and L-DOPA to relieve Parkinson's disease symptoms.[1071] Upon NIR irradiation, the silica microrods were excited to emit UV light. Following this, a molecular motor (similar to a gate) bound to the NP surface was excited via photoisomerization to release L-DOPA in a controlled manner (Figure 27C). In this way, multiple PRMs excited by different wavelengths can be combined into a composite PRMN. More commonly, thermosensitive compounds, such as lauric acid (LA) can be added to porous or hollow nanomaterials, allowing for controlled release of drugs, e.g., chemotherapeutic agents, during PTT (**Figure 28**A).

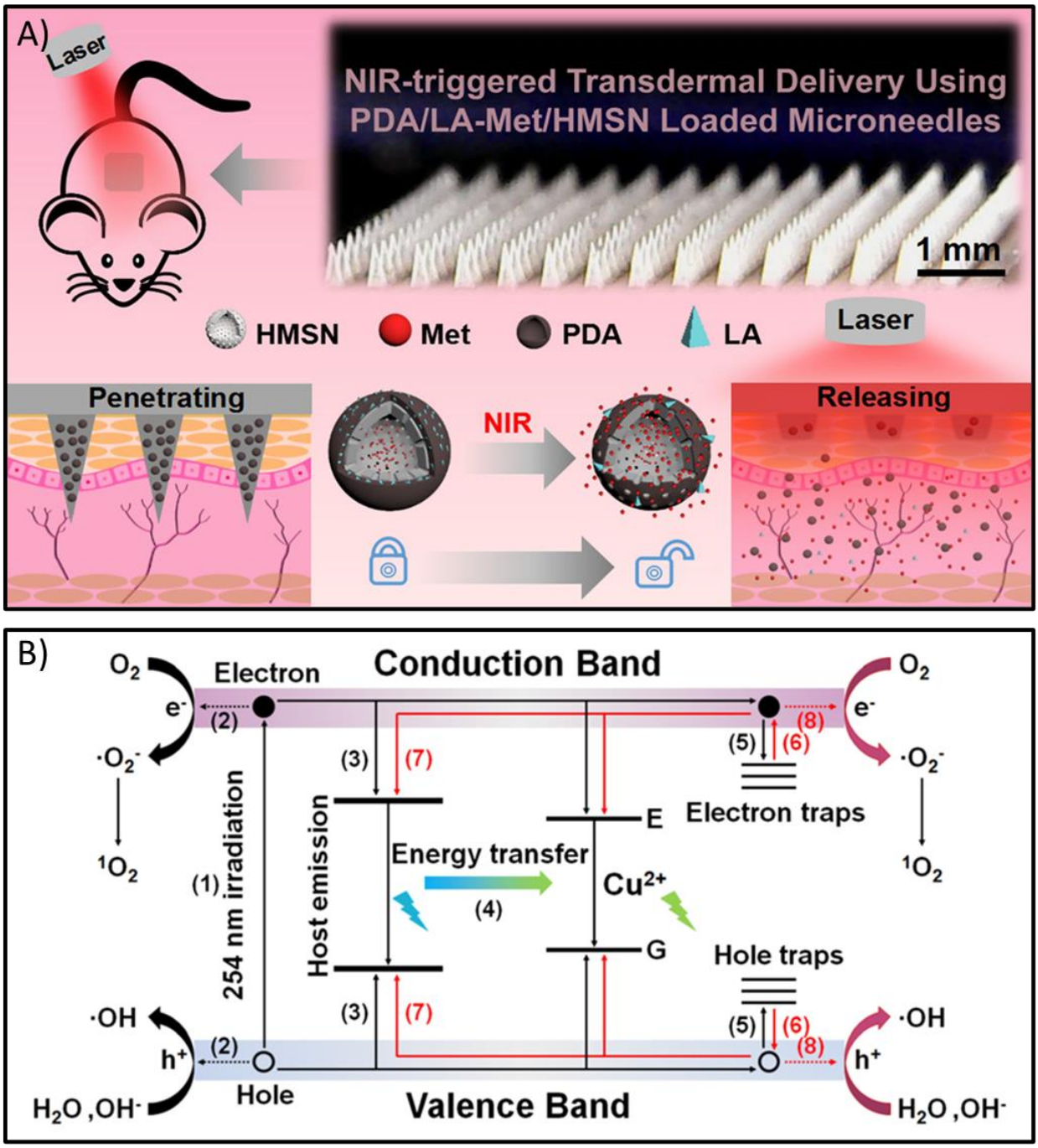

Figure 28: A) Heat-induced drug release using lauric acid as a thermosensitive trigger. Reprinted with permission from Ref [1075] (Copyright American Chemical Society, 2018). B) Proposed mechanisms for persistent luminescence-induced photocatalysis in Zn_2GeO_4:Cu^{2+} nanorods. Reprinted with permission from Ref [1076] (Copyright American Chemical Society, 2022).

Many different inorganic nano-PRMs have been used within MNs to trigger thermal effects, including gold,[1077–1083] magnetite (Fe_3O_4),[1084] Prussian blue (PB, $Fe_4[Fe(CN)_6]_3$),[1085] graphene oxide (GO),

copper sulfide (CuS), molybdenum disulfide (MoS_2),[1086] lanthanum hexaboride (LaB_6),[1087,1088] and bismuth sulfide (Bi_2S_3).[1089] Inorganic nanomaterials are attractive because of their multifunctionality, easy synthesis, chemical stability, mechanical strength, and tunability. For example, our lab recently reported a dissolvable polymeric PVA/PVP MN system that contained graphene oxide (GO) as the PRM and HA15 as a chemotherapeutic agent.[1090] The GO photothermal effect not only activated drug release at the melanoma tumor site, but also killed bacteria in situ to prevent infections during MN application. The GO also improved the tensile strength of the microneedles, improving their skin penetration. In non-MN applications, several inorganic NPs have shown strong photodynamic activities,[157,1091] although the lack of FDA approval and concerns over biocompatibility may be hinder their adoption.[1092] Regarding PDT in inorganic PRMs, higher-energy UV-Vis photons are usually required as they can easily induce interband transitions, enabling type I PDT. Comparatively, lower-energy NIR photons can only produce intraband transitions, which more rapidly dissipate their energy as heat via vibrational relaxation. However, NIR-driven PDT can still occur for inorganic PRMs when redox-sensitive molecules are adsorbed onto their surface, forming a charge-transfer complex.[1066,1069,1093,1094] NIR-driven PDT can also be performed in composite materials, wherein a Schottky junction forms and traps the electrons excited by NIR.[1095,1096] Dopants and impurities can also form electron-hole traps.[1097,1098] Certain dopants, such as lanthanide ions, can endow upconverting properties to some materials, allowing them to absorb multiple low-energy photons to produce emissions of greater energy.[1099–1101] Alternatively, up-conversion PRMs can be used for PDT. For example, Gong et al. recently used Zn_2GeO_4:Cu^{2+} luminescent nanorods for the treatment of methicillin-resistant *Staphylococcus aureus* (MRSA) infected wounds.[1076] Following pre-irradiation of the MNs with UV light, the nanorods displayed a persistent luminescence-induced PDT effect, generating ROS for several hours to eliminate wound bacteria (Figure 28B).

Organic pigments and dyes are also an important class of photothermal and photodynamic PRMs.[1064,1102] Among them, indocyanine green (ICG) is a widely studied FDA-approved photothermal agent for intravenous administration. Compared to inorganic NPs, organic dyes are biodegradable and safer for IV administration, but their rapid blood clearance and chemical stability are major disadvantages.[110] However, organic PRMs can also be assembled to form NPs or be conjugated with polymers to increase their stability and size, further slowing their clearance, and generate high photothermal or photodynamic efficiencies. For example, Lei et al. developed melanin@SiO_2 NPs for skin tumor PTT and wound healing using hyaluronic acid MNs. Following PTT, the released NPs could scavenge ROS to reduce inflammation and stimulate skin regeneration.[1103] In addition to dyes, other organic PRMs used with MNs include polydopamine (PDA) NPs (Figure 28B) and 5-aminolevulinic acid (ALA).[1075,1104,1105] Once delivered, ALA can be endogenously converted to protoporphyrin IX, a precursor to heme and chlorophyll, through a series of reactions in the cell.[1106] This molecule is responsive to red light (~630 nm) and has been widely used for

PDT. Organic molecules with similar structures, e.g., phthalocyanines and metal-center porphyrins, have also been explored for phototherapies with PRMNs.[1092,1107–1109]

5.2.2 Light Sources for Phototherapies

As mentioned earlier, visible and NIR light are typically chosen for most applications due to their low mutagenicity and greater tissue penetration than UV. Photons of these energies can be produced using several sources, with light emitting diodes (LEDs) and diode lasers being the most common. Both LEDs and lasers use electron-hole recombination to generate light, although the mechanisms and output differ significantly. In lasers, electron-hole pairs are generated and then amplified by stimulated emission.[1110] Stimulated emission is the process wherein a photon with the correct energy to generate an electron-hole pair can also induce recombination, generating a second photon with equal energy, phase, and direction. In LEDs, an electric current is used to generate the hole-pairs, which then recombine at a semiconductor junction.[1111] The light output of these sources is usually measured in watts (joules per second) per cm^2 of surface area (power density); however, it is important to note that power drops off with distance due to light scattering and diffraction, and thus the source-to-skin distance can also be an important clinical parameter. Depending on where the PRMN patch is located, patient movements, such as during breathing, could cause fluctuations in delivered power. While LEDs are significantly more cost effective, have a greater choice of emission wavelengths, and can treat larger areas than lasers, they also tend to have larger bandwidths, lower coherence, and low power densities. Therefore, LEDs are desirable for low-intensity therapies over large treatment areas. They are also easy to mass produce and implement. Conversely, lasers are preferred for phototherapies wherein high intensity light and/or small spot sizes are needed. However, lasers can pose additional risks, particularly to ocular tissue, caused by the scattering of high-intensity beams.

The main concern when using LEDs and lasers is their safety and ability to damage healthy tissue. While PRMs can preferentially absorb photons, the background absorbance of tissue can still be significant enough to result in burns or photochemical damage.[1112] Additionally, heating can also result in pain, even below the threshold for thermal burns, that may reduce patient compliance. Although PRMs mostly exert their effects locally, thermal expansion during high-intensity PTT could also result in damage to nearby healthy tissue. For patients with darker skin complexions, non-specific heating will also be greater because of the presence of a higher concentration of photoresponsive melanin in the skin. Joensen et al. notably found that continuous wave irradiation (810 nm) in darker skinned patients could result in 3–6 times more heating, with 62% of patients requesting exposure cessation.[1113] Thus, while phototherapies are generally considered safe, side effects can still occur and must be considered in designing experiments and clinical procedures, particularly for PTT, for each patient. According to the American National Standards Institute (ANSIZ136.1–2014), the safe power densities for visible and NIR is typically below 1 W/cm^2, which is

often exceeded in many published studies. Specifically, the safe power densities for light of 690, 808, 915, 980, and 1064 nm are ~0.20, 0.33, 0.54, 0.76, and 1 W/cm^2, respectively.[1114–1117] However, these limits depend not only on total power, but also on the irradiation time and the tissue affected. For example, the eyes are significantly more sensitive to irradiation than the skin, with the exposure limits for 532 nm light being 0.0025 W/cm^2 and 0.2 W/cm^2, respectively. Additionally, these standards are highly conservative and typically below pain thresholds.[1118] Notably, rapidly pulsed irradiation, which can reduce unwanted tissue heating by introducing cooling phases, can significantly reduce burn risks, allowing significantly more power (up to several W/cm^2) to be delivered safely.[1119,1120] For example, Santos Grandinétti et al. found no significant heating in patients with light, medium, and dark human skin using pulsed red and infrared lasers and LEDs.[1121] Therefore, pulsed lasers can be valuable for PDT and temperature-limited PTT, although most published reports still use continuous-wave sources.

5.2.3 Integration of MNs and PRMs

Polymers developed for MNs do not interact significantly with visible or NIR light, and thus PRMNs typically incorporate PRMs within their polymeric network or on their surface. Polymeric MNs can be constructed from various biocompatible polymers, with polyvinyl alcohol (PVA), polyvinylpyrrolidone (PVP), and hyaluronic acid (HA) being the most common for PRMNs. MNs can be categorized as solid, coated, hollow, swelling, or dissolvable (**Figure 29**A).[1122] Specifically, PRMNs use coated, swelling, or dissolvable MNs to deliver PRMs. In addition to these categories, some MN patches also feature a removable backing. Drug-coated MNs use water soluble drug formulations that dissolve off the MNs following insertion, after which the MNs can be removed. Swellable MNs are made with swellable polymers such as cross-linked hydrogels, that simultaneously extract interstitial fluid from the skin while permitting the release of preloaded APIs.[1123] Dissolvable MNs are made from water-soluble or biodegradable polymers that encapsulate APIs within the MN matrix that then dissolves after insertion, thereby releasing the encapsulated drug payload. In addition to being delivered via conventional MNs, photothermal PRMs allow for meltable MNs using thermosensitive polymers, such as polycaprolactone (PCL), for controlled drug release (Figure 29B and C).[1124] For example, Chen et al. used silica-coated lanthanum hexaboride (LaB_6@SiO_2) NPs to thermally degrade PCL MNs over several cycles, progressively releasing co-encapsulated doxorubicin (Figure 29D).[1125] Depending on the dissolution rate of the PRMs and the irradiation time, partial, total, or sustained drug release can be achieved. Photothermal PRMs can also be used to accelerate drug release, MN dissolution, and hydrogel swelling in non-meltable MNs as heat accelerates reaction kinetics and weakens chemical bonds.[1126–1128] Once released into the skin, drugs and PRMs either remain in place or enter the bloodstream through capillaries for systemic drug delivery. This depends on the ability of the drug to diffuse through the different layers of skin. Polymeric MNs are most

commonly fabricated through micromolding because of its excellent reproducibility, cost-efficiency, and scalability; however, for many polymers, the involvement of heat or UV irradiation during fabrication can pose issues for some encapsulated APIs.[1129]

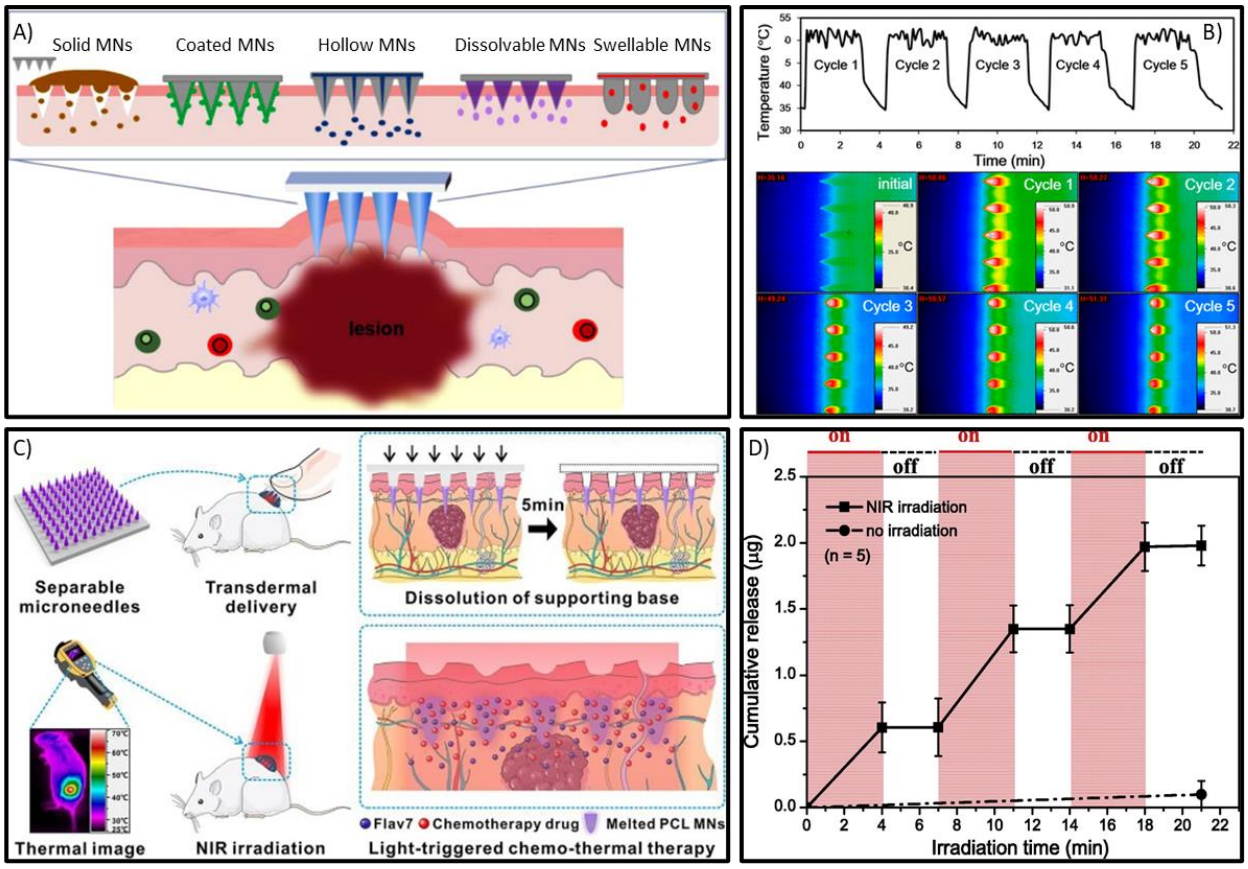

Figure 29: Microneedle types and delivery methods. A) Conventional MN designs. Reprinted with permission from Ref [1122] (Copyright Elsevier, 2021). B) Infrared camera images of meltable PRMNs over 5 cycles. Reprinted with permission from Ref [1088] (Copyright American Chemical Society, 2016). C) Chemotherapy drug release via synergistic photothermal therapy using dissolvable MNs. Reprinted with permission from Ref [1124] (Copyright Elsevier, 2022). B) Cumulative drug release over several irradiation cycles using meltable PRMNs. Reprinted with permission from Ref [1125] (Copyright Elsevier, 2015).

In addition to drug delivery and direct PTT or PDT, PRMNs are also used for synergistic and combination therapies. One example is PVP PRMNs that encapsulate CuO_2 NPs to treat superficial cancer.[1130] An advantage of this simple formulation is the multifunctional role of CuO_2 NPs, including its NIR-induced photothermal effect, Fenton toxicity, and glutathione depletion, thus combining PTT and CDT for effective cancer cell killing. Elsewhere, Zhou et al. fabricated PRMNs delivering a zeolitic imidazolate framework-8 (ZIF-8) metal-organic framework (MOF)-based core-shell nanomedicine for combined starvation therapy, PTT, and PDT (**Figure 30**A).[1131] The core of MOF encapsulated ICG and two enzymes,

i.e., glucose oxidase (Gox) and catalase (CAT), that sequentially degraded glucose, upregulated by cancer, into H_2O_2 and then O_2. The produced oxygen was then further converted to $^1O_2$ by ICG (type II PDT). Alternatively, the oxygen molecules could be used for glucose oxidation, forming a self-sustaining cycle, and minimizing hypoxia. Recently, the application of a novel photomechanical property of GO-encapsulated polymers, thermally triggered patch unfolding, was also exploited for MN technology to treat myocardial infarction through minimally invasive surgery.[1132] The PVA-based PRMN patch contained both GO and endothelial growth factor (VEGF). The folded MN patch was introduced into the chest cavity through a small incision (4 mm) and was unfolded with 10 s of NIR irradiation (Figure 30B). Importantly, because of the GO-enhanced strength, the unfolded MN patch easily pierced the heart surface with a sustainable release of VEGF, promoting neovascularization, reducing myocardial fibrosis, and restoring cardiac function.

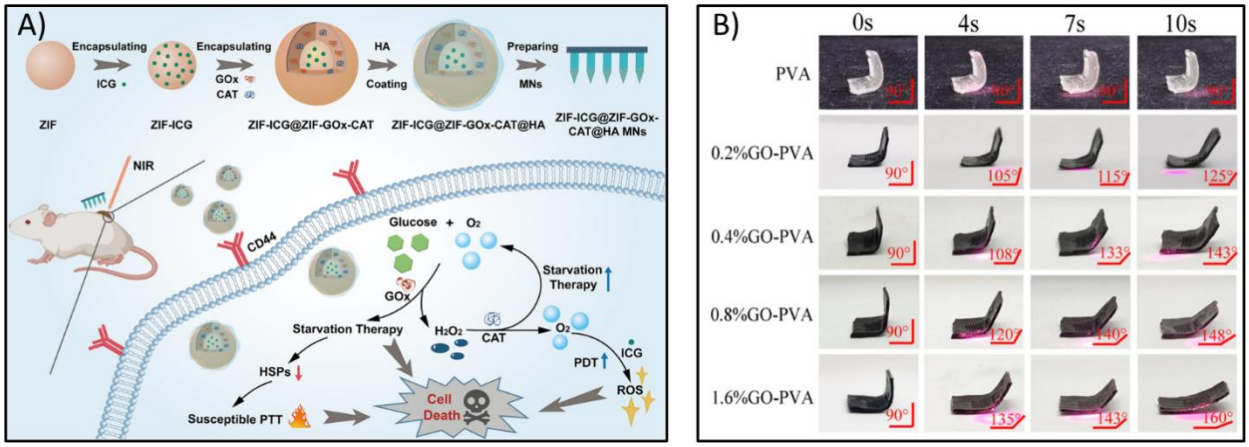

Figure 30: A) Synergistic anti-cancer therapy using starvation therapy, PTT, and PDT. Reprinted with permission from Ref [1131] (Copyright Elsevier, 2021). B) Unfolding of PVA PRMN patches containing GO. Reprinted with permission from Ref [1132] (Copyright American Chemical Society, 2021).

One key limitation of MNs is their inability to deliver high volumes of drugs or PRMs. Individual MNs typically carry a volume of ~10 nl each, which corresponds to a total patch volume of only 10 µl for a patch containing 1000 needles.[1133] Furthermore, within the MNs, only a small fraction of the volume is usually available for API loading since excipients must be included to facilitate manufacturing, provide mechanical strength, enable dissolution, etc. As such, PRMs with low potencies, i.e., poor quantum yield or photothermal transduction, are unlikely candidates for use within MNs. PRM or API doses can be increased either by increasing the number of MNs in each patch, which reduces their penetration ability, or by increasing patch area, which makes it more difficult to apply the patch uniformly.[1134] Therefore, more research is needed to develop fabrication methods and formulations that can maximize API loading and delivery. Notably, some PRMs, such as graphene oxide (GO) and molybdenum sulfide (MoS_2) nanosheets,

can improve MN mechanical strength, reducing the need for additional excipients and thus likely improving loading capacity.[1086,1090] Nevertheless, drug loading is a known problem for MN technology, and further work is needed to overcome this issue, although repeated dosing with painless patches may still be a preferred option to conventional injections. The use of concentrated freeze-dried powders has also been proposed as one method to improve API loading [1135,1136]; however, freeze drying may inhibit the activity of some APIs, such as attenuated viruses (vaccines),[1137–1139] thus making it unsuitable for some formulations.

5.3 PRMN Applications

MN-based DDSs can be activated and controlled by photoresponsive mechanisms for on-demand release and thus have promising applications in many disease treatments. MNs are compatible with various therapeutics, ranging from small molecules, such as doxorubicin (Dox), to macromolecules, including proteins, DNA, and siRNA.[1140] Currently, there are several stimuli-responsive DDSs using pH, hypoxia, ROS, and ultrasound, among others, to trigger cargo release [1141]; however, several key challenges remain. For example, pH-responsive DDSs can damage the endosomes of normal cells and high-intensity ultrasound-responsive DDSs may cause tumor metastasis.[1142] By comparison, low intensity photoresponsive DDSs are non-invasive and safe, causing minimal damage to surrounding tissue while offering excellent spatiotemporal control of drug release. In addition, PTT and PDT can be used for therapeutic modes on their own, allowing for synergistic and combination treatments,[110] while luminescent PRMs can be used for diagnostics. In this section, we review recent applications of PRMNs to cancer therapy, wound healing, diabetes treatment, and diagnostics, highlighting key innovations and common treatment strategies. In addition to these main applications, limited reports have also published using PRMNs for myocardial ischemia,[1132] Parkinson's disease,[1071] pain relief,[1073] and weight control.[1126,1143,1144] Notably, as previously described, several of these works used unique photoresponsive mechanisms, photocleavage, photoisomerization, and patch unfolding, to facilitate drug release.[1071,1132] Regarding weight control, current PRMNs use sublethal/mild PTT for heat-stimulated browning of white adipose tissue in combination with the small molecule drugs rosiglitazone or mirabegron.

5.3.1 PRMNs for Cancer Therapies

Cancer is a leading cause of death worldwide and its recurrent and aggressive nature requires multimodal therapies for effective treatment.[61,112,1145] Cancers evolve as a disease over several stages and can occur in any cell type of the body. The first two stages reflect the relative tumour size, while stage III indicates the potential for metastasis. The exact difference between a diagnosis of stage II or III differs for each cancer type. Finally, stage IV cancers are those that have spread to other parts of the body, corresponding to a low survival rate. To successfully treat cancers, all malignant cells must be killed or

made senescent, preventing their growth into new tumors. Traditional cancer therapies include chemotherapy, radiotherapy, and surgery. Although generally effective, these treatments have key limitations, such as systemic toxicity and limited selectivity. Additionally, tumors contain many subpopulations of cancer cells which may have, or develop, resistance to individual treatments. PRMNs are an alternative tool for superficial cancer treatment as they provide minimal invasiveness, low systemic toxicity, easy application, and spatiotemporal control over API release.[1031] Currently, several PRMNs have been successfully used for cancer therapies (**Table 5**). These include synergistic and multimodal phototherapy combinations with enzymatic cascades, chemotherapy, and immunotherapy. Due to dose limitations in MN patches, most PRMN formulations are ideal for treating localized early-stage cancers; however, by combining immunotherapy for anti-tumor vaccination, systemic responses can be triggered using PRMNs.

Table 5: Selected PRMNs for cancer therapies.

MN Materials	PRM	Light Source / Wavelength (nm)	Irradiation Power	Therapy	Adjunctive Agent(s)	Ref.
HA	ALA	N/A - 635	0.45 W	PDT	-	[1146]
	ALA	N/A - 635	0.2 W/cm^2	PDT + CDT +	CAT & Cu-$Ca_3(PO_4)_2$ NPs	[1147]
	Zn-phthalocyanine	Laser - 660	N/A	PDT + Immunotherapy	Anti-CTLA4 antibodies	[1107]
	Chlorin e6	Laser - 660	0.6 W/cm^2	PDT + Immunotherapy	-	[1148]
	ICG	Laser - 808	0.35 W/cm^2	PTT + Immunotherapy	Anti-aPD-1/aPD-L1 & anti-1-MT antibodies	[1149]
	ICG	Laser – 808	0.35 W/cm^2	PTT + Chemotherapy	Paclitaxel	[1150]
	ICG	Laser – 808	1.0 W/cm^2	PTT + Chemotherapy	Doxorubicin	[1151]
	IR-780	Laser – 808	1.0 W/cm^2	PTT + Chemotherapy	Paclitaxel	[1152]
	IR-780	Laser – 808	1.0 W/cm^2	PTT + Chemotherapy	Paclitaxel	[1153]
	Au Nanocages	Laser – 808	1.0 W/cm^2	PTT + Chemotherapy	Doxorubicin	[1078]
	Au Nanorods	Laser – 808	1.0 W/cm^2	PTT + Chemotherapy	Doxorubicin	[1077]
	Au Nanorods	Laser – 808	1.5 W/cm^2	PTT + Chemotherapy	5-Fluorouracil	[1154]
	IR-820	Laser – 808	1.0 W/cm^2	PTT + Immunotherapy	p53 DNA	[1155]
	IR-780	Laser – 808	1.0 W/cm^2	PTT + Immunotherapy	Autophagy inhibitor (CQ)	[1156]
	SiO_2@GA-Fe/PDA	Laser – 808	1.0 W/cm^2	PTT + CDT +	Fe ions	[1157]

				Chemotherapy		
	IR-820	Laser – 808	0.75 W/cm^2	PTT + Chemotherapy + Wound Healing	Curcumin	[1158]
	Melanin NPs	Pulsed (0.5 ms) Laser - 808	0.5 W/cm^2	PTT + Wound Healing	SiO_4^{4-}	[1103]
PLLA	Au Nanorods	Laser – 808	2.0 W/cm^2	PTT + Chemotherapy	Docetaxel	[1079]
PCL	LaB_6@SiO_2	Laser – 808	5.0-7.0 W/cm^2	PTT + Chemotherapy	Doxorubicin	[1087]
	LaB_6@SiO_2	Laser – 808	5 W/cm^2	PTT + Chemotherapy	Doxorubicin	[1125]
	Flav7	Laser – 808	1.0 W/cm^2	PTT + Chemotherapy	Doxorubicin	[1124]
	PB Nanocubes	Laser – 808	1.6 W/cm^2	PTT + Chemotherapy	Doxorubicin	[1159]
	LaB_6	Laser – 808	5.0 W/cm^2	PTT + Chemotherapy	Doxorubicin	[1088]
PVP	ICG	Laser – 808	0.34 W/cm^2	PTT + Chemotherapy	Doxorubicin	[1160]
	CuO_2 NPs	Laser – 808	0.75 W/cm^2	PTT + CDT	-	[1130]
	Poly(cyclopentadithiophene-*alt*-benzothiadiazole)	Laser – 808	1.0 W/cm^2	PTT + Immunotherapy	Polyinosinic–polycytidylic acid & Hyaluronidase	[1161]
	Nb_2C Nanosheets	Laser - 1064	1.0 W/cm^2	PTT	-	[1162]
PVA/PVP	ICG	Laser - 808	0.35 W/cm^2	PDT + Immunotherapy	Indoleamine 2,3-dioxygenase	[1163]
	ICG	Laser - 808	1.0 W/cm^2	PTT + Chemotherapy	Paclitaxel	[1164]
	NIR950 micelles	Laser - 808	1.0 W/cm^2	PTT	-	[1165]
	ICG@ZIF-8	Laser - 808	1.0 W/cm^2	PDT + PTT + Starvation Therapy	GOX & CAT	[1131]
	HA-CuS@ZIF-8	Laser - 808	1.0 W/cm^2	PTT + Chemotherapy	Camptothecin	[1166]
LA/PCL	CaO_2@Mn-PDA Nanoshells	Laser - 808	0.4-1.0 W/cm^2	PTT + CDT + Gas therapy	-	[1167]
	ICG	Laser - 808	0.4 W/cm^2	PTT + Chemotherapy	Doxorubicin	[1168]
PVA/ Chitosan/ PVP	Au@SiO_2 Nanoshells	Laser - 808	1.7 W/cm^2	PTT + Chemotherapy	Doxorubicin	[1080]
PVP/PCL	Cu-PDA NPs	Laser - 808	1.6 W/cm^2	PTT + CDT	-	[1169]
PVPVA	IR820	Laser - 808	0.1 W/cm^2	PDT + Chemotherapy	Cisplatin	[1170]

	Polyserotonin	Laser - 808	1.5 W/cm^2	PTT + Immunotherapy	β-catenin silencing DNAzyme	[1171]
MHA	Melanin	Laser - 808	1.0 W/cm^2	PTT + Immunotherapy	Tumor lysate & GM-CSF	[1172]
	BP-Gelatin Microspheres	Laser - 808	1.2 W/cm^2	PTT + Chemotherapy	Interferon γ & Dexamethasone	[1173]
HA/PVP	PDA Nanoshells	Laser - 808	0.9 W/cm^2	PTT + Starvation Therapy	GOX	[1174]
PMMA	SiO_2@Au Nanoaggregates	Laser - 808	0.5-1.0 W/cm^2	PTT	-	[1081]
PVP/CM/ HA	GO	Laser - 850	1.0 W/cm^2	PTT + Chemotherapy	HA15	[1090]

ALA, 5-aminolevulinic acid; CAT, catalase; CDT, chemodynamic therapy; CMC, carboxymethyl cellulose; CQ, chloroquine; CW, continuous wave; GOX, glucose oxidase; GM-CSF, granulocyte-macrophage colony-stimulating factor; HA, hyaluronic acid; ICG, indocyanine green; LA, lauric acid; MHA, methacrylated hyaluronic acid; MN, microneedle; PCL, polycaprolactone; PDA, polydopamine; PDT, photodynamic therapy; PLLA, poly(l-lactide); PMMA, polymethylmethacrylate; PRM, photoresponsive material; PTT, photothermal therapy; PVA, polyvinyl alcohol; PVP, polyvinylpyrrolidone; PVPVA, vinylpyrrolidone—vinyl acetate copolymer; ROS, reactive oxygen species; ST, starvation therapy.

Cancer immunotherapy involves activating or supressing the immune system to produce favorable tumor responses, which has gained increasing attention over the past few decades. Both immunotherapy and phototherapy benefit significantly from the high concentration of immune cells within the skin, allowing for easy immune activation.[1139] For example, Gu's group fabricated PRMNs encapsulating B16F10 tumor cell lysate (containing melanin) for sustained immunotherapy (**Figure 31**A).[1172] By using the photothermal heating of melanin to stimulate the release of local damage signals, immune cells could be stimulated to uptake tumor-antigens, promoting an immune response against both primary and metastatic tumors. The patch could also co-deliver a vaccine adjuvant (granulocyte-macrophage colony-stimulating factor, GM-CSF) that produced a synergistic immune response. In another example, Chen et al. exploited PDT-enhanced immunotherapy for cancer treatment.[1107] In this work, HA MNs were integrated with pH-sensitive dextran NPs containing Zn-phthalocyanine and anti-CTLA4 antibodies. When applied to skin tumors, the low tumor pH stimulated API release. PDT was then used to trigger the release of damage signals and tumor antigens whereas the antibodies served as an immune checkpoint inhibitor, enhancing the antitumor response (Figure 31B). PRMN-facilitated immunotherapy is still a new topic with vast opportunities for researchers to explore.

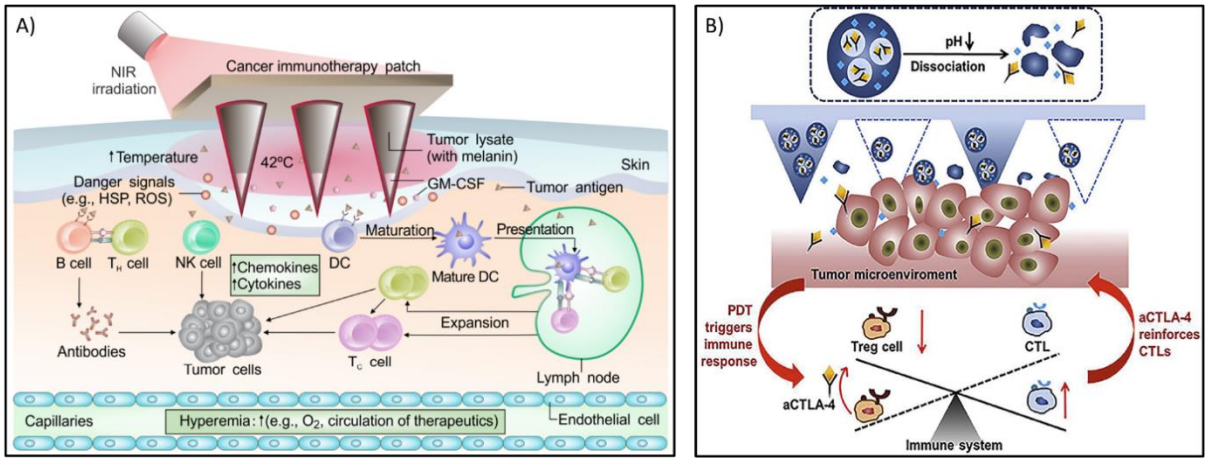

Figure 31: Cancer immunotherapy using PRMNs. (A) A schematic of a photoresponsive microneedle (PRMN)-based vaccination. Reprinted with permission from Ref [1172] (Copyright American Association for the Advancement of Science, 2017) (B) A schematic of MN-based photodynamic and immunotherapy and a possible mechanism for antitumor immune response. Reprinted with permission from Ref [1107] (Copyright Elsevier, 2019).

5.3.2 PRMNs for Wound Healing

Chronic wounds include skin damage, fungal infections, chronic ulcers, and non-melanoma skin cancers. Wound healing is a restoration process involving the replacement of destroyed or damaged tissue. This complex process involves inflammation, granulation, and tissue remodeling. Failures in any aspect may cause delayed healing.[1175,1176] MNs are promising for facilitating wound healing and infection treatment by altering inflammation, inactivating pathogens, and stimulating cell growth. Because of complications associated with systemic delivery and the ease-of-access of skin injuries and wounds, the logical strategy would be to apply therapies topically; however, any topical therapeutics must first diffuse through the outermost layer of damaged or dead cells to access healthy cells. Commonly, passive permeation requires the molecular weight of the API to be <0.5–0.6 kDa and be amphipathic.[1135] In addition, some wounds are continuously exuding fluid and can wash delivered therapeutics out of the wound bed.[1177] As a result, the local bioavailability of delivered drugs is lower than expected when they are applied topically. By comparison, MNs can effectively bypass the outermost skin layers and deliver specific doses of therapeutics to the wound area.

To date, PRMNs have been used for photodynamic antimicrobial chemotherapy (PACT), PTT, and gas therapy (**Table 6**). As biofilm development is often implicated in wound progression, potent therapeutic methodologies are required to eradicate persistent bacteria and accelerate wound healing. PACT provides an effective disinfection means for wound treatment via the PRMN platform. For example, Sun et al. fabricated PRMNs loaded with MOF-derived peroxidase-like nanozymes that not only converted light to heat but also increased its enzymatic activity to produce anti-bacterial ROS (**Figure 32**A).[1108] Wen et al.

showed another PACT example using MN-based PDT to treat acne vulgaris, an inflammatory skin disease.[1178] Therein, MNs delivered ICG encapsulated in a ZIF-8 MOF, which generated cytotoxic ROS, induced oxidative damage, and disrupted the metabolic activity of *Propionibacterium acnes* during irradiation. Additionally, Zn^{2+} released from ZIF-8 at low pH had additional antimicrobial effects. Some polymeric materials, such as hyaluronic acid (HA) and chitosan, have inherent antimicrobial activity and their use in MN fabrication may synergize with PR mechanisms.[1179,1180] Moving toward clinical applications of MNs, Petukhova et al. performed a small-scale clinical trial using ALA-encapsulated MNs for the treatment of actinic keratoses (pre-cancerous growths resulting from sun exposure) on 32 human participants.[1181] This system showed a high efficacy without causing pain as is often seen in conventional treatment methods.

Table 6: Selected PRMNs for wound healing.

MN materials	Wound Type	PRM	Light source / Wavelength	Irradiation Power	Type of therapy	Adjuvant Agent(s)	Ref.
N/A	Acne Scars	ALA	Laser - 633	0.08-0.1 W/cm^2	PACT	-	[1182]
Gantrez A-139 copolymer	Infection	MB	LED - 635	0.1 W/cm^2	PACT	-	[1183]
PVA	Infection	Zn_2GeO_4: Cu^{2+} NPs	N/A - 254 nm	N/A	PACT	-	[1076]
	Infection	PDA NPs	Laser - 808	0.5-2.0 W/cm^2	PTT	Levofloxacin + α-amylase	[1184]
	Muscle Damage	Carbonized wormwood	Laser - 808	3.0 W/cm^2	PTT	Prostaglandin E2	[1185]
	Infection	Metal-center Porphyrin	Laser - 808	1.0 W/cm^2	PACT	-	[1108]
	Infection	GO	Laser - 808	0.24 W/cm^2	PTT + GT	Nitric oxide	[1186]
MHA	Ischemic Perforator Flaps	Au Nanorods	Laser - 808	1.0 W/cm^2	PTT + GT	Nitric oxide	[1082]
	Infection	Fe_3O_4 NPs/ GO Nanosheets	Laser - 808	1.3 W/cm^2	PTT + CDT	-	[1187]
PVP/Col III	Infection	AMP-Cypate peptide	Laser - 808	1.5 W/cm^2	PTT	-	[1188]
PCL/Gelatin	Physical (Diabetes) & Infection	CaO_2@PDA Nanoshells	Laser - 808	1.6 W/cm^2	PTT + GT + IMT	Metformin	[1189]
HA	Infection	ICG	Laser - 808	0.3 W/cm^2	PACT + CDT	ZIF-8	[1178]
	Cancer Therapy & Infection	Melanin NPs	Pulsed (0.5 ms) Laser - 808	0.5 W/cm^2	PTT + Wound Healing	SiO_4^{4-}	[1103]

	Scar Healing	SiO_2 UCNPs	Laser - 980	0.5 W/cm^2	LPPC	mRNA	[1190]
PEG diacrylate	Physical	Mxene	N/A -808	N/A	PTT	Adenosine	[1191]
Gelatin Methacryloyl	Physical (Diabetes)	BP Quantum Dots	N/A - 808	1.56 W	PTT + GT	Hemoglobin	[1192]
PEGDA	Physical (Diabetes)	GO-MOF	N/A - 808	0.89 W/cm^2	PTT + GT	Nitric Oxide	[1193]
	Infection	Fe_3O_4 NPs	Laser - 808	1.0 W/cm^2	PTT + CTx	Doxycycline	[1084]

ALA, 5-aminolevulinic acid; BP, black phosphorus; Col III, recombinant human type III collagen; CDT, chemodynamic therapy; CTx, chemotherapy; CW, continues-wave; GT, gas therapy; GO, graphene oxide; HA, hyaluronic acid; ICG, indocyanine green; IMT, immunotherapy; LPPC, long-persistent photocatalysis; MB, methylene blue; MN, microneedle; MOF, metal-organic framework; NPs, nanoparticles; PACT, photodynamic antimicrobial chemotherapy; PDA, polydopamine; PDT, photodynamic therapy; PEG, polyethylene glycol; PEGDA, polyethylene glycol diacrylate; PRM, photoresponsive material; PTT, photothermal therapy; PVA, polyvinyl alcohol; PVP, polyvinylpyrrolidone; UCNP, upconverting nanoparticle; ZIF-8, zeolitic imidazolate framework-8.

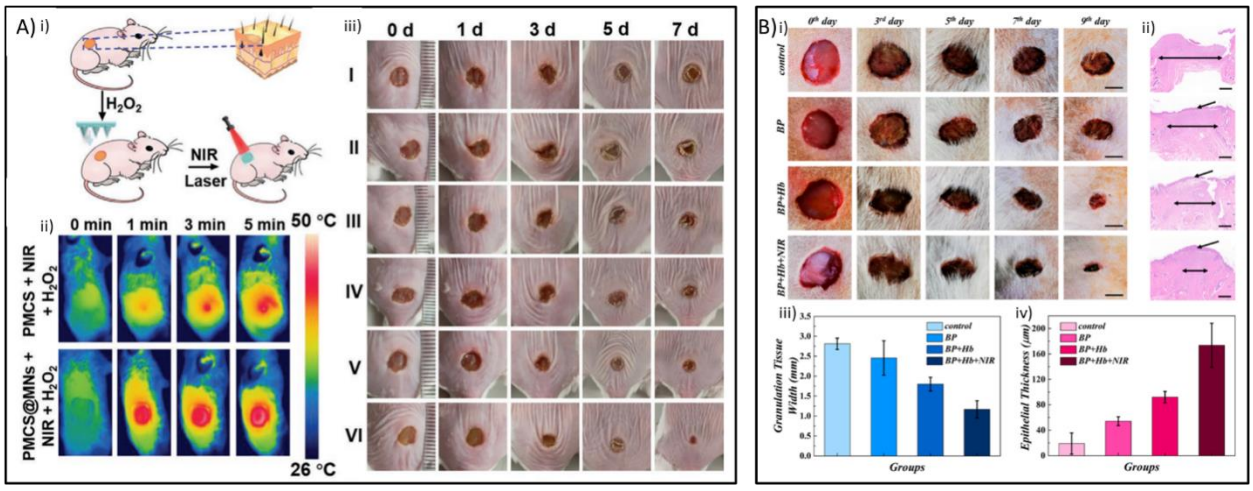

Figure 32: PRMNs for in vivo wound healing. (A) Bacterial wound healing using a metal-center porphyrin PRMN: (i) PRMN wound healing schematic, (ii) thermal images of PRMN-treated mice, and (iii) Staphylococcus-aureus-infected wounds on different days. Reprinted with permission from Ref [1108] (Copyright Wiley-VCH, 2021). (B) PRMNs using black phosphorus (BP) and hemoglobin (Hb) to facilitate wound healing: (i) Representative photos of the skin wounds of different groups. Scale bars = 0.5 cm. (ii) Corresponding H&E staining of the wound beds. Scale bars = 500 μm. (ii) Quantitative analysis of the granulation tissue width. (d) Quantitative analysis of epithelial thickness. Reprinted with permission from Ref [1192] (Copyright American Chemical Society, 2020).

In addition to bacteria eradication, the ideal PRMN can also remodel the wound microenvironment by promoting angiogenesis and suppressing inflammation. For example, Zhang et al. fabricated gelatin/PVA MNs containing black phosphorus quantum dots (BP QDs) as the PRM and hemoglobin as an oxygen delivery vehicle to facilitate wound healing.[1192] Wound oxygenation is considered a key

determinant of healing outcomes as oxygen is required for almost every step of the wound healing cascade.[1194–1196] Under NIR irradiation, the BP QDs increased the temperature of the MNs to facilitate oxygen release from hemoglobin, improving the recovery from diabetic wounds in a mouse model (Figure 32B). This work provides an example of gas therapy, which is considered as a promising green therapeutic strategy that minimize the adverse side effects to healthy tissues.[1197] Recently, the same group provided another excellent example using PRMNs deliver the therapeutic gas nitric oxide (NO). NO is an effective therapeutic gas for diabetic wound management as it, like oxygen, is involved in many steps of the wound healing process, including vasodilation and angiogenesis, signal transmission and integration, infection elimination, and immunoregulation.[1198–1200] Therein, Yao et al. reported a porous PRMN that used the photothermal property of GO-encapsulated MOF microparticles (GO-MOF MPs) to control the release of chemisorbed NO.[1193] The porous structure of the PRMN not only increased its surface area, leading to high NO adsorption capacity, but also ensure efficient NO release and diffusion. Such examples demonstrate that PRMN can provide multifunctional wound curing strategies by combining therapeutic delivery, pathogen destruction, and reduced inflammation. However, PRMNs for wound healing have not yet been extensively explored, and therefore there are many opportunities and gaps still available. Different pathogens and wound types, e.g., burns, infections, and cuts), require different therapeutic strategies, and comorbidities, such as diabetes or cancer, can further complicate treatment. Thus, further work on developing synergistic and multi-disease therapies should prove highly valuable.

5.3.3 Diabetes Treatment

As one of the fastest growing and most serious chronic diseases today, diabetes mellitus has gained intense research interest to develop effective yet economical therapies for its treatment. Diabetes is a metabolic disorder caused by either insufficient insulin production (type I, genetic autoimmune disorder) or utilization by the body (type II, adult-onset). This can result in several serious effects including delayed wound healing, nerve damage, cognitive impairment, hyperglycemia, and death. Currently, the main treatments for diabetes include insulin (a peptide hormone, 5.81 kDa) and metformin (a biguanide antihyperglycemic drug, 0.13 kDa). Importantly, insulin can be used to treat both type I and type II diabetes, but metformin can only be used for type II. Metformin is commonly delivered orally, while insulin must be delivered by injection. MN-based treatments can effectively deliver both drugs with high bioavailability by avoiding first-pass hepatic metabolism, gastrointestinal degradation, and providing precisely controlled drug release.[1201] Notably, like many drugs, the exact dose required for each patient depends on several factors, such as their body mass, metabolism rate, age, and diet. Infants can require as little as 5 IU of insulin, whereas overweight patients can require over 80 IU.[1135] Therefore, for MN patches, different doses

should be evaluated for efficacy, rather than a simplified 'one-dose fits all' approach. In the clinic, such flexibility is key to widespread adoption.

Recently, PRMNs have also been adopted for diabetes treatments via the controlled delivery of metformin and insulin.[1202,1203] Zhang et al. fabricated PVP PRMNs that could deliver metformin encapsulated in PDA- and LA-coated mesoporous SiO_2 NPs (Figure 28A).[1075] In vitro and in vivo analyses demonstrated photo-controllable drug release and an improved bioavailability of metformin compared to subcutaneous administration. Alternatively, Liu et al. used photothermal bismuth nanodots to control metformin release.[1089] These MNs produced a remarkable in vivo hypoglycaemic effect; however, compared to PDA, bismuth nanodots have some toxicity concerns.[1204,1205] Therefore, dosage-dependent toxicity and photothermal efficacy must be balanced. Notably, despite insulin being a heat-sensitive protein, Demir et al. successfully managed to deliver insulin via photothermal hydrogel MNs containing molybdenum sulfide (MoS_2) nanosheets (**Figure 33**A).[1086] The presence of MoS_2 improved the mechanical strength of MN patches and restricted the passive or burst release of insulin, minimizing unwanted dosing in both mice and pig models. Upon photothermal heating (980 nm, 0.5 W/cm^2, 10 min), insulin could be released without a noticeable loss in activity, which was attributed to the immobilization of insulin within the polymeric network of polyethylene glycol diacrylate (PEGDA). This strategy protects insulin and other biomolecules by providing a non-interacting environment that stabilizes their conformation via Van der Walls forces, hydrogen bonding, covalent bonding, etc.[1206–1208] Fan et al. also fabricated photothermal hydrogel-based PRMNs containing PEG-immobilized insulin and BP for diabetes treatment without a loss of insulin activity after PTT (Figure 33B).[1209] As such, use of PRMNs for insulin or metformin delivery may prove highly promising, although further work is needed to fully understand the heat response of drugs in different MN formulations. Recently, Montoya et al. published a review covering the use of different porous inorganic materials and organic polymers to improve the thermal stability of proteins, enzymes, and vaccines.[1207] These include several organic polymers that could be incorporated into PRMNs. Importantly, proteins can also be denatured upon physical contact with PRMs. Lee et al. demonstrated that insulin is denatured upon π-π adsorption on graphene whereas no denaturation was observed for electrostatic binding to GO.[1210,1211] By comparison to GO, MoS_2 nanosheets were calculated to have weaker interactions with insulin, further enhancing its stability.[1086]

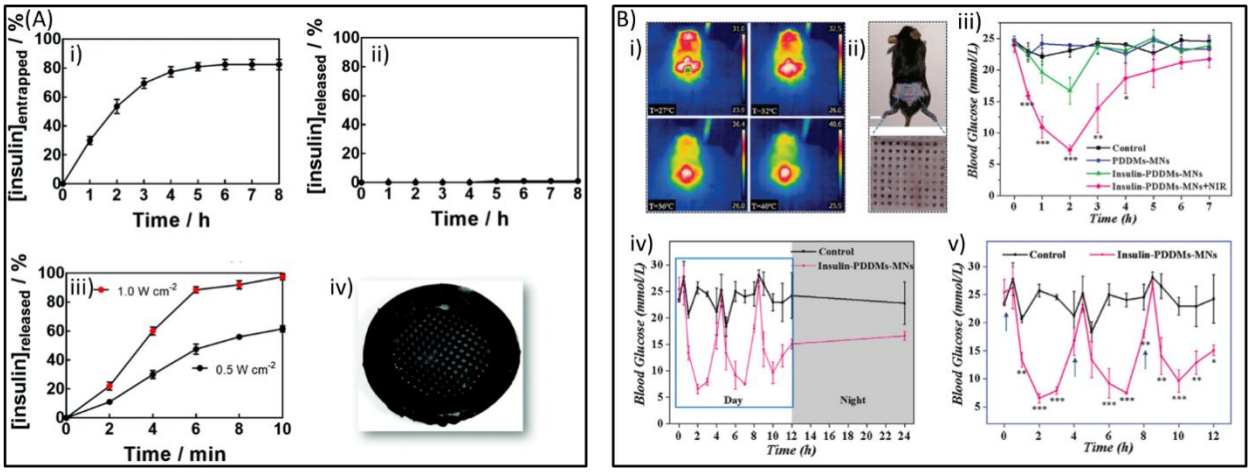

Figure 33: PRMNs for diabetes treatments. (A) Insulin loading and releasing using photothermal MoS_2 PRMNs: (i) Insulin loading at 4 °C over 8 h; (ii) passive drug release profile from the patch into PBS; (iii) in vitro release using different laser power densities at 980 nm for 10 min; and (iv) an SEM image of the patch after photothermal release experiments. Reprinted with permission from Ref [1086] (Copyright Royal Society of Chemistry, 2022). (B) In vivo antidiabetic study: (i) thermal imaging after PRMN insertion during NIR irradiation; (ii) dorsal skin photograph after MNs application; (iii) blood glucose level of diabetic mice undergoing different treatments; (iv) blood glucose level changes during treatment; and (v) a magnified view of daytime blood glucose changes. Reprinted with permission from Ref [1209] (Copyright Wiley-VCH, 2021).

5.3.4 Diagnostics

Another key application for PRMNs is imaging-based diagnostics. Unlike phototherapies, wherein heat or ROS are used, diagnostics use the luminescent properties of PRMs to provide important medical data in response to disease conditions. Some types of PRMs can also be used for photoacoustic, X-ray, and MRI imaging. One simple example of a diagnostic PRMN was provided by Babity et al., who used the decrease in detectable fluorescence as a marker for lymphedema monitoring.[1212] Lymphedema is a disorder characterized by a build-up of interstitial fluid in the extremities due to impaired lymphatic drainage. The authors used dissolvable PVP MNs to tattoo PEGylated Cy7.5 (an NIR fluorescent PRM) to the skin, allowing them to follow lymphatic drainage using in vivo mouse and rat models (**Figure 34**A and B). It was also determined that the MN length and the location of the PRM within the tips were critical to limit the background signal when the dye was not drained from the application site. Additionally, the authors also demonstrated this monitoring using a portable detection technology. This method was later used for a proof-of-concept clinical trial.[1213] Another interesting diagnostic tool for PRMNs is the use of surface-enhanced Raman spectroscopy (SERS) [1214]; a highly sensitive analytical technique that can enhance the detectable Raman signals of analytes by several orders of magnitude. This enhancement is due to the interaction of incoming light waves with localized surface plasmons, collective electron oscillations present

on NP surfaces. At particular wavelengths, the incoming photons and the surface plasmon can resonate, greatly enhancing the Raman scattering signal intensity of surface adsorbed analyte molecules.[1215] If the adsorbate is located in a nanogap between NPs, i.e., a 'hotspot,' the scattering intensity can be further enhanced. Charge transfer between NP surfaces and the adsorbed molecules is also believed to contribute to signal enhancement.[1216] Under ideal circumstances, this enhancement can allow for single-molecule detection.[1217] Using this technique, several papers have documented SERS PRMNs for the detection of bacteria and their metabolites,[1218,1219] pH and redox potential,[1220,1221] and glucose.[1222]

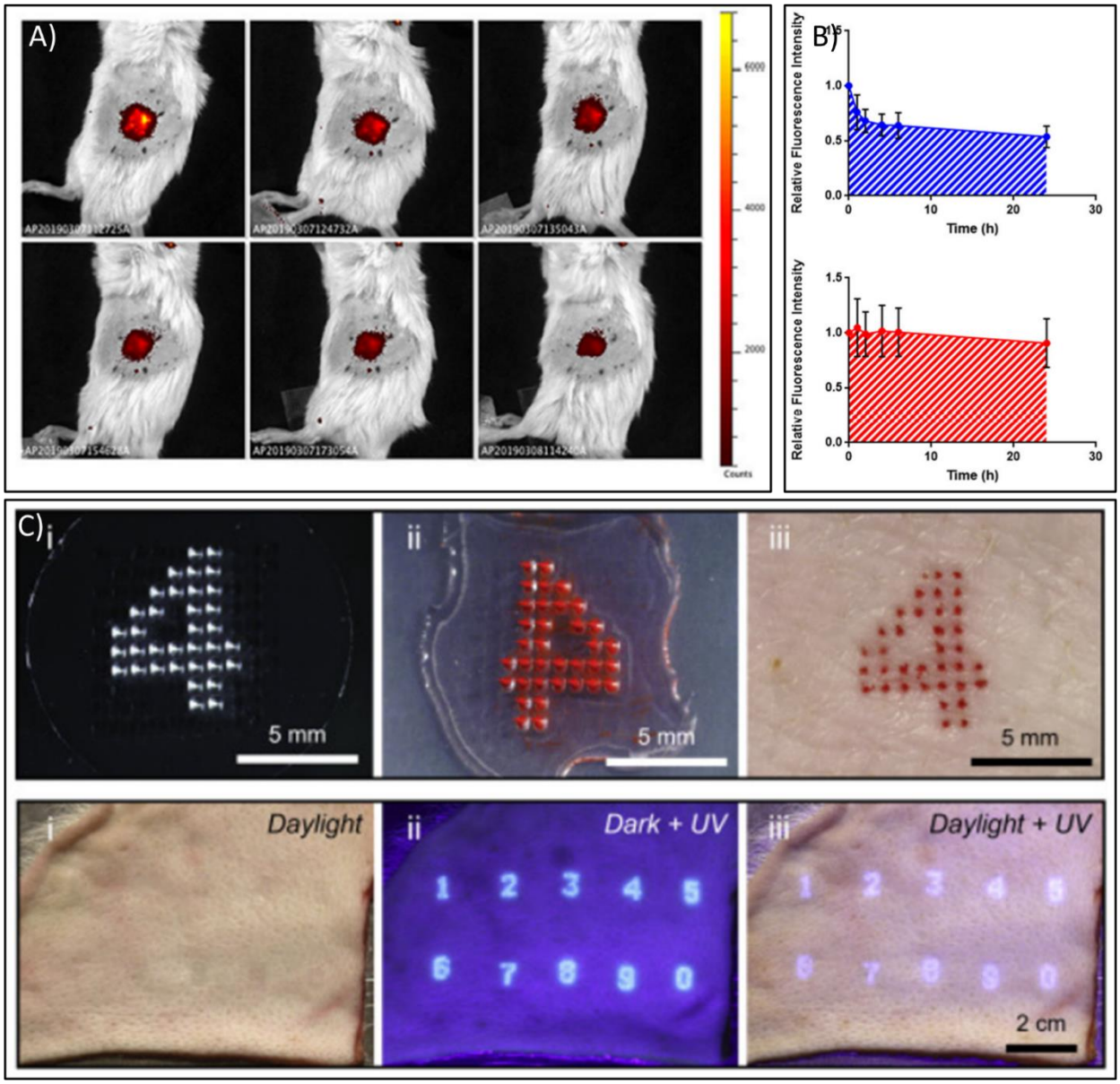

Figure 34: Diagnostic PRMNs. A) Fluorescent PRMs delivered via MNs for the monitoring of lymphatic drainage in mice, showing a decline over time. B) Comparison of fluorescence time for mice with functioning and impaired lymphatic drainage. Reprinted with permission from Ref [1212] (Copyright Elsevier, 2020). C) Representative

microscopy images of a MN patch tattoo. Top: (i) PDMN mold with a "4" pattern; (ii) PRMN loaded with Cy7.5; (iii) porcine skin tattooed by the MN patch ex vivo. Bottom: UV PRMN tattoos in (i) daylight, (ii) in the dark with UV, and (iii) in the day with UV. Reprinted with permission from Ref [1223] (Copyright Cell Press, 2022).

Key to the successful use of PRMNs for disease monitoring is using probes with fluorescence wavelengths that are not absorbed by biological tissue, i.e., NIR light. As such, Liu et al., developed Er^{3+} up-conversion NPs with both excitation (1530 nm) and emission (980 and 1180 nm) in the NIR-II window for the in vivo biosensing of H_2O_2.[1224] Furthermore, upon specific conditions, such as low or high pH, non-PRMs may undergo chemical changes into fluorescent PRMs, or vice versa, that can be detected under light irradiation. By using such conditions as a turn-on signal, the background noise of the probes can be minimized, and specific disorders could be detected. For example, tumor microenvironments are often hypoxic and acidic, diabetes results in higher glucose concentrations,[1225] and inflammation results in the production of ROS. As such, Babity et al. used Cy5 as a turn-on ROS-sensitive probe for the detection of skin inflammation.[1226] Turn off probes have also been developed, with Li et al., for example, using the quenching of fluorescent carbon QDs to measure interstitial Cu^{2+}.[1227] The integration of various stimuli-responsive materials to form smart MNs therefore hold good potential for disease monitoring and sensing. By adding fluorescent PRM to sensing MN sensors, the emitted light can be used as an indicator for when to apply follow-up treatments or use PTT for drug release; however, due to the low volume of the needles, multifunctionality must be balanced against chemical complexity and API loading capacity. Furthermore, some stimuli-responsive materials may generate painful toxic products. For example, glucose oxidase, an enzyme widely used for glucose sensing, produces both H_2O_2 and gluconic acid, which may damage tissue and cause pain or discomfort for patients.[992,1131,1228] Ideally, smart sensing systems should use a combination of materials to reduce the amount or type of unwanted products. In another approach Zheng et al., used fluorescent aptamer-coated hydrogel MNs to detect glucose, adenosine triphosphate, l-tyrosinamide, and thrombin *ex vivo*.[1229] In this way, multiple biomarkers could be detected without generating toxic products.

Diagnostic PRMNs can also be used to deliver medical tattoos containing patient information, such as identity, vaccination status,[1230] or the number of drug doses received. Importantly, the use of fluorescent PRMs allows for tattoos only visible using intense illumination of a specific wavelength (Figure 34B),[1223] although the ethics and risks of such a system should be carefully evaluated. For example, non-visible QR-code tattoos can provide an easy approach to access patient information for clinicians using specialized detectors; however, such devices could be used to discreetly obtain information without patient knowledge. Additionally, the chemotoxicity and phototoxicity of the long-lasting implanted materials must be carefully evaluated to ensure safety. Conventional tattoo ink is typically composed of multiple components, including nanomaterials, chemical binders, and pigments that are then injected into the dermis for long-term retention.

While these inks may be used with MNs, their interactions with any co-delivered therapeutics, e.g., vaccines, must be assessed for treatment efficacy. Notably, PRMNs could be used to create temporary medical tattoos that are slowly removed by lymphatic clearance. This approach could significantly improve security and patient compliance; however, because hospital stays can be of various lengths, the clearance rates of different PRMs should be more closely evaluated to optimize the number of patch applications. MN length should also be evaluated, as PRMs delivered at shallow depths can also be removed by the growth of new skin cells. For this reason, tattoo artists typically deliver ink to a depth of ~1.5–2 mm to avoid fading.

5.4 Conclusions and Outlook

While PRMNs have already demonstrated great promise for disease monitoring, controlled drug release, and potent multimodal disease treatments, the technology is still in its preliminary stage and several issues must be addressed to further advance its applications. First, the key to success in clinical applications is the development of a fundamental understanding of the mechanisms governing light-matter interactions. Such knowledge is critical for PRMN fabrication, optimization, and application while achieving high efficacy and low toxicity. For example, light penetration depth is mainly determined by its wavelength but is also affected by the materials used to prepare the backing layer of the MN patches and the properties of the skin, which varies among different body locations and patients. Sandby-Møller et al. found the mean thickness of the epidermis were 56.6, 70.3, and 81.5 μm at the forearm, shoulder, and buttock, respectively.[1231] Laurent et al. found that the average overall skin thickness (dermis + epidermis) was 2.54, 2.02, 1.91, and 1.55 mm at the suprascapular, deltoid, waist, and thigh.[1232] Many light wavelengths can therefore pass through the stratum corneum and epidermis of most patients; however, only certain wavelengths, i.e., NIR, can penetrate deeply into the dermis. The light source must be powerful enough to excite the PRMs to generate the expected therapeutical outcome, but not so strong as to induce adverse effects on the skin tissue. As noted by Joensen et al., consideration of the patient's skin pigmentation is also important for phototherapy safety.[1113] Factors, such as uneven or wrinkled skin, can further alter the average skin thickness and prevent uniform dose distribution. Patient age and sex are also known to influence skin thickness.[1233] Individual pain thresholds, immune responses, and API dose requirements should be considered in these designs. Finally, large-scale MN manufacture and storage with various compositions, particularly those containing temperature sensitive APIs, is still a critical issue that must be addressed before MNs can be widely and cost-effectively applied in clinical settings. While further work is needed, understanding and overcoming these issues can promote the development of personalized MN and PRMN patches. Compared to conventional MN patches, personal PRMN and smart-PRMN patches can offer improved control of drug release.

PRMNs also have inherent limitations. Like any other MN, they suffer from limited API loading capacities and thus are only applicable for delivering highly potent therapeutics that are effective at low doses. As such, released PRMs that have high reactivity, but poor clearance, may present chemical- or photo-toxicity. The discoloration of skin is another issue related to dyes, pigments, and NPs. Tatovic et al., for example, found that ultrasmall gold nanoparticles delivered via a MN system resulted in local changes in skin pigmentation for several months.[1234] More efforts are required to study the diffusion and clearance of various nanomaterials and therapeutics, including small molecules, polymers, and biologics with different physicochemical properties, within the skin (epidermis and dermis) and subcutaneous tissues. Therapeutics that are notably light- or heat-liable are also unsuitable for many PRMN designs. In addition to PTT, UV photo-crosslinking and heat treatments are commonly used for MN fabrication, which may inactivate encapsulated biologics or drug compounds. Unintended protein absorption onto nanomaterial surfaces could also lead to inactivation and unwanted immune responses.[110] Furthermore, due to the limited penetration of light compared to X-rays, invasive techniques are needed to deliver light to internal tumors or disease sites.

In summary, the combination of MNs with light may offer advanced technologies for phototherapies and medical diagnosis. Although several photoresponsive strategies have been exploited by PRMNs, there are still many photochemical reactions and photobiological approaches that can be used in novel PRMN designs. For example, UV-PRMNs may be explored as previous research showed great promise using UV-responsive polymers/drugs to treat wounds, although the technical concerns regarding the high phototoxicity and poor UV penetration must first be addressed. In addition, non-photoresponsive MNs have been explored for scalp, ocular, oral mucosal, gastrointestinal, ungual, anal, and vaginal drug administration [1235–1237]. As many of these locations can be easily irradiated with light, PRMNs could also be deployed for such treatments. While there are limited reports of MNs being used to deliver radiosensitizers, this strategy has not yet been examined using PRMNs; however, PDT and PTT have previously been reported to enhance RT. The use of PRMNs for vaccination against diseases other than cancer may also have advantages owing to the immunostimulatory effects of mild photothermal therapy. As such, further research into this technology should prove extremely valuable for global healthcare.

~ Chapter 6 ~

Accelerated Cascade Melanoma Therapy using Enzyme-Nanozyme-Integrated Dissolvable Polymeric Microneedles

The work presented in this chapter has been published as:

Singh, P.*, Chen, Y.*, **Youden, B.***, Oakley, D., Carrier, A., Oakes, K., Servos, M., Jiang, R., and Zhang, X. Accelerated Cascade Melanoma Therapy using Enzyme-Nanozyme-Integrated Dissolvable Polymeric Microneedles. *International Journal of Pharmaceutics*, **2024**, 652, 123814. DOI: 10.1016/j.ijpharm.2024.123814.

**These authors contributed equally to this work.*

Chapter Summary

Dissolvable polymeric microneedles (DPMNs) have emerged as a powerful technology for the localized treatment of diseases, such as melanoma. Herein, we fabricated a DPMN patch containing a potent enzyme-nanozyme composite that transforms the upregulated glucose consumption of cancerous cells into lethal reactive oxygen species *via* a cascade reaction accelerated by endogenous chloride ions and external near-infrared (NIR) irradiation. This was accomplished by combining glucose oxidase (Gox) with a NIR-responsive chloroperoxidase-like copper sulfide (CuS) nanozyme. In contrast with subcutaneous injection, the microneedle system highly localizes the treatment, enhancing nanomedicine uptake by the tumor and reducing its systemic exposure to the kidneys and spleen. NIR irradiation further controls the potency and toxicity of the formulation by thermally disabling Gox. In a mouse melanoma model, this unique combination of photothermal, starvation, and chemodynamic therapies resulted in complete tumor eradication (99.2 ± 0.8% reduction in tumor volume within 10 d) without producing signs of systemic toxicity. By comparison, other treatment combinations only resulted in a 42–76.5% reduction in tumor growth. The microneedle patch design is therefore not only highly potent but also with regulated toxicity and improved safety.

6.1 Introduction

Malignant melanoma is an aggressive cancer that causes ~75% of skin-cancer-related deaths and commonly occurs among the Caucasian population.[1238–1240] Current therapies including surgery, chemotherapy, and radiotherapy, have several limitations such as high costs and complex infrastructure requirements, severe side effects, long recovery times, scarring, and disappointing outcomes resulting from innate drug or radiation resistance.[1241] Therefore, the development of cost-effective, safe, and minimally

invasive treatment strategies is needed. In the past two decades, significant research efforts have been drawn to highly tunable nanomedicines that can combine multiple treatment modes into a single package.[59,1242,1243] Among these, catalytic platforms using chemodynamic therapy (CDT) that exploits potent reactive oxygen species (ROS) generated in situ, have gained particular attention.[154,981,1244–1249] These strategies use metallic nanoparticles (NPs) with enzyme-like activities (nanozymes), which have the advantages of low cost, high stability, and durability.[159,1250,1251] However, similar to many chemotherapeutics, concerns over the delivery efficiency and systemic toxicity of nanomedicines have limited their development and application.

Recently, copper sulfide (CuS)-based nanomaterials have emerged as catalytic platforms based on their peroxidase-like reactivity, which accelerates the conversion of the less toxic endogenous chemical hydrogen peroxide (H_2O_2) to potent ROS. Notably, the ROS generation of Cu-based Fenton-like systems is significantly enhanced by endogenous Cl^- (~110 mM).[112,784,987,1009,1010] This unique chloroperoxidase (CPO)-like activity has implications for the design and optimization of Cu-based Fenton therapeutics, particularly in the skin due to the presence of salt in sweat; however, this property has largely neither been studied nor accounted for.[1006] Additionally, compared to free copper ions, which can generate ROS at circumneutral pH and are thus toxic, CuS has demonstrated good biocompatibility due to its low dissolution rate and weak activity above pH 4–5.[1252–1254] The composition and crystal lattice of CuS also allows for photothermal therapy (PTT; the generation of heat by NIR photons). Together, these properties make CuS highly attractive for cancer therapy.

Despite their potential, a key limitation towards in vivo use of CuS and similar nanozymes is the low concentration of endogenous H_2O_2 in tumors ($\leq$ 100 μM), which is insufficient for killing cancerous cells that are normally resistant to oxidative stress.[1255,1256] To overcome this, our group developed a glucose oxidase-copper sulfide nanocomposite (Gox-CuS NC) that used tumor glucose as a source of H_2O_2. Due to their altered metabolism, cancer cells are highly susceptible to changes in glucose concentration, enabling Gox to act as a therapeutic agent by starving the tumor. The H_2O_2-could then be exploited by the CuS NPs for ROS generation in combination with external NIR irradiation and endogenous Cl^-. Therefore, this simple enzyme-nanozyme composite synergistically combined starvation therapy (ST), CDT, and PTT for effective melanoma treatment following intravenous injection. However, intravenous applications of Gox come with their own risk of systemic toxicity due to Gox's non-tissue-specific catalytic activity, resulting in side effects such as hypoglycemia. As such, it is challenging to deliver optimal doses that are safe but effective.[1246]

Since most superficial tumors are easily accessible, we propose the use of dissolvable polymeric microneedles (DPMNs) to deliver Gox-CuS. DPMNs are self-administrable arrays of micron-scale needles

that can painlessly deliver therapeutics through the superficial layers of the skin to treat both local and systematic diseases (depending on needle design).[1041,1043–1045,1133,1140,1257] Compared to injections, MNs can avoid mucosal irritation, first pass metabolism, and the need for specialized practitioner training. Furthermore, many DPMNs can retain the bioactivity of proteins, such as enzymes and antibodies, immobilized in the DPMN matrix under ambient storage conditions, facilitating their distribution and use in remote communities without the need for cold supply chains.[1043,1258–1262] The use of MNs to deliver agents for phototherapies has also recently demonstrated significant success.[113,1167,1189,1263] In the case of Gox-CuS, DPMNs would allow the nanomedicines to be efficiently delivered to skin tumor sites, reducing the need to protect Gox during circulation. Once the treatment has been applied, Gox can be denatured in the tumor/skin before entering the blood or lymph, either through photothermal deactivation or endogenous proteases. In this way, the NCs become self-limiting to prevent chronic or systemic toxicity. In combination with biocompatible CuS, endogenous Cl^-, and external NIR to generate significant levels of ROS and heat, the activity of even a small amount of Gox can be fully exploited in a controllable means without the risk of long-term toxicity. We hypothesized that delivering the Gox-CuS NCs using DPMNs may be a powerful strategy for melanoma treatment (**Scheme 4**) as it enhances the localized cargo delivery, thus improving both its treatment efficacy and safety. Herein, we validate the hypothesis and demonstrate the efficacy of this approach using a mouse model, highlighting an inexpensive, simple, and multimodal platform for cancer treatment.

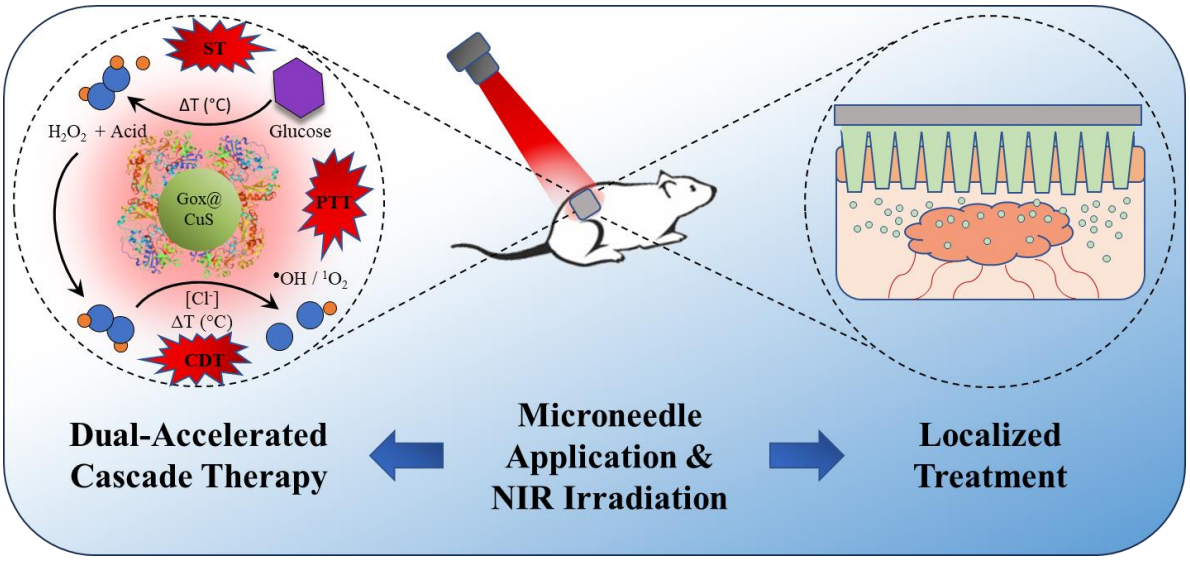

Scheme 4: Schematic for melanoma treatment using Gox-CuS in dissolvable polymeric microneedles (DPMNs).

6.2 Experimental

6.2.1 Materials

Copper chloride dihydrate ($CuCl_2$•$2H_2O$) was purchased from Shanghai Medin Co., Ltd. Sodium citrate was purchased from J&K Chemical Co., Ltd. Polyvinylpyrrolidone (PVP 30K, MW = 30000 g/mol) and poly(vinyl alcohol) (PVA 30K, MW = 30000 g/mol) was obtained from Sangon Biotech (Shanghai, China). Glucose oxidase (Gox) was purchased from J&K Chemical Co. Ltd., (China) 3-[4, 5-dimethylthiazol-2-yl]-2,5-diphenyl tetrazolium bromide (MTT) was purchased from Beyotime Institute of Biotechnology (Haimen, China). The MN mold was supplied by Zhongcheng 3D Technology Co., Ltd. (Beijing, China). The human breast cancer cell line MDA-MB-231 and human skin melanoma cell line A375 were obtained from the China Infrastructure of Cell Line Resource (Beijing, China). Fetal bovine serum (FBS) and the cell culture medium were obtained from Invitrogen Life Technologies (Carlsbad, CA, USA). ALT and AST assay kits were obtained from Elabscience Biotechnology Co. Ltd., (Wuhan, China). Sodium sulfide nonahydrate (Na_2S•$9H_2O$), acetic acid, sodium acetate, sodium chloride, 3,3',5,5'-tetramethylbenzidine (TMB), 2,2'-azino-bis(3-ethylbenzothiazoline-6-sulfonic acid) (ABTS), SnakeSkin™ 10 kDa molecular weight cutoff dialysis tubing, hydrogen peroxide (H_2O_2), isopropyl alcohol (IPA), and singlet oxygen sensor green (SOSG) were purchased from Thermo Fisher Scientific (Waltham, MA, USA). Sodium hydroxide (NaOH), hydrochloric acid (HCl), coumarin, and dimethyl sulfoxide (DMSO) were purchased from Alfa Aesar. All chemicals were used as received without further purification.

Sodium acetate buffers (NaOAc buffer, 0.1 M, pH 3.6–5.6) were prepared by mixing acetic acid and sodium acetate and adjusting the pH using HCl and NaOH. Stock solutions of terephthalic acid (TPA) were prepared by dissolving the pure sample in water, slowly adding 1 N NaOH with mixing until the sample dissolved, and then neutralizing the pH with an equal volume of 1 N HCl. Stock solutions of coumarin were prepared by dissolving the powder in water and stirring under low heat (<60 ºC). All UV-sensitive compounds were stored in the dark until use.

6.2.2 Fabrication and Characterization of CuS NPs and Gox-CuS NCs

CuS NPs were prepared as previously reported.[112,1016] Briefly, 10 mg of $CuCl_2$•$2H_2O$ and 10.7 mg of trisodium citrate were first dissolved into 30 mL of nanopure water and mixed using a magnetic stir bar. To this solution, 50 µL of a 743.92 mg/mL solution of Na_2S•$9H_2O$ was rapidly added and the temperature increased to 90 ºC. Following the addition of Na_2S, the pale blue copper solution rapidly turned to a dark golden brown, and then dark green indicating the formation of CuS. After 30 min of reacting under heat, the solution was removed from the hotplate, allowed to briefly cool, and then dialyzed against 2 L of

nanopure water to remove most impurities. The NPs were then stored at 4 ºC until use. For most experiments, NPs were used within 48 h to minimize the risk of Cu ion dissolution.

Gox (10 mg) was conjugated onto the CuS NPs by adding it to 30 mL of the prepared CuS NPs and shaking for 10 min. The nanocomposite was then separated from the free NPs and enzymes by size-exclusion chromatography using Sephadex G-50 pre-equilibrated with 0.1X PBS (pH 7.4). After separation, the nanocomposite was freeze-dried and stored in a freezer (-20 ºC) for future use. The synthesized NCs were also characterized by transmission electron microscopy (JEM-1400 TEM, 40–120 kV) to confirm the particle size and morphology.

6.2.3 CuS Catalysis and ROS Detection

All experiments were performed in 200 µL volumes in 96-well plates. To analyze ROS production broadly, ABTS and TMB oxidation were measured at 420 and 652 nm respectively with different combinations of NaCl (50 mM), CuS (200 µM), and H_2O_2 (200 mM) in NaAc buffer (pH 4.0, 50 mM). Coumarin oxidation to form umbelliferone (λ_{EX} = 325 nm, λ_{EM} = 452 nm) was performed as above by replacing ABTS or TMB with coumarin. SOSG oxidation (λ_{EX} = 485 nm, λ_{EM} = 504 nm) was performed in pH 5.5 MES buffer (100 mM) with 400 mM H_2O_2 and NaCl due to its lower sensitivity. For kinetic experiments, absorbance or fluorescence measurements were made every 30 s over 5–10 minutes. Hydroxyl radical scavenging experiments were performed as above but with the additional presence of 10% v/v IPA.

6.2.4 Fabrication of DPMN Patches

Briefly, the MN molds were treated with O_2 plasma (Mingheng Science and Technology Development Co., Ltd., Chengdu, China) for 20 s, and then 150 µL of polymer solution (50:50 PVP/PVA) was added immediately after. The MN polymerization was set at 40 ºC for 24 h. After that, the surfaces of the MNs were attached to adhesive tape and the MNs were gently peeled off from the mold and stored in a desiccator until use. To load the patches with Gox, CuS NPs, or Gox-CuS NCs, the above was performed with polymer solutions containing various concentrations of the therapeutics. Polymer solutions were sonicated to ensure polymer dissolution. All solutions were also centrifuged at 8000 rpm for 5 min to remove air bubbles.

6.2.5 Characterization of DPMN Patches

To check the dimensions and morphology of the Gox-CuS loaded MNs, the DPMN patches containing 50 nM CuS-Gox were broken into pieces and scattered onto conductive tape along with CuS and Gox-loaded patches. The samples were sputter-coated with 8 nm of platinum using a Leica SCD500

cryo sputter coater (Leica Microsystems, Vienna, Austria) for 30 s. After that, the samples were imaged under a ZEISS SUPRA 55 scanning electron microscope (SEM; Carl Zeiss, Oberkochen, Germany). Images were also taken using a cellphone camera and a 45× hand-held loupe microscope (YIMOO, Shenzhen, China). The distribution of the CuS NPs in MNs was also examined using FTIR.

The mechanical strength of DPMNs patches was measured using a Universal Testing Machine (AI-7000S, Gotech, Taiwan), with a plate moving speed and a maximum loading force of 10 μm/s and 50.0 N, respectively. Measurements were taken every 0.001 s to obtain the stress-true strain relationship. All the tests were performed in triplicate.

To examine the photothermal nature of the CuS-loaded DPMNs, patches were irradiated with NIR light (850 nm) at a power density of 1.5 W/cm^2 for 10 min. During irradiation, the temperature and morphological changes in the MNs were recorded by a FLIR infrared thermal imaging camera.

6.2.6 Skin Insertion Ability of the Gox-CuS DPMN Patches

PVP/PVA MNs with different CuS-Gox NP concentrations were applied to test the skin penetration ability. Initially, the abdominal skins of healthy Kunming strain mice (15–20 g, the Laboratory Animal Center of Southern Medical University) were isolated and washed with 75% ethanol followed twice by 0.9% NaCl. Residual water on the skin surface was removed using filter paper, and the skins were fixed on glass slides for use. Next, the DPMN patches were inserted into the skins gently and vertically, and a 200 g weight was placed on the surface of the patches for 5 min. After another 10 min for complete polymer dissolution, the patches were removed. The isolated skin sections were then put into a -80 ºC freezer for about 10 min before being embedded in an Opti-Mum Cutting Temperature (OCT) compound in a cryostat mold. The frozen samples were cut into 10 μm thick sections using a cryotome (Leica RM 2235, Leica Microsystems Nussloch GmbH, Nussloch, Germany) and viewed under an inverted microscope (Leica DMI4000B, Leica Co. Ltd., Bensheim, Germany).

6.2.7 Cell culture

MDA-MB-231, A375, and HEK-293 cells were cultured in RPMI-1640, DMEM, and EMEM media, respectively, supplemented with 10% FBS, 100 μg/mL penicillin, and 100 μg/mL streptomycin. The cells were cultured at 37 ºC in an atmosphere of 5% CO_2 and passaged every 2–4 d.

6.2.8 In Vitro Cytotoxicity assay

Cell viability was determined using the MTT assay. Briefly, MDA-MB-231 cells and A371 cells were first seeded in 96-well plates at a density of 5×10^3 cells/well. After attaching overnight, the medium was changed with fresh medium containing MN and CuS-Gox-MN solution. After an overnight treatment, MTT solution (0.5 mg/mL) was added into each well and incubated for 4 h. The solution was then replaced by 1-200 µL of DMSO and the absorbance was measured using a SpectraMax M5e (Molecular Devices, San Jose, CA, USA) at 570 nm. Samples were prepared in triplicate.

6.2.9 In Vivo Antitumor Efficacy of the DPMN Patches

The experimental procedures were designed based on the guidelines on animal care and use of Principles of Laboratory Animal Care (NIH publication no. 86-23, revised 1985) and approved by the Committee on Ethics of Shenzhen Glorybay Biotech Co., Ltd. (No. 12W-IACUC-22-0024).

Female BALB//c-nu/nu nude mice (11–13 g, 21–28 d) were supplied by Zhuhai BesTest Bio-Tech Co., Ltd. (Guangdong, China). The mice were used to evaluate the antitumor efficacy of CuS-Gox DPMNs in vivo when their body weight reached 10–13 g. In detail, 100 µL of a 5×10^6 cells/mL A375 cell suspension were subcutaneously injected into the left flank of the BALB/c-nu/nu mice. When the tumor volume grew to 70–100 mm^3, the mice were randomly divided into six groups (six mice per group): 1) a saline (PBS) control, 2) CuS NPs DPMNs, 3) CuS NPs DPMNs with NIR irradiation (λ = 850 nm, 1.5 W/cm^2, 10 min), 4) Gox DPMNs, 5) Gox-CuS DPMNs and, 6) Gox-CuS DPMNs with NIR irradiation. Each DPMN patch was inserted into the skin near the tumor site with a thumb press for 5 min and left in place for 20 min before being removed. The mice were treated and examined for tumor volume and body weight every 2 d, with a humane endpoint being established at a maximum tumor size of 2 cm in any direction. For larger tumors, animal behavior and signs of ulceration were also monitored to avoid undue stress. Based on these considerations, on day 11 all mice in each group were euthanized for further analysis.

6.2.10 Monitoring of Blood Glucose Levels

To evaluate the therapeutic efficacy of Gox delivery (starvation therapy) by DPMNs, the blood glucose level of each mouse was measured every other day with a glucometer (Sinocare Inc.) and digital glucose chip. The blood was collected from the tail of the mice to measure the blood glucose level.

6.2.11 In Vivo Toxicity Evaluation

Histological and hepatotoxicity evaluations were performed to examine the toxicity of the DPMN patches. For histological evaluation, on the day after the last treatment, two mice per group were euthanized at random, and sections of the main organs were collected and stained with hematoxylin and eosin. To examine liver toxicity, the blood of each group's mice was collected directly from the eyes 24 h post-injection. The blood samples were stored at 4 ºC overnight and then centrifuged at 3000 rpm for 20 min to separate the plasma. Plasma levels of AST and ALT were then assayed according to the protocols recommended by the manufacturer.

6.2.12 Blood Plasma Concentration of Gox-CuS

To monitor the blood plasma level of the Gox-CuS NCs 2 h after administration by DPMNs, treated mice were euthanized and blood was collected and stored in the refrigerator (4 ºC) for 4 h. In the next steps, samples were centrifuged at 3000 rpm for 20 min, plasma (100 µL) was collected, and then 2% v/v HNO_3 and H_2O_2 (50 µL) were added and stored for 2 d at room temperature. After that, the solvent was heated to evaporate until 5–10% remained. Finally, 1 mL water was added to the samples and sent for ICP-MS analysis (Thermo Fisher Scientific, model iCAPQ, instrument no KJ/JC094). The conditions for analysis in KED mode were: a radio frequency power of 1550 W, atomization chamber temperature of 2 ºC, sampling depth of 5.0 mm, and flow rates for plasma gas, carrier gas, auxiliary gas, and helium of 14.0 L/min, 0.80 L/min, 1.06 L/min, and 4.40 mL/min, respectively. All the samples were measured in triplicate.

6.2.13 Biodistribution Study

To evaluate the biodistribution of the Gox-CuS NCs 2 h after drug administration by DPMNs or tail-vein injection, the mice were euthanized and the major organs (liver, spleen, kidney, lungs, and heart) and tumor tissue were removed. Every organ was weighed and cut into small pieces and then treated with 1 mL of HNO_3 and 1 mL of H_2O_2 to dissolve and release Cu^{2+} into the medium. After 2 d incubation at 4 ºC, the HNO_3 and H_2O_2 were evaporated by heating to 100–110 ºC until 5–10% of the solution remained. To this, 2 mL of water was added to the samples, which were then centrifuged and filtered for ICP-MS analysis.

6.3 Results and Discussion

6.3.1 Synthesis and Characterization of CuS NPs and Gox-CuS NCs

CuS NPs were synthesized following an established approach using $CuCl_2 \cdot 2H_2O$ and $Na_2S \cdot 9H_2O$ as Cu^{2+} and S^{2-} precursors, respectively.[1016] The resultant spherical NPs were ~8 ± 2 nm in diameter (**Figure S28**), which were well-dispersed in water with a significant negative surface charge from citrate capping (ξ = -28 mV). Gox was conjugated to the CuS NP surfaces via adsorption by simple mixing (10 min) before separating the NCs using size-exclusion chromatography. The conjugation of Gox, which has roughly the same size as the NPs, approximately doubled the resulting NC size.[112]

6.3.2 Catalytic Mechanisms of CuS NPs

Unlike Gox, whose mechanism is well established, the chloroperoxidase-like activity of CuS NPs is less understood. We therefore first demonstrated the ability of the CuS NPs to effectively generate ROS by monitoring the oxidation of the colorimetric probes TMB and ABTS and the fluorescent probes coumarin and singlet oxygen sensor green (SOSG). TMB and ABTS are non-selective ROS probes that generate blue/green-colored radicals (λ_{max} = 652 and 420 nm, respectively) upon exposure to most oxidants, with the notable exception of H_2O_2.[1264] As such, their oxidation can be used to monitor the overall ROS generated in the system. When either probe was mixed with H_2O_2 alone, no significant changes were observed; however, when both H_2O_2 and CuS NPs were introduced in the solution under acidic conditions (**Figure S29**), the probes could be oxidized to produce visible signals (**Figure 35**A and B). Notably, TMB could be oxidized much more easily than ABTS, with significant oxidation of the latter only being observed in the presence of NaCl (Figure 35B and **Figure *S30***). We also demonstrate that Cl^- can accelerate the production of •OH that oxidizes coumarin in the presence of CuS and H_2O_2 (Figure 35C). Herein, coumarin is selectively converted to fluorescent umbelliferone (λ_{EX} = 325 nm, λ_{EM} = 452 nm) by reacting with •OH, which has the highest redox potential of the possible ROS species.[1265,1266] However, interestingly, the use of a high concentration of an •OH scavenger, isopropyl alcohol (IPA), did not inhibit TMB oxidation and only partially inhibited ABTS oxidation (Figure 35A and B). This suggests that while •OH is generated, other radicals, such as singlet oxygen, likely dominate. The generation of singlet oxygen was confirmed when using SOSG as a selective probe [1267]; importantly, Cl^- also accelerated the production of singlet oxygen, consistent with previous research of nanozymes exhibiting CPO-like activity.[784,987,1010]

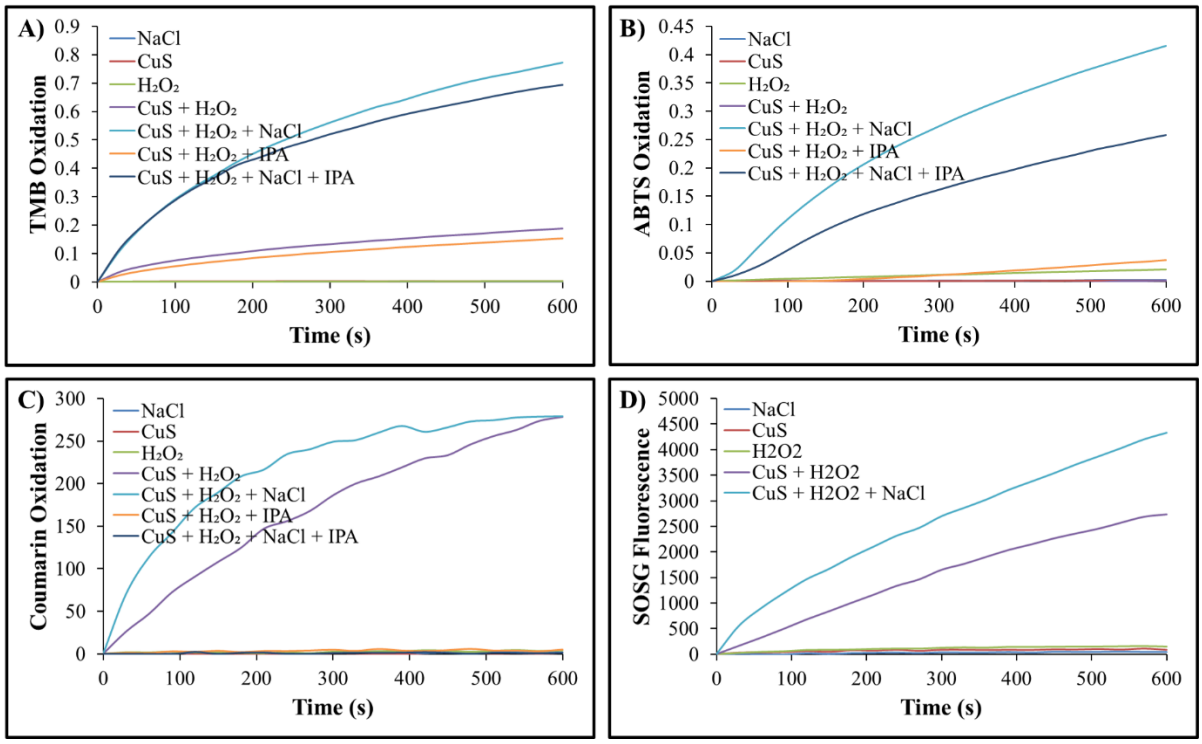

Figure 35: Measurements of generated ROS by (A) TMB, (B) ABTS, and (C) coumarin in the presence of different reactants and the •OH scavenger IPA. D) Measurements of singlet oxygen generation using SOSG.

The enhanced ROS production under NIR irradiation (808 nm, 1.0 W/cm^2) was also demonstrated using ABTS (**Figure 36**A). Notably, the enhanced ABTS oxidation rate due to NIR is independent of the acceleration provided by Cl^-. The accelerative effect from NIR appeared to increase more strongly with extended irradiation time, suggesting the acceleration may be due to the increase in temperature and thus the reaction kinetics, instead of photocatalysis. In contrast, Cl^- could rapidly increase the reaction rate from the beginning, indicating a different catalytic mechanism where Cl^- served as a co-catalyst. As such, the two accelerants could be combined to produce a synergistic effect, resulting in the overoxidation of ABTS into a yellow product (measured at 475 nm).[1268,1269] This can also be observed as a decrease in absorbance at 420 nm with increasing laser irradiation, showing a color change in sample solutions from blue to green/yellow (**Figure S31**). During extended reaction times, the yellow product could also be degraded in the presence of both accelerants. Since NIR irradiation is highly tunable in terms of its wavelength, power, focal point, and irradiation time, personalized microneedle treatments can be achieved according to the location, size, and depth of the tumor/skin lesion. Furthermore, NIR irradiation also provides a convenient means to control the toxicity of the Gox-CuS NC by decoupling the catalytic chain reaction as it can denature Gox via the strong photothermal effect on the CuS NP surfaces (**Figure S32**).

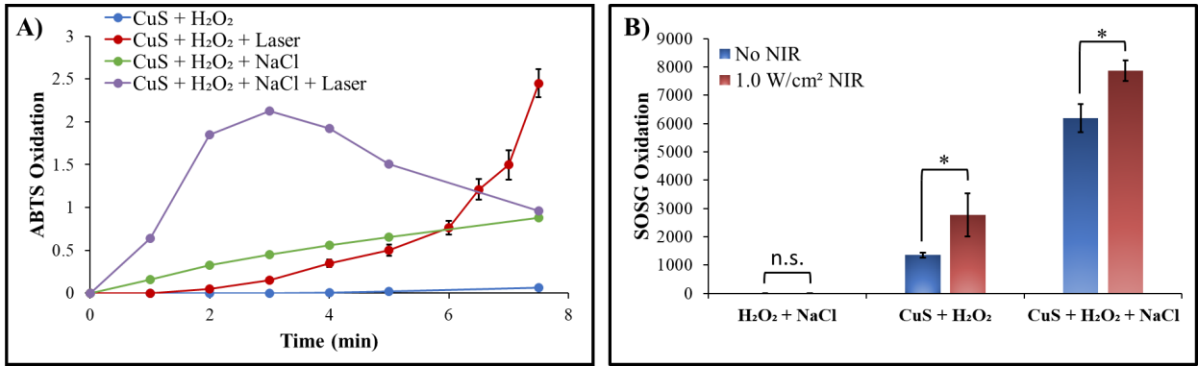

Figure 36: Effect of NIR irradiation time on the oxidation of ABTS (A) and SOSG (B) in the presence of different reactants. *$p < 0.05$. Error bars indicate the mean standard deviation ($n = 3$).

6.3.3 In Vitro Efficacy of the CuS NPs and Gox-CuS NCs

Due to their low dissolution rate and activity at circumneutral pH, CuS NPs are commonly found to be nontoxic without Gox to present them with sufficient acid and H_2O_2 concentrations.[1253] Herein, we demonstrate their biocompatibility using both an A375 melanoma cell model (**Figure 37**A; used to establish the in vivo model) and an MDA-MB-231 breast cancer model (Figure 37B; an independent control). Without Gox, CuS showed low toxicity; however, with Gox even a very dilute Gox-CuS NC solution (3–5 nM) could produce a significant cell-killing effect. Importantly, despite such potency, the ROS generated by the NC are short-lived (< 3.5 μs with a diffusion distance of < 300 nm within the body [1270]) and thus localize their reactivity within the tumor site, minimizing their systemic toxicity. When delivered via microneedles, this toxicity is further localized. Additionally, Gox as a protein will inevitably be degraded by cellular proteases, thus limiting its long-term toxicity even in the absence of NIR irradiation-based deactivation.

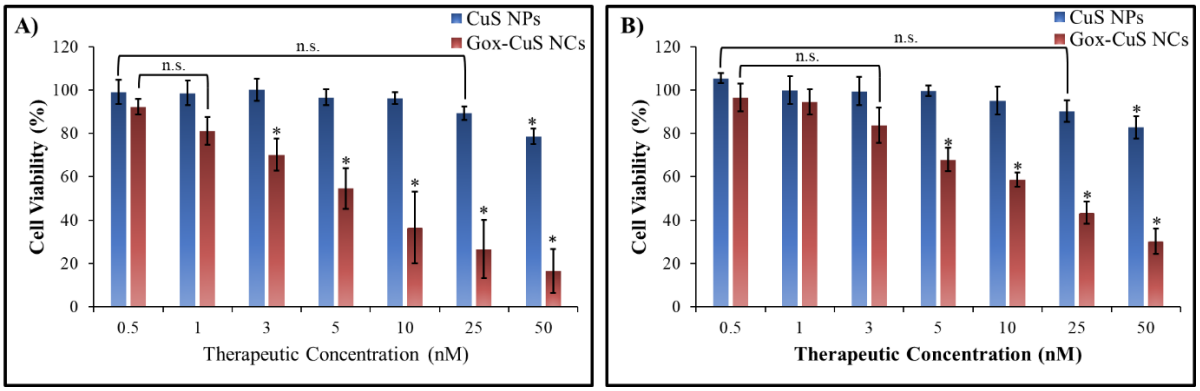

Figure 37: Cell viability assays of (A) A375 cells and (B) MDA-MB-231 cells after exposure to CuS NPs and Gox-CuS NCs. *$p < 0.05$. Error bars indicate the mean standard deviation ($n = 3$).

6.3.4 Fabrication and Application of Dissolvable Polymeric Microneedles (DPMNs)

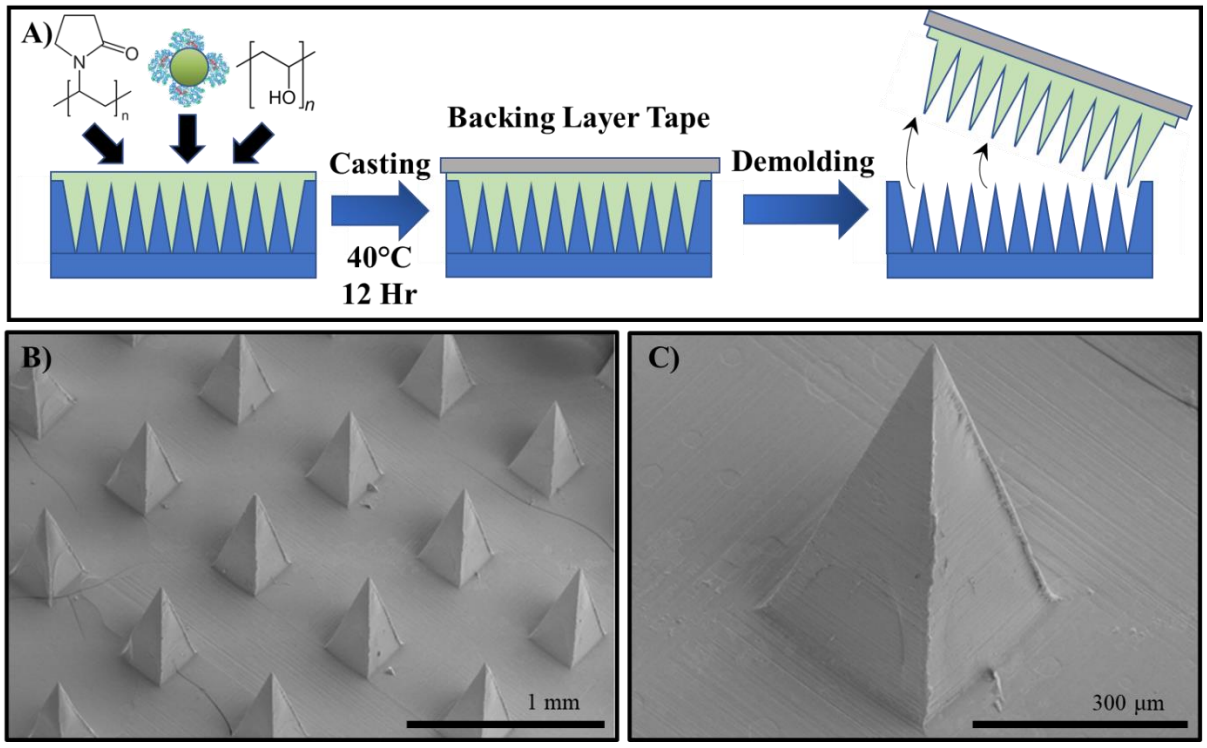

Figure 38: (A) Simplified schematic of the PVP/PVA-based DPMN patch fabrication. (B) DPMN patch morphology and (C) a single MN.

The microneedle (MN) fabrication procedure is simple and straightforward (**Figure 38**A). Sufficient mechanical strength for skin penetration was achieved by a combination of two common biocompatible polymers (1:1), polyvinylpyrrolidone (PVP) and polyvinyl alcohol (PVA), encapsulating the Gox-CuS NCs (Figure 38). The DPMN patches (**Figure 39**A) consisted of 10 × 10 square pyramidal MNs with a 250 µm base width, 700 µm height, ~10 µm tip width, and 800 µm needle center-to-center spacing. The mechanical strength of the fabricated CuS-Gox-DPMNs had a failure force of 0.189 N, which is larger than the threshold of 0.15 N required to penetrate the *stratum corneum* (Figure 39D inset). These low levels of force enable easy application by medical personnel or individual patients without the need for an applicator; however, caution must be made during transportation and handling to avoid prematurely breaking the needles.[1271] For application, the DPMN patches were applied to the mice manually for 5 min and then left in place for another 20 min (Figure 39B) until the MNs completely dissolved within the skin (Figure 39C).[1272] The application of the patches did not result in any long-term damage to the skin, though a temporary indentation was left immediately allowing patch removal (Figure 39D). Although the probability of microorganisms to enter the skin via holes created by MNs is negligible, the introduction of a self-sterilization mechanism into the MN design can minimize the risk.[1273] Similar to graphene oxide,[1090]

CuS NPs have been demonstrated effective in antibacterial applications both with and without NIR irradiation, which assisted in wound cleaning/healing.[1274–1276] After application, the patches can be easily disposed of due to their non-toxic biodegradable components and lack of sharps waste.

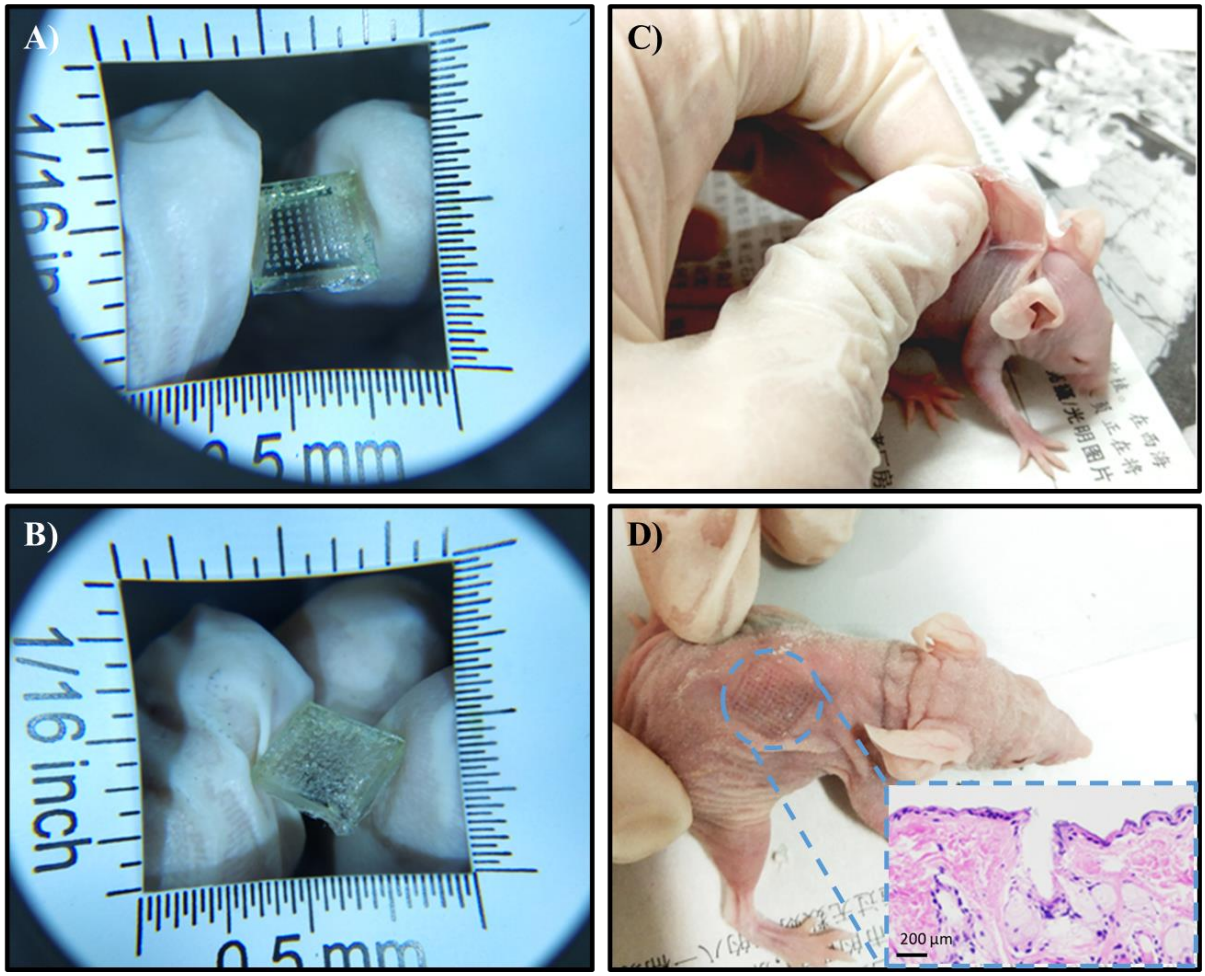

Figure 39:Skin insertion of CuS-Gox-MNs in a nude mouse. Photographs of MNs (A) before and (B) after insertion into the mouse skin, and the mouse (C) during and (D) after application, showing that MNs can puncture and then dissolve completely with little trauma. Inset: A representative histological image of mouse skin following MN insertion.

6.3.5 Photothermal Performance

The CuS NPs retained their photothermal properties after conjugation with Gox and encapsulation in the DPMNs. The photothermal performance of the patches was evaluated through laser irradiation of blank and Gox-CuS DPMNs in solutions (λ = 850 nm, 1.5 W/cm^2, 10 min, **Figure 40**A–D). During irradiation, the temperatures of the blank and Gox-CuS DPMNs increased by 2 and 13 ºC, respectively

(Figure 40E). This photothermal activity also remained after the in vivo application of DPMNs in mice (Figure 40F and G).

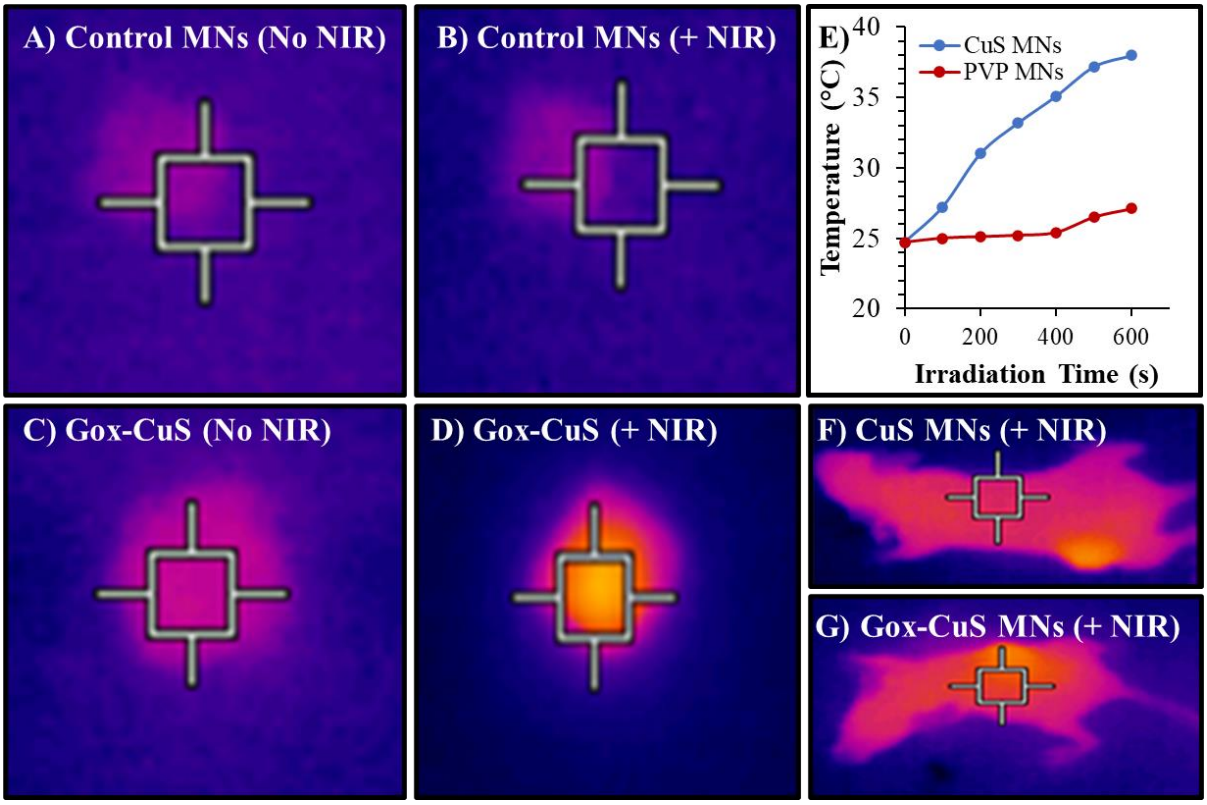

Figure 40: Photothermal efficiency of CuS-Gox DPMNs in comparison with control blank DPMNs. Thermal camera images of (A and B) control DPMNs and (C and D) Gox-CuS DPMNs before and after laser irradiation (λ = 850 nm, 10 min). (E) The temperature change of DPMNs as a function of irradiation time. Thermal camera images of (F) CuS NPs and (G) Gox-CuS NCs delivered in vivo within DPMNs after laser irradiation (10 min).

6.3.6 In Vivo Efficacy of DPMNs for Melanoma Treatment

The in vivo efficacy of the CuS-Gox-DPMNs was demonstrated through the treatment of A375 melanoma xenografts in BALB/c-nu/nu mice. Once the xenografts reached an average diameter of 6–8 mm, CuS-Gox or CuS DPMNs were applied and irradiated as described in Sections 2.4. and 2.5., respectively, every other day for 11 d. At this point, the tumor growth of the control group reached the humane endpoint. For treatment, laser irradiation (λ = 850 nm, 1.5 W/cm^2) was applied 10 min after patch application to allow Gox to catalyze glucose oxidation that enabled the build-up of H_2O_2 and a sufficient reduction in tumor pH. Intravenously delivered CuS NPs and Gox-CuS NCs were also performed for comparison. Thermal images (Figure 40F) following PTT indicated a significant amount of CuS or Gox-CuS NPs accumulated in the tumor site following patch application. After the total treatment period, our results showed that DPMNs

containing either CuS NPs, Gox, or Gox-CuS NCs showed various degrees of efficacy against the tumors (41.8 ± 9.1%, 64.3 ± 11.9%, and 74.2 ± 6.1% reductions in tumor growth/volume, respectively); however, only the Gox-CuS NCs combined with NIR irradiation were able to completely eradicate the tumor mass (99.2 ± 0.8%, **Figure 41**). NIR with CuS NPs alone was also only able to achieve a 76.5 ± 9.6% reduction in tumor growth. It is worth noting that the black and hard scar tissues dissected from the tumor sites in the Gox-CuS plus Laser group (Figure 41A) were not actually residual tumors. This is consistent with our previously reported observations for intravenous delivery and demonstrates the superior effectiveness of the multi-modal synergistic therapy combining ST, CDT, and PTT.[112] Importantly, this work demonstrates the efficacy of this multimodal nanoformulation delivered by DPMNs.

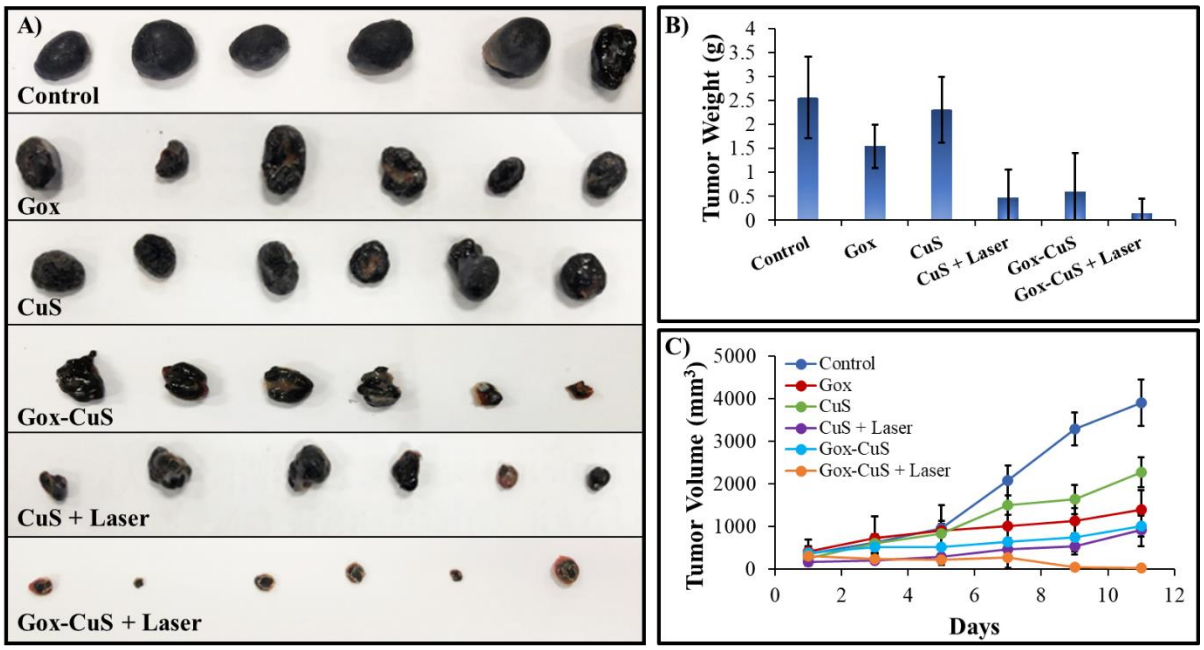

Figure 41: Antitumor efficacies of DPMNs for cancer therapies. (A) Digital photographs of representative tumor replicates treated with DPMNs. (B) Final tumor weights. (C) Changes to tumor volume during the treatment period. Error bars indicate the mean standard deviation (n = 3).

6.3.7 Biodistribution Study

To determine the biodistribution of the NPs and NCs following intravenous and transdermal delivery, we used ICP-MS to measure the total Cu content of the blood, tumors, and major organs of the mice. Notably, tumor tissue typically contains a higher concentration of free Cu^{2+} compared to normal tissue, presumably because Cu^{2+} can stimulate tumor cell proliferation.[1277,1278] As such, CuS NPs are useful for cancer therapy compared to other Cu NPs because of their lower dissolution rate.[1252] Injection is the most common delivery method for nanomedicine due to its rapid delivery; however, this method often has low patient compliance, poor tumor targeting, and results in a high systemic exposure via the bloodstream.

Conversely, while DPMNs are limited in their overall loading capacity they can directly deliver nanomedicines to the target site at highly localized concentrations. The blood plasma concentration after 2 h was unchanged for either delivery method (**Figure 42**A). This indicates that Gox-CuS NCs can be rapidly cleared from the blood when delivered via injection. In contrast, we observed very high concentrations of Cu at the tumor sites for both delivery methods, although DPMNs showed significantly greater delivery of Gox-Cus due to the localized application. This demonstrates the superior performance of DPMNs for delivering nanomedicines to the tumor tissue despite their low overall dose.

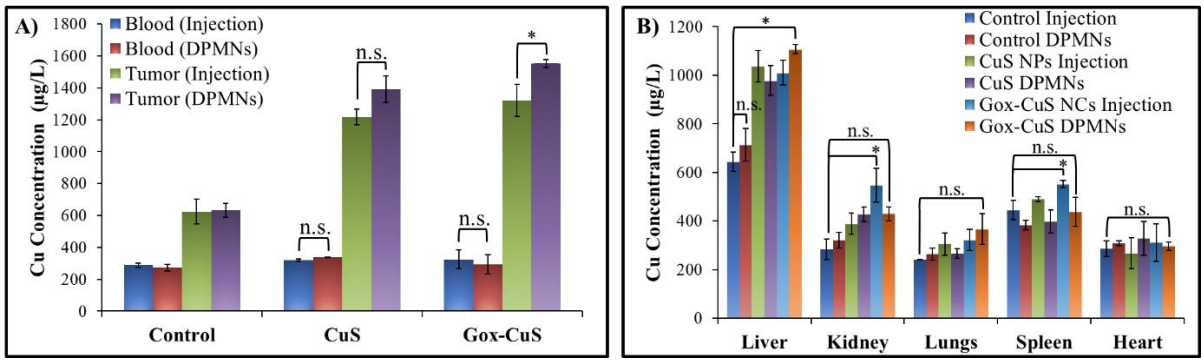

Figure 42: In vivo biodistribution of Gox-CuS NCs delivered via traditional injection or using DPMNs. (A) Blood plasma and tumor Cu concentration 2 h after administration. (B) Distribution of Cu in the liver, kidney, lungs, spleen, and heart. *$p < 0.05$. Error bars indicate the mean standard deviation ($n = 3$).

Different trends were observed when examining the Cu concentration in the major organs (Figure 42B). Fundamentally, the kidneys rapidly filter the smallest NPs (<6 nm, i.e., NPs degraded by cells or NIR irradiation) from the blood into the urine whereas the liver and spleen take up larger NPs for a slower degradation.[1279] Liver and spleen uptake is also aided by the lymphatic system. As such, both delivery methods resulted in NP or NC uptake by the liver. In addition, no increase in Cu was observed in the heart or lungs for either method. Notably, while intravenously delivered Gox-CuS NCs resulted in a higher Cu concentration in both the kidneys and spleen, no statistically significant increase was observed using DPMNs. Overall, injections showed a much higher degree of systemic exposure, and thus higher risk of toxicity, than DPMNs.

6.3.8 In Vivo Toxicity

Finally, we evaluated the off-target and systemic toxicity of the Gox-CuS DPMNs. The body weight of the mice did not change significantly during treatment (**Figure 43**A) and no significant changes to blood glucose were observed when using microneedles (Figure 43B and **Figure S34**A). This contrasted with injections containing Gox, wherein acute drops in blood glucose (from ~5 mM to 3.1 mM after 2 h) could be observed (**Figure S34**B). Despite being rapidly cleared from circulation, Gox can still impart toxic

effects by consuming blood glucose. Because a high concentration of the NCs was found in the kidneys following injections, we also evaluated the toxicity of the NPs and NCs to the kidneys using HEK-293 cells, a non-cancerous cell model for kidney toxicity studies. As seen in **Figure S33**, while the CuS NPs alone showed little toxicity to the kidney cells, the Gox-CuS NCs showed comparable toxicity to the cancerous cell lines. However, it should be noted that in vitro experiments often do not fully capture the in vivo toxicity. Histological images of the major organs did not show significant signs of damage following the various treatment conditions (Figure 43D and **Figure *S35***), indicating good biocompatibility for the Gox-CuS DPMNs. The levels of liver enzymes aspartate transaminase (AST) and alanine transaminase (ALT; Figure 43C), common indicators of liver function,[1280] were also similar to the control group for Gox-CuS DPMNs, suggesting no liver toxicity although the liver is the organ responsible for detoxifying the NCs. However, a slight increase in AST and ALT was observed for CuS DPMNs. The toxicity of CuS or Gox may vary between organs due to their unique metabolism and biochemical environments, i.e., glucose or H_2O_2 levels. While CuS has a lower dissolution rate than other NPs, they can still likely be degraded in the liver to produce toxic Cu^{2+}. Once deactivated in vivo, Gox conjugation may slow the degradation of the NPs by the liver, reducing their toxicity. Alternatively, the increased size of the NC relative to CuS NPs due to Gox conjugation may slow its diffusion within tissue matrices, reducing the potential oxidative stress. Overall, these results suggest the accumulation of Gox-CuS NCs in the organs does not pose a significant toxicity risk when using DPMNs.

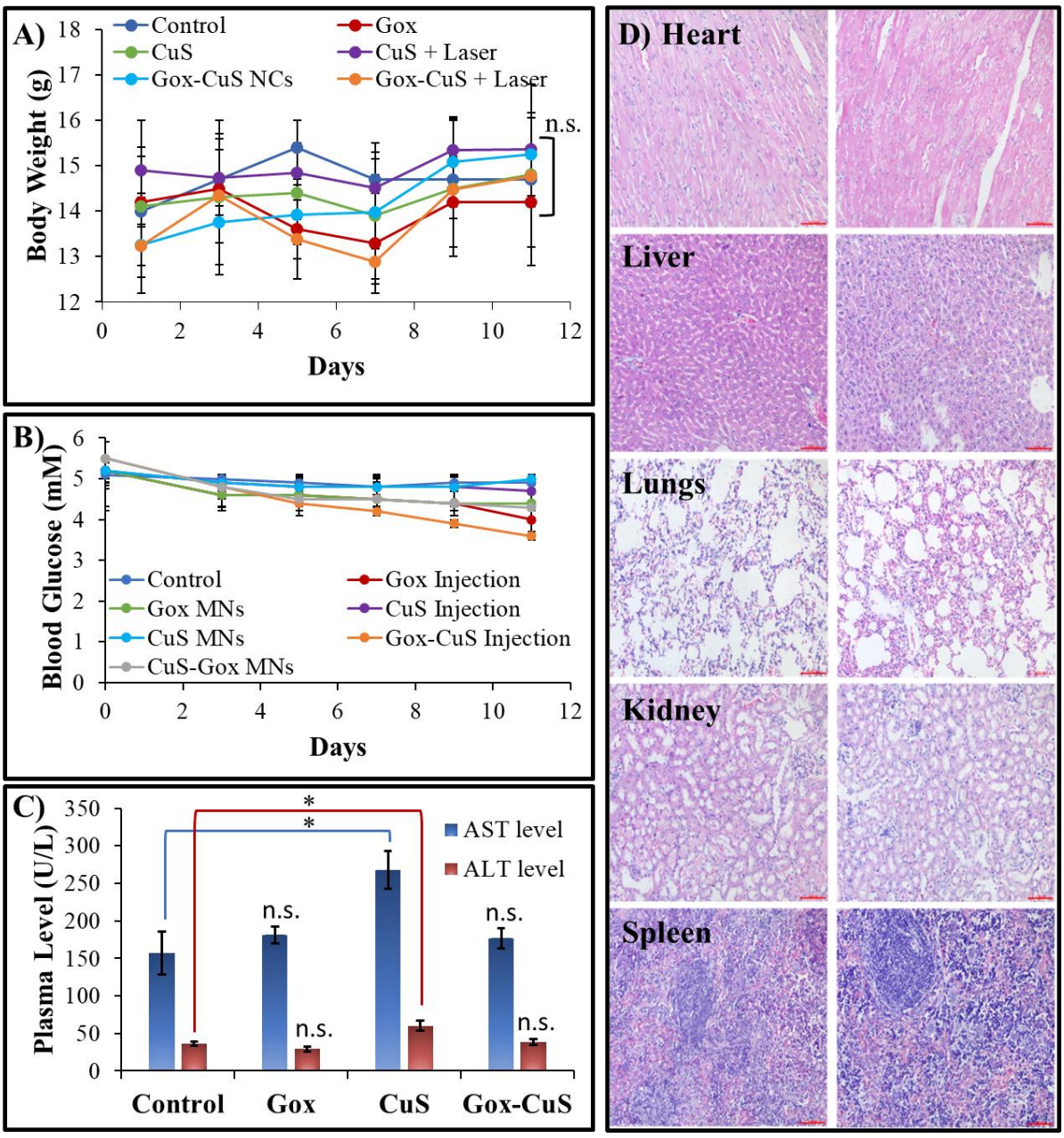

Figure 43: Toxicity of the Gox-CuS DPMNs. (A) Mouse body weight during treatment. (B) Changes to blood glucose throughout the treatment period in comparison to injection. (C) Changes in aspartate transaminase (AST) and alanine transaminase (ALT) levels (liver toxicity). (D) H&E histological staining of heart, liver, lungs, kidney, and spleen tissue slices from tumor-bearing mice after an 11-d treatment period with Gox-CuS DPMNs with (right) and without (left) NIR irradiation (scale bar = 100 μm). *$p < 0.05$. Error bars indicate the mean standard deviation ($n = 3$).

6.4 Conclusions

Herein, we have demonstrated a promising melanoma therapy using Gox-CuS NCs delivered by DPMNs. The NCs and DPMNs are easy to fabricate, store, and apply, and can generate sufficient levels of heat and ROS using endogenous energy sources (glucose and Cl^-). The efficacy of this approach stems from the dual roles of each component. The Gox enzyme initiates ST and activates the CuS nanozyme to enable chloride-accelerated CDT in a powerful cascade system. NIR irradiation can further enhance CuS-based CDT and activate PTT. PTT can then finally deactivate Gox to prevent systemic and long-term effects. Importantly, compared to delivery by injection, DPMNs improved NC uptake by the tumor tissue and reduced systemic toxicity. The resulting microneedle patch design is therefore low-cost, effective, and safe.

Nevertheless, several considerations must be taken for clinical translation. Admittedly, the adoption of a NIR light source, e.g., lasers, alongside the DPMN patches will increase the cost of the treatment; however, such cost could be minimized by using LEDs.[1281,1282] Other considerations include large-scale DPMN manufacturing, dose reproducibility, and patient feedback. Because the properties of the skin can vary significantly due to location, age, and co-morbidities, further work is needed to optimize this treatment for patients of different demographics. While applicators were not deemed necessary in this work, some scenarios may require them to ensure consistent delivery. Additionally, the co-loading of tracking dyes may serve as a probe to monitor drug release in real-time,[1283–1285] although this must be balanced against the limited delivery capacity of the MNs.

~ Chapter 7 ~

General Conclusions & Outlook

Chapter Summary

Chapter 7 summarizes of the conclusions of this thesis and provides a perspective on the future of the field of nanomedicine for the diagnosis and treatment of cancer and other diseases.

7.1 Research Conclusions

Nanomedicine is a diverse field that serves as an intersection of physics, biology, chemistry, materials science, and medicine. By combining these different perspectives, nanomedicine has and will continue to produce novel therapeutics and treatment strategies that will significantly improve oncology. Among the various advances, inorganic nanomaterials represent a potential next generation of powerful nanomedicines, taking advantage of fundamental physical and quantum effects for biomedical purposes. However, due to the complexity of nanomaterials and biological systems, significant gaps exist in our understanding of how nanoparticles (NPs) behave in the body, what risks they present, and under what conditions. While inorganic nanomedicines have been widely demonstrated as effective anticancer tools, legitimate concerns over their acute and long-term toxicity have hindered their emergence into the clinic. Many questions over the optimal design of various nanomaterial types for different treatments and their in vivo delivery also exist. In addition to slowing down research progress directly, this uncertainty also impacts the regulatory environment these materials are tested in. To overcome these hurdles, multiple perspectives must be combined and effectively communicated, both to academics and industry but also to regulators and the wider public. This thesis therefore describes efforts to improve the understanding, development, and design of novel next-generation metal-based nanomedicines for oncology using structure-activity relationships (SARs). The use of emerging microneedle (MN) technology to improve nanomedicine delivery was also evaluated and applied in this context.

In Chapters 1 and 2, the literature was comprehensively analyzed and a guiding framework for the design, application, and evaluation of nanomedicines was developed (the NSAF).[110] For clarity and simplicity, this framework was delineated into three complementary and interconnected layers detailing different levels of biological complexity. The NSAF can be viewed as both a general knowledge map and as a template for the design of more complex machine-learning algorithms. This knowledge-based approach can therefore be useful to academics, industry, and regulators in designing nanomedicines and evaluating their potential risks through pathway analysis.

In Chapter 3, SARs and the NSAF framework were applied to rationally design a gold-based nanomedicine (Lipogold) for image-guided radiation therapy (IGRT), photothermal therapy (PTT), and drug delivery.[111] Upon injection, nanomedicine circulation times and excretion rate are predominately a factor of size, with larger NPs circulating longer than smaller NPs. Large GNPs also typically support plasmons in the NIR region for phototherapies. Smaller GNPs, by contrast, can more easily penetrate cells and be excreted from the body but lack NIR-absorbance. In the context of IGRT, large GNPs can absorb more X-rays but are less effective at emitting Auger electrons than smaller NPs. For metallic nanomedicine, typically only one size range can be chosen, limiting some aspect of the design. By manipulating nanomaterial structure, this Chapter demonstrates one method to overcome this limitation by using liposomes as a biodegradable scaffold for small NPs. This produced a nanomedicine with a customizable core for drugs or contrast agents, the ability to biodegrade large Lipogold into small renal-clearable NPs, NIR absorbance, and a thin gold shell to maximize Auger emissions. Using clinical radiation equipment and in vitro models, the efficacy of each of these approaches were demonstrated. Lipogold was able to sensitize radiation-resistance prostate cancer cells to low doses of 6 MV X-rays and provide strong imaging contrast when combined with small molecule iohexol. PTT and drug delivery were also consistent with other Lipogold formulations (containing different liposome types) reported in the literature, further underscoring the customizability of the platform.

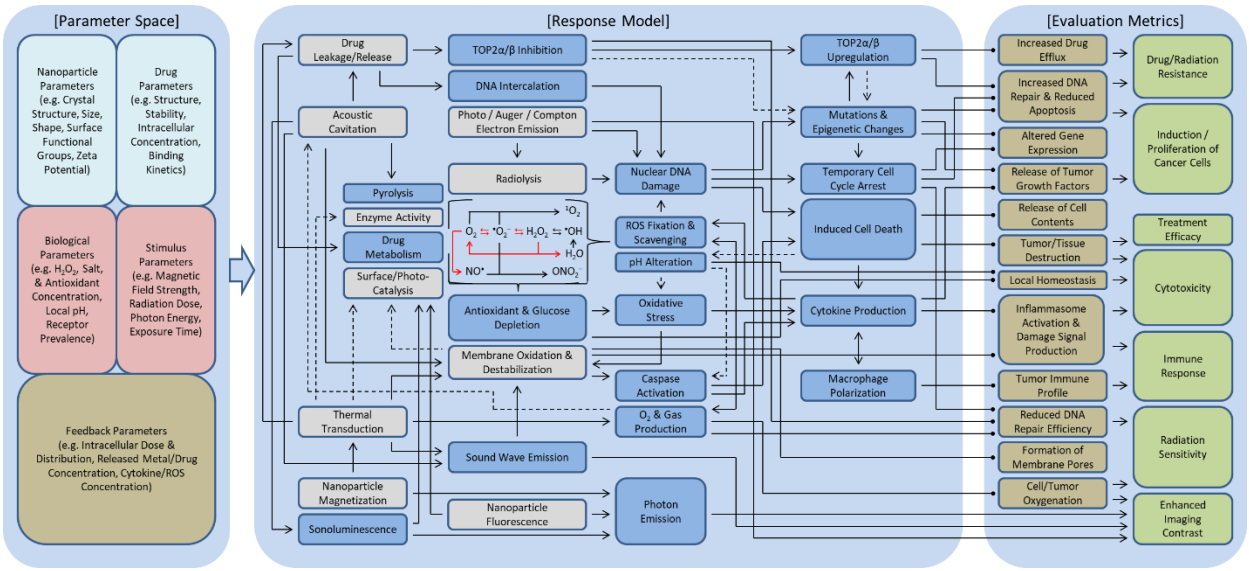

Figure 44: Updated NSAF Phase III (Dysregulation) diagram, including the action of glucose oxidase (Gox). Adapted with permission from Ref [110] (American Chemical Society, 2022).

Chapters 4-6 document the preclinical development of a CuS-based nanomedicine for superficial tumors such as melanoma. In Chapter 4, the CuS and Gox nanocomposite (Gox@CuS) was first developed and examined in situ, in vitro, and in vivo.[112] This formulation took advantage of both the properties of the

individual nanomaterial components and the tumor microenvironment (TME), converting tumor glucose into H_2O_2 and then ROS via a cascade reaction. While previously identified for copper ions and CuO, the chloride-accelerated Fenton-like reaction of CuS was also documented for the first time. **Figure 44** illustrates Phase III of the NSAF updated for the use of Gox. The combined treatment of starvation therapy, chemodynamic therapy, and photothermal therapy proved to be highly effective in a mouse melanoma model. However, while the intravenous injections used in Chapter 4 showed few signs of toxicity, the blood glucose level of the mice was found to vary widely. Gox's mechanism of action relies upon glucose consumption and the generation of H_2O_2 and acid, which can induce local or systemic effects depending on whether the reaction occurs in tissue or the blood. To improve the efficacy and safety profile of this simple nanoformulation, Microneedles were examined as a transdermal method that maximizes local delivery and limits pain, blood and off-target exposure, and first-past metabolism. In Chapter 5, another comprehensive review of the literature was provided to establish the viability, design considerations, and fabrication methods of microneedles containing light-responsive NPs such as Gox@CuS.[113] Other types of treatments were also examined to fully understand the advantages and limitations of this delivery system. Based on this additional review of an emerging, i.e., next-generation, nanomedicine delivery system, the Phase I diagram of the NSAF was updated to better reflect transdermal delivery pathways (**Figure 45**). Finally, in Chapter 6, Gox@CuS microneedles were validated in another mouse melanoma model, demonstrating an improved safety profile over injection without sacrificing potency.[114] Further exploration into the catalytic behavior of CuS was also performed, identifying the chloride-accelerated production of both $^{\bullet}OH$ and $^1O_2$. (and consequently O_2).

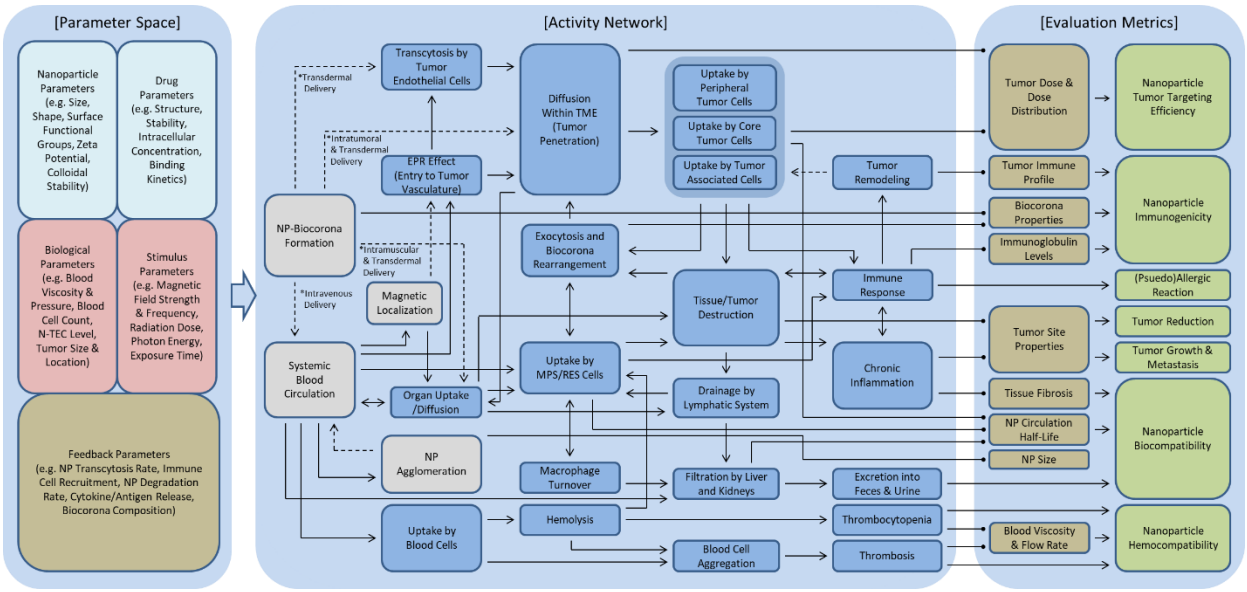

Figure 45: Updated NSAF Phase I (Biodistribution) diagram, including intramuscular delivery and nanoparticle diffusion in healthy tissue. Adapted with permission from Ref [110] (American Chemical Society, 2022).

7.2 Nanomedicine Case Study: SARS-CoV-2 Vaccines

The recent SARS-CoV-2 pandemic provided a unique case study on the understanding and application of nanomedicine. Indeed, the global pandemic response can be viewed as among the largest and successful clinical trials in history, with millions of patients receiving multiple doses. Although mRNA technology has much of the spotlight, the core feature of these vaccines that enable their efficacy are the liposome nanocarriers, which protect the mRNA from degradation until internalization by immune cells. Thus, it is difficult not to comment on this event and the implications for both organic and inorganic nanomedicines for oncology. While vaccination is distinct from cancer therapy, the overarching principles of using PEGylated liposomes for drug delivery, is shared between both applications. In the case of immunotherapy (cancer vaccination), the two treatments have little distinction. As such, significant insights can be gleamed from these nanomedicines (Spikevax® and Comirnaty®) and their application worldwide, including for metallic and metal-organic hybrid NPs. This also presents an opportunity to evaluate and further update the NSAF using more recent data.

First, in terms of efficacy, Spikevax® and Comirnaty® have given results comparable to that of traditional (viral vector) influenza vaccines, providing strong initial responses but waning (~15-50%) with time (1-6 months) as the virus evolves and antibody titers naturally decrease.[1286–1292] In this light, the vaccines can be considered a success and are attributed with a significant reduction in global deaths. When viewed in the context of immunotherapy, Spikevax® and Comirnaty® suggest that repeated doses of liposomal mRNA may be effective at inducing anticancer immune responses. In the case of hybrid nanomaterials such as Lipogold, the multifunctional treatment approach may assist in reducing the number of required doses. To assist in research to this end, the Phase I diagram of the NSAF has been updated to include intramuscular delivery (Figure 45) , although this method is currently poorly studied for inorganic nanomedicines.

Minor side-effects, including pain at and near the injection site and flu-like symptoms following the activation of the immune system and inflammation, were commonly expected and are largely unremarkable.[1293] Additionally, several serious side effects, i.e., PEG-induced anaphylaxis and CARPA, were identified early on with warnings provided to health practitioners and the public. The early guidance provided about this side-effect was based on the long history of liposome research both within and outside oncology. As a result, most reports indicate a very low incidence of anaphylactic responses (≤1 per 100,000),[1294–1296] although Spikevax® appears to have a notably higher immunogenicity and reactogenicity compared to Comirnaty® due to a higher rate of inducing anti-PEG antibodies.[1297] While both vaccines are PEGylated, differences in NP structure (i.e., PEG concentration or size), almost certainly cause this difference. Importantly, these antibodies may induce an accelerated blood clearance (ABC) effect on

subsequent doses or cause an increase in risk over time. Recent data suggests that two doses do not reduce the efficacy of a booster due to anti-PEG antibodies, although the long-term effects of multiple boosters are still unknown.[1298,1299] Overall, similarly rates of the above side-effects should also be expected for most inorganic NPs, but the causes and prevalence of CARPA are still unknown. Results with SPIONs suggest CARPA may be more common with inorganic materials due to ROS production, difference in NP coatings, and/or the presence of aggregates.[1300] Differences in patient demographics, i.e., genetic history, may also play a role in determining the incidence of these effects.

Importantly, Spikevax® and Comirnaty® have also been associated with several unexpected side-effects of significant concern, including the development of myo- and pericarditis in healthy young (<35-40) men and thrombosis (blood clotting).[1301–1303] In this light, the SARS-CoV-2 pandemic highlights new challenges, risks, and opportunities for nanomedicine research. Current estimates of the vaccine-induced myo- and pericarditis in men range from 0.41-53.76 per 100,000,[1304–1310] peaking in frequency following a 2nd dose. Estimates of overall thrombosis range from 0.02-0.56 per 100,000.[1311,1312] For a side effect to be considered 'very rare', it must typically occur in <0.1 per 100,000 individuals.[1311] By comparison, the age-adjusted mortality rate of the SARS-CoV-2 virus in the United States was 61.3 per 100,000 in 2022.[1313] By age, those <45 had a mortality of 0.5-5.2 per 100,000 while the risk above this range significantly increases up to 1224.2 per 100,000 for those ≥85. Those with comorbidities also represent the largest fraction of deaths overall. Thus, Spikevax® and Comirnaty® are critical for protecting many at risk groups, although some younger demographics may not experience substantial benefits without further refinements to the nanoformulations. While the incidence of these side-effects is low in comparison to the risks posed by cancers, such risks should nevertheless be overcome to improve healing and the long-term prognosis of the patient. Other serious side effects that have been reported but not yet casually established include thrombocytopenia, Bell's palsy, seizures, appendicitis, herpes zoster (shingles) reactivation, neurological complications, and autoimmune disorders, e.g., Guillain–Barré syndrome and autoimmune hepatitis.[1303,1314,1315]

Considering mechanisms and the implications for inorganic NPs, it is important to note that SARS-CoV-2 infections are also associated with both thrombosis and myo-/pericarditis at comparable or even higher rates.[1305,1316] This implicates the transcribed spike protein as a likely cause in both cases.[1294] Considering the behavior of NPs using the NSAF (Phases I and II), lipid NPs may diffuse into the blood stream from the injection site and then accumulate near the heart and facilitate toxicity. This mechanism suggests that metallic NPs are unlikely to induce myo- or pericarditis. Conversely, as noted in Phase I of the NSAF (Figure 45), many NPs are associated with thrombotic events by NP interactions with blood cells. Spikevax® and Comirnaty® also contain novel lipid components that have thus far been poorly studied. This

includes DMG-PEG-2000, ALC-0159, ALC-0315, and SM-102. Importantly, ALC-0315 and SM-102 are both cationic lipids, which are known to possess some toxicity to cells due to their strong interactions with cellular membranes. Since it is highly likely that these lipids will be used for additional liposomal formulations soon based on their success during the SARS-CoV-2 pandemic, significant efforts should be spent on studying the effects of these components on different organs and blood cells. For example, current evidence suggests that high concentrations of intravenous ALC-0315 has long-term liver retention and acute toxicity.[1317] Interestingly, recent evidence also implicates anti-platelet factor 4 antibodies for both SARS-CoV-2 infection- and vaccine-induced thrombosis.[1316] Anti-heart antibodies have also been suggested to play a role in infection-induced myo- and pericarditis.[1318] In these cases, the reported side-effects may be due to the cross-reactivity of anti-virus antibodies to tissue. This may be influenced by genetics and formulation or batch-specific parameters.

7.3 Future Perspectives & Conclusion

In this thesis, a novel method of viewing and understanding nanomedicine and several new nanomedicines for oncology applications were developed and tested. This provides both theoretical and practical contributions to the field. However, significant efforts are still needed to translate these advances into the clinic and regulatory use.

First, additionally work is needed to clarify, define, and integrate NSAF events with emerging data. This includes new biological discoveries, such as tertiary lymphoid structures or other unique cancer hallmarks, mechanisms of additional encapsulated/integrated APIs, and observations of unexpected/reported side effects from large scale clinical trials.[1319–1321] Following its initial development (Chapter 2), the NSAF was updated using the mechanisms and insights gained from Gox, Spikevax®, and Comirnaty® as examples of this process (Figure 44 and Figure 45). Additional delivery strategies, e.g., ocular and gastrointestinal delivery, should also be reviewed and integrated to account for a wider range of cancer types. However, these collective updates will quickly cause each Phase diagram to become increasingly visually cluttered. To minimize this issue, it is recommended that computer software be adopted to exploit dynamic graphic user interfaces (GUIs), which can group and filter events, project in 3D, and scale indefinitely, i.e., zooming in and out. The user-friendliness of these interfaces is always a challenge, although significant lessons can be derived from AI programs such as neural networks. This would allow the NSAF to contain as much as or as little information and complexity as necessary for its specific use. The development of a functional GUI could also help to accelerate the integration, evolution, and application of machine-learning algorithms as detailed in Chapter 2.

Following the proof-of-concept work in Chapter 3,[111] the next steps for Lipogold would be to optimize the liposome formulation for iohexol encapsulation and then evaluate IGRT in animal models. Thus far, the viability of Lipogold for in vivo drug delivery and PTT has been demonstrated elsewhere, which suggests good biocompatibility overall and a high likelihood of success.[901,940,948,1322] These works also demonstrate the ability to form Lipogold on different liposome compositions. One key limitation identified in Chapter 6 was that iohexol leakage was found to be very rapid, which possess a significant barrier for the transport and storage. In supervised but unpublished work, cholesterol content and lipid tail length were found to correlate with iohexol encapsulation, although more in-depth work is needed to identify the optimal liposome composition, including PEGylation or other surface modifications. Observations of non-lethal oxidative stress were observed in this work when cells were treated with Lipogold for 24 h as opposed to 48 hs. Further study should also therefore aim to evaluate this potential mechanism and minimize its risk. GNPs have been previously demonstrated as capable of depleting thiols or generating ROS in vivo and thus this may be an intrinsic part of Lipogold as a nanomaterial[1323,1324]; however, this may also be caused by other factors such as the ascorbic acid coating or shell thickness, which may be fine-tuned in the future.

Finally, since copper is one of the most reactive metal species, it is likely to take center-stage in chemodynamic therapies based on H_2O_2 and the Fenton reaction.[1325–1327] Among the various forms of nanocopper, CuS-based nanomedicines are emerging as a primary choice for nanomedicines due to their NIR-responsiveness, high biocompatibility, and stability.[1328] In Chapter 4 and 6, the in vivo effectiveness of Gox@CuS was demonstrated via conventional intravenous injection and a transdermal DPMN patch.[112,114] Due to their higher safety profile, these results suggest that Gox@CuS are a good candidate for clinical trials of melanoma and other superficial tumors. However, other recent work has suggested that CuS is less stable in oxidizing conditions and may induce toxicity under specific circumstances, with local O_2 and H_2O_2 concentrations being key parameters.[1329,1330] Other works have reported transformation in the CuS crystal structure following contact with H_2O_2 that can impact plasmon stability and the ability to perform PTT.[1331,1332] Therefore, preliminary work is currently underway investigating the interactions of H_2O_2 and CuS. In doing so, this should help elucidate key treatment parameters such as toxicity and the timing of PTT relative to the application of the DPMN patch and the generation of H_2O_2. Improvements to the mass-manufacturing and sterilization of DPMN patches should also be explored.

In conclusion, nanomedicine has extraordinary potential for the diagnosis and treatment of cancer and other diseases. Following the success of the SARS-CoV-2 pandemic, nanomedicines can be expected to see additional investment and study across the world. This includes next-generation metal-based nanomedicines that exploit unique chemical, physical, and quantum effects. For these nanomedicines to

reach the clinic, a firm understanding of their SARs is needed to optimize both their efficacy and safety. In this thesis, a guiding framework (NSAF) was developed to integrate and illustrate nanomedicine SARs for use by researchers, regulators, and industry. This provides structure and clarity to the complexity of the nanomedicine field while also identifying knowledge gaps and research opportunities. Two next-generation metallic nanomedicines, Lipogold and Gox@CuS, were then developed and evaluated for the first time, providing new and improved strategies for cancer imaging and therapy.

Letters of Copyright Permission

Copyright permissions for Chapters 2, 4, and 7 were obtained under the following agreement:

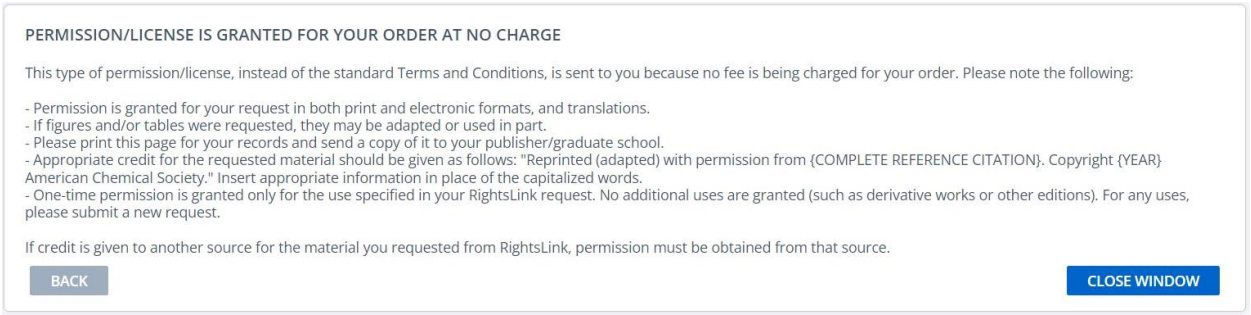

PERMISSION/LICENSE IS GRANTED FOR YOUR ORDER AT NO CHARGE

This type of permission/license, instead of the standard Terms and Conditions, is sent to you because no fee is being charged for your order. Please note the following:

- Permission is granted for your request in both print and electronic formats, and translations.
- If figures and/or tables were requested, they may be adapted or used in part.
- Please print this page for your records and send a copy of it to your publisher/graduate school.
- Appropriate credit for the requested material should be given as follows: "Reprinted (adapted) with permission from {COMPLETE REFERENCE CITATION}. Copyright {YEAR} American Chemical Society." Insert appropriate information in place of the capitalized words.
- One-time permission is granted only for the use specified in your RightsLink request. No additional uses are granted (such as derivative works or other editions). For any uses, please submit a new request.

If credit is given to another source for the material you requested from RightsLink, permission must be obtained from that source.

BACK CLOSE WINDOW

Copyright permissions for Chapters 3, 5, and 6 were obtained under the following agreement:

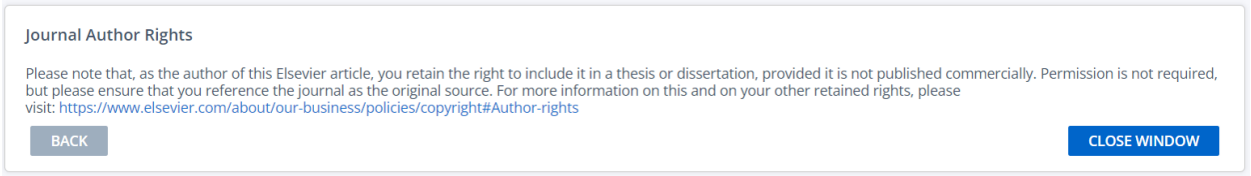

Journal Author Rights

Please note that, as the author of this Elsevier article, you retain the right to include it in a thesis or dissertation, provided it is not published commercially. Permission is not required, but please ensure that you reference the journal as the original source. For more information on this and on your other retained rights, please visit: https://www.elsevier.com/about/our-business/policies/copyright#Author-rights

BACK CLOSE WINDOW

References

(1) Hu, Z.; Sun, R.; Curtis, C. A Population Genetics Perspective on the Determinants of Intra-Tumor Heterogeneity. *Biochim. Biophys. Acta - Rev. Cancer* **2017**, *1867* (2), 109–126. https://doi.org/10.1016/j.bbcan.2017.03.001.

(2) Garner, H.; de Visser, K. E. Immune Crosstalk in Cancer Progression and Metastatic Spread: A Complex Conversation. *Nat. Rev. Immunol.* **2020**, *20* (8), 483–497. https://doi.org/10.1038/s41577-019-0271-z.

(3) Mareel, M.; Leroy, A. Clinical, Cellular, and Molecular Aspects of Cancer Invasion. *Physiol. Rev.* **2003**, *83* (2), 337–376. https://doi.org/10.1152/physrev.00024.2002.

(4) Nathanson, S. D. Insights into the Mechanisms of Lymph Node Metastasis. *Cancer* **2003**, *98* (2), 413–423. https://doi.org/10.1002/cncr.11464.

(5) Reymond, N.; d'Água, B. B.; Ridley, A. J. Crossing the Endothelial Barrier during Metastasis. *Nat. Rev. Cancer* **2013**, *13* (12), 858–870. https://doi.org/10.1038/nrc3628.

(6) Boutry, J.; Tissot, S.; Ujvari, B.; Capp, J.-P.; Giraudeau, M.; Nedelcu, A. M.; Thomas, F. The Evolution and Ecology of Benign Tumors. *Biochim. Biophys. Acta - Rev. Cancer* **2022**, *1877* (1), 188643. https://doi.org/10.1016/j.bbcan.2021.188643.

(7) Ferlay, J.; Colombet, M.; Soerjomataram, I.; Parkin, D. M.; Piñeros, M.; Znaor, A.; Bray, F. Cancer Statistics for the Year 2020: An Overview. *Int. J. Cancer* **2021**, *149* (4), 778–789. https://doi.org/10.1002/ijc.33588.

(8) Sung, H.; Ferlay, J.; Siegel, R. L.; Laversanne, M.; Soerjomataram, I.; Jemal, A.; Bray, F. Global Cancer Statistics 2020: GLOBOCAN Estimates of Incidence and Mortality Worldwide for 36 Cancers in 185 Countries. *CA. Cancer J. Clin.* **2021**, *71* (3), 209–249. https://doi.org/10.3322/caac.21660.

(9) Zheng, R.; Wang, S.; Zhang, S.; Zeng, H.; Chen, R.; Sun, K.; Li, L.; Bray, F.; Wei, W. Global, Regional, and National Lifetime Probabilities of Developing Cancer in 2020. *Sci. Bull.* **2023**, *68* (21), 2620–2628. https://doi.org/10.1016/j.scib.2023.09.041.

(10) Hanahan, D.; Weinberg, R. A. The Hallmarks of Cancer. *Cell* **2000**, *100* (1), 57–70. https://doi.org/10.1016/S0092-8674(00)81683-9.

(11) Hanahan, D.; Weinberg, R. A. Hallmarks of Cancer: The Next Generation. *Cell* **2011**, *144* (5), 646–674. https://doi.org/10.1016/j.cell.2011.02.013.

(12) Hanahan, D. Hallmarks of Cancer: New Dimensions. *Cancer Discov.* **2022**, *12* (1), 31–46. https://doi.org/10.1158/2159-8290.CD-21-1059.

(13) Martincorena, I.; Campbell, P. J. Somatic Mutation in Cancer and Normal Cells. *Science (80-.).* **2015**, *349* (6255), 1483–1489. https://doi.org/10.1126/science.aab4082.

(14) Crusz, S. M.; Balkwill, F. R. Inflammation and Cancer: Advances and New Agents. *Nat. Rev. Clin. Oncol.* **2015**, *12* (10), 584–596. https://doi.org/10.1038/nrclinonc.2015.105.

(15) Schneider, B. L.; Kulesz-Martin, M. Destructive Cycles: The Role of Genomic Instability and Adaptation in Carcinogenesis. *Carcinogenesis* **2004**, *25* (11), 2033–2044. https://doi.org/10.1093/carcin/bgh204.

(16) Wu, S.; Powers, S.; Zhu, W.; Hannun, Y. A. Substantial Contribution of Extrinsic Risk Factors to Cancer Development. *Nature* **2016**, *529* (7584), 43–47. https://doi.org/10.1038/nature16166.

(17) Tomasetti, C.; Vogelstein, B. Cancer Etiology. Variation in Cancer Risk among Tissues Can Be Explained by the Number of Stem Cell Divisions. *Science* **2015**, *347* (6217), 78–81. https://doi.org/10.1126/science.1260825.

(18) Sung, H.; Siegel, R. L.; Rosenberg, P. S.; Jemal, A. Emerging Cancer Trends among Young Adults in the

USA: Analysis of a Population-Based Cancer Registry. *Lancet. Public Heal.* **2019**, *4* (3), e137–e147. https://doi.org/10.1016/S2468-2667(18)30267-6.

(19) Pilleron, S.; Sarfati, D.; Janssen-Heijnen, M.; Vignat, J.; Ferlay, J.; Bray, F.; Soerjomataram, I. Global Cancer Incidence in Older Adults, 2012 and 2035: A Population-Based Study. *Int. J. Cancer* **2019**, *144* (1), 49–58. https://doi.org/10.1002/ijc.31664.

(20) Blokzijl, F.; de Ligt, J.; Jager, M.; Sasselli, V.; Roerink, S.; Sasaki, N.; Huch, M.; Boymans, S.; Kuijk, E.; Prins, P.; Nijman, I. J.; Martincorena, I.; Mokry, M.; Wiegerinck, C. L.; Middendorp, S.; Sato, T.; Schwank, G.; Nieuwenhuis, E. E. S.; Verstegen, M. M. A.; van der Laan, L. J. W.; de Jonge, J.; IJzermans, J. N. M.; Vries, R. G.; van de Wetering, M.; Stratton, M. R.; Clevers, H.; Cuppen, E.; van Boxtel, R. Tissue-Specific Mutation Accumulation in Human Adult Stem Cells during Life. *Nature* **2016**, *538* (7624), 260–264. https://doi.org/10.1038/nature19768.

(21) Li, Y.; Hecht, S. S. Carcinogenic Components of Tobacco and Tobacco Smoke: A 2022 Update. *Food Chem. Toxicol.* **2022**, *165*, 113179. https://doi.org/10.1016/j.fct.2022.113179.

(22) Safiri, S.; Nejadghaderi, S. A.; Abdollahi, M.; Carson-Chahhoud, K.; Kaufman, J. S.; Bragazzi, N. L.; Moradi-Lakeh, M.; Mansournia, M. A.; Sullman, M. J. M.; Almasi-Hashiani, A.; Taghizadieh, A.; Collins, G. S.; Kolahi, A.-A. Global, Regional, and National Burden of Cancers Attributable to Tobacco Smoking in 204 Countries and Territories, 1990-2019. *Cancer Med.* **2022**, *11* (13), 2662–2678. https://doi.org/10.1002/cam4.4647.

(23) de Martel, C.; Georges, D.; Bray, F.; Ferlay, J.; Clifford, G. M. Global Burden of Cancer Attributable to Infections in 2018: A Worldwide Incidence Analysis. *Lancet. Glob. Heal.* **2020**, *8* (2), e180–e190. https://doi.org/10.1016/S2214-109X(19)30488-7.

(24) Parkin, D. M. The Global Health Burden of Infection-Associated Cancers in the Year 2002. *Int. J. cancer* **2006**, *118* (12), 3030–3044. https://doi.org/10.1002/ijc.21731.

(25) Key, T. J.; Bradbury, K. E.; Perez-Cornago, A.; Sinha, R.; Tsilidis, K. K.; Tsugane, S. Diet, Nutrition, and Cancer Risk: What Do We Know and What Is the Way Forward? *BMJ* **2020**, *368*, m511. https://doi.org/10.1136/bmj.m511.

(26) Zhang, F. F.; Cudhea, F.; Shan, Z.; Michaud, D. S.; Imamura, F.; Eom, H.; Ruan, M.; Rehm, C. D.; Liu, J.; Du, M.; Kim, D.; Lizewski, L.; Wilde, P.; Mozaffarian, D. Preventable Cancer Burden Associated With Poor Diet in the United States. *JNCI cancer Spectr.* **2019**, *3* (2), pkz034. https://doi.org/10.1093/jncics/pkz034.

(27) Hart, S. N.; Polley, E. C.; Yussuf, A.; Yadav, S.; Goldgar, D. E.; Hu, C.; LaDuca, H.; Smith, L. P.; Fujimoto, J.; Li, S.; Couch, F. J.; Dolinsky, J. S. Mutation Prevalence Tables for Hereditary Cancer Derived from Multigene Panel Testing. *Hum. Mutat.* **2020**, *41* (8), e1–e6. https://doi.org/10.1002/humu.24053.

(28) Goodson, W. H. 3rd; Lowe, L.; Carpenter, D. O.; Gilbertson, M.; Manaf Ali, A.; Lopez de Cerain Salsamendi, A.; Lasfar, A.; Carnero, A.; Azqueta, A.; Amedei, A.; Charles, A. K.; Collins, A. R.; Ward, A.; Salzberg, A. C.; Colacci, A.; Olsen, A.-K.; Berg, A.; Barclay, B. J.; Zhou, B. P.; Blanco-Aparicio, C.; Baglole, C. J.; Dong, C.; Mondello, C.; Hsu, C.-W.; Naus, C. C.; Yedjou, C.; Curran, C. S.; Laird, D. W.; Koch, D. C.; Carlin, D. J.; Felsher, D. W.; Roy, D.; Brown, D. G.; Ratovitski, E.; Ryan, E. P.; Corsini, E.; Rojas, E.; Moon, E.-Y.; Laconi, E.; Marongiu, F.; Al-Mulla, F.; Chiaradonna, F.; Darroudi, F.; Martin, F. L.; Van Schooten, F. J.; Goldberg, G. S.; Wagemaker, G.; Nangami, G. N.; Calaf, G. M.; Williams, G.; Wolf, G. T.; Koppen, G.; Brunborg, G.; Lyerly, H. K.; Krishnan, H.; Ab Hamid, H.; Yasaei, H.; Sone, H.; Kondoh, H.; Salem, H. K.; Hsu, H.-Y.; Park, H. H.; Koturbash, I.; Miousse, I. R.; Scovassi, A. I.; Klaunig, J. E.; Vondráček, J.; Raju, J.; Roman, J.; Wise, J. P. S.; Whitfield, J. R.; Woodrick, J.; Christopher, J. A.; Ochieng, J.; Martinez-Leal, J. F.; Weisz, J.; Kravchenko, J.; Sun, J.; Prudhomme, K. R.; Narayanan, K. B.; Cohen-Solal, K. A.; Moorwood, K.; Gonzalez, L.; Soucek, L.; Jian, L.; D'Abronzo, L. S.; Lin, L.-T.; Li, L.; Gulliver, L.; McCawley, L. J.; Memeo, L.; Vermeulen, L.; Leyns, L.; Zhang, L.; Valverde, M.; Khatami, M.; Romano, M. F.; Chapellier, M.; Williams, M. A.; Wade, M.; Manjili, M. H.; Lleonart, M. E.; Xia, M.; Gonzalez, M. J.; Karamouzis, M. V; Kirsch-Volders, M.; Vaccari, M.; Kuemmerle, N. B.; Singh, N.; Cruickshanks, N.; Kleinstreuer, N.; van Larebeke, N.; Ahmed, N.; Ogunkua, O.; Krishnakumar, P. K.;

Vadgama, P.; Marignani, P. A.; Ghosh, P. M.; Ostrosky-Wegman, P.; Thompson, P. A.; Dent, P.; Heneberg, P.; Darbre, P.; Sing Leung, P.; Nangia-Makker, P.; Cheng, Q. S.; Robey, R. B.; Al-Temaimi, R.; Roy, R.; Andrade-Vieira, R.; Sinha, R. K.; Mehta, R.; Vento, R.; Di Fiore, R.; Ponce-Cusi, R.; Dornetshuber-Fleiss, R.; Nahta, R.; Castellino, R. C.; Palorini, R.; Abd Hamid, R.; Langie, S. A. S.; Eltom, S. E.; Brooks, S. A.; Ryeom, S.; Wise, S. S.; Bay, S. N.; Harris, S. A.; Papagerakis, S.; Romano, S.; Pavanello, S.; Eriksson, S.; Forte, S.; Casey, S. C.; Luanpitpong, S.; Lee, T.-J.; Otsuki, T.; Chen, T.; Massfelder, T.; Sanderson, T.; Guarnieri, T.; Hultman, T.; Dormoy, V.; Odero-Marah, V.; Sabbisetti, V.; Maguer-Satta, V.; Rathmell, W. K.; Engström, W.; Decker, W. K.; Bisson, W. H.; Rojanasakul, Y.; Luqmani, Y.; Chen, Z.; Hu, Z. Assessing the Carcinogenic Potential of Low-Dose Exposures to Chemical Mixtures in the Environment: The Challenge Ahead. *Carcinogenesis* **2015**, *36 Suppl 1* (Suppl 1), S254-96. https://doi.org/10.1093/carcin/bgv039.

(29) Whiteman, D. C.; Wilson, L. F. The Fractions of Cancer Attributable to Modifiable Factors: A Global Review. *Cancer Epidemiol.* **2016**, *44*, 203–221. https://doi.org/10.1016/j.canep.2016.06.013.

(30) Detterbeck, F. C.; Boffa, D. J.; Kim, A. W.; Tanoue, L. T. The Eighth Edition Lung Cancer Stage Classification. *Chest* **2017**, *151* (1), 193–203. https://doi.org/10.1016/j.chest.2016.10.010.

(31) Paner, G. P.; Stadler, W. M.; Hansel, D. E.; Montironi, R.; Lin, D. W.; Amin, M. B. Updates in the Eighth Edition of the Tumor-Node-Metastasis Staging Classification for Urologic Cancers. *Eur. Urol.* **2018**, *73* (4), 560–569. https://doi.org/10.1016/j.eururo.2017.12.018.

(32) Que, S. K. T.; Zwald, F. O.; Schmults, C. D. Cutaneous Squamous Cell Carcinoma: Incidence, Risk Factors, Diagnosis, and Staging. *J. Am. Acad. Dermatol.* **2018**, *78* (2), 237–247. https://doi.org/10.1016/j.jaad.2017.08.059.

(33) Gress, D. M.; Edge, S. B.; Greene, F. L.; Washington, M. K.; Asare, E. A.; Brierley, J. D.; Byrd, D. R.; Compton, C. C.; Jessup, J. M.; Winchester, D. P. Principles of Cancer Staging. In *AJCC Cancer Staging Manual*; Springer Switzerland, 2017; pp 3–30. https://doi.org/10.1007/978-3-319-40618-3_1.

(34) Hallek, M.; Cheson, B. D.; Catovsky, D.; Caligaris-Cappio, F.; Dighiero, G.; Döhner, H.; Hillmen, P.; Keating, M. J.; Montserrat, E.; Rai, K. R.; Kipps, T. J. Guidelines for the Diagnosis and Treatment of Chronic Lymphocytic Leukemia: A Report from the International Workshop on Chronic Lymphocytic Leukemia Updating the National Cancer Institute–Working Group 1996 Guidelines. *Blood* **2008**, *111* (12), 5446–5456. https://doi.org/10.1182/blood-2007-06-093906.

(35) Akeret, K.; Vasella, F.; Staartjes, V. E.; Velz, J.; Müller, T.; Neidert, M. C.; Weller, M.; Regli, L.; Serra, C.; Krayenbühl, N. Anatomical Phenotyping and Staging of Brain Tumours. *Brain* **2022**, *145* (3), 1162–1176. https://doi.org/10.1093/brain/awab352.

(36) Gupta, S.; Aitken, J. F.; Bartels, U.; Brierley, J.; Dolendo, M.; Friedrich, P.; Fuentes-Alabi, S.; Garrido, C. P.; Gatta, G.; Gospodarowicz, M.; Gross, T.; Howard, S. C.; Molyneux, E.; Moreno, F.; Pole, J. D.; Pritchard-Jones, K.; Ramirez, O.; Ries, L. A. G.; Rodriguez-Galindo, C.; Shin, H. Y.; Steliarova-Foucher, E.; Sung, L.; Supriyadi, E.; Swaminathan, R.; Torode, J.; Vora, T.; Kutluk, T.; Frazier, A. L. Paediatric Cancer Stage in Population-Based Cancer Registries: The Toronto Consensus Principles and Guidelines. *Lancet Oncol.* **2016**, *17* (4), e163–e172. https://doi.org/10.1016/S1470-2045(15)00539-2.

(37) Dagogo-Jack, I.; Shaw, A. T. Tumour Heterogeneity and Resistance to Cancer Therapies. *Nat. Rev. Clin. Oncol.* **2018**, *15* (2), 81–94. https://doi.org/10.1038/nrclinonc.2017.166.

(38) Renzi, C.; Lyratzopoulos, G. Comorbidity and the Diagnosis of Symptomatic-but-as-yet-Undiagnosed Cancer. *Br. J. Gen. Pract.* **2020**, *70* (698), e598–e599. https://doi.org/10.3399/bjgp20X712193.

(39) Zhou, Y.; Abel, G. A.; Hamilton, W.; Pritchard-Jones, K.; Gross, C. P.; Walter, F. M.; Renzi, C.; Johnson, S.; McPhail, S.; Elliss-Brookes, L.; Lyratzopoulos, G. Diagnosis of Cancer as an Emergency: A Critical Review of Current Evidence. *Nat. Rev. Clin. Oncol.* **2017**, *14* (1), 45–56. https://doi.org/10.1038/nrclinonc.2016.155.

(40) Sarma, E. A.; Silver, M. I.; Kobrin, S. C.; Marcus, P. M.; Ferrer, R. A. Cancer Screening: Health Impact, Prevalence, Correlates, and Interventions. *Psychol. Health* **2019**, *34* (9), 1036–1072.

https://doi.org/10.1080/08870446.2019.1584673.

(41) Vaidyanathan, R.; Soon, R. H.; Zhang, P.; Jiang, K.; Lim, C. T. Cancer Diagnosis: From Tumor to Liquid Biopsy and Beyond. *Lab Chip* **2019**, *19* (1), 11–34. https://doi.org/10.1039/C8LC00684A.

(42) Haber, D. A.; Velculescu, V. E. Blood-Based Analyses of Cancer: Circulating Tumor Cells and Circulating Tumor DNA. *Cancer Discov.* **2014**, *4* (6), 650–661. https://doi.org/10.1158/2159-8290.CD-13-1014.

(43) Shah, R.; Jones, E.; Vidart, V.; Kuppen, P. J. K.; Conti, J. A.; Francis, N. K. Biomarkers for Early Detection of Colorectal Cancer and Polyps: Systematic Review. *Cancer Epidemiol. Biomarkers Prev.* **2014**, *23* (9), 1712–1728. https://doi.org/10.1158/1055-9965.EPI-14-0412.

(44) Campos-Carrillo, A.; Weitzel, J. N.; Sahoo, P.; Rockne, R.; Mokhnatkin, J. V; Murtaza, M.; Gray, S. W.; Goetz, L.; Goel, A.; Schork, N.; Slavin, T. P. Circulating Tumor DNA as an Early Cancer Detection Tool. *Pharmacol. Ther.* **2020**, *207*, 107458. https://doi.org/10.1016/j.pharmthera.2019.107458.

(45) Philipson, T. J.; Durie, T.; Cong, Z.; Fendrick, A. M. The Aggregate Value of Cancer Screenings in the United States: Full Potential Value and Value Considering Adherence. *BMC Health Serv. Res.* **2023**, *23* (1), 829. https://doi.org/10.1186/s12913-023-09738-4.

(46) Crosby, D.; Bhatia, S.; Brindle, K. M.; Coussens, L. M.; Dive, C.; Emberton, M.; Esener, S.; Fitzgerald, R. C.; Gambhir, S. S.; Kuhn, P.; Rebbeck, T. R.; Balasubramanian, S. Early Detection of Cancer. *Science (80-.).* **2020**, *375* (6586), eaay9040. https://doi.org/10.1126/science.aay9040.

(47) Misra, R.; Acharya, S.; Sahoo, S. K. Cancer Nanotechnology: Application of Nanotechnology in Cancer Therapy. *Drug Discov. Today* **2010**, *15* (19), 842–850. https://doi.org/10.1016/j.drudis.2010.08.006.

(48) Mellman, I.; Coukos, G.; Dranoff, G. Cancer Immunotherapy Comes of Age. *Nature* **2011**, *480* (7378), 480–489. https://doi.org/10.1038/nature10673.

(49) Burstein, H. J.; Temin, S.; Anderson, H.; Buchholz, T. A.; Davidson, N. E.; Gelmon, K. E.; Giordano, S. H.; Hudis, C. A.; Rowden, D.; Solky, A. J.; Stearns, V.; Winer, E. P.; Griggs, J. J. Adjuvant Endocrine Therapy for Women with Hormone Receptor-Positive Breast Cancer: American Society of Clinical Oncology Clinical Practice Guideline Focused Update. *J. Clin. Oncol.* **2014**, *32* (21), 2255–2269. https://doi.org/10.1200/JCO.2013.54.2258.

(50) Canaparo, R.; Foglietta, F.; Barbero, N.; Serpe, L. The Promising Interplay between Sonodynamic Therapy and Nanomedicine. *Adv. Drug Deliv. Rev.* **2022**, *189*, 114495. https://doi.org/10.1016/j.addr.2022.114495.

(51) Ouyang, J.; Tang, Z.; Farokhzad, N.; Kong, N.; Kim, N. Y.; Feng, C.; Blake, S.; Xiao, Y.; Liu, C.; Xie, T.; Tao, W. Ultrasound Mediated Therapy: Recent Progress and Challenges in Nanoscience. *Nano Today* **2020**, *35*, 100949. https://doi.org/10.1016/j.nantod.2020.100949.

(52) Tay, Z. W.; Chandrasekharan, P.; Chiu-Lam, A.; Hensley, D. W.; Dhavalikar, R.; Zhou, X. Y.; Yu, E. Y.; Goodwill, P. W.; Zheng, B.; Rinaldi, C.; Conolly, S. M. Magnetic Particle Imaging-Guided Heating in Vivo Using Gradient Fields for Arbitrary Localization of Magnetic Hyperthermia Therapy. *ACS Nano* **2018**, *12* (4), 3699–3713. https://doi.org/10.1021/acsnano.8b00893.

(53) Ni, D.; Bu, W.; Ehlerding, E. B.; Cai, W.; Shi, J. Engineering of Inorganic Nanoparticles as Magnetic Resonance Imaging Contrast Agents. *Chem. Soc. Rev.* **2017**, *46* (23), 7438–7468. https://doi.org/10.1039/C7CS00316A.

(54) Ginn, S. L.; Amaya, A. K.; Alexander, I. E.; Edelstein, M.; Abedi, M. R. Gene Therapy Clinical Trials Worldwide to 2017: An Update. *J. Gene Med.* **2018**, *20* (5), e3015. https://doi.org/10.1002/jgm.3015.

(55) Ashton, J. R.; West, J. L.; Badea, C. T. In Vivo Small Animal Micro-CT Using Nanoparticle Contrast Agents. *Frontiers in Pharmacology*. Frontiers Research Foundation November 4, 2015, p 256. https://doi.org/10.3389/fphar.2015.00256.

(56) Seibert, J. A. X-Ray Imaging Physics for Nuclear Medicine Technologists. Part 1: Basic Principles of x-Ray Production. *Journal of Nuclear Medicine Technology*. Society of Nuclear Medicine September 1, 2004, pp

139–147.

(57) Yue, N. J. Principles and Practice of Brachytherapy Dosimetry. *Radiat. Meas.* **2006**, *41* (SUPPL. 1), S22–S27. https://doi.org/10.1016/j.radmeas.2007.01.001.

(58) Xie, Z.; Fan, T.; An, J.; Choi, W.; Duo, Y.; Ge, Y.; Zhang, B.; Nie, G.; Xie, N.; Zheng, T.; Chen, Y.; Zhang, H.; Kim, J. S. Emerging Combination Strategies with Phototherapy in Cancer Nanomedicine. *Chem. Soc. Rev.* **2020**, *49* (22), 8065–8087. https://doi.org/10.1039/D0CS00215A.

(59) Gao, D.; Guo, X.; Zhang, X.; Chen, S.; Wang, Y.; Chen, T.; Huang, G.; Gao, Y.; Tian, Z.; Yang, Z. Multifunctional Phototheranostic Nanomedicine for Cancer Imaging and Treatment. *Mater. Today Bio* **2020**, *5*, 100035. https://doi.org/10.1016/j.mtbio.2019.100035.

(60) Schieber, M.; Chandel, N. S. ROS Function in Redox Signaling and Oxidative Stress. *Curr. Biol.* **2014**, *24* (10), R453-62. https://doi.org/10.1016/j.cub.2014.03.034.

(61) Fan, W.; Yung, B.; Huang, P.; Chen, X. Nanotechnology for Multimodal Synergistic Cancer Therapy. *Chem. Rev.* **2017**, *117* (22), 13566–13638. https://doi.org/10.1021/acs.chemrev.7b00258.

(62) Chabner, B. A.; Roberts, T. G. Chemotherapy and the War on Cancer. *Nat. Rev. Cancer* **2005**, *5* (1), 65–72. https://doi.org/10.1038/nrc1529.

(63) Locati, M.; Mantovani, A.; Sica, A. Macrophage Activation and Polarization as an Adaptive Component of Innate Immunity. *Adv. Immunol.* **2013**, *120*, 163–184. https://doi.org/10.1016/B978-0-12-417028-5.00006-5.

(64) Zhu, S.; Wang, Y.; Tang, J.; Cao, M. Radiotherapy Induced Immunogenic Cell Death by Remodeling Tumor Immune Microenvironment. *Front. Immunol.* **2022**, *13*, 1074477. https://doi.org/10.3389/fimmu.2022.1074477.

(65) Jiang, M.; Zeng, J.; Zhao, L.; Zhang, M.; Ma, J.; Guan, X.; Zhang, W. Chemotherapeutic Drug-Induced Immunogenic Cell Death for Nanomedicine-Based Cancer Chemo–Immunotherapy. *Nanoscale* **2021**, *13* (41), 17218–17235. https://doi.org/10.1039/D1NR05512G.

(66) Radha, G.; Lopus, M. The Spontaneous Remission of Cancer: Current Insights and Therapeutic Significance. *Transl. Oncol.* **2021**, *14* (9), 101166. https://doi.org/10.1016/j.tranon.2021.101166.

(67) Jessy, T. Immunity over Inability: The Spontaneous Regression of Cancer. *J. Nat. Sci. Biol. Med.* **2011**, *2* (1), 43–49. https://doi.org/10.4103/0976-9668.82318.

(68) Brianna; Lee, S. H. Chemotherapy: How to Reduce Its Adverse Effects While Maintaining the Potency? *Med. Oncol.* **2023**, *40* (3), 88. https://doi.org/10.1007/s12032-023-01954-6.

(69) De Lombaerde, E.; De Wever, O.; De Geest, B. G. Delivery Routes Matter: Safety and Efficacy of Intratumoral Immunotherapy. *Biochim. Biophys. Acta - Rev. Cancer* **2021**, *1875* (2), 188526. https://doi.org/10.1016/j.bbcan.2021.188526.

(70) Krishnan, V.; Mitragotri, S. Nanoparticles for Topical Drug Delivery: Potential for Skin Cancer Treatment. *Adv. Drug Deliv. Rev.* **2020**, *153*, 87–108. https://doi.org/10.1016/j.addr.2020.05.011.

(71) Nagarkar, R.; Singh, M.; Nguyen, H. X.; Jonnalagadda, S. A Review of Recent Advances in Microneedle Technology for Transdermal Drug Delivery. *J. Drug Deliv. Sci. Technol.* **2020**, *59*, 101923. https://doi.org/10.1016/j.jddst.2020.101923.

(72) Jeong, W. Y.; Kwon, M.; Choi, H. E.; Kim, K. S. Recent Advances in Transdermal Drug Delivery Systems: A Review. *Biomater. Res.* **2024**, *25* (1), 24. https://doi.org/10.1186/s40824-021-00226-6.

(73) Thanki, K.; Gangwal, R. P.; Sangamwar, A. T.; Jain, S. Oral Delivery of Anticancer Drugs: Challenges and Opportunities. *J. Control. Release* **2013**, *170* (1), 15–40. https://doi.org/10.1016/j.jconrel.2013.04.020.

(74) Khan, A. R.; Liu, M.; Khan, M. W.; Zhai, G. Progress in Brain Targeting Drug Delivery System by Nasal Route. *J. Control. Release* **2017**, *268*, 364–389. https://doi.org/10.1016/j.jconrel.2017.09.001.

(75) Wu, W. Inorganic Nanomaterials for Printed Electronics: A Review. *Nanoscale* **2017**, *9* (22), 7342–7372. https://doi.org/10.1039/C7NR01604B.

(76) Khot, L. R.; Sankaran, S.; Maja, J. M.; Ehsani, R.; Schuster, E. W. Applications of Nanomaterials in Agricultural Production and Crop Protection: A Review. *Crop Prot.* **2012**, *35*, 64–70. https://doi.org/10.1016/j.cropro.2012.01.007.

(77) Pomerantseva, E.; Bonaccorso, F.; Feng, X.; Cui, Y.; Gogotsi, Y. Energy Storage: The Future Enabled by Nanomaterials. *Science (80-.).* **2019**, *366* (6468), eaan8285. https://doi.org/10.1126/science.aan8285.

(78) Edwards, E.; Brantley, C.; Ruffin, P. B. Overview of Nanotechnology in Military and Aerospace Applications. In *Nanotechnology Commercialization*; 2017; pp 133–176. https://doi.org/10.1002/9781119371762.ch5.

(79) Pelaz, B.; Alexiou, C.; Alvarez-Puebla, R. A.; Alves, F.; Andrews, A. M.; Ashraf, S.; Balogh, L. P.; Ballerini, L.; Bestetti, A.; Brendel, C.; Bosi, S.; Carril, M.; Chan, W. C. W.; Chen, C.; Chen, X.; Chen, X.; Cheng, Z.; Cui, D.; Du, J.; Dullin, C.; Escudero, A.; Feliu, N.; Gao, M.; George, M.; Gogotsi, Y.; Grünweller, A.; Gu, Z.; Halas, N. J.; Hampp, N.; Hartmann, R. K.; Hersam, M. C.; Hunziker, P.; Jian, J.; Jiang, X.; Jungebluth, P.; Kadhiresan, P.; Kataoka, K.; Khademhosseini, A.; Kopeček, J.; Kotov, N. A.; Krug, H. F.; Lee, D. S.; Lehr, C.-M.; Leong, K. W.; Liang, X.-J.; Ling Lim, M.; Liz-Marzán, L. M.; Ma, X.; Macchiarini, P.; Meng, H.; Möhwald, H.; Mulvaney, P.; Nel, A. E.; Nie, S.; Nordlander, P.; Okano, T.; Oliveira, J.; Park, T. H.; Penner, R. M.; Prato, M.; Puntes, V.; Rotello, V. M.; Samarakoon, A.; Schaak, R. E.; Shen, Y.; Sjöqvist, S.; Skirtach, A. G.; Soliman, M. G.; Stevens, M. M.; Sung, H.-W.; Tang, B. Z.; Tietze, R.; Udugama, B. N.; VanEpps, J. S.; Weil, T.; Weiss, P. S.; Willner, I.; Wu, Y.; Yang, L.; Yue, Z.; Zhang, Q.; Zhang, Q.; Zhang, X.-E.; Zhao, Y.; Zhou, X.; Parak, W. J. Diverse Applications of Nanomedicine. *ACS Nano* **2017**, *11* (3), 2313–2381. https://doi.org/10.1021/acsnano.6b06040.

(80) Baig, N.; Kammakakam, I.; Falath, W. Nanomaterials: A Review of Synthesis Methods, Properties, Recent Progress, and Challenges. *Mater. Adv.* **2021**, *2* (6), 1821–1871. https://doi.org/10.1039/D0MA00807A.

(81) Park, H.; Shin, D. J.; Yu, J. Categorization of Quantum Dots, Clusters, Nanoclusters, and Nanodots. *J. Chem. Educ.* **2021**, *98* (3), 703–709. https://doi.org/10.1021/acs.jchemed.0c01403.

(82) Semonin, O. E.; Luther, J. M.; Beard, M. C. Quantum Dots for Next-Generation Photovoltaics. *Mater. Today* **2012**, *15* (11), 508–515. https://doi.org/10.1016/S1369-7021(12)70220-1.

(83) Alshammari, B. H.; Lashin, M. M. A.; Mahmood, M. A.; Al-Mubaddel, F. S.; Ilyas, N.; Rahman, N.; Sohail, M.; Khan, A.; Abdullaev, S. S.; Khan, R. Organic and Inorganic Nanomaterials: Fabrication, Properties and Applications. *RSC Adv.* **2023**, *13* (20), 13735–13785. https://doi.org/10.1039/D3RA01421E.

(84) Hochella, M. F.; Mogk, D. W.; Ranville, J.; Allen, I. C.; Luther, G. W.; Marr, L. C.; McGrail, B. P.; Murayama, M.; Qafoku, N. P.; Rosso, K. M.; Sahai, N.; Schroeder, P. A.; Vikesland, P.; Westerhoff, P.; Yang, Y. Natural, Incidental, and Engineered Nanomaterials and Their Impacts on the Earth System. *Science (80-.).* **2019**, *363* (6434), eaau8299. https://doi.org/10.1126/science.aau8299.

(85) Du, Y.; Sheng, H.; Astruc, D.; Zhu, M. Atomically Precise Noble Metal Nanoclusters as Efficient Catalysts: A Bridge between Structure and Properties. *Chem. Rev.* **2020**, *120* (2), 526–622. https://doi.org/10.1021/acs.chemrev.8b00726.

(86) Montanarella, F.; Kovalenko, M. V. Three Millennia of Nanocrystals. *ACS Nano* **2022**, *16* (4), 5085–5102. https://doi.org/10.1021/acsnano.1c11159.

(87) Reibold, M.; Paufler, P.; Levin, A. A.; Kochmann, W.; Pätzke, N.; Meyer, D. C. Carbon Nanotubes in an Ancient Damascus Sabre. *Nature* **2006**, *444* (7117), 286. https://doi.org/10.1038/444286a.

(88) Barenholz, Y. Doxil®-the First FDA-Approved Nano-Drug: Lessons Learned. *J. Control. Release* **2012**, *160* (2), 117–134. https://doi.org/10.1016/j.jconrel.2012.03.020.

(89) Simeone, F. C.; Costa, A. L. Assessment of Cytotoxicity of Metal Oxide Nanoparticles on the Basis of Fundamental Physical–Chemical Parameters: A Robust Approach to Grouping. *Environ. Sci. Nano* **2019**, *6*

(10), 3102–3112. https://doi.org/10.1039/C9EN00785G.

(90) Lamon, L.; Asturiol, D.; Richarz, A.; Joossens, E.; Graepel, R.; Aschberger, K.; Worth, A. Grouping of Nanomaterials to Read-across Hazard Endpoints: From Data Collection to Assessment of the Grouping Hypothesis by Application of Chemoinformatic Techniques. *Part. Fibre Toxicol.* **2018**, *15* (1), 37. https://doi.org/10.1186/s12989-018-0273-1.

(91) Sukhanova, A.; Bozrova, S.; Sokolov, P.; Berestovoy, M.; Karaulov, A.; Nabiev, I. Dependence of Nanoparticle Toxicity on Their Physical and Chemical Properties. *Nanoscale Res. Lett.* **2018**, *13* (1), 44. https://doi.org/10.1186/s11671-018-2457-x.

(92) Oh, E.; Liu, R.; Nel, A.; Gemill, K. B.; Bilal, M.; Cohen, Y.; Medintz, I. L. Meta-Analysis of Cellular Toxicity for Cadmium-Containing Quantum Dots. *Nat. Nanotechnol.* **2016**, *11* (5), 479–486. https://doi.org/10.1038/nnano.2015.338.

(93) Shi, J.; Kantoff, P. W.; Wooster, R.; Farokhzad, O. C. Cancer Nanomedicine: Progress, Challenges and Opportunities. *Nat. Rev. Cancer* **2017**, *17* (1), 20–37. https://doi.org/10.1038/nrc.2016.108.

(94) Leong, H. S.; Butler, K. S.; Brinker, C. J.; Azzawi, M.; Conlan, S.; Dufés, C.; Owen, A.; Rannard, S.; Scott, C.; Chen, C.; Dobrovolskaia, M. A.; Kozlov, S. V; Prina-Mello, A.; Schmid, R.; Wick, P.; Caputo, F.; Boisseau, P.; Crist, R. M.; McNeil, S. E.; Fadeel, B.; Tran, L.; Hansen, S. F.; Hartmann, N. B.; Clausen, L. P. W.; Skjolding, L. M.; Baun, A.; Ågerstrand, M.; Gu, Z.; Lamprou, D. A.; Hoskins, C.; Huang, L.; Song, W.; Cao, H.; Liu, X.; Jandt, K. D.; Jiang, W.; Kim, B. Y. S.; Wheeler, K. E.; Chetwynd, A. J.; Lynch, I.; Moghimi, S. M.; Nel, A.; Xia, T.; Weiss, P. S.; Sarmento, B.; das Neves, J.; Santos, H. A.; Santos, L.; Mitragotri, S.; Little, S.; Peer, D.; Amiji, M. M.; Alonso, M. J.; Petri-Fink, A.; Balog, S.; Lee, A.; Drasler, B.; Rothen-Rutishauser, B.; Wilhelm, S.; Acar, H.; Harrison, R. G.; Mao, C.; Mukherjee, P.; Ramesh, R.; McNally, L. R.; Busatto, S.; Wolfram, J.; Bergese, P.; Ferrari, M.; Fang, R. H.; Zhang, L.; Zheng, J.; Peng, C.; Du, B.; Yu, M.; Charron, D. M.; Zheng, G.; Pastore, C. On the Issue of Transparency and Reproducibility in Nanomedicine. *Nat. Nanotechnol.* **2019**, *14* (7), 629–635. https://doi.org/10.1038/s41565-019-0496-9.

(95) Smith, A. M.; Nie, S. Semiconductor Nanocrystals: Structure, Properties, and Band Gap Engineering. *Acc. Chem. Res.* **2010**, *43* (2), 190–200. https://doi.org/10.1021/ar9001069.

(96) Juzenas, P.; Chen, W.; Sun, Y.-P.; Coelho, M. A. N.; Generalov, R.; Generalova, N.; Christensen, I. L. Quantum Dots and Nanoparticles for Photodynamic and Radiation Therapies of Cancer. *Adv. Drug Deliv. Rev.* **2008**, *60* (15), 1600–1614. https://doi.org/10.1016/j.addr.2008.08.004.

(97) Voinov, M. A.; Pagán, J. O. S.; Morrison, E.; Smirnova, T. I.; Smirnov, A. I. Surface-Mediated Production of Hydroxyl Radicals as a Mechanism of Iron Oxide Nanoparticle Biotoxicity. *J. Am. Chem. Soc.* **2011**, *133* (1), 35–41. https://doi.org/10.1021/ja104683w.

(98) Schlögl, R. Heterogeneous Catalysis. *Angew. Chem. Int. Ed. Engl.* **2015**, *54* (11), 3465—3520. https://doi.org/10.1002/anie.201410738.

(99) Bobo, D.; Robinson, K. J.; Islam, J.; Thurecht, K. J.; Corrie, S. R. Nanoparticle-Based Medicines: A Review of FDA-Approved Materials and Clinical Trials to Date. *Pharm. Res.* **2016**, *33* (10), 2373–2387. https://doi.org/10.1007/s11095-016-1958-5.

(100) Zhang, C.; Yan, L.; Wang, X.; Zhu, S.; Chen, C.; Gu, Z.; Zhao, Y. Progress, Challenges, and Future of Nanomedicine. *Nano Today* **2020**, *35*, 101008. https://doi.org/10.1016/j.nantod.2020.101008.

(101) Grodzinski, P.; Kircher, M.; Goldberg, M.; Gabizon, A. Integrating Nanotechnology into Cancer Care. *ACS Nano* **2019**, *13* (7), 7370–7376. https://doi.org/10.1021/acsnano.9b04266.

(102) Germain, M.; Caputo, F.; Metcalfe, S.; Tosi, G.; Spring, K.; Åslund, A. K. O.; Pottier, A.; Schiffelers, R.; Ceccaldi, A.; Schmid, R. Delivering the Power of Nanomedicine to Patients Today. *J. Control. Release* **2020**, *326*, 164–171. https://doi.org/10.1016/j.jconrel.2020.07.007.

(103) Sengupta, S. Cancer Nanomedicine: Lessons for Immuno-Oncology. *Trends in Cancer* **2017**, *3* (8), 551–

560. https://doi.org/10.1016/j.trecan.2017.06.006.

(104) Banik, B. L.; Fattahi, P.; Brown, J. L. Polymeric Nanoparticles: The Future of Nanomedicine. *WIREs Nanomedicine and Nanobiotechnology* **2016**, *8* (2), 271–299. https://doi.org/10.1002/wnan.1364.

(105) Palazzolo, S.; Bayda, S.; Hadla, M.; Caligiuri, I.; Corona, G.; Toffoli, G.; Rizzolio, F. The Clinical Translation of Organic Nanomaterials for Cancer Therapy: A Focus on Polymeric Nanoparticles, Micelles, Liposomes and Exosomes. *Curr. Med. Chem.* **2018**, *25* (34), 4224–4268. https://doi.org/10.2174/0929867324666170830113755.

(106) Bonvalot, S.; Rutkowski, P. L.; Thariat, J.; Carrère, S.; Ducassou, A.; Sunyach, M.-P.; Agoston, P.; Hong, A.; Mervoyer, A.; Rastrelli, M.; Moreno, V.; Li, R. K.; Tiangco, B.; Herraez, A. C.; Gronchi, A.; Mangel, L.; Sy-Ortin, T.; Hohenberger, P.; de Baère, T.; Le Cesne, A.; Helfre, S.; Saada-Bouzid, E.; Borkowska, A.; Anghel, R.; Co, A.; Gebhart, M.; Kantor, G.; Montero, A.; Loong, H. H.; Vergés, R.; Lapeire, L.; Dema, S.; Kacso, G.; Austen, L.; Moureau-Zabotto, L.; Servois, V.; Wardelmann, E.; Terrier, P.; Lazar, A. J.; Bovée, J. V. M. G.; Le Péchoux, C.; Papai, Z. NBTXR3, a First-in-Class Radioenhancer Hafnium Oxide Nanoparticle, plus Radiotherapy versus Radiotherapy Alone in Patients with Locally Advanced Soft-Tissue Sarcoma (Act.In.Sarc): A Multicentre, Phase 2-3, Randomised, Controlled Trial. *Lancet. Oncol.* **2019**, *20* (8), 1148–1159. https://doi.org/10.1016/S1470-2045(19)30326-2.

(107) Tang, Z.; Zhang, X.; Shu, Y.; Guo, M.; Zhang, H.; Tao, W. Insights from Nanotechnology in COVID-19 Treatment. *Nano Today* **2021**, *36*, 101019. https://doi.org/10.1016/j.nantod.2020.101019.

(108) Milane, L.; Amiji, M. Clinical Approval of Nanotechnology-Based SARS-CoV-2 MRNA Vaccines: Impact on Translational Nanomedicine. *Drug Deliv. Transl. Res.* **2021**, *11* (4), 1309–1315. https://doi.org/10.1007/s13346-021-00911-y.

(109) Ruiz-Hitzky, E.; Darder, M.; Wicklein, B.; Ruiz-Garcia, C.; Martín-Sampedro, R.; del Real, G.; Aranda, P. Nanotechnology Responses to COVID-19. *Adv. Healthc. Mater.* **2020**, *9* (19), 2000979. https://doi.org/10.1002/adhm.202000979.

(110) Youden, B.; Jiang, R.; Carrier, A. J.; Servos, M. R.; Zhang, X. A Nanomedicine Structure–Activity Framework for Research, Development, and Regulation of Future Cancer Therapies. *ACS Nano* **2022**, *16* (11), 17497–17551. https://doi.org/10.1021/acsnano.2c06337.

(111) Youden, B.; Wang, F.; Zhang, X.; Curry, D.; Majtenyi, N.; Shaaer, A.; Bingham, K.; Nguyen, Q.; Bragg, L.; Liu, J.; Servos, M.; Zhang, X.; Jiang, R. Degradable Multifunctional Gold-Liposomes as an All-in-One Theranostic Platform for Image-Guided Radiotherapy. *Int. J. Pharm.* **2022**, *629*, 122413. https://doi.org/10.1016/j.ijpharm.2022.122413.

(112) Singh, P.; Youden, B.; Yang, Y.; Chen, Y.; Carrier, A.; Cui, S.; Oakes, K.; Servos, M.; Jiang, R.; Zhang, X. Synergistic Multimodal Cancer Therapy Using Glucose Oxidase@CuS Nanocomposites. *ACS Appl. Mater. Interfaces* **2021**, *13* (35), 41464–41472. https://doi.org/10.1021/acsami.1c12235.

(113) Singh, P.; Youden, B.; Carrier, A.; Oakes, K.; Servos, M.; Jiang, R.; Lin, S.; Nguyen, T. D.; Zhang, X. Photoresponsive Polymeric Microneedles: An Innovative Way to Monitor and Treat Diseases. *J. Control. Release* **2023**, *353*, 1050–1067. https://doi.org/10.1016/j.jconrel.2022.12.036.

(114) Singh, P.; Chen, Y.; Youden, B.; Oakley, D.; Carrier, A.; Oakes, K.; Servos, M.; Jiang, R.; Zhang, X. Accelerated Cascade Melanoma Therapy Using Enzyme-Nanozyme-Integrated Dissolvable Polymeric Microneedles. *Int. J. Pharm.* **2024**, *652*, 123814. https://doi.org/10.1016/j.ijpharm.2024.123814.

(115) Lancet, T. GLOBOCAN 2018: Counting the Toll of Cancer. *Lancet* **2018**, *392* (10152), 985. https://doi.org/10.1016/S0140-6736(18)32252-9.

(116) Bray, F.; Ferlay, J.; Soerjomataram, I.; Siegel, R. L.; Torre, L. A.; Jemal, A. Global Cancer Statistics 2018: GLOBOCAN Estimates of Incidence and Mortality Worldwide for 36 Cancers in 185 Countries. *CA. Cancer J. Clin.* **2018**, *68* (6), 394–424. https://doi.org/10.3322/caac.21492.

(117) Siamof, C. M.; Goel, S.; Cai, W. Moving Beyond the Pillars of Cancer Treatment: Perspectives From

Nanotechnology. *Front. Chem.* **2020**, *8*, 1088. https://doi.org/10.3389/fchem.2020.598100.

(118) Han, X.; Xu, K.; Taratula, O.; Farsad, K. Applications of Nanoparticles in Biomedical Imaging. *Nanoscale* **2019**, *11* (3), 799–819. https://doi.org/10.1039/C8NR07769J.

(119) van der Meel, R.; Sulheim, E.; Shi, Y.; Kiessling, F.; Mulder, W. J. M.; Lammers, T. Smart Cancer Nanomedicine. *Nat. Nanotechnol.* **2019**, *14* (11), 1007–1017. https://doi.org/10.1038/s41565-019-0567-y.

(120) Beltrán-Gracia, E.; López-Camacho, A.; Higuera-Ciapara, I.; Velázquez-Fernández, J. B.; Vallejo-Cardona, A. A. Nanomedicine Review: Clinical Developments in Liposomal Applications. *Cancer Nanotechnol.* **2019**, *10* (1), 11. https://doi.org/10.1186/s12645-019-0055-y.

(121) Anselmo, A. C.; Mitragotri, S. Nanoparticles in the Clinic: An Update. *Bioeng. Transl. Med.* **2019**, *4* (3), e10143. https://doi.org/10.1002/btm2.10143.

(122) Bulbake, U.; Doppalapudi, S.; Kommineni, N.; Khan, W. Liposomal Formulations in Clinical Use: An Updated Review. *Pharmaceutics* **2017**, *9* (2), 12. https://doi.org/10.3390/pharmaceutics9020012.

(123) Anselmo, A. C.; Mitragotri, S. Nanoparticles in the Clinic: An Update Post COVID-19 Vaccines. *Bioeng. Transl. Med.* **2021**, *n/a* (n/a), e10246. https://doi.org/10.1002/btm2.10246.

(124) Bayda, S.; Hadla, M.; Palazzolo, S.; Riello, P.; Corona, G.; Toffoli, G.; Rizzolio, F. Inorganic Nanoparticles for Cancer Therapy: A Transition from Lab to Clinic. *Curr. Med. Chem.* **2018**, *25* (34), 4269–4303. https://doi.org/10.2174/0929867325666171229141156.

(125) Khalid, K.; Tan, X.; Mohd Zaid, H. F.; Tao, Y.; Lye Chew, C.; Chu, D.-T.; Lam, M. K.; Ho, Y.-C.; Lim, J. W.; Chin Wei, L. Advanced in Developmental Organic and Inorganic Nanomaterial: A Review. *Bioengineered* **2020**, *11* (1), 328–355. https://doi.org/10.1080/21655979.2020.1736240.

(126) Paris, J. L.; Baeza, A.; Vallet-Regí, M. Overcoming the Stability, Toxicity, and Biodegradation Challenges of Tumor Stimuli-Responsive Inorganic Nanoparticles for Delivery of Cancer Therapeutics. *Expert Opin. Drug Deliv.* **2019**, *16* (10), 1095–1112. https://doi.org/10.1080/17425247.2019.1662786.

(127) Kankala, R. K.; Zhang, H.; Liu, C.-G.; Kanubaddi, K. R.; Lee, C.-H.; Wang, S.-B.; Cui, W.; Santos, H. A.; Lin, K.; Chen, A.-Z. Metal Species–Encapsulated Mesoporous Silica Nanoparticles: Current Advancements and Latest Breakthroughs. *Adv. Funct. Mater.* **2019**, *29* (43), 1902652. https://doi.org/10.1002/adfm.201902652.

(128) Marchal, S.; Hor, A. El; Millard, M.; Gillon, V.; Bezdetnaya, L. Anticancer Drug Delivery: An Update on Clinically Applied Nanotherapeutics. *Drugs* **2015**, *75* (14), 1601–1611. https://doi.org/10.1007/s40265-015-0453-3.

(129) Vakili-Ghartavol, R.; Momtazi-Borojeni, A. A.; Vakili-Ghartavol, Z.; Aiyelabegan, H. T.; Jaafari, M. R.; Rezayat, S. M.; Arbabi Bidgoli, S. Toxicity Assessment of Superparamagnetic Iron Oxide Nanoparticles in Different Tissues. *Artif. cells, nanomedicine, Biotechnol.* **2020**, *48* (1), 443–451. https://doi.org/10.1080/21691401.2019.1709855.

(130) Park, S.; Aalipour, A.; Vermesh, O.; Yu, J. H.; Gambhir, S. S. Towards Clinically Translatable in Vivo Nanodiagnostics. *Nat. Rev. Mater.* **2017**, *2* (5), 17014. https://doi.org/10.1038/natrevmats.2017.14.

(131) Khandel, P.; Yadaw, R. K.; Soni, D. K.; Kanwar, L.; Shahi, S. K. Biogenesis of Metal Nanoparticles and Their Pharmacological Applications: Present Status and Application Prospects. *J. Nanostructure Chem.* **2018**, *8* (3), 217–254. https://doi.org/10.1007/s40097-018-0267-4.

(132) Weissig, V.; Pettinger, T. K.; Murdock, N. Nanopharmaceuticals (Part 1): Products on the Market. *Int. J. Nanomedicine* **2014**, *9*, 4357–4373. https://doi.org/10.2147/IJN.S46900.

(133) Sharifi-Rad, J.; Quispe, C.; Butnariu, M.; Rotariu, L. S.; Sytar, O.; Sestito, S.; Rapposelli, S.; Akram, M.; Iqbal, M.; Krishna, A.; Kumar, N. V. A.; Braga, S. S.; Cardoso, S. M.; Jafernik, K.; Ekiert, H.; Cruz-Martins, N.; Szopa, A.; Villagran, M.; Mardones, L.; Martorell, M.; Docea, A. O.; Calina, D. Chitosan Nanoparticles as a Promising Tool in Nanomedicine with Particular Emphasis on Oncological Treatment.

Cancer Cell Int. **2021**, *21* (1), 318. https://doi.org/10.1186/s12935-021-02025-4.

(134) Dias, A. P.; da Silva Santos, S.; da Silva, J. V.; Parise-Filho, R.; Igne Ferreira, E.; Seoud, O. El; Giarolla, J. Dendrimers in the Context of Nanomedicine. *Int. J. Pharm.* **2020**, *573*, 118814. https://doi.org/10.1016/j.ijpharm.2019.118814.

(135) O'Brien, M. E. R.; Wigler, N.; Inbar, M.; Rosso, R.; Grischke, E.; Santoro, A.; Catane, R.; Kieback, D. G.; Tomczak, P.; Ackland, S. P.; Orlandi, F.; Mellars, L.; Alland, L.; Tendler, C. Reduced Cardiotoxicity and Comparable Efficacy in a Phase III Trial of Pegylated Liposomal Doxorubicin HCl (CAELYX/Doxil) versus Conventional Doxorubicin for First-Line Treatment of Metastatic Breast Cancer. *Ann. Oncol. Off. J. Eur. Soc. Med. Oncol.* **2004**, *15* (3), 440–449. https://doi.org/10.1093/annonc/mdh097.

(136) Guimarães, P. P. G.; Gaglione, S.; Sewastianik, T.; Carrasco, R. D.; Langer, R.; Mitchell, M. J. Nanoparticles for Immune Cytokine TRAIL-Based Cancer Therapy. *ACS Nano* **2018**, *12* (2), 912–931. https://doi.org/10.1021/acsnano.7b05876.

(137) Pramanik, A.; Xu, Z.; Shamsuddin, S. H.; Khaled, Y. S.; Ingram, N.; Maisey, T.; Tomlinson, D.; Coletta, P. L.; Jayne, D.; Hughes, T. A.; Tyler, A. I. I.; Millner, P. A. Affimer Tagged Cubosomes: Targeting of Carcinoembryonic Antigen Expressing Colorectal Cancer Cells Using In Vitro and In Vivo Models. *ACS Appl. Mater. Interfaces* **2022**, *14* (9), 11078–11091. https://doi.org/10.1021/acsami.1c21655.

(138) Fang, J.; Nakamura, H.; Maeda, H. The EPR Effect: Unique Features of Tumor Blood Vessels for Drug Delivery, Factors Involved, and Limitations and Augmentation of the Effect. *Advanced Drug Delivery Reviews*. March 18, 2011, pp 136–151. https://doi.org/10.1016/j.addr.2010.04.009.

(139) Bae, Y. H.; Park, K. Targeted Drug Delivery to Tumors: Myths, Reality and Possibility. *Journal of Controlled Release*. Elsevier B.V. August 10, 2011, pp 198–205. https://doi.org/10.1016/j.jconrel.2011.06.001.

(140) Nel, A.; Ruoslahti, E.; Meng, H. New Insights into "Permeability" as in the Enhanced Permeability and Retention Effect of Cancer Nanotherapeutics. *ACS Nano* **2017**, *11* (10), 9567–9569. https://doi.org/10.1021/acsnano.7b07214.

(141) Golombek, S. K.; May, J. N.; Theek, B.; Appold, L.; Drude, N.; Kiessling, F.; Lammers, T. Tumor Targeting via EPR: Strategies to Enhance Patient Responses. *Advanced Drug Delivery Reviews*. Elsevier B.V. May 1, 2018, pp 17–38. https://doi.org/10.1016/j.addr.2018.07.007.

(142) Sindhwani, S.; Syed, A. M.; Ngai, J.; Kingston, B. R.; Maiorino, L.; Rothschild, J.; MacMillan, P.; Zhang, Y.; Rajesh, N. U.; Hoang, T.; Wu, J. L. Y.; Wilhelm, S.; Zilman, A.; Gadde, S.; Sulaiman, A.; Ouyang, B.; Lin, Z.; Wang, L.; Egeblad, M.; Chan, W. C. W. The Entry of Nanoparticles into Solid Tumours. *Nat. Mater.* **2020**, *19* (5), 566–575. https://doi.org/10.1038/s41563-019-0566-2.

(143) Crist, R. M.; Dasa, S. S. K.; Liu, C. H.; Clogston, J. D.; Dobrovolskaia, M. A.; Stern, S. T. Challenges in the Development of Nanoparticle-Based Imaging Agents: Characterization and Biology. *WIREs Nanomedicine and Nanobiotechnology* **2021**, *13* (1), e1665. https://doi.org/10.1002/wnan.1665.

(144) Chen, D.; Ganesh, S.; Wang, W.; Amiji, M. Protein Corona-Enabled Systemic Delivery and Targeting of Nanoparticles. *AAPS J.* **2020**, *22* (4), 83. https://doi.org/10.1208/s12248-020-00464-x.

(145) Giulimondi, F.; Digiacomo, L.; Pozzi, D.; Palchetti, S.; Vulpis, E.; Capriotti, A. L.; Chiozzi, R. Z.; Laganà, A.; Amenitsch, H.; Masuelli, L.; Peruzzi, G.; Mahmoudi, M.; Screpanti, I.; Zingoni, A.; Caracciolo, G. Interplay of Protein Corona and Immune Cells Controls Blood Residency of Liposomes. *Nat. Commun.* **2019**, *10* (1), 3686. https://doi.org/10.1038/s41467-019-11642-7.

(146) Allen, T. M.; Cullis, P. R. Liposomal Drug Delivery Systems: From Concept to Clinical Applications. *Adv. Drug Deliv. Rev.* **2013**, *65* (1), 36–48. https://doi.org/10.1016/j.addr.2012.09.037.

(147) Zylberberg, C.; Matosevic, S. Pharmaceutical Liposomal Drug Delivery: A Review of New Delivery Systems and a Look at the Regulatory Landscape. *Drug Deliv.* **2016**, *23* (9), 3319–3329. https://doi.org/10.1080/10717544.2016.1177136.

(148) Hua, S.; Wu, S. Y. The Use of Lipid-Based Nanocarriers for Targeted Pain Therapies. *Front. Pharmacol.* **2013**, *4*, 143. https://doi.org/10.3389/fphar.2013.00143.

(149) Sercombe, L.; Veerati, T.; Moheimani, F.; Wu, S. Y.; Sood, A. K.; Hua, S. Advances and Challenges of Liposome Assisted Drug Delivery. *Front. Pharmacol.* **2015**, *6*, 286. https://doi.org/10.3389/fphar.2015.00286.

(150) Schöttler, S.; Becker, G.; Winzen, S.; Steinbach, T.; Mohr, K.; Landfester, K.; Mailänder, V.; Wurm, F. R. Protein Adsorption Is Required for Stealth Effect of Poly(Ethylene Glycol)- and Poly(Phosphoester)-Coated Nanocarriers. *Nat. Nanotechnol.* **2016**, *11* (4), 372–377. https://doi.org/10.1038/nnano.2015.330.

(151) Lorusso, D.; Di Stefano, A.; Carone, V.; Fagotti, A.; Pisconti, S.; Scambia, G. Pegylated Liposomal Doxorubicin-Related Palmar-Plantar Erythrodysesthesia (‘Hand-Foot’ Syndrome). *Ann. Oncol.* **2007**, *18* (7), 1159–1164. https://doi.org/10.1093/annonc/mdl477.

(152) Fukuda, A.; Tahara, K.; Hane, Y.; Matsui, T.; Sasaoka, S.; Hatahira, H.; Motooka, Y.; Hasegawa, S.; Naganuma, M.; Abe, J.; Nakao, S.; Takeuchi, H.; Nakamura, M. Comparison of the Adverse Event Profiles of Conventional and Liposomal Formulations of Doxorubicin Using the FDA Adverse Event Reporting System. *PLoS One* **2017**, *12* (9), e0185654–e0185654. https://doi.org/10.1371/journal.pone.0185654.

(153) Brucker, J.; Mayer, C.; Gebauer, G.; Mallmann, P.; Belau, A. K.; Schneeweiss, A.; Sohn, C.; Eichbaum, M. Non-Pegylated Liposomal Doxorubicin for Patients with Recurrent Ovarian Cancer: A Multicentric Phase II Trial. *Oncol. Lett.* **2016**, *12* (2), 1211–1215. https://doi.org/10.3892/ol.2016.4740.

(154) Yang, B.; Chen, Y.; Shi, J. Reactive Oxygen Species (ROS)-Based Nanomedicine. *Chem. Rev.* **2019**, *119* (8), 4881–4985. https://doi.org/10.1021/acs.chemrev.8b00626.

(155) Auffan, M.; Rose, J.; Bottero, J.-Y.; Lowry, G. V; Jolivet, J.-P.; Wiesner, M. R. Towards a Definition of Inorganic Nanoparticles from an Environmental, Health and Safety Perspective. *Nat. Nanotechnol.* **2009**, *4* (10), 634–641. https://doi.org/10.1038/nnano.2009.242.

(156) Kim, D.; Kim, J.; Park, Y. Il; Lee, N.; Hyeon, T. Recent Development of Inorganic Nanoparticles for Biomedical Imaging. *ACS Cent. Sci.* **2018**, *4* (3), 324–336. https://doi.org/10.1021/acscentsci.7b00574.

(157) Zhang, L.; Zhu, C.; Huang, R.; Ding, Y.; Ruan, C.; Shen, X.-C. Mechanisms of Reactive Oxygen Species Generated by Inorganic Nanomaterials for Cancer Therapeutics. *Front. Chem.* **2021**, *9*, 630969. https://doi.org/10.3389/fchem.2021.630969.

(158) Hadjipanayis, C. G.; Bonder, M. J.; Balakrishnan, S.; Wang, X.; Mao, H.; Hadjipanayis, G. C. Metallic Iron Nanoparticles for MRI Contrast Enhancement and Local Hyperthermia. *Small* **2008**, *4* (11), 1925–1929. https://doi.org/10.1002/smll.200800261.

(159) Wang, X.; Zhong, X.; Liu, Z.; Cheng, L. Recent Progress of Chemodynamic Therapy-Induced Combination Cancer Therapy. *Nano Today* **2020**, *35*, 100946. https://doi.org/10.1016/j.nantod.2020.100946.

(160) Jaque, D.; Martínez Maestro, L.; Del Rosal, B.; Haro-Gonzalez, P.; Benayas, A.; Plaza, J. L.; Martín Rodríguez, E.; García Solé, J. Nanoparticles for Photothermal Therapies. *Nanoscale* **2014**, *6* (16), 9494–9530. https://doi.org/10.1039/c4nr00708e.

(161) Gavilán, H.; Avugadda, S. K.; Fernández-Cabada, T.; Soni, N.; Cassani, M.; Mai, B. T.; Chantrell, R.; Pellegrino, T. Magnetic Nanoparticles and Clusters for Magnetic Hyperthermia: Optimizing Their Heat Performance and Developing Combinatorial Therapies to Tackle Cancer. *Chem. Soc. Rev.* **2021**, *50* (20), 11614–11667. https://doi.org/10.1039/D1CS00427A.

(162) Tang, Z.; Liu, Y.; He, M.; Bu, W. Chemodynamic Therapy: Tumour Microenvironment-Mediated Fenton and Fenton-like Reactions. *Angew. Chem. Int. Ed. Engl.* **2019**, *58* (4), 946–956. https://doi.org/10.1002/anie.201805664.

(163) Xie, J.; Gong, L.; Zhu, S.; Yong, Y.; Gu, Z.; Zhao, Y. Emerging Strategies of Nanomaterial-Mediated Tumor Radiosensitization. *Adv. Mater.* **2019**, *31* (3), 1802244. https://doi.org/10.1002/adma.201802244.

(164) Frtús, A.; Smolková, B.; Uzhytchak, M.; Lunova, M.; Jirsa, M.; Kubinová, Š.; Dejneka, A.; Lunov, O. Analyzing the Mechanisms of Iron Oxide Nanoparticles Interactions with Cells: A Road from Failure to Success in Clinical Applications. *J. Control. Release* **2020**, *328*, 59–77. https://doi.org/10.1016/j.jconrel.2020.08.036.

(165) Her, S.; Jaffray, D. A.; Allen, C. Gold Nanoparticles for Applications in Cancer Radiotherapy: Mechanisms and Recent Advancements. *Adv. Drug Deliv. Rev.* **2017**, *109*, 84–101. https://doi.org/10.1016/j.addr.2015.12.012.

(166) Liu, Y.; Zhang, P.; Li, F.; Jin, X.; Li, J.; Chen, W.; Li, Q. Metal-Based *NanoEnhancers* for Future Radiotherapy: Radiosensitizing and Synergistic Effects on Tumor Cells. *Theranostics* **2018**, *8* (7), 1824–1849. https://doi.org/10.7150/thno.22172.

(167) Delaney, G. P.; Barton, M. B. Evidence-Based Estimates of the Demand for Radiotherapy. *Clin. Oncol.* **2015**, *27* (2), 70–76. https://doi.org/10.1016/j.clon.2014.10.005.

(168) Zubizarreta, E.; Van Dyk, J.; Lievens, Y. Analysis of Global Radiotherapy Needs and Costs by Geographic Region and Income Level. *Clin. Oncol.* **2017**, *29* (2), 84–92. https://doi.org/10.1016/j.clon.2016.11.011.

(169) Hall, E. J.; Giaccia, A. J. *Radiobiology for the Radiologist: Seventh Edition*; Wolters Kluwer Health Adis (ESP), 2012.

(170) Baskar, R.; Dai, J.; Wenlong, N.; Yeo, R.; Yeoh, K. W. Biological Response of Cancer Cells to Radiation Treatment. *Front. Mol. Biosci.* **2014**, *1*. https://doi.org/10.3389/fmolb.2014.00024.

(171) Mikkelsen, R. B.; Wardman, P. Biological Chemistry of Reactive Oxygen and Nitrogen and Radiation-Induced Signal Transduction Mechanisms. *Oncogene* **2003**, *22* (37), 5734–5754. https://doi.org/10.1038/sj.onc.1206663.

(172) Cui, L.; Her, S.; Borst, G. R.; Bristow, R. G.; Jaffray, D. A.; Allen, C. Radiosensitization by Gold Nanoparticles: Will They Ever Make It to the Clinic? *Radiother. Oncol.* **2017**, *124* (3), 344–356. https://doi.org/10.1016/j.radonc.2017.07.007.

(173) Burrell, R. A.; McGranahan, N.; Bartek, J.; Swanton, C. The Causes and Consequences of Genetic Heterogeneity in Cancer Evolution. *Nature* **2013**, *501* (7467), 338–345. https://doi.org/10.1038/nature12625.

(174) Vilalta, M.; Rafat, M.; Graves, E. E. Effects of Radiation on Metastasis and Tumor Cell Migration. *Cell. Mol. Life Sci.* **2016**, *73* (16), 2999–3007. https://doi.org/10.1007/s00018-016-2210-5.

(175) Gordon Steel, G.; Peckham, M. J. Exploitable Mechanisms in Combined Radiotherapy-Chemotherapy: The Concept of Additivity. *Int. J. Radiat. Oncol. Biol. Phys.* **1979**, *5* (1), 85–91. https://doi.org/10.1016/0360-3016(79)90044-0.

(176) Seiwert, T. Y.; Salama, J. K.; Vokes, E. E. The Concurrent Chemoradiation Paradigm - General Principles. *Nat. Clin. Pract. Oncol.* **2007**, *4* (2), 86–100. https://doi.org/10.1038/ncponc0714.

(177) Thariat, J.; Hannoun-Levi, J. M.; Sun Myint, A.; Vuong, T.; Gérard, J. P. Past, Present, and Future of Radiotherapy for the Benefit of Patients. *Nature Reviews Clinical Oncology*. Nat Rev Clin Oncol January 2013, pp 52–60. https://doi.org/10.1038/nrclinonc.2012.203.

(178) Lawrence, T. S.; Blackstock, A. W.; McGinn, C. The Mechanism of Action of Radiosensitization of Conventional Chemotherapeutic Agents. *Semin. Radiat. Oncol.* **2003**, *13* (1), 13–21. https://doi.org/10.1053/srao.2003.50002.

(179) Wilson, G. D.; Bentzen, S. M.; Harari, P. M. Biologic Basis for Combining Drugs with Radiation. *Semin. Radiat. Oncol.* **2006**, *16* (1), 2–9. https://doi.org/10.1016/j.semradonc.2005.08.001.

(180) Gorlick, R.; Banerjee, D. Fluoropyrimidine Resistance in Colon Cancer. *Expert Rev. Anticancer Ther.* **2002**, *2* (4), 409–416. https://doi.org/10.1586/14737140.2.4.409.

(181) Stordal, B.; Davey, M. Understanding Cisplatin Resistance Using Cellular Models. *IUBMB Life* **2007**, *59* (11), 696–699. https://doi.org/10.1080/15216540701636287.

(182) Ahmad, S. S.; Crittenden, M. R.; Tran, P. T.; Kluetz, P. G.; Blumenthal, G. M.; Bulbeck, H.; Baird, R. D.; Williams, K. J.; Illidge, T.; Hahn, S. M.; Lawrence, T. S.; Spears, P. A.; Walker, A. J.; Sharma, R. A. Clinical Development of Novel Drug-Radiotherapy Combinations. *Clin. Cancer Res.* **2019**, *25* (5), 1455–1461. https://doi.org/10.1158/1078-0432.CCR-18-2466.

(183) Schuemann, J.; Bagley, A. F.; Berbeco, R.; Bromma, K.; Butterworth, K. T.; Byrne, H. L.; Chithrani, B. D.; Cho, S. H.; Cook, J. R.; Favaudon, V.; Gholami, Y. H.; Gargioni, E.; Hainfeld, J. F.; Hespeels, F.; Heuskin, A.-C.; Ibeh, U. M.; Kuncic, Z.; Kunjachan, S.; Lacombe, S.; Lucas, S.; Lux, F.; McMahon, S.; Nevozhay, D.; Ngwa, W.; Payne, J. D.; Penninckx, S.; Porcel, E.; Prise, K. M.; Rabus, H.; Ridwan, S. M.; Rudek, B.; Sanche, L.; Singh, B.; Smilowitz, H. M.; Sokolov, K. V; Sridhar, S.; Stanishevskiy, Y.; Sung, W.; Tillement, O.; Virani, N.; Yantasee, W.; Krishnan, S. Roadmap for Metal Nanoparticles in Radiation Therapy: Current Status, Translational Challenges, and Future Directions. *Phys. Med. Biol.* **2020**, *65* (21), 21RM02. https://doi.org/10.1088/1361-6560/ab9159.

(184) Schuemann, J.; Berbeco, R.; Chithrani, D. B.; Cho, S. H.; Kumar, R.; McMahon, S. J.; Sridhar, S.; Krishnan, S. Roadmap to Clinical Use of Gold Nanoparticles for Radiation Sensitization. *Int. J. Radiat. Oncol. Biol. Phys.* **2016**, *94* (1), 189–205. https://doi.org/10.1016/j.ijrobp.2015.09.032.

(185) Butterworth, K. T.; McMahon, S. J.; Taggart, L. E.; Prise, K. M. Radiosensitization by Gold Nanoparticles: Effective at Megavoltage Energies and Potential Role of Oxidative Stress. *Transl. Cancer Res.* **2013**, *2* (4), 269–279. https://doi.org/10.21037/1514.

(186) Hainfeld, J. F.; Slatkin, D. N.; Smilowitz, H. M. The Use of Gold Nanoparticles to Enhance Radiotherapy in Mice. *Phys. Med. Biol.* **2004**, *49* (18), N309--N315. https://doi.org/10.1088/0031-9155/49/18/n03.

(187) Hainfeld, J. F.; Slatkin, D. N.; Focella, T. M.; Smilowitz, H. M. Gold Nanoparticles: A New X-Ray Contrast Agent. *Br. J. Radiol.* **2006**, *79* (939), 248–253. https://doi.org/10.1259/bjr/13169882.

(188) Mühlebach, S. Regulatory Challenges of Nanomedicines and Their Follow-on Versions: A Generic or Similar Approach? *Adv. Drug Deliv. Rev.* **2018**, *131*, 122–131. https://doi.org/10.1016/j.addr.2018.06.024.

(189) Paradise, J. Regulating Nanomedicine at the Food and Drug Administration. *AMA J. ethics* **2019**, *21* (4), E347-355. https://doi.org/10.1001/amajethics.2019.347.

(190) Foulkes, R.; Man, E.; Thind, J.; Yeung, S.; Joy, A.; Hoskins, C. The Regulation of Nanomaterials and Nanomedicines for Clinical Application: Current and Future Perspectives. *Biomater. Sci.* **2020**, *8* (17), 4653–4664. https://doi.org/10.1039/D0BM00558D.

(191) Ventola, C. L. Progress in Nanomedicine: Approved and Investigational Nanodrugs. *Pharmacol. Ther.* **2017**, *42* (12), 742–755. https://doi.org/10.1021/acsbiomaterials.8b01181.

(192) Ragelle, H.; Danhier, F.; Préat, V.; Langer, R.; Anderson, D. G. Nanoparticle-Based Drug Delivery Systems: A Commercial and Regulatory Outlook as the Field Matures. *Expert Opin. Drug Deliv.* **2017**, *14* (7), 851–864. https://doi.org/10.1080/17425247.2016.1244187.

(193) U.S. Food and Drug Administration. *Final Guidance for Industry - Liposome Drug Products: Chemistry, Manufacturing, and Controls; Human Pharmacokinetics and Bioavailability; and Labeling Documentation*; 2018. https://doi.org/https://www.fda.gov/media/70837/download.

(194) U.S. Food and Drug Administration. *Final Guidance for Industry - Considering Whether an FDA-Regulated Product Involves the Application of Nanotechnology*; 2014. https://doi.org/https://www.fda.gov/media/88423/download.

(195) U.S. Food and Drug Administration. *Draft Guidance for Industry - Drug Products, Including Biological Products, That Contain Nanomaterials*; 2017. https://doi.org/https://www.fda.gov/media/109910/download.

(196) Soares, S.; Sousa, J.; Pais, A.; Vitorino, C. Nanomedicine: Principles, Properties, and Regulatory Issues.

Front. Chem. **2018**, *6*, 360. https://doi.org/10.3389/fchem.2018.00360.

(197) Hannon, G.; Prina-Mello, A. Endotoxin Contamination of Engineered Nanomaterials: Overcoming the Hurdles Associated with Endotoxin Testing. *WIREs Nanomedicine and Nanobiotechnology* **2021**, *13* (6), e1738. https://doi.org/10.1002/wnan.1738.

(198) Mello, D. F.; Trevisan, R.; Rivera, N.; Geitner, N. K.; Di Giulio, R. T.; Wiesner, M. R.; Hsu-Kim, H.; Meyer, J. N. Caveats to the Use of MTT, Neutral Red, Hoechst and Resazurin to Measure Silver Nanoparticle Cytotoxicity. *Chem. Biol. Interact.* **2020**, *315*, 108868. https://doi.org/10.1016/j.cbi.2019.108868.

(199) Kroll, A.; Pillukat, M. H.; Hahn, D.; Schnekenburger, J. Interference of Engineered Nanoparticles with in Vitro Toxicity Assays. *Arch. Toxicol.* **2012**, *86* (7), 1123–1136. https://doi.org/10.1007/s00204-012-0837-z.

(200) Chen, Y.; Yang, Y.; Zeng, X.; Feng, J. L.; Oakes, K.; Zhang, X.; Cui, S. Microfluidic Chip Interfacing Microdialysis and Mass Spectrometry for in Vivo Monitoring of Nanomedicine Pharmacokinetics in Real Time. *J. Chromatogr. A* **2022**, *1683*, 463520. https://doi.org/10.1016/j.chroma.2022.463520.

(201) Emily, M.; Ioanna, N.; Scott, B.; Beat, F. Reflections on FDA Draft Guidance for Products Containing Nanomaterials: Is the Abbreviated New Drug Application (ANDA) a Suitable Pathway for Nanomedicines? *AAPS J.* **2018**, *20* (5), 92. https://doi.org/10.1208/s12248-018-0255-0.

(202) European Commision; Joint Research Centre; Box, H.; Bremer-Hoffmann, S.; Gaitan, S.; Del Pozo, A.; Elk, M.; Geertsma, R.; Gainza Lafuente, E.; Roesslein, M.; Owen, A.; Halamoda-Kenzaoui, B. *Anticipation of Regulatory Needs for Nanotechnology-Enabled Health Products : The REFINE White Paper*; Publications Office, 2019. https://doi.org/doi/10.2760/596822.

(203) Blumenfeld, P.; Pfeffer, R. M.; Symon, Z.; Den, R. B.; Dicker, A. P.; Raben, D.; Lawrence, Y. R. The Lag Time in Initiating Clinical Testing of New Drugs in Combination with Radiation Therapy, a Significant Barrier to Progress? *Br. J. Cancer* **2014**, *111* (7), 1305–1309. https://doi.org/10.1038/bjc.2014.448.

(204) Bhardwaj, V.; Kaushik, A.; Khatib, Z. M.; Nair, M.; McGoron, A. J. Recalcitrant Issues and New Frontiers in Nano-Pharmacology . *Frontiers in Pharmacology* . 2019, p 1369.

(205) Metselaar, J. M.; Lammers, T. Challenges in Nanomedicine Clinical Translation. *Drug Deliv. Transl. Res.* **2020**, *10* (3), 721–725. https://doi.org/10.1007/s13346-020-00740-5.

(206) Kad, A.; Pundir, A.; Arya, S. K.; Bhardwaj, N.; Khatri, M. An Elucidative Review to Analytically Sieve the Viability of Nanomedicine Market. *J. Pharm. Innov.* **2022**, *17* (1), 249–265. https://doi.org/10.1007/s12247-020-09495-5.

(207) He, H.; Liu, L.; Morin, E. E.; Liu, M.; Schwendeman, A. Survey of Clinical Translation of Cancer Nanomedicines-Lessons Learned from Successes and Failures. *Acc. Chem. Res.* **2019**, *52* (9), 2445–2461. https://doi.org/10.1021/acs.accounts.9b00228.

(208) Youn, Y. S.; Bae, Y. H. Perspectives on the Past, Present, and Future of Cancer Nanomedicine. *Adv. Drug Deliv. Rev.* **2018**, *130*, 3–11. https://doi.org/10.1016/j.addr.2018.05.008.

(209) Farjadian, F.; Ghasemi, A.; Gohari, O.; Roointan, A.; Karimi, M.; Hamblin, M. R. Nanopharmaceuticals and Nanomedicines Currently on the Market: Challenges and Opportunities. *Nanomedicine (Lond).* **2019**, *14* (1), 93–126. https://doi.org/10.2217/nnm-2018-0120.

(210) Wang, C.; Graham, D. J.; Kane, R. C.; Xie, D.; Wernecke, M.; Levenson, M.; MaCurdy, T. E.; Houstoun, M.; Ryan, Q.; Wong, S.; Mott, K.; Sheu, T.-C.; Limb, S.; Worrall, C.; Kelman, J. A.; Reichman, M. E. Comparative Risk of Anaphylactic Reactions Associated With Intravenous Iron Products. *JAMA* **2015**, *314* (19), 2062–2068. https://doi.org/10.1001/jama.2015.15572.

(211) Heymans, S.; Cooper, L. T. Myocarditis after COVID-19 MRNA Vaccination: Clinical Observations and Potential Mechanisms. *Nat. Rev. Cardiol.* **2022**, *19* (2), 75–77. https://doi.org/10.1038/s41569-021-00662-w.

(212) Maderal, A. D.; Vivas, A. C.; Eaglstein, W. H.; Kirsner, R. S. The FDA and Designing Clinical Trials for Chronic Cutaneous Ulcers. *Semin. Cell Dev. Biol.* **2012**, *23* (9), 993–999. https://doi.org/10.1016/j.semcdb.2012.09.014.

(213) Baig, B.; Halim, S. A.; Farrukh, A.; Greish, Y.; Amin, A. Current Status of Nanomaterial-Based Treatment for Hepatocellular Carcinoma. *Biomed. Pharmacother.* **2019**, *116*, 108852. https://doi.org/10.1016/j.biopha.2019.108852.

(214) Rasmussen, K.; Rauscher, H.; Mech, A.; Riego Sintes, J.; Gilliland, D.; González, M.; Kearns, P.; Moss, K.; Visser, M.; Groenewold, M.; Bleeker, E. A. J. Physico-Chemical Properties of Manufactured Nanomaterials - Characterisation and Relevant Methods. An Outlook Based on the OECD Testing Programme. *Regul. Toxicol. Pharmacol.* **2018**, *92*, 8–28. https://doi.org/10.1016/j.yrtph.2017.10.019.

(215) Sarmento, B. Have Nanomedicines Progressed as Much as We'd Hoped for in Drug Discovery and Development? *Expert Opin. Drug Discov.* **2019**, *14* (8), 723–725. https://doi.org/10.1080/17460441.2019.1621286.

(216) Labouta, H. I.; Asgarian, N.; Rinker, K.; Cramb, D. T. Meta-Analysis of Nanoparticle Cytotoxicity via Data-Mining the Literature. *ACS Nano* **2019**, *13* (2), 1583–1594. https://doi.org/10.1021/acsnano.8b07562.

(217) Zhang, H.; Ji, Z.; Xia, T.; Meng, H.; Low-Kam, C.; Liu, R.; Pokhrel, S.; Lin, S.; Wang, X.; Liao, Y.-P.; Wang, M.; Li, L.; Rallo, R.; Damoiseaux, R.; Telesca, D.; Mädler, L.; Cohen, Y.; Zink, J. I.; Nel, A. E. Use of Metal Oxide Nanoparticle Band Gap to Develop a Predictive Paradigm for Oxidative Stress and Acute Pulmonary Inflammation. *ACS Nano* **2012**, *6* (5), 4349–4368. https://doi.org/10.1021/nn3010087.

(218) Fadeel, B.; Fornara, A.; Toprak, M. S.; Bhattacharya, K. Keeping It Real: The Importance of Material Characterization in Nanotoxicology. *Biochem. Biophys. Res. Commun.* **2015**, *468* (3), 498–503. https://doi.org/10.1016/j.bbrc.2015.06.178.

(219) Zheng, R.; Zhang, H. Regulation of Electronic Properties of Metal Oxide Nanoparticles to Reveal Their Toxicity Mechanism and Safe-by-Design Approach. *Adv. Biol.* **2021**, *5* (2), 2000220. https://doi.org/10.1002/adbi.202000220.

(220) Qiu, T. A.; Clement, P. L.; Haynes, C. L. Linking Nanomaterial Properties to Biological Outcomes: Analytical Chemistry Challenges in Nanotoxicology for the next Decade. *Chem. Commun.* **2018**, *54* (91), 12787–12803. https://doi.org/10.1039/C8CC06473C.

(221) Corbo, C.; Molinaro, R.; Parodi, A.; Toledano Furman, N. E.; Salvatore, F.; Tasciotti, E. The Impact of Nanoparticle Protein Corona on Cytotoxicity, Immunotoxicity and Target Drug Delivery. *Nanomedicine (Lond).* **2016**, *11* (1), 81–100. https://doi.org/10.2217/nnm.15.188.

(222) Oomen, A. G.; Steinhäuser, K. G.; Bleeker, E. A. J.; van Broekhuizen, F.; Sips, A.; Dekkers, S.; Wijnhoven, S. W. P.; Sayre, P. G. Risk Assessment Frameworks for Nanomaterials: Scope, Link to Regulations, Applicability, and Outline for Future Directions in View of Needed Increase in Efficiency. *NanoImpact* **2018**, *9*, 1–13. https://doi.org/10.1016/j.impact.2017.09.001.

(223) Liu, Y.; Zhu, S.; Gu, Z.; Chen, C.; Zhao, Y. Toxicity of Manufactured Nanomaterials. *Particuology* **2022**, *69*, 31–48. https://doi.org/10.1016/j.partic.2021.11.007.

(224) Faria, M.; Björnmalm, M.; Thurecht, K. J.; Kent, S. J.; Parton, R. G.; Kavallaris, M.; Johnston, A. P. R.; Gooding, J. J.; Corrie, S. R.; Boyd, B. J.; Thordarson, P.; Whittaker, A. K.; Stevens, M. M.; Prestidge, C. A.; Porter, C. J. H.; Parak, W. J.; Davis, T. P.; Crampin, E. J.; Caruso, F. Minimum Information Reporting in Bio-Nano Experimental Literature. *Nat. Nanotechnol.* **2018**, *13* (9), 777–785. https://doi.org/10.1038/s41565-018-0246-4.

(225) Kempson, I. Mechanisms of Nanoparticle Radiosensitization. *WIREs Nanomedicine and Nanobiotechnology* **2021**, *13* (1), e1656. https://doi.org/10.1002/wnan.1656.

(226) Zhang, Q.; Li, J.; Middleton, A.; Bhattacharya, S.; Conolly, R. B. Bridging the Data Gap From in Vitro Toxicity Testing to Chemical Safety Assessment Through Computational Modeling. *Front. Public Heal.*

2018, *6*, 261. https://doi.org/10.3389/fpubh.2018.00261.

(227) Bremer-Hoffmann, S.; Halamoda-Kenzaoui, B.; Borgos, S. E. Identification of Regulatory Needs for Nanomedicines. *J. Interdiscip. Nanomedicine* **2018**, *3* (1), 4–15. https://doi.org/10.1002/jin2.34.

(228) Villeneuve, D. L.; Coady, K.; Escher, B. I.; Mihaich, E.; Murphy, C. A.; Schlekat, T.; Garcia-Reyero, N. High-Throughput Screening and Environmental Risk Assessment: State of the Science and Emerging Applications. *Environ. Toxicol. Chem.* **2019**, *38* (1), 12–26. https://doi.org/10.1002/etc.4315.

(229) Avila, A. M.; Bebenek, I.; Bonzo, J. A.; Bourcier, T.; Davis Bruno, K. L.; Carlson, D. B.; Dubinion, J.; Elayan, I.; Harrouk, W.; Lee, S.-L.; Mendrick, D. L.; Merrill, J. C.; Peretz, J.; Place, E.; Saulnier, M.; Wange, R. L.; Yao, J.; Zhao, D.; Brown, P. C. An FDA/CDER Perspective on Nonclinical Testing Strategies: Classical Toxicology Approaches and New Approach Methodologies (NAMs). *Regul. Toxicol. Pharmacol.* **2020**, *114*, 104662. https://doi.org/10.1016/j.yrtph.2020.104662.

(230) Lamon, L.; Aschberger, K.; Asturiol, D.; Richarz, A.; Worth, A. Grouping of Nanomaterials to Read-across Hazard Endpoints: A Review. *Nanotoxicology* **2019**, *13* (1), 100–118. https://doi.org/10.1080/17435390.2018.1506060.

(231) Gerloff, K.; Landesmann, B.; Worth, A.; Munn, S.; Palosaari, T.; Whelan, M. The Adverse Outcome Pathway Approach in Nanotoxicology. *Comput. Toxicol.* **2017**, *1*, 3–11. https://doi.org/10.1016/j.comtox.2016.07.001.

(232) Halappanavar, S.; Ede, J. D.; Shatkin, J. A.; Krug, H. F. A Systematic Process for Identifying Key Events for Advancing the Development of Nanomaterial Relevant Adverse Outcome Pathways. *NanoImpact* **2019**, *15*, 100178. https://doi.org/10.1016/j.impact.2019.100178.

(233) Vietti, G.; Lison, D.; van den Brule, S. Mechanisms of Lung Fibrosis Induced by Carbon Nanotubes: Towards an Adverse Outcome Pathway (AOP). *Part. Fibre Toxicol.* **2016**, *13* (1), 1–23. https://doi.org/10.1186/s12989-016-0123-y.

(234) Gomes, S. I. L.; Scott-Fordsmand, J. J.; Amorim, M. J. B. Alternative Test Methods for (Nano)Materials Hazards Assessment: Challenges and Recommendations for Regulatory Preparedness. *Nano Today* **2021**, *40*, 101242. https://doi.org/10.1016/j.nantod.2021.101242.

(235) Jeong, J.; Song, T.; Chatterjee, N.; Choi, I.; Cha, Y. K.; Choi, J. Developing Adverse Outcome Pathways on Silver Nanoparticle-Induced Reproductive Toxicity via Oxidative Stress in the Nematode Caenorhabditis Elegans Using a Bayesian Network Model. *Nanotoxicology* **2018**, *12* (10), 1182–1197. https://doi.org/10.1080/17435390.2018.1529835.

(236) Ma, Y. B.; Lu, C. J.; Junaid, M.; Jia, P. P.; Yang, L.; Zhang, J. H.; Pei, D. S. Potential Adverse Outcome Pathway (AOP) of Silver Nanoparticles Mediated Reproductive Toxicity in Zebrafish. *Chemosphere* **2018**, *207*, 320–328. https://doi.org/10.1016/j.chemosphere.2018.05.019.

(237) Labib, S.; Williams, A.; Yauk, C. L.; Nikota, J. K.; Wallin, H.; Vogel, U.; Halappanavar, S. Nano-Risk Science: Application of Toxicogenomics in an Adverse Outcome Pathway Framework for Risk Assessment of Multi-Walled Carbon Nanotubes. *Part. Fibre Toxicol.* **2016**, *13* (1), 1–17. https://doi.org/10.1186/s12989-016-0125-9.

(238) Muller, E. B.; Lin, S.; Nisbet, R. M. Quantitative Adverse Outcome Pathway Analysis of Hatching in Zebrafish with CuO Nanoparticles. *Environ. Sci. Technol.* **2015**, *49* (19), 11817–11824. https://doi.org/10.1021/acs.est.5b01837.

(239) Gomes, S. I. L.; Roca, C. P.; Pegoraro, N.; Trindade, T.; Scott-Fordsmand, J. J.; Amorim, M. J. B. High-Throughput Tool to Discriminate Effects of NMs (Cu-NPs, Cu-Nanowires, CuNO3, and Cu Salt Aged): Transcriptomics in Enchytraeus Crypticus. *Nanotoxicology* **2018**, *12* (4), 325–340. https://doi.org/10.1080/17435390.2018.1446559.

(240) Desai, N. Challenges in Development of Nanoparticle-Based Therapeutics. *AAPS J.* **2012**, *14* (2), 282–295. https://doi.org/10.1208/s12248-012-9339-4.

(241) Agrahari, V.; Hiremath, P. Challenges Associated and Approaches for Successful Translation of Nanomedicines into Commercial Products. *Nanomedicine* **2017**, *12* (8), 819–823. https://doi.org/10.2217/nnm-2017-0039.

(242) Ciccarese, F.; Raimondi, V.; Sharova, E.; Silic-Benussi, M.; Ciminale, V. Nanoparticles as Tools to Target Redox Homeostasis in Cancer Cells. *Antioxidants*. 2020.

(243) Abdal Dayem, A.; Hossain, M. K.; Lee, S. Bin; Kim, K.; Saha, S. K.; Yang, G.-M.; Choi, H. Y.; Cho, S.-G. The Role of Reactive Oxygen Species (ROS) in the Biological Activities of Metallic Nanoparticles. *Int. J. Mol. Sci.* **2017**, *18* (1), 120. https://doi.org/10.3390/ijms18010120.

(244) Ede, J. D.; Lobaskin, V.; Vogel, U.; Lynch, I.; Halappanavar, S.; Doak, S. H.; Roberts, M. G.; Shatkin, J. A. Translating Scientific Advances in the AOP Framework to Decision Making for Nanomaterials. *Nanomaterials* **2020**, *10* (6), 1229. https://doi.org/10.3390/nano10061229.

(245) Spinu, N.; Bal-Price, A.; Cronin, M. T. D.; Enoch, S. J.; Madden, J. C.; Worth, A. P. Development and Analysis of an Adverse Outcome Pathway Network for Human Neurotoxicity. *Arch. Toxicol.* **2019**, *93* (10), 2759–2772. https://doi.org/10.1007/s00204-019-02551-1.

(246) Villeneuve, D. L.; Crump, D.; Garcia-Reyero, N.; Hecker, M.; Hutchinson, T. H.; LaLone, C. A.; Landesmann, B.; Lettieri, T.; Munn, S.; Nepelska, M.; Ottinger, M. A.; Vergauwen, L.; Whelan, M. Adverse Outcome Pathway (AOP) Development I: Strategies and Principles. *Toxicol. Sci.* **2014**, *142* (2), 312–320. https://doi.org/10.1093/toxsci/kfu199.

(247) Dogra, P.; Butner, J. D.; Ruiz Ramírez, J.; Chuang, Y.; Noureddine, A.; Jeffrey Brinker, C.; Cristini, V.; Wang, Z. A Mathematical Model to Predict Nanomedicine Pharmacokinetics and Tumor Delivery. *Comput. Struct. Biotechnol. J.* **2020**, *18*, 518–531. https://doi.org/10.1016/j.csbj.2020.02.014.

(248) Ho, Y. T.; Kamm, R. D.; Kah, J. C. Y. Influence of Protein Corona and Caveolae-Mediated Endocytosis on Nanoparticle Uptake and Transcytosis. *Nanoscale* **2018**, *10* (26), 12386–12397. https://doi.org/10.1039/C8NR02393J.

(249) Karmali, P. P.; Simberg, D. Interactions of Nanoparticles with Plasma Proteins: Implication on Clearance and Toxicity of Drug Delivery Systems. *Expert Opin. Drug Deliv.* **2011**, *8* (3), 343–357. https://doi.org/10.1517/17425247.2011.554818.

(250) Szebeni, J. Complement Activation-Related Pseudoallergy: A New Class of Drug-Induced Acute Immune Toxicity. *Toxicology* **2005**, *216* (2–3), 106–121. https://doi.org/10.1016/j.tox.2005.07.023.

(251) Gustafson, H. H.; Holt-Casper, D.; Grainger, D. W.; Ghandehari, H. Nanoparticle Uptake: The Phagocyte Problem. *Nano Today* **2015**, *10* (4), 487–510. https://doi.org/10.1016/j.nantod.2015.06.006.

(252) Zhang, Y.-N.; Poon, W.; Tavares, A. J.; McGilvray, I. D.; Chan, W. C. W. Nanoparticle-Liver Interactions: Cellular Uptake and Hepatobiliary Elimination. *J. Control. Release* **2016**, *240*, 332–348. https://doi.org/10.1016/j.jconrel.2016.01.020.

(253) Du, B.; Yu, M.; Zheng, J. Transport and Interactions of Nanoparticles in the Kidneys. *Nat. Rev. Mater.* **2018**, *3* (10), 358–374. https://doi.org/10.1038/s41578-018-0038-3.

(254) Choi, H. S.; Liu, W.; Misra, P.; Tanaka, E.; Zimmer, J. P.; Itty Ipe, B.; Bawendi, M. G.; Frangioni, J. V. Renal Clearance of Quantum Dots. *Nat. Biotechnol.* **2007**, *25* (10), 1165–1170. https://doi.org/10.1038/nbt1340.

(255) Foroozandeh, P.; Aziz, A. A. Merging Worlds of Nanomaterials and Biological Environment: Factors Governing Protein Corona Formation on Nanoparticles and Its Biological Consequences. *Nanoscale Res. Lett.* **2015**, *10* (1), 221. https://doi.org/10.1186/s11671-015-0922-3.

(256) Barui, A. K.; Oh, J. Y.; Jana, B.; Kim, C.; Ryu, J.-H. Cancer-Targeted Nanomedicine: Overcoming the Barrier of the Protein Corona. *Adv. Ther.* **2020**, *3* (1), 1900124. https://doi.org/10.1002/adtp.201900124.

(257) Cai, R.; Chen, C. The Crown and the Scepter: Roles of the Protein Corona in Nanomedicine. *Adv. Mater.*

2019, *31* (45), 1805740. https://doi.org/10.1002/adma.201805740.

(258) Baimanov, D.; Cai, R.; Chen, C. Understanding the Chemical Nature of Nanoparticle–Protein Interactions. *Bioconjug. Chem.* **2019**, *30* (7), 1923–1937. https://doi.org/10.1021/acs.bioconjchem.9b00348.

(259) Nguyen, V. H.; Lee, B.-J. Protein Corona: A New Approach for Nanomedicine Design. *Int. J. Nanomedicine* **2017**, *12*, 3137–3151. https://doi.org/10.2147/IJN.S129300.

(260) Tedja, R.; Lim, M.; Amal, R.; Marquis, C. Effects of Serum Adsorption on Cellular Uptake Profile and Consequent Impact of Titanium Dioxide Nanoparticles on Human Lung Cell Lines. *ACS Nano* **2012**, *6* (5), 4083–4093. https://doi.org/10.1021/nn3004845.

(261) Sun, H.; Jiang, C.; Wu, L.; Bai, X.; Zhai, S. Cytotoxicity-Related Bioeffects Induced by Nanoparticles: The Role of Surface Chemistry. *Front. Bioeng. Biotechnol.* **2019**, *7*, 414. https://doi.org/10.3389/fbioe.2019.00414.

(262) Rampado, R.; Crotti, S.; Caliceti, P.; Pucciarelli, S.; Agostini, M. Recent Advances in Understanding the Protein Corona of Nanoparticles and in the Formulation of "Stealthy" Nanomaterials. *Front. Bioeng. Biotechnol.* **2020**, *8*, 166. https://doi.org/10.3389/fbioe.2020.00166.

(263) Walkey, C. D.; Olsen, J. B.; Song, F.; Liu, R.; Guo, H.; Olsen, D. W. H.; Cohen, Y.; Emili, A.; Chan, W. C. W. Protein Corona Fingerprinting Predicts the Cellular Interaction of Gold and Silver Nanoparticles. *ACS Nano* **2014**, *8* (3), 2439–2455. https://doi.org/10.1021/nn406018q.

(264) Palchetti, S.; Digiacomo, L.; Pozzi, D.; Peruzzi, G.; Micarelli, E.; Mahmoudi, M.; Caracciolo, G. Nanoparticles-Cell Association Predicted by Protein Corona Fingerprints. *Nanoscale* **2016**, *8* (25), 12755–12763. https://doi.org/10.1039/C6NR03898K.

(265) Mohammad-Beigi, H.; Hayashi, Y.; Zeuthen, C. M.; Eskandari, H.; Scavenius, C.; Juul-Madsen, K.; Vorup-Jensen, T.; Enghild, J. J.; Sutherland, D. S. Mapping and Identification of Soft Corona Proteins at Nanoparticles and Their Impact on Cellular Association. *Nat. Commun.* **2020**, *11* (1), 4535. https://doi.org/10.1038/s41467-020-18237-7.

(266) Papi, M.; Caputo, D.; Palmieri, V.; Coppola, R.; Palchetti, S.; Bugli, F.; Martini, C.; Digiacomo, L.; Pozzi, D.; Caracciolo, G. Clinically Approved PEGylated Nanoparticles Are Covered by a Protein Corona That Boosts the Uptake by Cancer Cells. *Nanoscale* **2017**, *9* (29), 10327–10334. https://doi.org/10.1039/c7nr03042h.

(267) Hadjidemetriou, M.; Al-Ahmady, Z.; Kostarelos, K. Time-Evolution of in Vivo Protein Corona onto Blood-Circulating PEGylated Liposomal Doxorubicin (DOXIL) Nanoparticles. *Nanoscale* **2016**, *8* (13), 6948–6957. https://doi.org/10.1039/C5NR09158F.

(268) Berrecoso, G.; Crecente-Campo, J.; Alonso, M. J. Unveiling the Pitfalls of the Protein Corona of Polymeric Drug Nanocarriers. *Drug Deliv. Transl. Res.* **2020**, *10* (3), 730–750. https://doi.org/10.1007/s13346-020-00745-0.

(269) Cedervall, T.; Lynch, I.; Lindman, S.; Berggård, T.; Thulin, E.; Nilsson, H.; Dawson, K. A.; Linse, S. Understanding the Nanoparticle-Protein Corona Using Methods to Quantify Exchange Rates and Affinities of Proteins for Nanoparticles. *Proc. Natl. Acad. Sci. U. S. A.* **2007**, *104* (7), 2050–2055. https://doi.org/10.1073/pnas.0608582104.

(270) Lundqvist, M.; Stigler, J.; Elia, G.; Lynch, I.; Cedervall, T.; Dawson, K. A. Nanoparticle Size and Surface Properties Determine the Protein Corona with Possible Implications for Biological Impacts. *Proc. Natl. Acad. Sci. U. S. A.* **2008**, *105* (38), 14265–14270. https://doi.org/10.1073/pnas.0805135105.

(271) Su, G.; Zhou, X.; Zhou, H.; Li, Y.; Zhang, X.; Liu, Y.; Cao, D.; Yan, B. Size-Dependent Facilitation of Cancer Cell Targeting by Proteins Adsorbed on Nanoparticles. *ACS Appl. Mater. Interfaces* **2016**, *8* (44), 30037–30047. https://doi.org/10.1021/acsami.6b10967.

(272) Corbo, C.; Molinaro, R.; Tabatabaei, M.; Farokhzad, O. C.; Mahmoudi, M. Personalized Protein Corona on

Nanoparticles and Its Clinical Implications. *Biomater. Sci.* **2017**, *5* (3), 378–387. https://doi.org/10.1039/c6bm00921b.

(273) Schaaij-Visser, T. B. M.; de Wit, M.; Lam, S. W.; Jiménez, C. R. The Cancer Secretome, Current Status and Opportunities in the Lung, Breast and Colorectal Cancer Context. *Biochim. Biophys. Acta - Proteins Proteomics* **2013**, *1834* (11), 2242–2258. https://doi.org/10.1016/j.bbapap.2013.01.029.

(274) Mitchell, M. J.; Billingsley, M. M.; Haley, R. M.; Wechsler, M. E.; Peppas, N. A.; Langer, R. Engineering Precision Nanoparticles for Drug Delivery. *Nat. Rev. Drug Discov.* **2021**, *20* (2), 101–124. https://doi.org/10.1038/s41573-020-0090-8.

(275) Elechalawar, C. K.; Hossen, M. N.; McNally, L.; Bhattacharya, R.; Mukherjee, P. Analysing the Nanoparticle-Protein Corona for Potential Molecular Target Identification. *J. Control. Release* **2020**, *322*, 122–136. https://doi.org/10.1016/j.jconrel.2020.03.008.

(276) Monopoli, M. P.; Walczyk, D.; Campbell, A.; Elia, G.; Lynch, I.; Bombelli, F. B.; Dawson, K. A. Physical-Chemical Aspects of Protein Corona: Relevance to in Vitro and in Vivo Biological Impacts of Nanoparticles. *J. Am. Chem. Soc.* **2011**, *133* (8), 2525–2534. https://doi.org/10.1021/ja107583h.

(277) Zhang, T.-X.; Zhu, G.-Y.; Lu, B.-Y.; Zhang, C.-L.; Peng, Q. Concentration-Dependent Protein Adsorption at the Nano–Bio Interfaces of Polymeric Nanoparticles and Serum Proteins. *Nanomedicine* **2017**, *12* (22), 2757–2769. https://doi.org/10.2217/nnm-2017-0238.

(278) Wang, J.; Jensen, U. B.; Jensen, G. V; Shipovskov, S.; Balakrishnan, V. S.; Otzen, D.; Pedersen, J. S.; Besenbacher, F.; Sutherland, D. S. Soft Interactions at Nanoparticles Alter Protein Function and Conformation in a Size Dependent Manner. *Nano Lett.* **2011**, *11* (11), 4985–4991. https://doi.org/10.1021/nl202940k.

(279) Miclăuş, T.; Bochenkov, V. E.; Ogaki, R.; Howard, K. A.; Sutherland, D. S. Spatial Mapping and Quantification of Soft and Hard Protein Coronas at Silver Nanocubes. *Nano Lett.* **2014**, *14* (4), 2086–2093. https://doi.org/10.1021/nl500277c.

(280) Raoufi, M.; Hajipour, M. J.; Kamali Shahri, S. M.; Schoen, I.; Linn, U.; Mahmoudi, M. Probing Fibronectin Conformation on a Protein Corona Layer around Nanoparticles. *Nanoscale* **2018**, *10* (3), 1228–1233. https://doi.org/10.1039/c7nr06970g.

(281) Ge, C.; Tian, J.; Zhao, Y.; Chen, C.; Zhou, R.; Chai, Z. Towards Understanding of Nanoparticle–Protein Corona. *Arch. Toxicol.* **2015**, *89* (4), 519–539. https://doi.org/10.1007/s00204-015-1458-0.

(282) Francia, V.; Yang, K.; Deville, S.; Reker-Smit, C.; Nelissen, I.; Salvati, A. Corona Composition Can Affect the Mechanisms Cells Use to Internalize Nanoparticles. *ACS Nano* **2019**, *13* (10), 11107–11121. https://doi.org/10.1021/acsnano.9b03824.

(283) Mortimer, G. M.; Butcher, N. J.; Musumeci, A. W.; Deng, Z. J.; Martin, D. J.; Minchin, R. F. Cryptic Epitopes of Albumin Determine Mononuclear Phagocyte System Clearance of Nanomaterials. *ACS Nano* **2014**, *8* (4), 3357–3366. https://doi.org/10.1021/nn405830g.

(284) Schwenk, J. M.; Omenn, G. S.; Sun, Z.; Campbell, D. S.; Baker, M. S.; Overall, C. M.; Aebersold, R.; Moritz, R. L.; Deutsch, E. W. The Human Plasma Proteome Draft of 2017: Building on the Human Plasma PeptideAtlas from Mass Spectrometry and Complementary Assays. *J. Proteome Res.* **2017**, *16* (12), 4299–4310. https://doi.org/10.1021/acs.jproteome.7b00467.

(285) Gorshkov, V.; Bubis, J. A.; Solovyeva, E. M.; Gorshkov, M. V; Kjeldsen, F. Protein Corona Formed on Silver Nanoparticles in Blood Plasma Is Highly Selective and Resistant to Physicochemical Changes of the Solution. *Environ. Sci. Nano* **2019**, *6* (4), 1089–1098. https://doi.org/10.1039/c8en01054d.

(286) Cedervall, T.; Lynch, I.; Foy, M.; Berggård, T.; Donnelly, S. C.; Cagney, G.; Linse, S.; Dawson, K. A. Detailed Identification of Plasma Proteins Adsorbed on Copolymer Nanoparticles. *Angew. Chemie Int. Ed.* **2007**, *46* (30), 5754–5756. https://doi.org/10.1002/anie.200700465.

(287) Aliyandi, A.; Zuhorn, I. S.; Salvati, A. Disentangling Biomolecular Corona Interactions With Cell Receptors and Implications for Targeting of Nanomedicines. *Front. Bioeng. Biotechnol.* **2020**, *8*, 1409. https://doi.org/10.3389/fbioe.2020.599454.

(288) Dobrovolskaia, M. A.; Shurin, M.; Shvedova, A. A. Current Understanding of Interactions between Nanoparticles and the Immune System. *Toxicol. Appl. Pharmacol.* **2016**, *299*, 78–89. https://doi.org/10.1016/j.taap.2015.12.022.

(289) Duan, Y.; Coreas, R.; Liu, Y.; Bitounis, D.; Zhang, Z.; Parviz, D.; Strano, M.; Demokritou, P.; Zhong, W. Prediction of Protein Corona on Nanomaterials by Machine Learning Using Novel Descriptors. *NanoImpact* **2020**, *17*, 100207. https://doi.org/10.1016/j.impact.2020.100207.

(290) Findlay, M. R.; Freitas, D. N.; Mobed-Miremadi, M.; Wheeler, K. E. Machine Learning Provides Predictive Analysis into Silver Nanoparticle Protein Corona Formation from Physicochemical Properties. *Environ. Sci. Nano* **2018**, *5* (1), 64–71. https://doi.org/10.1039/C7EN00466D.

(291) Lazarovits, J.; Sindhwani, S.; Tavares, A. J.; Zhang, Y.; Song, F.; Audet, J.; Krieger, J. R.; Syed, A. M.; Stordy, B.; Chan, W. C. W. Supervised Learning and Mass Spectrometry Predicts the in Vivo Fate of Nanomaterials. *ACS Nano* **2019**, *13* (7), 8023–8034. https://doi.org/10.1021/acsnano.9b02774.

(292) Bigdeli, A.; Palchetti, S.; Pozzi, D.; Hormozi-Nezhad, M. R.; Baldelli Bombelli, F.; Caracciolo, G.; Mahmoudi, M. Exploring Cellular Interactions of Liposomes Using Protein Corona Fingerprints and Physicochemical Properties. *ACS Nano* **2016**, *10* (3), 3723–3737. https://doi.org/10.1021/acsnano.6b00261.

(293) Barrán-Berdón, A. L.; Pozzi, D.; Caracciolo, G.; Capriotti, A. L.; Caruso, G.; Cavaliere, C.; Riccioli, A.; Palchetti, S.; Laganà, A. Time Evolution of Nanoparticle–Protein Corona in Human Plasma: Relevance for Targeted Drug Delivery. *Langmuir* **2013**, *29* (21), 6485–6494. https://doi.org/10.1021/la401192x.

(294) VROMAN, L.; LUKOSEVICIUS, A. ELLIPSOMETER RECORDINGS OF CHANGES IN OPTICAL THICKNESS OF ADSORBED FILMS ASSOCIATED WITH SURFACE ACTIVATION OF BLOOD CLOTTING. *Nature* **1964**, *204*, 701–703. https://doi.org/10.1038/204701b0.

(295) Vroman, L.; Adams, A. L.; Fischer, G. C.; Munoz, P. C. Interaction of High Molecular Weight Kininogen, Factor XII, and Fibrinogen in Plasma at Interfaces. *Blood* **1980**, *55* (1), 156–159.

(296) Chakraborty, D.; Ethiraj, K. R.; Mukherjee, A. Understanding the Relevance of Protein Corona in Nanoparticle-Based Therapeutics and Diagnostics. *RSC Adv.* **2020**, *10* (45), 27161–27172. https://doi.org/10.1039/D0RA05241H.

(297) Larson, T. A.; Joshi, P. P.; Sokolov, K. Preventing Protein Adsorption and Macrophage Uptake of Gold Nanoparticles via a Hydrophobic Shield. *ACS Nano* **2012**, *6* (10), 9182–9190. https://doi.org/10.1021/nn3035155.

(298) Angioletti-Uberti, S.; Ballauff, M.; Dzubiella, J. Competitive Adsorption of Multiple Proteins to Nanoparticles: The Vroman Effect Revisited. *Mol. Phys.* **2018**, *116* (21–22), 3154–3163. https://doi.org/10.1080/00268976.2018.1467056.

(299) Ke, P. C.; Lin, S.; Parak, W. J.; Davis, T. P.; Caruso, F. A Decade of the Protein Corona. *ACS Nano* **2017**, *11* (12), 11773–11776. https://doi.org/10.1021/acsnano.7b08008.

(300) Palchetti, S.; Pozzi, D.; Capriotti, A. L.; Barbera, G. La; Chiozzi, R. Z.; Digiacomo, L.; Peruzzi, G.; Caracciolo, G.; Laganà, A. Influence of Dynamic Flow Environment on Nanoparticle-Protein Corona: From Protein Patterns to Uptake in Cancer Cells. *Colloids Surfaces B Biointerfaces* **2017**, *153*, 263–271. https://doi.org/10.1016/j.colsurfb.2017.02.037.

(301) Palchetti, S.; Colapicchioni, V.; Digiacomo, L.; Caracciolo, G.; Pozzi, D.; Capriotti, A. L.; La Barbera, G.; Laganà, A. The Protein Corona of Circulating PEGylated Liposomes. *Biochim. Biophys. Acta - Biomembr.* **2016**, *1858* (2), 189–196. https://doi.org/10.1016/j.bbamem.2015.11.012.

(302) Yu, J.; Yin, W.; Peng, T.; Chang, Y.; Zu, Y.; Li, J.; He, X.; Ma, X.; Gu, Z.; Zhao, Y. Biodistribution,

Excretion, and Toxicity of Polyethyleneimine Modified NaYF4:Yb,Er Upconversion Nanoparticles in Mice via Different Administration Routes. *Nanoscale* **2017**, *9* (13), 4497–4507. https://doi.org/10.1039/C7NR00078B.

(303) Zhao, Y.; Sultan, D.; Liu, Y. 2 - Biodistribution, Excretion, and Toxicity of Nanoparticles. In *Micro and Nano Technologies*; Cui, W., Zhao, X. B. T.-T. B., Eds.; Elsevier, 2019; pp 27–53. https://doi.org/10.1016/B978-0-12-815341-3.00002-X.

(304) Bimbo, L. M.; Sarparanta, M.; Santos, H. A.; Airaksinen, A. J.; Mäkilä, E.; Laaksonen, T.; Peltonen, L.; Lehto, V.-P.; Hirvonen, J.; Salonen, J. Biocompatibility of Thermally Hydrocarbonized Porous Silicon Nanoparticles and Their Biodistribution in Rats. *ACS Nano* **2010**, *4* (6), 3023–3032. https://doi.org/10.1021/nn901657w.

(305) Mukherjee, S.; Bollu, V. S.; Roy, A.; Nethi, S. K.; Madhusudana, K.; Kumar, J. M.; Sistla, R.; Patra, C. R. Acute Toxicity, Biodistribution, and Pharmacokinetics Studies of Pegylated Platinum Nanoparticles in Mouse Model. *Adv. NanoBiomed Res.* **2021**, *1* (7), 2000082. https://doi.org/10.1002/anbr.202000082.

(306) Dölen, Y.; Valente, M.; Tagit, O.; Jäger, E.; Van Dinther, E. A. W.; van Riessen, N. K.; Hruby, M.; Gileadi, U.; Cerundolo, V.; Figdor, C. G. Nanovaccine Administration Route Is Critical to Obtain Pertinent INKt Cell Help for Robust Anti-Tumor T and B Cell Responses. *Oncoimmunology* **2020**, *9* (1), 1738813. https://doi.org/10.1080/2162402X.2020.1738813.

(307) Manzano, M.; Vallet-Regí, M. Mesoporous Silica Nanoparticles for Drug Delivery. *Adv. Funct. Mater.* **2020**, *30* (2), 1902634. https://doi.org/10.1002/adfm.201902634.

(308) Mangal, S.; Gao, W.; Li, T.; Zhou, Q. T. Pulmonary Delivery of Nanoparticle Chemotherapy for the Treatment of Lung Cancers: Challenges and Opportunities. *Acta Pharmacol. Sin.* **2017**, *38* (6), 782–797. https://doi.org/10.1038/aps.2017.34.

(309) Cao, S.; Xu, S.; Wang, H.; Ling, Y.; Dong, J.; Xia, R.; Sun, X. Nanoparticles: Oral Delivery for Protein and Peptide Drugs. *AAPS PharmSciTech* **2019**, *20* (5), 190. https://doi.org/10.1208/s12249-019-1325-z.

(310) Wong, C. Y.; Al-Salami, H.; Dass, C. R. The Role of Chitosan on Oral Delivery of Peptide-Loaded Nanoparticle Formulation. *J. Drug Target.* **2018**, *26* (7), 551–562. https://doi.org/10.1080/1061186X.2017.1400552.

(311) Tsoi, K. M.; MacParland, S. A.; Ma, X.-Z.; Spetzler, V. N.; Echeverri, J.; Ouyang, B.; Fadel, S. M.; Sykes, E. A.; Goldaracena, N.; Kaths, J. M.; Conneely, J. B.; Alman, B. A.; Selzner, M.; Ostrowski, M. A.; Adeyi, O. A.; Zilman, A.; McGilvray, I. D.; Chan, W. C. W. Mechanism of Hard-Nanomaterial Clearance by the Liver. *Nat. Mater.* **2016**, *15* (11), 1212–1221. https://doi.org/10.1038/nmat4718.

(312) Wang, B.; He, X.; Zhang, Z.; Zhao, Y.; Feng, W. Metabolism of Nanomaterials in Vivo: Blood Circulation and Organ Clearance. *Acc. Chem. Res.* **2013**, *46* (3), 761–769. https://doi.org/10.1021/ar2003336.

(313) Tee, J. K.; Peng, F.; Ho, H. K. Effects of Inorganic Nanoparticles on Liver Fibrosis: Optimizing a Double-Edged Sword for Therapeutics. *Biochem. Pharmacol.* **2019**, *160*, 24–33. https://doi.org/10.1016/j.bcp.2018.12.003.

(314) de la Harpe, K. M.; Kondiah, P. P. D.; Choonara, Y. E.; Marimuthu, T.; du Toit, L. C.; Pillay, V. The Hemocompatibility of Nanoparticles: A Review of Cell-Nanoparticle Interactions and Hemostasis. *Cells* **2019**, *8* (10), 1209. https://doi.org/10.3390/cells8101209.

(315) Ilinskaya, A. N.; Dobrovolskaia, M. A. Nanoparticles and the Blood Coagulation System. Part II: Safety Concerns. *Nanomedicine (Lond).* **2013**, *8* (6), 969–981. https://doi.org/10.2217/nnm.13.49.

(316) Lee, E.-J.; Cines, D. B.; Gernsheimer, T.; Kessler, C.; Michel, M.; Tarantino, M. D.; Semple, J. W.; Arnold, D. M.; Godeau, B.; Lambert, M. P.; Bussel, J. B. Thrombocytopenia Following Pfizer and Moderna SARS-CoV-2 Vaccination. *Am. J. Hematol.* **2021**, *96* (5), 534–537. https://doi.org/10.1002/ajh.26132.

(317) Kadkhoda, K. Post-Adenoviral-Based COVID-19 Vaccines Thrombosis: A Proposed Mechanism. *J.*

Thromb. Haemost. **2021**, *19* (7), 1831–1832. https://doi.org/10.1111/jth.15348.

(318) Tripathy, N.; Wang, J.; Tung, M.; Conway, C.; Chung, E. J. Transdermal Delivery of Kidney-Targeting Nanoparticles Using Dissolvable Microneedles. *Cell. Mol. Bioeng.* **2020**, *13* (5), 475–486. https://doi.org/10.1007/s12195-020-00622-3.

(319) Amani, H.; Shahbazi, M.-A.; D'Amico, C.; Fontana, F.; Abbaszadeh, S.; Santos, H. A. Microneedles for Painless Transdermal Immunotherapeutic Applications. *J. Control. Release* **2021**, *330*, 185–217. https://doi.org/10.1016/j.jconrel.2020.12.019.

(320) Borgheti-Cardoso, L. N.; Viegas, J. S. R.; Silvestrini, A. V. P.; Caron, A. L.; Praça, F. G.; Kravicz, M.; Bentley, M. V. L. B. Nanotechnology Approaches in the Current Therapy of Skin Cancer. *Adv. Drug Deliv. Rev.* **2020**, *153*, 109–136. https://doi.org/10.1016/j.addr.2020.02.005.

(321) Hozayen, W. G.; Mahmoud, A. M.; Desouky, E. M.; El-Nahass, E.-S.; Soliman, H. A.; Farghali, A. A. Cardiac and Pulmonary Toxicity of Mesoporous Silica Nanoparticles Is Associated with Excessive ROS Production and Redox Imbalance in Wistar Rats. *Biomed. Pharmacother.* **2019**, *109*, 2527–2538. https://doi.org/10.1016/j.biopha.2018.11.093.

(322) Avsievich, T.; Popov, A.; Bykov, A.; Meglinski, I. Mutual Interaction of Red Blood Cells Influenced by Nanoparticles. *Sci. Rep.* **2019**, *9* (1), 5147. https://doi.org/10.1038/s41598-019-41643-x.

(323) Hannon, G.; Lysaght, J.; Liptrott, N. J.; Prina-Mello, A. Immunotoxicity Considerations for Next Generation Cancer Nanomedicines. *Adv. Sci.* **2019**, *6* (19), 1900133. https://doi.org/10.1002/advs.201900133.

(324) Shang, L.; Nienhaus, K.; Nienhaus, G. U. Engineered Nanoparticles Interacting with Cells: Size Matters. *J. Nanobiotechnology* **2014**, *12* (1), 5. https://doi.org/10.1186/1477-3155-12-5.

(325) Davenport, R. D. Pathophysiology of Hemolytic Transfusion Reactions. *Semin. Hematol.* **2005**, *42* (3), 165–168. https://doi.org/10.1053/j.seminhematol.2005.04.006.

(326) L'Acqua, C.; Hod, E. New Perspectives on the Thrombotic Complications of Haemolysis. *Br. J. Haematol.* **2015**, *168* (2), 175–185. https://doi.org/10.1111/bjh.13183.

(327) Ataga, K. I. Hypercoagulability and Thrombotic Complications in Hemolytic Anemias. *Haematologica* **2009**, *94* (11), 1481–1484. https://doi.org/10.3324/haematol.2009.013672.

(328) Byrnes, J. R.; Wolberg, A. S. Red Blood Cells in Thrombosis. *Blood* **2017**, *130* (16), 1795–1799. https://doi.org/10.1182/blood-2017-03-745349.

(329) Mehri, R.; Mavriplis, C.; Fenech, M. Red Blood Cell Aggregates and Their Effect on Non-Newtonian Blood Viscosity at Low Hematocrit in a Two-Fluid Low Shear Rate Microfluidic System. *PLoS One* **2018**, *13* (7), e0199911. https://doi.org/10.1371/journal.pone.0199911.

(330) Barshtein, G.; Arbell, D.; Yedgar, S. Hemodynamic Functionality of Transfused Red Blood Cells in the Microcirculation of Blood Recipients. *Front. Physiol.* **2018**, *9*, 41. https://doi.org/10.3389/fphys.2018.00041.

(331) Walton, B. L.; Lehmann, M.; Skorczewski, T.; Holle, L. A.; Beckman, J. D.; Cribb, J. A.; Mooberry, M. J.; Wufsus, A. R.; Cooley, B. C.; Homeister, J. W.; Pawlinski, R.; Falvo, M. R.; Key, N. S.; Fogelson, A. L.; Neeves, K. B.; Wolberg, A. S. Elevated Hematocrit Enhances Platelet Accumulation Following Vascular Injury. *Blood* **2017**, *129* (18), 2537–2546. https://doi.org/10.1182/blood-2016-10-746479.

(332) Fogelson, A. L.; Neeves, K. B. Fluid Mechanics of Blood Clot Formation. *Annu. Rev. Fluid Mech.* **2015**, *47*, 377–403. https://doi.org/10.1146/annurev-fluid-010814-014513.

(333) Zhao, Y.; Sun, X.; Zhang, G.; Trewyn, B. G.; Slowing, I. I.; Lin, V. S.-Y. Interaction of Mesoporous Silica Nanoparticles with Human Red Blood Cell Membranes: Size and Surface Effects. *ACS Nano* **2011**, *5* (2), 1366–1375. https://doi.org/10.1021/nn103077k.

(334) He, Z.; Liu, J.; Du, L. The Unexpected Effect of PEGylated Gold Nanoparticles on the Primary Function of

Erythrocytes. *Nanoscale* **2014**, *6* (15), 9017–9024. https://doi.org/10.1039/c4nr01857e.

(335) Haute, D. Van; Berlin, J. M. Challenges in Realizing Selectivity for Nanoparticle Biodistribution and Clearance: Lessons from Gold Nanoparticles. *Ther. Deliv.* **2017**, *8* (9), 763–774. https://doi.org/10.4155/tde-2017-0057.

(336) Huang, Y.; Jiang, K.; Zhang, X.; Chung, E. J. The Effect of Size, Charge, and Peptide Ligand Length on Kidney Targeting by Small, Organic Nanoparticles. *Bioeng. Transl. Med.* **2020**, *5* (3), e10173. https://doi.org/10.1002/btm2.10173.

(337) Ota, Z.; Makino, H.; Takaya, Y.; Ofuji, T. Molecular Sieve in Renal Glomerular and Tubular Basement Membranes as Revealed by Electron Microscopy. *Ren. Physiol.* **1980**, *3* (1–6), 317–323. https://doi.org/10.1159/000172777.

(338) Brenner, B. M.; Bohrer, M. P.; Baylis, C.; Deen, W. M. Determinants of Glomerular Permselectivity: Insights Derived from Observations in Vivo. *Kidney Int.* **1977**, *12* (4), 229–237. https://doi.org/10.1038/ki.1977.107.

(339) Hashizume, H.; Baluk, P.; Morikawa, S.; McLean, J. W.; Thurston, G.; Roberge, S.; Jain, R. K.; McDonald, D. M. Openings between Defective Endothelial Cells Explain Tumor Vessel Leakiness. *Am. J. Pathol.* **2000**, *156* (4), 1363–1380. https://doi.org/10.1016/S0002-9440(10)65006-7.

(340) Ernsting, M. J.; Murakami, M.; Roy, A.; Li, S.-D. Factors Controlling the Pharmacokinetics, Biodistribution and Intratumoral Penetration of Nanoparticles. *J. Control. Release* **2013**, *172* (3), 782–794. https://doi.org/10.1016/j.jconrel.2013.09.013.

(341) Cataldi, M.; Vigliotti, C.; Mosca, T.; Cammarota, M.; Capone, D. Emerging Role of the Spleen in the Pharmacokinetics of Monoclonal Antibodies, Nanoparticles and Exosomes. *Int. J. Mol. Sci.* **2017**, *18* (6), 1249. https://doi.org/10.3390/ijms18061249.

(342) Perrault, S. D.; Walkey, C.; Jennings, T.; Fischer, H. C.; Chan, W. C. W. Mediating Tumor Targeting Efficiency of Nanoparticles through Design. *Nano Lett.* **2009**, *9* (5), 1909–1915. https://doi.org/10.1021/nl900031y.

(343) Wei, Y.; Quan, L.; Zhou, C.; Zhan, Q. Factors Relating to the Biodistribution & Clearance of Nanoparticles & Their Effects on in Vivo Application. *Nanomedicine* **2018**, *13* (12), 1495–1512. https://doi.org/10.2217/nnm-2018-0040.

(344) Lankoff, A.; Sandberg, W. J.; Wegierek-Ciuk, A.; Lisowska, H.; Refsnes, M.; Sartowska, B.; Schwarze, P. E.; Meczynska-Wielgosz, S.; Wojewodzka, M.; Kruszewski, M. The Effect of Agglomeration State of Silver and Titanium Dioxide Nanoparticles on Cellular Response of HepG2, A549 and THP-1 Cells. *Toxicol. Lett.* **2012**, *208* (3), 197–213. https://doi.org/10.1016/j.toxlet.2011.11.006.

(345) Kettler, K.; Giannakou, C.; de Jong, W. H.; Hendriks, A. J.; Krystek, P. Uptake of Silver Nanoparticles by Monocytic THP-1 Cells Depends on Particle Size and Presence of Serum Proteins. *J. Nanoparticle Res.* **2016**, *18* (9), 286. https://doi.org/10.1007/s11051-016-3595-7.

(346) Liu, D.; Mori, A.; Huang, L. Role of Liposome Size and RES Blockade in Controlling Biodistribution and Tumor Uptake of GM1-Containing Liposomes. *Biochim. Biophys. Acta* **1992**, *1104* (1), 95–101. https://doi.org/10.1016/0005-2736(92)90136-a.

(347) Anselmo, A. C.; Mitragotri, S. Impact of Particle Elasticity on Particle-Based Drug Delivery Systems. *Adv. Drug Deliv. Rev.* **2017**, *108*, 51–67. https://doi.org/10.1016/j.addr.2016.01.007.

(348) Chen, L.; Li, X.; Zhang, Y.; Chen, T.; Xiao, S.; Liang, H. Morphological and Mechanical Determinants of Cellular Uptake of Deformable Nanoparticles. *Nanoscale* **2018**, *10* (25), 11969–11979. https://doi.org/10.1039/C8NR01521J.

(349) Hu, G.; Guo, M.; Xu, J.; Wu, F.; Fan, J.; Huang, Q.; Yang, G.; Lv, Z.; Wang, X.; Jin, Y. Nanoparticles Targeting Macrophages as Potential Clinical Therapeutic Agents Against Cancer and Inflammation. *Front.*

Immunol. **2019**, *10*, 1998. https://doi.org/10.3389/fimmu.2019.01998.

(350) Akter, M.; Sikder, M. T.; Rahman, M. M.; Ullah, A. K. M. A.; Hossain, K. F. B.; Banik, S.; Hosokawa, T.; Saito, T.; Kurasaki, M. A Systematic Review on Silver Nanoparticles-Induced Cytotoxicity: Physicochemical Properties and Perspectives. *J. Adv. Res.* **2018**, *9*, 1–16. https://doi.org/10.1016/j.jare.2017.10.008.

(351) Charles, S.; Jomini, S.; Fessard, V.; Bigorgne-Vizade, E.; Rousselle, C.; Michel, C. Assessment of the in Vitro Genotoxicity of TiO2 Nanoparticles in a Regulatory Context. *Nanotoxicology* **2018**, *12* (4), 357–374. https://doi.org/10.1080/17435390.2018.1451567.

(352) Brohi, R. D.; Wang, L.; Talpur, H. S.; Wu, D.; Khan, F. A.; Bhattarai, D.; Rehman, Z.-U.; Farmanullah, F.; Huo, L.-J. Toxicity of Nanoparticles on the Reproductive System in Animal Models: A Review. *Front. Pharmacol.* **2017**, *8*, 606. https://doi.org/10.3389/fphar.2017.00606.

(353) Huang, H.; Feng, W.; Chen, Y.; Shi, J. Inorganic Nanoparticles in Clinical Trials and Translations. *Nano Today* **2020**, *35*, 100972. https://doi.org/10.1016/j.nantod.2020.100972.

(354) Halappanavar, S.; van den Brule, S.; Nymark, P.; Gaté, L.; Seidel, C.; Valentino, S.; Zhernovkov, V.; Høgh Danielsen, P.; De Vizcaya, A.; Wolff, H.; Stöger, T.; Boyadziev, A.; Poulsen, S. S.; Sørli, J. B.; Vogel, U. Adverse Outcome Pathways as a Tool for the Design of Testing Strategies to Support the Safety Assessment of Emerging Advanced Materials at the Nanoscale. *Part. Fibre Toxicol.* **2020**, *17* (1), 16. https://doi.org/10.1186/s12989-020-00344-4.

(355) Lai, X.; Zhao, H.; Zhang, Y.; Guo, K.; Xu, Y.; Chen, S.; Zhang, J. Intranasal Delivery of Copper Oxide Nanoparticles Induces Pulmonary Toxicity and Fibrosis in C57BL/6 Mice. *Sci. Rep.* **2018**, *8* (1), 4499. https://doi.org/10.1038/s41598-018-22556-7.

(356) Hong, F.; Ji, J.; Ze, X.; Zhou, Y.; Ze, Y. Liver Inflammation and Fibrosis Induced by Long-Term Exposure to Nano Titanium Dioxide (TiO_2) Nanoparticles in Mice and Its Molecular Mechanism. *J. Biomed. Nanotechnol.* **2020**, *16* (5), 616–625. https://doi.org/10.1166/jbn.2020.2921.

(357) Sadauskas, E.; Wallin, H.; Stoltenberg, M.; Vogel, U.; Doering, P.; Larsen, A.; Danscher, G. Kupffer Cells Are Central in the Removal of Nanoparticles from the Organism. *Part. Fibre Toxicol.* **2007**, *4*, 10. https://doi.org/10.1186/1743-8977-4-10.

(358) Cho, W.-S.; Cho, M.; Jeong, J.; Choi, M.; Cho, H.-Y.; Han, B. S.; Kim, S. H.; Kim, H. O.; Lim, Y. T.; Chung, B. H.; Jeong, J. Acute Toxicity and Pharmacokinetics of 13 Nm-Sized PEG-Coated Gold Nanoparticles. *Toxicol. Appl. Pharmacol.* **2009**, *236* (1), 16–24. https://doi.org/10.1016/j.taap.2008.12.023.

(359) Cho, W.-S.; Cho, M.; Jeong, J.; Choi, M.; Han, B. S.; Shin, H.-S.; Hong, J.; Chung, B. H.; Jeong, J.; Cho, M.-H. Size-Dependent Tissue Kinetics of PEG-Coated Gold Nanoparticles. *Toxicol. Appl. Pharmacol.* **2010**, *245* (1), 116–123. https://doi.org/10.1016/j.taap.2010.02.013.

(360) Briley-Saebo, K.; Bjørnerud, A.; Grant, D.; Ahlstrom, H.; Berg, T.; Kindberg, G. M. Hepatic Cellular Distribution and Degradation of Iron Oxide Nanoparticles Following Single Intravenous Injection in Rats: Implications for Magnetic Resonance Imaging. *Cell Tissue Res.* **2004**, *316* (3), 315–323. https://doi.org/10.1007/s00441-004-0884-8.

(361) Johnston, H. J.; Semmler-Behnke, M.; Brown, D. M.; Kreyling, W.; Tran, L.; Stone, V. Evaluating the Uptake and Intracellular Fate of Polystyrene Nanoparticles by Primary and Hepatocyte Cell Lines in Vitro. *Toxicol. Appl. Pharmacol.* **2010**, *242* (1), 66–78. https://doi.org/10.1016/j.taap.2009.09.015.

(362) Schluep, T.; Hwang, J.; Hildebrandt, I. J.; Czernin, J.; Choi, C. H. J.; Alabi, C. A.; Mack, B. C.; Davis, M. E. Pharmacokinetics and Tumor Dynamics of the Nanoparticle IT-101 from PET Imaging and Tumor Histological Measurements. *Proc. Natl. Acad. Sci. U. S. A.* **2009**, *106* (27), 11394–11399. https://doi.org/10.1073/pnas.0905487106.

(363) Balasubramanian, S. K.; Jittiwat, J.; Manikandan, J.; Ong, C.-N.; Yu, L. E.; Ong, W.-Y. Biodistribution of Gold Nanoparticles and Gene Expression Changes in the Liver and Spleen after Intravenous Administration

in Rats. *Biomaterials* **2010**, *31* (8), 2034–2042. https://doi.org/10.1016/j.biomaterials.2009.11.079.

(364) Kolosnjaj-Tabi, J.; Javed, Y.; Lartigue, L.; Volatron, J.; Elgrabli, D.; Marangon, I.; Pugliese, G.; Caron, B.; Figuerola, A.; Luciani, N.; Pellegrino, T.; Alloyeau, D.; Gazeau, F. The One Year Fate of Iron Oxide Coated Gold Nanoparticles in Mice. *ACS Nano* **2015**, *9* (8), 7925–7939. https://doi.org/10.1021/acsnano.5b00042.

(365) Levy, M.; Luciani, N.; Alloyeau, D.; Elgrabli, D.; Deveaux, V.; Pechoux, C.; Chat, S.; Wang, G.; Vats, N.; Gendron, F.; Factor, C.; Lotersztajn, S.; Luciani, A.; Wilhelm, C.; Gazeau, F. Long Term in Vivo Biotransformation of Iron Oxide Nanoparticles. *Biomaterials* **2011**, *32* (16), 3988–3999. https://doi.org/10.1016/j.biomaterials.2011.02.031.

(366) Xia, T.; Kovochich, M.; Liong, M.; Mädler, L.; Gilbert, B.; Shi, H.; Yeh, J. I.; Zink, J. I.; Nel, A. E. Comparison of the Mechanism of Toxicity of Zinc Oxide and Cerium Oxide Nanoparticles Based on Dissolution and Oxidative Stress Properties. *ACS Nano* **2008**, *2* (10), 2121–2134. https://doi.org/10.1021/nn800511k.

(367) Sadauskas, E.; Danscher, G.; Stoltenberg, M.; Vogel, U.; Larsen, A.; Wallin, H. Protracted Elimination of Gold Nanoparticles from Mouse Liver. *Nanomedicine Nanotechnology, Biol. Med.* **2009**, *5* (2), 162–169. https://doi.org/10.1016/j.nano.2008.11.002.

(368) Disdier, C.; Devoy, J.; Cosnefroy, A.; Chalansonnet, M.; Herlin-Boime, N.; Brun, E.; Lund, A.; Mabondzo, A. Tissue Biodistribution of Intravenously Administrated Titanium Dioxide Nanoparticles Revealed Blood-Brain Barrier Clearance and Brain Inflammation in Rat. *Part. Fibre Toxicol.* **2015**, *12*, 27. https://doi.org/10.1186/s12989-015-0102-8.

(369) Chevallier, P.; Walter, A.; Garofalo, A.; Veksler, I.; Lagueux, J.; Bégin-Colin, S.; Felder-Flesch, D.; Fortin, M.-A. Tailored Biological Retention and Efficient Clearance of Pegylated Ultra-Small MnO Nanoparticles as Positive MRI Contrast Agents for Molecular Imaging. *J. Mater. Chem. B* **2014**, *2* (13), 1779–1790. https://doi.org/10.1039/C3TB21634A.

(370) Alsaleh, N. B.; Brown, J. M. Engineered Nanomaterials and Type I Allergic Hypersensitivity Reactions. *Front. Immunol.* **2020**, *11*, 222. https://doi.org/10.3389/fimmu.2020.00222.

(371) Szebeni, J.; Simberg, D.; González-Fernández, Á.; Barenholz, Y.; Dobrovolskaia, M. A. Roadmap and Strategy for Overcoming Infusion Reactions to Nanomedicines. *Nat. Nanotechnol.* **2018**, *13* (12), 1100–1108. https://doi.org/10.1038/s41565-018-0273-1.

(372) Dispenza, M. C. Classification of Hypersensitivity Reactions. *Allergy asthma Proc.* **2019**, *40* (6), 470–473. https://doi.org/10.2500/aap.2019.40.4274.

(373) Moghimi, S. M.; Andersen, A. J.; Ahmadvand, D.; Wibroe, P. P.; Andresen, T. L.; Hunter, A. C. Material Properties in Complement Activation. *Adv. Drug Deliv. Rev.* **2011**, *63* (12), 1000–1007. https://doi.org/10.1016/j.addr.2011.06.002.

(374) Chen, F.; Wang, G.; Griffin, J. I.; Brenneman, B.; Banda, N. K.; Holers, V. M.; Backos, D. S.; Wu, L.; Moghimi, S. M.; Simberg, D. Complement Proteins Bind to Nanoparticle Protein Corona and Undergo Dynamic Exchange in Vivo. *Nat. Nanotechnol.* **2017**, *12* (4), 387–393. https://doi.org/10.1038/nnano.2016.269.

(375) Moghimi, S. M.; Simberg, D.; Skotland, T.; Yaghmur, A.; Hunter, A. C. The Interplay Between Blood Proteins, Complement, and Macrophages on Nanomedicine Performance and Responses. *J. Pharmacol. Exp. Ther.* **2019**, *370* (3), 581 LP – 592. https://doi.org/10.1124/jpet.119.258012.

(376) Szebeni, J. Complement Activation-Related Pseudoallergy: A Stress Reaction in Blood Triggered by Nanomedicines and Biologicals. *Mol. Immunol.* **2014**, *61* (2), 163–173. https://doi.org/10.1016/j.molimm.2014.06.038.

(377) Szebeni, J.; Muggia, F.; Gabizon, A.; Barenholz, Y. Activation of Complement by Therapeutic Liposomes and Other Lipid Excipient-Based Therapeutic Products: Prediction and Prevention. *Adv. Drug Deliv. Rev.* **2011**, *63* (12), 1020–1030. https://doi.org/10.1016/j.addr.2011.06.017.

(378) La-Beck, N. M.; Islam, M. R.; Markiewski, M. M. Nanoparticle-Induced Complement Activation: Implications for Cancer Nanomedicine. *Front. Immunol.* **2020**, *11*, 603039. https://doi.org/10.3389/fimmu.2020.603039.

(379) Moghimi, S. M. Nanomedicine Safety in Preclinical and Clinical Development: Focus on Idiosyncratic Injection/Infusion Reactions. *Drug Discov. Today* **2018**, *23* (5), 1034–1042. https://doi.org/10.1016/j.drudis.2017.11.006.

(380) Banda, N. K.; Mehta, G.; Chao, Y.; Wang, G.; Inturi, S.; Fossati-Jimack, L.; Botto, M.; Wu, L.; Moghimi, S. M.; Simberg, D. Mechanisms of Complement Activation by Dextran-Coated Superparamagnetic Iron Oxide (SPIO) Nanoworms in Mouse versus Human Serum. *Part. Fibre Toxicol.* **2014**, *11* (1), 64. https://doi.org/10.1186/s12989-014-0064-2.

(381) Halamoda-Kenzaoui, B.; Bremer-Hoffmann, S. Main Trends of Immune Effects Triggered by Nanomedicines in Preclinical Studies. *Int. J. Nanomedicine* **2018**, *13*, 5419–5431. https://doi.org/10.2147/IJN.S168808.

(382) Fadeel, B. Hide and Seek: Nanomaterial Interactions With the Immune System. *Front. Immunol.* **2019**, *10*, 133. https://doi.org/10.3389/fimmu.2019.00133.

(383) Fontenot, A. P.; Falta, M. T.; Kappler, J. W.; Dai, S.; McKee, A. S. Beryllium-Induced Hypersensitivity: Genetic Susceptibility and Neoantigen Generation. *J. Immunol.* **2016**, *196* (1), 22–27. https://doi.org/10.4049/jimmunol.1502011.

(384) Watanabe, H.; Nakanishi, T.; Umetsu, M.; Kumagai, I. Human Anti-Gold Antibodies: Biofunctionalization of Gold Nanoparticles and Surfaces with Anti-Gold Antibodies. *J. Biol. Chem.* **2008**, *283* (51), 36031–36038. https://doi.org/10.1074/jbc.M805547200.

(385) Izhaky, D.; Pecht, I. What Else Can the Immune System Recognize? *Proc. Natl. Acad. Sci. U. S. A.* **1998**, *95* (20), 11509–11510. https://doi.org/10.1073/pnas.95.20.11509.

(386) Silva, A. L.; Peres, C.; Conniot, J.; Matos, A. I.; Moura, L.; Carreira, B.; Sainz, V.; Scomparin, A.; Satchi-Fainaro, R.; Préat, V.; Florindo, H. F. Nanoparticle Impact on Innate Immune Cell Pattern-Recognition Receptors and Inflammasomes Activation. *Semin. Immunol.* **2017**, *34*, 3–24. https://doi.org/10.1016/j.smim.2017.09.003.

(387) Walkey, C. D.; Olsen, J. B.; Guo, H.; Emili, A.; Chan, W. C. W. Nanoparticle Size and Surface Chemistry Determine Serum Protein Adsorption and Macrophage Uptake. *J. Am. Chem. Soc.* **2012**, *134* (4), 2139–2147. https://doi.org/10.1021/ja2084338.

(388) Garay, R. P.; El-Gewely, R.; Armstrong, J. K.; Garratty, G.; Richette, P. Antibodies against Polyethylene Glycol in Healthy Subjects and in Patients Treated with PEG-Conjugated Agents. *Expert opinion on drug delivery*. England November 2012, pp 1319–1323. https://doi.org/10.1517/17425247.2012.720969.

(389) Sroda, K.; Rydlewski, J.; Langner, M.; Kozubek, A.; Grzybek, M.; Sikorski, A. F. Repeated Injections of PEG-PE Liposomes Generate Anti-PEG Antibodies. *Cell. Mol. Biol. Lett.* **2005**, *10* (1), 37–47.

(390) Ganson, N. J.; Povsic, T. J.; Sullenger, B. A.; Alexander, J. H.; Zelenkofske, S. L.; Sailstad, J. M.; Rusconi, C. P.; Hershfield, M. S. Pre-Existing Anti-Polyethylene Glycol Antibody Linked to First-Exposure Allergic Reactions to Pegnivacogin, a PEGylated RNA Aptamer. *The Journal of allergy and clinical immunology*. May 2016, pp 1610-1613.e7. https://doi.org/10.1016/j.jaci.2015.10.034.

(391) Armstrong, J. K. The Occurrence, Induction, Specificity and Potential Effect of Antibodies against Poly(Ethylene Glycol) BT - PEGylated Protein Drugs: Basic Science and Clinical Applications; Veronese, F. M., Ed.; Birkhäuser Basel: Basel, 2009; pp 147–168. https://doi.org/10.1007/978-3-7643-8679-5_9.

(392) Richter, A. W.; Akerblom, E. Polyethylene Glycol Reactive Antibodies in Man: Titer Distribution in Allergic Patients Treated with Monomethoxy Polyethylene Glycol Modified Allergens or Placebo, and in Healthy Blood Donors. *Int. Arch. Allergy Appl. Immunol.* **1984**, *74* (1), 36–39. https://doi.org/10.1159/000233512.

(393) Sellaturay, P.; Nasser, S.; Islam, S.; Gurugama, P.; Ewan, P. W. Polyethylene Glycol (PEG) Is a Cause of Anaphylaxis to the Pfizer/BioNTech MRNA COVID-19 Vaccine. *Clin. Exp. Allergy* **2021**, *51* (6), 861–863. https://doi.org/10.1111/cea.13874.

(394) Cabanillas, B.; Akdis, C. A.; Novak, N. COVID-19 Vaccine Anaphylaxis: IgE, Complement or What Else? A Reply to: "COVID-19 Vaccine Anaphylaxis: PEG or Not?" *Allergy* **2021**, *76* (6), 1938–1940. https://doi.org/10.1111/all.14725.

(395) Borgsteede, S. D.; Geersing, T. H.; Tempels-Pavlica, Ž. Other Excipients than PEG Might Cause Serious Hypersensitivity Reactions in COVID-19 Vaccines. *Allergy* **2021**, *76* (6), 1941–1942. https://doi.org/10.1111/all.14774.

(396) Padín-González, E.; Lancaster, P.; Bottini, M.; Gasco, P.; Tran, L.; Fadeel, B.; Wilkins, T.; Monopoli, M. P. Understanding the Role and Impact of Poly (Ethylene Glycol) (PEG) on Nanoparticle Formulation: Implications for COVID-19 Vaccines. *Front. Bioeng. Biotechnol.* **2022**, *10*, 882363. https://doi.org/10.3389/fbioe.2022.882363.

(397) Ishida, T.; Ichihara, M.; Wang, X.; Yamamoto, K.; Kimura, J.; Majima, E.; Kiwada, H. Injection of PEGylated Liposomes in Rats Elicits PEG-Specific IgM, Which Is Responsible for Rapid Elimination of a Second Dose of PEGylated Liposomes. *J. Control. Release* **2006**, *112* (1), 15–25. https://doi.org/10.1016/j.jconrel.2006.01.005.

(398) Judge, A.; McClintock, K.; Phelps, J. R.; Maclachlan, I. Hypersensitivity and Loss of Disease Site Targeting Caused by Antibody Responses to PEGylated Liposomes. *Mol. Ther.* **2006**, *13* (2), 328–337. https://doi.org/10.1016/j.ymthe.2005.09.014.

(399) El Sayed, M. M.; Takata, H.; Shimizu, T.; Kawaguchi, Y.; Abu Lila, A. S.; Elsadek, N. E.; Alaaeldin, E.; Ishima, Y.; Ando, H.; Kamal, A.; Sarhan, H. A.; Ishida, T. Hepatosplenic Phagocytic Cells Indirectly Contribute to Anti-PEG IgM Production in the Accelerated Blood Clearance (ABC) Phenomenon against PEGylated Liposomes: Appearance of an Unexplained Mechanism in the ABC Phenomenon. *J. Control. Release* **2020**, *323*, 102–109. https://doi.org/10.1016/j.jconrel.2020.04.011.

(400) Chen, B.-M.; Cheng, T.-L.; Roffler, S. R. Polyethylene Glycol Immunogenicity: Theoretical, Clinical, and Practical Aspects of Anti-Polyethylene Glycol Antibodies. *ACS Nano* **2021**, *15* (9), 14022–14048. https://doi.org/10.1021/acsnano.1c05922.

(401) Hadjesfandiari, N.; Parambath, A. 13 - Stealth Coatings for Nanoparticles: Polyethylene Glycol Alternatives. In *Woodhead Publishing Series in Biomaterials*; Woodhead Publishing, 2018; pp 345–361. https://doi.org/10.1016/B978-0-08-101750-0.00013-1.

(402) Bludau, H.; Czapar, A. E.; Pitek, A. S.; Shukla, S.; Jordan, R.; Steinmetz, N. F. POxylation as an Alternative Stealth Coating for Biomedical Applications. *Eur. Polym. J.* **2017**, *88*, 679–688. https://doi.org/10.1016/j.eurpolymj.2016.10.041.

(403) d'Avanzo, N.; Celia, C.; Barone, A.; Carafa, M.; Di Marzio, L.; Santos, H. A.; Fresta, M. Immunogenicity of Polyethylene Glycol Based Nanomedicines: Mechanisms, Clinical Implications and Systematic Approach. *Adv. Ther.* **2020**, *3* (3), 1900170. https://doi.org/10.1002/adtp.201900170.

(404) Fontana, F.; Lindstedt, H.; Correia, A.; Chiaro, J.; Kari, O. K.; Ndika, J.; Alenius, H.; Buck, J.; Sieber, S.; Mäkilä, E.; Salonen, J.; Urtti, A.; Cerullo, V.; Hirvonen, J. T.; Santos, H. A. Influence of Cell Membrane Wrapping on the Cell−Porous Silicon Nanoparticle Interactions. *Adv. Healthc. Mater.* **2020**, *9* (17), 2000529. https://doi.org/10.1002/adhm.202000529.

(405) Han, H.; Bártolo, R.; Li, J.; Shahbazi, M.-A.; Santos, H. A. Biomimetic Platelet Membrane-Coated Nanoparticles for Targeted Therapy. *Eur. J. Pharm. Biopharm.* **2022**, *172*, 1–15. https://doi.org/10.1016/j.ejpb.2022.01.004.

(406) Yong, T.; Zhang, X.; Bie, N.; Zhang, H.; Zhang, X.; Li, F.; Hakeem, A.; Hu, J.; Gan, L.; Santos, H. A.; Yang, X. Tumor Exosome-Based Nanoparticles Are Efficient Drug Carriers for Chemotherapy. *Nat. Commun.* **2019**, *10* (1), 3838. https://doi.org/10.1038/s41467-019-11718-4.

(407) Jakobsson, U.; Mäkilä, E.; Rahikkala, A.; Imlimthan, S.; Lampuoti, J.; Ranjan, S.; Heino, J.; Jalkanen, P.; Köster, U.; Mizohata, K.; Santos, H. A.; Salonen, J.; Airaksinen, A. J.; Sarparanta, M.; Helariutta, K. Preparation and in Vivo Evaluation of Red Blood Cell Membrane Coated Porous Silicon Nanoparticles Implanted with 155Tb. *Nucl. Med. Biol.* **2020**, *84–85*, 102–110. https://doi.org/10.1016/j.nucmedbio.2020.04.001.

(408) Chen, L.; Hong, W.; Ren, W.; Xu, T.; Qian, Z.; He, Z. Recent Progress in Targeted Delivery Vectors Based on Biomimetic Nanoparticles. *Signal Transduct. Target. Ther.* **2021**, *6* (1), 225. https://doi.org/10.1038/s41392-021-00631-2.

(409) Jiang, Y.; Krishnan, N.; Zhou, J.; Chekuri, S.; Wei, X.; Kroll, A. V; Yu, C. L.; Duan, Y.; Gao, W.; Fang, R. H.; Zhang, L. Engineered Cell-Membrane-Coated Nanoparticles Directly Present Tumor Antigens to Promote Anticancer Immunity. *Adv. Mater.* **2020**, *32* (30), 2001808. https://doi.org/10.1002/adma.202001808.

(410) Ochyl, L. J.; Bazzill, J. D.; Park, C.; Xu, Y.; Kuai, R.; Moon, J. J. PEGylated Tumor Cell Membrane Vesicles as a New Vaccine Platform for Cancer Immunotherapy. *Biomaterials* **2018**, *182*, 157–166. https://doi.org/10.1016/j.biomaterials.2018.08.016.

(411) Brenner, J. S.; Mitragotri, S.; Muzykantov, V. R. Red Blood Cell Hitchhiking: A Novel Approach for Vascular Delivery of Nanocarriers. *Annu. Rev. Biomed. Eng.* **2021**, *23* (1), 225–248. https://doi.org/10.1146/annurev-bioeng-121219-024239.

(412) Li, J.; Cheng, Q.; Yue, L.; Gao, C.; Wei, J.; Ding, Y.; Wang, Y.; Zheng, Y.; Wang, R. Macrophage-Hitchhiking Supramolecular Aggregates of CuS Nanoparticles for Enhanced Tumor Deposition and Photothermal Therapy. *Nanoscale Horizons* **2021**, *6* (11), 907–912. https://doi.org/10.1039/D1NH00291K.

(413) Brenner, J. S.; Pan, D. C.; Myerson, J. W.; Marcos-Contreras, O. A.; Villa, C. H.; Patel, P.; Hekierski, H.; Chatterjee, S.; Tao, J.-Q.; Parhiz, H.; Bhamidipati, K.; Uhler, T. G.; Hood, E. D.; Kiseleva, R. Y.; Shuvaev, V. S.; Shuvaeva, T.; Khoshnejad, M.; Johnston, I.; Gregory, J. V; Lahann, J.; Wang, T.; Cantu, E.; Armstead, W. M.; Mitragotri, S.; Muzykantov, V. Red Blood Cell-Hitchhiking Boosts Delivery of Nanocarriers to Chosen Organs by Orders of Magnitude. *Nat. Commun.* **2018**, *9* (1), 2684. https://doi.org/10.1038/s41467-018-05079-7.

(414) Dhaliwal, A.; Zheng, G. Improving Accessibility of EPR-Insensitive Tumor Phenotypes Using EPR-Adaptive Strategies: Designing a New Perspective in Nanomedicine Delivery. *Theranostics* **2019**, *9* (26), 8091–8108. https://doi.org/10.7150/thno.37204.

(415) Petersen, G. H.; Alzghari, S. K.; Chee, W.; Sankari, S. S.; La-Beck, N. M. Meta-Analysis of Clinical and Preclinical Studies Comparing the Anticancer Efficacy of Liposomal versus Conventional Non-Liposomal Doxorubicin. *J. Control. Release* **2016**, *232*, 255–264. https://doi.org/10.1016/j.jconrel.2016.04.028.

(416) Cabral, H.; Matsumoto, Y.; Mizuno, K.; Chen, Q.; Murakami, M.; Kimura, M.; Terada, Y.; Kano, M. R.; Miyazono, K.; Uesaka, M.; Nishiyama, N.; Kataoka, K. Accumulation of Sub-100 Nm Polymeric Micelles in Poorly Permeable Tumours Depends on Size. *Nat. Nanotechnol.* **2011**, *6* (12), 815–823. https://doi.org/10.1038/nnano.2011.166.

(417) Stylianopoulos, T.; Jain, R. K. Combining Two Strategies to Improve Perfusion and Drug Delivery in Solid Tumors. *Proc. Natl. Acad. Sci. U. S. A.* **2013**, *110* (46), 18632–18637. https://doi.org/10.1073/pnas.1318415110.

(418) Nichols, J. W.; Bae, Y. H. EPR: Evidence and Fallacy. *J. Control. Release* **2014**, *190*, 451–464. https://doi.org/10.1016/j.jconrel.2014.03.057.

(419) Hansen, A. E.; Petersen, A. L.; Henriksen, J. R.; Boerresen, B.; Rasmussen, P.; Elema, D. R.; af Rosenschöld, P. M.; Kristensen, A. T.; Kjær, A.; Andresen, T. L. Positron Emission Tomography Based Elucidation of the Enhanced Permeability and Retention Effect in Dogs with Cancer Using Copper-64 Liposomes. *ACS Nano* **2015**, *9* (7), 6985–6995. https://doi.org/10.1021/acsnano.5b01324.

(420) Carmeliet, P.; Jain, R. K. Molecular Mechanisms and Clinical Applications of Angiogenesis. *Nature* **2011**,

473 (7347), 298–307. https://doi.org/10.1038/nature10144.

(421) Maeda, H. Toward a Full Understanding of the EPR Effect in Primary and Metastatic Tumors as Well as Issues Related to Its Heterogeneity. *Adv. Drug Deliv. Rev.* **2015**, *91*, 3–6. https://doi.org/10.1016/j.addr.2015.01.002.

(422) Prabhakar, U.; Maeda, H.; Jain, R. K.; Sevick-Muraca, E. M.; Zamboni, W.; Farokhzad, O. C.; Barry, S. T.; Gabizon, A.; Grodzinski, P.; Blakey, D. C. Challenges and Key Considerations of the Enhanced Permeability and Retention Effect for Nanomedicine Drug Delivery in Oncology. *Cancer research*. April 2013, pp 2412–2417. https://doi.org/10.1158/0008-5472.CAN-12-4561.

(423) Wilhelm, S.; Tavares, A. J.; Dai, Q.; Ohta, S.; Audet, J.; Dvorak, H. F.; Chan, W. C. W. Analysis of Nanoparticle Delivery to Tumours. *Nat. Rev. Mater.* **2016**, *1* (5), 16014. https://doi.org/10.1038/natrevmats.2016.14.

(424) McNeil, S. E. Evaluation of Nanomedicines: Stick to the Basics. *Nat. Rev. Mater.* **2016**, *1* (10), 16073. https://doi.org/10.1038/natrevmats.2016.73.

(425) Price, L. S. L.; Stern, S. T.; Deal, A. M.; Kabanov, A. V; Zamboni, W. C. A Reanalysis of Nanoparticle Tumor Delivery Using Classical Pharmacokinetic Metrics. *Sci. Adv.* **2020**, *6* (29), eaay9249. https://doi.org/10.1126/sciadv.aay9249.

(426) Khedri, M.; Afsharchi, F.; Souderjani, A. H.; Rezvantalab, S.; Didandeh, M.; Maleki, R.; Musaie, K.; Santos, H. A.; Shahbazi, M.-A. Molecular Scale Study on the Interactions of Biocompatible Nanoparticles with Macrophage Membrane and Blood Proteins. *Nano Sel.* **2022**, *n/a* (n/a). https://doi.org/10.1002/nano.202200043.

(427) Kingston, B. R.; Lin, Z. P.; Ouyang, B.; MacMillan, P.; Ngai, J.; Syed, A. M.; Sindhwani, S.; Chan, W. C. W. Specific Endothelial Cells Govern Nanoparticle Entry into Solid Tumors. *ACS Nano* **2021**, *15* (9), 14080–14094. https://doi.org/10.1021/acsnano.1c04510.

(428) Verhoef, J. J. F.; Anchordoquy, T. J. Questioning the Use of PEGylation for Drug Delivery. *Drug Deliv. Transl. Res.* **2013**, *3* (6), 499–503. https://doi.org/10.1007/s13346-013-0176-5.

(429) Carnovale, C.; Bryant, G.; Shukla, R.; Bansal, V. Identifying Trends in Gold Nanoparticle Toxicity and Uptake: Size, Shape, Capping Ligand, and Biological Corona. *ACS Omega* **2019**, *4* (1), 242–256. https://doi.org/10.1021/acsomega.8b03227.

(430) Lesniak, A.; Salvati, A.; Santos-Martinez, M. J.; Radomski, M. W.; Dawson, K. A.; Åberg, C. Nanoparticle Adhesion to the Cell Membrane and Its Effect on Nanoparticle Uptake Efficiency. *J. Am. Chem. Soc.* **2013**, *135* (4), 1438–1444. https://doi.org/10.1021/ja309812z.

(431) Guarnieri, D.; Guaccio, A.; Fusco, S.; Netti, P. A. Effect of Serum Proteins on Polystyrene Nanoparticle Uptake and Intracellular Trafficking in Endothelial Cells. *J. Nanoparticle Res.* **2011**, *13* (9), 4295. https://doi.org/10.1007/s11051-011-0375-2.

(432) Salvati, A.; Pitek, A. S.; Monopoli, M. P.; Prapainop, K.; Bombelli, F. B.; Hristov, D. R.; Kelly, P. M.; Åberg, C.; Mahon, E.; Dawson, K. A. Transferrin-Functionalized Nanoparticles Lose Their Targeting Capabilities When a Biomolecule Corona Adsorbs on the Surface. *Nat. Nanotechnol.* **2013**, *8* (2), 137–143. https://doi.org/10.1038/nnano.2012.237.

(433) Smith, P. J.; Giroud, M.; Wiggins, H. L.; Gower, F.; Thorley, J. A.; Stolpe, B.; Mazzolini, J.; Dyson, R. J.; Rappoport, J. Z. Cellular Entry of Nanoparticles via Serum Sensitive Clathrin-Mediated Endocytosis, and Plasma Membrane Permeabilization. *Int. J. Nanomedicine* **2012**, *7*, 2045–2055. https://doi.org/10.2147/IJN.S29334.

(434) Jiang, Y.; Huo, S.; Mizuhara, T.; Das, R.; Lee, Y.-W.; Hou, S.; Moyano, D. F.; Duncan, B.; Liang, X.-J.; Rotello, V. M. The Interplay of Size and Surface Functionality on the Cellular Uptake of Sub-10 Nm Gold Nanoparticles. *ACS Nano* **2015**, *9* (10), 9986–9993. https://doi.org/10.1021/acsnano.5b03521.

(435) Brun, E.; Sicard – Roselli, C. Could Nanoparticle Corona Characterization Help for Biological Consequence Prediction? *Cancer Nanotechnol.* **2014**, *5* (1), 7. https://doi.org/10.1186/s12645-014-0007-5.

(436) Holback, H.; Yeo, Y. Intratumoral Drug Delivery with Nanoparticulate Carriers. *Pharm. Res.* **2011**, *28* (8), 1819–1830. https://doi.org/10.1007/s11095-010-0360-y.

(437) Lu, W.; Xiong, C.; Zhang, R.; Shi, L.; Huang, M.; Zhang, G.; Song, S.; Huang, Q.; Liu, G.; Li, C. Receptor-Mediated Transcytosis: A Mechanism for Active Extravascular Transport of Nanoparticles in Solid Tumors. *J. Control. Release* **2012**, *161* (3), 959–966. https://doi.org/10.1016/j.jconrel.2012.05.014.

(438) Liu, Y.; Huo, Y.; Yao, L.; Xu, Y.; Meng, F.; Li, H.; Sun, K.; Zhou, G.; Kohane, D. S.; Tao, K. Transcytosis of Nanomedicine for Tumor Penetration. *Nano Lett.* **2019**, *19* (11), 8010–8020. https://doi.org/10.1021/acs.nanolett.9b03211.

(439) Park, J.; Choi, Y.; Chang, H.; Um, W.; Ryu, J. H.; Kwon, I. C. Alliance with EPR Effect: Combined Strategies to Improve the EPR Effect in the Tumor Microenvironment. *Theranostics* **2019**, *9* (26), 8073–8090. https://doi.org/10.7150/thno.37198.

(440) Tuma, P. L.; Hubbard, A. L. Transcytosis: Crossing Cellular Barriers. *Physiol. Rev.* **2003**, *83* (3), 871–932. https://doi.org/10.1152/physrev.00001.2003.

(441) Poller, W. C.; Ramberger, E.; Boehm-Sturm, P.; Mueller, S.; Möller, K.; Löwa, N.; Wiekhorst, F.; Wagner, S.; Taupitz, M.; Schellenberger, E.; Baumann, G.; Stangl, K.; Stangl, V.; Ludwig, A. Uptake of Citrate-Coated Iron Oxide Nanoparticles into Atherosclerotic Lesions in Mice Occurs via Accelerated Transcytosis through Plaque Endothelial Cells. *Nano Res.* **2016**, *9* (11), 3437–3452. https://doi.org/10.1007/s12274-016-1220-9.

(442) Jing, X.; Yang, F.; Shao, C.; Wei, K.; Xie, M.; Shen, H.; Shu, Y. Role of Hypoxia in Cancer Therapy by Regulating the Tumor Microenvironment. *Mol. Cancer* **2019**, *18* (1), 157. https://doi.org/10.1186/s12943-019-1089-9.

(443) Zhang, B.; Hu, Y.; Pang, Z. Modulating the Tumor Microenvironment to Enhance Tumor Nanomedicine Delivery. *Front. Pharmacol.* **2017**, *8*, 952. https://doi.org/10.3389/fphar.2017.00952.

(444) Padera, T. P.; Stoll, B. R.; Tooredman, J. B.; Capen, D.; Tomaso, E. di; Jain, R. K. Cancer Cells Compress Intratumour Vessels. *Nature* **2004**, *427* (6976), 695. https://doi.org/10.1038/427695a.

(445) Heldin, C.-H.; Rubin, K.; Pietras, K.; Östman, A. High Interstitial Fluid Pressure — an Obstacle in Cancer Therapy. *Nat. Rev. Cancer* **2004**, *4* (10), 806–813. https://doi.org/10.1038/nrc1456.

(446) Rofstad, E. K.; Galappathi, K.; Mathiesen, B. S. Tumor Interstitial Fluid Pressure—A Link between Tumor Hypoxia, Microvascular Density, and Lymph Node Metastasis. *Neoplasia* **2014**, *16* (7), 586–594. https://doi.org/10.1016/j.neo.2014.07.003.

(447) Muz, B.; de la Puente, P.; Azab, F.; Azab, A. K. The Role of Hypoxia in Cancer Progression, Angiogenesis, Metastasis, and Resistance to Therapy. *Hypoxia (Auckland, N.Z.)* **2015**, *3*, 83–92. https://doi.org/10.2147/HP.S93413.

(448) Semenza, G. L. Cancer-Stromal Cell Interactions Mediated by Hypoxia-Inducible Factors Promote Angiogenesis, Lymphangiogenesis, and Metastasis. *Oncogene* **2013**, *32* (35), 4057–4063. https://doi.org/10.1038/onc.2012.578.

(449) Vaupel, P.; Mayer, A. Hypoxia in Cancer: Significance and Impact on Clinical Outcome. *Cancer Metastasis Rev.* **2007**, *26* (2), 225–239. https://doi.org/10.1007/s10555-007-9055-1.

(450) Eales, K. L.; Hollinshead, K. E. R.; Tennant, D. A. Hypoxia and Metabolic Adaptation of Cancer Cells. *Oncogenesis* **2016**, *5* (1), e190–e190. https://doi.org/10.1038/oncsis.2015.50.

(451) Graham, K.; Unger, E. Overcoming Tumor Hypoxia as a Barrier to Radiotherapy, Chemotherapy and Immunotherapy in Cancer Treatment. *Int. J. Nanomedicine* **2018**, *13*, 6049–6058. https://doi.org/10.2147/IJN.S140462.

(452) Baran, N.; Konopleva, M. Molecular Pathways: Hypoxia-Activated Prodrugs in Cancer Therapy. *Clin. cancer Res. an Off. J. Am. Assoc. Cancer Res.* **2017**, *23* (10), 2382–2390. https://doi.org/10.1158/1078-0432.CCR-16-0895.

(453) Keith, B.; Johnson, R. S.; Simon, M. C. HIF1α and HIF2α: Sibling Rivalry in Hypoxic Tumour Growth and Progression. *Nat. Rev. Cancer* **2011**, *12* (1), 9–22. https://doi.org/10.1038/nrc3183.

(454) Forristal, C. E.; Winkler, I. G.; Nowlan, B.; Barbier, V.; Walkinshaw, G.; Levesque, J.-P. Pharmacologic Stabilization of HIF-1α Increases Hematopoietic Stem Cell Quiescence in Vivo and Accelerates Blood Recovery after Severe Irradiation. *Blood* **2013**, *121* (5), 759–769. https://doi.org/10.1182/blood-2012-02-408419.

(455) Li, Y.; An, L.; Lin, J.; Tian, Q.; Yang, S. Smart Nanomedicine Agents for Cancer, Triggered by PH, Glutathione, H(2)O(2), or H(2)S. *Int. J. Nanomedicine* **2019**, *14*, 5729–5749. https://doi.org/10.2147/IJN.S210116.

(456) Sharma, A.; Arambula, J. F.; Koo, S.; Kumar, R.; Singh, H.; Sessler, J. L.; Kim, J. S. Hypoxia-Targeted Drug Delivery. *Chem. Soc. Rev.* **2019**, *48* (3), 771–813. https://doi.org/10.1039/c8cs00304a.

(457) Miao, L.; Newby, J. M.; Lin, C. M.; Zhang, L.; Xu, F.; Kim, W. Y.; Forest, M. G.; Lai, S. K.; Milowsky, M. I.; Wobker, S. E.; Huang, L. The Binding Site Barrier Elicited by Tumor-Associated Fibroblasts Interferes Disposition of Nanoparticles in Stroma-Vessel Type Tumors. *ACS Nano* **2016**, *10* (10), 9243–9258. https://doi.org/10.1021/acsnano.6b02776.

(458) Roode, L. E.; Brighton, H.; Bo, T.; Perry, J. L.; Parrott, M. C.; Kersey, F.; Luft, J. C.; Bear, J. E.; DeSimone, J. M.; Davis, I. J. Subtumoral Analysis of PRINT Nanoparticle Distribution Reveals Targeting Variation Based on Cellular and Particle Properties. *Nanomedicine Nanotechnology, Biol. Med.* **2016**, *12* (4), 1053–1062. https://doi.org/10.1016/j.nano.2015.12.382.

(459) Yokoi, K.; Kojic, M.; Milosevic, M.; Tanei, T.; Ferrari, M.; Ziemys, A. Capillary-Wall Collagen as a Biophysical Marker of Nanotherapeutic Permeability into the Tumor Microenvironment. *Cancer Res.* **2014**, *74* (16), 4239–4246. https://doi.org/10.1158/0008-5472.CAN-13-3494.

(460) MacParland, S. A.; Tsoi, K. M.; Ouyang, B.; Ma, X.-Z.; Manuel, J.; Fawaz, A.; Ostrowski, M. A.; Alman, B. A.; Zilman, A.; Chan, W. C. W.; McGilvray, I. D. Phenotype Determines Nanoparticle Uptake by Human Macrophages from Liver and Blood. *ACS Nano* **2017**, *11* (3), 2428–2443. https://doi.org/10.1021/acsnano.6b06245.

(461) Duan, Q.; Zhang, H.; Zheng, J.; Zhang, L. Turning Cold into Hot: Firing up the Tumor Microenvironment. *Trends in cancer* **2020**, *6* (7), 605–618. https://doi.org/10.1016/j.trecan.2020.02.022.

(462) Baci, D.; Bosi, A.; Gallazzi, M.; Rizzi, M.; Noonan, D. M.; Poggi, A.; Bruno, A.; Mortara, L. The Ovarian Cancer Tumor Immune Microenvironment (TIME) as Target for Therapy: A Focus on Innate Immunity Cells as Therapeutic Effectors. *Int. J. Mol. Sci.* **2020**, *21* (9).

(463) Barrett, R. L.; Puré, E. Cancer-Associated Fibroblasts and Their Influence on Tumor Immunity and Immunotherapy. *Elife* **2020**, *9*, e57243. https://doi.org/10.7554/eLife.57243.

(464) Korangath, P.; Barnett, J. D.; Sharma, A.; Henderson, E. T.; Stewart, J.; Yu, S.-H.; Kandala, S. K.; Yang, C.-T.; Caserto, J. S.; Hedayati, M.; Armstrong, T. D.; Jaffee, E.; Gruettner, C.; Zhou, X. C.; Fu, W.; Hu, C.; Sukumar, S.; Simons, B. W.; Ivkov, R. Nanoparticle Interactions with Immune Cells Dominate Tumor Retention and Induce T Cell–Mediated Tumor Suppression in Models of Breast Cancer. *Sci. Adv.* **2020**, *6* (13), eaay1601. https://doi.org/10.1126/sciadv.aay1601.

(465) Provenzano, P. P.; Cuevas, C.; Chang, A. E.; Goel, V. K.; Von Hoff, D. D.; Hingorani, S. R. Enzymatic Targeting of the Stroma Ablates Physical Barriers to Treatment of Pancreatic Ductal Adenocarcinoma. *Cancer Cell* **2012**, *21* (3), 418–429. https://doi.org/10.1016/j.ccr.2012.01.007.

(466) Zhang, B.; Jiang, T.; Shen, S.; She, X.; Tuo, Y.; Hu, Y.; Pang, Z.; Jiang, X. Cyclopamine Disrupts Tumor Extracellular Matrix and Improves the Distribution and Efficacy of Nanotherapeutics in Pancreatic Cancer.

Biomaterials **2016**, *103*, 12–21. https://doi.org/10.1016/j.biomaterials.2016.06.048.

(467) Shi, Y.; van der Meel, R.; Chen, X.; Lammers, T. The EPR Effect and beyond: Strategies to Improve Tumor Targeting and Cancer Nanomedicine Treatment Efficacy. *Theranostics* **2020**, *10* (17), 7921–7924. https://doi.org/10.7150/thno.49577.

(468) Ojha, T.; Pathak, V.; Shi, Y.; Hennink, W. E.; Moonen, C. T. W.; Storm, G.; Kiessling, F.; Lammers, T. Pharmacological and Physical Vessel Modulation Strategies to Improve EPR-Mediated Drug Targeting to Tumors. *Adv. Drug Deliv. Rev.* **2017**, *119*, 44–60. https://doi.org/10.1016/j.addr.2017.07.007.

(469) Brown, T. D.; Habibi, N.; Wu, D.; Lahann, J.; Mitragotri, S. Effect of Nanoparticle Composition, Size, Shape, and Stiffness on Penetration Across the Blood–Brain Barrier. *ACS Biomater. Sci. Eng.* **2020**, *6* (9), 4916–4928. https://doi.org/10.1021/acsbiomaterials.0c00743.

(470) Zhou, Y.; Peng, Z.; Seven, E. S.; Leblanc, R. M. Crossing the Blood-Brain Barrier with Nanoparticles. *J. Control. Release* **2018**, *270*, 290–303. https://doi.org/10.1016/j.jconrel.2017.12.015.

(471) Power, E. A.; Rechberger, J. S.; Gupta, S.; Schwartz, J. D.; Daniels, D. J.; Khatua, S. Drug Delivery across the Blood-Brain Barrier for the Treatment of Pediatric Brain Tumors – An Update. *Adv. Drug Deliv. Rev.* **2022**, *185*, 114303. https://doi.org/10.1016/j.addr.2022.114303.

(472) Krol, S.; Macrez, R.; Docagne, F.; Defer, G.; Laurent, S.; Rahman, M.; Hajipour, M. J.; Kehoe, P. G.; Mahmoudi, M. Therapeutic Benefits from Nanoparticles: The Potential Significance of Nanoscience in Diseases with Compromise to the Blood Brain Barrier. *Chem. Rev.* **2013**, *113* (3), 1877–1903. https://doi.org/10.1021/cr200472g.

(473) Ding, S.; Khan, A. I.; Cai, X.; Song, Y.; Lyu, Z.; Du, D.; Dutta, P.; Lin, Y. Overcoming Blood–Brain Barrier Transport: Advances in Nanoparticle-Based Drug Delivery Strategies. *Mater. Today* **2020**, *37*, 112–125. https://doi.org/10.1016/j.mattod.2020.02.001.

(474) Saraiva, C.; Praça, C.; Ferreira, R.; Santos, T.; Ferreira, L.; Bernardino, L. Nanoparticle-Mediated Brain Drug Delivery: Overcoming Blood–Brain Barrier to Treat Neurodegenerative Diseases. *J. Control. Release* **2016**, *235*, 34–47. https://doi.org/10.1016/j.jconrel.2016.05.044.

(475) Snipstad, S.; Vikedal, K.; Maardalen, M.; Kurbatskaya, A.; Sulheim, E.; Davies, C. de L. Ultrasound and Microbubbles to Beat Barriers in Tumors: Improving Delivery of Nanomedicine. *Adv. Drug Deliv. Rev.* **2021**, *177*, 113847. https://doi.org/10.1016/j.addr.2021.113847.

(476) Poon, C.; McMahon, D.; Hynynen, K. Noninvasive and Targeted Delivery of Therapeutics to the Brain Using Focused Ultrasound. *Neuropharmacology* **2017**, *120*, 20–37. https://doi.org/10.1016/j.neuropharm.2016.02.014.

(477) Roovers, S.; Segers, T.; Lajoinie, G.; Deprez, J.; Versluis, M.; De Smedt, S. C.; Lentacker, I. The Role of Ultrasound-Driven Microbubble Dynamics in Drug Delivery: From Microbubble Fundamentals to Clinical Translation. *Langmuir* **2019**, *35* (31), 10173–10191. https://doi.org/10.1021/acs.langmuir.8b03779.

(478) Lee, H.; Kim, H.; Han, H.; Lee, M.; Lee, S.; Yoo, H.; Chang, J. H.; Kim, H. Microbubbles Used for Contrast Enhanced Ultrasound and Theragnosis: A Review of Principles to Applications. *Biomed. Eng. Lett.* **2017**, *7* (2), 59–69. https://doi.org/10.1007/s13534-017-0016-5.

(479) Alheshibri, M.; Craig, V. S. J. Armoured Nanobubbles; Ultrasound Contrast Agents under Pressure. *J. Colloid Interface Sci.* **2019**, *537*, 123–131. https://doi.org/10.1016/j.jcis.2018.10.108.

(480) Konar, M.; Mathew, A.; Dasgupta, S. Effect of Silica Nanoparticles on the Amyloid Fibrillation of Lysozyme. *ACS Omega* **2019**, *4* (1), 1015–1026. https://doi.org/10.1021/acsomega.8b03169.

(481) Jaragh-Alhadad, L. A.; Falahati, M. Copper Oxide Nanoparticles Promote Amyloid-β-Triggered Neurotoxicity through Formation of Oligomeric Species as a Prelude to Alzheimer's Diseases. *Int. J. Biol. Macromol.* **2022**, *207*, 121–129. https://doi.org/10.1016/j.ijbiomac.2022.03.006.

(482) John, T.; Gladytz, A.; Kubeil, C.; Martin, L. L.; Risselada, H. J.; Abel, B. Impact of Nanoparticles on

Amyloid Peptide and Protein Aggregation: A Review with a Focus on Gold Nanoparticles. *Nanoscale* **2018**, *10* (45), 20894–20913. https://doi.org/10.1039/C8NR04506B.

(483) Rees, P.; Wills, J. W.; Brown, M. R.; Barnes, C. M.; Summers, H. D. The Origin of Heterogeneous Nanoparticle Uptake by Cells. *Nat. Commun.* **2019**, *10* (1), 2341. https://doi.org/10.1038/s41467-019-10112-4.

(484) Yameen, B.; Choi, W. Il; Vilos, C.; Swami, A.; Shi, J.; Farokhzad, O. C. Insight into Nanoparticle Cellular Uptake and Intracellular Targeting. *J. Control. Release* **2014**, *190*, 485–499. https://doi.org/10.1016/j.jconrel.2014.06.038.

(485) Brocato, T. A.; Coker, E. N.; Durfee, P. N.; Lin, Y.-S.; Townson, J.; Wyckoff, E. F.; Cristini, V.; Brinker, C. J.; Wang, Z. Understanding the Connection between Nanoparticle Uptake and Cancer Treatment Efficacy Using Mathematical Modeling. *Sci. Rep.* **2018**, *8* (1), 7538. https://doi.org/10.1038/s41598-018-25878-8.

(486) Zhao, J.; Stenzel, M. H. Entry of Nanoparticles into Cells: The Importance of Nanoparticle Properties. *Polym. Chem.* **2018**, *9* (3), 259–272. https://doi.org/10.1039/C7PY01603D.

(487) Fu, X.; Shi, Y.; Qi, T.; Qiu, S.; Huang, Y.; Zhao, X.; Sun, Q.; Lin, G. Precise Design Strategies of Nanomedicine for Improving Cancer Therapeutic Efficacy Using Subcellular Targeting. *Signal Transduct. Target. Ther.* **2020**, *5* (1), 262. https://doi.org/10.1038/s41392-020-00342-0.

(488) Kube, S.; Hersch, N.; Naumovska, E.; Gensch, T.; Hendriks, J.; Franzen, A.; Landvogt, L.; Siebrasse, J.-P.; Kubitscheck, U.; Hoffmann, B.; Merkel, R.; Csiszár, A. Fusogenic Liposomes as Nanocarriers for the Delivery of Intracellular Proteins. *Langmuir* **2017**, *33* (4), 1051–1059. https://doi.org/10.1021/acs.langmuir.6b04304.

(489) Sokolova, V.; Mekky, G.; van der Meer, S. B.; Seeds, M. C.; Atala, A. J.; Epple, M. Transport of Ultrasmall Gold Nanoparticles (2 Nm) across the Blood–Brain Barrier in a Six-Cell Brain Spheroid Model. *Sci. Rep.* **2020**, *10* (1), 18033. https://doi.org/10.1038/s41598-020-75125-2.

(490) Liu, C.-G.; Han, Y.-H.; Kankala, R. K.; Wang, S.-B.; Chen, A.-Z. Subcellular Performance of Nanoparticles in Cancer Therapy. *Int. J. Nanomedicine* **2020**, *15*, 675–704. https://doi.org/10.2147/IJN.S226186.

(491) Zhang, Z.; Wang, T.; Yang, R.; Fu, S.; Guan, L.; Hou, T.; Mu, W.; Pang, X.; Liang, S.; Liu, Y.; Zhang, N. Small Morph Nanoparticles for Deep Tumor Penetration via Caveolae-Mediated Transcytosis. *ACS Appl. Mater. Interfaces* **2020**, *12* (34), 38499–38511. https://doi.org/10.1021/acsami.0c06872.

(492) Oh, P.; Borgström, P.; Witkiewicz, H.; Li, Y.; Borgström, B. J.; Chrastina, A.; Iwata, K.; Zinn, K. R.; Baldwin, R.; Testa, J. E.; Schnitzer, J. E. Live Dynamic Imaging of Caveolae Pumping Targeted Antibody Rapidly and Specifically across Endothelium in the Lung. *Nat. Biotechnol.* **2007**, *25* (3), 327–337. https://doi.org/10.1038/nbt1292.

(493) Yamada, Y.; Harashima, H. Enhancement in Selective Mitochondrial Association by Direct Modification of a Mitochondrial Targeting Signal Peptide on a Liposomal Based Nanocarrier. *Mitochondrion* **2013**, *13* (5), 526–532. https://doi.org/10.1016/j.mito.2012.09.001.

(494) Zhao, Z.; Ukidve, A.; Kim, J.; Mitragotri, S. Targeting Strategies for Tissue-Specific Drug Delivery. *Cell* **2020**, *181* (1), 151–167. https://doi.org/10.1016/j.cell.2020.02.001.

(495) Madni, A.; Rehman, S.; Sultan, H.; Khan, M. M.; Ahmad, F.; Raza, M. R.; Rai, N.; Parveen, F. Mechanistic Approaches of Internalization, Subcellular Trafficking, and Cytotoxicity of Nanoparticles for Targeting the Small Intestine. *AAPS PharmSciTech* **2020**, *22* (1), 3. https://doi.org/10.1208/s12249-020-01873-z.

(496) Antunes, F.; Cadenas, E.; Brunk, U. T. Apoptosis Induced by Exposure to a Low Steady-State Concentration of H2O2 Is a Consequence of Lysosomal Rupture. *Biochem. J.* **2001**, *356* (2), 549–555. https://doi.org/10.1042/bj3560549.

(497) Liu, C.-G.; Han, Y.-H.; Zhang, J.-T.; Kankala, R. K.; Wang, S.-B.; Chen, A.-Z. Rerouting Engineered Metal-Dependent Shapes of Mesoporous Silica Nanocontainers to Biodegradable Janus-Type (Sphero-

Ellipsoid) Nanoreactors for Chemodynamic Therapy. *Chem. Eng. J.* **2019**, *370*, 1188–1199. https://doi.org/10.1016/j.cej.2019.03.272.

(498) Sabella, S.; Carney, R. P.; Brunetti, V.; Malvindi, M. A.; Al-Juffali, N.; Vecchio, G.; Janes, S. M.; Bakr, O. M.; Cingolani, R.; Stellacci, F.; Pompa, P. P. A General Mechanism for Intracellular Toxicity of Metal-Containing Nanoparticles. *Nanoscale* **2014**, *6* (12), 7052–7061. https://doi.org/10.1039/c4nr01234h.

(499) Zhao, F.; Zhao, Y.; Liu, Y.; Chang, X.; Chen, C.; Zhao, Y. Cellular Uptake, Intracellular Trafficking, and Cytotoxicity of Nanomaterials. *Small* **2011**, *7* (10), 1322–1337. https://doi.org/10.1002/smll.201100001.

(500) Wu, X.-S.; Elias, S.; Liu, H.; Heureaux, J.; Wen, P. J.; Liu, A. P.; Kozlov, M. M.; Wu, L.-G. Membrane Tension Inhibits Rapid and Slow Endocytosis in Secretory Cells. *Biophys. J.* **2017**, *113* (11), 2406–2414. https://doi.org/10.1016/j.bpj.2017.09.035.

(501) Rueda-Gensini, L.; Cifuentes, J.; Castellanos, M. C.; Puentes, P. R.; Serna, J. A.; Muñoz-Camargo, C.; Cruz, J. C. Tailoring Iron Oxide Nanoparticles for Efficient Cellular Internalization and Endosomal Escape. *Nanomaterials* **2020**, *10* (9).

(502) Sahay, G.; Alakhova, D. Y.; Kabanov, A. V. Endocytosis of Nanomedicines. *J. Control. Release* **2010**, *145* (3), 182–195. https://doi.org/10.1016/j.jconrel.2010.01.036.

(503) Behzadi, S.; Serpooshan, V.; Tao, W.; Hamaly, M. A.; Alkawareek, M. Y.; Dreaden, E. C.; Brown, D.; Alkilany, A. M.; Farokhzad, O. C.; Mahmoudi, M. Cellular Uptake of Nanoparticles: Journey inside the Cell. *Chem. Soc. Rev.* **2017**, *46* (14), 4218–4244. https://doi.org/10.1039/c6cs00636a.

(504) Donahue, N. D.; Acar, H.; Wilhelm, S. Concepts of Nanoparticle Cellular Uptake, Intracellular Trafficking, and Kinetics in Nanomedicine. *Adv. Drug Deliv. Rev.* **2019**, *143*, 68–96. https://doi.org/10.1016/j.addr.2019.04.008.

(505) Derakhshankhah, H.; Jafari, S. Cell Penetrating Peptides: A Concise Review with Emphasis on Biomedical Applications. *Biomed. Pharmacother.* **2018**, *108*, 1090–1096. https://doi.org/10.1016/j.biopha.2018.09.097.

(506) Huang, K.; Ma, H.; Liu, J.; Huo, S.; Kumar, A.; Wei, T.; Zhang, X.; Jin, S.; Gan, Y.; Wang, P. C.; He, S.; Zhang, X.; Liang, X.-J. Size-Dependent Localization and Penetration of Ultrasmall Gold Nanoparticles in Cancer Cells, Multicellular Spheroids, and Tumors in Vivo. *ACS Nano* **2012**, *6* (5), 4483–4493. https://doi.org/10.1021/nn301282m.

(507) Kostarelos, K.; Lacerda, L.; Pastorin, G.; Wu, W.; Wieckowski, S.; Luangsivilay, J.; Godefroy, S.; Pantarotto, D.; Briand, J.-P.; Muller, S.; Prato, M.; Bianco, A. Cellular Uptake of Functionalized Carbon Nanotubes Is Independent of Functional Group and Cell Type. *Nat. Nanotechnol.* **2007**, *2* (2), 108–113. https://doi.org/10.1038/nnano.2006.209.

(508) Zhu, M.; Nie, G.; Meng, H.; Xia, T.; Nel, A.; Zhao, Y. Physicochemical Properties Determine Nanomaterial Cellular Uptake, Transport, and Fate. *Acc. Chem. Res.* **2013**, *46* (3), 622–631. https://doi.org/10.1021/ar300031y.

(509) Hillaireau, H.; Couvreur, P. Nanocarriers' Entry into the Cell: Relevance to Drug Delivery. *Cell. Mol. Life Sci.* **2009**, *66* (17), 2873–2896. https://doi.org/10.1007/s00018-009-0053-z.

(510) Foroozandeh, P.; Aziz, A. A. Insight into Cellular Uptake and Intracellular Trafficking of Nanoparticles. *Nanoscale Res. Lett.* **2018**, *13* (1), 339. https://doi.org/10.1186/s11671-018-2728-6.

(511) Pauwels, A.-M.; Trost, M.; Beyaert, R.; Hoffmann, E. Patterns, Receptors, and Signals: Regulation of Phagosome Maturation. *Trends Immunol.* **2017**, *38* (6), 407–422. https://doi.org/10.1016/j.it.2017.03.006.

(512) Underhill, D. M.; Goodridge, H. S. Information Processing during Phagocytosis. *Nature reviews. Immunology*. Inflammatory Bowel & Immunobiology Research Institute, Department of Biomedical Sciences, Cedars-Sinai Medical Center, 8,700 Beverly Boulevard, Los Angeles, California 90048, USA. David.Underhill@csmc.edu 2012, pp 492–502. https://doi.org/10.1038/nri3244.

(513) Mosser, D. M.; Edwards, J. P. Exploring the Full Spectrum of Macrophage Activation. *Nat. Rev. Immunol.*

2008, *8* (12), 958–969. https://doi.org/10.1038/nri2448.

(514) Dobrovolskaia, M. A.; McNeil, S. E. Immunological Properties of Engineered Nanomaterials. *Nat. Nanotechnol.* **2007**, *2* (8), 469–478. https://doi.org/10.1038/nnano.2007.223.

(515) Bartneck, M.; Keul, H. A.; Singh, S.; Czaja, K.; Bornemann, J.; Bockstaller, M.; Moeller, M.; Zwadlo-Klarwasser, G.; Groll, J. Rapid Uptake of Gold Nanorods by Primary Human Blood Phagocytes and Immunomodulatory Effects of Surface Chemistry. *ACS Nano* **2010**, *4* (6), 3073–3086. https://doi.org/10.1021/nn100262h.

(516) Kirchhausen, T. Clathrin. *Annu. Rev. Biochem.* **2000**, *69*, 699–727. https://doi.org/10.1146/annurev.biochem.69.1.699.

(517) Conner, S. D.; Schmid, S. L. Regulated Portals of Entry into the Cell. *Nature* **2003**, *422* (6927), 37–44. https://doi.org/10.1038/nature01451.

(518) Cocucci, E.; Aguet, F.; Boulant, S.; Kirchhausen, T. The First Five Seconds in the Life of a Clathrin-Coated Pit. *Cell* **2012**, *150* (3), 495–507. https://doi.org/10.1016/j.cell.2012.05.047.

(519) Schmid, E. M.; Ford, M. G. J.; Burtey, A.; Praefcke, G. J. K.; Peak-Chew, S.-Y.; Mills, I. G.; Benmerah, A.; McMahon, H. T. Role of the AP2 Beta-Appendage Hub in Recruiting Partners for Clathrin-Coated Vesicle Assembly. *PLoS Biol.* **2006**, *4* (9), e262. https://doi.org/10.1371/journal.pbio.0040262.

(520) Collins, A.; Warrington, A.; Taylor, K. A.; Svitkina, T. Structural Organization of the Actin Cytoskeleton at Sites of Clathrin-Mediated Endocytosis. *Curr. Biol.* **2011**, *21* (14), 1167–1175. https://doi.org/10.1016/j.cub.2011.05.048.

(521) Kaksonen, M.; Roux, A. Mechanisms of Clathrin-Mediated Endocytosis. *Nat. Rev. Mol. Cell Biol.* **2018**, *19* (5), 313–326. https://doi.org/10.1038/nrm.2017.132.

(522) McMahon, H. T.; Boucrot, E. Molecular Mechanism and Physiological Functions of Clathrin-Mediated Endocytosis. *Nat. Rev. Mol. Cell Biol.* **2011**, *12* (8), 517–533. https://doi.org/10.1038/nrm3151.

(523) Antonny, B.; Burd, C.; De Camilli, P.; Chen, E.; Daumke, O.; Faelber, K.; Ford, M.; Frolov, V. A.; Frost, A.; Hinshaw, J. E.; Kirchhausen, T.; Kozlov, M. M.; Lenz, M.; Low, H. H.; McMahon, H.; Merrifield, C.; Pollard, T. D.; Robinson, P. J.; Roux, A.; Schmid, S. Membrane Fission by Dynamin: What We Know and What We Need to Know. *EMBO J.* **2016**, *35* (21), 2270–2284. https://doi.org/10.15252/embj.201694613.

(524) Popova, N. V; Deyev, I. E.; Petrenko, A. G. Clathrin-Mediated Endocytosis and Adaptor Proteins. *Acta Naturae* **2013**, *5* (3), 62–73.

(525) Lee, S. H.; Park, D. J.; Yun, W. S.; Park, J.-E.; Choi, J. S.; Key, J.; Seo, Y. J. Endocytic Trafficking of Polymeric Clustered Superparamagnetic Iron Oxide Nanoparticles in Mesenchymal Stem Cells. *J. Control. Release* **2020**, *326*, 408–418. https://doi.org/10.1016/j.jconrel.2020.07.032.

(526) Xu, S.; Olenyuk, B. Z.; Okamoto, C. T.; Hamm-Alvarez, S. F. Targeting Receptor-Mediated Endocytotic Pathways with Nanoparticles: Rationale and Advances. *Adv. Drug Deliv. Rev.* **2013**, *65* (1), 121–138. https://doi.org/10.1016/j.addr.2012.09.041.

(527) Bitsikas, V.; Corrêa, I. R. J.; Nichols, B. J. Clathrin-Independent Pathways Do Not Contribute Significantly to Endocytic Flux. *Elife* **2014**, *3*, e03970. https://doi.org/10.7554/eLife.03970.

(528) Wang, H.; Zhang, H.; Xiang, Y.; Pan, W.; Li, N.; Tang, B. An Efficient Strategy for Cancer Therapy Using a Tumor- and Lysosome-Targeted Organic Photothermal Agent. *Nanoscale* **2021**, *13* (19), 8790–8794. https://doi.org/10.1039/D1NR01547H.

(529) Allal, A. S.; Richter, M.; Russo, M.; Rouzaud, M.; Dulguerov, P.; Kurtz, J. M. Dose Variation at Bone/Titanium Interfaces Using Titanium Hollow Screw Osseointegrating Reconstruction Plates. *Int. J. Radiat. Oncol. Biol. Phys.* **1998**, *40* (1), 215–219. https://doi.org/10.1016/s0360-3016(97)00587-7.

(530) Anderson, R. G. The Caveolae Membrane System. *Annu. Rev. Biochem.* **1998**, *67*, 199–225.

https://doi.org/10.1146/annurev.biochem.67.1.199.

(531) Pelkmans, L.; Helenius, A. Endocytosis via Caveolae. *Traffic* **2002**, *3* (5), 311–320. https://doi.org/10.1034/j.1600-0854.2002.30501.x.

(532) Salatin, S.; Yari Khosroushahi, A. Overviews on the Cellular Uptake Mechanism of Polysaccharide Colloidal Nanoparticles. *J. Cell. Mol. Med.* **2017**, *21* (9), 1668–1686. https://doi.org/10.1111/jcmm.13110.

(533) Parton, R. G.; Howes, M. T. Revisiting Caveolin Trafficking: The End of the Caveosome. *J. Cell Biol.* **2010**, *191* (3), 439–441. https://doi.org/10.1083/jcb.201009093.

(534) Cheng, J. P. X.; Nichols, B. J. Caveolae: One Function or Many? *Trends Cell Biol.* **2016**, *26* (3), 177–189. https://doi.org/10.1016/j.tcb.2015.10.010.

(535) Hayer, A.; Stoeber, M.; Ritz, D.; Engel, S.; Meyer, H. H.; Helenius, A. Caveolin-1 Is Ubiquitinated and Targeted to Intralumenal Vesicles in Endolysosomes for Degradation. *J. Cell Biol.* **2010**, *191* (3), 615–629. https://doi.org/10.1083/jcb.201003086.

(536) Parton, R. G.; McMahon, K.-A.; Wu, Y. Caveolae: Formation, Dynamics, and Function. *Curr. Opin. Cell Biol.* **2020**, *65*, 8–16. https://doi.org/10.1016/j.ceb.2020.02.001.

(537) Taggart, M. J. Smooth Muscle Excitation-Contraction Coupling: A Role for Caveolae and Caveolins? *Physiology* **2001**, *16* (2), 61–65. https://doi.org/10.1152/physiologyonline.2001.16.2.61.

(538) Thorn, H.; Stenkula, K. G.; Karlsson, M.; Ortegren, U.; Nystrom, F. H.; Gustavsson, J.; Stralfors, P. Cell Surface Orifices of Caveolae and Localization of Caveolin to the Necks of Caveolae in Adipocytes. *Mol. Biol. Cell* **2003**, *14* (10), 3967–3976. https://doi.org/10.1091/mbc.e03-01-0050.

(539) Wang, Z.; Tiruppathi, C.; Cho, J.; Minshall, R. D.; Malik, A. B. Delivery of Nanoparticle: Complexed Drugs across the Vascular Endothelial Barrier via Caveolae. *IUBMB Life* **2011**, *63* (8), 659–667. https://doi.org/10.1002/iub.485.

(540) Chatterjee, M.; Ben-Josef, E.; Robb, R.; Vedaie, M.; Seum, S.; Thirumoorthy, K.; Palanichamy, K.; Harbrecht, M.; Chakravarti, A.; Williams, T. M. Caveolae-Mediated Endocytosis Is Critical for Albumin Cellular Uptake and Response to Albumin-Bound Chemotherapy. *Cancer Res.* **2017**, *77* (21), 5925–5937. https://doi.org/10.1158/0008-5472.CAN-17-0604.

(541) Hawkins, M. J.; Soon-Shiong, P.; Desai, N. Protein Nanoparticles as Drug Carriers in Clinical Medicine. *Adv. Drug Deliv. Rev.* **2008**, *60* (8), 876–885. https://doi.org/10.1016/j.addr.2007.08.044.

(542) Kumari, S.; Mg, S.; Mayor, S. Endocytosis Unplugged: Multiple Ways to Enter the Cell. *Cell Res.* **2010**, *20* (3), 256–275. https://doi.org/10.1038/cr.2010.19.

(543) de Almeida, M.; Susnik, E.; Drasler, B.; Taladriz-Blanco, P.; Petri-Fink, A.; Rothen-Rutishauser, B. Understanding Nanoparticle Endocytosis to Improve Targeting Strategies in Nanomedicine. *Chem. Soc. Rev.* **2021**. https://doi.org/10.1039/D0CS01127D.

(544) Sandvig, K.; Pust, S.; Skotland, T.; van Deurs, B. Clathrin-Independent Endocytosis: Mechanisms and Function. *Curr. Opin. Cell Biol.* **2011**, *23* (4), 413–420. https://doi.org/10.1016/j.ceb.2011.03.007.

(545) Manzanares, D.; Ceña, V. Endocytosis: The Nanoparticle and Submicron Nanocompounds Gateway into the Cell. *Pharmaceutics* **2020**, *12* (4), 371. https://doi.org/10.3390/pharmaceutics12040371.

(546) Lu, Y.; Low, P. S. Folate-Mediated Delivery of Macromolecular Anticancer Therapeutic Agents. *Adv. Drug Deliv. Rev.* **2012**, *64*, 342–352. https://doi.org/10.1016/j.addr.2012.09.020.

(547) Ding, L.; Zhu, X.; Wang, Y.; Shi, B.; Ling, X.; Chen, H.; Nan, W.; Barrett, A.; Guo, Z.; Tao, W.; Wu, J.; Shi, X. Intracellular Fate of Nanoparticles with Polydopamine Surface Engineering and a Novel Strategy for Exocytosis-Inhibiting, Lysosome Impairment-Based Cancer Therapy. *Nano Lett.* **2017**, *17* (11), 6790–6801. https://doi.org/10.1021/acs.nanolett.7b03021.

(548) Kasper, J.; Hermanns, M. I.; Bantz, C.; Utech, S.; Koshkina, O.; Maskos, M.; Brochhausen, C.; Pohl, C.; Fuchs, S.; Unger, R. E.; Kirkpatrick, C. J. Flotillin-Involved Uptake of Silica Nanoparticles and Responses of an Alveolar-Capillary Barrier in Vitro. *Eur. J. Pharm. Biopharm. Off. J. Arbeitsgemeinschaft fur Pharm. Verfahrenstechnik e.V* **2013**, *84* (2), 275–287. https://doi.org/10.1016/j.ejpb.2012.10.011.

(549) Bohmer, N.; Jordan, A. Caveolin-1 and CDC42 Mediated Endocytosis of Silica-Coated Iron Oxide Nanoparticles in HeLa Cells. *Beilstein J. Nanotechnol.* **2015**, *6*, 167–176. https://doi.org/10.3762/bjnano.6.16.

(550) Swanson, J. A.; Yoshida, S. Macropinosomes as Units of Signal Transduction. *Philos. Trans. R. Soc. London. Ser. B, Biol. Sci.* **2019**, *374* (1765), 20180157. https://doi.org/10.1098/rstb.2018.0157.

(551) Kerr, M. C.; Teasdale, R. D. Defining Macropinocytosis. *Traffic* **2009**, *10* (4), 364–371. https://doi.org/10.1111/j.1600-0854.2009.00878.x.

(552) Gratton, S. E. A.; Ropp, P. A.; Pohlhaus, P. D.; Luft, J. C.; Madden, V. J.; Napier, M. E.; DeSimone, J. M. The Effect of Particle Design on Cellular Internalization Pathways. *Proc. Natl. Acad. Sci.* **2008**, *105* (33), 11613 LP – 11618. https://doi.org/10.1073/pnas.0801763105.

(553) Falcone, S.; Cocucci, E.; Podini, P.; Kirchhausen, T.; Clementi, E.; Meldolesi, J. Macropinocytosis: Regulated Coordination of Endocytic and Exocytic Membrane Traffic Events. *J. Cell Sci.* **2006**, *119* (Pt 22), 4758–4769. https://doi.org/10.1242/jcs.03238.

(554) Ding, L.; Yao, C.; Yin, X.; Li, C.; Huang, Y.; Wu, M.; Wang, B.; Guo, X.; Wang, Y.; Wu, M. Size, Shape, and Protein Corona Determine Cellular Uptake and Removal Mechanisms of Gold Nanoparticles. *Small* **2018**, *14* (42), 1801451. https://doi.org/10.1002/smll.201801451.

(555) Jiang, W.; Kim, B. Y. S.; Rutka, J. T.; Chan, W. C. W. Nanoparticle-Mediated Cellular Response Is Size-Dependent. *Nature nanotechnology*. England March 2008, pp 145–150. https://doi.org/10.1038/nnano.2008.30.

(556) Wang, S.-H.; Lee, C.-W.; Chiou, A.; Wei, P.-K. Size-Dependent Endocytosis of Gold Nanoparticles Studied by Three-Dimensional Mapping of Plasmonic Scattering Images. *J. Nanobiotechnology* **2010**, *8* (1), 33. https://doi.org/10.1186/1477-3155-8-33.

(557) Lu, F.; Wu, S.-H.; Hung, Y.; Mou, C.-Y. Size Effect on Cell Uptake in Well-Suspended, Uniform Mesoporous Silica Nanoparticles. *Small* **2009**, *5* (12), 1408–1413. https://doi.org/10.1002/smll.200900005.

(558) Chithrani, B. D.; Ghazani, A. A.; Chan, W. C. W. Determining the Size and Shape Dependence of Gold Nanoparticle Uptake into Mammalian Cells. *Nano Lett.* **2006**, *6* (4), 662–668. https://doi.org/10.1021/nl052396o.

(559) Hoshyar, N.; Gray, S.; Han, H.; Bao, G. The Effect of Nanoparticle Size on in Vivo Pharmacokinetics and Cellular Interaction. *Nanomedicine (Lond).* **2016**, *11* (6), 673–692. https://doi.org/10.2217/nnm.16.5.

(560) Yuan, H.; Li, J.; Bao, G.; Zhang, S. Variable Nanoparticle-Cell Adhesion Strength Regulates Cellular Uptake. *Phys. Rev. Lett.* **2010**, *105* (13), 138101. https://doi.org/10.1103/PhysRevLett.105.138101.

(561) Elias, D. R.; Poloukhtine, A.; Popik, V.; Tsourkas, A. Effect of Ligand Density, Receptor Density, and Nanoparticle Size on Cell Targeting. *Nanomedicine* **2013**, *9* (2), 194–201. https://doi.org/10.1016/j.nano.2012.05.015.

(562) Huajian, G.; Wendong, S.; B., F. L. Mechanics of Receptor-Mediated Endocytosis. *Proc. Natl. Acad. Sci.* **2005**, *102* (27), 9469–9474. https://doi.org/10.1073/pnas.0503879102.

(563) Mortensen, N. P.; Hurst, G. B.; Wang, W.; Foster, C. M.; Nallathamby, P. D.; Retterer, S. T. Dynamic Development of the Protein Corona on Silica Nanoparticles: Composition and Role in Toxicity. *Nanoscale* **2013**, *5* (14), 6372–6380. https://doi.org/10.1039/c3nr33280b.

(564) Izak-Nau, E.; Voetz, M.; Eiden, S.; Duschl, A.; Puntes, V. F. Altered Characteristics of Silica Nanoparticles in Bovine and Human Serum: The Importance of Nanomaterial Characterization Prior to Its Toxicological

Evaluation. *Part. Fibre Toxicol.* **2013**, *10* (1), 56. https://doi.org/10.1186/1743-8977-10-56.

(565) Albanese, A.; Chan, W. C. W. Effect of Gold Nanoparticle Aggregation on Cell Uptake and Toxicity. *ACS Nano* **2011**, *5* (7), 5478–5489. https://doi.org/10.1021/nn2007496.

(566) Meng, H.; Yang, S.; Li, Z.; Xia, T.; Chen, J.; Ji, Z.; Zhang, H.; Wang, X.; Lin, S.; Huang, C.; Zhou, Z. H.; Zink, J. I.; Nel, A. E. Aspect Ratio Determines the Quantity of Mesoporous Silica Nanoparticle Uptake by a Small GTPase-Dependent Macropinocytosis Mechanism. *ACS Nano* **2011**, *5* (6), 4434–4447. https://doi.org/10.1021/nn103344k.

(567) Dasgupta, S.; Auth, T.; Gompper, G. Shape and Orientation Matter for the Cellular Uptake of Nonspherical Particles. *Nano Lett.* **2014**, *14* (2), 687–693. https://doi.org/10.1021/nl403949h.

(568) Li, Z.; Sun, L.; Zhang, Y.; Dove, A. P.; O'Reilly, R. K.; Chen, G. Shape Effect of Glyco-Nanoparticles on Macrophage Cellular Uptake and Immune Response. *ACS Macro Lett.* **2016**, *5* (9), 1059–1064. https://doi.org/10.1021/acsmacrolett.6b00419.

(569) Hao, N.; Li, L.; Zhang, Q.; Huang, X.; Meng, X.; Zhang, Y.; Chen, D.; Tang, F.; Li, L. The Shape Effect of PEGylated Mesoporous Silica Nanoparticles on Cellular Uptake Pathway in Hela Cells. *Microporous Mesoporous Mater.* **2012**, *162*, 14–23. https://doi.org/10.1016/j.micromeso.2012.05.040.

(570) Herd, H.; Daum, N.; Jones, A. T.; Huwer, H.; Ghandehari, H.; Lehr, C.-M. Nanoparticle Geometry and Surface Orientation Influence Mode of Cellular Uptake. *ACS Nano* **2013**, *7* (3), 1961–1973. https://doi.org/10.1021/nn304439f.

(571) Ma, N.; Wu, F.-G.; Zhang, X.; Jiang, Y.-W.; Jia, H.-R.; Wang, H.-Y.; Li, Y.-H.; Liu, P.; Gu, N.; Chen, Z. Shape-Dependent Radiosensitization Effect of Gold Nanostructures in Cancer Radiotherapy: Comparison of Gold Nanoparticles, Nanospikes, and Nanorods. *ACS Appl. Mater. Interfaces* **2017**, *9* (15), 13037–13048. https://doi.org/10.1021/acsami.7b01112.

(572) Arnida; Malugin, A.; Ghandehari, H. Cellular Uptake and Toxicity of Gold Nanoparticles in Prostate Cancer Cells: A Comparative Study of Rods and Spheres. *J. Appl. Toxicol.* **2010**, *30* (3), 212–217. https://doi.org/10.1002/jat.1486.

(573) Shen, Z.; Ye, H.; Yi, X.; Li, Y. Membrane Wrapping Efficiency of Elastic Nanoparticles during Endocytosis: Size and Shape Matter. *ACS Nano* **2019**, *13* (1), 215–228. https://doi.org/10.1021/acsnano.8b05340.

(574) Guo, P.; Liu, D.; Subramanyam, K.; Wang, B.; Yang, J.; Huang, J.; Auguste, D. T.; Moses, M. A. Nanoparticle Elasticity Directs Tumor Uptake. *Nat. Commun.* **2018**, *9* (1), 130. https://doi.org/10.1038/s41467-017-02588-9.

(575) Palomba, R.; Palange, A. L.; Rizzuti, I. F.; Ferreira, M.; Cervadoro, A.; Barbato, M. G.; Canale, C.; Decuzzi, P. Modulating Phagocytic Cell Sequestration by Tailoring Nanoconstruct Softness. *ACS Nano* **2018**, *12* (2), 1433–1444. https://doi.org/10.1021/acsnano.7b07797.

(576) Anselmo, A. C.; Zhang, M.; Kumar, S.; Vogus, D. R.; Menegatti, S.; Helgeson, M. E.; Mitragotri, S. Elasticity of Nanoparticles Influences Their Blood Circulation, Phagocytosis, Endocytosis, and Targeting. *ACS Nano* **2015**, *9* (3), 3169–3177. https://doi.org/10.1021/acsnano.5b00147.

(577) Maxfield, F. R.; McGraw, T. E. Endocytic Recycling. *Nat. Rev. Mol. Cell Biol.* **2004**, *5* (2), 121–132. https://doi.org/10.1038/nrm1315.

(578) Jovic, M.; Sharma, M.; Rahajeng, J.; Caplan, S. The Early Endosome: A Busy Sorting Station for Proteins at the Crossroads. *Histol. Histopathol.* **2010**, *25* (1), 99–112. https://doi.org/10.14670/HH-25.99.

(579) Aoyama, M.; Yoshioka, Y.; Arai, Y.; Hirai, H.; Ishimoto, R.; Nagano, K.; Higashisaka, K.; Nagai, T.; Tsutsumi, Y. Intracellular Trafficking of Particles inside Endosomal Vesicles Is Regulated by Particle Size. *J. Control. Release* **2017**, *260*, 183–193. https://doi.org/10.1016/j.jconrel.2017.06.007.

(580) Liu, M.; Li, Q.; Liang, L.; Li, J.; Wang, K.; Li, J.; Lv, M.; Chen, N.; Song, H.; Lee, J.; Shi, J.; Wang, L.;

Lal, R.; Fan, C. Real-Time Visualization of Clustering and Intracellular Transport of Gold Nanoparticles by Correlative Imaging. *Nat. Commun.* **2017**, *8* (1), 15646. https://doi.org/10.1038/ncomms15646.

(581) Grant, B. D.; Donaldson, J. G. Pathways and Mechanisms of Endocytic Recycling. *Nat. Rev. Mol. Cell Biol.* **2009**, *10* (9), 597–608. https://doi.org/10.1038/nrm2755.

(582) Zhang, J.; Chang, D.; Yang, Y.; Zhang, X.; Tao, W.; Jiang, L.; Liang, X.; Tsai, H.; Huang, L.; Mei, L. Systematic Investigation on the Intracellular Trafficking Network of Polymeric Nanoparticles. *Nanoscale* **2017**, *9* (9), 3269–3282. https://doi.org/10.1039/C7NR00532F.

(583) Willmann, W.; Dringen, R. Monitoring of the Cytoskeleton-Dependent Intracellular Trafficking of Fluorescent Iron Oxide Nanoparticles by Nanoparticle Pulse-Chase Experiments in C6 Glioma Cells. *Neurochem. Res.* **2018**, *43* (11), 2055–2071. https://doi.org/10.1007/s11064-018-2627-3.

(584) Mindell, J. A. Lysosomal Acidification Mechanisms. *Annu. Rev. Physiol.* **2012**, *74*, 69–86. https://doi.org/10.1146/annurev-physiol-012110-142317.

(585) Dominska, M.; Dykxhoorn, D. M. Breaking down the Barriers: SiRNA Delivery and Endosome Escape. *J. Cell Sci.* **2010**, *123* (Pt 8), 1183–1189. https://doi.org/10.1242/jcs.066399.

(586) Hsu, V. W.; Bai, M.; Li, J. Getting Active: Protein Sorting in Endocytic Recycling. *Nature reviews. Molecular cell biology*. England April 2012, pp 323–328. https://doi.org/10.1038/nrm3332.

(587) Anding, A. L.; Baehrecke, E. H. Cleaning House: Selective Autophagy of Organelles. *Dev. Cell* **2017**, *41* (1), 10–22. https://doi.org/10.1016/j.devcel.2017.02.016.

(588) Klionsky, D. J. Autophagy: From Phenomenology to Molecular Understanding in Less than a Decade. *Nat. Rev. Mol. Cell Biol.* **2007**, *8* (11), 931–937. https://doi.org/10.1038/nrm2245.

(589) Mizushima, N. Autophagy: Process and Function. *Genes Dev.* **2007**, *21* (22), 2861–2873. https://doi.org/10.1101/gad.1599207.

(590) Sun, Q.; Fan, J.; Billiar, T. R.; Scott, M. J. Inflammasome and Autophagy Regulation - a Two-Way Street. *Mol. Med.* **2017**, *23*, 188–195. https://doi.org/10.2119/molmed.2017.00077.

(591) Mohammadinejad, R.; Moosavi, M. A.; Tavakol, S.; Vardar, D. Ö.; Hosseini, A.; Rahmati, M.; Dini, L.; Hussain, S.; Mandegary, A.; Klionsky, D. J. Necrotic, Apoptotic and Autophagic Cell Fates Triggered by Nanoparticles. *Autophagy* **2019**, *15* (1), 4–33. https://doi.org/10.1080/15548627.2018.1509171.

(592) Wang, J.; Yu, Y.; Lu, K.; Yang, M.; Li, Y.; Zhou, X.; Sun, Z. Silica Nanoparticles Induce Autophagy Dysfunction via Lysosomal Impairment and Inhibition of Autophagosome Degradation in Hepatocytes. *Int. J. Nanomedicine* **2017**, *12*, 809–825. https://doi.org/10.2147/IJN.S123596.

(593) Ma, X.; Wu, Y.; Jin, S.; Tian, Y.; Zhang, X.; Zhao, Y.; Yu, L.; Liang, X.-J. Gold Nanoparticles Induce Autophagosome Accumulation through Size-Dependent Nanoparticle Uptake and Lysosome Impairment. *ACS Nano* **2011**, *5* (11), 8629–8639. https://doi.org/10.1021/nn202155y.

(594) Panja, P.; Debnath, K.; Jana, N. R.; Jana, N. R. Surface Chemistry- and Intracellular Trafficking-Dependent Autophagy Induction by Iron Oxide Nanoparticles. *ACS Appl. Bio Mater.* **2020**, *3* (9), 5974–5983. https://doi.org/10.1021/acsabm.0c00640.

(595) Tang, D.; Kang, R.; Coyne, C. B.; Zeh, H. J.; Lotze, M. T. PAMPs and DAMPs: Signal 0s That Spur Autophagy and Immunity. *Immunol. Rev.* **2012**, *249* (1), 158–175. https://doi.org/10.1111/j.1600-065X.2012.01146.x.

(596) Kreyling, W. G.; Abdelmonem, A. M.; Ali, Z.; Alves, F.; Geiser, M.; Haberl, N.; Hartmann, R.; Hirn, S.; de Aberasturi, D. J.; Kantner, K.; Khadem-Saba, G.; Montenegro, J.-M.; Rejman, J.; Rojo, T.; de Larramendi, I. R.; Ufartes, R.; Wenk, A.; Parak, W. J. In Vivo Integrity of Polymer-Coated Gold Nanoparticles. *Nat. Nanotechnol.* **2015**, *10* (7), 619–623. https://doi.org/10.1038/nnano.2015.111.

(597) Fröhlich, E. Cellular Elimination of Nanoparticles. *Environ. Toxicol. Pharmacol.* **2016**, *46*, 90–94.

https://doi.org/10.1016/j.etap.2016.07.003.

(598) Martens, T. F.; Remaut, K.; Demeester, J.; De Smedt, S. C.; Braeckmans, K. Intracellular Delivery of Nanomaterials: How to Catch Endosomal Escape in the Act. *Nano Today* **2014**, *9* (3), 344–364. https://doi.org/10.1016/j.nantod.2014.04.011.

(599) Wang, F.; Wang, Y.-C.; Dou, S.; Xiong, M.-H.; Sun, T.-M.; Wang, J. Doxorubicin-Tethered Responsive Gold Nanoparticles Facilitate Intracellular Drug Delivery for Overcoming Multidrug Resistance in Cancer Cells. *ACS Nano* **2011**, *5* (5), 3679–3692. https://doi.org/10.1021/nn200007z.

(600) Sangtani, A.; Petryayeva, E.; Wu, M.; Susumu, K.; Oh, E.; Huston, A. L.; Lasarte-Aragones, G.; Medintz, I. L.; Algar, W. R.; Delehanty, J. B. Intracellularly Actuated Quantum Dot–Peptide–Doxorubicin Nanobioconjugates for Controlled Drug Delivery via the Endocytic Pathway. *Bioconjug. Chem.* **2018**, *29* (1), 136–148. https://doi.org/10.1021/acs.bioconjchem.7b00658.

(601) Vermeulen, L. M. P.; De Smedt, S. C.; Remaut, K.; Braeckmans, K. The Proton Sponge Hypothesis: Fable or Fact? *Eur. J. Pharm. Biopharm.* **2018**, *129*, 184–190. https://doi.org/10.1016/j.ejpb.2018.05.034.

(602) Chen, J.; Li, J.; Zhou, J.; Lin, Z.; Cavalieri, F.; Czuba-Wojnilowicz, E.; Hu, Y.; Glab, A.; Ju, Y.; Richardson, J. J.; Caruso, F. Metal–Phenolic Coatings as a Platform to Trigger Endosomal Escape of Nanoparticles. *ACS Nano* **2019**, *13* (10), 11653–11664. https://doi.org/10.1021/acsnano.9b05521.

(603) Horie, M.; Tabei, Y. Role of Oxidative Stress in Nanoparticles Toxicity. *Free Radic. Res.* **2020**, 1–12. https://doi.org/10.1080/10715762.2020.1859108.

(604) Yu, Z.; Li, Q.; Wang, J.; Yu, Y.; Wang, Y.; Zhou, Q.; Li, P. Reactive Oxygen Species-Related Nanoparticle Toxicity in the Biomedical Field. *Nanoscale Res. Lett.* **2020**, *15* (1), 115. https://doi.org/10.1186/s11671-020-03344-7.

(605) Yang, W.; Wang, L.; Mettenbrink, E. M.; DeAngelis, P. L.; Wilhelm, S. Nanoparticle Toxicology. *Annu. Rev. Pharmacol. Toxicol.* **2021**, *61* (1), 269–289. https://doi.org/10.1146/annurev-pharmtox-032320-110338.

(606) Kang, J. H.; Jang, W. Y.; Ko, Y. T. The Effect of Surface Charges on the Cellular Uptake of Liposomes Investigated by Live Cell Imaging. *Pharm. Res.* **2017**, *34* (4), 704–717. https://doi.org/10.1007/s11095-017-2097-3.

(607) Liu, X.; Huang, N.; Li, H.; Jin, Q.; Ji, J. Surface and Size Effects on Cell Interaction of Gold Nanoparticles with Both Phagocytic and Nonphagocytic Cells. *Langmuir* **2013**, *29* (29), 9138–9148. https://doi.org/10.1021/la401556k.

(608) Zhang, M.; Zhou, X.; Iijima, S.; Yudasaka, M. Small-Sized Carbon Nanohorns Enabling Cellular Uptake Control. *Small* **2012**, *8* (16), 2524–2531. https://doi.org/10.1002/smll.201102595.

(609) Chung, T.-H.; Wu, S.-H.; Yao, M.; Lu, C.-W.; Lin, Y.-S.; Hung, Y.; Mou, C.-Y.; Chen, Y.-C.; Huang, D.-M. The Effect of Surface Charge on the Uptake and Biological Function of Mesoporous Silica Nanoparticles in 3T3-L1 Cells and Human Mesenchymal Stem Cells. *Biomaterials* **2007**, *28* (19), 2959–2966. https://doi.org/10.1016/j.biomaterials.2007.03.006.

(610) Ma, N.; Ma, C.; Li, C.; Wang, T.; Tang, Y.; Wang, H.; Moul, X.; Chen, Z.; Hel, N. Influence of Nanoparticle Shape, Size, and Surface Functionalization on Cellular Uptake. *J. Nanosci. Nanotechnol.* **2013**, *13* (10), 6485–6498. https://doi.org/10.1166/jnn.2013.7525.

(611) Chen, J.; Hessler, J. A.; Putchakayala, K.; Panama, B. K.; Khan, D. P.; Hong, S.; Mullen, D. G.; DiMaggio, S. C.; Som, A.; Tew, G. N.; Lopatin, A. N.; Baker, J. R.; Holl, M. M. B.; Orr, B. G. Cationic Nanoparticles Induce Nanoscale Disruption in Living Cell Plasma Membranes. *J. Phys. Chem. B* **2009**, *113* (32), 11179–11185. https://doi.org/10.1021/jp9033936.

(612) El Badawy, A. M.; Silva, R. G.; Morris, B.; Scheckel, K. G.; Suidan, M. T.; Tolaymat, T. M. Surface Charge-Dependent Toxicity of Silver Nanoparticles. *Environ. Sci. Technol.* **2011**, *45* (1), 283–287.

https://doi.org/10.1021/es1034188.

(613) Fröhlich, E. The Role of Surface Charge in Cellular Uptake and Cytotoxicity of Medical Nanoparticles. *Int. J. Nanomedicine* **2012**, *7*, 5577–5591. https://doi.org/10.2147/IJN.S36111.

(614) Schaeublin, N. M.; Braydich-Stolle, L. K.; Schrand, A. M.; Miller, J. M.; Hutchison, J.; Schlager, J. J.; Hussain, S. M. Surface Charge of Gold Nanoparticles Mediates Mechanism of Toxicity. *Nanoscale* **2011**, *3* (2), 410–420. https://doi.org/10.1039/C0NR00478B.

(615) Xiao, K.; Li, Y.; Luo, J.; Lee, J. S.; Xiao, W.; Gonik, A. M.; Agarwal, R. G.; Lam, K. S. The Effect of Surface Charge on in Vivo Biodistribution of PEG-Oligocholic Acid Based Micellar Nanoparticles. *Biomaterials* **2011**, *32* (13), 3435–3446. https://doi.org/10.1016/j.biomaterials.2011.01.021.

(616) Limbach, L. K.; Li, Y.; Grass, R. N.; Brunner, T. J.; Hintermann, M. A.; Muller, M.; Gunther, D.; Stark, W. J. Oxide Nanoparticle Uptake in Human Lung Fibroblasts: Effects of Particle Size, Agglomeration, and Diffusion at Low Concentrations. *Environ. Sci. Technol.* **2005**, *39* (23), 9370–9376. https://doi.org/10.1021/es051043o.

(617) Tantra, R.; Tompkins, J.; Quincey, P. Characterisation of the De-Agglomeration Effects of Bovine Serum Albumin on Nanoparticles in Aqueous Suspension. *Colloids Surfaces B Biointerfaces* **2010**, *75* (1), 275–281. https://doi.org/10.1016/j.colsurfb.2009.08.049.

(618) Calatayud, M. P.; Sanz, B.; Raffa, V.; Riggio, C.; Ibarra, M. R.; Goya, G. F. The Effect of Surface Charge of Functionalized Fe3O4 Nanoparticles on Protein Adsorption and Cell Uptake. *Biomaterials* **2014**, *35* (24), 6389–6399. https://doi.org/10.1016/j.biomaterials.2014.04.009.

(619) Tan, Y.; Zhu, X.; Wu, D.; Song, E.; Song, Y. Compromised Autophagic Effect of Polystyrene Nanoplastics Mediated by Protein Corona Was Recovered after Lysosomal Degradation of Corona. *Environ. Sci. Technol.* **2020**, *54* (18), 11485–11493. https://doi.org/10.1021/acs.est.0c04097.

(620) Wang, F.; Yu, L.; Monopoli, M. P.; Sandin, P.; Mahon, E.; Salvati, A.; Dawson, K. A. The Biomolecular Corona Is Retained during Nanoparticle Uptake and Protects the Cells from the Damage Induced by Cationic Nanoparticles until Degraded in the Lysosomes. *Nanomedicine* **2013**, *9* (8), 1159–1168. https://doi.org/10.1016/j.nano.2013.04.010.

(621) Stepien, G.; Moros, M.; Pérez-Hernández, M.; Monge, M.; Gutiérrez, L.; Fratila, R. M.; las Heras, M. de; Menao Guillén, S.; Puente Lanzarote, J. J.; Solans, C.; Pardo, J.; de la Fuente, J. M. Effect of Surface Chemistry and Associated Protein Corona on the Long-Term Biodegradation of Iron Oxide Nanoparticles In Vivo. *ACS Appl. Mater. Interfaces* **2018**, *10* (5), 4548–4560. https://doi.org/10.1021/acsami.7b18648.

(622) Bourquin, J.; Milosevic, A.; Hauser, D.; Lehner, R.; Blank, F.; Petri-Fink, A.; Rothen-Rutishauser, B. Biodistribution, Clearance, and Long-Term Fate of Clinically Relevant Nanomaterials. *Adv. Mater.* **2018**, *30* (19), e1704307. https://doi.org/10.1002/adma.201704307.

(623) Nag, O. K.; Delehanty, J. B. Active Cellular and Subcellular Targeting of Nanoparticles for Drug Delivery. *Pharmaceutics* **2019**, *11* (10), 543. https://doi.org/10.3390/pharmaceutics11100543.

(624) Sakhrani, N. M.; Padh, H. Organelle Targeting: Third Level of Drug Targeting. *Drug Des. Devel. Ther.* **2013**, *7*, 585–599. https://doi.org/10.2147/DDDT.S45614.

(625) Ma, X.; Gong, N.; Zhong, L.; Sun, J.; Liang, X.-J. Future of Nanotherapeutics: Targeting the Cellular Sub-Organelles. *Biomaterials* **2016**, *97*, 10–21. https://doi.org/10.1016/j.biomaterials.2016.04.026.

(626) Wang, G.; Norton, A. S.; Pokharel, D.; Song, Y.; Hill, R. A. KDEL Peptide Gold Nanoconstructs: Promising Nanoplatforms for Drug Delivery. *Nanomedicine* **2013**, *9* (3), 366–374. https://doi.org/10.1016/j.nano.2012.09.002.

(627) Boyoglu, C.; He, Q.; Willing, G.; Boyoglu-Barnum, S.; Dennis, V. A.; Pillai, S.; Singh, S. R. Microscopic Studies of Various Sizes of Gold Nanoparticles and Their Cellular Localizations. *ISRN Nanotechnol.* **2013**, *2013*, 123838. https://doi.org/10.1155/2013/123838.

(628) Larsen, J. D.; Ross, N. L.; Sullivan, M. O. Requirements for the Nuclear Entry of Polyplexes and Nanoparticles during Mitosis. *J. Gene Med.* **2012**, *14* (9–10), 580–589. https://doi.org/10.1002/jgm.2669.

(629) Maimon, T.; Elad, N.; Dahan, I.; Medalia, O. The Human Nuclear Pore Complex as Revealed by Cryo-Electron Tomography. *Structure* **2012**, *20* (6), 998–1006. https://doi.org/10.1016/j.str.2012.03.025.

(630) Huo, S.; Jin, S.; Ma, X.; Xue, X.; Yang, K.; Kumar, A.; Wang, P. C.; Zhang, J.; Hu, Z.; Liang, X.-J. Ultrasmall Gold Nanoparticles as Carriers for Nucleus-Based Gene Therapy Due to Size-Dependent Nuclear Entry. *ACS Nano* **2014**, *8* (6), 5852–5862. https://doi.org/10.1021/nn5008572.

(631) Yang, C.; Uertz, J.; Yohan, D.; Chithrani, B. D. Peptide Modified Gold Nanoparticles for Improved Cellular Uptake, Nuclear Transport, and Intracellular Retention. *Nanoscale* **2014**, *6* (20), 12026–12033. https://doi.org/10.1039/c4nr02535k.

(632) Pan, L.; He, Q.; Liu, J.; Chen, Y.; Ma, M.; Zhang, L.; Shi, J. Nuclear-Targeted Drug Delivery of TAT Peptide-Conjugated Monodisperse Mesoporous Silica Nanoparticles. *J. Am. Chem. Soc.* **2012**, *134* (13), 5722–5725. https://doi.org/10.1021/ja211035w.

(633) Torchilin, V. P. Tat Peptide-Mediated Intracellular Delivery of Pharmaceutical Nanocarriers. *Adv. Drug Deliv. Rev.* **2008**, *60* (4–5), 548–558. https://doi.org/10.1016/j.addr.2007.10.008.

(634) Han, L.; Tang, C.; Yin, C. PH-Responsive Core-Shell Structured Nanoparticles for Triple-Stage Targeted Delivery of Doxorubicin to Tumors. *ACS Appl. Mater. Interfaces* **2016**, *8* (36), 23498–23508. https://doi.org/10.1021/acsami.6b07173.

(635) Fan, Y.; Li, C.; Li, F.; Chen, D. PH-Activated Size Reduction of Large Compound Nanoparticles for in Vivo Nucleus-Targeted Drug Delivery. *Biomaterials* **2016**, *85*, 30–39. https://doi.org/10.1016/j.biomaterials.2016.01.057.

(636) Li, H.; Yan, W.; Suo, X.; Peng, H.; Yang, X.; Li, Z.; Zhang, J.; Liu, D. Nucleus-Targeted Nano Delivery System Eradicates Cancer Stem Cells by Combined Thermotherapy and Hypoxia-Activated Chemotherapy. *Biomaterials* **2019**, *200*, 1–14. https://doi.org/10.1016/j.biomaterials.2019.01.048.

(637) Li, N.; Sun, Q.; Yu, Z.; Gao, X.; Pan, W.; Wan, X.; Tang, B. Nuclear-Targeted Photothermal Therapy Prevents Cancer Recurrence with Near-Infrared Triggered Copper Sulfide Nanoparticles. *ACS Nano* **2018**, *12* (6), 5197–5206. https://doi.org/10.1021/acsnano.7b06870.

(638) Pan, W.; Gong, S.; Wang, J.; Yu, L.; Chen, Y.; Li, N.; Tang, B. A Nuclear-Targeted Titanium Dioxide Radiosensitizer for Cell Cycle Regulation and Enhanced Radiotherapy. *Chem. Commun.* **2019**, *55* (56), 8182–8185. https://doi.org/10.1039/C9CC01651A.

(639) Peng, H.; Tang, J.; Zheng, R.; Guo, G.; Dong, A.; Wang, Y.; Yang, W. Nuclear-Targeted Multifunctional Magnetic Nanoparticles for Photothermal Therapy. *Adv. Healthc. Mater.* **2017**, *6* (7).

(640) Oh, E.; Delehanty, J. B.; Sapsford, K. E.; Susumu, K.; Goswami, R.; Blanco-Canosa, J. B.; Dawson, P. E.; Granek, J.; Shoff, M.; Zhang, Q.; Goering, P. L.; Huston, A.; Medintz, I. L. Cellular Uptake and Fate of PEGylated Gold Nanoparticles Is Dependent on Both Cell-Penetration Peptides and Particle Size. *ACS Nano* **2011**, *5* (8), 6434–6448. https://doi.org/10.1021/nn201624c.

(641) Dalal, C.; Jana, N. R. Multivalency Effect of TAT-Peptide-Functionalized Nanoparticle in Cellular Endocytosis and Subcellular Trafficking. *J. Phys. Chem. B* **2017**, *121* (14), 2942–2951. https://doi.org/10.1021/acs.jpcb.6b12182.

(642) Tang, P. S.; Sathiamoorthy, S.; Lustig, L. C.; Ponzielli, R.; Inamoto, I.; Penn, L. Z.; Shin, J. A.; Chan, W. C. W. The Role of Ligand Density and Size in Mediating Quantum Dot Nuclear Transport. *Small* **2014**, *10* (20), 4182–4192. https://doi.org/10.1002/smll.201401056.

(643) Misra, R.; Sahoo, S. K. Intracellular Trafficking of Nuclear Localization Signal Conjugated Nanoparticles for Cancer Therapy. *Eur. J. Pharm. Sci.* **2010**, *39* (1), 152–163. https://doi.org/10.1016/j.ejps.2009.11.010.

(644) Dong, L.; Gopalan, V.; Holland, O.; Neuzil, J. Mitocans Revisited: Mitochondrial Targeting as Efficient

Anti-Cancer Therapy. *Int. J. Mol. Sci.* **2020**, *21* (21), 7941. https://doi.org/10.3390/ijms21217941.

(645) DeBerardinis, R. J.; Chandel, N. S. We Need to Talk about the Warburg Effect. *Nat. Metab.* **2020**, *2* (2), 127–129. https://doi.org/10.1038/s42255-020-0172-2.

(646) Choudhary, D.; Goykar, H.; Karanwad, T.; Kannaujia, S.; Gadekar, V.; Misra, M. An Understanding of Mitochondria and Its Role in Targeting Nanocarriers for Diagnosis and Treatment of Cancer. *Asian J. Pharm. Sci.* **2020**.

(647) Weinberg, S. E.; Chandel, N. S. Targeting Mitochondria Metabolism for Cancer Therapy. *Nat. Chem. Biol.* **2015**, *11* (1), 9–15. https://doi.org/10.1038/nchembio.1712.

(648) Marrache, S.; Dhar, S. The Energy Blocker inside the Power House: Mitochondria Targeted Delivery of 3-Bromopyruvate. *Chem. Sci.* **2015**, *6* (3), 1832–1845. https://doi.org/10.1039/C4SC01963F.

(649) Dilip, A.; Cheng, G.; Joseph, J.; Kunnimalaiyaan, S.; Kalyanaraman, B.; Kunnimalaiyaan, M.; Gamblin, T. C. Mitochondria-Targeted Antioxidant and Glycolysis Inhibition: Synergistic Therapy in Hepatocellular Carcinoma. *Anticancer. Drugs* **2013**, *24* (9), 881–888. https://doi.org/10.1097/CAD.0b013e32836442c6.

(650) Jeena, M. T.; Kim, S.; Jin, S.; Ryu, J.-H. Recent Progress in Mitochondria-Targeted Drug and Drug-Free Agents for Cancer Therapy. *Cancers (Basel).* **2019**, *12* (1), 4. https://doi.org/10.3390/cancers12010004.

(651) Robertson, J. D.; Gogvadze, V.; Zhivotovsky, B.; Orrenius, S. Distinct Pathways for Stimulation of Cytochrome c Release by Etoposide. *J. Biol. Chem.* **2000**, *275* (42), 32438–32443. https://doi.org/10.1074/jbc.C000518200.

(652) Kidd, J. F.; Pilkington, M. F.; Schell, M. J.; Fogarty, K. E.; Skepper, J. N.; Taylor, C. W.; Thorn, P. Paclitaxel Affects Cytosolic Calcium Signals by Opening the Mitochondrial Permeability Transition Pore. *J. Biol. Chem.* **2002**, *277* (8), 6504–6510. https://doi.org/10.1074/jbc.M106802200.

(653) Costantini, P.; Jacotot, E.; Decaudin, D.; Kroemer, G. Mitochondrion as a Novel Target of Anticancer Chemotherapy. *J. Natl. Cancer Inst.* **2000**, *92* (13), 1042–1053. https://doi.org/10.1093/jnci/92.13.1042.

(654) Zorova, L. D.; Popkov, V. A.; Plotnikov, E. Y.; Silachev, D. N.; Pevzner, I. B.; Jankauskas, S. S.; Babenko, V. A.; Zorov, S. D.; Balakireva, A. V; Juhaszova, M.; Sollott, S. J.; Zorov, D. B. Mitochondrial Membrane Potential. *Anal. Biochem.* **2018**, *552*, 50–59. https://doi.org/10.1016/j.ab.2017.07.009.

(655) Rovini, A.; Heslop, K.; Hunt, E. G.; Morris, M. E.; Fang, D.; Gooz, M.; Gerencser, A. A.; Maldonado, E. N. Quantitative Analysis of Mitochondrial Membrane Potential Heterogeneity in Unsynchronized and Synchronized Cancer Cells. *FASEB J.* **2021**, *35* (1), e21148. https://doi.org/10.1096/fj.202001693R.

(656) Zhang, B.; Wang, D.; Guo, F.; Xuan, C. Mitochondrial Membrane Potential and Reactive Oxygen Species in Cancer Stem Cells. *Fam. Cancer* **2015**, *14* (1), 19–23. https://doi.org/10.1007/s10689-014-9757-9.

(657) Assanhou, A. G.; Li, W.; Zhang, L.; Xue, L.; Kong, L.; Sun, H.; Mo, R.; Zhang, C. Reversal of Multidrug Resistance by Co-Delivery of Paclitaxel and Lonidamine Using a TPGS and Hyaluronic Acid Dual-Functionalized Liposome for Cancer Treatment. *Biomaterials* **2015**, *73*, 284–295. https://doi.org/10.1016/j.biomaterials.2015.09.022.

(658) Battogtokh, G.; Cho, Y.-Y.; Lee, J. Y.; Lee, H. S.; Kang, H. C. Mitochondrial-Targeting Anticancer Agent Conjugates and Nanocarrier Systems for Cancer Treatment. *Front. Pharmacol.* **2018**, *9*, 922. https://doi.org/10.3389/fphar.2018.00922.

(659) Liu, D.; Jin, F.; Shu, G.; Xu, X.; Qi, J.; Kang, X.; Yu, H.; Lu, K.; Jiang, S.; Han, F.; You, J.; Du, Y.; Ji, J. Enhanced Efficiency of Mitochondria-Targeted Peptide SS-31 for Acute Kidney Injury by PH-Responsive and AKI-Kidney Targeted Nanopolyplexes. *Biomaterials* **2019**, *211*, 57–67. https://doi.org/10.1016/j.biomaterials.2019.04.034.

(660) Ruttala, H. B.; Ramasamy, T.; Ruttala, R. R. T.; Tran, T. H.; Jeong, J.-H.; Choi, H.-G.; Ku, S. K.; Yong, C. S.; Kim, J. O. Mitochondria-Targeting Multi-Metallic ZnCuO Nanoparticles and IR780 for Efficient Photodynamic and Photothermal Cancer Treatments. *J. Mater. Sci. Technol.* **2021**, *86*, 139–150.

https://doi.org/10.1016/j.jmst.2021.01.035.

(661) Chakraborty, A.; Jana, N. R. Design and Synthesis of Triphenylphosphonium Functionalized Nanoparticle Probe for Mitochondria Targeting and Imaging. *J. Phys. Chem. C* **2015**, *119* (5), 2888–2895. https://doi.org/10.1021/jp511870e.

(662) Li, W.-Q.; Wang, Z.; Hao, S.; He, H.; Wan, Y.; Zhu, C.; Sun, L.-P.; Cheng, G.; Zheng, S.-Y. Mitochondria-Targeting Polydopamine Nanoparticles To Deliver Doxorubicin for Overcoming Drug Resistance. *ACS Appl. Mater. Interfaces* **2017**, *9* (20), 16793–16802. https://doi.org/10.1021/acsami.7b01540.

(663) Qu, Q.; Ma, X.; Zhao, Y. Targeted Delivery of Doxorubicin to Mitochondria Using Mesoporous Silica Nanoparticle Nanocarriers. *Nanoscale* **2015**, *7* (40), 16677–16686. https://doi.org/10.1039/C5NR05139H.

(664) Henninger, C.; Fritz, G. Statins in Anthracycline-Induced Cardiotoxicity: Rac and Rho, and the Heartbreakers. *Cell Death Dis.* **2018**, *8* (1), e2564–e2564. https://doi.org/10.1038/cddis.2016.418.

(665) Christidi, E.; Brunham, L. R. Regulated Cell Death Pathways in Doxorubicin-Induced Cardiotoxicity. *Cell Death Dis.* **2021**, *12* (4), 339. https://doi.org/10.1038/s41419-021-03614-x.

(666) Rawat, P. S.; Jaiswal, A.; Khurana, A.; Bhatti, J. S.; Navik, U. Doxorubicin-Induced Cardiotoxicity: An Update on the Molecular Mechanism and Novel Therapeutic Strategies for Effective Management. *Biomed. Pharmacother.* **2021**, *139*, 111708. https://doi.org/10.1016/j.biopha.2021.111708.

(667) Makwana, V.; Karanjia, J.; Haselhorst, T.; Anoopkumar-Dukie, S.; Rudrawar, S. Liposomal Doxorubicin as Targeted Delivery Platform: Current Trends in Surface Functionalization. *Int. J. Pharm.* **2021**, *593*, 120117. https://doi.org/10.1016/j.ijpharm.2020.120117.

(668) Liou, G.-Y.; Storz, P. Reactive Oxygen Species in Cancer. *Free Radic. Res.* **2010**, *44* (5), 479–496. https://doi.org/10.3109/10715761003667554.

(669) Reczek, C. R.; Chandel, N. S. The Two Faces of Reactive Oxygen Species in Cancer. *Annu. Rev. Cancer Biol.* **2017**, *1* (1), 79–98. https://doi.org/10.1146/annurev-cancerbio-041916-065808.

(670) Miki, H.; Funato, Y. Regulation of Intracellular Signalling through Cysteine Oxidation by Reactive Oxygen Species. *J. Biochem.* **2012**, *151* (3), 255–261. https://doi.org/10.1093/jb/mvs006.

(671) Perillo, B.; Di Donato, M.; Pezone, A.; Di Zazzo, E.; Giovannelli, P.; Galasso, G.; Castoria, G.; Migliaccio, A. ROS in Cancer Therapy: The Bright Side of the Moon. *Exp. Mol. Med.* **2020**, *52* (2), 192–203. https://doi.org/10.1038/s12276-020-0384-2.

(672) Sabharwal, S. S.; Schumacker, P. T. Mitochondrial ROS in Cancer: Initiators, Amplifiers or an Achilles' Heel? *Nat. Rev. Cancer* **2014**, *14* (11), 709–721. https://doi.org/10.1038/nrc3803.

(673) Trachootham, D.; Alexandre, J.; Huang, P. Targeting Cancer Cells by ROS-Mediated Mechanisms: A Radical Therapeutic Approach? *Nat. Rev. Drug Discov.* **2009**, *8* (7), 579–591. https://doi.org/10.1038/nrd2803.

(674) Kumar, B.; Koul, S.; Khandrika, L.; Meacham, R. B.; Koul, H. K. Oxidative Stress Is Inherent in Prostate Cancer Cells and Is Required for Aggressive Phenotype. *Cancer Res.* **2008**, *68* (6), 1777–1785. https://doi.org/10.1158/0008-5472.CAN-07-5259.

(675) Safford, S. E.; Oberley, T. D.; Urano, M.; St Clair, D. K. Suppression of Fibrosarcoma Metastasis by Elevated Expression of Manganese Superoxide Dismutase. *Cancer Res.* **1994**, *54* (16), 4261–4265.

(676) Toyokuni, S.; Okamoto, K.; Yodoi, J.; Hiai, H. Persistent Oxidative Stress in Cancer. *FEBS Lett.* **1995**, *358* (1), 1–3. https://doi.org/10.1016/0014-5793(94)01368-b.

(677) Kawanishi, S.; Hiraku, Y.; Pinlaor, S.; Ma, N. Oxidative and Nitrative DNA Damage in Animals and Patients with Inflammatory Diseases in Relation to Inflammation-Related Carcinogenesis. *Biol. Chem.* **2006**, *387* (4), 365–372. https://doi.org/10.1515/BC.2006.049.

(678) Martínez-Sánchez, G.; Giuliani, A. Cellular Redox Status Regulates Hypoxia Inducible Factor-1 Activity. Role in Tumour Development. *J. Exp. Clin. Cancer Res.* **2007**, *26* (1), 39–50.

(679) Chen, E. I.; Hewel, J.; Krueger, J. S.; Tiraby, C.; Weber, M. R.; Kralli, A.; Becker, K.; Yates, J. R. 3rd; Felding-Habermann, B. Adaptation of Energy Metabolism in Breast Cancer Brain Metastases. *Cancer Res.* **2007**, *67* (4), 1472–1486. https://doi.org/10.1158/0008-5472.CAN-06-3137.

(680) Gorrini, C.; Harris, I. S.; Mak, T. W. Modulation of Oxidative Stress as an Anticancer Strategy. *Nat. Rev. Drug Discov.* **2013**, *12* (12), 931–947. https://doi.org/10.1038/nrd4002.

(681) Yun, J.; Mullarky, E.; Lu, C.; Bosch, K. N.; Kavalier, A.; Rivera, K.; Roper, J.; Chio, I. I. C.; Giannopoulou, E. G.; Rago, C.; Muley, A.; Asara, J. M.; Paik, J.; Elemento, O.; Chen, Z.; Pappin, D. J.; Dow, L. E.; Papadopoulos, N.; Gross, S. S.; Cantley, L. C. Vitamin C Selectively Kills KRAS and BRAF Mutant Colorectal Cancer Cells by Targeting GAPDH. *Science (80-.).* **2015**, *350* (6266), 1391–1396. https://doi.org/10.1126/science.aaa5004.

(682) Zhang, D.; Zhou, T.; He, F.; Rong, Y.; Lee, S. H.; Wu, S.; Zuo, L. Reactive Oxygen Species Formation and Bystander Effects in Gradient Irradiation on Human Breast Cancer Cells. *Oncotarget* **2016**, *7* (27), 41622–41636. https://doi.org/10.18632/oncotarget.9517.

(683) Wang, H.; Jiang, H.; Van De Gucht, M.; De Ridder, M. Hypoxic Radioresistance: Can ROS Be the Key to Overcome It? *Cancers*. 2019.

(684) Gilles, M.; Brun, E.; Sicard-Roselli, C. Quantification of Hydroxyl Radicals and Solvated Electrons Produced by Irradiated Gold Nanoparticles Suggests a Crucial Role of Interfacial Water. *J. Colloid Interface Sci.* **2018**, *525*, 31–38. https://doi.org/10.1016/j.jcis.2018.04.017.

(685) Dixon, S. J.; Lemberg, K. M.; Lamprecht, M. R.; Skouta, R.; Zaitsev, E. M.; Gleason, C. E.; Patel, D. N.; Bauer, A. J.; Cantley, A. M.; Yang, W. S.; Morrison, B.; Stockwell, B. R. Ferroptosis: An Iron-Dependent Form of Nonapoptotic Cell Death. *Cell* **2012**, *149* (5), 1060–1072. https://doi.org/10.1016/j.cell.2012.03.042.

(686) Angelé-Martínez, C.; Nguyen, K. V. T.; Ameer, F. S.; Anker, J. N.; Brumaghim, J. L. Reactive Oxygen Species Generation by Copper(II) Oxide Nanoparticles Determined by DNA Damage Assays and EPR Spectroscopy. *Nanotoxicology* **2017**, *11* (2), 278–288. https://doi.org/10.1080/17435390.2017.1293750.

(687) Kim, S.-Y.; Kim, S.-J.; Kim, B.-J.; Rah, S.-Y.; Chung, S. M.; Im, M.-J.; Kim, U.-H. Doxorubicin-Induced Reactive Oxygen Species Generation and Intracellular Ca2+ Increase Are Reciprocally Modulated in Rat Cardiomyocytes. *Exp. Mol. Med.* **2006**, *38* (5), 535–545. https://doi.org/10.1038/emm.2006.63.

(688) Cheng, N. N.; Starkewolf, Z.; Davidson, R. A.; Sharmah, A.; Lee, C.; Lien, J.; Guo, T. Chemical Enhancement by Nanomaterials under X-Ray Irradiation. *J. Am. Chem. Soc.* **2012**, *134* (4), 1950–1953. https://doi.org/10.1021/ja210239k.

(689) Misawa, M.; Takahashi, J. Generation of Reactive Oxygen Species Induced by Gold Nanoparticles under X-Ray and UV Irradiations. *Nanomedicine* **2011**, *7* (5), 604–614. https://doi.org/10.1016/j.nano.2011.01.014.

(690) Butterworth, K. T.; McMahon, S. J.; Currell, F. J.; Prise, K. M. Physical Basis and Biological Mechanisms of Gold Nanoparticle Radiosensitization. *Nanoscale* **2012**, *4* (16), 4830–4838. https://doi.org/10.1039/c2nr31227a.

(691) Xu, C.; Qu, X. Cerium Oxide Nanoparticle: A Remarkably Versatile Rare Earth Nanomaterial for Biological Applications. *NPG Asia Mater.* **2014**, *6* (3), e90–e90. https://doi.org/10.1038/am.2013.88.

(692) Liu, L.; Corma, A. Metal Catalysts for Heterogeneous Catalysis: From Single Atoms to Nanoclusters and Nanoparticles. *Chem. Rev.* **2018**, *118* (10), 4981–5079. https://doi.org/10.1021/acs.chemrev.7b00776.

(693) Boronat, M.; Leyva-Pérez, A.; Corma, A. Theoretical and Experimental Insights into the Origin of the Catalytic Activity of Subnanometric Gold Clusters: Attempts to Predict Reactivity with Clusters and Nanoparticles of Gold. *Acc. Chem. Res.* **2014**, *47* (3), 834–844. https://doi.org/10.1021/ar400068w.

(694) Zobel, M. Observing Structural Reorientations at Solvent{--}nanoparticle Interfaces by X-Ray Diffraction {--} Putting Water in the Spotlight. *Acta Crystallogr. Sect. A* **2016**, *72* (6), 621–631. https://doi.org/10.1107/S2053273316013516.

(695) Zobel, M.; Neder, R. B.; Kimber, S. A. J. Universal Solvent Restructuring Induced by Colloidal Nanoparticles. *Science (80-.).* **2015**, *347* (6219), 292 LP – 294. https://doi.org/10.1126/science.1261412.

(696) Liu, R. Adsorption and Dissociation of H2O on Au(111) Surface: A DFT Study. *Comput. Theor. Chem.* **2013**, *1019*, 141–145. https://doi.org/10.1016/j.comptc.2013.07.009.

(697) Guerreiro, A.; Chatterton, N.; Crabb, E. M.; Golding, J. P. A Comparison of the Radiosensitisation Ability of 22 Different Element Metal Oxide Nanoparticles Using Clinical Megavoltage X-Rays. *Cancer Nanotechnol.* **2019**, *10* (1), 10. https://doi.org/10.1186/s12645-019-0057-9.

(698) Fu, J.; Li, T.; Yang, Y.; Jiang, L.; Wang, W.; Fu, L.; Zhu, Y.; Hao, Y. Activatable Nanomedicine for Overcoming Hypoxia-Induced Resistance to Chemotherapy and Inhibiting Tumor Growth by Inducing Collaborative Apoptosis and Ferroptosis in Solid Tumors. *Biomaterials* **2021**, *268*, 120537. https://doi.org/10.1016/j.biomaterials.2020.120537.

(699) Weinberg, F.; Ramnath, N.; Nagrath, D. Reactive Oxygen Species in the Tumor Microenvironment: An Overview. *Cancers (Basel).* **2019**, *11* (8).

(700) Liang, H.; Wu, Y.; Ou, X.-Y.; Li, J.-Y.; Li, J. Au@Pt Nanoparticles as Catalase Mimics to Attenuate Tumor Hypoxia and Enhance Immune Cell-Mediated Cytotoxicity. *Nanotechnology* **2017**, *28* (46), 465702. https://doi.org/10.1088/1361-6528/aa8d9c.

(701) Ranji-Burachaloo, H.; Gurr, P. A.; Dunstan, D. E.; Qiao, G. G. Cancer Treatment through Nanoparticle-Facilitated Fenton Reaction. *ACS Nano* **2018**, *12* (12), 11819–11837. https://doi.org/10.1021/acsnano.8b07635.

(702) You, C.; Gao, Z.; Wu, H.; Sun, K.; Ning, L.; Lin, F.; Sun, B.; Wang, F. Reactive Oxygen Species Mediated Theranostics Using a Fenton Reaction Activable Lipo-Polymersome. *J. Mater. Chem. B* **2019**, *7* (2), 314–323. https://doi.org/10.1039/C8TB02947D.

(703) Nosaka, Y.; Nosaka, A. Y. Generation and Detection of Reactive Oxygen Species in Photocatalysis. *Chem. Rev.* **2017**, *117* (17), 11302–11336. https://doi.org/10.1021/acs.chemrev.7b00161.

(704) Li, J.; Liu, W.; Wu, X.; Gao, X. Mechanism of PH-Switchable Peroxidase and Catalase-like Activities of Gold, Silver, Platinum and Palladium. *Biomaterials* **2015**, *48*, 37–44. https://doi.org/10.1016/j.biomaterials.2015.01.012.

(705) Tang, Z.; Zhao, P.; Wang, H.; Liu, Y.; Bu, W. Biomedicine Meets Fenton Chemistry. *Chem. Rev.* **2021**, *121* (4), 1981–2019. https://doi.org/10.1021/acs.chemrev.0c00977.

(706) Yi, Q.; Ji, J.; Shen, B.; Dong, C.; Liu, J.; Zhang, J.; Xing, M. Singlet Oxygen Triggered by Superoxide Radicals in a Molybdenum Cocatalytic Fenton Reaction with Enhanced REDOX Activity in the Environment. *Environ. Sci. Technol.* **2019**, *53* (16), 9725–9733. https://doi.org/10.1021/acs.est.9b01676.

(707) Yang, Z.; Qian, J.; Yu, A.; Pan, B. Singlet Oxygen Mediated Iron-Based Fenton-like Catalysis under Nanoconfinement. *Proc. Natl. Acad. Sci.* **2019**, *116* (14), 6659–6664. https://doi.org/10.1073/PNAS.1819382116.

(708) Bokare, A. D.; Choi, W. Review of Iron-Free Fenton-like Systems for Activating H2O2 in Advanced Oxidation Processes. *J. Hazard. Mater.* **2014**, *275*, 121–135. https://doi.org/10.1016/j.jhazmat.2014.04.054.

(709) Chudal, L.; Pandey, N. K.; Phan, J.; Johnson, O.; Lin, L.; Yu, H.; Shu, Y.; Huang, Z.; Xing, M.; Liu, J. P.; Chen, M. L.; Chen, W. Copper-Cysteamine Nanoparticles as a Heterogeneous Fenton-Like Catalyst for Highly Selective Cancer Treatment. *ACS Appl. Bio Mater.* **2020**, *3* (3), 1804–1814. https://doi.org/10.1021/acsabm.0c00098.

(710) Chen, W.; Chen, J.; Feng, Y.-B.; Hong, L.; Chen, Q.-Y.; Wu, L.-F.; Lin, X.-H.; Xia, X.-H. Peroxidase-like

Activity of Water-Soluble Cupric Oxide Nanoparticles and Its Analytical Application for Detection of Hydrogen Peroxide and Glucose. *Analyst* **2012**, *137* (7), 1706–1712. https://doi.org/10.1039/c2an35072f.

(711) Gao, L.; Zhuang, J.; Nie, L.; Zhang, J.; Zhang, Y.; Gu, N.; Wang, T.; Feng, J.; Yang, D.; Perrett, S.; Yan, X. Intrinsic Peroxidase-like Activity of Ferromagnetic Nanoparticles. *Nat. Nanotechnol.* **2007**, *2* (9), 577–583. https://doi.org/10.1038/nnano.2007.260.

(712) Yoshihisa, Y.; Zhao, Q.-L.; Hassan, M. A.; Wei, Z.-L.; Furuichi, M.; Miyamoto, Y.; Kondo, T.; Shimizu, T. SOD/Catalase Mimetic Platinum Nanoparticles Inhibit Heat-Induced Apoptosis in Human Lymphoma U937 and HH Cells. *Free Radic. Res.* **2011**, *45* (3), 326–335. https://doi.org/10.3109/10715762.2010.532494.

(713) Yang, N.; Xiao, W.; Song, X.; Wang, W.; Dong, X. Recent Advances in Tumor Microenvironment Hydrogen Peroxide-Responsive Materials for Cancer Photodynamic Therapy. *Nano-Micro Lett.* **2020**, *12* (1), 15. https://doi.org/10.1007/s40820-019-0347-0.

(714) Doskey, C. M.; Buranasudja, V.; Wagner, B. A.; Wilkes, J. G.; Du, J.; Cullen, J. J.; Buettner, G. R. Tumor Cells Have Decreased Ability to Metabolize H2O2: Implications for Pharmacological Ascorbate in Cancer Therapy. *Redox Biol.* **2016**, *10*, 274–284. https://doi.org/10.1016/j.redox.2016.10.010.

(715) Forman, H. J.; Maiorino, M.; Ursini, F. Signaling Functions of Reactive Oxygen Species. *Biochemistry* **2010**, *49* (5), 835–842. https://doi.org/10.1021/bi9020378.

(716) Park, W. H. Hydrogen Peroxide Inhibits the Growth of Lung Cancer Cells via the Induction of Cell Death and G1-phase Arrest. *Oncol. Rep.* **2018**, *40* (3), 1787–1794. https://doi.org/10.3892/or.2018.6535.

(717) Sen, S.; Kawahara, B.; Chaudhuri, G. Maintenance of Higher H2O2 Levels, and Its Mechanism of Action to Induce Growth in Breast Cancer Cells: Important Roles of Bioactive Catalase and PP2A. *Free Radic. Biol. Med.* **2012**, *53* (8), 1541–1551. https://doi.org/10.1016/j.freeradbiomed.2012.06.030.

(718) Lennicke, C.; Rahn, J.; Lichtenfels, R.; Wessjohann, L. A.; Seliger, B. Hydrogen Peroxide - Production, Fate and Role in Redox Signaling of Tumor Cells. *Cell Commun. Signal.* **2015**, *13*, 39. https://doi.org/10.1186/s12964-015-0118-6.

(719) Yu, L.; Chen, Y.; Chen, H. H2O2-Responsive Theranostic Nanomedicine. *Chinese Chem. Lett.* **2017**, *28* (9), 1841–1850. https://doi.org/10.1016/j.cclet.2017.05.023.

(720) Khalil, T. T.; Bazzi, R.; Roux, S.; Fromm, M. The Contribution of Hydrogen Peroxide to the Radiosensitizing Effect of Gold Nanoparticles. *Colloids Surfaces B Biointerfaces* **2019**, *175*, 606–613. https://doi.org/10.1016/j.colsurfb.2018.12.041.

(721) Manke, A.; Wang, L.; Rojanasakul, Y. Mechanisms of Nanoparticle-Induced Oxidative Stress and Toxicity. *BioMed Research International*. 2013.

(722) Chen, Z.; Yin, J.-J.; Zhou, Y.-T.; Zhang, Y.; Song, L.; Song, M.; Hu, S.; Gu, N. Dual Enzyme-like Activities of Iron Oxide Nanoparticles and Their Implication for Diminishing Cytotoxicity. *ACS Nano* **2012**, *6* (5), 4001–4012. https://doi.org/10.1021/nn300291r.

(723) Chen, Q.; Feng, L.; Liu, J.; Zhu, W.; Dong, Z.; Wu, Y.; Liu, Z. Intelligent Albumin–MnO2 Nanoparticles as PH-/H2O2-Responsive Dissociable Nanocarriers to Modulate Tumor Hypoxia for Effective Combination Therapy. *Adv. Mater.* **2016**, *28* (33), 7129–7136. https://doi.org/10.1002/adma.201601902.

(724) Lin, L.-S.; Huang, T.; Song, J.; Ou, X.-Y.; Wang, Z.; Deng, H.; Tian, R.; Liu, Y.; Wang, J.-F.; Liu, Y.; Yu, G.; Zhou, Z.; Wang, S.; Niu, G.; Yang, H.-H.; Chen, X. Synthesis of Copper Peroxide Nanodots for H2O2 Self-Supplying Chemodynamic Therapy. *J. Am. Chem. Soc.* **2019**, *141* (25), 9937–9945. https://doi.org/10.1021/jacs.9b03457.

(725) Huang, X.; Deng, G.; Han, Y.; Yang, G.; Zou, R.; Zhang, Z.; Sun, S.; Hu, J. Right Cu2−xS@MnS Core–Shell Nanoparticles as a Photo/H2O2-Responsive Platform for Effective Cancer Theranostics. *Adv. Sci.* **2019**, *6* (20), 1901461. https://doi.org/10.1002/advs.201901461.

(726) Gao, S.; Jin, Y.; Ge, K.; Li, Z.; Liu, H.; Dai, X.; Zhang, Y.; Chen, S.; Liang, X.; Zhang, J. Self-Supply of O2 and H2O2 by a Nanocatalytic Medicine to Enhance Combined Chemo/Chemodynamic Therapy. *Adv. Sci.* **2019**, *6* (24), 1902137. https://doi.org/10.1002/advs.201902137.

(727) Lin, T.; Zhao, X.; Zhao, S.; Yu, H.; Cao, W.; Chen, W.; Wei, H.; Guo, H. O(2)-Generating MnO(2) Nanoparticles for Enhanced Photodynamic Therapy of Bladder Cancer by Ameliorating Hypoxia. *Theranostics* **2018**, *8* (4), 990–1004. https://doi.org/10.7150/thno.22465.

(728) Kankala, R. K.; Liu, C.-G.; Yang, D.-Y.; Wang, S.-B.; Chen, A.-Z. Ultrasmall Platinum Nanoparticles Enable Deep Tumor Penetration and Synergistic Therapeutic Abilities through Free Radical Species-Assisted Catalysis to Combat Cancer Multidrug Resistance. *Chem. Eng. J.* **2020**, *383*, 123138. https://doi.org/10.1016/j.cej.2019.123138.

(729) Chen, Y.; Zhong, H.; Wang, J.; Wan, X.; Li, Y.; Pan, W.; Li, N.; Tang, B. Catalase-like Metal–Organic Framework Nanoparticles to Enhance Radiotherapy in Hypoxic Cancer and Prevent Cancer Recurrence. *Chem. Sci.* **2019**, *10* (22), 5773–5778. https://doi.org/10.1039/C9SC00747D.

(730) Pan, W.; Cui, B.; Gao, P.; Ge, Y.; Li, N.; Tang, B. A Cancer Cell Membrane-Camouflaged Nanoreactor for Enhanced Radiotherapy against Cancer Metastasis. *Chem. Commun.* **2020**, *56* (4), 547–550. https://doi.org/10.1039/C9CC07878A.

(731) Lousada, C. M.; Yang, M.; Nilsson, K.; Jonsson, M. Catalytic Decomposition of Hydrogen Peroxide on Transition Metal and Lanthanide Oxides. *J. Mol. Catal. A Chem.* **2013**, *379*, 178–184. https://doi.org/10.1016/j.molcata.2013.08.017.

(732) Pham, A. N.; Xing, G.; Miller, C. J.; Waite, T. D. Fenton-like Copper Redox Chemistry Revisited: Hydrogen Peroxide and Superoxide Mediation of Copper-Catalyzed Oxidant Production. *J. Catal.* **2013**, *301*, 54–64. https://doi.org/10.1016/j.jcat.2013.01.025.

(733) Peng, J.; Yang, Q.; Li, W.; Tan, L.; Xiao, Y.; Chen, L.; Hao, Y.; Qian, Z. Erythrocyte-Membrane-Coated Prussian Blue/Manganese Dioxide Nanoparticles as H2O2-Responsive Oxygen Generators To Enhance Cancer Chemotherapy/Photothermal Therapy. *ACS Appl. Mater. Interfaces* **2017**, *9* (51), 44410–44422. https://doi.org/10.1021/acsami.7b17022.

(734) Sharma, V.; Jeevanandam, P. Synthesis of Copper Sulfide Nanoparticles by Thermal Decomposition Approach and Morphology Dependent Peroxidase-Like Activity. *J. Nanosci. Nanotechnol.* **2020**, *20* (5), 2763–2780. https://doi.org/10.1166/jnn.2020.17432.

(735) Guan, J.; Peng, J.; Jin, X. Synthesis of Copper Sulfide Nanorods as Peroxidase Mimics for the Colorimetric Detection of Hydrogen Peroxide. *Anal. Methods* **2015**, *7* (13), 5454–5461. https://doi.org/10.1039/c5ay00895f.

(736) Mulenos, M. R.; Liu, J.; Lujan, H.; Guo, B.; Lichtfouse, E.; Sharma, V. K.; Sayes, C. M. Copper, Silver, and Titania Nanoparticles Do Not Release Ions under Anoxic Conditions and Release Only Minute Ion Levels under Oxic Conditions in Water: Evidence for the Low Toxicity of Nanoparticles. *Environ. Chem. Lett.* **2020**, 1–10. https://doi.org/10.1007/s10311-020-00985-z.

(737) Rehn, B.; Seiler, F.; Rehn, S.; Bruch, J.; Maier, M. Investigations on the Inflammatory and Genotoxic Lung Effects of Two Types of Titanium Dioxide: Untreated and Surface Treated. *Toxicol. Appl. Pharmacol.* **2003**, *189* (2), 84–95. https://doi.org/10.1016/S0041-008X(03)00092-9.

(738) Fujita, K.; Fujita, K.; Horie, M.; Kato, H.; Endoh, S.; Suzuki, M.; Nakamura, A.; Miyauchi, A.; Yamamoto, K.; Kinugasa, S.; Nishio, K.; Yoshida, Y.; Iwahashi, H.; Nakanishi, J. Effects of Ultrafine TiO2 Particles on Gene Expression Profile in Human Keratinocytes without Illumination: Involvement of Extracellular Matrix and Cell Adhesion. *Toxicol. Lett.* **2009**, *191* (2–3), 109–117. https://doi.org/10.1016/j.toxlet.2009.08.011.

(739) Li, M.; Yin, J. J.; Wamer, W. G.; Lo, Y. M. Mechanistic Characterization of Titanium Dioxide Nanoparticle-Induced Toxicity Using Electron Spin Resonance. *J. Food Drug Anal.* **2014**, *22* (1), 76–85. https://doi.org/10.1016/j.jfda.2014.01.006.

(740) Skocaj, M.; Filipic, M.; Petkovic, J.; Novak, S. Titanium Dioxide in Our Everyday Life; Is It Safe? *Radiol. Oncol.* **2011**, *45* (4), 227–247. https://doi.org/10.2478/v10019-011-0037-0.

(741) Smith, C. W.; Chen, Y.-S.; Nandu, N.; Kachwala, M.; Yigit, M. V. The Analysis of Zirconium (IV) Oxide (ZrO2) Nanoparticles for Peroxidase Activity. *J. Anal. Test.* **2019**, *3* (3), 246–252. https://doi.org/10.1007/s41664-019-00101-3.

(742) Hiroki, A.; LaVerne, J. A. Decomposition of Hydrogen Peroxide at Water−Ceramic Oxide Interfaces. *J. Phys. Chem. B* **2005**, *109* (8), 3364–3370. https://doi.org/10.1021/jp046405d.

(743) Singh, K. R. B.; Nayak, V.; Sarkar, T.; Singh, R. P. Cerium Oxide Nanoparticles: Properties, Biosynthesis and Biomedical Application. *RSC Adv.* **2020**, *10* (45), 27194–27214. https://doi.org/10.1039/D0RA04736H.

(744) Long, T. C.; Saleh, N.; Tilton, R. D.; Lowry, G. V; Veronesi, B. Titanium Dioxide (P25) Produces Reactive Oxygen Species in Immortalized Brain Microglia (BV2): Implications for Nanoparticle Neurotoxicity. *Environ. Sci. Technol.* **2006**, *40* (14), 4346–4352. https://doi.org/10.1021/es060589n.

(745) Park, E.-J.; Yi, J.; Chung, K.-H.; Ryu, D.-Y.; Choi, J.; Park, K. Oxidative Stress and Apoptosis Induced by Titanium Dioxide Nanoparticles in Cultured BEAS-2B Cells. *Toxicol. Lett.* **2008**, *180* (3), 222–229. https://doi.org/10.1016/j.toxlet.2008.06.869.

(746) Saquib, Q.; Al-Khedhairy, A. A.; Siddiqui, M. A.; Abou-Tarboush, F. M.; Azam, A.; Musarrat, J. Titanium Dioxide Nanoparticles Induced Cytotoxicity, Oxidative Stress and DNA Damage in Human Amnion Epithelial (WISH) Cells. *Toxicol. In Vitro* **2012**, *26* (2), 351–361. https://doi.org/10.1016/j.tiv.2011.12.011.

(747) Shi, H.; Magaye, R.; Castranova, V.; Zhao, J. Titanium Dioxide Nanoparticles: A Review of Current Toxicological Data. *Part. Fibre Toxicol.* **2013**, *10* (1), 15. https://doi.org/10.1186/1743-8977-10-15.

(748) Gea, M.; Bonetta, S.; Iannarelli, L.; Giovannozzi, A. M.; Maurino, V.; Bonetta, S.; Hodoroaba, V.-D.; Armato, C.; Rossi, A. M.; Schilirò, T. Shape-Engineered Titanium Dioxide Nanoparticles (TiO2-NPs): Cytotoxicity and Genotoxicity in Bronchial Epithelial Cells. *Food Chem. Toxicol.* **2019**, *127*, 89–100. https://doi.org/10.1016/j.fct.2019.02.043.

(749) Kongseng, S.; Yoovathaworn, K.; Wongprasert, K.; Chunhabundit, R.; Sukwong, P.; Pissuwan, D. Cytotoxic and Inflammatory Responses of TiO2 Nanoparticles on Human Peripheral Blood Mononuclear Cells. *J. Appl. Toxicol.* **2016**, *36* (10), 1364–1373. https://doi.org/10.1002/jat.3342.

(750) Ma, Y.; Guo, Y.; Wu, S.; Lv, Z.; Zhang, Q.; Ke, Y. Titanium Dioxide Nanoparticles Induce Size-Dependent Cytotoxicity and Genomic DNA Hypomethylation in Human Respiratory Cells. *RSC Adv.* **2017**, *7* (38), 23560–23572. https://doi.org/10.1039/C6RA28272E.

(751) He, Q.; Zhou, X.; Liu, Y.; Gou, W.; Cui, J.; Li, Z.; Wu, Y.; Zuo, D. Titanium Dioxide Nanoparticles Induce Mouse Hippocampal Neuron Apoptosis via Oxidative Stress- and Calcium Imbalance-Mediated Endoplasmic Reticulum Stress. *Environ. Toxicol. Pharmacol.* **2018**, *63*, 6–15. https://doi.org/10.1016/j.etap.2018.08.003.

(752) Zhao, H.; Chen, L.; Zhong, G.; Huang, Y.; Zhang, X.; Chu, C.; Chen, L.; Wang, M. Titanium Dioxide Nanoparticles Induce Mitochondrial Dynamic Imbalance and Damage in HT22 Cells. *J. Nanomater.* **2019**, *2019*, 4607531. https://doi.org/10.1155/2019/4607531.

(753) Gurr, J.-R.; Wang, A. S. S.; Chen, C.-H.; Jan, K.-Y. Ultrafine Titanium Dioxide Particles in the Absence of Photoactivation Can Induce Oxidative Damage to Human Bronchial Epithelial Cells. *Toxicology* **2005**, *213* (1–2), 66–73. https://doi.org/10.1016/j.tox.2005.05.007.

(754) Lipovsky, A.; levitski, L.; Tzitrinovich, Z.; Gedanken, A.; Lubart, R. The Different Behavior of Rutile and Anatase Nanoparticles in Forming Oxy Radicals Upon Illumination with Visible Light: An EPR Study. *Photochem. Photobiol.* **2012**, *88* (1), 14–20. https://doi.org/10.1111/j.1751-1097.2011.01015.x.

(755) Fenoglio, I.; Greco, G.; Livraghi, S.; Fubini, B. Non-UV-Induced Radical Reactions at the Surface of TiO2 Nanoparticles That May Trigger Toxic Responses. *Chem. – A Eur. J.* **2009**, *15* (18), 4614–4621.

https://doi.org/10.1002/chem.200802542.

(756) Sánchez, L. D.; Taxt-Lamolle, S. F. M.; Hole, E. O.; Krivokapić, A.; Sagstuen, E.; Haugen, H. J. TiO2 Suspension Exposed to H2O2 in Ambient Light or Darkness: Degradation of Methylene Blue and EPR Evidence for Radical Oxygen Species. *Appl. Catal. B Environ.* **2013**, *142–143*, 662–667. https://doi.org/10.1016/j.apcatb.2013.05.017.

(757) Wiedmer, D.; Sagstuen, E.; Welch, K.; Haugen, H. J.; Tiainen, H. Oxidative Power of Aqueous Non-Irradiated TiO2-H2O2 Suspensions: Methylene Blue Degradation and the Role of Reactive Oxygen Species. *Appl. Catal. B Environ.* **2016**, *198*, 9–15. https://doi.org/10.1016/j.apcatb.2016.05.036.

(758) Pele, L. C.; Thoree, V.; Bruggraber, S. F. A.; Koller, D.; Thompson, R. P. H.; Lomer, M. C.; Powell, J. J. Pharmaceutical/Food Grade Titanium Dioxide Particles Are Absorbed into the Bloodstream of Human Volunteers. *Part. Fibre Toxicol.* **2015**, *12*, 26. https://doi.org/10.1186/s12989-015-0101-9.

(759) Trouiller, B.; Reliene, R.; Westbrook, A.; Solaimani, P.; Schiestl, R. H. Titanium Dioxide Nanoparticles Induce DNA Damage and Genetic Instability <Em>In Vivo</Em> in Mice. *Cancer Res.* **2009**, *69* (22), 8784 LP – 8789. https://doi.org/10.1158/0008-5472.CAN-09-2496.

(760) Li, B.; Ze, Y.; Sun, Q.; Zhang, T.; Sang, X.; Cui, Y.; Wang, X.; Gui, S.; Tan, D.; Zhu, M.; Zhao, X.; Sheng, L.; Wang, L.; Hong, F.; Tang, M. Molecular Mechanisms of Nanosized Titanium Dioxide–Induced Pulmonary Injury in Mice. *PLoS One* **2013**, *8* (2), e55563.

(761) Rosa, S.; Connolly, C.; Schettino, G.; Butterworth, K. T.; Prise, K. M. Biological Mechanisms of Gold Nanoparticle Radiosensitization. *Cancer Nanotechnol.* **2017**, *8* (1).

(762) Haruta, M. When Gold Is Not Noble: Catalysis by Nanoparticles. *Chem. Rec.* **2003**, *3* (2), 75–87. https://doi.org/10.1002/tcr.10053.

(763) Mateo, D.; Morales, P.; Ávalos, A.; Haza, A. I. Oxidative Stress Contributes to Gold Nanoparticle-Induced Cytotoxicity in Human Tumor Cells. *Toxicol. Mech. Methods* **2014**, *24* (3), 161–172. https://doi.org/10.3109/15376516.2013.869783.

(764) Behravesh, E.; Kumar, N.; Balme, Q.; Roine, J.; Salonen, J.; Schukarev, A.; Mikkola, J.-P.; Peurla, M.; Aho, A.; Eränen, K.; Murzin, D. Y.; Salmi, T. Synthesis and Characterization of Au Nano Particles Supported Catalysts for Partial Oxidation of Ethanol: Influence of Solution PH, Au Nanoparticle Size, Support Structure and Acidity. *J. Catal.* **2017**, *353*, 223–238. https://doi.org/10.1016/j.jcat.2017.07.014.

(765) Butterworth, K. T.; Coulter, J. A.; Jain, S.; Forker, J.; McMahon, S. J.; Schettino, G.; Prise, K. M.; Currell, F. J.; Hirst, D. G. Evaluation of Cytotoxicity and Radiation Enhancement Using 1.9 Nm Gold Particles: Potential Application for Cancer Therapy. *Nanotechnology* **2010**, *21* (29), 295101. https://doi.org/10.1088/0957-4484/21/29/295101.

(766) Pan, Y.; Leifert, A.; Ruau, D.; Neuss, S.; Bornemann, J.; Schmid, G.; Brandau, W.; Simon, U.; Jahnen-Dechent, W. Gold Nanoparticles of Diameter 1.4 Nm Trigger Necrosis by Oxidative Stress and Mitochondrial Damage. *Small* **2009**, *5* (18), 2067–2076. https://doi.org/10.1002/smll.200900466.

(767) Ionita, P.; Conte, M.; Gilbert, B. C.; Chechik, V. Gold Nanoparticle-Initiated Free Radical Oxidations and Halogen Abstractions. *Org. Biomol. Chem.* **2007**, *5* (21), 3504–3509. https://doi.org/10.1039/b711573c.

(768) Conte, M.; Wilson, K.; Chechik, V. Radical Intermediates in Chloroform Reactions over Triphenylphosphine-Protected Au Nanoparticles. *Org. Biomol. Chem.* **2009**, *7* (7), 1361–1367. https://doi.org/10.1039/b819627c.

(769) Zhang, Z.; Berg, A.; Levanon, H.; Fessenden, R. W.; Meisel, D. On the Interactions of Free Radicals with Gold Nanoparticles. *J. Am. Chem. Soc.* **2003**, *125* (26), 7959–7963. https://doi.org/10.1021/ja034830z.

(770) Taggart, L. E.; McMahon, S. J.; Currell, F. J.; Prise, K. M.; Butterworth, K. T. The Role of Mitochondrial Function in Gold Nanoparticle Mediated Radiosensitisation. *Cancer Nanotechnol.* **2014**, *5* (1), 5. https://doi.org/10.1186/s12645-014-0005-7.

(771) Dudek, J. Role of Cardiolipin in Mitochondrial Signaling Pathways . *Frontiers in Cell and Developmental Biology* . 2017, p 90.

(772) Redza-Dutordoir, M.; Averill-Bates, D. A. Activation of Apoptosis Signalling Pathways by Reactive Oxygen Species. *Biochim. Biophys. Acta - Mol. Cell Res.* **2016**, *1863* (12), 2977–2992. https://doi.org/10.1016/j.bbamcr.2016.09.012.

(773) Richardson, R. B.; Harper, M.-E. Mitochondrial Stress Controls the Radiosensitivity of the Oxygen Effect: Implications for Radiotherapy. *Oncotarget* **2016**, *7* (16), 21469–21483. https://doi.org/10.18632/oncotarget.7412.

(774) Jv, Y.; Li, B.; Cao, R. Positively-Charged Gold Nanoparticles as Peroxidiase Mimic and Their Application in Hydrogen Peroxide and Glucose Detection. *Chem. Commun.* **2010**, *46* (42), 8017–8019. https://doi.org/10.1039/C0CC02698K.

(775) Wang, S.; Chen, W.; Liu, A.-L.; Hong, L.; Deng, H.-H.; Lin, X.-H. Comparison of the Peroxidase-Like Activity of Unmodified, Amino-Modified, and Citrate-Capped Gold Nanoparticles. *ChemPhysChem* **2012**, *13* (5), 1199–1204. https://doi.org/10.1002/cphc.201100906.

(776) He, W.; Zhou, Y.-T.; Wamer, W. G.; Hu, X.; Wu, X.; Zheng, Z.; Boudreau, M. D.; Yin, J.-J. Intrinsic Catalytic Activity of Au Nanoparticles with Respect to Hydrogen Peroxide Decomposition and Superoxide Scavenging. *Biomaterials* **2013**, *34* (3), 765–773. https://doi.org/10.1016/j.biomaterials.2012.10.010.

(777) Liu, Y.; Wu, H.; Li, M.; Yin, J.-J.; Nie, Z. PH Dependent Catalytic Activities of Platinum Nanoparticles with Respect to the Decomposition of Hydrogen Peroxide and Scavenging of Superoxide and Singlet Oxygen. *Nanoscale* **2014**, *6* (20), 11904–11910. https://doi.org/10.1039/C4NR03848G.

(778) Cao, G.-J.; Chen, Y.; Chen, X.; Weng, P.; Lin, R.-G. Intrinsic Catalytic Activity of Rhodium Nanoparticles with Respect to Reactive Oxygen Species Scavenging: Implication for Diminishing Cytotoxicity. *J. Environ. Sci. Heal. Part C* **2019**, *37* (1), 14–25. https://doi.org/10.1080/10590501.2019.1555319.

(779) Sobańska, K.; Pietrzyk, P.; Sojka, Z. Generation of Reactive Oxygen Species via Electroprotic Interaction of H2O2 with ZrO2 Gel: Ionic Sponge Effect and PH-Switchable Peroxidase- and Catalase-Like Activity. *ACS Catal.* **2017**, *7* (4), 2935–2947. https://doi.org/10.1021/acscatal.7b00189.

(780) Liu, X.; Li, X.; Xu, W.; Zhang, X.; Huang, Z.; Wang, F.; Liu, J. Sub-Angstrom Gold Nanoparticle/Liposome Interfaces Controlled by Halides. *Langmuir* **2018**, *34* (22), 6628–6635. https://doi.org/10.1021/acs.langmuir.8b01138.

(781) Wood, P. M. The Redox Potential of the System Oxygen—Superoxide. *FEBS Lett.* **1974**, *44* (1), 22–24. https://doi.org/10.1016/0014-5793(74)80297-8.

(782) Yan, J.; Xu, X.; Zhou, J.; Liu, C.; Zhang, L.; Wang, D.; Yang, F.; Zhang, H. Fabrication of a PH/Redox-Triggered Mesoporous Silica-Based Nanoparticle with Microfluidics for Anticancer Drugs Doxorubicin and Paclitaxel Codelivery. *ACS Appl. Bio Mater.* **2020**, *3* (2), 1216–1225. https://doi.org/10.1021/acsabm.9b01111.

(783) Zhang, H.; Qu, X.; Chen, H.; Kong, H.; Ding, R.; Chen, D.; Zhang, X.; Pei, H.; Santos, H. A.; Hai, M.; Weitz, D. A. Fabrication of Calcium Phosphate-Based Nanocomposites Incorporating DNA Origami, Gold Nanorods, and Anticancer Drugs for Biomedical Applications. *Adv. Healthc. Mater.* **2017**, *6* (20), 1700664. https://doi.org/10.1002/adhm.201700664.

(784) Wang, L.; Hou, J.; Liu, S.; Carrier, A. J.; Guo, T.; Liang, Q.; Oakley, D.; Zhang, X. CuO Nanoparticles as Haloperoxidase-Mimics: Chloride-Accelerated Heterogeneous Cu-Fenton Chemistry for H2O2 and Glucose Sensing. *Sensors Actuators B Chem.* **2019**, *287*, 180–184. https://doi.org/10.1016/j.snb.2019.02.030.

(785) Castillo, M. H.; Button, T. M.; Doerr, R.; Homs, M. I.; Pruett, C. W.; Pearce, J. I. Effects of Radiotherapy on Mandibular Reconstruction Plates. *Am. J. Surg.* **1988**, *156* (4), 261–263. https://doi.org/10.1016/S0002-9610(88)80287-3.

(786) Delacroix, S.; Rymel, J.; Smith, P. J.; Clubb, B. S. The Effects of Steel and Titanium Mandibular Reconstruction Plates on Photon and Electron Beams. *Br. J. Radiol.* **1990**, *63* (752), 642–645. https://doi.org/10.1259/0007-1285-63-752-642.

(787) Cho, S. H. Estimation of Tumour Dose Enhancement Due to Gold Nanoparticles during Typical Radiation Treatments: A Preliminary Monte Carlo Study. *Phys. Med. Biol.* **2005**, *50* (15), N163-73. https://doi.org/10.1088/0031-9155/50/15/N01.

(788) Roeske, J. C.; Nunez, L.; Hoggarth, M.; Labay, E.; Weichselbaum, R. R. Characterization of the Theorectical Radiation Dose Enhancement from Nanoparticles. *Technol. Cancer Res. Treat.* **2007**, *6* (5), 395–401. https://doi.org/10.1177/153303460700600504.

(789) Jain, S.; Hirst, D. G.; O'Sullivan, J. M. Gold Nanoparticles as Novel Agents for Cancer Therapy. *Br. J. Radiol.* **2012**, *85* (1010), 101–113. https://doi.org/10.1259/bjr/59448833.

(790) Jones, B. L.; Krishnan, S.; Cho, S. H. Estimation of Microscopic Dose Enhancement Factor around Gold Nanoparticles by Monte Carlo Calculations. *Med. Phys.* **2010**, *37* (7), 3809–3816. https://doi.org/10.1118/1.3455703.

(791) Hubbell, J. H.; Seltzer, S. M. *Tables of X-Ray Mass Attenuation Coefficients and Mass Energy-Absorption Coefficients 1 KeV to 20 MeV for Elements z = 1 to 92 and 48 Additional Substances of Dosimetric Interest*; United States, 1995.

(792) Auger, P. *Sur Les Rayons β Secondaires Produit Dans Un Gaz Par Des Rayons X.*; 1925.

(793) Howell, R. W. Auger Processes in the 21st Century. In *International Journal of Radiation Biology*; NIH Public Access, 2008; Vol. 84, pp 959–975. https://doi.org/10.1080/09553000802395527.

(794) Coster, D.; L. Kronig, R. De. New Type of Auger Effect and Its Influence on the X-Ray Spectrum. *Physica* **1935**, *2* (1), 13–24. https://doi.org/10.1016/S0031-8914(35)90060-X.

(795) Rezaee, M.; Hunting, D. J.; Sanche, L. Correlation between Energy Deposition and Molecular Damage from Auger Electrons: A Case Study of Ultra-Low Energy (5-18 EV) Electron Interactions with DNA. *Med. Phys.* **2014**, *41* (7).

(796) Buchegger, F.; Perillo-Adamer, F.; Dupertuis, Y. M.; Delaloye, A. B. Auger Radiation Targeted into DNA: A Therapy Perspective. *Eur. J. Nucl. Med. Mol. Imaging* **2006**, *33* (11), 1352–1363. https://doi.org/10.1007/s00259-006-0187-2.

(797) McMahon, S. J.; Hyland, W. B.; Muir, M. F.; Coulter, J. A.; Jain, S.; Butterworth, K. T.; Schettino, G.; Dickson, G. R.; Hounsell, A. R.; O'Sullivan, J. M.; Prise, K. M.; Hirst, D. G.; Currell, F. J. Biological Consequences of Nanoscale Energy Deposition near Irradiated Heavy Atom Nanoparticles. *Sci. Rep.* **2011**, *1*.

(798) Lin, Y.; McMahon, S. J.; Scarpelli, M.; Paganetti, H.; Schuemann, J. Comparing Gold Nano-Particle Enhanced Radiotherapy with Protons, Megavoltage Photons and Kilovoltage Photons: A Monte Carlo Simulation. *Phys. Med. Biol.* **2014**, *59* (24), 7675–7689. https://doi.org/10.1088/0031-9155/59/24/7675.

(799) McMahon, S. J.; Paganetti, H.; Prise, K. M. Optimising Element Choice for Nanoparticle Radiosensitisers. *Nanoscale* **2016**, *8* (1), 581–589. https://doi.org/10.1039/C5NR07089A.

(800) Dong, Y. C.; Hajfathalian, M.; Maidment, P. S. N.; Hsu, J. C.; Naha, P. C.; Si-Mohamed, S.; Breuilly, M.; Kim, J.; Chhour, P.; Douek, P.; Litt, H. I.; Cormode, D. P. Effect of Gold Nanoparticle Size on Their Properties as Contrast Agents for Computed Tomography. *Sci. Rep.* **2019**, *9* (1), 14912. https://doi.org/10.1038/s41598-019-50332-8.

(801) Stewart, C.; Konstantinov, K.; McKinnon, S.; Guatelli, S.; Lerch, M.; Rosenfeld, A.; Tehei, M.; Corde, S. First Proof of Bismuth Oxide Nanoparticles as Efficient Radiosensitisers on Highly Radioresistant Cancer Cells. *Phys. Medica* **2016**, *32* (11), 1444–1452. https://doi.org/10.1016/j.ejmp.2016.10.015.

(802) Lim, S. N.; Pradhan, A. K.; Barth, R. F.; Nahar, S. N.; Nakkula, R. J.; Yang, W.; Palmer, A. M.; Turro, C.;

Weldon, M.; Bell, E. H.; Mo, X. Tumoricidal Activity of Low-Energy 160-KV versus 6-MV X-Rays against Platinum-Sensitized F98 Glioma Cells. *J. Radiat. Res.* **2015**, *56* (1), 77–89. https://doi.org/10.1093/jrr/rru084.

(803) Scarboro, S. B.; Followill, D. S.; Howell, R. M.; Kry, S. F. Variations in Photon Energy Spectra of a 6 MV Beam and Their Impact on TLD Response. *Med. Phys.* **2011**, *38* (5), 2619–2628. https://doi.org/10.1118/1.3575419.

(804) Maqbool, M.; Muhammad, W.; Shahid, M.; Ahmad, M.; Matiullah, M. Accuracy Checks of Physical Beam Modifier Factors Algorithm Used in Computerized Treatment Planning System for a 15 MV Photon Beam. *Reports Pract. Oncol. Radiother.* **2009**, *14* (6), 214–220. https://doi.org/10.1016/j.rpor.2009.12.002.

(805) Tsiamas, P.; Liu, B.; Cifter, F.; Ngwa, W. F.; Berbeco, R. I.; Kappas, C.; Theodorou, K.; Marcus, K.; Makrigiorgos, M. G.; Sajo, E.; Zygmanski, P. Impact of Beam Quality on Megavoltage Radiotherapy Treatment Techniques Utilizing Gold Nanoparticles for Dose Enhancement. *Phys. Med. Biol.* **2013**, *58* (3), 451–464. https://doi.org/10.1088/0031-9155/58/3/451.

(806) Cashmore, J. Surface Dose Variations in 6 and 10 MV Flattened and Flattening Filter-Free (FFF) Photon Beams. *J. Appl. Clin. Med. Phys.* **2016**, *17* (5), 293–307. https://doi.org/10.1120/jacmp.v17i5.6284.

(807) Harada, H.; Inoue, M.; Itasaka, S.; Hirota, K.; Morinibu, A.; Shinomiya, K.; Zeng, L.; Ou, G.; Zhu, Y.; Yoshimura, M.; McKenna, W. G.; Muschel, R. J.; Hiraoka, M. Cancer Cells That Survive Radiation Therapy Acquire HIF-1 Activity and Translocate towards Tumour Blood Vessels. *Nat. Commun.* **2012**, *3* (1), 783. https://doi.org/10.1038/ncomms1786.

(808) Brown, J. M.; Wilson, W. R. Exploiting Tumour Hypoxia in Cancer Treatment. *Nat. Rev. Cancer* **2004**, *4* (6), 437–447. https://doi.org/10.1038/nrc1367.

(809) Epel, B.; Maggio, M. C.; Barth, E. D.; Miller, R. C.; Pelizzari, C. A.; Krzykawska-Serda, M.; Sundramoorthy, S. V; Aydogan, B.; Weichselbaum, R. R.; Tormyshev, V. M.; Halpern, H. J. Oxygen-Guided Radiation Therapy. *Int. J. Radiat. Oncol.* **2019**, *103* (4), 977–984. https://doi.org/10.1016/j.ijrobp.2018.10.041.

(810) Kobiela, J.; Spychalski, P.; Marvaso, G.; Ciardo, D.; Dell'Acqua, V.; Kraja, F.; Błażyńska-Spychalska, A.; Łachiński, A. J.; Surgo, A.; Glynne-Jones, R.; Jereczek-Fossa, B. A. Ablative Stereotactic Radiotherapy for Oligometastatic Colorectal Cancer: Systematic Review. *Crit. Rev. Oncol. Hematol.* **2018**, *129*, 91–101. https://doi.org/10.1016/j.critrevonc.2018.06.005.

(811) Lehrer, E. J.; Singh, R.; Wang, M.; Chinchilli, V. M.; Trifiletti, D. M.; Ost, P.; Siva, S.; Meng, M.; Tchelebi, L.; Zaorsky, N. G. Safety and Survival Rates Associated With Ablative Stereotactic Radiotherapy for Patients With Oligometastatic Cancer: A Systematic Review and Meta-Analysis. *JAMA Oncol.* **2021**, *7* (1), 92–106. https://doi.org/10.1001/jamaoncol.2020.6146.

(812) Hanna, G. G.; Murray, L.; Patel, R.; Jain, S.; Aitken, K. L.; Franks, K. N.; van As, N.; Tree, A.; Hatfield, P.; Harrow, S.; McDonald, F.; Ahmed, M.; Saran, F. H.; Webster, G. J.; Khoo, V.; Landau, D.; Eaton, D. J.; Hawkins, M. A. UK Consensus on Normal Tissue Dose Constraints for Stereotactic Radiotherapy. *Clin. Oncol.* **2018**, *30* (1), 5–14. https://doi.org/10.1016/j.clon.2017.09.007.

(813) Spencer, K. L.; van der Velden, J. M.; Wong, E.; Seravalli, E.; Sahgal, A.; Chow, E.; Verlaan, J.-J.; Verkooijen, H. M.; van der Linden, Y. M. Systematic Review of the Role of Stereotactic Radiotherapy for Bone Metastases. *JNCI J. Natl. Cancer Inst.* **2019**, *111* (10), 1023–1032. https://doi.org/10.1093/jnci/djz101.

(814) Ong, W. L.; Siva, S.; Milne, R. L.; Foroudi, F.; Millar, J. L. Trend in Stereotactic Radiation Therapy Use for Management of Bone and Brain Metastases in Patients with Renal Cell Carcinoma in Australia. *Oncologist* **2021**, *26* (7), e1288–e1289. https://doi.org/10.1002/onco.13792.

(815) Paciotti, M.; Schmidt, A. L.; Ravi, P.; McKay, R. R.; Trinh, Q.-D.; Choueiri, T. K. Temporal Trends and Predictors in the Use of Stereotactic Body Radiotherapy for Treatment of Metastatic Renal Cell Carcinoma in the U.S. *Oncologist* **2021**, *26* (5), e905–e906. https://doi.org/10.1002/onco.13736.

(816) Wegner, R. E.; Abel, S.; Vemana, G.; Mao, S.; Fuhrer, R. Utilization of Stereotactic Ablative Body Radiation Therapy for Intact Renal Cell Carcinoma: Trends in Treatment and Predictors of Outcome. *Adv. Radiat. Oncol.* **2020**, *5* (1), 85–91. https://doi.org/10.1016/j.adro.2019.07.018.

(817) Najafi, M.; Fardid, R.; Hadadi, G.; Fardid, M. The Mechanisms of Radiation-Induced Bystander Effect. *J. Biomed. Phys. Eng.* **2014**, *4* (4), 163–172.

(818) Elahi, N.; Kamali, M.; Baghersad, M. H. Recent Biomedical Applications of Gold Nanoparticles: A Review. *Talanta* **2018**, *184*, 537–556. https://doi.org/10.1016/j.talanta.2018.02.088.

(819) Cho, S. H.; Jones, B. L.; Krishnan, S. The Dosimetric Feasibility of Gold Nanoparticle-Aided Radiation Therapy (GNRT) via Brachytherapy Using Low-Energy Gamma-/x-Ray Sources. *Phys. Med. Biol.* **2009**, *54* (16), 4889–4905. https://doi.org/10.1088/0031-9155/54/16/004.

(820) Laprise-Pelletier, M.; Simão, T.; Fortin, M.-A. Gold Nanoparticles in Radiotherapy and Recent Progress in Nanobrachytherapy. *Adv. Healthc. Mater.* **2018**, *7* (16), 1701460. https://doi.org/10.1002/adhm.201701460.

(821) Su, X.-Y.; Liu, P.-D.; Wu, H.; Gu, N. Enhancement of Radiosensitization by Metal-Based Nanoparticles in Cancer Radiation Therapy. *Cancer Biol. Med.* **2014**, *11* (2), 86–91. https://doi.org/10.7497/j.issn.2095-3941.2014.02.003.

(822) Rastinehad, A. R.; Anastos, H.; Wajswol, E.; Winoker, J. S.; Sfakianos, J. P.; Doppalapudi, S. K.; Carrick, M. R.; Knauer, C. J.; Taouli, B.; Lewis, S. C.; Tewari, A. K.; Schwartz, J. A.; Canfield, S. E.; George, A. K.; West, J. L.; Halas, N. J. Gold Nanoshell-Localized Photothermal Ablation of Prostate Tumors in a Clinical Pilot Device Study. *Proc. Natl. Acad. Sci. U. S. A.* **2019**, *116* (37), 18590–18596. https://doi.org/10.1073/pnas.1906929116.

(823) Stern, J. M.; Kibanov Solomonov, V. V; Sazykina, E.; Schwartz, J. A.; Gad, S. C.; Goodrich, G. P. Initial Evaluation of the Safety of Nanoshell-Directed Photothermal Therapy in the Treatment of Prostate Disease. *Int. J. Toxicol.* **2016**, *35* (1), 38–46. https://doi.org/10.1177/1091581815600170.

(824) Libutti, S. K.; Paciotti, G. F.; Byrnes, A. A.; Alexander, H. R. J.; Gannon, W. E.; Walker, M.; Seidel, G. D.; Yuldasheva, N.; Tamarkin, L. Phase I and Pharmacokinetic Studies of CYT-6091, a Novel PEGylated Colloidal Gold-RhTNF Nanomedicine. *Clin. cancer Res. an Off. J. Am. Assoc. Cancer Res.* **2010**, *16* (24), 6139–6149. https://doi.org/10.1158/1078-0432.CCR-10-0978.

(825) Penninckx, S.; Heuskin, A.-C.; Michiels, C.; Lucas, S. Gold Nanoparticles as a Potent Radiosensitizer: A Transdisciplinary Approach from Physics to Patient. *Cancers (Basel).* **2020**, *12* (8), 2021. https://doi.org/10.3390/cancers12082021.

(826) Choi, B. J.; Jung, K. O.; Graves, E. E.; Pratx, G. A Gold Nanoparticle System for the Enhancement of Radiotherapy and Simultaneous Monitoring of Reactive-Oxygen-Species Formation. *Nanotechnology* **2018**, *29* (50), 504001. https://doi.org/10.1088/1361-6528/aae272.

(827) Geng, F.; Song, K.; Xing, J. Z.; Yuan, C.; Yan, S.; Yang, Q.; Chen, J.; Kong, B. Thio-Glucose Bound Gold Nanoparticles Enhance Radio-Cytotoxic Targeting of Ovarian Cancer. *Nanotechnology* **2011**, *22* (28), 285101. https://doi.org/10.1088/0957-4484/22/28/285101.

(828) Chang, J.; Taylor, R. D.; Davidson, R. A.; Sharmah, A.; Guo, T. Electron Paramagnetic Resonance Spectroscopy Investigation of Radical Production by Gold Nanoparticles in Aqueous Solutions Under X-Ray Irradiation. *J. Phys. Chem. A* **2016**, *120* (18), 2815–2823. https://doi.org/10.1021/acs.jpca.6b01755.

(829) Rodriguez, E. C.; Pracht, M.; Rolland, Y.; De Baere, T.; Nguyen, T. V. F.; Bronowicki, J. P.; Vendrely, V.; Cunha, A. S.; Baumann, A. S.; Croisé-Laurent, V.; Rio, E.; Le Sourd, S.; Gustin, P.; Perret, C.; Peiffert, D.; Deutsch, E. Hafnium Oxide Nanoparticles Activated by SBRT for the Treatment of Hepatocellular Carcinoma and Liver Metastasis: A Phase I/II Trial. *Int. J. Radiat. Oncol. Biol. Phys.* **2019**, *105* (1), S110–S111. https://doi.org/10.1016/j.ijrobp.2019.06.605.

(830) Hoffmann, C.; Calugaru, V.; Borcoman, E.; Moreno, V.; Calvo, E.; Liem, X.; Salas, S.; Doger, B.; Jouffroy, T.; Mirabel, X.; Rodriguez, J.; Chilles, A.; Bernois, K.; Dimitriu, M.; Fakhry, N.; Hee Kam, S. W.; Le

Tourneau, C. Phase I Dose-Escalation Study of NBTXR3 Activated by Intensity-Modulated Radiation Therapy in Elderly Patients with Locally Advanced Squamous Cell Carcinoma of the Oral Cavity or Oropharynx. *Eur. J. Cancer* **2021**, *146*, 135–144. https://doi.org/10.1016/j.ejca.2021.01.007.

(831) Bonvalot, S.; Le Pechoux, C.; De Baere, T.; Kantor, G.; Buy, X.; Stoeckle, E.; Terrier, P.; Sargos, P.; Coindre, J. M.; Lassau, N.; Ait Sarkouh, R.; Dimitriu, M.; Borghi, E.; Levy, L.; Deutsch, E.; Soria, J.-C. First-in-Human Study Testing a New Radioenhancer Using Nanoparticles (NBTXR3) Activated by Radiation Therapy in Patients with Locally Advanced Soft Tissue Sarcomas. *Clin. Cancer Res.* **2017**, *23* (4), 908–917. https://doi.org/10.1158/1078-0432.CCR-16-1297.

(832) Maggiorella, L.; Barouch, G.; Devaux, C.; Pottier, A.; Deutsch, E.; Bourhis, J.; Borghi, E.; Levy, L. Nanoscale Radiotherapy with Hafnium Oxide Nanoparticles. *Future Oncol.* **2012**, *8* (9), 1167–1181. https://doi.org/10.2217/fon.12.96.

(833) Pottier, A.; Borghi, E.; Levy, L. New Use of Metals as Nanosized Radioenhancers. *Anticancer Res.* **2014**, *34* (1), 443–453.

(834) Shiryaeva, E. S.; Baranova, I. A.; Kiselev, G. O.; Morozov, V. N.; Belousov, A. V; Sherstiuk, A. A.; Kolyvanova, M. A.; Krivoshapkin, P. V; Feldman, V. I. Hafnium Oxide as a Nanoradiosensitizer under X-Ray Irradiation of Aqueous Organic Systems: A Model Study Using the Spin-Trapping Technique and Monte Carlo Simulations. *J. Phys. Chem. C* **2019**, *123* (45), 27375–27384. https://doi.org/10.1021/acs.jpcc.9b08387.

(835) Marill, J.; Anesary, N. M.; Zhang, P.; Vivet, S.; Borghi, E.; Levy, L.; Pottier, A. Hafnium Oxide Nanoparticles: Toward an in Vitropredictive Biological Effect? *Radiat. Oncol.* **2014**, *9* (1), 150. https://doi.org/10.1186/1748-717X-9-150.

(836) Fakhardo, A. F.; Anastasova, E. I.; Gabdullina, S. R.; Solovyeva, A. S.; Saparova, V. B.; Chrishtop, V. V; Koshevaya, E. D.; Krivoshapkina, E. F.; Krivoshapkin, P. V; Kiselev, G. O.; Kalikina, P. A.; Koshel, E. I.; Shtil, A. A.; Vinogradov, V. V. Toxicity Patterns of Clinically Relevant Metal Oxide Nanoparticles. *ACS Appl. Bio Mater.* **2019**, *2* (10), 4427–4435. https://doi.org/10.1021/acsabm.9b00615.

(837) Field, J. A.; Luna-Velasco, A.; Boitano, S. A.; Shadman, F.; Ratner, B. D.; Barnes, C.; Sierra-Alvarez, R. Cytotoxicity and Physicochemical Properties of Hafnium Oxide Nanoparticles. *Chemosphere* **2011**, *84* (10), 1401–1407. https://doi.org/10.1016/j.chemosphere.2011.04.067.

(838) Jayaraman, V.; Bhavesh, G.; Chinnathambi, S.; Ganesan, S.; Aruna, P. Synthesis and Characterization of Hafnium Oxide Nanoparticles for Bio-Safety. *Mater. Express* **2014**, *4* (5), 375–383. https://doi.org/10.1166/mex.2014.1190.

(839) Kumar, N.; George, B. P. A.; Abrahamse, H.; Parashar, V.; Ray, S. S.; Ngila, J. C. A Novel Approach to Low-Temperature Synthesis of Cubic HfO2 Nanostructures and Their Cytotoxicity. *Sci. Rep.* **2017**, *7* (1), 9351. https://doi.org/10.1038/s41598-017-07753-0.

(840) Shin, D. Y.; Kim, G. Y.; Li, W.; Choi, B. T.; Kim, N. D.; Kang, H. S.; Choi, Y. H. Implication of Intracellular ROS Formation, Caspase-3 Activation and Egr-1 Induction in Platycodon D-Induced Apoptosis of U937 Human Leukemia Cells. *Biomed. Pharmacother.* **2009**, *63* (2), 86–94. https://doi.org/10.1016/j.biopha.2008.08.001.

(841) Higuchi, M.; Honda, T.; Proske, R. J.; Yeh, E. T. H. Regulation of Reactive Oxygen Species-Induced Apoptosis and Necrosis by Caspase 3-like Proteases. *Oncogene* **1998**, *17* (21), 2753–2760. https://doi.org/10.1038/sj.onc.1202211.

(842) Li, Y.; Qi, Y.; Zhang, H.; Xia, Z.; Xie, T.; Li, W.; Zhong, D.; Zhu, H.; Zhou, M. Gram-Scale Synthesis of Highly Biocompatible and Intravenous Injectable Hafnium Oxide Nanocrystal with Enhanced Radiotherapy Efficacy for Cancer Theranostic. *Biomaterials* **2020**, *226*, 119538. https://doi.org/10.1016/j.biomaterials.2019.119538.

(843) Lousada, C. M.; Jonsson, M. Kinetics, Mechanism, and Activation Energy of H2O2 Decomposition on the Surface of ZrO2. *J. Phys. Chem. C* **2010**, *114* (25), 11202–11208. https://doi.org/10.1021/jp1028933.

(844) Yang, M.; Jonsson, M. Surface Reactivity of Hydroxyl Radicals Formed upon Catalytic Decomposition of H2O2 on ZrO2. *J. Mol. Catal. A Chem.* **2015**, *400*, 49–55. https://doi.org/10.1016/j.molcata.2015.02.002.

(845) Shang, Y.; Wang, Q.; Li, J.; Liu, H.; Zhao, Q.; Huang, X.; Dong, H.; Chen, W.; Gui, R.; Nie, X. Zirconia Nanoparticles Induce HeLa Cell Death Through Mitochondrial Apoptosis and Autophagy Pathways Mediated by ROS . *Frontiers in Chemistry* . 2021, p 80.

(846) Huang, P.; Li, Z.; Lin, J.; Yang, D.; Gao, G.; Xu, C.; Bao, L.; Zhang, C.; Wang, K.; Song, H.; Hu, H.; Cui, D. Photosensitizer-Conjugated Magnetic Nanoparticles for in Vivo Simultaneous Magnetofluorescent Imaging and Targeting Therapy. *Biomaterials* **2011**, *32* (13), 3447–3458. https://doi.org/10.1016/j.biomaterials.2011.01.032.

(847) Juarranz, Á.; Jaén, P.; Sanz-Rodríguez, F.; Cuevas, J.; González, S. Photodynamic Therapy of Cancer. Basic Principles and Applications. *Clin. Transl. Oncol.* **2008**, *10* (3), 148–154. https://doi.org/10.1007/s12094-008-0172-2.

(848) Calixto, G. M.; Bernegossi, J.; De Freitas, L. M.; Fontana, C. R.; Chorilli, M. Nanotechnology-Based Drug Delivery Systems for Photodynamic Therapy of Cancer: A Review. *Molecules*. 2016.

(849) Chen, D.; Xu, Q.; Wang, W.; Shao, J.; Huang, W.; Dong, X. Type I Photosensitizers Revitalizing Photodynamic Oncotherapy. *Small* **2021**, *17* (31), 2006742. https://doi.org/10.1002/smll.202006742.

(850) Wang, Y.-Y.; Liu, Y.-C.; Sun, H.; Guo, D.-S. Type I Photodynamic Therapy by Organic–Inorganic Hybrid Materials: From Strategies to Applications. *Coord. Chem. Rev.* **2019**, *395*, 46–62. https://doi.org/10.1016/j.ccr.2019.05.016.

(851) Lovell, J. F.; Liu, T. W. B.; Chen, J.; Zheng, G. Activatable Photosensitizers for Imaging and Therapy. *Chem. Rev.* **2010**, *110* (5), 2839–2857. https://doi.org/10.1021/cr900236h.

(852) Riethmüller, M.; Burger, N.; Bauer, G. Singlet Oxygen Treatment of Tumor Cells Triggers Extracellular Singlet Oxygen Generation, Catalase Inactivation and Reactivation of Intercellular Apoptosis-Inducing Signaling. *Redox Biol.* **2015**, *6*, 157–168. https://doi.org/10.1016/j.redox.2015.07.006.

(853) Guo, H.; Qian, H.; Idris, N. M.; Zhang, Y. Singlet Oxygen-Induced Apoptosis of Cancer Cells Using Upconversion Fluorescent Nanoparticles as a Carrier of Photosensitizer. *Nanomedicine* **2010**, *6* (3), 486–495. https://doi.org/10.1016/j.nano.2009.11.004.

(854) Bergs, J. W. J.; Franken, N. A. P.; Haveman, J.; Geijsen, E. D.; Crezee, J.; van Bree, C. Hyperthermia, Cisplatin and Radiation Trimodality Treatment: A Promising Cancer Treatment? A Review from Preclinical Studies to Clinical Application. *Int. J. Hyperth.* **2007**, *23* (4), 329–341. https://doi.org/10.1080/02656730701378684.

(855) Zagar, T. M.; Oleson, J. R.; Vujaskovic, Z.; Dewhirst, M. W.; Craciunescu, O. I.; Blackwell, K. L.; Prosnitz, L. R.; Jones, E. L. Hyperthermia Combined with Radiation Therapy for Superficial Breast Cancer and Chest Wall Recurrence: A Review of the Randomised Data. *Int. J. Hyperth.* **2010**, *26* (7), 612–617. https://doi.org/10.3109/02656736.2010.487194.

(856) Y. Harima K. Harima, V. V. Ostapenko, Y. Tanaka, S. Sawada, K. N. A Randomized Clinical Trial of Radiation Therapy versus Thermoradiotherapy in Stage IIIB Cervical Carcinoma. *Int. J. Hyperth.* **2001**, *17* (2), 97–105. https://doi.org/10.1080/02656730010001333.

(857) Datta, N. R.; Rogers, S.; Ordóñez, S. G.; Puric, E.; Bodis, S. Hyperthermia and Radiotherapy in the Management of Head and Neck Cancers: A Systematic Review and Meta-Analysis. *Int. J. Hyperth.* **2016**, *32* (1), 31–40. https://doi.org/10.3109/02656736.2015.1099746.

(858) Song, G.; Liang, C.; Yi, X.; Zhao, Q.; Cheng, L.; Yang, K.; Liu, Z. Perfluorocarbon-Loaded Hollow Bi2Se3 Nanoparticles for Timely Supply of Oxygen under Near-Infrared Light to Enhance the Radiotherapy of Cancer. *Adv. Mater.* **2016**, *28* (14), 2716–2723. https://doi.org//10.1002/adma.201504617.

(859) Kong, G.; Braun, R. D.; Dewhirst, M. W. Hyperthermia Enables Tumor-Specific Nanoparticle Delivery:

Effect of Particle Size. *Cancer Res.* **2000**, *60* (16), 4440–4445.

(860) Gormley, A. J.; Larson, N.; Banisadr, A.; Robinson, R.; Frazier, N.; Ray, A.; Ghandehari, H. Plasmonic Photothermal Therapy Increases the Tumor Mass Penetration of HPMA Copolymers. *J. Control. Release* **2013**, *166* (2), 130–138. https://doi.org/10.1016/j.jconrel.2012.12.007.

(861) Grüll, H.; Langereis, S. Hyperthermia-Triggered Drug Delivery from Temperature-Sensitive Liposomes Using MRI-Guided High Intensity Focused Ultrasound. *J. Control. Release* **2012**, *161* (2), 317–327. https://doi.org/10.1016/j.jconrel.2012.04.041.

(862) Zhao, J.; Nguyen, S. C.; Ye, R.; Ye, B.; Weller, H.; Somorjai, G. A.; Alivisatos, A. P.; Toste, F. D. A Comparison of Photocatalytic Activities of Gold Nanoparticles Following Plasmonic and Interband Excitation and a Strategy for Harnessing Interband Hot Carriers for Solution Phase Photocatalysis. *ACS Cent. Sci.* **2017**, *3* (5), 482–488. https://doi.org/10.1021/acscentsci.7b00122.

(863) Brongersma, M. L.; Halas, N. J.; Nordlander, P. Plasmon-Induced Hot Carrier Science and Technology. *Nat. Nanotechnol.* **2015**, *10* (1), 25–34. https://doi.org/10.1038/nnano.2014.311.

(864) Kolwas, K.; Derkachova, A. Impact of the Interband Transitions in Gold and Silver on the Dynamics of Propagating and Localized Surface Plasmons. *Nanomater. (Basel, Switzerland)* **2020**, *10* (7), 1411. https://doi.org/10.3390/nano10071411.

(865) Lee, C.; Park, Y.; Park, J. Y. Hot Electrons Generated by Intraband and Interband Transition Detected Using a Plasmonic Cu/TiO2 Nanodiode. *RSC Adv.* **2019**, *9* (32), 18371–18376. https://doi.org/10.1039/C9RA02601K.

(866) Li, F.; Du, Y.; Liu, J.; Sun, H.; Wang, J.; Li, R.; Kim, D.; Hyeon, T.; Ling, D. Responsive Assembly of Upconversion Nanoparticles for PH-Activated and Near-Infrared-Triggered Photodynamic Therapy of Deep Tumors. *Adv. Mater.* **2018**, *30* (35), 1802808. https://doi.org/10.1002/adma.201802808.

(867) Deng, K.; Li, C.; Huang, S.; Xing, B.; Jin, D.; Zeng, Q.; Hou, Z.; Lin, J. Recent Progress in Near Infrared Light Triggered Photodynamic Therapy. *Small* **2017**, *13* (44), 1702299. https://doi.org/10.1002/smll.201702299.

(868) Zhang, X.; Chen, Y. L.; Liu, R.-S.; Tsai, D. P. Plasmonic Photocatalysis. *Reports Prog. Phys.* **2013**, *76* (4), 46401. https://doi.org/10.1088/0034-4885/76/4/046401.

(869) Yu, Z.; Sun, Q.; Pan, W.; Li, N.; Tang, B. A Near-Infrared Triggered Nanophotosensitizer Inducing Domino Effect on Mitochondrial Reactive Oxygen Species Burst for Cancer Therapy. *ACS Nano* **2015**, *9* (11), 11064–11074. https://doi.org/10.1021/acsnano.5b04501.

(870) Gao, K.; Tu, W.; Yu, X.; Ahmad, F.; Zhang, X.; Wu, W.; An, X.; Chen, X.; Li, W. W-Doped TiO(2) Nanoparticles with Strong Absorption in the NIR-II Window for Photoacoustic/CT Dual-Modal Imaging and Synergistic Thermoradiotherapy of Tumors. *Theranostics* **2019**, *9* (18), 5214–5226. https://doi.org/10.7150/thno.33574.

(871) Ren, W.; Yan, Y.; Zeng, L.; Shi, Z.; Gong, A.; Schaaf, P.; Wang, D.; Zhao, J.; Zou, B.; Yu, H.; Chen, G.; Brown, E. M. B.; Wu, A. A Near Infrared Light Triggered Hydrogenated Black TiO 2 for Cancer Photothermal Therapy. *Adv. Healthc. Mater.* **2015**, *4* (10), 1526–1536. https://doi.org/10.1002/adhm.v4.10.

(872) Qin, Y.; Ding, Z.; Guo, W.; Guo, X.; Hou, C.; Jiang, B.-P.; Liu, C.-G.; Shen, X.-C. A Full Solar Light Spectrum Responsive B@ZrO2–OV Photocatalyst: A Synergistic Strategy for Visible-to-NIR Photon Harvesting. *ACS Sustain. Chem. Eng.* **2020**, *8* (34), 13039–13047. https://doi.org/10.1021/acssuschemeng.0c04380.

(873) Sun, L.; Jiao, X.; Liu, W.; Wang, Y.; Cao, Y.; Bao, S.-J.; Xu, Z.; Kang, Y.; Xue, P. Novel Oxygen-Deficient Zirconia (ZrO2–x) for Fluorescence/Photoacoustic Imaging-Guided Photothermal/Photodynamic Therapy for Cancer. *ACS Appl. Mater. Interfaces* **2019**, *11* (44), 41127–41139. https://doi.org/10.1021/acsami.9b16604.

(874) Huang, X.; Neretina, S.; El-Sayed, M. A. Gold Nanorods: From Synthesis and Properties to Biological and Biomedical Applications. *Adv. Mater.* **2009**, *21* (48), 4880–4910. https://doi.org/10.1002/adma.200802789.

(875) Kim, M.; Lee, J.-H.; Nam, J.-M. Plasmonic Photothermal Nanoparticles for Biomedical Applications. *Adv. Sci.* **2019**, *6* (17), 1900471. https://doi.org/10.1002/advs.201900471.

(876) Amendola, V.; Pilot, R.; Frasconi, M.; Maragò, O. M.; Iatì, M. A. Surface Plasmon Resonance in Gold Nanoparticles: A Review. *J. Phys. Condens. Matter* **2017**, *29* (20), 203002. https://doi.org/10.1088/1361-648x/aa60f3.

(877) Jang, Y. J.; Chung, K.; Lee, J. S.; Choi, C. H.; Lim, J. W.; Kim, D. H. Plasmonic Hot Carriers Imaging: Promise and Outlook. *ACS Photonics* **2018**, *5* (12), 4711–4723. https://doi.org/10.1021/acsphotonics.8b01021.

(878) Melikyan, A.; Minassian, H. On Surface Plasmon Damping in Metallic Nanoparticles. *Appl. Phys. B* **2004**, *78* (3), 453–455. https://doi.org/10.1007/s00340-004-1403-z.

(879) Furube, A.; Hashimoto, S. Insight into Plasmonic Hot-Electron Transfer and Plasmon Molecular Drive: New Dimensions in Energy Conversion and Nanofabrication. *NPG Asia Mater.* **2017**, *9* (12), e454–e454. https://doi.org/10.1038/am.2017.191.

(880) Link, S.; El-Sayed, M. A. Optical Properties and Ultrafast Dynamics of Metallic Nanocrystals. *Annu. Rev. Phys. Chem.* **2003**, *54* (1), 331–366. https://doi.org/10.1146/annurev.physchem.54.011002.103759.

(881) Clavero, C. Plasmon-Induced Hot-Electron Generation at Nanoparticle/Metal-Oxide Interfaces for Photovoltaic and Photocatalytic Devices. *Nat. Photonics* **2014**, *8* (2), 95–103. https://doi.org/10.1038/nphoton.2013.238.

(882) Kim, Y.; Smith, J. G.; Jain, P. K. Harvesting Multiple Electron–Hole Pairs Generated through Plasmonic Excitation of Au Nanoparticles. *Nat. Chem.* **2018**, *10* (7), 763–769. https://doi.org/10.1038/s41557-018-0054-3.

(883) Verma, R.; Belgamwar, R.; Polshettiwar, V. Plasmonic Photocatalysis for CO2 Conversion to Chemicals and Fuels. *ACS Mater. Lett.* **2021**, *3* (5), 574–598. https://doi.org/10.1021/acsmaterialslett.1c00081.

(884) Jain, P. K. Taking the Heat Off of Plasmonic Chemistry. *J. Phys. Chem. C* **2019**, *123* (40), 24347–24351. https://doi.org/10.1021/acs.jpcc.9b08143.

(885) Liu, Y.; Bhattarai, P.; Dai, Z.; Chen, X. Photothermal Therapy and Photoacoustic Imaging via Nanotheranostics in Fighting Cancer. *Chem. Soc. Rev.* **2019**, *48* (7), 2053–2108. https://doi.org/10.1039/C8CS00618K.

(886) Huang, X.; El-Sayed, M. A. Plasmonic Photo-Thermal Therapy (PPTT). *Alexandria J. Med.* **2011**, *47* (1), 1–9. https://doi.org/10.1016/j.ajme.2011.01.001.

(887) Hu, Y.; Chi, C.; Wang, S.; Wang, L.; Liang, P.; Liu, F.; Shang, W.; Wang, W.; Zhang, F.; Li, S.; Shen, H.; Yu, X.; Liu, H.; Tian, J. A Comparative Study of Clinical Intervention and Interventional Photothermal Therapy for Pancreatic Cancer. *Adv. Mater.* **2017**, *29* (33), 1700448. https://doi.org/10.1002/adma.201700448.

(888) Pan, D.; Kim, B.; Wang, L. V; Lanza, G. M. A Brief Account of Nanoparticle Contrast Agents for Photoacoustic Imaging. *WIREs Nanomedicine and Nanobiotechnology* **2013**, *5* (6), 517–543. https://doi.org/10.1002/wnan.1231.

(889) Luan, X.; Pan, Y.; Gao, Y.; Song, Y. Recent Near-Infrared Light-Activated Nanomedicine toward Precision Cancer Therapy. *J. Mater. Chem. B* **2021**, *9* (35), 7076–7099. https://doi.org/10.1039/D1TB00671A.

(890) Melamed, J. R.; Edelstein, R. S.; Day, E. S. Elucidating the Fundamental Mechanisms of Cell Death Triggered by Photothermal Therapy. *ACS Nano* **2015**, *9* (1), 6–11. https://doi.org/10.1021/acsnano.5b00021.

(891) Zhang, Y.; Zhan, X.; Xiong, J.; Peng, S.; Huang, W.; Joshi, R.; Cai, Y.; Liu, Y.; Li, R.; Yuan, K.; Zhou, N.;

Min, W. Temperature-Dependent Cell Death Patterns Induced by Functionalized Gold Nanoparticle Photothermal Therapy in Melanoma Cells. *Sci. Rep.* **2018**, *8* (1), 8720. https://doi.org/10.1038/s41598-018-26978-1.

(892) Zhao, H.; Chen, H.; Guo, Z.; Zhang, W.; Yu, H.; Zhuang, Z.; Zhong, H.; Liu, Z. In Situ Photothermal Activation of Necroptosis Potentiates Black Phosphorus-Mediated Cancer Photo-Immunotherapy. *Chem. Eng. J.* **2020**, *394*, 124314. https://doi.org/10.1016/j.cej.2020.124314.

(893) Tang, R.; Xu, J.; Zhang, B.; Liu, J.; Liang, C.; Hua, J.; Meng, Q.; Yu, X.; Shi, S. Ferroptosis, Necroptosis, and Pyroptosis in Anticancer Immunity. *J. Hematol. Oncol.* **2020**, *13* (1), 110. https://doi.org/10.1186/s13045-020-00946-7.

(894) Krysko, O.; Aaes, T. L.; Kagan, V. E.; D'Herde, K.; Bachert, C.; Leybaert, L.; Vandenabeele, P.; Krysko, D. V. Necroptotic Cell Death in Anti-Cancer Therapy. *Immunol. Rev.* **2017**, *280* (1), 207–219. https://doi.org/10.1111/imr.12583.

(895) Moros, M.; Lewinska, A.; Merola, F.; Ferraro, P.; Wnuk, M.; Tino, A.; Tortiglione, C. Gold Nanorods and Nanoprisms Mediate Different Photothermal Cell Death Mechanisms In Vitro and In Vivo. *ACS Appl. Mater. Interfaces* **2020**, *12* (12), 13718–13730. https://doi.org/10.1021/acsami.0c02022.

(896) Ou, L.; Lin, S.; Song, B.; Liu, J.; Lai, R.; Shao, L. The Mechanisms of Graphene-Based Materials-Induced Programmed Cell Death: A Review of Apoptosis, Autophagy, and Programmed Necrosis. *Int. J. Nanomedicine* **2017**, *12*, 6633–6646. https://doi.org/10.2147/IJN.S140526.

(897) Rastinehad, A. R.; Anastos, H.; Wajswol, E.; Winoker, J. S.; Sfakianos, J. P.; Doppalapudi, S. K.; Carrick, M. R.; Knauer, C. J.; Taouli, B.; Lewis, S. C.; Tewari, A. K.; Schwartz, J. A.; Canfield, S. E.; George, A. K.; West, J. L.; Halas, N. J. Gold Nanoshell-Localized Photothermal Ablation of Prostate Tumors in a Clinical Pilot Device Study. *Proc. Natl. Acad. Sci.* **2019**, *116* (37), 18590–18596. https://doi.org/10.1073/PNAS.1906929116.

(898) Thi, T. T.; Suys, E. J. A.; Lee, J. S.; Nguyen, D. H.; Park, K. D.; Truong, N. P. Lipid-Based Nanoparticles in the Clinic and Clinical Trials: From Cancer Nanomedicine to COVID-19 Vaccines. *Vaccines*. 2021.

(899) Dou, Y.; Hynynen, K.; Allen, C. To Heat or Not to Heat: Challenges with Clinical Translation of Thermosensitive Liposomes. *J. Control. Release* **2017**, *249*, 63–73. https://doi.org/10.1016/j.jconrel.2017.01.025.

(900) Kneidl, B.; Peller, M.; Winter, G.; Lindner, L. H.; Hossann, M. Thermosensitive Liposomal Drug Delivery Systems: State of the Art Review. *Int. J. Nanomedicine* **2014**, *9*, 4387–4398. https://doi.org/10.2147/IJN.S49297.

(901) Rengan, A. K.; Jagtap, M.; De, A.; Banerjee, R.; Srivastava, R. Multifunctional Gold Coated Thermo-Sensitive Liposomes for Multimodal Imaging and Photo-Thermal Therapy of Breast Cancer Cells. *Nanoscale* **2014**, *6* (2), 916–923. https://doi.org/10.1039/C3NR04448C.

(902) Liu, X.; Zhang, Y.; Wang, Y.; Zhu, W.; Li, G.; Ma, X.; Zhang, Y.; Chen, S.; Tiwari, S.; Shi, K.; Zhang, S.; Fan, H. M.; Zhao, Y. X.; Liang, X.-J. Comprehensive Understanding of Magnetic Hyperthermia for Improving Antitumor Therapeutic Efficacy. *Theranostics* **2020**, *10* (8), 3793–3815. https://doi.org/10.7150/thno.40805.

(903) Dennis, C. L.; Ivkov, R. Physics of Heat Generation Using Magnetic Nanoparticles for Hyperthermia. *Int. J. Hyperth.* **2013**, *29* (8), 715–729. https://doi.org/10.3109/02656736.2013.836758.

(904) Wahajuddin; Arora, S. Superparamagnetic Iron Oxide Nanoparticles: Magnetic Nanoplatforms as Drug Carriers. *Int. J. Nanomedicine* **2012**, *7*, 3445–3471. https://doi.org/10.2147/IJN.S30320.

(905) Wu, K.; Su, D.; Liu, J.; Saha, R.; Wang, J.-P. Magnetic Nanoparticles in Nanomedicine: A Review of Recent Advances. *Nanotechnology* **2019**, *30* (50), 502003. https://doi.org/10.1088/1361-6528/ab4241.

(906) Kafrouni, L.; Savadogo, O. Recent Progress on Magnetic Nanoparticles for Magnetic Hyperthermia. *Prog.*

Biomater. **2016**, *5* (3), 147–160. https://doi.org/10.1007/s40204-016-0054-6.

(907) Sharma, S. K.; Shrivastava, N.; Rossi, F.; Tung, L. D.; Thanh, N. T. K. Nanoparticles-Based Magnetic and Photo Induced Hyperthermia for Cancer Treatment. *Nano Today* **2019**, *29*, 100795. https://doi.org/10.1016/j.nantod.2019.100795.

(908) Choi, V.; Rajora, M. A.; Zheng, G. Activating Drugs with Sound: Mechanisms Behind Sonodynamic Therapy and the Role of Nanomedicine. *Bioconjug. Chem.* **2020**, *31* (4), 967–989. https://doi.org/10.1021/acs.bioconjchem.0c00029.

(909) Lafond, M.; Yoshizawa, S.; Umemura, S. Sonodynamic Therapy: Advances and Challenges in Clinical Translation. *J. Ultrasound Med.* **2019**, *38* (3), 567–580. https://doi.org/10.1002/jum.14733.

(910) Adir, O.; Poley, M.; Chen, G.; Froim, S.; Krinsky, N.; Shklover, J.; Shainsky-Roitman, J.; Lammers, T.; Schroeder, A. Integrating Artificial Intelligence and Nanotechnology for Precision Cancer Medicine. *Adv. Mater.* **2020**, *32* (13), 1901989. https://doi.org/10.1002/adma.201901989.

(911) Stillman, N. R.; Kovacevic, M.; Balaz, I.; Hauert, S. In Silico Modelling of Cancer Nanomedicine, across Scales and Transport Barriers. *npj Comput. Mater.* **2020**, *6* (1), 92. https://doi.org/10.1038/s41524-020-00366-8.

(912) Tao, H.; Wu, T.; Aldeghi, M.; Wu, T. C.; Aspuru-Guzik, A.; Kumacheva, E. Nanoparticle Synthesis Assisted by Machine Learning. *Nat. Rev. Mater.* **2021**, *6* (8), 701–716. https://doi.org/10.1038/s41578-021-00337-5.

(913) Chen, C.; Yaari, Z.; Apfelbaum, E.; Grodzinski, P.; Shamay, Y.; Heller, D. A. Merging Data Curation and Machine Learning to Improve Nanomedicines. *Adv. Drug Deliv. Rev.* **2022**, *183*, 114172. https://doi.org/10.1016/j.addr.2022.114172.

(914) Florindo, H. F.; Madi, A.; Satchi-Fainaro, R. Challenges in the Implementation of MIRIBEL Criteria on Nanobiomed Manuscripts. *Nat. Nanotechnol.* **2019**, *14* (7), 627–628. https://doi.org/10.1038/s41565-019-0498-7.

(915) Chetwynd, A. J.; Wheeler, K. E.; Lynch, I. Best Practice in Reporting Corona Studies: Minimum Information about Nanomaterial Biocorona Experiments (MINBE). *Nano Today* **2019**, *28*, 100758. https://doi.org/10.1016/j.nantod.2019.06.004.

(916) Poon, W.; Kingston, B. R.; Ouyang, B.; Ngo, W.; Chan, W. C. W. A Framework for Designing Delivery Systems. *Nat. Nanotechnol.* **2020**, *15* (10), 819–829. https://doi.org/10.1038/s41565-020-0759-5.

(917) Ban, Z.; Yuan, P.; Yu, F.; Peng, T.; Zhou, Q.; Hu, X. Machine Learning Predicts the Functional Composition of the Protein Corona and the Cellular Recognition of Nanoparticles. *Proc. Natl. Acad. Sci.* **2020**, *117* (19), 10492–10499. https://doi.org/10.1073/pnas.1919755117.

(918) Boehnke, N.; Straehla, J. P.; Safford, H. C.; Kocak, M.; Rees, M. G.; Ronan, M.; Rosenberg, D.; Adelmann, C. H.; Chivukula, R. R.; Nabar, N.; Berger, A. G.; Lamson, N. G.; Cheah, J. H.; Li, H.; Roth, J. A.; Koehler, A. N.; Hammond, P. T. Massively Parallel Pooled Screening Reveals Genomic Determinants of Nanoparticle Delivery. *Science (80-.).* **2022**, *377* (6604), eabm5551. https://doi.org/10.1126/science.abm5551.

(919) Singh, A. V.; Ansari, M. H. D.; Rosenkranz, D.; Maharjan, R. S.; Kriegel, F. L.; Gandhi, K.; Kanase, A.; Singh, R.; Laux, P.; Luch, A. Artificial Intelligence and Machine Learning in Computational Nanotoxicology: Unlocking and Empowering Nanomedicine. *Adv. Healthc. Mater.* **2020**, *9* (17), 1901862. https://doi.org/10.1002/adhm.201901862.

(920) Baskar, R.; Lee, K. A.; Yeo, R.; Yeoh, K. W. Cancer and Radiation Therapy: Current Advances and Future Directions. *Int. J. Med. Sci.* **2012**, *9* (3), 193–199. https://doi.org/10.7150/ijms.3635.

(921) McKelvey, K. J.; Hudson, A. L.; Back, M.; Eade, T.; Diakos, C. I. Radiation, Inflammation and the Immune Response in Cancer. *Mamm. Genome* **2018**, *29* (11), 843–865. https://doi.org/10.1007/s00335-018-9777-0.

(922) Yin, M.; Liu, X.; Lei, Z.; Gao, Y.; Liu, J.; Tian, S.; Liang, Z.; Wang, Y.; Meng, F.; Luo, L. Precisely Translating Computed Tomography Diagnosis Accuracy into Therapeutic Intervention by a Carbon-Iodine Conjugated Polymer. *Nat. Commun.* **2022**, *13* (1), 2625. https://doi.org/10.1038/s41467-022-30263-1.

(923) Solbak, M. S.; Henning, M. K.; England, A.; Martinsen, A. C.; Aaløkken, T. M.; Johansen, S. Impact of Iodine Concentration and Scan Parameters on Image Quality, Contrast Enhancement and Radiation Dose in Thoracic CT. *Eur. Radiol. Exp.* **2020**, *4* (1), 57. https://doi.org/10.1186/s41747-020-00184-z.

(924) Kweon, S.; Lee, H.-J.; Hyung, W. J.; Suh, J.; Lim, J. S.; Lim, S.-J. Liposomes Coloaded with Iopamidol/Lipiodol as a RES-Targeted Contrast Agent for Computed Tomography Imaging. *Pharm. Res.* **2010**, *27* (7), 1408–1415. https://doi.org/10.1007/s11095-010-0135-5.

(925) Hainfeld, J. F.; Ridwan, S. M.; Stanishevskiy, Y.; Smilowitz, N. R.; Davis, J.; Smilowitz, H. M. Small, Long Blood Half-Life Iodine Nanoparticle for Vascular and Tumor Imaging. *Sci. Rep.* **2018**, *8* (1), 13803. https://doi.org/10.1038/s41598-018-31940-2.

(926) Morozov, V. N.; Belousov, A. V; Zverev, V. I.; Shtil, A. A.; Kolyvanova, M. A.; Krivoshapkin, P. V. The Prospects of Metal Oxide Nanoradiosensitizers: The Effect of the Elemental Composition of Particles and Characteristics of Radiation Sources on Enhancement of the Adsorbed Dose. *Biophysics (Oxf).* **2020**, *65* (4), 533–540. https://doi.org/10.1134/S0006350920040107.

(927) Chan, W. C. W. Nanomedicine 2.0. *Acc. Chem. Res.* **2017**, *50* (3), 627–632. https://doi.org/10.1021/acs.accounts.6b00629.

(928) Howard, K. A. Nanomedicine: Working Towards Defining the Field BT - Nanomedicine; Howard, K. A., Vorup-Jensen, T., Peer, D., Eds.; Springer New York: New York, NY, 2016; pp 1–12. https://doi.org/10.1007/978-1-4939-3634-2_1.

(929) Chen, Y.; Yang, J.; Fu, S.; Wu, J. Gold Nanoparticles as Radiosensitizers in Cancer Radiotherapy. *Int. J. Nanomedicine* **2020**, *15*, 9407–9430. https://doi.org/10.2147/IJN.S272902.

(930) McMahon, S. J.; Hyland, W. B.; Muir, M. F.; Coulter, J. A.; Jain, S.; Butterworth, K. T.; Schettino, G.; Dickson, G. R.; Hounsell, A. R.; O'Sullivan, J. M.; Prise, K. M.; Hirst, D. G.; Currell, F. J. Biological Consequences of Nanoscale Energy Deposition near Irradiated Heavy Atom Nanoparticles. *Sci. Rep.* **2011**, *1*. https://doi.org/10.1038/srep00018.

(931) Sharifi, M.; Attar, F.; Saboury, A. A.; Akhtari, K.; Hooshmand, N.; Hasan, A.; El-Sayed, M. A.; Falahati, M. Plasmonic Gold Nanoparticles: Optical Manipulation, Imaging, Drug Delivery and Therapy. *J. Control. Release* **2019**, *311–312*, 170–189. https://doi.org/10.1016/j.jconrel.2019.08.032.

(932) Xiong, W.; Mazid, R.; Yap, L. W.; Li, X.; Cheng, W. Plasmonic Caged Gold Nanorods for Near-Infrared Light Controlled Drug Delivery. *Nanoscale* **2014**, *6* (23), 14388–14393. https://doi.org/10.1039/C4NR04400B.

(933) Liu, J.; Detrembleur, C.; De Pauw-Gillet, M.-C.; Mornet, S.; Jérôme, C.; Duguet, E. Gold Nanorods Coated with Mesoporous Silica Shell as Drug Delivery System for Remote Near Infrared Light-Activated Release and Potential Phototherapy. *Small* **2015**, *11* (19), 2323–2332. https://doi.org/10.1002/smll.201402145.

(934) Troutman, T. S.; Barton, J. K.; Romanowski, M. Biodegradable Plasmon Resonant Nanoshells. *Adv. Mater.* **2008**, *20* (13), 2604–2608. https://doi.org/10.1002/adma.200703026.

(935) Leung, S. J.; Troutman, T. S.; Romanowski, M. Plasmon Resonant Gold-Coated Liposomes for Spectrally Coded Content Release. In *Proc.SPIE*; 2009; Vol. 7190. https://doi.org/10.1117/12.808315.

(936) Troutman, T. S.; Leung, S. J.; Romanowski, M. Light-Induced Content Release from Plasmon-Resonant Liposomes. *Adv. Mater.* **2009**, *21* (22), 2334–2338. https://doi.org/10.1002/adma.200900018.

(937) Sugikawa, K.; Kadota, T.; Yasuhara, K.; Ikeda, A. Anisotropic Self-Assembly of Citrate-Coated Gold Nanoparticles on Fluidic Liposomes. *Angew. Chemie Int. Ed.* **2016**, *55* (12), 4059–4063. https://doi.org/10.1002/anie.201511785.

(938) Jin, Y.; Gao, X. Spectrally Tunable Leakage-Free Gold Nanocontainers. *J. Am. Chem. Soc.* **2009**, *131* (49), 17774–17776. https://doi.org/10.1021/ja9076765.

(939) Leung, S. J.; Romanowski, M. NIR-Activated Content Release from Plasmon Resonant Liposomes for Probing Single-Cell Responses. *ACS Nano* **2012**, *6* (11), 9383–9391. https://doi.org/10.1021/nn304434a.

(940) Luo, L.; Bian, Y.; Liu, Y.; Zhang, X.; Wang, M.; Xing, S.; Li, L.; Gao, D. Combined Near Infrared Photothermal Therapy and Chemotherapy Using Gold Nanoshells Coated Liposomes to Enhance Antitumor Effect. *Small* **2016**, *12* (30), 4103–4112. https://doi.org/10.1002/smll.201503961.

(941) Leung, S. J.; Kachur, X. M.; Bobnick, M. C.; Romanowski, M. Wavelength-Selective Light-Induced Release from Plasmon Resonant Liposomes. *Adv. Funct. Mater.* **2011**, *21* (6), 1113–1121. https://doi.org/10.1002/adfm.201002373.

(942) Wang, M.; Liu, Y.; Zhang, X.; Luo, L.; Li, L.; Xing, S.; He, Y.; Cao, W.; Zhu, R.; Gao, D. Gold Nanoshell Coated Thermo-PH Dual Responsive Liposomes for Resveratrol Delivery and Chemo-Photothermal Synergistic Cancer Therapy. *J. Mater. Chem. B* **2017**, *5* (11), 2161–2171. https://doi.org/10.1039/C7TB00258K.

(943) Knights-Mitchell, S. S.; Romanowski, M. Near-Infrared Activated Release of Doxorubicin from Plasmon Resonant Liposomes. *Nanotheranostics* **2018**, *2* (4), 295–305. https://doi.org/10.7150/ntno.22544.

(944) Wang, S.; Xin, J.; Zhang, L.; Zhou, Y.; Yao, C.; Wang, B.; Wang, J.; Zhang, Z. Cantharidin-Encapsulated Thermal-Sensitive Liposomes Coated with Gold Nanoparticles for Enhanced Photothermal Therapy on A431 Cells. *Int. J. Nanomedicine* **2018**, *13*, 2143–2160. https://doi.org/10.2147/IJN.S156240.

(945) Singh, S. P.; Alvi, S. B.; Pemmaraju, D. B.; Singh, A. D.; Manda, S. V.; Srivastava, R.; Rengan, A. K. NIR Triggered Liposome Gold Nanoparticles Entrapping Curcumin as in Situ Adjuvant for Photothermal Treatment of Skin Cancer. *Int. J. Biol. Macromol.* **2018**, *110*, 375–382. https://doi.org/10.1016/j.ijbiomac.2017.11.163.

(946) Oh, J.; Yoon, H.-J.; Park, J.-H. Plasmonic Liposomes for Synergistic Photodynamic and Photothermal Therapy. *J. Mater. Chem. B* **2014**, *2* (17), 2592–2597. https://doi.org/10.1039/C3TB21452D.

(947) Koga, K.; Tagami, T.; Ozeki, T. Gold Nanoparticle-Coated Thermosensitive Liposomes for the Triggered Release of Doxorubicin, and Photothermal Therapy Using a near-Infrared Laser. *Colloids Surfaces A Physicochem. Eng. Asp.* **2021**, *626*, 127038. https://doi.org/10.1016/j.colsurfa.2021.127038.

(948) Rengan, A. K.; Bukhari, A. B.; Pradhan, A.; Malhotra, R.; Banerjee, R.; Srivastava, R.; De, A. In Vivo Analysis of Biodegradable Liposome Gold Nanoparticles as Efficient Agents for Photothermal Therapy of Cancer. *Nano Lett.* **2015**, *15* (2), 842–848. https://doi.org/10.1021/nl5045378.

(949) Li, X.; Hirsh, D. J.; Cabral-Lilly, D.; Zirkel, A.; Gruner, S. M.; Janoff, A. S.; Perkins, W. R. Doxorubicin Physical State in Solution and inside Liposomes Loaded via a PH Gradient. *Biochim. Biophys. Acta - Biomembr.* **1998**, *1415* (1), 23–40. https://doi.org/10.1016/S0005-2736(98)00175-8.

(950) Zheng, J.; Perkins, G.; Kirilova, A.; Allen, C.; Jaffray, D. A. Multimodal Contrast Agent for Combined Computed Tomography and Magnetic Resonance Imaging Applications. *Invest. Radiol.* **2006**, *41* (3). https://doi.org/10.1097/01.rli.0000186568.50265.64.

(951) Delama, A.; Teixeira, M. I.; Dorati, R.; Genta, I.; Conti, B.; Lamprou, D. A. Microfluidic Encapsulation Method to Produce Stable Liposomes Containing Iohexol. *J. Drug Deliv. Sci. Technol.* **2019**, *54*, 101340. https://doi.org/10.1016/j.jddst.2019.101340.

(952) Yang, S.; Zhu, W.; Wang, Z.; Xiao, Y.; Mao, P.; Qu, L.; Hu, Y.; Wang, J. Thermosensitive Liposomes Encapsulating Anti-Cancer Agent Lomustine, and Contrast Medium Iohexol, for Thermochemotherapy: Preparation, Characterization, and In Vivo Evaluation. *J. Nanosci. Nanotechnol.* **2020**, *20* (10), 6070–6076. https://doi.org/10.1166/jnn.2020.18590.

(953) El Assri, S.; Sam, H.; El Assri, A.; Bentata, Y.; Saalaoui, E.; Rochdi, C.; Sebbar, E.-H.; Choukri, M. Iohexol

Assay for Direct Determination of Glomerular Filtration Rate: Optimization and Development of an HPLC-UV Method for Measurement in Serum and Urine. *Clin. Chim. Acta* **2020**, *508*, 115–121. https://doi.org/10.1016/j.cca.2020.04.038.

(954) Drazenovic, J.; Wang, H.; Roth, K.; Zhang, J.; Ahmed, S.; Chen, Y.; Bothun, G.; Wunder, S. L. Effect of Lamellarity and Size on Calorimetric Phase Transitions in Single Component Phosphatidylcholine Vesicles. *Biochim. Biophys. Acta - Biomembr.* **2015**, *1848* (2), 532–543. https://doi.org/10.1016/j.bbamem.2014.10.003.

(955) Tournebize, J.; Sapin-Minet, A.; Bartosz, G.; Leroy, P.; Boudier, A. Pitfalls of Assays Devoted to Evaluation of Oxidative Stress Induced by Inorganic Nanoparticles. *Talanta* **2013**, *116*, 753–763. https://doi.org/10.1016/j.talanta.2013.07.077.

(956) Stepanenko, A. A.; Dmitrenko, V. V. Pitfalls of the MTT Assay: Direct and off-Target Effects of Inhibitors Can Result in over/Underestimation of Cell Viability. *Gene* **2015**, *574* (2), 193–203. https://doi.org/10.1016/j.gene.2015.08.009.

(957) Rai, Y.; Pathak, R.; Kumari, N.; Sah, D. K.; Pandey, S.; Kalra, N.; Soni, R.; Dwarakanath, B. S.; Bhatt, A. N. Mitochondrial Biogenesis and Metabolic Hyperactivation Limits the Application of MTT Assay in the Estimation of Radiation Induced Growth Inhibition. *Sci. Rep.* **2018**, *8* (1), 1531. https://doi.org/10.1038/s41598-018-19930-w.

(958) Podgórski, R.; Wojasiński, M.; Ciach, T. Nanofibrous Materials Affect the Reaction of Cytotoxicity Assays. *Sci. Rep.* **2022**, *12* (1), 9047. https://doi.org/10.1038/s41598-022-13002-w.

(959) Orsinger, G. V; Williams, J. D.; Romanowski, M. Intracellular Light-Induced Release of Signaling Molecules from Gold-Coated Liposomes. In *Proc.SPIE*; 2014; Vol. 8955. https://doi.org/10.1117/12.2040854.

(960) Wee, T. I.; Jeon, Y. W.; Cho, Y. J.; Cho, S. K.; Ha, J.; Lee, J. W.; Cho, S. H.; Han, H. D.; Shin, B. C. Preparation of Gold Coated Liposomes for CT Contrast Medium. *J. Korean Chem. Soc.* **2013**, *57* (5), 634–639.

(961) Bernstein, A. L.; Dhanantwari, A.; Jurcova, M.; Cheheltani, R.; Naha, P. C.; Ivanc, T.; Shefer, E.; Cormode, D. P. Improved Sensitivity of Computed Tomography towards Iodine and Gold Nanoparticle Contrast Agents via Iterative Reconstruction Methods. *Sci. Rep.* **2016**, *6* (1), 26177. https://doi.org/10.1038/srep26177.

(962) Xu, C.; Tung, G. A.; Sun, S. Size and Concentration Effect of Gold Nanoparticles on X-Ray Attenuation As Measured on Computed Tomography. *Chem. Mater.* **2008**, *20* (13), 4167–4169. https://doi.org/10.1021/cm8008418.

(963) Chen, Z.; Li, Y.; Airan, R.; Han, Z.; Xu, J.; Chan, K. W. Y.; Xu, Y.; Bulte, J. W. M.; van Zijl, P. C. M.; McMahon, M. T.; Zhou, S.; Liu, G. CT and CEST MRI Bimodal Imaging of the Intratumoral Distribution of Iodinated Liposomes. *Quant. Imaging Med. Surg.* **2019**, *9* (9), 1579–1591. https://doi.org/10.21037/qims.2019.06.10.

(964) Mukundan, S. J.; Ghaghada, K. B.; Badea, C. T.; Kao, C.-Y.; Hedlund, L. W.; Provenzale, J. M.; Johnson, G. A.; Chen, E.; Bellamkonda, R. V; Annapragada, A. A Liposomal Nanoscale Contrast Agent for Preclinical CT in Mice. *AJR. Am. J. Roentgenol.* **2006**, *186* (2), 300–307. https://doi.org/10.2214/AJR.05.0523.

(965) Bromma, K.; Cicon, L.; Beckham, W.; Chithrani, D. B. Gold Nanoparticle Mediated Radiation Response among Key Cell Components of the Tumour Microenvironment for the Advancement of Cancer Nanotechnology. *Sci. Rep.* **2020**, *10* (1), 12096. https://doi.org/10.1038/s41598-020-68994-0.

(966) Pansare, K.; Raj Singh, S.; Chakravarthy, V.; Gupta, N.; Hole, A.; Gera, P.; Sarin, R.; Murali Krishna, C. Raman Spectroscopy: An Exploratory Study to Identify Post-Radiation Cell Survival. *Appl. Spectrosc.* **2020**, *74* (5), 553–562. https://doi.org/10.1177/0003702820908352.

(967) Andreucci, M.; Faga, T.; Serra, R.; De Sarro, G.; Michael, A. Update on the Renal Toxicity of Iodinated Contrast Drugs Used in Clinical Medicine. *Drug. Healthc. Patient Saf.* **2017**, *9*, 25–37. https://doi.org/10.2147/DHPS.S122207.

(968) Wang, Y.; Ren, K.; Xie, L.; Sun, W.; Liu, Y.; Li, S. Effect of Repeated Injection of Iodixanol on Renal Function in Healthy Wistar Rats Using Functional MRI. *Biomed Res. Int.* **2018**, *2018*, 7272485. https://doi.org/10.1155/2018/7272485.

(969) Sadat, U. Radiographic Contrast-Media-Induced Acute Kidney Injury: Pathophysiology and Prophylactic Strategies. *ISRN Radiol.* **2013**, *2013*, 496438. https://doi.org/10.5402/2013/496438.

(970) Anik, M. I.; Mahmud, N.; Al Masud, A.; Hasan, M. Gold Nanoparticles (GNPs) in Biomedical and Clinical Applications: A Review. *Nano Sel.* **2022**, *3* (4), 792–828. https://doi.org/10.1002/nano.202100255.

(971) Danila, D.; Partha, R.; Elrod, D. B.; Lackey, M.; Casscells, S. W.; Conyers, J. L. Antibody-Labeled Liposomes for CT Imaging of Atherosclerotic Plaques: In Vitro Investigation of an Anti-ICAM Antibody-Labeled Liposome Containing Iohexol for Molecular Imaging of Atherosclerotic Plaques via Computed Tomography. *Texas Hear. Inst. J.* **2009**, *36* (5), 393–403.

(972) Lou, D.; Tian, Y.; Zhang, Y.; Yin, J.; Yang, T.; He, C.; Ma, M.; Yu, W.; Gu, N. Peroxidase-Like Activity of Gold Nanoparticles and Their Gold Staining Enhanced ELISA Application. *J. Nanosci. Nanotechnol.* **2018**, *18* (2), 951–958. https://doi.org/10.1166/jnn.2018.13977.

(973) Fasoli, E. Protein Corona: Dr. Jekyll and Mr. Hyde of Nanomedicine. *Biotechnol. Appl. Biochem.* **2021**, *68* (6), 1139–1152. https://doi.org/10.1002/bab.2035.

(974) Kobos, L.; Shannahan, J. Biocorona-Induced Modifications in Engineered Nanomaterial–Cellular Interactions Impacting Biomedical Applications. *WIREs Nanomedicine and Nanobiotechnology* **2020**, *12* (3), e1608. https://doi.org/10.1002/wnan.1608.

(975) Guan, J.; Shen, Q.; Zhang, Z.; Jiang, Z.; Yang, Y.; Lou, M.; Qian, J.; Lu, W.; Zhan, C. Enhanced Immunocompatibility of Ligand-Targeted Liposomes by Attenuating Natural IgM Absorption. *Nat. Commun.* **2018**, *9* (1), 2982. https://doi.org/10.1038/s41467-018-05384-1.

(976) Dos Santos, N.; Allen, C.; Doppen, A.-M.; Anantha, M.; Cox, K. A. K.; Gallagher, R. C.; Karlsson, G.; Edwards, K.; Kenner, G.; Samuels, L.; Webb, M. S.; Bally, M. B. Influence of Poly(Ethylene Glycol) Grafting Density and Polymer Length on Liposomes: Relating Plasma Circulation Lifetimes to Protein Binding. *Biochim. Biophys. Acta - Biomembr.* **2007**, *1768* (6), 1367–1377. https://doi.org/10.1016/j.bbamem.2006.12.013.

(977) Nakhaei, P.; Margiana, R.; Bokov, D. O.; Abdelbasset, W. K.; Jadidi Kouhbanani, M. A.; Varma, R. S.; Marofi, F.; Jarahian, M.; Beheshtkhoo, N. Liposomes: Structure, Biomedical Applications, and Stability Parameters With Emphasis on Cholesterol. *Front. Bioeng. Biotechnol.* **2021**, *9*. https://doi.org/10.3389/fbioe.2021.705886.

(978) Dizon, D. S.; Hensley, M. L.; Poynor, E. A.; Sabbatini, P.; Aghajanian, C.; Hummer, A.; Venkatraman, E.; Spriggs, D. R. Retrospective Analysis of Carboplatin and Paclitaxel as Initial Second-Line Therapy for Recurrent Epithelial Ovarian Carcinoma: Application toward a Dynamic Disease State Model of Ovarian Cancer. *J. Clin. Oncol.* **2002**, *20* (5), 1238–1247. https://doi.org/10.1200/JCO.2002.20.5.1238.

(979) Pienta, K. J.; Partin, A. W.; Coffey, D. S. Cancer as a Disease of DNA Organization and Dynamic Cell Structure. *Cancer Res.* **1989**, *49* (10), 2525–2532.

(980) Wang, M.; Wang, D.; Chen, Q.; Li, C.; Li, Z.; Lin, J. Recent Advances in Glucose-Oxidase-Based Nanocomposites for Tumor Therapy. *Small* **2019**, *15* (51), 1903895. https://doi.org/10.1002/smll.201903895.

(981) Fu, L.-H.; Qi, C.; Lin, J.; Huang, P. Catalytic Chemistry of Glucose Oxidase in Cancer Diagnosis and Treatment. *Chem. Soc. Rev.* **2018**, *47* (17), 6454–6472. https://doi.org/10.1039/C7CS00891K.

(982) Gao, P.; Shi, M.; Wei, R.; Pan, W.; Liu, X.; Li, N.; Tang, B. A Biomimetic MOF Nanoreactor Enables Synergistic Suppression of Intracellular Defense Systems for Augmented Tumor Ablation. *Chem. Commun.* **2020**, *56* (6), 924–927. https://doi.org/10.1039/C9CC08498C.

(983) Yu, Z.; Zhou, P.; Pan, W.; Li, N.; Tang, B. A Biomimetic Nanoreactor for Synergistic Chemiexcited Photodynamic Therapy and Starvation Therapy Against Tumor Metastasis. *Nat. Commun.* **2018**, *9* (1), 5044. https://doi.org/10.1038/s41467-018-07197-8.

(984) Bubici, C.; Papa, S. Editorial: The Warburg Effect Regulation Under Siege: The Intertwined Pathways in Health and Disease. *Front. Cell Dev. Biol.* **2019**, *7*, 80. https://doi.org/10.3389/fcell.2019.00080.

(985) Denko, N. C. Hypoxia, HIF1 and Glucose Metabolism in the Solid Tumour. *Nat. Rev. Cancer* **2008**, *8* (9), 705–713. https://doi.org/10.1038/nrc2468.

(986) Vander Heiden, M. G.; Cantley, L. C.; Thompson, C. B. Understanding the Warburg Effect: The Metabolic Requirements of Cell Proliferation. *Science* **2009**, *324* (5930), 1029–1033. https://doi.org/10.1126/science.1160809.

(987) Carrier, A.; Nganou, C.; Oakley, D.; Chen, Y.; Oakes, K.; MacQuarrie, S.; Zhang, X. Selective Generation of Singlet Oxygen in Chloride Accelerated Copper Fenton Chemistry. *ChemRxiv* **2018**. https://doi.org/10.26434/chemrxiv.7364225.v1.

(988) Carrier, A.; Hamid, S.; Oakley, D.; Oakes, K.; Zhang, X. Singlet Oxygen Generation in Classical Fenton Chemistry. *ChemRxiv* **2019**. https://doi.org/10.26434/chemrxiv.7730654.v1.

(989) Huo, M.; Wang, L.; Chen, Y.; Shi, J. Tumor-Selective Catalytic Nanomedicine by Nanocatalyst Delivery. *Nat. Commun.* **2017**, *8* (1), 357. https://doi.org/10.1038/s41467-017-00424-8.

(990) Zhang, C.; Zhang, L.; Wu, W.; Gao, F.; Li, R.-Q.; Song, W.; Zhuang, Z.-N.; Liu, C.-J.; Zhang, X.-Z. Artificial Super Neutrophils for Inflammation Targeting and HClO Generation against Tumors and Infections. *Adv. Mater.* **2019**, *31* (19), e1901179. https://doi.org/10.1002/adma.201901179.

(991) Fan, W.; Lu, N.; Huang, P.; Liu, Y.; Yang, Z.; Wang, S.; Yu, G.; Liu, Y.; Hu, J.; He, Q.; Qu, J.; Wang, T.; Chen, X. Glucose-Responsive Sequential Generation of Hydrogen Peroxide and Nitric Oxide for Synergistic Cancer Starving-Like/Gas Therapy. *Angew. Chemie Int. Ed.* **2017**, *56* (5), 1229–1233. https://doi.org/10.1002/anie.201610682.

(992) Wang, C.; Yang, J.; Dong, C.; Shi, S. Glucose Oxidase-Related Cancer Therapies. *Adv. Ther.* **2020**, *3* (10), 2000110. https://doi.org/10.1002/adtp.202000110.

(993) Li, S.-Y.; Cheng, H.; Xie, B.-R.; Qiu, W.-X.; Zeng, J.-Y.; Li, C.-X.; Wan, S.-S.; Zhang, L.; Liu, W.-L.; Zhang, X.-Z. Cancer Cell Membrane Camouflaged Cascade Bioreactor for Cancer Targeted Starvation and Photodynamic Therapy. *ACS Nano* **2017**, *11* (7), 7006–7018. https://doi.org/10.1021/acsnano.7b02533.

(994) Bonifert, G.; Folkes, L.; Gmeiner, C.; Dachs, G.; Spadiut, O. Recombinant Horseradish Peroxidase Variants for Targeted Cancer Treatment. *Cancer Med.* **2016**, *5* (6), 1194–1203. https://doi.org/10.1002/cam4.668.

(995) Tan, H.; Guo, S.; Dinh, N.-D.; Luo, R.; Jin, L.; Chen, C.-H. Heterogeneous Multi-Compartmental Hydrogel Particles as Synthetic Cells for Incompatible Tandem Reactions. *Nat. Commun.* **2017**, *8* (1), 663. https://doi.org/10.1038/s41467-017-00757-4.

(996) Xiang, H.; Feng, W.; Chen, Y. Single-Atom Catalysts in Catalytic Biomedicine. *Adv. Mater.* **2020**, *32* (8), 1905994. https://doi.org/10.1002/adma.201905994.

(997) Yang, B.; Ding, L.; Yao, H.; Chen, Y.; Shi, J. A Metal-Organic Framework (MOF) Fenton Nanoagent-Enabled Nanocatalytic Cancer Therapy in Synergy with Autophagy Inhibition. *Adv. Mater.* **2020**, *32* (12), 1907152. https://doi.org/10.1002/adma.201907152.

(998) Zhou, J.; Li, M.; Hou, Y.; Luo, Z.; Chen, Q.; Cao, H.; Huo, R.; Xue, C.; Sutrisno, L.; Hao, L.; Cao, Y.; Ran, H.; Lu, L.; Li, K.; Cai, K. Engineering of a Nanosized Biocatalyst for Combined Tumor Starvation and Low-Temperature Photothermal Therapy. *ACS Nano* **2018**, *12* (3), 2858–2872.

https://doi.org/10.1021/acsnano.8b00309.

(999) Fu, L.-H.; Hu, Y.-R.; Qi, C.; He, T.; Jiang, S.; Jiang, C.; He, J.; Qu, J.; Lin, J.; Huang, P. Biodegradable Manganese-Doped Calcium Phosphate Nanotheranostics for Traceable Cascade Reaction-Enhanced Anti-Tumor Therapy. *ACS Nano* **2019**, *13* (12), 13985–13994. https://doi.org/10.1021/acsnano.9b05836.

(1000) Zhang, Y.; Yang, Y.; Jiang, S.; Li, F.; Lin, J.; Wang, T.; Huang, P. Degradable Silver-Based Nanoplatform for Synergistic Cancer Starving-like/Metal Ion Therapy. *Mater. Horizons* **2019**, *6* (1), 169–175. https://doi.org/10.1039/C8MH00908B.

(1001) Zhang, Y.; Wang, F.; Liu, C.; Wang, Z.; Kang, L.; Huang, Y.; Dong, K.; Ren, J.; Qu, X. Nanozyme Decorated Metal–Organic Frameworks for Enhanced Photodynamic Therapy. *ACS Nano* **2018**, *12* (1), 651–661. https://doi.org/10.1021/acsnano.7b07746.

(1002) Zhang, Y.-H.; Qiu, W.-X.; Zhang, M.; Zhang, L.; Zhang, X.-Z. MnO2 Motor: A Prospective Cancer-Starving Therapy Promoter. *ACS Appl. Mater. Interfaces* **2018**, *10* (17), 15030–15039. https://doi.org/10.1021/acsami.8b01818.

(1003) Feng, L.; Xie, R.; Wang, C.; Gai, S.; He, F.; Yang, D.; Yang, P.; Lin, J. Magnetic Targeting, Tumor Microenvironment-Responsive Intelligent Nanocatalysts for Enhanced Tumor Ablation. *ACS Nano* **2018**, *12* (11), 11000–11012. https://doi.org/10.1021/acsnano.8b05042.

(1004) Dong, L.; Li, K.; Wen, D.; Lu, Y.; Du, K.; Zhang, M.; Gao, X.; Feng, J.; Zhang, H. A Highly Active (102) Surface-Induced Rapid Fegradation of a CuS Nanotheranostic Platform for in Situ T1-Weighted Magnetic Resonance Imaging-Guided Synergistic Therapy. *Nanoscale* **2019**, *11* (27), 12853–12857. https://doi.org/10.1039/C9NR03830B.

(1005) Li, Y.; Lu, W.; Huang, Q.; Li, C.; Chen, W. Copper Sulfide Nanoparticles for Photothermal Ablation of Tumor Cells. *Nanomedicine* **2010**, *5* (8), 1161–1171. https://doi.org/10.2217/nnm.10.85.

(1006) Wang, S.; Riedinger, A.; Li, H.; Fu, C.; Liu, H.; Li, L.; Liu, T.; Tan, L.; Barthel, M. J.; Pugliese, G.; De Donato, F.; Scotto D'Abbusco, M.; Meng, X.; Manna, L.; Meng, H.; Pellegrino, T. Plasmonic Copper Sulfide Nanocrystals Exhibiting Near-Infrared Photothermal and Photodynamic Therapeutic Effects. *ACS Nano* **2015**, *9* (2), 1788–1800. https://doi.org/10.1021/nn506687t.

(1007) Ku, G.; Zhou, M.; Song, S.; Huang, Q.; Hazle, J.; Li, C. Copper Sulfide Nanoparticles As a New Class of Photoacoustic Contrast Agent for Deep Tissue Imaging at 1064 Nm. *ACS Nano* **2012**, *6* (8), 7489–7496. https://doi.org/10.1021/nn302782y.

(1008) Yi, X.; Chen, L.; Chen, J.; Maiti, D.; Chai, Z.; Liu, Z.; Yang, K. Biomimetic Copper Sulfide for Chemo-Radiotherapy: Enhanced Uptake and Reduced Efflux of Nanoparticles for Tumor Cells under Ionizing Radiation. *Adv. Funct. Mater.* **2018**, *28* (9), 1705161. https://doi.org/10.1002/adfm.201705161.

(1009) Shan, Z.; Lu, M.; Wang, L.; MacDonald, B.; MacInnis, J.; Mkandawire, M.; Zhang, X.; Oakes, K. D. Chloride Accelerated Fenton Chemistry for the Ultrasensitive and Selective Colorimetric Detection of Copper. *Chem. Commun.* **2016**, *52* (10), 2087–2090. https://doi.org/10.1039/C5CC07446K.

(1010) Wang, L.; Miao, Y.; Lu, M.; Shan, Z.; Lu, S.; Hou, J.; Yang, Q.; Liang, X.; Zhou, T.; Curry, D.; Oakes, K.; Zhang, X. Chloride-Accelerated Cu-Fenton Chemistry for Biofilm Removal. *Chem. Commun.* **2017**, *53* (43), 5862–5865. https://doi.org/10.1039/C7CC00928C.

(1011) Li, Y.; Zhao, J.; Shang, E.; Xia, X.; Niu, J.; Crittenden, J. Effects of Chloride Ions on Dissolution, ROS Generation, and Toxicity of Silver Nanoparticles under UV Irradiation. *Environ. Sci. Technol.* **2018**, *52* (8), 4842–4849. https://doi.org/10.1021/acs.est.7b04547.

(1012) Choudhary, V. R.; Samanta, C. Role of Chloride or Bromide Anions and Protons for Promoting the Selective Oxidation of H2 by O2 to H2O2 over Supported Pd Catalysts in an Aqueous Medium. *J. Catal.* **2006**, *238* (1), 28–38. https://doi.org/10.1016/j.jcat.2005.11.024.

(1013) Raineri, M.; Winkler, E. L.; Torres, T. E.; Vasquez Mansilla, M.; Nadal, M. S.; Zysler, R. D.; Lima, E.

Effects of Biological Buffer Solutions on the Peroxidase-like Catalytic Activity of Fe3O4 Nanoparticles. *Nanoscale* **2019**, *11* (39), 18393–18406. https://doi.org/10.1039/C9NR05799D.

(1014) Chen, L.; Hu, H.; Chen, Y.; Gao, J.; Li, G. Plasmonic Cu2−xS Nanoparticles: A Brief Introduction of Optical Properties and Applications. *Mater. Adv.* **2021**, *2* (3), 907–926. https://doi.org/10.1039/D0MA00837K.

(1015) Nichela, D. A.; Berkovic, A. M.; Costante, M. R.; Juliarena, M. P.; García Einschlag, F. S. Nitrobenzene Degradation in Fenton-like Systems Using Cu(II) as Catalyst. Comparison between Cu(II)- and Fe(III)-Based Systems. *Chem. Eng. J.* **2013**, *228*, 1148–1157. https://doi.org/10.1016/j.cej.2013.05.002.

(1016) Gao, W.; Sun, Y.; Cai, M.; Zhao, Y.; Cao, W.; Liu, Z.; Cui, G.; Tang, B. Copper Sulfide Nanoparticles as a Photothermal Switch for TRPV1 Signaling to Attenuate Atherosclerosis. *Nat. Commun.* **2018**, *9* (1), 1–10. https://doi.org/10.1038/s41467-017-02657-z.

(1017) Liu, Y.; Jin, H.; Zou, W.; Guo, R. Protein-Mediated Sponge-like Copper Sulfide as an Ingenious and Efficient Peroxidase Mimic for Colorimetric Glucose Sensing. *RSC Adv.* **2020**, *10* (48), 28819–28826. https://doi.org/10.1039/D0RA05496H.

(1018) Gullino, P. M.; Clark, S. H.; Grantham, F. H. The Interstitial Fluid Of Solid Tumors. *Cancer Res.* **1964**, *24*, 780–794.

(1019) Chakraborty, K.; Leung, K.; Krishnan, Y. High Lumenal Chloride in the Lysosome Is Critical for Lysosome Function. *Elife* **2017**, *6*, e28862. https://doi.org/10.7554/eLife.28862.

(1020) Glorieux, C.; Zamocky, M.; Sandoval, J. M.; Verrax, J.; Calderon, P. B. Regulation of Catalase Expression in Healthy and Cancerous Cells. *Free Radic. Biol. Med.* **2015**, *87*, 84–97. https://doi.org/10.1016/j.freeradbiomed.2015.06.017.

(1021) Fan, Z.; Jiang, B.; Zhu, Q.; Xiang, S.; Tu, L.; Yang, Y.; Zhao, Q.; Huang, D.; Han, J.; Su, G.; Ge, D.; Hou, Z. Tumor-Specific Endogenous FeII-Activated, MRI-Guided Self-Targeting Gadolinium-Coordinated Theranostic Nanoplatforms for Amplification of ROS and Enhanced Chemodynamic Chemotherapy. *ACS Appl. Mater. Interfaces* **2020**, *12* (13), 14884–14904. https://doi.org/10.1021/acsami.0c00970.

(1022) Chou, T.-C. Drug Combination Studies and Their Synergy Quantification Using the Chou-Talalay Method. *Cancer Res.* **2010**, *70* (2), 440 LP – 446. https://doi.org/10.1158/0008-5472.CAN-09-1947.

(1023) Ghirardi, M. L.; Dubini, A.; Yu, J.; Maness, P.-C. Photobiological Hydrogen-Producing Systems. *Chem. Soc. Rev.* **2009**, *38* (1), 52–61. https://doi.org/10.1039/B718939G.

(1024) Yun, S. H.; Kwok, S. J. J. Light in Diagnosis, Therapy and Surgery. *Nat. Biomed. Eng.* **2017**, *1* (1), 8. https://doi.org/10.1038/s41551-016-0008.

(1025) Rwei, A. Y.; Wang, W.; Kohane, D. S. Photoresponsive Nanoparticles for Drug Delivery. *Nano Today* **2015**, *10* (4), 451–467. https://doi.org/10.1016/j.nantod.2015.06.004.

(1026) Gai, S.; Yang, G.; Yang, P.; He, F.; Lin, J.; Jin, D.; Xing, B. Recent Advances in Functional Nanomaterials for Light–Triggered Cancer Therapy. *Nano Today* **2018**, *19*, 146–187. https://doi.org/10.1016/j.nantod.2018.02.010.

(1027) Garland, M. J.; Cassidy, C. M.; Woolfson, D.; Donnelly, R. F. Designing Photosensitizers for Photodynamic Therapy: Strategies, Challenges and Promising Developments. *Future Med. Chem.* **2009**, *1* (4), 667–691. https://doi.org/10.4155/fmc.09.55.

(1028) Xue, C.; Sutrisno, L.; Li, M.; Zhu, W.; Fei, Y.; Liu, C.; Wang, X.; Cai, K.; Hu, Y.; Luo, Z. Implantable Multifunctional Black Phosphorus Nanoformulation-Deposited Biodegradable Scaffold for Combinational Photothermal/ Chemotherapy and Wound Healing. *Biomaterials* **2021**, *269*, 120623. https://doi.org/10.1016/j.biomaterials.2020.120623.

(1029) Pham, T. C.; Nguyen, V.-N.; Choi, Y.; Lee, S.; Yoon, J. Recent Strategies to Develop Innovative Photosensitizers for Enhanced Photodynamic Therapy. *Chem. Rev.* **2021**, *121* (21), 13454–13619.

https://doi.org/10.1021/acs.chemrev.1c00381.

(1030) Alvarez-Lorenzo, C.; Bromberg, L.; Concheiro, A. Light-Sensitive Intelligent Drug Delivery Systems. *Photochem. Photobiol.* **2009**, *85* (4), 848–860. https://doi.org/10.1111/j.1751-1097.2008.00530.x.

(1031) Rapp, T. L.; DeForest, C. A. Targeting Drug Delivery with Light: A Highly Focused Approach. *Adv. Drug Deliv. Rev.* **2021**, *171*, 94–107. https://doi.org/10.1016/j.addr.2021.01.009.

(1032) Liu, W.; Dong, X.; Liu, Y.; Sun, Y. Photoresponsive Materials for Intensified Modulation of Alzheimer's Amyloid-β Protein Aggregation: A Review. *Acta Biomater.* **2021**, *123*, 93–109. https://doi.org/10.1016/j.actbio.2021.01.018.

(1033) Son, J.; Yi, G.; Yoo, J.; Park, C.; Koo, H.; Choi, H. S. Light-Responsive Nanomedicine for Biophotonic Imaging and Targeted Therapy. *Adv. Drug Deliv. Rev.* **2019**, *138*, 133–147. https://doi.org/10.1016/j.addr.2018.10.002.

(1034) Jiang, B.; Liu, X.; Yang, C.; Yang, Z.; Luo, J.; Kou, S.; Liu, K.; Sun, F. Injectable, Photoresponsive Hydrogels for Delivering Neuroprotective Proteins Enabled by Metal-Directed Protein Assembly. *Sci. Adv.* **2022**, *6* (41), eabc4824. https://doi.org/10.1126/sciadv.abc4824.

(1035) Tomatsu, I.; Peng, K.; Kros, A. Photoresponsive Hydrogels for Biomedical Applications. *Adv. Drug Deliv. Rev.* **2011**, *63* (14–15), 1257–1266. https://doi.org/10.1016/j.addr.2011.06.009.

(1036) Li, J.; Pu, K. Development of Organic Semiconducting Materials for Deep-Tissue Optical Imaging, Phototherapy and Photoactivation. *Chem. Soc. Rev.* **2019**, *48* (1), 38–71. https://doi.org/10.1039/C8CS00001H.

(1037) Ta, T.; Porter, T. M. Thermosensitive Liposomes for Localized Delivery and Triggered Release of Chemotherapy. *J. Control. Release* **2013**, *169* (1–2), 112–125. https://doi.org/10.1016/j.jconrel.2013.03.036.

(1038) Cai, Y.; Wei, Z.; Song, C.; Tang, C.; Han, W.; Dong, X. Optical Nano-Agents in the Second near-Infrared Window for Biomedical Applications. *Chem. Soc. Rev.* **2019**, *48* (1), 22–37. https://doi.org/10.1039/C8CS00494C.

(1039) Zhao, H.; Xu, J.; Wan, J.; Huang, W.; Zhao, Y.; Yang, X. A Versatile Strategy for Improving Phototherapeutic Efficacy on Deep-Sited Tumor by Tissue Optical Clearing Technique. *Nano Today* **2021**, *36*, 101058. https://doi.org/10.1016/j.nantod.2020.101058.

(1040) Paudel, K. S.; Milewski, M.; Swadley, C. L.; Brogden, N. K.; Ghosh, P.; Stinchcomb, A. L. Challenges and Opportunities in Dermal/Transdermal Delivery. *Ther. Deliv.* **2010**, *1* (1), 109–131. https://doi.org/10.4155/tde.10.16.

(1041) Tuan-Mahmood, T.-M.; McCrudden, M. T. C.; Torrisi, B. M.; McAlister, E.; Garland, M. J.; Singh, T. R. R.; Donnelly, R. F. Microneedles for Intradermal and Transdermal Drug Delivery. *Eur. J. Pharm. Sci.* **2013**, *50* (5), 623–637. https://doi.org/10.1016/j.ejps.2013.05.005.

(1042) Hu, X.; Zhang, H.; Wang, Z.; Shiu, C. Y. A.; Gu, Z. Microneedle Array Patches Integrated with Nanoparticles for Therapy and Diagnosis. *Small Struct.* **2021**, *2* (4), 2000097. https://doi.org/10.1002/sstr.202000097.

(1043) Singh, P.; Carrier, A.; Chen, Y.; Lin, S.; Wang, J.; Cui, S.; Zhang, X. Polymeric Microneedles for Controlled Transdermal Drug Delivery. *J. Control. Release* **2019**, *315*, 97–113. https://doi.org/10.1016/j.jconrel.2019.10.022.

(1044) Rzhevskiy, A. S.; Singh, T. R. R.; Donnelly, R. F.; Anissimov, Y. G. Microneedles as the Technique of Drug Delivery Enhancement in Diverse Organs and Tissues. *J. Control. Release* **2018**, *270*, 184–202. https://doi.org/10.1016/j.jconrel.2017.11.048.

(1045) Chen, J.; Ren, H.; Zhou, P.; Zheng, S.; Du, B.; Liu, X.; Xiao, F. Microneedle-Mediated Drug Delivery for Cutaneous Diseases. *Front. Bioeng. Biotechnol.* **2022**, *10*. https://doi.org/10.3389/fbioe.2022.1032041.

(1046) Tran, K. T. M.; Gavitt, T. D.; Farrell, N. J.; Curry, E. J.; Mara, A. B.; Patel, A.; Brown, L.; Kilpatrick, S.; Piotrowska, R.; Mishra, N.; Szczepanek, S. M.; Nguyen, T. D. Transdermal Microneedles for the Programmable Burst Release of Multiple Vaccine Payloads. *Nat. Biomed. Eng.* **2021**, *5* (9), 998–1007. https://doi.org/10.1038/s41551-020-00650-4.

(1047) Li, W.; Terry, R. N.; Tang, J.; Feng, M. R.; Schwendeman, S. P.; Prausnitz, M. R. Rapidly Separable Microneedle Patch for the Sustained Release of a Contraceptive. *Nat. Biomed. Eng.* **2019**, *3* (3), 220–229. https://doi.org/10.1038/s41551-018-0337-4.

(1048) Yu, J.; Zhang, Y.; Ye, Y.; DiSanto, R.; Sun, W.; Ranson, D.; Ligler, F. S.; Buse, J. B.; Gu, Z. Microneedle-Array Patches Loaded with Hypoxia-Sensitive Vesicles Provide Fast Glucose-Responsive Insulin Delivery. *Proc. Natl. Acad. Sci.* **2015**, *112* (27), 8260–8265. https://doi.org/10.1073/pnas.1505405112.

(1049) Bhatnagar, S.; Dave, K.; Venuganti, V. V. K. Microneedles in the Clinic. *J. Control. Release* **2017**, *260*, 164–182. https://doi.org/10.1016/j.jconrel.2017.05.029.

(1050) Zhi, D.; Yang, T.; O'Hagan, J.; Zhang, S.; Donnelly, R. F. Microneedles for Photodynamic and Photothermal Therapy. *J. Control. Release* **2020**, *325*, 52–71. https://doi.org/10.1016/j.jconrel.2020.06.032.

(1051) Elman, M.; Lebzelter, J. Light Therapy in the Treatment of Acne Vulgaris. *Dermatologic Surg.* **2004**, *30* (2), 139–146. https://doi.org/10.1111/j.1524-4725.2004.30053.x.

(1052) Tipnis, N. P.; Burgess, D. J. Sterilization of Implantable Polymer-Based Medical Devices: A Review. *Int. J. Pharm.* **2018**, *544* (2), 455–460. https://doi.org/10.1016/j.ijpharm.2017.12.003.

(1053) Wang, X.; Tian, F.; Soni, S. S.; Gonzalez-Lima, F.; Liu, H. Interplay between Up-Regulation of Cytochrome-c-Oxidase and Hemoglobin Oxygenation Induced by near-Infrared Laser. *Sci. Rep.* **2016**, *6* (1), 30540. https://doi.org/10.1038/srep30540.

(1054) Meng, Z.; Hou, W.; Zhou, H.; Zhou, L.; Chen, H.; Wu, C. Therapeutic Considerations and Conjugated Polymer-Based Photosensitizers for Photodynamic Therapy. *Macromol. Rapid Commun.* **2018**, *39* (5), 1700614. https://doi.org/10.1002/marc.201700614.

(1055) Weng, X.-L.; Liu, J.-Y. Strategies for Maximizing Photothermal Conversion Efficiency Based on Organic Dyes. *Drug Discov. Today* **2021**, *26* (8), 2045–2052. https://doi.org/10.1016/j.drudis.2021.03.009.

(1056) Li, J.; Zhang, W.; Ji, W.; Wang, J.; Wang, N.; Wu, W.; Wu, Q.; Hou, X.; Hu, W.; Li, L. Near Infrared Photothermal Conversion Materials: Mechanism, Preparation, and Photothermal Cancer Therapy Applications. *J. Mater. Chem. B* **2021**, *9* (38), 7909–7926. https://doi.org/10.1039/D1TB01310F.

(1057) Bensadoun, R.-J.; Epstein, J. B.; Nair, R. G.; Barasch, A.; Raber-Durlacher, J. E.; Migliorati, C.; Genot-Klastersky, M.-T.; Treister, N.; Arany, P.; Lodewijckx, J.; Robijns, J.; World Association for Laser Therapy. Safety and Efficacy of Photobiomodulation Therapy in Oncology: A Systematic Review. *Cancer Med.* **2020**, *9* (22), 8279–8300. https://doi.org/10.1002/cam4.3582.

(1058) Zein, R.; Selting, W.; Hamblin, M. R. Review of Light Parameters and Photobiomodulation Efficacy: Dive into Complexity. *J. Biomed. Opt.* **2018**, *23* (12), 1–17. https://doi.org/10.1117/1.JBO.23.12.120901.

(1059) Ren, Y.; Liu, H.; Liu, X.; Zheng, Y.; Li, Z.; Li, C.; Yeung, K. W. K.; Zhu, S.; Liang, Y.; Cui, Z.; Wu, S. Photoresponsive Materials for Antibacterial Applications. *Cell Reports Phys. Sci.* **2020**, *1* (11), 100245. https://doi.org/10.1016/j.xcrp.2020.100245.

(1060) Raza, A.; Hayat, U.; Rasheed, T.; Bilal, M.; Iqbal, H. M. N. "Smart" Materials-Based near-Infrared Light-Responsive Drug Delivery Systems for Cancer Treatment: A Review. *J. Mater. Res. Technol.* **2019**, *8* (1), 1497–1509. https://doi.org/10.1016/j.jmrt.2018.03.007.

(1061) Zhao, J.; Zhong, D.; Zhou, S. NIR-I-to-NIR-II Fluorescent Nanomaterials for Biomedical Imaging and Cancer Therapy. *J. Mater. Chem. B* **2018**, *6* (3), 349–365. https://doi.org/10.1039/c7tb02573d.

(1062) Ruggiero, E.; Alonso-de Castro, S.; Habtemariam, A.; Salassa, L. Upconverting Nanoparticles for the near Infrared Photoactivation of Transition Metal Complexes: New Opportunities and Challenges in Medicinal

Inorganic Photochemistry. *Dalt. Trans.* **2016**, *45* (33), 13012–13020. https://doi.org/10.1039/C6DT01428C.

(1063) Lee, H. P.; Gaharwar, A. K. Light-Responsive Inorganic Biomaterials for Biomedical Applications. *Adv. Sci.* **2020**, *7* (17), 2000863. https://doi.org/10.1002/advs.202000863.

(1064) Nguyen, V.-N.; Zhao, Z.; Tang, B. Z.; Yoon, J. Organic Photosensitizers for Antimicrobial Phototherapy. *Chem. Soc. Rev.* **2022**, *51* (9), 3324–3340. https://doi.org/10.1039/D1CS00647A.

(1065) Chen, H.; Zhao, Y. Applications of Light-Responsive Systems for Cancer Theranostics. *ACS Appl. Mater. Interfaces* **2018**, *10* (25), 21021–21034. https://doi.org/10.1021/acsami.8b01114.

(1066) Linic, S.; Christopher, P.; Ingram, D. B. Plasmonic-Metal Nanostructures for Efficient Conversion of Solar to Chemical Energy. *Nat. Mater.* **2011**, *10* (12), 911–921. https://doi.org/10.1038/nmat3151.

(1067) Sun, J.; Du, K.; Diao, J.; Cai, X.; Feng, F.; Wang, S. GSH and H2O2 Co-Activatable Mitochondria-Targeted Photodynamic Therapy under Normoxia and Hypoxia. *Angew. Chemie Int. Ed.* **2020**, *59* (29), 12122–12128. https://doi.org/10.1002/anie.202003895.

(1068) George, B. P.; Chota, A.; Sarbadhikary, P.; Abrahamse, H. Fundamentals and Applications of Metal Nanoparticle- Enhanced Singlet Oxygen Generation for Improved Cancer Photodynamic Therapy. *Front. Chem.* **2022**, *10*, 964674. https://doi.org/10.3389/fchem.2022.964674.

(1069) Ge, H.; Du, J.; Long, S.; Xia, X.; Zheng, J.; Xu, N.; Yao, Q.; Fan, J.; Peng, X. Near-Infrared Light Triggered H2 Generation for Enhanced Photothermal/Photodynamic Therapy against Hypoxic Tumor. *Adv. Healthc. Mater.* **2022**, *11* (3), 2101449. https://doi.org/10.1002/adhm.202101449.

(1070) Sai, D. L.; Lee, J.; Nguyen, D. L.; Kim, Y.-P. Tailoring Photosensitive ROS for Advanced Photodynamic Therapy. *Exp. Mol. Med.* **2021**, *53* (4), 495–504. https://doi.org/10.1038/s12276-021-00599-7.

(1071) Zhou, X.; Li, B.; Guo, M.; Peng, W.; Wang, D.; Guo, Q.; Wang, S.; Ming, D.; Zheng, B. Microneedle Patch Based on Molecular Motor as a Spatio-Temporal Controllable Dosing Strategy of L-DOPA for Parkinson's Disease. *Chem. Eng. J.* **2022**, *427*, 131555. https://doi.org/10.1016/j.cej.2021.131555.

(1072) Kim, S.; Lee, H.; Choi, H.; Yoo, K.-Y.; Yoon, H. Investigation on Photopolymerization of PEGDA to Fabricate High-Aspect-Ratio Microneedles. *RSC Adv.* **2022**, *12* (16), 9550–9555. https://doi.org/10.1039/D2RA00189F.

(1073) Hardy, J. G.; Larrañeta, E.; Donnelly, R. F.; McGoldrick, N.; Migalska, K.; McCrudden, M. T. C.; Irwin, N. J.; Donnelly, L.; McCoy, C. P. Hydrogel-Forming Microneedle Arrays Made from Light-Responsive Materials for On-Demand Transdermal Drug Delivery. *Mol. Pharm.* **2016**, *13* (3), 907–914. https://doi.org/10.1021/acs.molpharmaceut.5b00807.

(1074) Zheng, Z.; Ye, H.; Wang, J.; Zhang, T.; You, Q.; Li, H.; He, R.; Chen, Y.; Zhang, W.; Cao, Y. Visible-Light-Controllable Drug Release from Multilayer-Coated Microneedles. *J. Mater. Chem. B* **2017**, *5* (34), 7014–7017. https://doi.org/10.1039/C7TB01546A.

(1075) Zhang, Y.; Jiang, G.; Hong, W.; Gao, M.; Xu, B.; Zhu, J.; Song, G.; Liu, T. Polymeric Microneedles Integrated with Metformin-Loaded and PDA/LA-Coated Hollow Mesoporous SiO2 for NIR-Triggered Transdermal Delivery on Diabetic Rats. *ACS Appl. Bio Mater.* **2018**, *1* (6), 1906–1917. https://doi.org/10.1021/acsabm.8b00470.

(1076) Gong, J.-H.; Chen, L.-J.; Zhao, X.; Yan, X.-P. Persistent Production of Reactive Oxygen Species with Zn2GeO4:Cu Nanorod-Loaded Microneedles for Methicillin-Resistant Staphylococcus Aureus Infectious Wound Healing. *ACS Appl. Mater. Interfaces* **2022**, *14* (15), 17142–17152. https://doi.org/10.1021/acsami.2c02503.

(1077) Hao, Y.; Chen, Y.; Lei, M.; Zhang, T.; Cao, Y.; Peng, J.; Chen, L.; Qian, Z. Near-Infrared Responsive PEGylated Gold Nanorod and Doxorubicin Loaded Dissolvable Hyaluronic Acid Microneedles for Human Epidermoid Cancer Therapy. *Adv. Ther.* **2018**, *1* (2), 1800008. https://doi.org/10.1002/adtp.201800008.

(1078) Dong, L.; Li, Y.; Li, Z.; Xu, N.; Liu, P.; Du, H.; Zhang, Y.; Huang, Y.; Zhu, J.; Ren, G.; Xie, J.; Wang, K.;

Zhou, Y.; Shen, C.; Zhu, J.; Tao, J. Au Nanocage-Strengthened Dissolving Microneedles for Chemo-Photothermal Combined Therapy of Superficial Skin Tumors. *ACS Appl. Mater. Interfaces* **2018**, *10* (11), 9247–9256. https://doi.org/10.1021/acsami.7b18293.

(1079) Hao, Y.; Dong, M.; Zhang, T.; Peng, J.; Jia, Y.; Cao, Y.; Qian, Z. Novel Approach of Using Near-Infrared Responsive PEGylated Gold Nanorod Coated Poly(l-Lactide) Microneedles to Enhance the Antitumor Efficiency of Docetaxel-Loaded MPEG-PDLLA Micelles for Treating an A431 Tumor. *ACS Appl. Mater. Interfaces* **2017**, *9* (18), 15317–15327. https://doi.org/10.1021/acsami.7b03604.

(1080) Moreira, A. F.; Rodrigues, C. F.; Jacinto, T. A.; Miguel, S. P.; Costa, E. C.; Correia, I. J. Poly (Vinyl Alcohol)/Chitosan Layer-by-Layer Microneedles for Cancer Chemo-Photothermal Therapy. *Int. J. Pharm.* **2020**, *576*, 118907. https://doi.org/10.1016/j.ijpharm.2019.118907.

(1081) Ziesmer, J.; Sondén, I.; Thersleff, T.; Sotiriou, G. A. Highly Efficient Near-IR Photothermal Microneedles with Flame-Made Plasmonic Nanoaggregates for Reduced Intradermal Nanoparticle Deposition. *Adv. Mater. Interfaces* **2022**, *9* (34), 2201540. https://doi.org/10.1002/admi.202201540.

(1082) Liu, L.; Wang, Q.; Liao, H.; Ye, J.; Huang, J.; Li, S.; Peng, H.; Yu, X.; Wen, H.; Wang, X. Soluble Microneedle Patch with Photothermal and NO-Release Properties for Painless and Precise Treatment of Ischemic Perforator Flaps. *J. Mater. Chem. B* **2021**, *9* (37), 7725–7733. https://doi.org/10.1039/D1TB00491C.

(1083) Cárcamo-Martínez, Á.; Mallon, B.; Domínguez-Robles, J.; Cordeiro, A. S.; Celentano, M.; Larrañeta, E.; Bell, S. E. J.; Donnelly, R. F. Plasmonic Photothermal Microneedle Arrays and Single Needles for Minimally-Invasive Deep in-Skin Hyperthermia. *J. Mater. Chem. B* **2020**, *8* (25), 5425–5433. https://doi.org/10.1039/D0TB00962H.

(1084) Cui, J.; Huang, J.; Yan, Y.; Chen, W.; Wen, J.; Wu, X.; Liu, J.; Liu, H.; Huang, C. Ferroferric Oxide Loaded Near-Infrared Triggered Photothermal Microneedle Patch for Controlled Drug Release. *J. Colloid Interface Sci.* **2022**, *617*, 718–729. https://doi.org/10.1016/j.jcis.2022.03.046.

(1085) Yu, W.; Jiang, G.; Zhang, Y.; Liu, D.; Xu, B.; Zhou, J. Near-Infrared Light Triggered and Separable Microneedles for Transdermal Delivery of Metformin in Diabetic Rats. *J. Mater. Chem. B* **2017**, *5* (48), 9507–9513. https://doi.org/10.1039/C7TB02236K.

(1086) Demir, B.; Rosselle, L.; Voronova, A.; Pagneux, Q.; Quenon, A.; Gmyr, V.; Jary, D.; Hennuyer, N.; Staels, B.; Hubert, T.; Abderrahmani, A.; Plaisance, V.; Pawlowski, V.; Boukherroub, R.; Vignoud, S.; Szunerits, S. Innovative Transdermal Delivery of Insulin Using Gelatin Methacrylate-Based Microneedle Patches in Mice and Mini-Pigs. *Nanoscale horizons* **2022**, *7* (2), 174–184. https://doi.org/10.1039/d1nh00596k.

(1087) Chen, M.-C.; Ling, M.-H.; Wang, K.-W.; Lin, Z.-W.; Lai, B.-H.; Chen, D.-H. Near-Infrared Light-Responsive Composite Microneedles for on-Demand Transdermal Drug Delivery. *Biomacromolecules* **2015**, *16* (5), 1598–1607. https://doi.org/10.1021/acs.biomac.5b00185.

(1088) Chen, M.-C.; Lin, Z.-W.; Ling, M.-H. Near-Infrared Light-Activatable Microneedle System for Treating Superficial Tumors by Combination of Chemotherapy and Photothermal Therapy. *ACS Nano* **2016**, *10* (1), 93–101. https://doi.org/10.1021/acsnano.5b05043.

(1089) Liu, D.; Zhang, Y.; Jiang, G.; Yu, W.; Xu, B.; Zhu, J. Fabrication of Dissolving Microneedles with Thermal-Responsive Coating for NIR-Triggered Transdermal Delivery of Metformin on Diabetic Rats. *ACS Biomater. Sci. Eng.* **2018**, *4* (5), 1687–1695. https://doi.org/10.1021/acsbiomaterials.8b00159.

(1090) Chen, Y.; Yang, Y.; Xian, Y.; Singh, P.; Feng, J.; Cui, S.; Carrier, A.; Oakes, K.; Luan, T.; Zhang, X. Multifunctional Graphene-Oxide-Reinforced Dissolvable Polymeric Microneedles for Transdermal Drug Delivery. *ACS Appl. Mater. Interfaces* **2020**, *12* (1), 352–360. https://doi.org/10.1021/acsami.9b19518.

(1091) Younis, M. R.; He, G.; Qu, J.; Lin, J.; Huang, P.; Xia, X.-H. Inorganic Nanomaterials with Intrinsic Singlet Oxygen Generation for Photodynamic Therapy. *Adv. Sci.* **2021**, *8* (21), 2102587. https://doi.org/10.1002/advs.202102587.

(1092) Song, X.; Chen, Q.; Liu, Z. Recent Advances in the Development of Organic Photothermal Nano-Agents. *Nano Res.* **2015**, *8* (2), 340–354. https://doi.org/10.1007/s12274-014-0620-y.

(1093) Meng, X.; Liu, L.; Ouyang, S.; Xu, H.; Wang, D.; Zhao, N.; Ye, J. Nanometals for Solar-to-Chemical Energy Conversion: From Semiconductor-Based Photocatalysis to Plasmon-Mediated Photocatalysis and Photo-Thermocatalysis. *Adv. Mater.* **2016**, *28* (32), 6781–6803. https://doi.org/10.1002/adma.201600305.

(1094) Kale, M. J.; Avanesian, T.; Christopher, P. Direct Photocatalysis by Plasmonic Nanostructures. *ACS Catal.* **2014**, *4* (1), 116–128. https://doi.org/10.1021/cs400993w.

(1095) Xu, X.; Luo, F.; Tang, W.; Hu, J.; Zeng, H.; Zhou, Y. Enriching Hot Electrons via NIR-Photon-Excited Plasmon in WS2@Cu Hybrids for Full-Spectrum Solar Hydrogen Evolution. *Adv. Funct. Mater.* **2018**, *28* (43), 1804055. https://doi.org/10.1002/adfm.201804055.

(1096) Kumar, V.; O'Donnell, S.; Zoellner, B.; Martinez, J.; Wang, G.; Maggard, P. A. Interfacing Plasmonic Nanoparticles with Ferroelectrics for Hot-Carrier-Driven Photocatalysis: Impact of Schottky Barrier Height. *ACS Appl. Energy Mater.* **2019**, *2* (10), 7690–7699. https://doi.org/10.1021/acsaem.9b01682.

(1097) Haneef, H. F.; Zeidell, A. M.; Jurchescu, O. D. Charge Carrier Traps in Organic Semiconductors: A Review on the Underlying Physics and Impact on Electronic Devices. *J. Mater. Chem. C* **2020**, *8* (3), 759–787. https://doi.org/10.1039/C9TC05695E.

(1098) Hiramoto, M.; Kikuchi, M.; Izawa, S. Parts-per-Million-Level Doping Effects in Organic Semiconductor Films and Organic Single Crystals. *Adv. Mater.* **2019**, *31* (1), 1801236. https://doi.org/10.1002/adma.201801236.

(1099) Demirbas, U.; Thesinga, J.; Kellert, M.; Pergament, M.; Kärtner, F. X. Temperature and Doping Dependence of Fluorescence Lifetime in Yb:YLF (Role of Impurities). *Opt. Mater. (Amst).* **2021**, *112*, 110792. https://doi.org/10.1016/j.optmat.2020.110792.

(1100) Fu, H.; Hu, C.; Liu, J.; Zhang, Q.; Xu, J. Y.; Jiang, G. J.; Liu, M. An Overview of Boosting Lanthanide Upconversion Luminescence through Chemical Methods and Physical Strategies. *CrystEngComm* **2022**, *24* (44), 7698–7717. https://doi.org/10.1039/D2CE01206E.

(1101) Chen, D.; Wang, Y. Impurity Doping: A Novel Strategy for Controllable Synthesis of Functional Lanthanide Nanomaterials. *Nanoscale* **2013**, *5* (11), 4621–4637. https://doi.org/10.1039/C3NR00368J.

(1102) Luo, S.; Zhang, E.; Su, Y.; Cheng, T.; Shi, C. A Review of NIR Dyes in Cancer Targeting and Imaging. *Biomaterials* **2011**, *32* (29), 7127–7138. https://doi.org/10.1016/j.biomaterials.2011.06.024.

(1103) Lei, Q.; He, D.; Ding, L.; Kong, F.; He, P.; Huang, J.; Guo, J.; Brinker, C. J.; Luo, G.; Zhu, W.; Yu, Y. Microneedle Patches Integrated with Biomineralized Melanin Nanoparticles for Simultaneous Skin Tumor Photothermal Therapy and Wound Healing. *Adv. Funct. Mater.* **2022**, *32* (22), 2113269. https://doi.org/10.1002/adfm.202113269.

(1104) Li, H.; Yin, D.; Li, W.; Tang, Q.; Zou, L.; Peng, Q. Polydopamine-Based Nanomaterials and Their Potentials in Advanced Drug Delivery and Therapy. *Colloids Surfaces B Biointerfaces* **2021**, *199*, 111502. https://doi.org/10.1016/j.colsurfb.2020.111502.

(1105) Mahmoudi, K.; Garvey, K. L.; Bouras, A.; Cramer, G.; Stepp, H.; Jesu Raj, J. G.; Bozec, D.; Busch, T. M.; Hadjipanayis, C. G. 5-Aminolevulinic Acid Photodynamic Therapy for the Treatment of High-Grade Gliomas. *J. Neurooncol.* **2019**, *141* (3), 595–607. https://doi.org/10.1007/s11060-019-03103-4.

(1106) Collaud, S.; Juzeniene, A.; Moan, J.; Lange, N. On the Selectivity of 5-Aminolevulinic Acid-Induced Protoporphyrin IX Formation. *Curr. Med. Chem. Anticancer. Agents* **2004**, *4* (3), 301–316. https://doi.org/10.2174/1568011043352984.

(1107) Chen, S.-X.; Ma, M.; Xue, F.; Shen, S.; Chen, Q.; Kuang, Y.; Liang, K.; Wang, X.; Chen, H. Construction of Microneedle-Assisted Co-Delivery Platform and Its Combining Photodynamic/Immunotherapy. *J. Control. Release* **2020**, *324*, 218–227. https://doi.org/10.1016/j.jconrel.2020.05.006.

(1108) Sun, Y.; Liu, J.; Wang, H.; Li, S.; Pan, X.; Xu, B.; Yang, H.; Wu, Q.; Li, W.; Su, X.; Huang, Z.; Guo, X.; Liu, H. NIR Laser-Triggered Microneedle-Based Liquid Band-Aid for Wound Care. *Adv. Funct. Mater.* **2021**, *31* (29), 2100218. https://doi.org/10.1002/adfm.202100218.

(1109) Moreira, L. M.; Vieira dos Santos, F.; Lyon, J. P.; Maftoum-Costa, M.; Pacheco-Soares, C.; Soares da Silva, N. Photodynamic Therapy: Porphyrins and Phthalocyanines as Photosensitizers. *Aust. J. Chem.* **2008**, *61* (10), 741–754.

(1110) Heiskanen, V.; Hamblin, M. R. Photobiomodulation: Lasers vs. Light Emitting Diodes? *Photochem. Photobiol. Sci.* **2018**, *17* (8), 1003–1017. https://doi.org/10.1039/C8PP00176F.

(1111) Yeh, N. G.; Wu, C.-H.; Cheng, T. C. Light-Emitting Diodes—Their Potential in Biomedical Applications. *Renew. Sustain. Energy Rev.* **2010**, *14* (8), 2161–2166. https://doi.org/10.1016/j.rser.2010.02.015.

(1112) Bozkurt, A.; Onaral, B. Safety Assessment of near Infrared Light Emitting Diodes for Diffuse Optical Measurements. *Biomed. Eng. Online* **2004**, *3* (1), 9. https://doi.org/10.1186/1475-925X-3-9.

(1113) Joensen, J.; Demmink, J. H.; Johnson, M. I.; Iversen, V. V; Lopes-Martins, R. Á. B.; Bjordal, J. M. The Thermal Effects of Therapeutic Lasers with 810 and 904 Nm Wavelengths on Human Skin. *Photomed. Laser Surg.* **2011**, *29* (3), 145–153. https://doi.org/10.1089/pho.2010.2793.

(1114) Li, Y.; Xu, H.; Li, H.; Zhong, S. Controlled Preparation and Photothermal Properties of Polydopamine Submicrospheres. *Inorg. Chem. Commun.* **2021**, *124*, 108395. https://doi.org/10.1016/j.inoche.2020.108395.

(1115) Yang, Y.; Fan, X.; Li, L.; Yang, Y.; Nuernisha, A.; Xue, D.; He, C.; Qian, J.; Hu, Q.; Chen, H.; Liu, J.; Huang, W. Semiconducting Polymer Nanoparticles as Theranostic System for Near-Infrared-II Fluorescence Imaging and Photothermal Therapy under Safe Laser Fluence. *ACS Nano* **2020**, *14* (2), 2509–2521. https://doi.org/10.1021/acsnano.0c00043.

(1116) Lei, Z.; Zhang, W.; Li, B.; Guan, G.; Huang, X.; Peng, X.; Zou, R.; Hu, J. A Full-Spectrum-Absorption from Nickel Sulphide Nanoparticles for Efficient NIR-II Window Photothermal Therapy. *Nanoscale* **2019**, *11* (42), 20161–20170. https://doi.org/10.1039/C9NR04005F.

(1117) Huda, K.; Swan, K. F.; Gambala, C. T.; Pridjian, G. C.; Bayer, C. L. Towards Transabdominal Functional Photoacoustic Imaging of the Placenta: Improvement in Imaging Depth Through Optimization of Light Delivery. *Ann. Biomed. Eng.* **2021**, *49* (8), 1861–1873. https://doi.org/10.1007/s10439-021-02777-0.

(1118) Reidenbach, H.-D. Temporary Blinding Limits versus Maximum Permissible Exposure – A Paradigm Change in Risk Assessment for Visible Optical Radiation. *Phys. Procedia* **2014**, *56*, 1366–1376. https://doi.org/10.1016/j.phpro.2014.08.065.

(1119) Yadav, A.; Gupta, A. Noninvasive Red and Near-Infrared Wavelength-Induced Photobiomodulation: Promoting Impaired Cutaneous Wound Healing. *Photodermatol. Photoimmunol. Photomed.* **2017**, *33* (1), 4–13. https://doi.org/10.1111/phpp.12282.

(1120) Hashmi, J. T.; Huang, Y.-Y.; Sharma, S. K.; Kurup, D. B.; De Taboada, L.; Carroll, J. D.; Hamblin, M. R. Effect of Pulsing in Low-Level Light Therapy. *Lasers Surg. Med.* **2010**, *42* (6), 450–466. https://doi.org/10.1002/lsm.20950.

(1121) Grandinétti, V. dos S.; Miranda, E. F.; Johnson, D. S.; de Paiva, P. R. V.; Tomazoni, S. S.; Vanin, A. A.; Albuquerque-Pontes, G. M.; Frigo, L.; Marcos, R. L.; de Carvalho, P. de T. C.; Leal-Junior, E. C. P. The Thermal Impact of Phototherapy with Concurrent Super-Pulsed Lasers and Red and Infrared LEDs on Human Skin. *Lasers Med. Sci.* **2015**, *30* (5), 1575–1581. https://doi.org/10.1007/s10103-015-1755-0.

(1122) Yang, D.; Chen, M.; Sun, Y.; Jin, Y.; Lu, C.; Pan, X.; Quan, G.; Wu, C. Microneedle-Mediated Transdermal Drug Delivery for Treating Diverse Skin Diseases. *Acta Biomater.* **2021**, *121*, 119–133. https://doi.org/10.1016/j.actbio.2020.12.004.

(1123) Al-Kasasbeh, R.; Brady, A. J.; Courtenay, A. J.; Larrañeta, E.; McCrudden, M. T. C.; O'Kane, D.; Liggett, S.; Donnelly, R. F. Evaluation of the Clinical Impact of Repeat Application of Hydrogel-Forming

Microneedle Array Patches. *Drug Deliv. Transl. Res.* **2020**, *10* (3), 690–705. https://doi.org/10.1007/s13346-020-00727-2.

(1124) Wang, H.; Wang, W.; Li, C.; Xu, A.; Qiu, B.; Li, F.; Ding, W. Flav7 + DOX Co-Loaded Separable Microneedle for Light-Triggered Chemo-Thermal Therapy of Superficial Tumors. *Chem. Eng. J.* **2022**, *428*, 131913. https://doi.org/10.1016/j.cej.2021.131913.

(1125) Chen, M.-C.; Wang, K.-W.; Chen, D.-H.; Ling, M.-H.; Liu, C.-Y. Remotely Triggered Release of Small Molecules from LaB6@SiO2-Loaded Polycaprolactone Microneedles. *Acta Biomater.* **2015**, *13*, 344–353. https://doi.org/10.1016/j.actbio.2014.11.040.

(1126) Peng, H.; Zhang, C.; Wang, M.; Zhang, W.; Xu, B.; Yan, X.; Xin, H.; Wang, X. Black Phosphorus Modified Soluble Microneedle Patch for Painless, Effective and Accurate Body Slimming. *Appl. Mater. Today* **2020**, *19*, 100577. https://doi.org/10.1016/j.apmt.2020.100577.

(1127) Park, J.-H.; Kim, C. B.; Lee, H.-J.; Roh, J. Y.; Lee, J. M.; Kim, H. J.; Park, J.-H. Development and Clinical Study of the Use of Infrared Radiation to Accelerate the Dissolution Rate of a Microneedle Array Patch (MAP). *Drug Deliv. Transl. Res.* **2020**, *10* (3), 791–800. https://doi.org/10.1007/s13346-020-00710-x.

(1128) Amer, M.; Ni, X.; Xian, M.; Chen, R. K. Photo-Responsive Hydrogel Microneedles With Interlocking Control for Easy Extraction in Sustained Ocular Drug Delivery. *J. Eng. Sci. Med. Diagnostics Ther.* **2021**, *5* (1). https://doi.org/10.1115/1.4052627.

(1129) Liu, T.; Luo, G.; Xing, M. Biomedical Applications of Polymeric Microneedles for Transdermal Therapeutic Delivery and Diagnosis: Current Status and Future Perspectives. *Adv. Ther.* **2020**, *3* (9), 1900140. https://doi.org/10.1002/adtp.201900140.

(1130) Chen, J.; Cao, Y.; Lin, S.; Niu, H.; Zhang, H.; Guan, L.; Shu, C.; Wu, A.; Bian, Y.; Zhu, Y. A Responsive Microneedle System for Efficient Anti-Melanoma by Combining Self-Enhanced Chemodynamic Therapy with Photothermal Therapy. *Chem. Eng. J.* **2022**, *431*, 133466. https://doi.org/10.1016/j.cej.2021.133466.

(1131) Zhou, Y.; Niu, B.; Zhao, Y.; Fu, J.; Wen, T.; Liao, K.; Quan, G.; Pan, X.; Wu, C. Multifunctional Nanoreactors-Integrated Microneedles for Cascade Reaction-Enhanced Cancer Therapy. *J. Control. Release* **2021**, *339*, 335–349. https://doi.org/10.1016/j.jconrel.2021.09.041.

(1132) Fan, Z.; Wei, Y.; Yin, Z.; Huang, H.; Liao, X.; Sun, L.; Liu, B.; Liu, F. Near-Infrared Light-Triggered Unfolding Microneedle Patch for Minimally Invasive Treatment of Myocardial Ischemia. *ACS Appl. Mater. Interfaces* **2021**, *13* (34), 40278–40289. https://doi.org/10.1021/acsami.1c09658.

(1133) Li, W.; Li, S.; Fan, X.; Prausnitz, M. R. Microneedle Patch Designs to Increase Dose Administered to Human Subjects. *J. Control. Release* **2021**, *339*, 350–360. https://doi.org/10.1016/j.jconrel.2021.09.036.

(1134) Gill, H. S.; Denson, D. D.; Burris, B. A.; Prausnitz, M. R. Effect of Microneedle Design on Pain in Human Volunteers. *Clin. J. Pain* **2008**, *24* (7), 585–594. https://doi.org/10.1097/AJP.0b013e31816778f9.

(1135) Li, W. X.; Zhang, X. P.; Chen, B. Z.; Fei, W. M.; Cui, Y.; Zhang, C. Y.; Guo, X. D. An Update on Microneedle-Based Systems for Diabetes. *Drug Deliv. Transl. Res.* **2022**, *12* (10), 2275–2286. https://doi.org/10.1007/s13346-021-01113-2.

(1136) Arsiccio, A.; Giorsello, P.; Marenco, L.; Pisano, R. Considerations on Protein Stability During Freezing and Its Impact on the Freeze-Drying Cycle: A Design Space Approach. *J. Pharm. Sci.* **2020**, *109* (1), 464–475. https://doi.org/10.1016/j.xphs.2019.10.022.

(1137) Hansen, L. J. J.; Daoussi, R.; Vervaet, C.; Remon, J.-P.; De Beer, T. R. M. Freeze-Drying of Live Virus Vaccines: A Review. *Vaccine* **2015**, *33* (42), 5507–5519. https://doi.org/10.1016/j.vaccine.2015.08.085.

(1138) Abla, K. K.; Mehanna, M. M. Freeze-Drying: A Flourishing Strategy to Fabricate Stable Pharmaceutical and Biological Products. *Int. J. Pharm.* **2022**, *628*, 122233. https://doi.org/10.1016/j.ijpharm.2022.122233.

(1139) Chu, L. Y.; Ye, L.; Dong, K.; Compans, R. W.; Yang, C.; Prausnitz, M. R. Enhanced Stability of Inactivated Influenza Vaccine Encapsulated in Dissolving Microneedle Patches. *Pharm. Res.* **2016**, *33* (4), 868–878.

https://doi.org/10.1007/s11095-015-1833-9.

(1140) Ingrole, R. S. J.; Azizoglu, E.; Dul, M.; Birchall, J. C.; Gill, H. S.; Prausnitz, M. R. Trends of Microneedle Technology in the Scientific Literature, Patents, Clinical Trials and Internet Activity. *Biomaterials* **2021**, *267*, 120491. https://doi.org/10.1016/j.biomaterials.2020.120491.

(1141) Makvandi, P.; Jamaledin, R.; Chen, G.; Baghbantaraghdari, Z.; Zare, E. N.; Di Natale, C.; Onesto, V.; Vecchione, R.; Lee, J.; Tay, F. R.; Netti, P.; Mattoli, V.; Jaklenec, A.; Gu, Z.; Langer, R. Stimuli-Responsive Transdermal Microneedle Patches. *Mater. Today* **2021**, *47*, 206–222. https://doi.org/10.1016/j.mattod.2021.03.012.

(1142) Zhou, Y.; Ye, H.; Chen, Y.; Zhu, R.; Yin, L. Photoresponsive Drug/Gene Delivery Systems. *Biomacromolecules* **2018**, *19* (6), 1840–1857. https://doi.org/10.1021/acs.biomac.8b00422.

(1143) Zan, P.; Than, A.; Zhang, W.; Cai, H. X.; Zhao, W.; Chen, P. Transdermal Photothermal-Pharmacotherapy to Remodel Adipose Tissue for Obesity and Metabolic Disorders. *ACS Nano* **2022**, *16* (2), 1813–1825. https://doi.org/10.1021/acsnano.1c06410.

(1144) Peng, H.; Zhou, Y.; Zhang, C.; Wang, M.; Zhao, S.; Xu, Y.; Zhang, W.; Xin, H.; Wang, X. An Accurate and Dual-Effective Body Slimming Method through a Soluble Microneedle Patch with Variable Temperature. *J. Mater. Chem. B* **2021**, *9* (2), 421–427. https://doi.org/10.1039/D0TB01547D.

(1145) Xu, M.; Zhou, L.; Zheng, L.; Zhou, Q.; Liu, K.; Mao, Y.; Song, S. Sonodynamic Therapy-Derived Multimodal Synergistic Cancer Therapy. *Cancer Lett.* **2021**, *497*, 229–242. https://doi.org/10.1016/j.canlet.2020.10.037.

(1146) Zhao, X.; Li, X.; Zhang, P.; Du, J.; Wang, Y. Tip-Loaded Fast-Dissolving Microneedle Patches for Photodynamic Therapy of Subcutaneous Tumor. *J. Control. Release* **2018**, *286*, 201–209. https://doi.org/10.1016/j.jconrel.2018.07.038.

(1147) He, G.; Li, Y.; Younis, M. R.; Fu, L.-H.; He, T.; Lei, S.; Lin, J.; Huang, P. Synthetic Biology-Instructed Transdermal Microneedle Patch for Traceable Photodynamic Therapy. *Nat. Commun.* **2022**, *13* (1), 6238. https://doi.org/10.1038/s41467-022-33837-1.

(1148) Bian, Q.; Huang, L.; Xu, Y.; Wang, R.; Gu, Y.; Yuan, A.; Ma, X.; Hu, J.; Rao, Y.; Xu, D.; Wang, H.; Gao, J. A Facile Low-Dose Photosensitizer-Incorporated Dissolving Microneedles-Based Composite System for Eliciting Antitumor Immunity and the Abscopal Effect. *ACS Nano* **2021**, *15* (12), 19468–19479. https://doi.org/10.1021/acsnano.1c06225.

(1149) Yang, P.; Chen, M.; Qin, W.; Shi, C.; Bai, X.; Quan, G.; Pan, X.; Wu, C. Effective Photothermal Therapy Mediated by Indocyanine Green Nanoparticle Tip-Loaded Microneedles to Enhance Checkpoint Inhibitor Immunotherapy for Melanoma Treatment. *ACS Appl. Nano Mater.* **2021**, *4* (6), 5921–5931. https://doi.org/10.1021/acsanm.1c00832.

(1150) Peng, T.; Huang, Y.; Feng, X.; Zhu, C.; Ma, X.; Wang, X.; Bai, X.; Pan, X.; Wu, C. Dissolving Microneedles Loading TPGS Biphasic Functionalized PLGA Nanoparticles for Efficient Chemo-Photothermal Combined Therapy of Melanoma. *Adv. Ther.* **2020**, *3* (6), 1900190. https://doi.org/10.1002/adtp.201900190.

(1151) Wu, B.; Fu, J.; Zhou, Y.; Luo, S.; Zhao, Y.; Quan, G.; Pan, X.; Wu, C. Tailored Core–shell Dual Metal–Organic Frameworks as a Versatile Nanomotor for Effective Synergistic Antitumor Therapy. *Acta Pharm. Sin. B* **2020**, *10* (11), 2198–2211. https://doi.org/10.1016/j.apsb.2020.07.025.

(1152) Qin, W.; Quan, G.; Sun, Y.; Chen, M.; Yang, P.; Feng, D.; Wen, T.; Hu, X.; Pan, X.; Wu, C. Dissolving Microneedles with Spatiotemporally Controlled Pulsatile Release Nanosystem for Synergistic Chemo-Photothermal Therapy of Melanoma. *Theranostics* **2020**, *10* (18), 8179–8196. https://doi.org/10.7150/thno.44194.

(1153) Sun, Y.; Chen, M.; Yang, D.; Qin, W.; Quan, G.; Wu, C.; Pan, X. Self-Assembly Nanomicelle-Microneedle Patches with Enhanced Tumor Penetration for Superior Chemo-Photothermal Therapy. *Nano Res.* **2022**, *15*

(3), 2335–2346. https://doi.org/10.1007/s12274-021-3817-x.

(1154) Hao, Y.; Chen, Y.; He, X.; Yang, F.; Han, R.; Yang, C.; Li, W.; Qian, Z. Near-Infrared Responsive 5-Fluorouracil and Indocyanine Green Loaded MPEG-PCL Nanoparticle Integrated with Dissolvable Microneedle for Skin Cancer Therapy. *Bioact. Mater.* **2020**, *5* (3), 542–552. https://doi.org/10.1016/j.bioactmat.2020.04.002.

(1155) Xu, Q.; Li, X.; Zhang, P.; Wang, Y. Rapidly Dissolving Microneedle Patch for Synergistic Gene and Photothermal Therapy of Subcutaneous Tumor. *J. Mater. Chem. B* **2020**, *8* (19), 4331–4339. https://doi.org/10.1039/D0TB00105H.

(1156) Chen, M.; Yang, D.; Sun, Y.; Liu, T.; Wang, W.; Fu, J.; Wang, Q.; Bai, X.; Quan, G.; Pan, X.; Wu, C. In Situ Self-Assembly Nanomicelle Microneedles for Enhanced Photoimmunotherapy via Autophagy Regulation Strategy. *ACS Nano* **2021**, *15* (2), 3387–3401. https://doi.org/10.1021/acsnano.0c10396.

(1157) Liao, K.; Niu, B.; Dong, H.; He, L.; Zhou, Y.; Sun, Y.; Yang, D.; Wu, C.; Pan, X.; Quan, G. A Spark to the Powder Keg: Microneedle-Based Antitumor Nanomedicine Targeting Reactive Oxygen Species Accumulation for Chemodynamic/Photothermal/Chemotherapy. *J. Colloid Interface Sci.* **2022**, *628*, 189–203. https://doi.org/10.1016/j.jcis.2022.08.042.

(1158) Shan, Y.; Tan, B.; Zhang, M.; Xie, X.; Liao, J. Restorative Biodegradable Two-Layered Hybrid Microneedles for Melanoma Photothermal/Chemo Co-Therapy and Wound Healing. *J. Nanobiotechnology* **2022**, *20* (1), 238. https://doi.org/10.1186/s12951-022-01426-5.

(1159) Yu, W.; Li, X.; Huang, Y.; Chen, Y.; Gao, Q.; Wang, Y.; Ji, J. Build an Implanted "Arsenal": Detachable Microneedles for NIR-Triggered Cancer Photothermo-Chemotherapy. *Biomater. Sci.* **2021**, *9* (13), 4737–4745. https://doi.org/10.1039/D1BM00520K.

(1160) Pei, P.; Yang, F.; Liu, J.; Hu, H.; Du, X.; Hanagata, N.; Zhao, S.; Zhu, Y. Composite-Dissolving Microneedle Patches for Chemotherapy and Photothermal Therapy in Superficial Tumor Treatment. *Biomater. Sci.* **2018**, *6* (6), 1414–1423. https://doi.org/10.1039/C8BM00005K.

(1161) He, T.; Luo, Y.; Zhang, Q.; Men, Z.; Su, T.; Fan, L.; Chen, H.; Shen, T. Hyalase-Mediated Cascade Degradation of a Matrix Barrier and Immune Cell Penetration by a Photothermal Microneedle for Efficient Anticancer Therapy. *ACS Appl. Mater. Interfaces* **2021**, *13* (23), 26790–26799. https://doi.org/10.1021/acsami.1c06725.

(1162) Lin, S.; Lin, H.; Yang, M.; Ge, M.; Chen, Y.; Zhu, Y. A Two-Dimensional MXene Potentiates a Therapeutic Microneedle Patch for Photonic Implantable Medicine in the Second NIR Biowindow. *Nanoscale* **2020**, *12* (18), 10265–10276. https://doi.org/10.1039/D0NR01444C.

(1163) Chen, M.; Quan, G.; Wen, T.; Yang, P.; Qin, W.; Mai, H.; Sun, Y.; Lu, C.; Pan, X.; Wu, C. Cold to Hot: Binary Cooperative Microneedle Array-Amplified Photoimmunotherapy for Eliciting Antitumor Immunity and the Abscopal Effect. *ACS Appl. Mater. Interfaces* **2020**, *12* (29), 32259–32269. https://doi.org/10.1021/acsami.0c05090.

(1164) Peng, T.; Huang, Y.; Feng, X.; Zhu, C.; Yin, S.; Wang, X.; Bai, X.; Pan, X.; Wu, C. TPGS/Hyaluronic Acid Dual-Functionalized PLGA Nanoparticles Delivered through Dissolving Microneedles for Markedly Improved Chemo-Photothermal Combined Therapy of Superficial Tumor. *Acta Pharm. Sin. B* **2021**, *11* (10), 3297–3309. https://doi.org/10.1016/j.apsb.2020.11.013.

(1165) Wei, S.; Quan, G.; Lu, C.; Pan, X.; Wu, C. Dissolving Microneedles Integrated with PH-Responsive Micelles Containing AIEgen with Ultra-Photostability for Enhancing Melanoma Photothermal Therapy. *Biomater. Sci.* **2020**, *8* (20), 5739–5750. https://doi.org/10.1039/D0BM00914H.

(1166) Zhao, Y.; Zhou, Y.; Yang, D.; Gao, X.; Wen, T.; Fu, J.; Wen, X.; Quan, G.; Pan, X.; Wu, C. Intelligent and Spatiotemporal Drug Release Based on Multifunctional Nanoparticle-Integrated Dissolving Microneedle System for Synergetic Chemo-Photothermal Therapy to Eradicate Melanoma. *Acta Biomater.* **2021**, *135*, 164–178. https://doi.org/10.1016/j.actbio.2021.09.009.

(1167) Ruan, L.; Song, G.; Zhang, X.; Liu, T.; Sun, Y.; Zhu, J.; Zeng, Z.; Jiang, G. Transdermal Delivery of Multifunctional CaO2@Mn-PDA Nanoformulations by Microneedles for NIR-Induced Synergistic Therapy against Skin Melanoma. *Biomater. Sci.* **2021**, *9* (20), 6830–6841. https://doi.org/10.1039/D1BM01117K.

(1168) Song, G.; Jiang, G.; Liu, T.; Zhang, X.; Zeng, Z.; Wang, R.; Li, P.; Yang, Y. Separable Microneedles for Synergistic Chemo-Photothermal Therapy against Superficial Skin Tumors. *ACS Biomater. Sci. Eng.* **2020**, *6* (7), 4116–4125. https://doi.org/10.1021/acsbiomaterials.0c00793.

(1169) Song, G.; Sun, Y.; Liu, T.; Zhang, X.; Zeng, Z.; Wang, R.; Li, P.; Li, C.; Jiang, G. Transdermal Delivery of Cu-Doped Polydopamine Using Microneedles for Photothermal and Chemodynamic Synergistic Therapy against Skin Melanoma. *Chem. Eng. J.* **2021**, *426*, 130790. https://doi.org/10.1016/j.cej.2021.130790.

(1170) Fu, J.; Li, C.; Liu, Y.; Chen, M.; Zhang, Q.; Yu, X.; Wu, B.; Li, J.; Du, L.; Dang, Y.; Wu, D.; Wei, M.; Lin, Z.; Lei, X. The Microneedles Carrying Cisplatin and IR820 to Perform Synergistic Chemo-Photodynamic Therapy against Breast Cancer. *J. Nanobiotechnology* **2020**, *18* (1), 146. https://doi.org/10.1186/s12951-020-00697-0.

(1171) Zhu, J.; Chang, R.; Wei, B.; Fu, Y.; Chen, X.; Liu, H.; Zhou, W. Photothermal Nano-Vaccine Promoting Antigen Presentation and Dendritic Cells Infiltration for Enhanced Immunotherapy of Melanoma via Transdermal Microneedles Delivery. *Res. (Washington, D.C.)* **2022**, *2022*, 9816272. https://doi.org/10.34133/2022/9816272.

(1172) Ye, Y.; Wang, C.; Zhang, X.; Hu, Q.; Zhang, Y.; Liu, Q.; Wen, D.; Milligan, J.; Bellotti, A.; Huang, L.; Dotti, G.; Gu, Z. A Melanin-Mediated Cancer Immunotherapy Patch. *Sci. Immunol.* **2017**, *2* (17), eaan5692. https://doi.org/10.1126/sciimmunol.aan5692.

(1173) Fan, L.; Zhang, X.; Nie, M.; Xu, Y.; Wang, Y.; Shang, L.; Zhao, Y.; Zhao, Y. Photothermal Responsive Microspheres-Triggered Separable Microneedles for Versatile Drug Delivery. *Adv. Funct. Mater.* **2022**, *32* (13), 2110746. https://doi.org/10.1002/adfm.202110746.

(1174) Zeng, Y.; Zhou, H.; Ding, J.; Zhou, W. Cell Membrane Inspired Nano-Shell Enabling Long-Acting Glucose Oxidase for Melanoma Starvation Therapy via Microneedles-Based Percutaneous Delivery. *Theranostics* **2021**, *11* (17), 8270–8282. https://doi.org/10.7150/thno.60758.

(1175) Gurtner, G. C.; Werner, S.; Barrandon, Y.; Longaker, M. T. Wound Repair and Regeneration. *Nature* **2008**, *453* (7193), 314–321. https://doi.org/10.1038/nature07039.

(1176) Guo, B.; Dong, R.; Liang, Y.; Li, M. Haemostatic Materials for Wound Healing Applications. *Nat. Rev. Chem.* **2021**, *5* (11), 773–791. https://doi.org/10.1038/s41570-021-00323-z.

(1177) Barnum, L.; Samandari, M.; Schmidt, T. A.; Tamayol, A. Microneedle Arrays for the Treatment of Chronic Wounds. *Expert Opin. Drug Deliv.* **2020**, *17* (12), 1767–1780. https://doi.org/10.1080/17425247.2020.1819787.

(1178) Wen, T.; Lin, Z.; Zhao, Y.; Zhou, Y.; Niu, B.; Shi, C.; Lu, C.; Wen, X.; Zhang, M.; Quan, G.; Wu, C.; Pan, X. Bioresponsive Nanoarchitectonics-Integrated Microneedles for Amplified Chemo-Photodynamic Therapy against Acne Vulgaris. *ACS Appl. Mater. Interfaces* **2021**, *13* (41), 48433–48448. https://doi.org/10.1021/acsami.1c15673.

(1179) Romanò, C. L.; De Vecchi, E.; Bortolin, M.; Morelli, I.; Drago, L. Hyaluronic Acid and Its Composites as a Local Antimicrobial/Antiadhesive Barrier. *J. bone Jt. Infect.* **2017**, *2* (1), 63–72. https://doi.org/10.7150/jbji.17705.

(1180) Yilmaz Atay, H. Antibacterial Activity of Chitosan-Based Systems. *Functional Chitosan: Drug Delivery and Biomedical Applications*. March 2020, pp 457–489. https://doi.org/10.1007/978-981-15-0263-7_15.

(1181) Petukhova, T. A.; Hassoun, L. A.; Foolad, N.; Barath, M.; Sivamani, R. K. Effect of Expedited Microneedle-Assisted Photodynamic Therapy for Field Treatment of Actinic Keratoses: A Randomized Clinical Trial. *JAMA Dermatology* **2017**, *153* (7), 637–643. https://doi.org/10.1001/jamadermatol.2017.0849.

(1182) Yan, D.; Zhao, H.; Li, C.; Xia, A.; Zhang, J.; Zhang, S.; Yun, Q.; Li, X.; Huang, F.; Tian, Y. A Clinical Study of Carbon Dioxide Lattice Laser–Assisted or Microneedle-Assisted 5-Aminolevulinic Acid–Based Photodynamic Therapy for the Treatment of Hypertrophic Acne Scars. *Photodermatol. Photoimmunol. Photomed.* **2022**, *38* (1), 53–59. https://doi.org/10.1111/phpp.12716.

(1183) Caffarel-Salvador, E.; Kearney, M.-C.; Mairs, R.; Gallo, L.; Stewart, S. A.; Brady, A. J.; Donnelly, R. F. Methylene Blue-Loaded Dissolving Microneedles: Potential Use in Photodynamic Antimicrobial Chemotherapy of Infected Wounds. *Pharmaceutics* **2015**, *7* (4), 397–412. https://doi.org/10.3390/pharmaceutics7040397.

(1184) Yu, X.; Zhao, J.; Fan, D. A Dissolving Microneedle Patch for Antibiotic/Enzymolysis/Photothermal Triple Therapy against Bacteria and Their Biofilms. *Chem. Eng. J.* **2022**, *437*, 135475. https://doi.org/10.1016/j.cej.2022.135475.

(1185) Zhang, C.; Jia, S.; Huang, J.; Peng, H.; Zhang, J.; Liu, L.; Zhang, W.; Xin, H.; Wang, X. A Carbonized Wormwood Modified Photothermal Microneedle Patch for the Repair of Damaged Skeletal Muscles. *J. Mater. Chem. B* **2021**, *9* (38), 8014–8020. https://doi.org/10.1039/D1TB00610J.

(1186) Ma, C. J.; He, Y.; Jin, X.; Zhang, Y.; Zhang, X.; Li, Y.; Xu, M.; Liu, K.; Yao, Y.; Lu, F. Light-Regulated Nitric Oxide Release from Hydrogel-Forming Microneedles Integrated with Graphene Oxide for Biofilm-Infected-Wound Healing. *Biomater. Adv.* **2022**, *134*, 112555. https://doi.org/10.1016/j.msec.2021.112555.

(1187) Zhu, W.; Mei, J.; Zhang, X.; Zhou, J.; Xu, D.; Su, Z.; Fang, S.; Wang, J.; Zhang, X.; Zhu, C. Photothermal Nanozyme-Based Microneedle Patch against Refractory Bacterial Biofilm Infection via Iron-Actuated Janus Ion Therapy. *Adv. Mater.* **2022**, *n/a* (n/a), 2207961. https://doi.org/10.1002/adma.202207961.

(1188) Lei, X.; Li, M.; Wang, C.; Cui, P.; Qiu, L.; Zhou, S.; Jiang, P.; Li, H.; Zhao, D.; Ni, X.; Wang, J.; Xia, J. Degradable Microneedle Patches Loaded with Antibacterial Gelatin Nanoparticles to Treat Staphylococcal Infection-Induced Chronic Wounds. *Int. J. Biol. Macromol.* **2022**, *217*, 55–65. https://doi.org/10.1016/j.ijbiomac.2022.07.021.

(1189) Zeng, Z.; Jiang, G.; Sun, Y.; Aharodnikau, U. E.; Yunusov, K. E.; Gao, X.; Liu, T.; Solomevich, S. O. Rational Design of Flexible Microneedles Coupled with CaO2@PDA-Loaded Nanofiber Films for Skin Wound Healing on Diabetic Rats. *Biomater. Sci.* **2022**, *10* (18), 5326–5339. https://doi.org/10.1039/D2BM00861K.

(1190) Wang, M.; Han, Y.; Yu, X.; Liang, L.; Chang, H.; Yeo, D. C.; Wiraja, C.; Wee, M. L.; Liu, L.; Liu, X.; Xu, C. Upconversion Nanoparticle Powered Microneedle Patches for Transdermal Delivery of SiRNA. *Adv. Healthc. Mater.* **2020**, *9* (2), 1900635. https://doi.org/10.1002/adhm.201900635.

(1191) Sun, L.; Fan, L.; Bian, F.; Chen, G.; Wang, Y.; Zhao, Y. MXene-Integrated Microneedle Patches with Innate Molecule Encapsulation for Wound Healing. *Res. (Washington, D.C.)* **2021**, *2021*, 9838490. https://doi.org/10.34133/2021/9838490.

(1192) Zhang, X.; Chen, G.; Liu, Y.; Sun, L.; Sun, L.; Zhao, Y. Black Phosphorus-Loaded Separable Microneedles as Responsive Oxygen Delivery Carriers for Wound Healing. *ACS Nano* **2020**, *14* (5), 5901–5908. https://doi.org/10.1021/acsnano.0c01059.

(1193) Yao, S.; Wang, Y.; Chi, J.; Yu, Y.; Zhao, Y.; Luo, Y.; Wang, Y. Porous MOF Microneedle Array Patch with Photothermal Responsive Nitric Oxide Delivery for Wound Healing. *Adv. Sci.* **2022**, *9* (3), 2103449. https://doi.org/10.1002/advs.202103449.

(1194) Frykberg, R. G. Topical Wound Oxygen Therapy in the Treatment of Chronic Diabetic Foot Ulcers. *Medicina (Kaunas).* **2021**, *57* (9). https://doi.org/10.3390/medicina57090917.

(1195) de Smet, G. H. J.; Kroese, L. F.; Menon, A. G.; Jeekel, J.; van Pelt, A. W. J.; Kleinrensink, G.-J.; Lange, J. F. Oxygen Therapies and Their Effects on Wound Healing. *Wound Repair Regen.* **2017**, *25* (4), 591–608. https://doi.org/10.1111/wrr.12561.

(1196) Castilla, D. M.; Liu, Z.-J.; Velazquez, O. C. Oxygen: Implications for Wound Healing. *Advances in wound*

care. United States December 2012, pp 225–230. https://doi.org/10.1089/wound.2011.0319.

(1197) Jin, Q.; Deng, Y.; Jia, F.; Tang, Z.; Ji, J. Gas Therapy: An Emerging "Green" Strategy for Anticancer Therapeutics. *Adv. Ther.* **2018**, *1* (6), 1800084. https://doi.org/10.1002/adtp.201800084.

(1198) Witte, M. B.; Barbul, A. Role of Nitric Oxide in Wound Repair. *Am. J. Surg.* **2002**, *183* (4), 406–412. https://doi.org/10.1016/S0002-9610(02)00815-2.

(1199) Schäffer, M. R.; Tantry, U.; Gross, S. S.; Wasserkrug, H. L.; Barbul, A. Nitric Oxide Regulates Wound Healing. *J. Surg. Res.* **1996**, *63* (1), 237–240. https://doi.org/10.1006/jsre.1996.0254.

(1200) Luo, J.; Chen, A. F. Nitric Oxide: A Newly Discovered Function on Wound Healing. *Acta Pharmacol. Sin.* **2005**, *26* (3), 259–264. https://doi.org/10.1111/j.1745-7254.2005.00058.x.

(1201) Jin, X.; Zhu, D. D.; Chen, B. Z.; Ashfaq, M.; Guo, X. D. Insulin Delivery Systems Combined with Microneedle Technology. *Adv. Drug Deliv. Rev.* **2018**, *127*, 119–137. https://doi.org/10.1016/j.addr.2018.03.011.

(1202) Liu, T.; Jiang, G.; Song, G.; Zhu, J.; Yang, Y. Fabrication of Separable Microneedles with Phase Change Coating for NIR-Triggered Transdermal Delivery of Metformin on Diabetic Rats. *Biomed. Microdevices* **2020**, *22* (1), 12. https://doi.org/10.1007/s10544-019-0468-8.

(1203) Zhang, Y.; Wang, D.; Gao, M.; Xu, B.; Zhu, J.; Yu, W.; Liu, D.; Jiang, G. Separable Microneedles for Near-Infrared Light-Triggered Transdermal Delivery of Metformin in Diabetic Rats. *ACS Biomater. Sci. Eng.* **2018**, *4* (8), 2879–2888. https://doi.org/10.1021/acsbiomaterials.8b00642.

(1204) Badrigilan, S.; Heydarpanahi, F.; Choupani, J.; Jaymand, M.; Samadian, H.; Hoseini-Ghahfarokhi, M.; Webster, T. J.; Tayebi, L. A Review on the Biodistribution, Pharmacokinetics and Toxicity of Bismuth-Based Nanomaterials. *Int. J. Nanomedicine* **2020**, *15*, 7079–7096. https://doi.org/10.2147/IJN.S250001.

(1205) Luo, Y.; Wang, C.; Qiao, Y.; Hossain, M.; Ma, L.; Su, M. In Vitro Cytotoxicity of Surface Modified Bismuth Nanoparticles. *J. Mater. Sci. Mater. Med.* **2012**, *23* (10), 2563–2573. https://doi.org/10.1007/s10856-012-4716-1.

(1206) Tadepalli, S.; Yim, J.; Cao, S.; Wang, Z.; Naik, R. R.; Singamaneni, S. Metal–Organic Framework Encapsulation for the Preservation and Photothermal Enhancement of Enzyme Activity. *Small* **2018**, *14* (7), 1702382. https://doi.org/10.1002/smll.201702382.

(1207) Montoya, N. A.; Roth, R. E.; Funk, E. K.; Gao, P.; Corbin, D. R.; Shiflett, M. B. Review on Porous Materials for the Thermal Stabilization of Proteins. *Microporous Mesoporous Mater.* **2022**, *333*, 111750. https://doi.org/10.1016/j.micromeso.2022.111750.

(1208) Jintapattanakit, A.; Junyaprasert, V. B.; Mao, S.; Sitterberg, J.; Bakowsky, U.; Kissel, T. Peroral Delivery of Insulin Using Chitosan Derivatives: A Comparative Study of Polyelectrolyte Nanocomplexes and Nanoparticles. *Int. J. Pharm.* **2007**, *342* (1), 240–249. https://doi.org/10.1016/j.ijpharm.2007.05.015.

(1209) Fan, L.; Zhang, X.; Liu, X.; Sun, B.; Li, L.; Zhao, Y. Responsive Hydrogel Microcarrier-Integrated Microneedles for Versatile and Controllable Drug Delivery. *Adv. Healthc. Mater.* **2021**, *10* (9), 2002249. https://doi.org/10.1002/adhm.202002249.

(1210) Lee, W. C.; Lim, C. H. Y. X.; Shi, H.; Tang, L. A. L.; Wang, Y.; Lim, C. T.; Loh, K. P. Origin of Enhanced Stem Cell Growth and Differentiation on Graphene and Graphene Oxide. *ACS Nano* **2011**, *5* (9), 7334–7341. https://doi.org/10.1021/nn202190c.

(1211) Teodorescu, F.; Oz, Y.; Quéniat, G.; Abderrahmani, A.; Foulon, C.; Lecoeur, M.; Sanyal, R.; Sanyal, A.; Boukherroub, R.; Szunerits, S. Photothermally Triggered On-Demand Insulin Release from Reduced Graphene Oxide Modified Hydrogels. *J. Control. release Off. J. Control. Release Soc.* **2017**, *246*, 164–173. https://doi.org/10.1016/j.jconrel.2016.10.028.

(1212) Babity, S.; Polomska, A. K.; Couture, F.; Bonmarin, M.; Fehr, D.; Detmar, M.; Brambilla, D. Rational Design of a Fluorescent Microneedle Tattoo for Minimally Invasive Monitoring of Lymphatic Function. *J.*

Control. Release **2020**, *327*, 350–359. https://doi.org/10.1016/j.jconrel.2020.08.017.

(1213) Polomska, A.; Gousopoulos, E.; Fehr, D.; Bachmann, A.; Bonmarin, M.; Detmar, M.; Lindenblatt, N. Development and Clinical Validation of the LymphMonitor Technology to Quantitatively Assess Lymphatic Function. *Diagnostics (Basel, Switzerland)* **2021**, *11* (10). https://doi.org/10.3390/diagnostics11101873.

(1214) Kolluru, C.; Gupta, R.; Jiang, Q.; Williams, M.; Gholami Derami, H.; Cao, S.; Noel, R. K.; Singamaneni, S.; Prausnitz, M. R. Plasmonic Paper Microneedle Patch for On-Patch Detection of Molecules in Dermal Interstitial Fluid. *ACS Sensors* **2019**, *4* (6), 1569–1576. https://doi.org/10.1021/acssensors.9b00258.

(1215) Sharma, B.; Frontiera, R. R.; Henry, A.-I.; Ringe, E.; Van Duyne, R. P. SERS: Materials, Applications, and the Future. *Mater. Today* **2012**, *15* (1), 16–25. https://doi.org/10.1016/S1369-7021(12)70017-2.

(1216) Xia, L.; Chen, M.; Zhao, X.; Zhang, Z.; Xia, J.; Xu, H.; Sun, M. Visualized Method of Chemical Enhancement Mechanism on SERS and TERS. *J. Raman Spectrosc.* **2014**, *45* (7), 533–540. https://doi.org/10.1002/jrs.4504.

(1217) Cardinal, M. F.; Vander Ende, E.; Hackler, R. A.; McAnally, M. O.; Stair, P. C.; Schatz, G. C.; Van Duyne, R. P. Expanding Applications of SERS through Versatile Nanomaterials Engineering. *Chem. Soc. Rev.* **2017**, *46* (13), 3886–3903. https://doi.org/10.1039/C7CS00207F.

(1218) Mei, R.; Wang, Y.; Shi, S.; Zhao, X.; Zhang, Z.; Wang, X.; Shen, D.; Kang, Q.; Chen, L. Highly Sensitive and Reliable Internal-Standard Surface-Enhanced Raman Scattering Microneedles for Determination of Bacterial Metabolites as Infection Biomarkers in Skin Interstitial Fluid. *Anal. Chem.* **2022**, *94* (46), 16069–16078. https://doi.org/10.1021/acs.analchem.2c03208.

(1219) Wang, Y.; Ni, H.; Li, H.; Chen, J.; Zhang, D.; Fu, L. Plasmonic Microneedle Arrays for Rapid Extraction, SERS Detection, and Inactivation of Bacteria. *Chem. Eng. J.* **2022**, *442*, 136140. https://doi.org/10.1016/j.cej.2022.136140.

(1220) Pan, C.; Li, X.; Sun, J.; Li, Z.; Zhang, L.; Qian, W.; Wang, P.; Dong, J. A Multiplexed SERS-Active Microneedle for Simultaneous Redox Potential and PH Measurements in Rat Joints. *ACS Appl. Bio Mater.* **2019**, *2* (5), 2102–2108. https://doi.org/10.1021/acsabm.9b00117.

(1221) Park, J. E.; Yonet-Tanyeri, N.; Vander Ende, E.; Henry, A.-I.; Perez White, B. E.; Mrksich, M.; Van Duyne, R. P. Plasmonic Microneedle Arrays for in Situ Sensing with Surface-Enhanced Raman Spectroscopy (SERS). *Nano Lett.* **2019**, *19* (10), 6862–6868. https://doi.org/10.1021/acs.nanolett.9b02070.

(1222) Ju, J.; Hsieh, C.-M.; Tian, Y.; Kang, J.; Chia, R.; Chang, H.; Bai, Y.; Xu, C.; Wang, X.; Liu, Q. Surface Enhanced Raman Spectroscopy Based Biosensor with a Microneedle Array for Minimally Invasive In Vivo Glucose Measurements. *ACS Sensors* **2020**, *5* (6), 1777–1785. https://doi.org/10.1021/acssensors.0c00444.

(1223) Li, S.; Kim, Y.; Lee, J. W.; Prausnitz, M. R. Microneedle Patch Tattoos. *iScience* **2022**, *25* (10), 105014. https://doi.org/10.1016/j.isci.2022.105014.

(1224) Liu, L.; Wang, S.; Zhao, B.; Pei, P.; Fan, Y.; Li, X.; Zhang, F. Er3+ Sensitized 1530 Nm to 1180 Nm Second Near-Infrared Window Upconversion Nanocrystals for In Vivo Biosensing. *Angew. Chemie Int. Ed.* **2018**, *57* (25), 7518–7522. https://doi.org/10.1002/anie.201802889.

(1225) Cui, Y.; Duan, W.; Jin, Y.; Wo, F.; Xi, F.; Wu, J. Ratiometric Fluorescent Nanohybrid for Noninvasive and Visual Monitoring of Sweat Glucose. *ACS Sensors* **2020**, *5* (7), 2096–2105. https://doi.org/10.1021/acssensors.0c00718.

(1226) Babity, S.; Couture, F.; Campos, E. V. R.; Hedtrich, S.; Hagen, R.; Fehr, D.; Bonmarin, M.; Brambilla, D. A Naked Eye-Invisible Ratiometric Fluorescent Microneedle Tattoo for Real-Time Monitoring of Inflammatory Skin Conditions. *Adv. Healthc. Mater.* **2022**, *11* (6), 2102070. https://doi.org/10.1002/adhm.202102070.

(1227) Li, J.; Lu, H.; Wang, Y.; Yang, S.; Zhang, Y.; Wei, W.; Qiao, Y.; Dai, W.; Ge, R.; Dong, H. Interstitial

Fluid Biomarkers' Minimally Invasive Monitoring Using Microneedle Sensor Arrays. *Anal. Chem.* **2022**, *94* (2), 968–974. https://doi.org/10.1021/acs.analchem.1c03827.

(1228) Mohammadpour, F.; Hadizadeh, F.; Tafaghodi, M.; Sadri, K.; Mohammadpour, A. H.; Kalani, M. R.; Gholami, L.; Mahmoudi, A.; Chamani, J. Preparation, in Vitro and in Vivo Evaluation of PLGA/Chitosan Based Nano-Complex as a Novel Insulin Delivery Formulation. *Int. J. Pharm.* **2019**, *572*, 118710. https://doi.org/10.1016/j.ijpharm.2019.118710.

(1229) Zheng, H.; GhavamiNejad, A.; GhavamiNejad, P.; Samarikhalaj, M.; Giacca, A.; Poudineh, M. Hydrogel Microneedle-Assisted Assay Integrating Aptamer Probes and Fluorescence Detection for Reagentless Biomarker Quantification. *ACS Sensors* **2022**, *7* (8), 2387–2399. https://doi.org/10.1021/acssensors.2c01033.

(1230) McHugh, K. J.; Jing, L.; Severt, S. Y.; Cruz, M.; Sarmadi, M.; Jayawardena, H. S. N.; Perkinson, C. F.; Larusson, F.; Rose, S.; Tomasic, S.; Graf, T.; Tzeng, S. Y.; Sugarman, J. L.; Vlasic, D.; Peters, M.; Peterson, N.; Wood, L.; Tang, W.; Yeom, J.; Collins, J.; Welkhoff, P. A.; Karchin, A.; Tse, M.; Gao, M.; Bawendi, M. G.; Langer, R.; Jaklenec, A. Biocompatible Near-Infrared Quantum Dots Delivered to the Skin by Microneedle Patches Record Vaccination. *Sci. Transl. Med.* **2019**, *11* (523), eaay7162. https://doi.org/10.1126/scitranslmed.aay7162.

(1231) Sandby-Møller, J.; Poulsen, T.; Wulf, H. C. Epidermal Thickness at Different Body Sites: Relationship to Age, Gender, Pigmentation, Blood Content, Skin Type and Smoking Habits. *Acta Derm. Venereol.* **2003**, *83* (6), 410–413. https://doi.org/10.1080/00015550310015419.

(1232) Laurent, A.; Mistretta, F.; Bottigioli, D.; Dahel, K.; Goujon, C.; Nicolas, J. F.; Hennino, A.; Laurent, P. E. Echographic Measurement of Skin Thickness in Adults by High Frequency Ultrasound to Assess the Appropriate Microneedle Length for Intradermal Delivery of Vaccines. *Vaccine* **2007**, *25* (34), 6423–6430. https://doi.org/10.1016/j.vaccine.2007.05.046.

(1233) Derraik, J. G. B.; Rademaker, M.; Cutfield, W. S.; Pinto, T. E.; Tregurtha, S.; Faherty, A.; Peart, J. M.; Drury, P. L.; Hofman, P. L. Effects of Age, Gender, BMI, and Anatomical Site on Skin Thickness in Children and Adults with Diabetes. *PLoS One* **2014**, *9* (1), e86637.

(1234) Tatovic, D.; McAteer, M. A.; Barry, J.; Barrientos, A.; Rodríguez Terradillos, K.; Perera, I.; Kochba, E.; Levin, Y.; Dul, M.; Coulman, S. A.; Birchall, J. C.; von Ruhland, C.; Howell, A.; Stenson, R.; Alhadj Ali, M.; Luzio, S. D.; Dunseath, G.; Cheung, W. Y.; Holland, G.; May, K.; Ingram, J. R.; Chowdhury, M. M. U.; Wong, F. S.; Casas, R.; Dayan, C.; Ludvigsson, J. Safety of the Use of Gold Nanoparticles Conjugated with Proinsulin Peptide and Administered by Hollow Microneedles as an Immunotherapy in Type 1 Diabetes. *Immunother. Adv.* **2022**, *2* (1), ltac002. https://doi.org/10.1093/immadv/ltac002.

(1235) Lee, J. W.; Prausnitz, M. R. Drug Delivery Using Microneedle Patches: Not Just for Skin. *Expert Opin. Drug Deliv.* **2018**, *15* (6), 541–543. https://doi.org/10.1080/17425247.2018.1471059.

(1236) Voronova, A.; Prieto, C.; Pardo-Figuerez, M.; Lagaron, J. M.; Sanyal, A.; Demir, B.; Hubert, T.; Plaisance, V.; Pawlowski, V.; Vignoud-Despond, S.; Barras, A.; Abderrahmani, A.; Boukherroub, R.; Szunerits, S. Photothermal Activatable Mucoadhesive Fiber Mats for On-Demand Delivery of Insulin via Buccal and Corneal Mucosa. *ACS Appl. Bio Mater.* **2022**, *5* (2), 771–778. https://doi.org/10.1021/acsabm.1c01161.

(1237) Xia, D.; Toy, R.; Pradhan, P.; Hejri, A.; Chae, J.; Grossniklaus, H. E.; Cursiefen, C.; Roy, K.; Prausnitz, M. R. Enhanced Immune Responses to Vaccine Antigens in the Corneal Stroma. *J. Control. Release* **2022**, S0168-3659(22)00798-2. https://doi.org/10.1016/j.jconrel.2022.11.045.

(1238) Arrangoiz, R.; Dorantes, J.; Cordera, F.; Muñoz, M.; Paquentin, E.; Luque-de-León, E. Melanoma Review: Epidemiology, Risk Factors, Diagnosis and Staging. *J. Cancer Treat. Res.* **2016**, *Volume 4*, Pages:1-15. https://doi.org/10.11648/j.jctr.20160401.11.

(1239) Conforti, C.; Zalaudek, I. Epidemiology and Risk Factors of Melanoma: A Review. *Dermatol. Pract. Concept.* **2021**, *11* (Suppl 1), e2021161S-e2021161S. https://doi.org/10.5826/dpc.11S1a161S.

(1240) Berk-Krauss, J.; Stein, J. A.; Weber, J.; Polsky, D.; Geller, A. C. New Systematic Therapies and Trends in

Cutaneous Melanoma Deaths Among US Whites, 1986–2016. *Am. J. Public Health* **2020**, *110* (5), 731–733. https://doi.org/10.2105/AJPH.2020.305567.

(1241) Mkhobongo, B.; Chandran, R.; Abrahamse, H. Impact of Aluminium Phthalocyanine Nanoconjugate on Melanoma Stem Cells. *Artif. Cells, Nanomedicine, Biotechnol.* **2023**, *51* (1), 334–345. https://doi.org/10.1080/21691401.2023.2233568.

(1242) Zhou, Y.; Fan, S.; Feng, L.; Huang, X.; Chen, X. Manipulating Intratumoral Fenton Chemistry for Enhanced Chemodynamic and Chemodynamic-Synergized Multimodal Therapy. *Adv. Mater.* **2021**, *33* (48), 2104223. https://doi.org/10.1002/adma.202104223.

(1243) Wang, S.; Yu, G.; Yang, W.; Wang, Z.; Jacobson, O.; Tian, R.; Deng, H.; Lin, L.; Chen, X. Photodynamic-Chemodynamic Cascade Reactions for Efficient Drug Delivery and Enhanced Combination Therapy. *Adv. Sci.* **2021**, *8* (10), 2002927. https://doi.org/10.1002/advs.202002927.

(1244) Han, H.; Li, J.; Santos, H. A. Recent Advances in Fenton and Fenton-like Reaction Mediated Nanoparticle in Cancer Therapy. *Biomed. Technol.* **2023**, *3*, 40–51. https://doi.org/10.1016/j.bmt.2022.12.004.

(1245) Yang, B.; Chen, Y.; Shi, J. Nanocatalytic Medicine. *Adv. Mater.* **2019**, *31* (39), 1901778. https://doi.org/10.1002/adma.201901778.

(1246) Fu, L.-H.; Qi, C.; Hu, Y.-R.; Lin, J.; Huang, P. Glucose Oxidase-Instructed Multimodal Synergistic Cancer Therapy. *Adv. Mater.* **2019**, *31* (21), e1808325. https://doi.org/10.1002/adma.201808325.

(1247) Wang, S.; Yu, G.; Wang, Z.; Jacobson, O.; Lin, L.-S.; Yang, W.; Deng, H.; He, Z.; Liu, Y.; Chen, Z.-Y.; Chen, X. Enhanced Antitumor Efficacy by a Cascade of Reactive Oxygen Species Generation and Drug Release. *Angew. Chemie Int. Ed.* **2019**, *58* (41), 14758–14763. https://doi.org/10.1002/anie.201908997.

(1248) Tian, Q.; Xue, F.; Wang, Y.; Cheng, Y.; An, L.; Yang, S.; Chen, X.; Huang, G. Recent Advances in Enhanced Chemodynamic Therapy Strategies. *Nano Today* **2021**, *39*, 101162. https://doi.org/10.1016/j.nantod.2021.101162.

(1249) Chota, A.; George, B. P.; Abrahamse, H. Reactive Oxygen Species–Induced Cancer Cell Death: A Therapeutic Approach. In *Handbook of Oxidative Stress in Cancer: Therapeutic Aspects*; Springer, 2022; pp 3793–3808. https://doi.org/10.1007/978-981-16-5422-0_202.

(1250) Sun, Q.; Wang, Z.; Liu, B.; He, F.; Gai, S.; Yang, P.; Yang, D.; Li, C.; Lin, J. Recent Advances on Endogenous/Exogenous Stimuli-Triggered Nanoplatforms for Enhanced Chemodynamic Therapy. *Coord. Chem. Rev.* **2022**, *451*, 214267. https://doi.org/10.1016/j.ccr.2021.214267.

(1251) Shan, J.; Zhang, X.; Wang, L.; Zhao, Y. Spatiotemporal Catalytic Nanozymes Microneedle Patches with Opposite Properties for Wound Management. *Small* **2023**, *n/a* (n/a), 2302347. https://doi.org/10.1002/smll.202302347.

(1252) Kent, R. D.; Vikesland, P. J. Dissolution and Persistence of Copper-Based Nanomaterials in Undersaturated Solutions with Respect to Cupric Solid Phases. *Environ. Sci. Technol.* **2016**, *50* (13), 6772–6781. https://doi.org/10.1021/acs.est.5b04719.

(1253) Argueta-Figueroa, L.; Martínez-Alvarez, O.; Santos-Cruz, J.; Garcia-Contreras, R.; Acosta-Torres, L. S.; de la Fuente-Hernández, J.; Arenas-Arrocena, M. C. Nanomaterials Made of Non-Toxic Metallic Sulfides: A Systematic Review of Their Potential Biomedical Applications. *Mater. Sci. Eng. C* **2017**, *76*, 1305–1315. https://doi.org/10.1016/j.msec.2017.02.120.

(1254) Guo, L.; Yan, D. D.; Yang, D.; Li, Y.; Wang, X.; Zalewski, O.; Yan, B.; Lu, W. Combinatorial Photothermal and Immuno Cancer Therapy Using Chitosan-Coated Hollow Copper Sulfide Nanoparticles. *ACS Nano* **2014**, *8* (6), 5670–5681. https://doi.org/10.1021/nn5002112.

(1255) Ning, S.; Zhang, X.; Suo, M.; Lyu, M.; Pan, Y.; Jiang, Y.; Yang, H.; Yip Lam, J. W.; Zhang, T.; Pan, L.; Tang, B. Z. Platelet-Derived Exosomes Hybrid Liposomes Facilitate Uninterrupted Singlet Oxygen Generation to Enhance Breast Cancer Immunotherapy. *Cell Reports Phys. Sci.* **2023**, *4* (7), 101505.

https://doi.org/10.1016/j.xcrp.2023.101505.

(1256) Wang, J.; Zhang, Y.; Archibong, E.; Ligler, F. S.; Gu, Z. Leveraging H2O2 Levels for Biomedical Applications. *Adv. Biosyst.* **2017**, *1* (9), 1700084. https://doi.org/10.1002/adbi.201700084.

(1257) Bauleth-Ramos, T.; El-Sayed, N.; Fontana, F.; Lobita, M.; Shahbazi, M.-A.; Santos, H. A. Recent Approaches for Enhancing the Performance of Dissolving Microneedles in Drug Delivery Applications. *Mater. Today* **2023**, *63*, 239–287. https://doi.org/10.1016/j.mattod.2022.12.007.

(1258) Larrañeta, E.; Lutton, R. E. M.; Woolfson, A. D.; Donnelly, R. F. Microneedle Arrays as Transdermal and Intradermal Drug Delivery Systems: Materials Science, Manufacture and Commercial Development. *Mater. Sci. Eng. R Reports* **2016**, *104*, 1–32. https://doi.org/10.1016/j.mser.2016.03.001.

(1259) Tran, K. T. M.; Le, T. T.; Agrahari, V.; Peet, M. M.; Ouattara, L. A.; Anderson, S. M.; Le-Kim, T. H.; Singh, O. N.; Doncel, G. F.; Nguyen, T. D. Single-Administration Long-Acting Microarray Patch with Ultrahigh Loading Capacity and Multiple Releases of Thermally Stable Antibodies. *Mol. Pharm.* **2023**, *20* (5), 2352–2361. https://doi.org/10.1021/acs.molpharmaceut.2c00919.

(1260) Tran, K. T. M.; Gavitt, T. D.; Le, T. T.; Graichen, A.; Lin, F.; Liu, Y.; Tulman, E. R.; Szczepanek, S. M.; Nguyen, T. D. A Single-Administration Microneedle Skin Patch for Multi-Burst Release of Vaccine against SARS-CoV-2. *Adv. Mater. Technol.* **2023**, *8* (3), 2200905. https://doi.org/10.1002/admt.202200905.

(1261) Park, J.-H.; Allen, M. G.; Prausnitz, M. R. Polymer Microneedles for Controlled-Release Drug Delivery. *Pharm. Res.* **2006**, *23* (5), 1008–1019. https://doi.org/10.1007/s11095-006-0028-9.

(1262) Mistilis, M. J.; Joyce, J. C.; Esser, E. S.; Skountzou, I.; Compans, R. W.; Bommarius, A. S.; Prausnitz, M. R. Long-Term Stability of Influenza Vaccine in a Dissolving Microneedle Patch. *Drug Deliv. Transl. Res.* **2017**, *7* (2), 195–205. https://doi.org/10.1007/s13346-016-0282-2.

(1263) Shan, J.; Zhang, X.; Cheng, Y.; Song, C.; Chen, G.; Gu, Z.; Zhao, Y. Glucose Metabolism-Inspired Catalytic Patches for NIR-II Phototherapy of Diabetic Wound Infection. *Acta Biomater.* **2023**, *157*, 200–209. https://doi.org/10.1016/j.actbio.2022.12.001.

(1264) Karim, M. N.; Singh, M.; Weerathunge, P.; Bian, P.; Zheng, R.; Dekiwadia, C.; Ahmed, T.; Walia, S.; Della Gaspera, E.; Singh, S.; Ramanathan, R.; Bansal, V. Visible-Light-Triggered Reactive-Oxygen-Species-Mediated Antibacterial Activity of Peroxidase-Mimic CuO Nanorods. *ACS Appl. Nano Mater.* **2018**, *1* (4), 1694–1704. https://doi.org/10.1021/acsanm.8b00153.

(1265) Payra, S.; Likhitha Reddy, K.; Sharma, R. S.; Singh, S.; Roy, S. A Trade-off between Adsorption and Photocatalysis over ZIF-Derived Composite. *J. Hazard. Mater.* **2020**, *393*, 122491. https://doi.org/10.1016/j.jhazmat.2020.122491.

(1266) Manikkoth, S. T.; Thulasi, K. M.; Palantavida, S.; Kizhakkekilikoodayil Vijayan, B. In-Situ Synthesis of Titania Nanosheet – CdS Nanoparticle Composites by Combined Hydrothermal – Selective Adsorption and Reaction for Enhanced Photocatalytic Activity. *Mater. Today Proc.* **2021**, *41*, 660–664. https://doi.org/10.1016/j.matpr.2020.05.374.

(1267) Ingenbosch, K. N.; Quint, S.; Dyllick-Brenzinger, M.; Wunschik, D. S.; Kiebist, J.; Süss, P.; Liebelt, U.; Zuhse, R.; Menyes, U.; Scheibner, K.; Mayer, C.; Opwis, K.; Gutmann, J. S.; Hoffmann-Jacobsen, K. Singlet-Oxygen Generation by Peroxidases and Peroxygenases for Chemoenzymatic Synthesis. *ChemBioChem* **2021**, *22* (2), 398–407. https://doi.org/10.1002/cbic.202000326.

(1268) Tsiakiri, E. P.; Sompatzi, E.; Voukia, F.; Sotiropoulos, S.; Pantazaki, A. A. Biocatalytic and Bioelectrolytic Decolorization of Simulated Melanoidin Wastewaters by Saccharomyces Cerevisiae Cells Suspended and Conjugated on Silica and Alumina. *J. Environ. Chem. Eng.* **2020**, *8* (5), 104078. https://doi.org/10.1016/j.jece.2020.104078.

(1269) Kadnikova, E. N.; Kostić, N. M. Oxidation of ABTS by Hydrogen Peroxide Catalyzed by Horseradish Peroxidase Encapsulated into Sol–Gel Glass.: Effects of Glass Matrix on Reactivity. *J. Mol. Catal. B Enzym.* **2002**, *18* (1), 39–48. https://doi.org/10.1016/S1381-1177(02)00057-7.

(1270) Skovsen, E.; Snyder, J. W.; Lambert, J. D. C.; Ogilby, P. R. Lifetime and Diffusion of Singlet Oxygen in a Cell. *J. Phys. Chem. B* **2005**, *109* (18), 8570–8573. https://doi.org/10.1021/jp051163i.

(1271) Azmana, M.; Mahmood, S.; Hilles, A. R.; Mandal, U. K.; Saeed Al-Japairai, K. A.; Raman, S. Transdermal Drug Delivery System through Polymeric Microneedle: A Recent Update. *J. Drug Deliv. Sci. Technol.* **2020**, *60*, 101877. https://doi.org/10.1016/j.jddst.2020.101877.

(1272) Mangang, K. N.; Thakran, P.; Halder, J.; Yadav, K. S.; Ghosh, G.; Pradhan, D.; Rath, G.; Rai, V. K. PVP-Microneedle Array for Drug Delivery: Mechanical Insight, Biodegradation, and Recent Advances. *J. Biomater. Sci. Polym. Ed.* **2023**, *34* (7), 986–1017. https://doi.org/10.1080/09205063.2022.2155778.

(1273) Salwa; Chevala, N. T.; Jitta, S. R.; Marques, S. M.; Vaz, V. M.; Kumar, L. Polymeric Microneedles for Transdermal Delivery of Nanoparticles: Frontiers of Formulation, Sterility and Stability Aspects. *J. Drug Deliv. Sci. Technol.* **2021**, *65*, 102711. https://doi.org/10.1016/j.jddst.2021.102711.

(1274) Nain, A.; Wei, S.-C.; Lin, Y.-F.; Tseng, Y.-T.; Mandal, R. P.; Huang, Y.-F.; Huang, C.-C.; Tseng, F.-G.; Chang, H.-T. Copper Sulfide Nanoassemblies for Catalytic and Photoresponsive Eradication of Bacteria from Infected Wounds. *ACS Appl. Mater. Interfaces* **2021**, *13* (7), 7865–7878. https://doi.org/10.1021/acsami.0c18999.

(1275) Ayaz Ahmed, K. B.; Anbazhagan, V. Synthesis of Copper Sulfide Nanoparticles and Evaluation of in Vitro Antibacterial Activity and in Vivo Therapeutic Effect in Bacteria-Infected Zebrafish. *RSC Adv.* **2017**, *7* (58), 36644–36652. https://doi.org/10.1039/C7RA05636B.

(1276) Wang, W.; Li, B.; Yang, H.; Lin, Z.; Chen, L.; Li, Z.; Ge, J.; Zhang, T.; Xia, H.; Li, L.; Lu, Y. Efficient Elimination of Multidrug-Resistant Bacteria Using Copper Sulfide Nanozymes Anchored to Graphene Oxide Nanosheets. *Nano Res.* **2020**, *13* (8), 2156–2164. https://doi.org/10.1007/s12274-020-2824-7.

(1277) Gupte, A.; Mumper, R. J. Elevated Copper and Oxidative Stress in Cancer Cells as a Target for Cancer Treatment. *Cancer Treat. Rev.* **2009**, *35* (1), 32–46. https://doi.org/10.1016/j.ctrv.2008.07.004.

(1278) Wang, J.; Luo, C.; Shan, C.; You, Q.; Lu, J.; Elf, S.; Zhou, Y.; Wen, Y.; Vinkenborg, J. L.; Fan, J.; Kang, H.; Lin, R.; Han, D.; Xie, Y.; Karpus, J.; Chen, S.; Ouyang, S.; Luan, C.; Zhang, N.; Ding, H.; Merkx, M.; Liu, H.; Chen, J.; Jiang, H.; He, C. Inhibition of Human Copper Trafficking by a Small Molecule Significantly Attenuates Cancer Cell Proliferation. *Nat. Chem.* **2015**, *7* (12), 968–979. https://doi.org/10.1038/nchem.2381.

(1279) Guo, L.; Panderi, I.; Yan, D. D.; Szulak, K.; Li, Y.; Chen, Y.-T.; Ma, H.; Niesen, D. B.; Seeram, N.; Ahmed, A.; Yan, B.; Pantazatos, D.; Lu, W. A Comparative Study of Hollow Copper Sulfide Nanoparticles and Hollow Gold Nanospheres on Degradability and Toxicity. *ACS Nano* **2013**, *7* (10), 8780–8793. https://doi.org/10.1021/nn403202w.

(1280) Rahmani, J.; Miri, A.; Namjoo, I.; Zamaninour, N.; Maljaei, M. B.; Zhou, K.; Cerneviciute, R.; Mousavi, S. M.; Varkaneh, H. K.; Salehisahlabadi, A. Elevated Liver Enzymes and Cardiovascular Mortality: A Systematic Review and Dose–Response Meta-Analysis of More than One Million Participants. *Eur. J. Gastroenterol. Hepatol.* **2019**, *31* (5), 555–562. https://doi.org/10.1097/MEG.0000000000001353.

(1281) Shao, Y.; Dong, K.; Lu, X.; Gao, B.; He, B. Bioinspired 3D-Printed MXene and Spidroin-Based Near-Infrared Light-Responsive Microneedle Scaffolds for Efficient Wound Management. *ACS Appl. Mater. Interfaces* **2022**, *14* (51), 56525–56534. https://doi.org/10.1021/acsami.2c16277.

(1282) Chang, K.; Gao, D.; Qi, Q.; Liu, Y.; Yuan, Z. Engineering Biocompatible Benzodithiophene-Based Polymer Dots with Tunable Absorptions as High-Efficiency Theranostic Agents for Multiscale Photoacoustic Imaging-Guided Photothermal Therapy. *Biomater. Sci.* **2019**, *7* (4), 1486–1492. https://doi.org/10.1039/C8BM01577E.

(1283) Lopez-Ramirez, M. A.; Soto, F.; Wang, C.; Rueda, R.; Shukla, S.; Silva-Lopez, C.; Kupor, D.; McBride, D. A.; Pokorski, J. K.; Nourhani, A.; Steinmetz, N. F.; Shah, N. J.; Wang, J. Built-In Active Microneedle Patch with Enhanced Autonomous Drug Delivery. *Adv. Mater.* **2020**, *32* (1), 1905740. https://doi.org/10.1002/adma.201905740.

(1284) Kennedy, J.; Larrañeta, E.; McCrudden, M. T. C.; McCrudden, C. M.; Brady, A. J.; Fallows, S. J.; McCarthy, H. O.; Kissenpfennig, A.; Donnelly, R. F. In Vivo Studies Investigating Biodistribution of Nanoparticle-Encapsulated Rhodamine B Delivered via Dissolving Microneedles. *J. Control. Release* **2017**, *265*, 57–65. https://doi.org/10.1016/j.jconrel.2017.04.022.

(1285) Ito, Y.; Hirono, M.; Fukushima, K.; Sugioka, N.; Takada, K. Two-Layered Dissolving Microneedles Formulated with Intermediate-Acting Insulin. *Int. J. Pharm.* **2012**, *436* (1), 387–393. https://doi.org/10.1016/j.ijpharm.2012.06.047.

(1286) Piechotta, V.; Harder, T. Waning of COVID-19 Vaccine Effectiveness: Individual and Public Health Risk. *Lancet (London, England)* **2022**, *399* (10328), 887–889. https://doi.org/10.1016/S0140-6736(22)00282-3.

(1287) Feikin, D. R.; Higdon, M. M.; Abu-Raddad, L. J.; Andrews, N.; Araos, R.; Goldberg, Y.; Groome, M. J.; Huppert, A.; O'Brien, K. L.; Smith, P. G.; Wilder-Smith, A.; Zeger, S.; Deloria Knoll, M.; Patel, M. K. Duration of Effectiveness of Vaccines against SARS-CoV-2 Infection and COVID-19 Disease: Results of a Systematic Review and Meta-Regression. *Lancet (London, England)* **2022**, *399* (10328), 924–944. https://doi.org/10.1016/S0140-6736(22)00152-0.

(1288) Menni, C.; May, A.; Polidori, L.; Louca, P.; Wolf, J.; Capdevila, J.; Hu, C.; Ourselin, S.; Steves, C. J.; Valdes, A. M.; Spector, T. D. COVID-19 Vaccine Waning and Effectiveness and Side-Effects of Boosters: A Prospective Community Study from the ZOE COVID Study. *Lancet Infect. Dis.* **2022**, *22* (7), 1002–1010. https://doi.org/10.1016/S1473-3099(22)00146-3.

(1289) Ferdinands, J. M.; Rao, S.; Dixon, B. E.; Mitchell, P. K.; DeSilva, M. B.; Irving, S. A.; Lewis, N.; Natarajan, K.; Stenehjem, E.; Grannis, S. J.; Han, J.; McEvoy, C.; Ong, T. C.; Naleway, A. L.; Reese, S. E.; Embi, P. J.; Dascomb, K.; Klein, N. P.; Griggs, E. P.; Konatham, D.; Kharbanda, A. B.; Yang, D.-H.; Fadel, W. F.; Grisel, N.; Goddard, K.; Patel, P.; Liao, I.-C.; Birch, R.; Valvi, N. R.; Reynolds, S.; Arndorfer, J.; Zerbo, O.; Dickerson, M.; Murthy, K.; Williams, J.; Bozio, C. H.; Blanton, L.; Verani, J. R.; Schrag, S. J.; Dalton, A. F.; Wondimu, M. H.; Link-Gelles, R.; Azziz-Baumgartner, E.; Barron, M. A.; Gaglani, M.; Thompson, M. G.; Fireman, B. Waning 2-Dose and 3-Dose Effectiveness of MRNA Vaccines Against COVID-19–Associated Emergency Department and Urgent Care Encounters and Hospitalizations Among Adults During Periods of Delta and Omicron Variant Predominance — VISION Network, 10 States, Aug. *MMWR. Morb. Mortal. Wkly. Rep.* **2022**, *71* (7), 255–263. https://doi.org/10.15585/mmwr.mm7107e2.

(1290) Thompson, M. G.; Natarajan, K.; Irving, S. A.; Rowley, E. A.; Griggs, E. P.; Gaglani, M.; Klein, N. P.; Grannis, S. J.; DeSilva, M. B.; Stenehjem, E.; Reese, S. E.; Dickerson, M.; Naleway, A. L.; Han, J.; Konatham, D.; McEvoy, C.; Rao, S.; Dixon, B. E.; Dascomb, K.; Lewis, N.; Levy, M. E.; Patel, P.; Liao, I.-C.; Kharbanda, A. B.; Barron, M. A.; Fadel, W. F.; Grisel, N.; Goddard, K.; Yang, D.-H.; Wondimu, M. H.; Murthy, K.; Valvi, N. R.; Arndorfer, J.; Fireman, B.; Dunne, M. M.; Embi, P.; Azziz-Baumgartner, E.; Zerbo, O.; Bozio, C. H.; Reynolds, S.; Ferdinands, J.; Williams, J.; Link-Gelles, R.; Schrag, S. J.; Verani, J. R.; Ball, S.; Ong, T. C. Effectiveness of a Third Dose of MRNA Vaccines Against COVID-19-Associated Emergency Department and Urgent Care Encounters and Hospitalizations Among Adults During Periods of Delta and Omicron Variant Predominance - VISION Network, 10 States, August 2021-. *MMWR. Morb. Mortal. Wkly. Rep.* **2022**, *71* (4), 139–145. https://doi.org/10.15585/mmwr.mm7104e3.

(1291) Lau, J. J.; Cheng, S. M. S.; Leung, K.; Lee, C. K.; Hachim, A.; Tsang, L. C. H.; Yam, K. W. H.; Chaothai, S.; Kwan, K. K. H.; Chai, Z. Y. H.; Lo, T. H. K.; Mori, M.; Wu, C.; Valkenburg, S. A.; Amarasinghe, G. K.; Lau, E. H. Y.; Hui, D. S. C.; Leung, G. M.; Peiris, M.; Wu, J. T. Real-World COVID-19 Vaccine Effectiveness against the Omicron BA.2 Variant in a SARS-CoV-2 Infection-Naive Population. *Nat. Med.* **2023**, *29* (2), 348–357. https://doi.org/10.1038/s41591-023-02219-5.

(1292) Yan, V. K. C.; Wan, E. Y. F.; Ye, X.; Mok, A. H. Y.; Lai, F. T. T.; Chui, C. S. L.; Li, X.; Wong, C. K. H.; Li, P. H.; Ma, T.; Qin, S.; Lau, C. S.; Wong, I. C. K.; Chan, E. W. Y. Waning Effectiveness against COVID-19-Related Hospitalization, Severe Complications, and Mortality with Two to Three Doses of CoronaVac and BNT162b2: A Case-Control Study. *Emerg. Microbes Infect.* **2023**, *12* (1), 2209201. https://doi.org/10.1080/22221751.2023.2209201.

(1293) Menni, C.; Klaser, K.; May, A.; Polidori, L.; Capdevila, J.; Louca, P.; Sudre, C. H.; Nguyen, L. H.; Drew, D. A.; Merino, J.; Hu, C.; Selvachandran, S.; Antonelli, M.; Murray, B.; Canas, L. S.; Molteni, E.; Graham,

M. S.; Modat, M.; Joshi, A. D.; Mangino, M.; Hammers, A.; Goodman, A. L.; Chan, A. T.; Wolf, J.; Steves, C. J.; Valdes, A. M.; Ourselin, S.; Spector, T. D. Vaccine Side-Effects and SARS-CoV-2 Infection after Vaccination in Users of the COVID Symptom Study App in the UK: A Prospective Observational Study. *Lancet Infect. Dis.* **2021**, *21* (7), 939–949. https://doi.org/10.1016/S1473-3099(21)00224-3.

(1294) Stowe, J.; Miller, E.; Andrews, N.; Whitaker, H. J. Risk of Myocarditis and Pericarditis after a COVID-19 MRNA Vaccine Booster and after COVID-19 in Those with and without Prior SARS-CoV-2 Infection: A Self-Controlled Case Series Analysis in England. *PLOS Med.* **2023**, *20* (6), e1004245. https://doi.org/10.1371/journal.pmed.1004245.

(1295) Shimabukuro, T. T.; Cole, M.; Su, J. R. Reports of Anaphylaxis After Receipt of MRNA COVID-19 Vaccines in the US—December 14, 2020-January 18, 2021. *JAMA* **2021**, *325* (11), 1101–1102. https://doi.org/10.1001/jama.2021.1967.

(1296) Moghimi, S. M. Allergic Reactions and Anaphylaxis to LNP-Based COVID-19 Vaccines. *Mol. Ther.* **2021**, *29* (3), 898–900. https://doi.org/10.1016/j.ymthe.2021.01.030.

(1297) Carreño, J. M.; Singh, G.; Tcheou, J.; Srivastava, K.; Gleason, C.; Muramatsu, H.; Desai, P.; Aberg, J. A.; Miller, R. L.; study group, P.; Pardi, N.; Simon, V.; Krammer, F. MRNA-1273 but Not BNT162b2 Induces Antibodies against Polyethylene Glycol (PEG) Contained in MRNA-Based Vaccine Formulations. *Vaccine* **2022**, *40* (42), 6114–6124. https://doi.org/10.1016/j.vaccine.2022.08.024.

(1298) Guerrini, G.; Gioria, S.; Sauer, A. V; Lucchesi, S.; Montagnani, F.; Pastore, G.; Ciabattini, A.; Medaglini, D.; Calzolai, L. Monitoring Anti-PEG Antibodies Level upon Repeated Lipid Nanoparticle-Based COVID-19 Vaccine Administration. *Int. J. Mol. Sci.* **2022**, *23* (16). https://doi.org/10.3390/ijms23168838.

(1299) Ju, Y.; Carreño, J. M.; Simon, V.; Dawson, K.; Krammer, F.; Kent, S. J. Impact of Anti-PEG Antibodies Induced by SARS-CoV-2 MRNA Vaccines. *Nat. Rev. Immunol.* **2023**, *23* (3), 135–136. https://doi.org/10.1038/s41577-022-00825-x.

(1300) Fülöp, T.; Nemes, R.; Mészáros, T.; Urbanics, R.; Kok, R. J.; Jackman, J. A.; Cho, N.-J.; Storm, G.; Szebeni, J. Complement Activation in Vitro and Reactogenicity of Low-Molecular Weight Dextran-Coated SPIONs in the Pig CARPA Model: Correlation with Physicochemical Features and Clinical Information. *J. Control. Release* **2018**, *270*, 268–274. https://doi.org/10.1016/j.jconrel.2017.11.043.

(1301) Goyal, M.; Ray, I.; Mascarenhas, D.; Kunal, S.; Sachdeva, R. A.; Ish, P. Myocarditis Post-SARS-CoV-2 Vaccination: A Systematic Review. *QJM An Int. J. Med.* **2023**, *116* (1), 7–25. https://doi.org/10.1093/qjmed/hcac064.

(1302) Yasmin, F.; Najeeb, H.; Naeem, U.; Moeed, A.; Atif, A. R.; Asghar, M. S.; Nimri, N.; Saleem, M.; Bandyopadhyay, D.; Krittanawong, C.; Fadelallah Eljack, M. M.; Tahir, M. J.; Waqar, F. Adverse Events Following COVID-19 MRNA Vaccines: A Systematic Review of Cardiovascular Complication, Thrombosis, and Thrombocytopenia. *Immunity, Inflamm. Dis.* **2023**, *11* (3), e807. https://doi.org/10.1002/iid3.807.

(1303) Trougakos, I. P.; Terpos, E.; Alexopoulos, H.; Politou, M.; Paraskevis, D.; Scorilas, A.; Kastritis, E.; Andreakos, E.; Dimopoulos, M. A. Adverse Effects of COVID-19 MRNA Vaccines: The Spike Hypothesis. *Trends Mol. Med.* **2022**, *28* (7), 542–554. https://doi.org/10.1016/j.molmed.2022.04.007.

(1304) Mevorach, D.; Anis, E.; Cedar, N.; Bromberg, M.; Haas, E. J.; Nadir, E.; Olsha-Castell, S.; Arad, D.; Hasin, T.; Levi, N.; Asleh, R.; Amir, O.; Meir, K.; Cohen, D.; Dichtiar, R.; Novick, D.; Hershkovitz, Y.; Dagan, R.; Leitersdorf, I.; Ben-Ami, R.; Miskin, I.; Saliba, W.; Muhsen, K.; Levi, Y.; Green, M. S.; Keinan-Boker, L.; Alroy-Preis, S. Myocarditis after BNT162b2 MRNA Vaccine against Covid-19 in Israel. *N. Engl. J. Med.* **2021**, *385* (23), 2140–2149. https://doi.org/10.1056/NEJMoa2109730.

(1305) Patone, M.; Mei, X. W.; Handunnetthi, L.; Dixon, S.; Zaccardi, F.; Shankar-Hari, M.; Watkinson, P.; Khunti, K.; Harnden, A.; Coupland, C. A. C.; Channon, K. M.; Mills, N. L.; Sheikh, A.; Hippisley-Cox, J. Risk of Myocarditis After Sequential Doses of COVID-19 Vaccine and SARS-CoV-2 Infection by Age and Sex. *Circulation* **2022**, *146* (10), 743–754. https://doi.org/10.1161/CIRCULATIONAHA.122.059970.

(1306) Knudsen, B.; Prasad, V. COVID-19 Vaccine Induced Myocarditis in Young Males: A Systematic Review. *Eur. J. Clin. Invest.* **2023**, *53* (4), e13947. https://doi.org/10.1111/eci.13947.

(1307) Straus, W.; Urdaneta, V.; Esposito, D. B.; Mansi, J. A.; Sanz Rodriguez, C.; Burton, P.; Vega, J. M. Analysis of Myocarditis Among 252 Million MRNA-1273 Recipients Worldwide. *Clin. Infect. Dis.* **2023**, *76* (3), e544–e552. https://doi.org/10.1093/cid/ciac446.

(1308) Mevorach, D.; Anis, E.; Cedar, N.; Hasin, T.; Bromberg, M.; Goldberg, L.; Levi, N.; Perzon, O.; Magadle, N.; Barhoum, B.; Parnassa, E.; Dichtiar, R.; Hershkovitz, Y.; Green, M. S.; Ash, N.; Keinan-Boker, L.; Alroy-Preis, S. Myocarditis After BNT162b2 COVID-19 Third Booster Vaccine in Israel. *Circulation*. United States September 2022, pp 802–804. https://doi.org/10.1161/CIRCULATIONAHA.122.060961.

(1309) Ishisaka, Y.; Watanabe, A.; Aikawa, T.; Kanaoka, K.; Takagi, H.; Wiley, J.; Yasuhara, J.; Kuno, T. Overview of SARS-CoV-2 Infection and Vaccine Associated Myocarditis Compared to Non-COVID-19-Associated Myocarditis: A Systematic Review and Meta-Analysis. *Int. J. Cardiol.* **2024**, *395*, 131401. https://doi.org/10.1016/j.ijcard.2023.131401.

(1310) Ammirati, E.; Conti, N.; Palazzini, M.; Rocchetti, M.; Spangaro, A.; Garascia, A.; Lupi, L.; Cereda, A. Fulminant Myocarditis Temporally Associated with COVID-19 Vaccination. *Curr. Cardiol. Rep.* **2024**. https://doi.org/10.1007/s11886-024-02021-w.

(1311) Fan, B. E.; Shen, J. Y.; Lim, X. R.; Tu, T. M.; Chang, C. C. R.; Khin, H. S. W.; Koh, J. S.; Rao, J. P.; Lau, S. L.; Tan, G. B.; Chia, Y. W.; Tay, K. Y.; Hameed, S.; Umapathi, T.; Ong, K. H.; Prasad, B. M. R. V. Cerebral Venous Thrombosis Post BNT162b2 MRNA SARS-CoV-2 Vaccination: A Black Swan Event. *Am. J. Hematol.* **2021**, *96* (9), E357–E361. https://doi.org/10.1002/ajh.26272.

(1312) Fan, B. E.; Ling, R. R.; Ramanathan, K.; Leung, B. P. L.; Lim, X. R.; Chadachan, V. M.; Thirugnanam, U.; Stegner, D.; Tu, T. M. COVID-19 MRNA Vaccine-Associated Cerebral Venous Thrombosis: Rare Adverse Event or Coincidence? *Am. J. Hematol.* **2023**, *98* (1), E4–E7. https://doi.org/10.1002/ajh.26773.

(1313) Ahmad, F. B.; Cisewski, J. A.; Xu, J.; Anderson, R. N. COVID-19 Mortality Update - United States, 2022. *MMWR. Morb. Mortal. Wkly. Rep.* **2023**, *72* (18), 493–496. https://doi.org/10.15585/mmwr.mm7218a4.

(1314) García-Grimshaw, M.; Ceballos-Liceaga, S. E.; Hernández-Vanegas, L. E.; Núñez, I.; Hernández-Valdivia, N.; Carrillo-García, D. A.; Michel-Chávez, A.; Galnares-Olalde, J. A.; Carbajal-Sandoval, G.; Del Mar Saniger-Alba, M.; Carrillo-Mezo, R. A.; Fragoso-Saavedra, S.; Espino-Ojeda, A.; Blaisdell-Vidal, C.; Mosqueda-Gómez, J. L.; Sierra-Madero, J.; Pérez-Padilla, R.; Alomía-Zegarra, J. L.; López-Gatell, H.; Díaz-Ortega, J. L.; Reyes-Terán, G.; Arauz, A.; Valdés-Ferrer, S. I. Neurologic Adverse Events among 704,003 First-Dose Recipients of the BNT162b2 MRNA COVID-19 Vaccine in Mexico: A Nationwide Descriptive Study. *Clin. Immunol.* **2021**, *229*, 108786. https://doi.org/10.1016/j.clim.2021.108786.

(1315) Iba, T.; Levy, J. H. Thrombosis and Thrombocytopenia in COVID-19 and after COVID-19 Vaccination. *Trends Cardiovasc. Med.* **2022**, *32* (5), 249–256. https://doi.org/10.1016/j.tcm.2022.02.008.

(1316) Zheng, X.; Gao, F.; Wang, L.; Meng, Y.; Ageno, W.; Qi, X. Incidence and Outcomes of Splanchnic Vein Thrombosis after Diagnosis of COVID-19 or COVID-19 Vaccination: A Systematic Review and Meta-Analysis. *J. Thromb. Thrombolysis* **2023**, *55* (1), 18–31. https://doi.org/10.1007/s11239-022-02732-3.

(1317) Ferraresso, F.; Strilchuk, A. W.; Juang, L. J.; Poole, L. G.; Luyendyk, J. P.; Kastrup, C. J. Comparison of DLin-MC3-DMA and ALC-0315 for SiRNA Delivery to Hepatocytes and Hepatic Stellate Cells. *Mol. Pharm.* **2022**, *19* (7), 2175–2182. https://doi.org/10.1021/acs.molpharmaceut.2c00033.

(1318) Blagova, O.; Lutokhina, Y.; Kogan, E.; Kukleva, A.; Ainetdinova, D.; Novosadov, V.; Rud', R.; Savina, P.; Zaitsev, A.; Fomin, V. Chronic Biopsy Proven Post-COVID Myoendocarditis with SARS-Cov-2 Persistence and High Level of Antiheart Antibodies. *Clin. Cardiol.* **2022**, *45* (9), 952–959. https://doi.org/10.1002/clc.23886.

(1319) Aoyama, S.; Nakagawa, R.; Mulé, J. J.; Mailloux, A. W. Inducible Tertiary Lymphoid Structures: Promise and Challenges for Translating a New Class of Immunotherapy. *Front. Immunol.* **2021**, *12*. https://doi.org/10.3389/fimmu.2021.675538.

(1320) Schumacher, T. N.; Thommen, D. S. Tertiary Lymphoid Structures in Cancer. *Science (80-.).* **2024**, *375* (6576), eabf9419. https://doi.org/10.1126/science.abf9419.

(1321) Li, R.; Berglund, A.; Zemp, L.; Dhillon, J.; Putney, R.; Kim, Y.; Jain, R. K.; Grass, G. D.; Conejo-Garcia, J.; Mulé, J. J. The 12-CK Score: Global Measurement of Tertiary Lymphoid Structures. *Front. Immunol.* **2021**, *12*. https://doi.org/10.3389/fimmu.2021.694079.

(1322) Zhang, X.; Liu, Y.; Luo, L.; Li, L.; Xing, S.; Yin, T.; Bian, K.; Zhu, R.; Gao, D. A Chemo-Photothermal Synergetic Antitumor Drug Delivery System: Gold Nanoshell Coated Wedelolactone Liposome. *Mater. Sci. Eng. C* **2019**, *101*, 505–512. https://doi.org/10.1016/j.msec.2019.04.006.

(1323) Makhdoumi, P.; Karimi, H.; Khazaei, M. Review on Metal-Based Nanoparticles: Role of Reactive Oxygen Species in Renal Toxicity. *Chem. Res. Toxicol.* **2020**, *33* (10), 2503–2514. https://doi.org/10.1021/acs.chemrestox.9b00438.

(1324) Niu, B.; Liao, K.; Zhou, Y.; Wen, T.; Quan, G.; Pan, X.; Wu, C. Application of Glutathione Depletion in Cancer Therapy: Enhanced ROS-Based Therapy, Ferroptosis, and Chemotherapy. *Biomaterials* **2021**, *277*, 121110. https://doi.org/10.1016/j.biomaterials.2021.121110.

(1325) Jia, C.; Guo, Y.; Wu, F.-G. Chemodynamic Therapy via Fenton and Fenton-Like Nanomaterials: Strategies and Recent Advances. *Small* **2022**, *18* (6), 2103868. https://doi.org/10.1002/smll.202103868.

(1326) Hao, Y.-N.; Zhang, W.-X.; Gao, Y.-R.; Wei, Y.-N.; Shu, Y.; Wang, J.-H. State-of-the-Art Advances of Copper-Based Nanostructures in the Enhancement of Chemodynamic Therapy. *J. Mater. Chem. B* **2021**, *9* (2), 250–266. https://doi.org/10.1039/D0TB02360D.

(1327) Dong, C.; Feng, W.; Xu, W.; Yu, L.; Xiang, H.; Chen, Y.; Zhou, J. The Coppery Age: Copper (Cu)-Involved Nanotheranostics. *Adv. Sci.* **2020**, *7* (21), 2001549. https://doi.org/10.1002/advs.202001549.

(1328) Poudel, K.; Gautam, M.; Jin, S. G.; Choi, H.-G.; Yong, C. S.; Kim, J. O. Copper Sulfide: An Emerging Adaptable Nanoplatform in Cancer Theranostics. *Int. J. Pharm.* **2019**, *562*, 135–150. https://doi.org/10.1016/j.ijpharm.2019.03.043.

(1329) Wang, Z.; von dem Bussche, A.; Kabadi, P. K.; Kane, A. B.; Hurt, R. H. Biological and Environmental Transformations of Copper-Based Nanomaterials. *ACS Nano* **2013**, *7* (10), 8715–8727. https://doi.org/10.1021/nn403080y.

(1330) Ma, R.; Stegemeier, J.; Levard, C.; Dale, J. G.; Noack, C. W.; Yang, T.; Brown, G. E.; Lowry, G. V. Sulfidation of Copper Oxide Nanoparticles and Properties of Resulting Copper Sulfide. *Environ. Sci. Nano* **2014**, *1* (4), 347–357. https://doi.org/10.1039/C4EN00018H.

(1331) He, H.; Sun, M.; Wu, D.; Di, G.; Fei, X. Cu(III) Generation and Air Sparging Extend Catalytic Effectiveness of Cu2S/H2O2 from Neutral to Acidic Condition: Performance and Mechanism in Comparison with CuS/H2O2. *J. Clean. Prod.* **2021**, *278*, 123572. https://doi.org/10.1016/j.jclepro.2020.123572.

(1332) Raj, S. I.; Jaiswal, A. Nanoscale Transformation in CuS Fenton-like Catalyst for Highly Selective and Enhanced Dye Degradation. *J. Photochem. Photobiol. A Chem.* **2021**, *410*, 113158. https://doi.org/10.1016/j.jphotochem.2021.113158.

(1333) Tang, Y.; Ji, Y.; Yi, C.; Cheng, D.; Wang, B.; Fu, Y.; Xu, Y.; Qian, X.; Choonara, Y. E.; Pillay, V.; Zhu, W.; Liu, Y.; Nie, Z. Self-Accelerating H_2O_2-Responsive Plasmonic Nanovesicles for Synergistic Chemo/Starving Therapy of Tumors. *Theranostics* **2020**, *10* (19), 8691–8704. https://doi.org/10.7150/thno.45392.

(1334) Deng, Z.; Fang, C.; Ma, X.; Li, X.; Zeng, Y.-J.; Peng, X. One Stone Two Birds: Zr-Fc Metal–Organic Framework Nanosheet for Synergistic Photothermal and Chemodynamic Cancer Therapy. *ACS Appl. Mater. Interfaces* **2020**, *12* (18), 20321–20330. https://doi.org/10.1021/acsami.0c06648.

(1335) Ma, S.; Xie, J.; Wang, L.; Zhou, Z.; Luo, X.; Yan, J.; Ran, G. Hetero-Core–Shell BiNS–Fe@Fe as a Potential Theranostic Nanoplatform for Multimodal Imaging-Guided Simultaneous Photothermal–

Photodynamic and Chemodynamic Treatment. *ACS Appl. Mater. Interfaces* **2021**, *13* (9), 10728–10740. https://doi.org/10.1021/acsami.0c21579.

(1336) Sun, P.; Deng, Q.; Kang, L.; Sun, Y.; Ren, J.; Qu, X. A Smart Nanoparticle-Laden and Remote-Controlled Self-Destructive Macrophage for Enhanced Chemo/Chemodynamic Synergistic Therapy. *ACS Nano* **2020**, *14* (10), 13894–13904. https://doi.org/10.1021/acsnano.0c06290.

(1337) Fang, C.; Deng, Z.; Cao, G.; Chu, Q.; Wu, Y.; Li, X.; Peng, X.; Han, G. Co–Ferrocene MOF/Glucose Oxidase as Cascade Nanozyme for Effective Tumor Therapy. *Adv. Funct. Mater.* **2020**, *30* (16), 1910085. https://doi.org/10.1002/adfm.201910085.

(1338) Lyu, M.; Zhu, D.; Kong, X.; Yang, Y.; Ding, S.; Zhou, Y.; Quan, H.; Duo, Y.; Bao, Z. Glutathione-Depleting Nanoenzyme and Glucose Oxidase Combination for Hypoxia Modulation and Radiotherapy Enhancement. *Adv. Healthc. Mater.* **2020**, *9* (11), 1901819. https://doi.org/10.1002/adhm.201901819.

(1339) Zhang, D.-Y.; Huang, F.; Ma, Y.; Liang, G.; Peng, Z.; Guan, S.; Zhai, J. Tumor Microenvironment-Responsive Theranostic Nanoplatform for Guided Molecular Dynamic/Photodynamic Synergistic Therapy. *ACS Appl. Mater. Interfaces* **2021**, *13* (15), 17392–17403. https://doi.org/10.1021/acsami.1c03277.

(1340) Ranji-Burachaloo, H.; Reyhani, A.; Gurr, P. A.; Dunstan, D. E.; Qiao, G. G. Combined Fenton and Starvation Therapies Using Hemoglobin and Glucose Oxidase. *Nanoscale* **2019**, *11* (12), 5705–5716. https://doi.org/10.1039/C8NR09107B.

(1341) He, S.; Jiang, Y.; Li, J.; Pu, K. Semiconducting Polycomplex Nanoparticles for Photothermal Ferrotherapy of Cancer. *Angew. Chemie Int. Ed.* **2020**, *59* (26), 10633–10638. https://doi.org/10.1002/anie.202003004.

(1342) Zhao, Z.; Xu, K.; Fu, C.; Liu, H.; Lei, M.; Bao, J.; Fu, A.; Yu, Y.; Zhang, W. Interfacial Engineered Gadolinium Oxide Nanoparticles for Magnetic Resonance Imaging Guided Microenvironment-Mediated Synergetic Chemodynamic/Photothermal Therapy. *Biomaterials* **2019**, *219*, 119379. https://doi.org/10.1016/j.biomaterials.2019.119379.

(1343) Zhang, M.; Liu, X.; Luo, Q.; Wang, Q.; Zhao, L.; Deng, G.; Ge, R.; Zhang, L.; Hu, J.; Lu, J. Tumor Environment Responsive Degradable CuS@mSiO2@MnO2/DOX for MRI Guided Synergistic Chemo-Photothermal Therapy and Chemodynamic Therapy. *Chem. Eng. J.* **2020**, *389*, 124450. https://doi.org/10.1016/j.cej.2020.124450.

(1344) Xiao, S.; Lu, Y.; Feng, M.; Dong, M.; Cao, Z.; Zhang, X.; Chen, Y.; Liu, J. Multifunctional FeS2 Theranostic Nanoparticles for Photothermal-Enhanced Chemodynamic/Photodynamic Cancer Therapy and Photoacoustic Imaging. *Chem. Eng. J.* **2020**, *396*, 125294. https://doi.org/10.1016/j.cej.2020.125294.

(1345) Zhang, L.; Yang, Z.; He, W.; Ren, J.; Wong, C.-Y. One-Pot Synthesis of a Self-Reinforcing Cascade Bioreactor for Combined Photodynamic/Chemodynamic/Starvation Therapy. *J. Colloid Interface Sci.* **2021**, *599*, 543–555. https://doi.org/10.1016/j.jcis.2021.03.173.

(1346) Han, R.; Xiao, Y.; Yang, Q.; Pan, M.; Hao, Y.; He, X.; Peng, J.; Qian, Z. Ag2S Nanoparticle-Mediated Multiple Ablations Reinvigorates the Immune Response for Enhanced Cancer Photo-Immunotherapy. *Biomaterials* **2021**, *264*, 120451. https://doi.org/10.1016/j.biomaterials.2020.120451.

(1347) Wang, Y.; Li, Z.; Hu, Y.; Liu, J.; Guo, M.; Wei, H.; Zheng, S.; Jiang, T.; Sun, X.; Ma, Z.; Sun, Y.; Besenbacher, F.; Chen, C.; Yu, M. Photothermal Conversion-Coordinated Fenton-like and Photocatalytic Reactions of Cu2-XSe-Au Janus Nanoparticles for Tri-Combination Antitumor Therapy. *Biomaterials* **2020**, *255*, 120167. https://doi.org/10.1016/j.biomaterials.2020.120167.

(1348) Zhang, F.; Han, X.; Hu, Y.; Wang, S.; Liu, S.; Pan, X.; Wang, H.; Ma, J.; Wang, W.; Li, S.; Wu, Q.; Shen, H.; Yu, X.; Yuan, Q.; Liu, H. Interventional Photothermal Therapy Enhanced Brachytherapy: A New Strategy to Fight Deep Pancreatic Cancer. *Adv. Sci.* **2019**, *6* (5), 1801507. https://doi.org/10.1002/advs.201801507.

(1349) Li, Q.; Sun, L.; Hou, M.; Chen, Q.; Yang, R.; Zhang, L.; Xu, Z.; Kang, Y.; Xue, P. Phase-Change Material Packaged within Hollow Copper Sulfide Nanoparticles Carrying Doxorubicin and Chlorin E6 for

Fluorescence-Guided Trimodal Therapy of Cancer. *ACS Appl. Mater. Interfaces* **2019**, *11* (1), 417–429. https://doi.org/10.1021/acsami.8b19667.

(1350) Wang, Y.; An, L.; Lin, J.; Tian, Q.; Yang, S. A Hollow Cu9S8 Theranostic Nanoplatform Based on a Combination of Increased Active Sites and Photothermal Performance in Enhanced Chemodynamic Therapy. *Chem. Eng. J.* **2020**, *385*, 123925. https://doi.org/10.1016/j.cej.2019.123925.

(1351) Gu, X.; Qiu, Y.; Lin, M.; Cui, K.; Chen, G.; Chen, Y.; Fan, C.; Zhang, Y.; Xu, L.; Chen, H.; Wan, J.-B.; Lu, W.; Xiao, Z. CuS Nanoparticles as a Photodynamic Nanoswitch for Abrogating Bypass Signaling To Overcome Gefitinib Resistance. *Nano Lett.* **2019**, *19* (5), 3344–3352. https://doi.org/10.1021/acs.nanolett.9b01065.

(1352) Zhang, X.; He, C.; Chen, Y.; Chen, C.; Yan, R.; Fan, T.; Gai, Y.; Yang, T.; Lu, Y.; Xiang, G. Cyclic Reactions-Mediated Self-Supply of H2O2 and O2 for Cooperative Chemodynamic/Starvation Cancer Therapy. *Biomaterials* **2021**, *275*, 120987. https://doi.org/10.1016/j.biomaterials.2021.120987.

Appendices

~ Appendix 1 ~

Supplemental Information for Chapter 3

The work presented in this appendix has been published as supplementary information for:

Youden, B., Wang, F., Zhang, X., Curry, D., Majtenyi, N., Shaaer, A., Bingham, K., Nguyen, Q., Bragg, L., Liu, J., Servos, M., Zhang, X., and Jiang, R. Degradable Multifunctional Gold-Liposomes as an All-in-One Theranostic Platform for Image-Guided Radiotherapy. *International Journal of Pharmaceutics*, **2022**, 629 (15), 122413. DOI: 10.1016/j.ijpharm.2022.122413.

Preliminary data for this work was also presented and published as a conference abstract (The American Association of Physicists in Medicine, 2018 Annual Meeting):

Youden, B., Jiang, R., Zhang, X. and Servos, M. Radio-Photothermal Therapy of Prostate Cancer Cells Using Gold-Lipid Nanoshells. In *Medical Physics*, **2018**, 45 (6), E342-E343. 111 River St., Hoboken 07030-5774, NJ USA: Wiley.

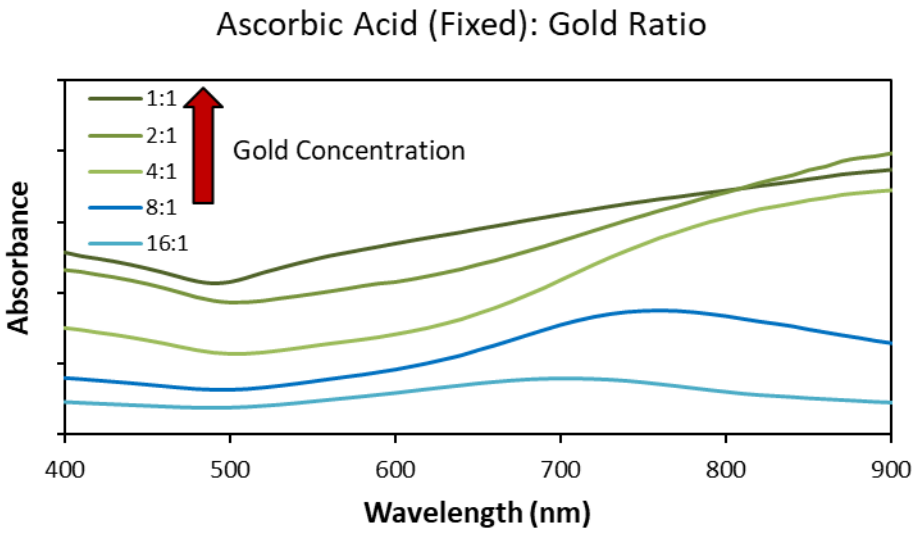

Figure S1: UV-Vis spectrum of different Lipogold plasmons LSPRs following storage at 4ºC for 48 h.

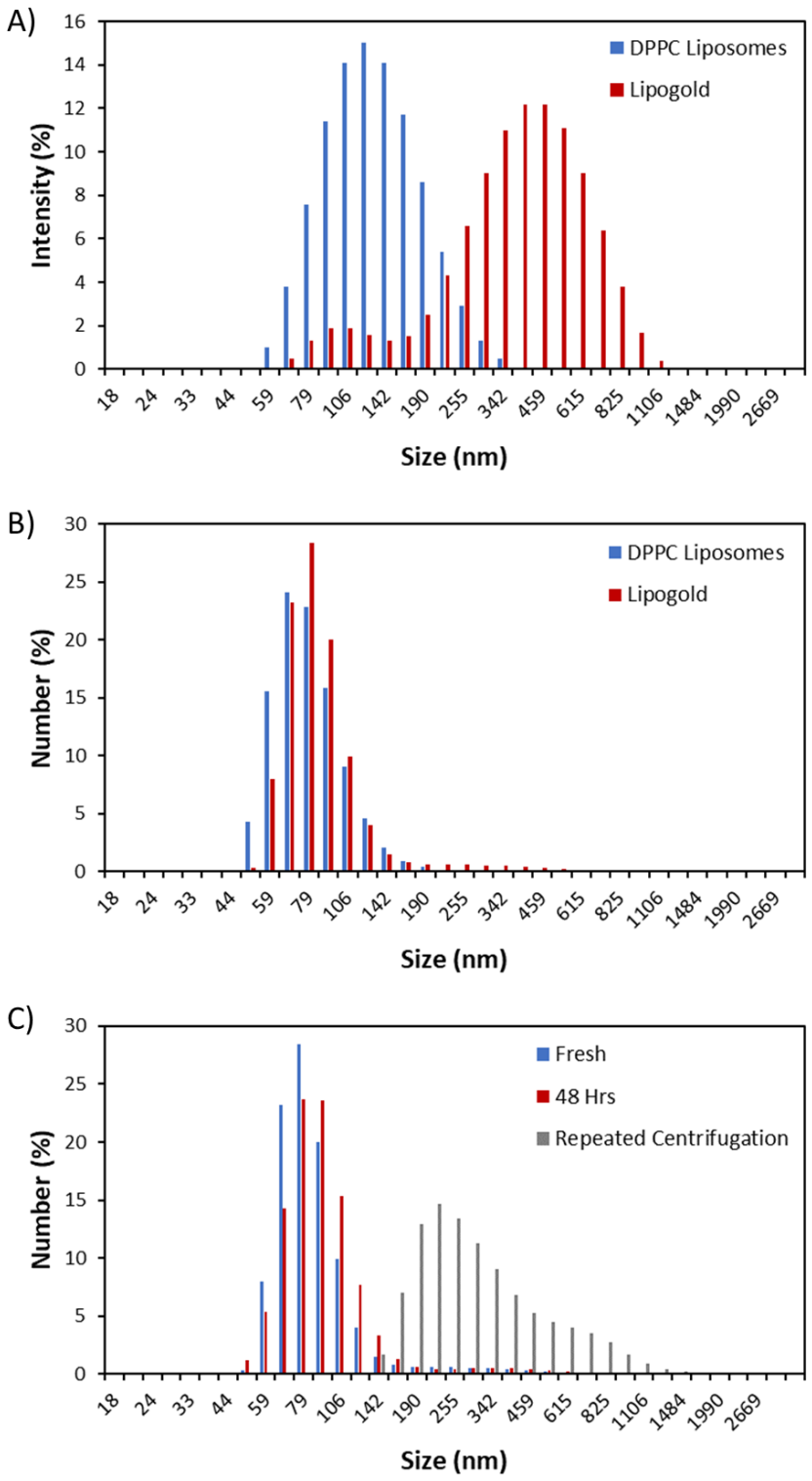

Figure S2: Representative dynamic light scattering (DLS) size distributions for uncoated DPPC liposomes and Lipogold using intensity-weighted (A) and number-weighted (B) measurements. C) Number-weighted measurements of Lipogold immediately after synthesis, after 48 h at 4°C, and after multiple centrifugations.

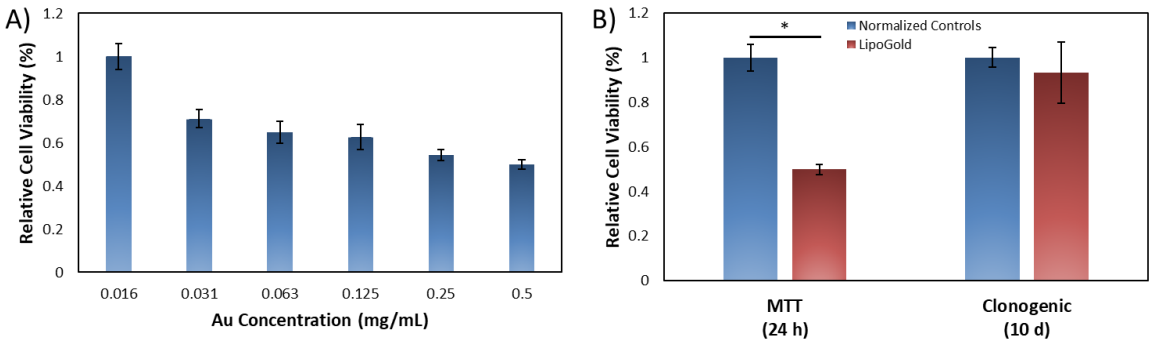

Figure S3: In vitro toxicity of Lipogold to DU-145 cells. A) MTT assay performed after 24 h of incubation. B) Comparison of MTT assay (24 h) to clonogenic assay (10 d). $n = 3$ with errors bars representing the standard deviation. $*p < 0.05$.

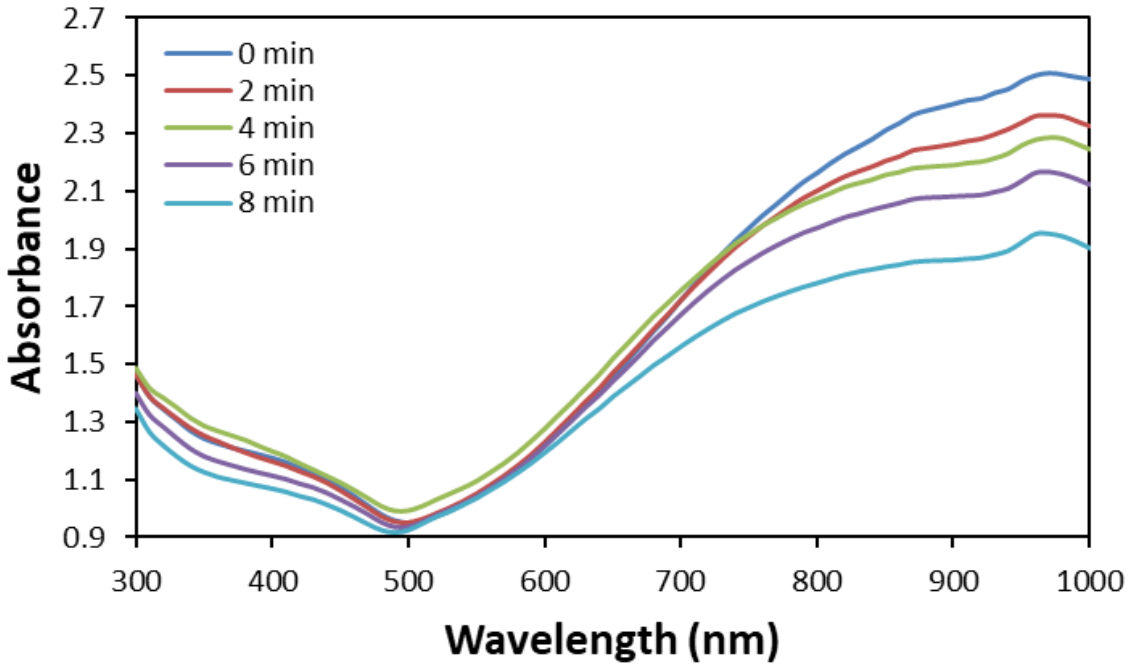

Figure S4: Degradation of Lipogold as measured via the loss of the LSPR during exposure to an 808 nm laser in 2 min on/off cycles.

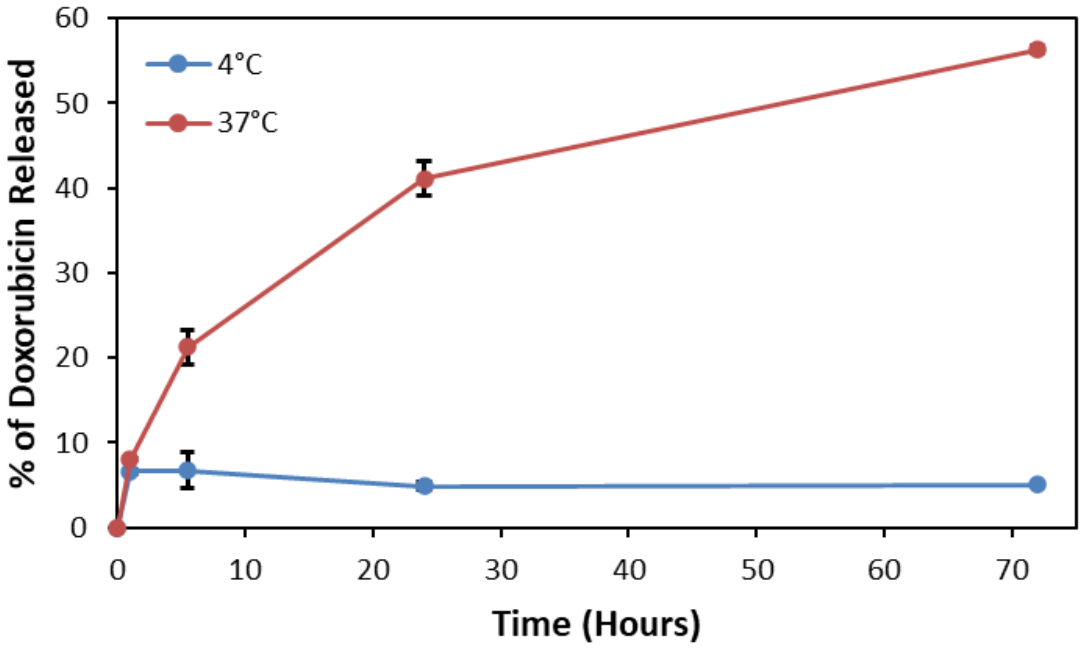

Figure S5: Leakage of DOX from Lipogold over 72 h at 4°C and 37°C.

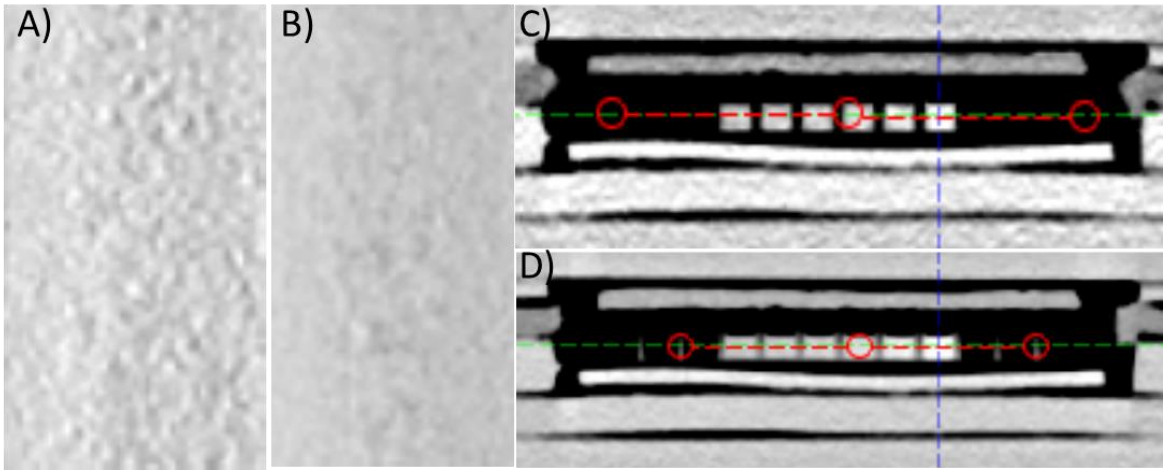

Figure S6: Representative phantom noise produced at 70 kV (A) and 120 kV (B). Data collection for Lipogold at 70 and 120 kV (C and D, respectively). The HU per slice was measured along the red line, with the circles representing the ends and center of the measured area (10 cm). The red, blue, and green lines indicate the centering of the image in the analysis software.

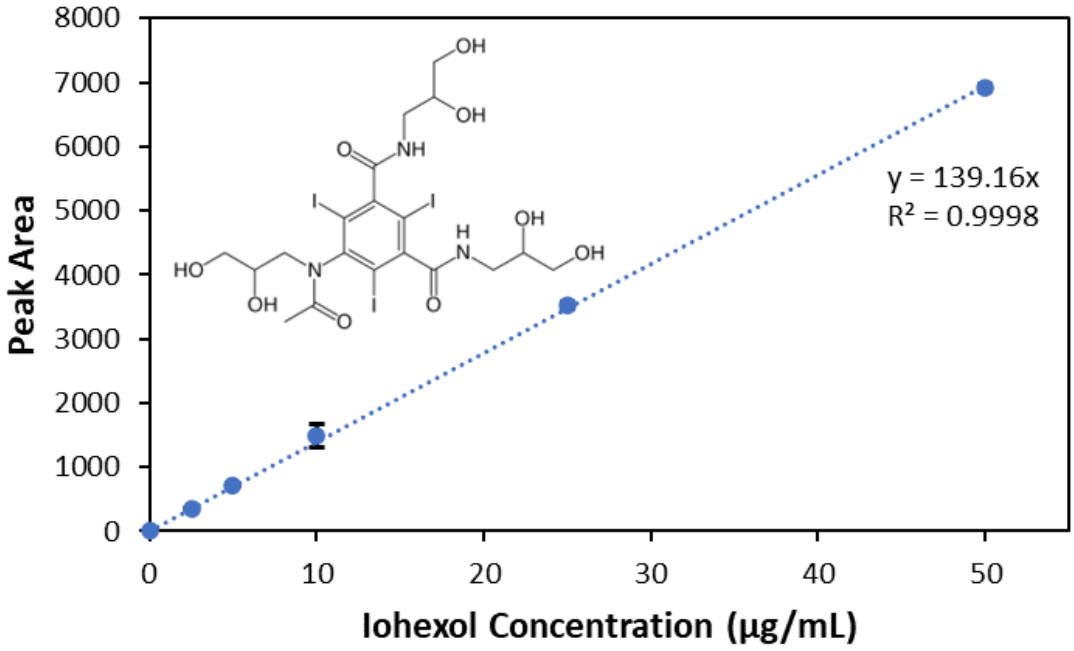

Figure S7: Calibration curve of iohexol measured via HPLC method. *n* = 3 with errors bars representing the standard deviation.

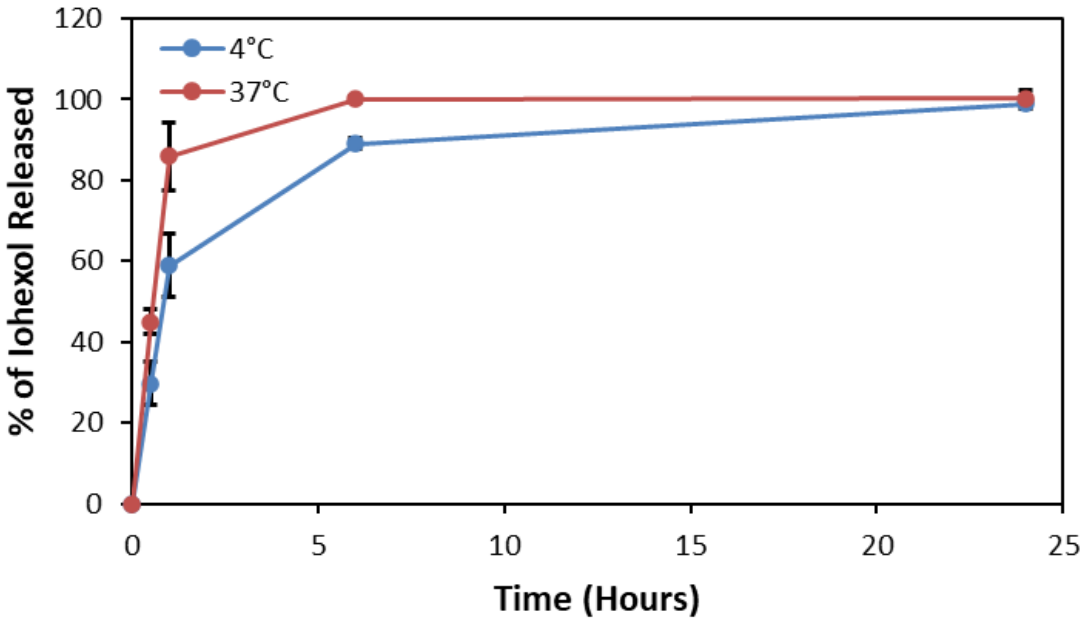

Figure S8: Diffusion of free iohexol across the dialysis membrane.

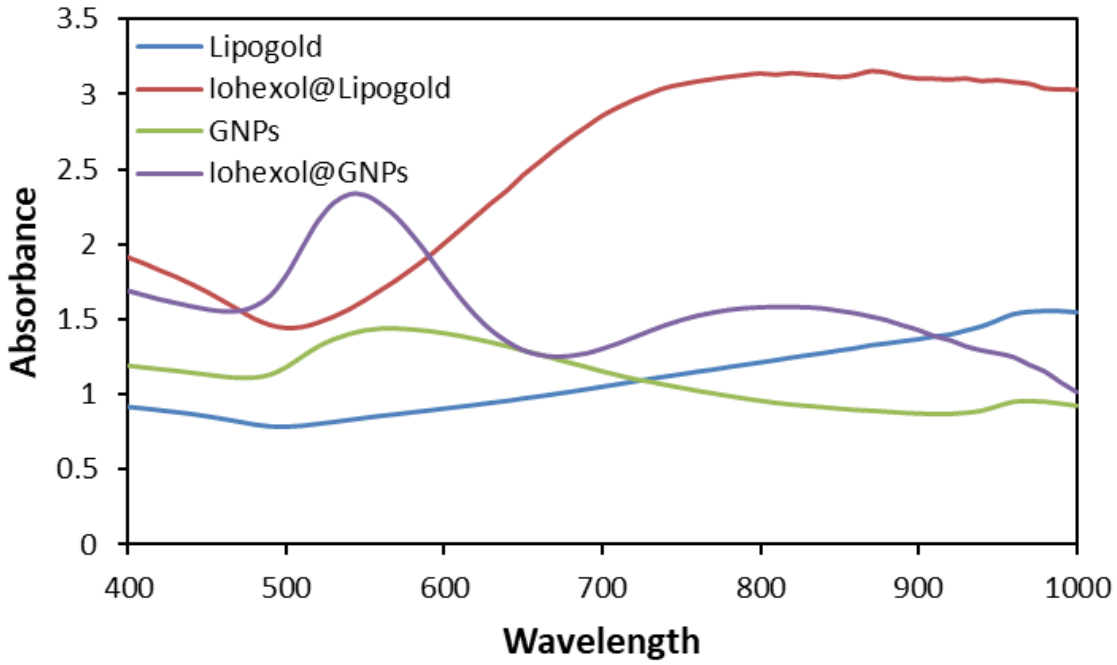

Figure S9: UV-Vis-NIR absorption spectra of Lipogold or GNPs (without a liposome template) prepared in the presence or absence of iohexol.

~ Appendix 2 ~

Supplemental Information for Chapter 4

The work presented in this appendix has been published as supplementary information for:

Singh, P.*, **Youden, B.**, Yang, Y., Chen, Y., Carrier, A., Cui, S., Oakes, K., Servos, M., Jiang, R. and Zhang, X. Synergistic multimodal cancer therapy using glucose oxidase@CuS nanocomposites. *ACS Applied Materials & Interfaces*, **2021**, 13 (35), pp.41464-41472. DOI: 10.1021/acsami.1c12235.

**These authors contributed equally to this work.*

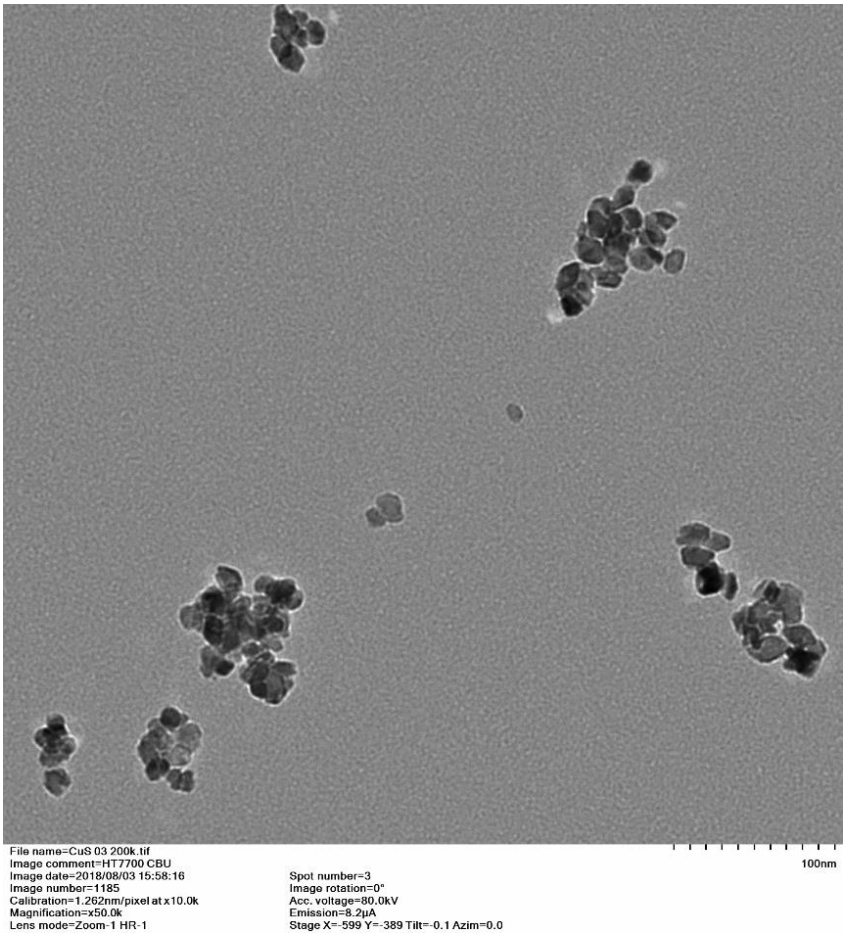

Figure S10: A transmission electron micrograph of the CuS nanoparticles.

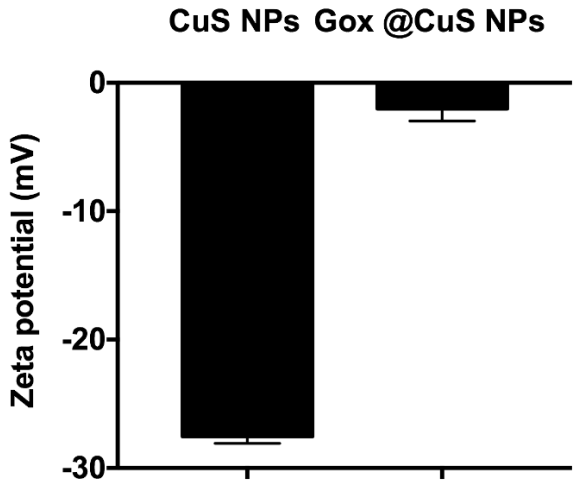

Figure S11: Zeta potentials of the CuS and Gox@CuS nanoparticles (NPs). Error bars indicate standard deviation (*n* = 3).

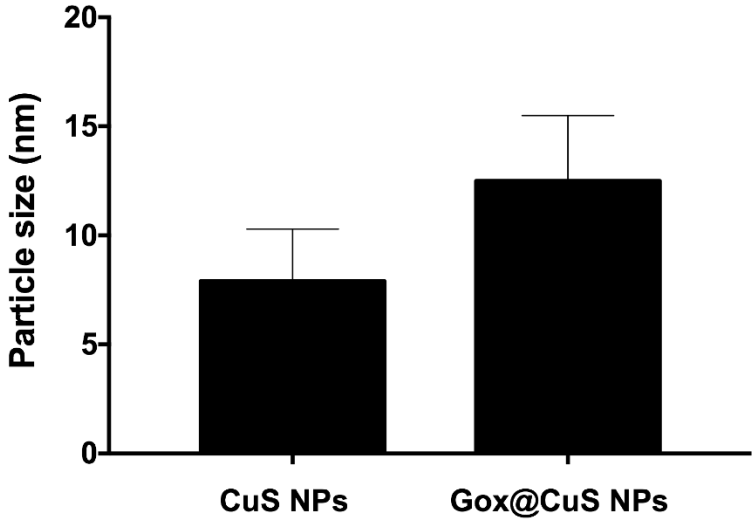

Figure S12: The hydrodynamic sizes of the CuS and Gox@CuS nanoparticles (NPs) measured by dynamic light scattering. Error bars indicate standard deviation (*n* = 3).

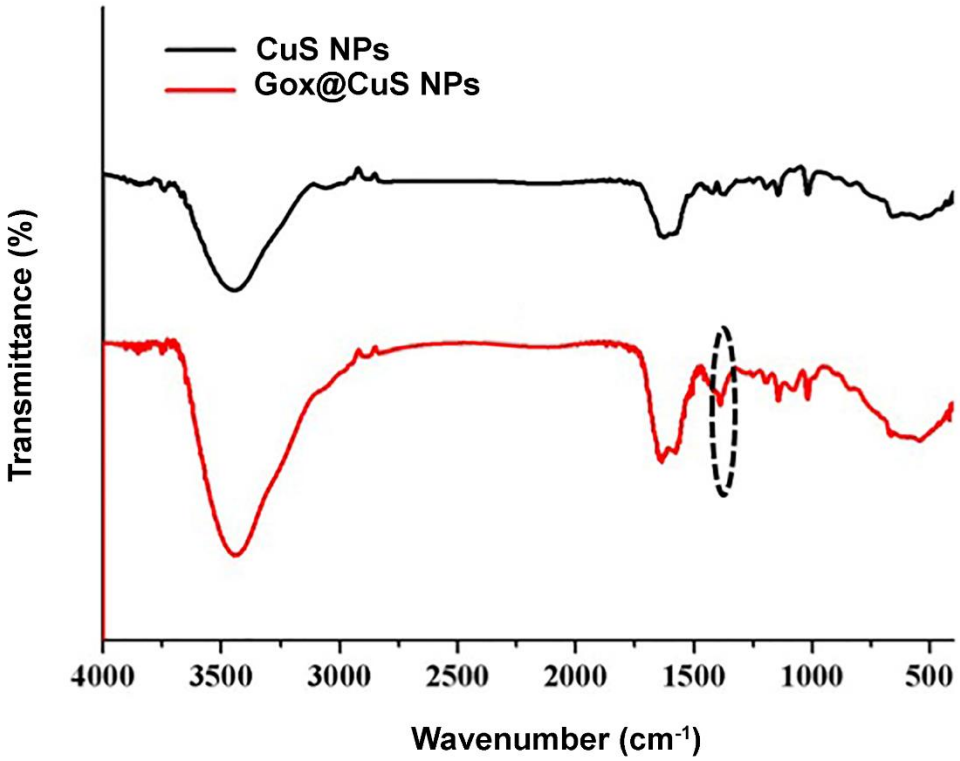

Figure S13: Fourier transform-infrared spectra of the CuS and Gox@CuS nanoparticles. The peak at 1450 cm^{-1} was assigned to C-O stretching and OH bending of Gox in the nanoparticles.

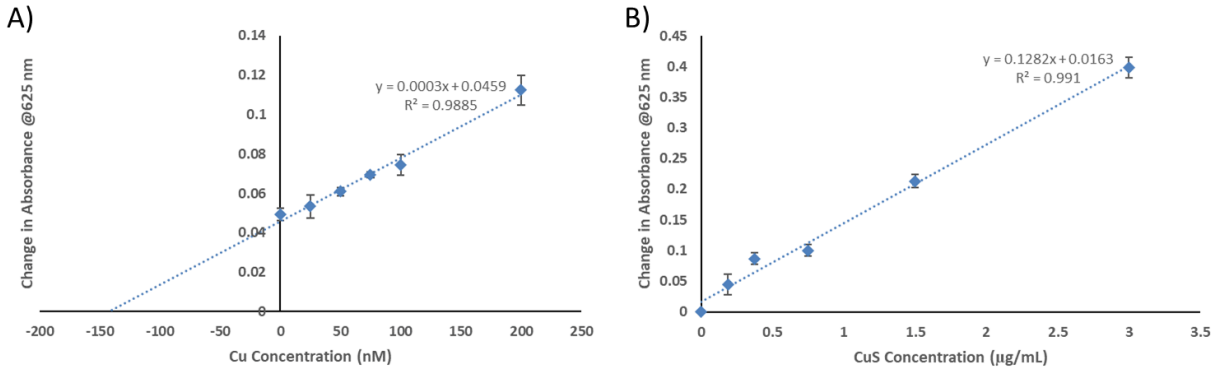

Figure S14: Quantification of copper and CuS. A) Standard addition curve for Cu^{2+} detection, and B) calibration curve for CuS detection following cellular uptake using the chloride-accelerated copper Fenton reaction with H_2O_2 and 3,3',5,5'-tetramethylbenzidine. Error bars represent standard deviation (n = 3).

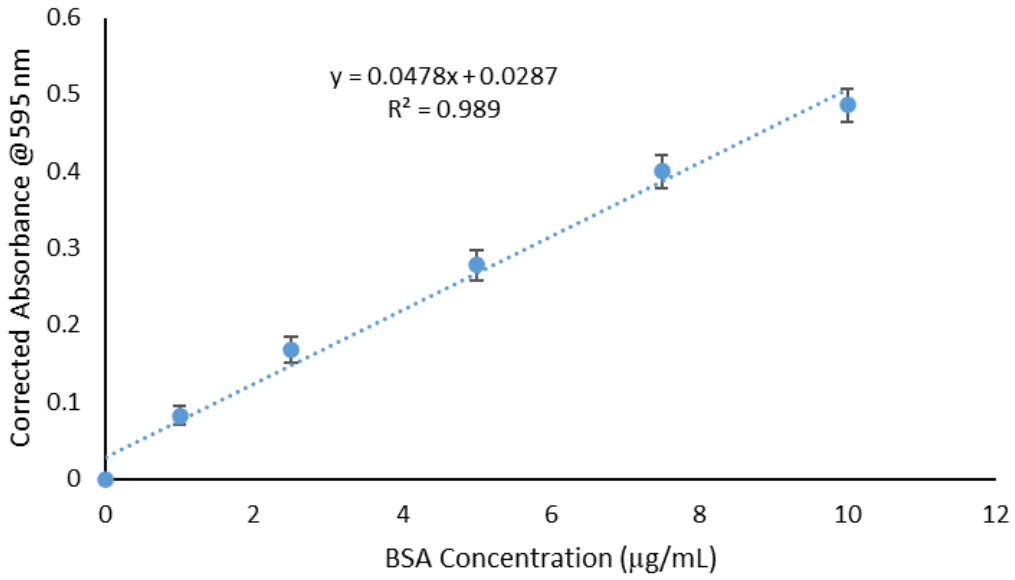

Figure S15: Standard bovine serum albumin (BSA) protein calibration curve used to quantify Gox during the Bradford assay. Error bars represent standard deviation (n = 3).

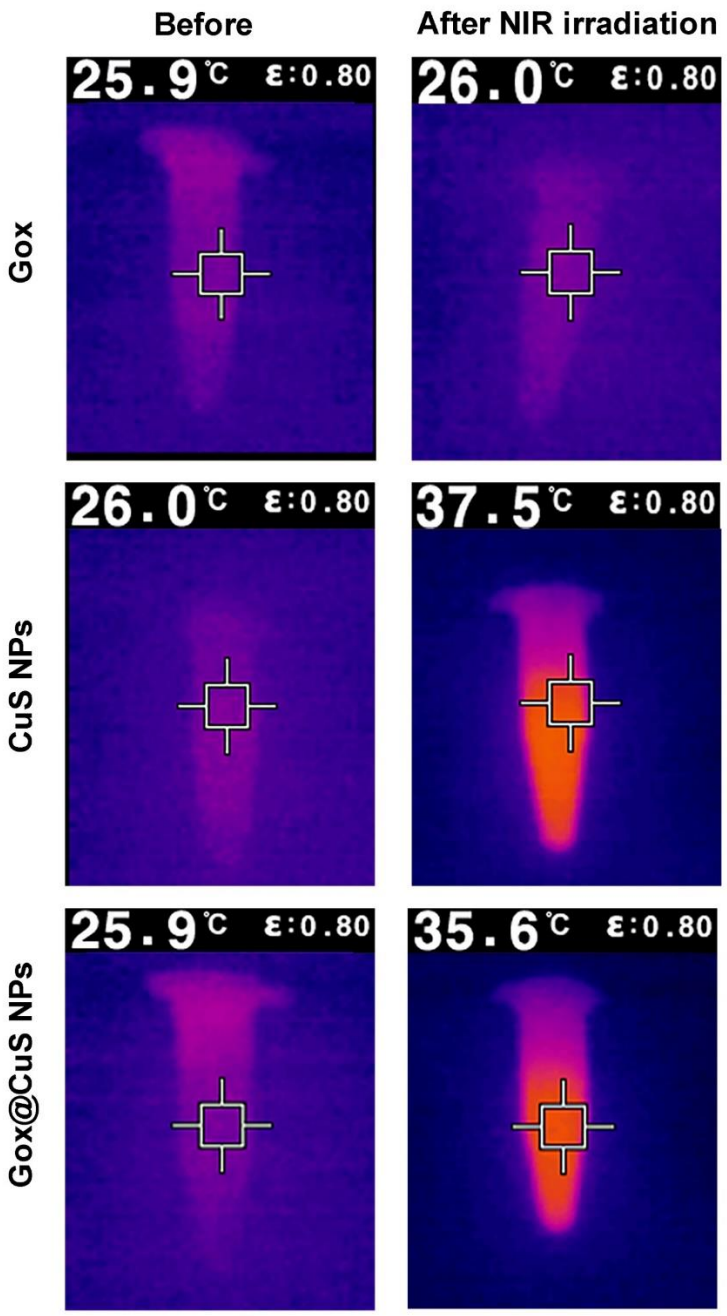

Figure S16: Infrared thermal imaging of Gox, CuS nanoparticles (NPs) and Gox@CuS NPs ([NP] = 10 μg/mL) with near infrared irradiation (980 nm, 5 W/cm^2) for 300 s.

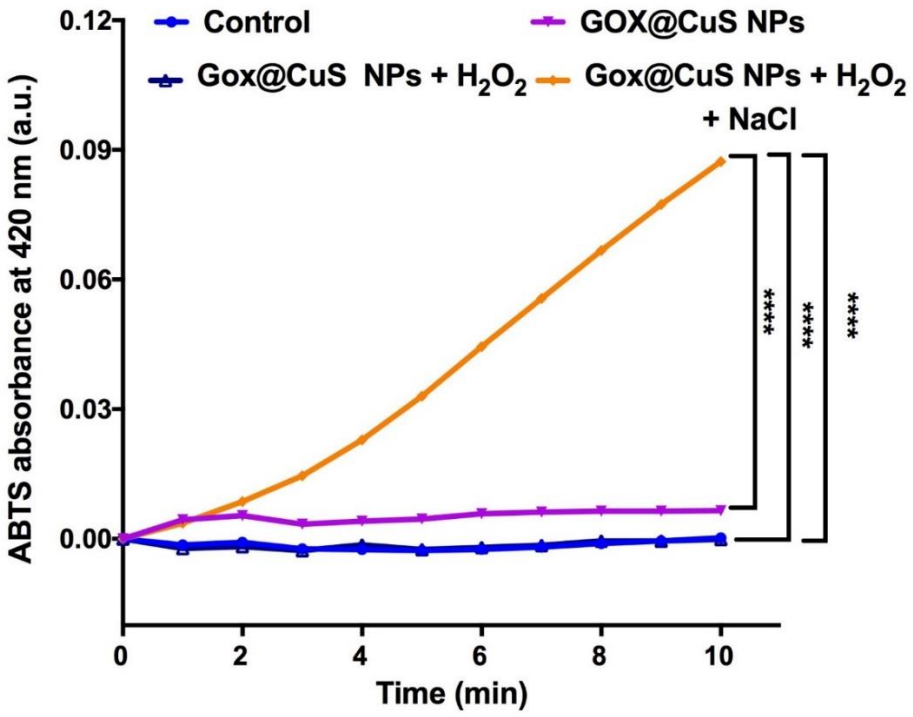

Figure S17: The Fenton catalytic activity of Gox@CuS nanoparticles (NPs). 2,2'-Azino-bis(3-ethylbenzthiazoline-6-sulfonic acid) (ABTS, 250 μM) oxidation catalyzed by Gox@CuS NPs (10 μg/mL) and H_2O_2 (200 mM) in the presence and absence of NaCl (100 mM).

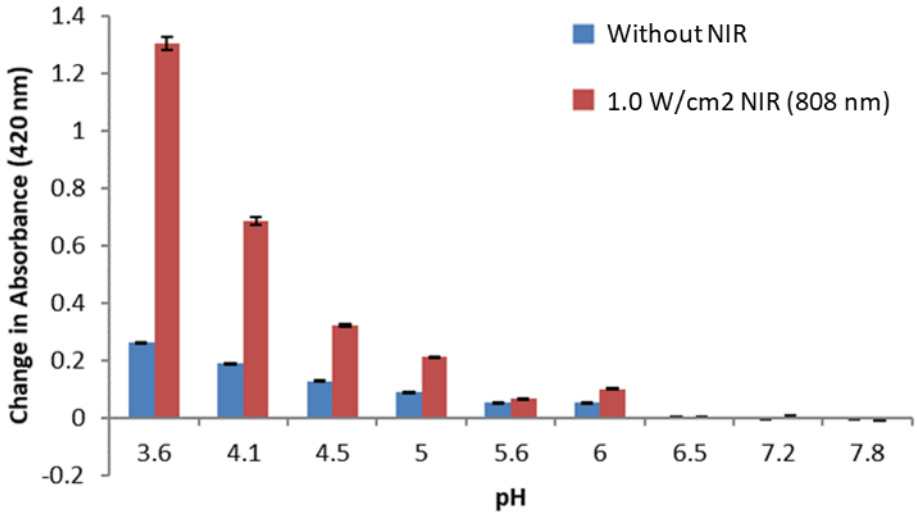

Figure S18: 2,2'-Azino-bis(3-ethylbenzthiazoline-6-sulfonic acid) (ABTS, 250 μM) oxidation catalyzed by CuS nanoparticles (10 μg/mL), NaCl (100 mM), and H_2O_2 (100 mM) at different pHs with or without near infrared (NIR) irradiation (1.5 W/cm^2). Error bars represent standard deviation (n = 3).

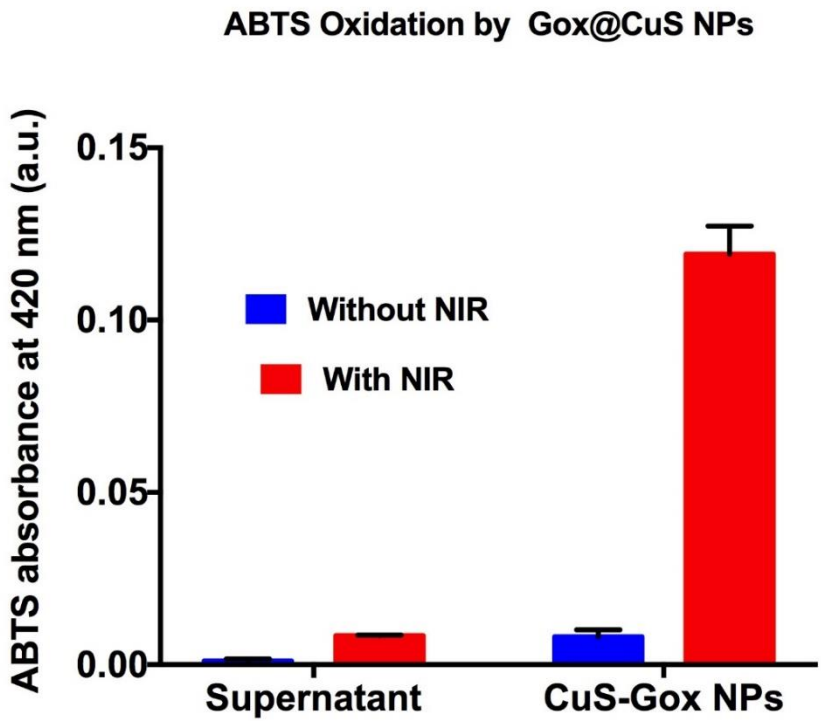

Figure S19: 2,2'-Azino-bis(3-ethylbenzthiazoline-6-sulfonic acid) (ABTS) oxidation catalyzed by Cu^{2+} leached from Gox@CuS nanoparticles (NPs) and the parent NPs with and without near infrared (NIR) irradiation. Error bars represent standard deviation (n = 3).

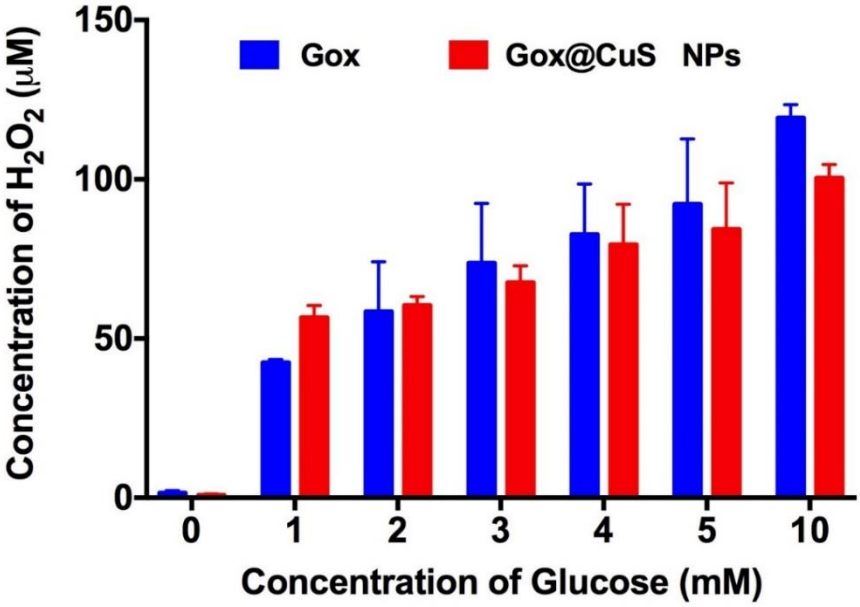

Figure S20: In vitro catalytic H_2O_2 production by Gox and Gox@CuS nanoparticles (NPs) with different initial glucose concentrations after 5 min. Error bars represent standard deviation (n = 3).

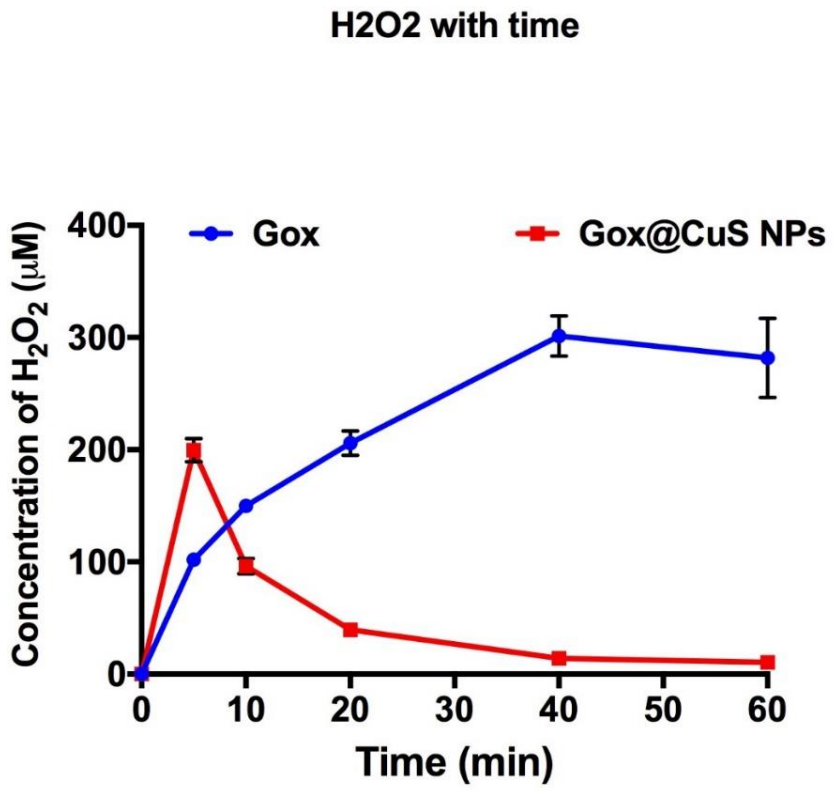

Figure S21: In vitro H_2O_2 generation by Gox and Gox@CuS nanoparticles (NPs) over time. CuS NPs decompose the H_2O_2 generated by glucose oxidation, producing reactive oxygen species. Error bars represent standard deviation (n = 3).

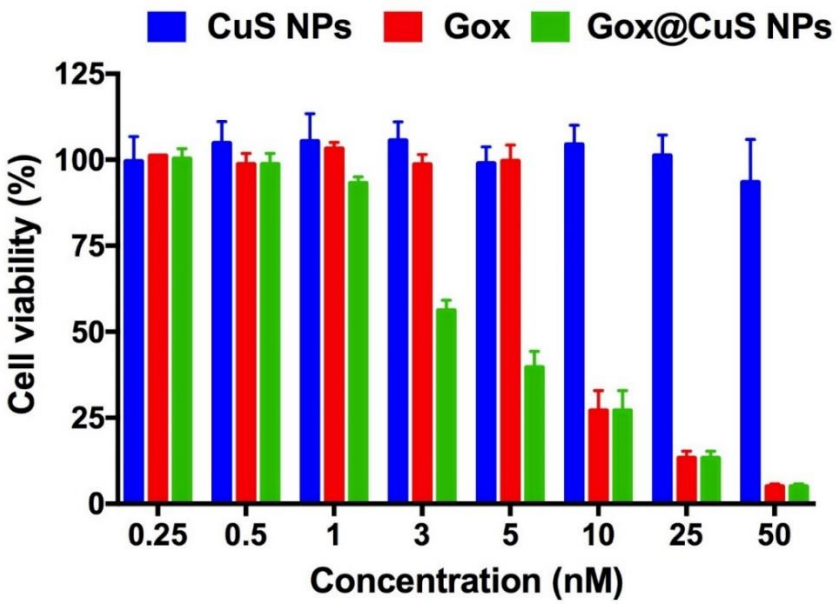

Figure S22: In vitro toxicity of Gox@CuS nanoparticles (NPs) in MDA-MB-231 cells. Error bars represent standard deviation (n = 3).

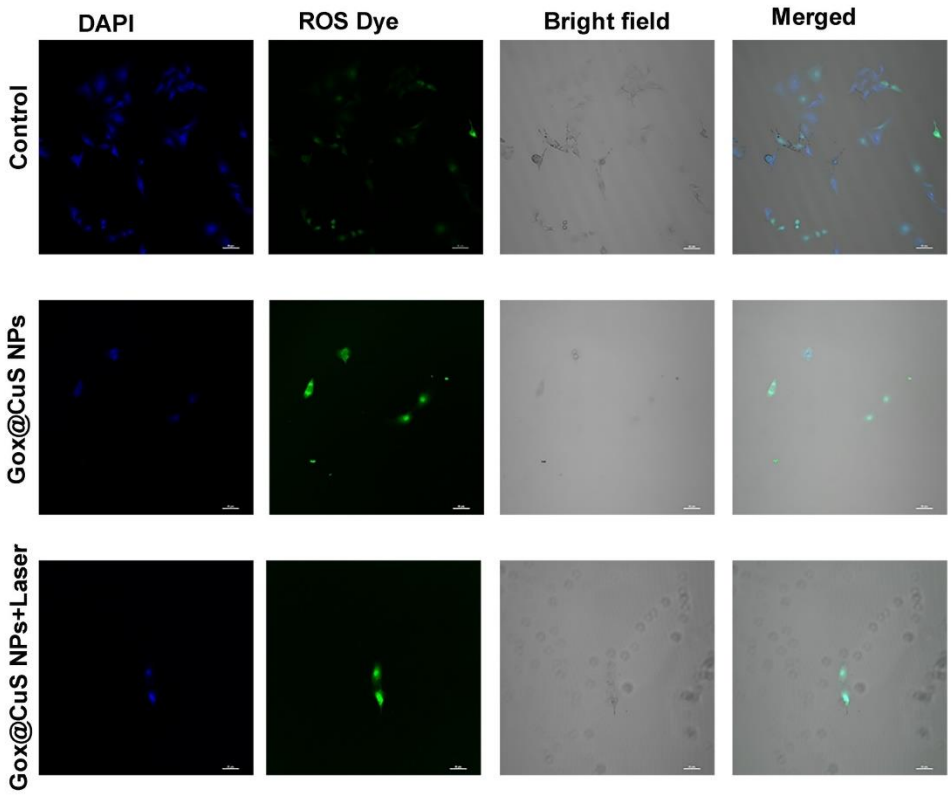

Figure S23: The intracellular reactive oxygen species (ROS) level shown by confocal laser scanning microscopy images of B16F10 cells incubated for 4 h with Gox@CuS nanoparticles (NPs) with or without a brief near infrared (NIR) irradiation (5 s). [CuS NPs] = 2 nM. Scale bars: 50 μm**.**

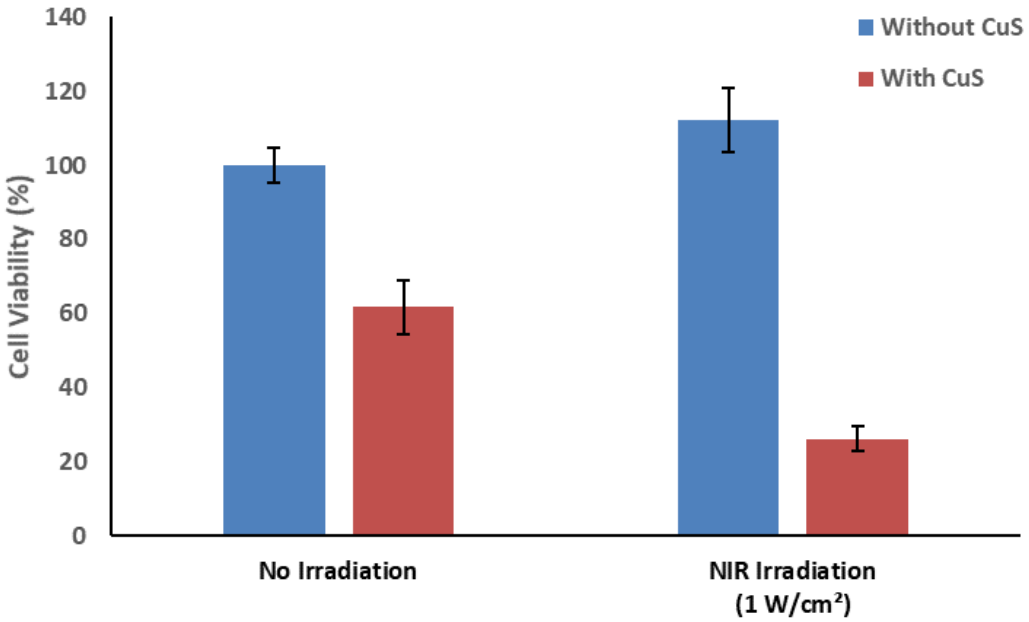

Figure S24: Cell viability of PC-3 prostate cancer cells after treatment with 30 μg/mL CuS nanoparticles (NPs) and 5 min of near infrared (NIR) irradiation (808 nm). Error bars represent standard deviation (*n* = 3).

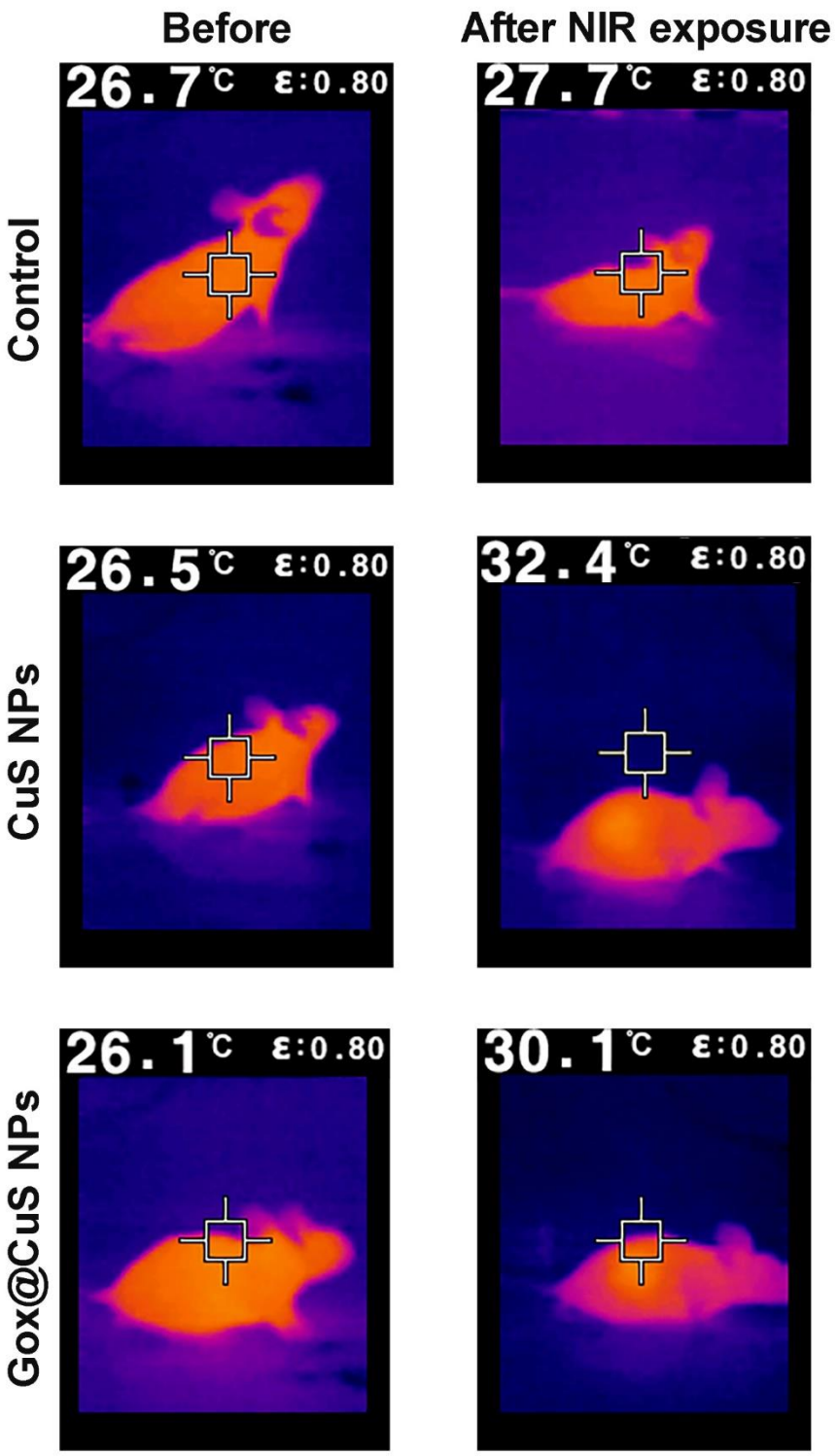

Figure S25: In vivo infrared thermal imaging of mice from control, CuS nanoparticle (NP), and Gox@CuS NP groups with near infrared (NIR) irradiation after drug administration ([NPs] = 200 nM, 980 nm, 5 W/cm^2 for 300 s).

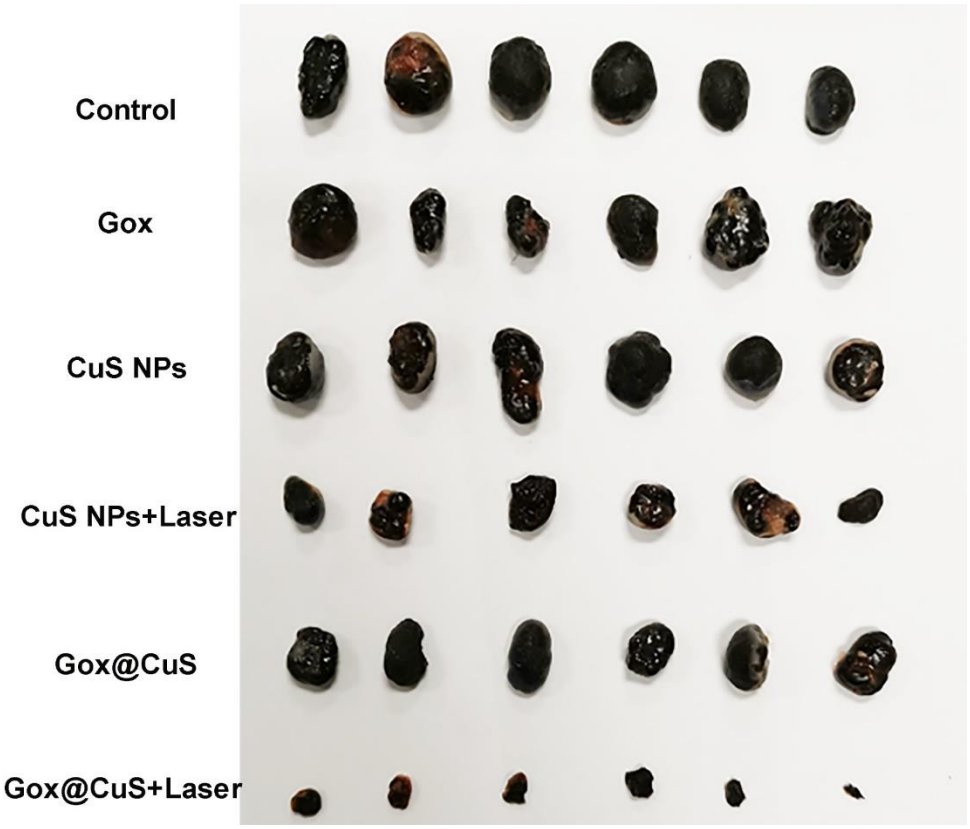

Figure S26: Therapeutic effect of Gox@CuS nanoparticles (NPs) after 10 d of treatment with almost complete eradication of the tumors.

Figure S27: Images of mice after 10 d of treatment using Gox@CuS nanoparticles (NPs) with near infrared (NIR) irradiation, showing all mice were cured with a dark black scar.

Table S1: Energy dispersive X-ray analysis of the atomic fraction of the CuS nanoparticles (NPs) and Gox@CuS NPs. (N/D: not detectable).

Metal	CuS NPs (atom%)	Gox@CuS NPs (atom%)
Cu	70	33.2
S	30	4.5
C	N/D	55.4
N	N/D	3.6
O	N/D	3.3

Table S2: Literature comparison of recent multimodal anticancer nanomedicines in terms of their methodologies and toxicities.

Reference #	Nanoformulation	Applications	In Vivo Treatment/Safety Assessments	IC50(s) (μg/mL)
Tang et al., 2020 (Theranostics)[1333]	Tirapazamine and Gox encapsulated gold nanovesicles	-CDT -Starvation Therapy	-Mice euthanized after 15 d -Body weight & tumor volume -Histology	7.9–22.1 μg/mL
Deng et al., 2020 (*ACS Appl. Mater. Interfaces*)[1334]	Zr-ferrocene (Fc) MOF nanosheet	-CDT -PTT	-Mice euthanized after 14 d -Body weight & tumor volume -Histology	N/A
Ma et al., 2021 (*ACS Appl. Mater. Interfaces*)[1335]	Bi-Fe core-shell NP	-CDT -PDT -PTT	-Mice euthanized after 14 d -Body weight & tumor volume -Histology	N/A
Yang et al., 2020 (*ACS Nano*)[1115]	Semiconducting polymer NP	-PTT -Fluorescence Imaging	-Mice euthanized after 14 & 28 d -Body weight & tumor volume -Histology	N/A
Sun et al., 2020 (*ACS Nano*)[1336]	Doxorubicin (Dox)-loaded mesoporous carbon nanosphere (MnO_2 shell)	-CDT -Chemotherapy -Hypoxia relief	-Mice euthanized after 14 d -Body weight & tumor volume -Histology	N/A
Fang et al., 2020 (*Adv. Funct. Mater.*)[1337]	Gox-loaded Co–fc MOFs	-CDT -Starvation Therapy	-Mice euthanized after 14 d -Body weight & tumor volume -Histology	*7–15 μg/mL
Lyu et al., 2020 (*Adv. Healthc. Mater.*)[1338]	Fe_3O_4@MnO_2 core-shell nanozyme	-CDT -Hypoxia relief -MRI imaging -Radiation Therapy	-Mice euthanized after 18 d -Body weight & tumor volume -Histology	*100 μg/mL
Zhang et al., 2021 (*ACS Appl. Mater. Interfaces*)[1339]	Sinoporphyrin sodium loaded-ZnO_2 NPs	-CDT -PDT -Fluorescence Imaging	-Mice euthanized after 15 d -Body weight & tumor volume -Histology	*~0.5 μg/mL
Ranji-Burachaloo et al., 2019 (*Nanoscale*)[1340]	Gox & hemoglobin encapsulated zeolitic imidazolate framework-8 (ZIF-8) MOFs	-CDT -Starvation Therapy	N/A	1.54–17.01 μg/mL

Fan et al., 2020 (*ACS Appl. Mater. Interfaces*)[1021]	Methotrexate, gadolinium, and artesunate NPs	-CDT -MRI Imaging -Chemotherapy	-Mice euthanized after 21 d -Body weight & tumor volume -Histology -Hemolysis assay -Serum analysis	9.8–19.2 μg/mL
Pu et al., 2020 (*Angew. Chem. Int. Ed.*)[1341]	Iron-chelating semiconductor polymer NP	-CDT -PTT	-Mice euthanized after 14 d -Body weight & tumor volume -Histology -Hemolysis assay	N/A
Zhao et al., 2020 (*Biomaterials*)[1342]	Mn-doped Gd_2O_3 NPs	-CDT -PTT -MRI Imaging	-Mice euthanized after 14 d -Body weight & tumor volume -Histology	*~25–50 μg/mL
Zhang et al., 2020 (*Chem. Eng. J.*)[1343]	Dox loaded CuS@mSiO$_2$@MnO$_2$ nanocomposites	-CDT -PTT -MRI Imaging -Hypoxia Relief	-Mice euthanized after 14 d -Body weight & tumor volume -Histology	*~50–80 μg/mL
Xiao et al., 2020 (*Chem. Eng. J.*)[1344]	L-Buthionine-sulfoximine modified FeS_2 NPs	-CDT -PDT -PTT -Photoacoustic Imaging -Immunotherapy	-Mice euthanized after 21 d -Body weight & tumor volume -Histology -Serum analysis	*~5–10 μg/mL Fe
Zhang et al., 2021 (*J. Colloid Interface Sci.*)[1345]	Chlorin e6 (Ce6)/Gox@ZIF-8/polydopamine@ MnO_2 nanocomposites	-CDT -PDT -Hypoxia Relief -Starvation Therapy	-Mice euthanized after 14 d -Body weight & tumor volume -Histology -Serum analysis	44.134–124.072 μg/mL
Han et al., 2021 (Biomaterials)[1346]	Ag_2S NPs	-PTT -Photoacoustic Imaging -Immunotherapy	-Mice euthanized after 12 d -Body weight & tumor volume -Histology -Immune profiling -Serum analysis	N/A
Wang et al., 2020 (*Biomaterials*)[1347]	$Cu_{2-x}Se$-Au Janus NPs	-CDT -PDT -PTT -Photoacoustic Imaging -CT Imaging	-Mice euthanized after 16 d -Body weight & tumor volume -Histology	477.6–2076.8 μg/mL
Zhang et al., 2019 (*Adv. Sci.*)[1348]	Honeycomb-like gold NPs	-PTT -Brachytherapy (w/ ^{125}I seeds) -Photoacoustic Imaging	-Mice euthanized after 13 d -Body weight & tumor volume -Histology	*~100 μg/mL
Li et al., 2019 (*ACS Appl. Mater. Interfaces*)[1349]	Ce6 & Dox loaded hollow-CuS-1-tetradecanol NPs	-PTT -PDT -Chemotherapy -Fluorescence Imaging	-Mice euthanized after 14 d -Body weight & tumor volume -Histology	*~15–30 μg/mL
Wang et al., 2020 (*Chem. Eng. J.*)[1350]	Hollow-Cu_9S_8 NPs	-CDT -PTT -Photoacoustic Imaging	-Mice euthanized after 18 d -Body weight & tumor volume -Histology -Serum analysis	N/A

Huo et al., 2017 (*Nat. Commun*)[989]	Gox-Fe_3O_4 NPs	-CDT -PTT -Starvation Therapy	-Mice euthanized after 15 d -Body weight & tumor volume -Histology	*~3–6 μg/mL
Gu et al., 2019 (*Nano. Lett.*)[1351]	CuS NPs with Gefitinib	-PDT -PTT -Chemotherapy	-Mice euthanized after 22 d -Body weight & tumor volume -Histology -Serum analysis	N/A
Zhang et al., 2018 (Mater. Horiz.)[1000]	Gox-Ag Nanocubes	-CDT -Starvation Therapy	-Survival analysis until tumor volume reached 2 cm^2 -Histology -Serum analysis	N/A
Zhang et al., 2021 (*Biomaterials*)[1352]	PEGylated liposomes encapsulating $Fe(OH)_3$-doped CaO_2 NPs & Gox	-CDT -Starvation Therapy -Hypoxia Relief	-Mice euthanized after 16 d -Body weight & tumor volume -Histology	*~0.3 μg/mL Gox
This work	Gox-CuS NPs	-CDT -PDT -PTT -Starvation Therapy	-Mice euthanized after 14 d -Body weight & tumor volume -Histology -Serum analysis	~0.1 μg/mL CuS

N/A: Not Available/ Not Reported; CDT: chemodynamic therapy; PDT: photodynamic therapy; PTT: photothermal therapy.
*: Calculated IC values (not reported in the papers).

~ Appendix 3 ~

Supplemental Information for Chapter 6

The work presented in this appendix has been published as supplementary information for:

Singh, P.*, Chen, Y.*, **Youden, B.***, Oakley, D., Carrier, A., Oakes, K., Servos, M., Jiang, R., and Zhang, X. Accelerated Cascade Melanoma Therapy using Enzyme-Nanozyme-Integrated Dissolvable Polymeric Microneedles. *International Journal of Pharmaceutics*, **2024**, 652, 123814. DOI: 10.1016/j.ijpharm.2024.123814.

**These authors contributed equally to this work.*

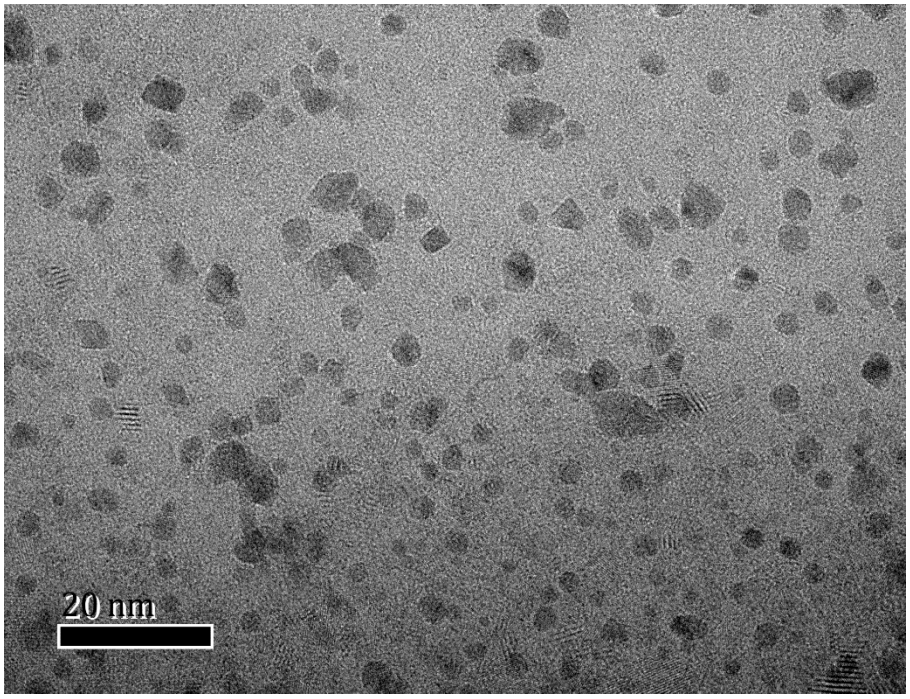

Figure S28: TEM images of the Gox-CuS NCs, showing ultra-small nanoparticles (8 ± 2 nm) with roughly spherical shapes.

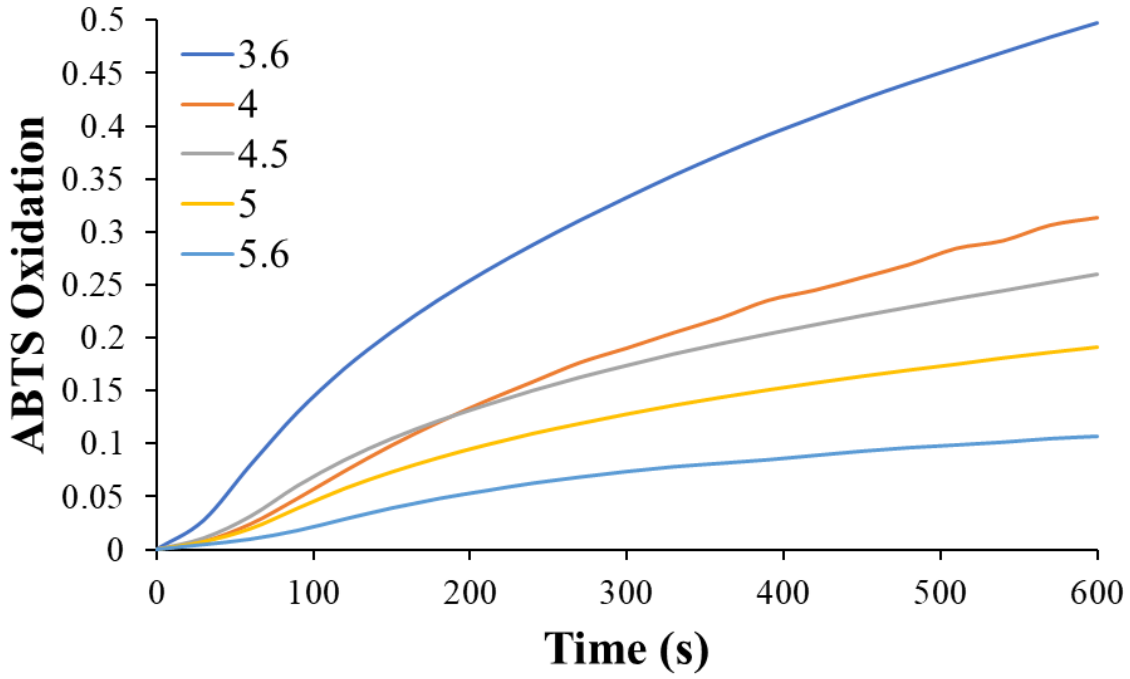

Figure S29: Effect of pH on the oxidation rate of ABTS (500 µM) by CuS NPs (200 µM). Arbitrary H_2O_2 and NaCl concentrations (200 and 100 mM, respectively) were used.

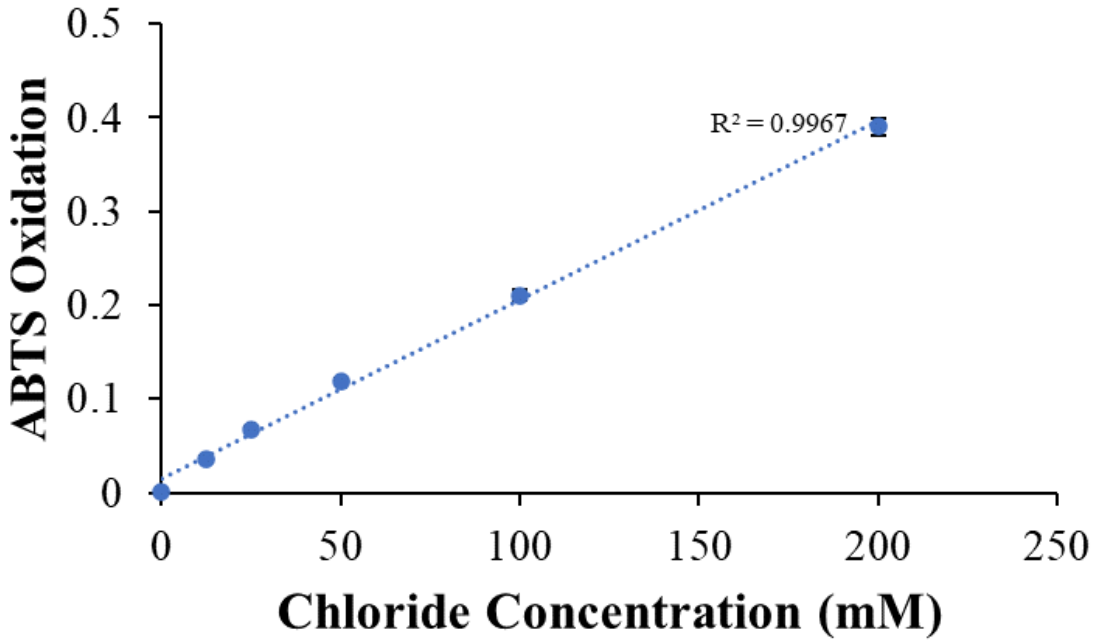

Figure S30: Effect of [Cl^-] on the oxidation of ABTS (500 µM) by CuS NPs (200 µM) and H_2O_2 (200 mM). All measurements were taken 10 min after the addition of H_2O_2. Error bars indicate the mean standard deviation (n = 3).

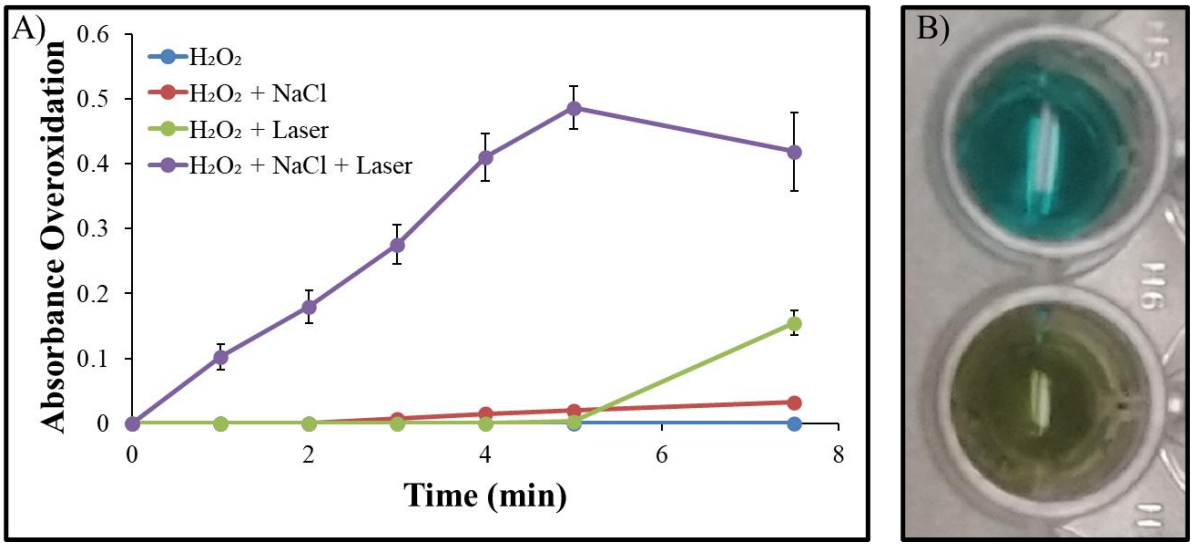

Figure S31: Overoxidation of ABTS into a yellow species. A) Effects of Cl- (200 mM) and/or NIR irradiation (808 nm, 1.0 W/cm2) on ABTS overoxidation. B) Visual appearance of oxidized $ABTS^{+}$ product (top) and overoxidized $ABTS^{2+}$ product (bottom) in aqueous solutions. Error bars indicate the mean standard deviation (n = 3).

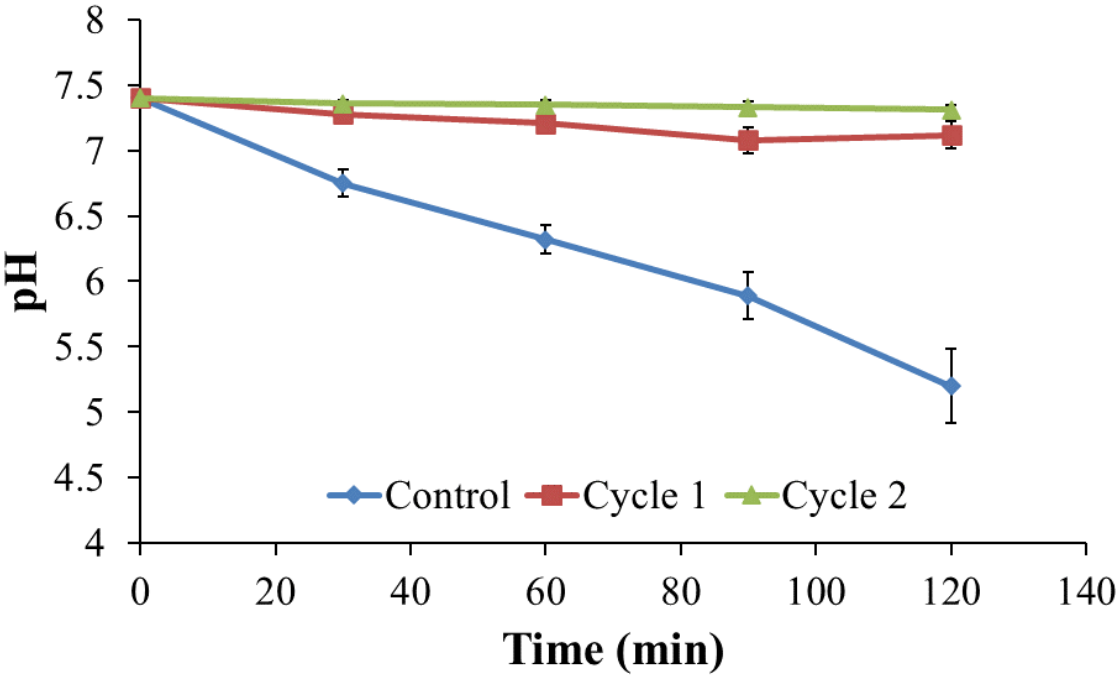

Figure S32: Photothermal deactivation of Gox on CuS surfaces. Each cycle of irradiation consisted of 5 minutes of laser irradiation (808 nm) at 1.0 W/cm^2. Samples were prepared in 0.1X PBS (pH 7.4) containing 5 mM glucose. Control is the Gox-CuS NCs without NIR irradiation. Here, the pH decrease over time indicates the activity of Gox on glucose oxidation; after NIR irradiation, Gox was deactivated and unable to catalyze glucose oxidation. Therefore, in in vivo experiments (Section 6.3.6), NIR laser irradiation was applied 10 min after MN application so that Gox

could enable glucose oxidation, H_2O_2 build-up, and pH drop within the tumor tissue (Equation 3). Error bars indicate the mean standard deviation (n = 3).

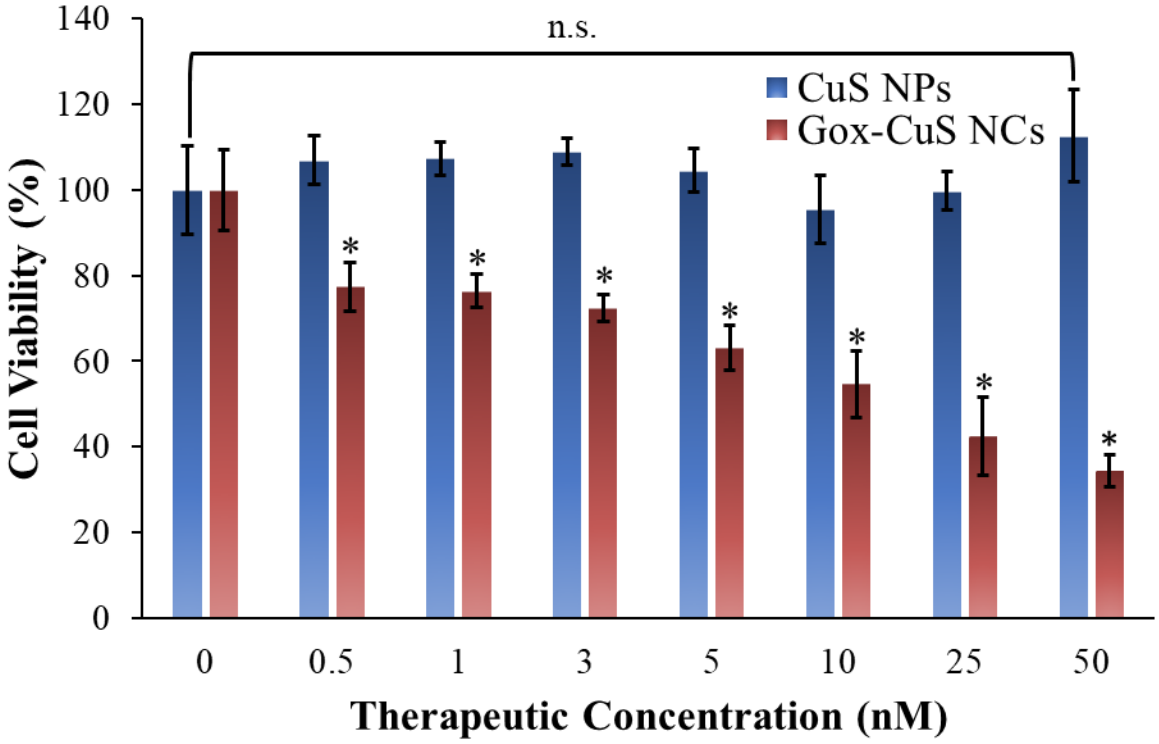

Figure S33: Cell viability assay of HEK293 cells after exposure to CuS NPs and Gox-CuS NCs. *p < 0.05. Error bars indicate the mean standard deviation (n = 3).

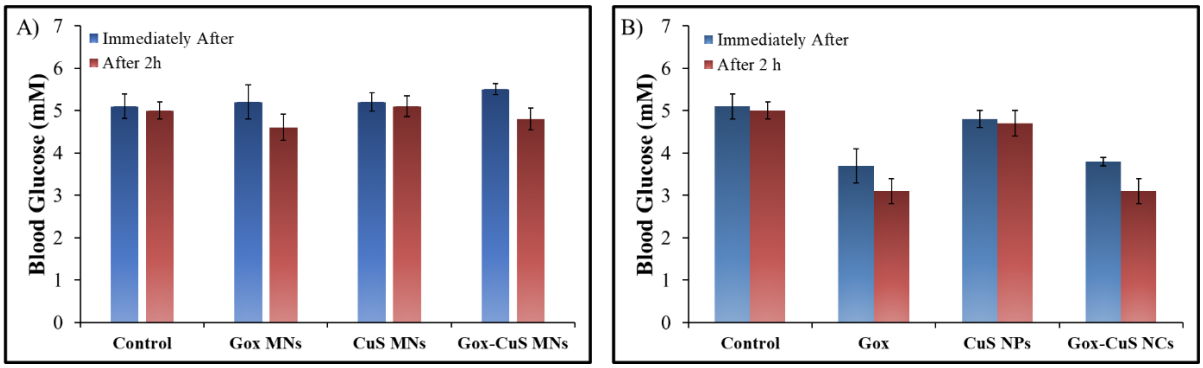

Figure S34: Blood glucose levels following A) DPMN patch application or B) injection. *p < 0.05. Error bars indicate the mean standard deviation (n = 3).

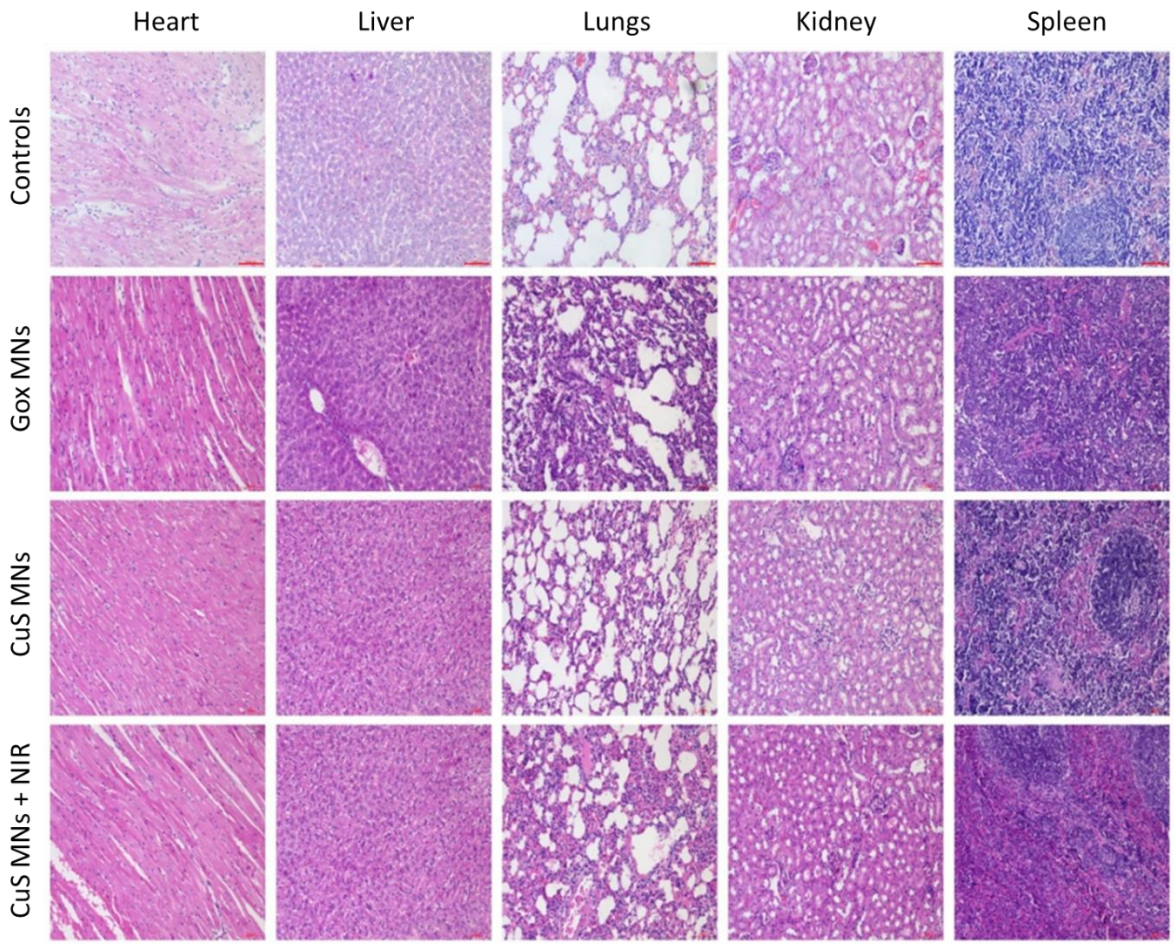

Figure S35: Histological analysis of various body organs of mice after the 10-d treatment using DPMNs.